NASA/CP-2003-212155

Atmospheric Ionizing Radiation (AIR): Analysis, Results, and Lessons Learned From the June 1997 ER-2 Campaign

Edited by:

J. W. Wilson, I. W. Jones, and D. L. Maiden
Langley Research Center, Hampton, Virginia

P. Goldhagen
DOE Environmental Measurements Laboratory, New York, New York

February 2003

The NASA STI Program Office . . . in Profile

Since its founding, NASA has been dedicated to the advancement of aeronautics and space science. The NASA Scientific and Technical Information (STI) Program Office plays a key part in helping NASA maintain this important role.

The NASA STI Program Office is operated by Langley Research Center, the lead center for NASA's scientific and technical information. The NASA STI Program Office provides access to the NASA STI Database, the largest collection of aeronautical and space science STI in the world. The Program Office is also NASA's institutional mechanism for disseminating the results of its research and development activities. These results are published by NASA in the NASA STI Report Series, which includes the following report types:

- TECHNICAL PUBLICATION. Reports of completed research or a major significant phase of research that present the results of NASA programs and include extensive data or theoretical analysis. Includes compilations of significant scientific and technical data and information deemed to be of continuing reference value. NASA counterpart of peer-reviewed formal professional papers, but having less stringent limitations on manuscript length and extent of graphic presentations.

- TECHNICAL MEMORANDUM. Scientific and technical findings that are preliminary or of specialized interest, e.g., quick release reports, working papers, and bibliographies that contain minimal annotation. Does not contain extensive analysis.

- CONTRACTOR REPORT. Scientific and technical findings by NASA-sponsored contractors and grantees.

- CONFERENCE PUBLICATION. Collected papers from scientific and technical conferences, symposia, seminars, or other meetings sponsored or co-sponsored by NASA.

- SPECIAL PUBLICATION. Scientific, technical, or historical information from NASA programs, projects, and missions, often concerned with subjects having substantial public interest.

- TECHNICAL TRANSLATION. English-language translations of foreign scientific and technical material pertinent to NASA's mission.

Specialized services that complement the STI Program Office's diverse offerings include creating custom thesauri, building customized databases, organizing and publishing research results ... even providing videos.

For more information about the NASA STI Program Office, see the following:

- Access the NASA STI Program Home Page at ***http://www.sti.nasa.gov***

- E-mail your question via the Internet to help@sti.nasa.gov

- Fax your question to the NASA STI Help Desk at (301) 621-0134

- Phone the NASA STI Help Desk at (301) 621-0390

- Write to:
  NASA STI Help Desk
  NASA Center for AeroSpace Information
  7121 Standard Drive
  Hanover, MD 21076-1320

NASA/CP-2003-212155

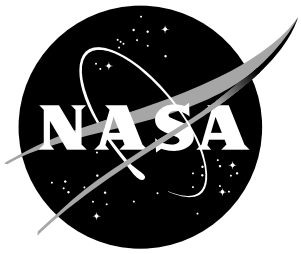

Atmospheric Ionizing Radiation (AIR): Analysis, Results, and Lessons Learned From the June 1997 ER-2 Campaign

Edited by:

J. W. Wilson, I. W. Jones, and D. L. Maiden
Langley Research Center, Hampton, Virginia

P. Goldhagen
DOE Environmental Measurements Laboratory, New York, New York

Proceedings of a workshop sponsored by the National Aeronautics and Space Administration, Washington, D.C., and held at Langley Research Center, Hampton, Virginia
March 30-31, 1998

National Aeronautics and
Space Administration

Langley Research Center
Hampton, Virginia 23681-2199

February 2003

The use of trademarks or names of manufacturers in the report is for accurate reporting and does not constitute an official endorsement, either expressed or implied, of such products or manufacturers by the National Aeronautics and Space Administration.

Available from:

NASA Center for AeroSpace Information (CASI)
7121 Standard Drive
Hanover, MD 21076-1320
(301) 621-0390

National Technical Information Service (NTIS)
5285 Port Royal Road
Springfield, VA 22161-2171
(703) 605-6000

Preface

It was the foresight of Trutz Foelsche of the NASA Langley Research Center who first identified neutrons as an important unresolved issue relative to high-altitude supersonic commercial operations. Furthermore, Foelsche first suggested that solar particle events may be a major concern to high-altitude operations in the polar regions where the geomagnetic cutoffs are low and low-energy protons produced by solar related activity could impact operations. A program for the understanding of biologically important radiation components above 60,000 ft altitudes produced by background galactic cosmic rays (GCR) and to make radiation measurements during a solar particle event (SPE) was directed by Foelsche over the major portion of solar cycle 20 from 1965 through 1971. That program demonstrated that neutrons are the dominant contributor to high altitude exposures and that solar particle events can give large contributions to exposures over a few hour time periods requiring real-time radiation monitoring during high-altitude operations and the development of evasive techniques to reduce exposure. Aside from the possible exposure during a large solar particle event, the radiation levels from the background GCR were found to be within acceptable levels for radiation workers although the high-altitude exposures were considered high for even an occupationally exposed group. At the close of that activity, several issues were identified as remaining unresolved issues. Among these issues was the uncertainty of the neutron spectrum above the measurements of the Langley program of about 10 MeV. The measurements of this early Langley program are the basis of the first atmospheric ionizing radiation (*AIR*) model.

It was a growing concern of the 1980's that the solid tumors observed in the World War II a-bomb survivors were higher than anticipated on the basis of the earlier observations of leukemia incidence. Earlier estimates of cancer risk coefficients were made assuming that the solid tumors, which appear many decades after the exposure, would be no greater than the leukemia incidence, which mostly occurred in the first decade. Data on solid tumor deaths in the 1960's and 1970's were observed to be about five times greater than previously assumed placing great doubt on the exposure limits used in radiation protection practice. Recommended exposure limits were radically reduced in the 1990 recommendations of the International Commission on Radiological Protection. It now became of concern that subsonic commercial operations may be adversely affected by exposure limitations in spite of the reduced levels of radiation exposure rates at subsonic altitudes. At the same time that recommended limits declined, the relative biological effectiveness (RBE) of neutrons was found to be higher than previously estimated resulting in a fifty- percent increase in neutron exposure contributions which are so important to aircraft operations. At the same time, new analysis techniques for high-energy neutron multisphere spectrometers developed by Ferenc Hajnal of the DOE Environmental Measurements Laboratory were used to reanalyze subsonic aircraft measurements and evidence of an underestimate of the high-energy neutron spectrum (above 10 MeV) in prior analysis was observed which results in even higher estimates of neutron exposures in aircraft

operations. The concerned European Communities held a workshop in Luxembourg on the "Radiation Exposure of Civil Aircrew" in June of 1991 to address these issues.

The United States initiated a program to assess the technology required for an environmentally safe and operationally efficient High Speed Civil Transport (HSCT) for entrance on the world market after the turn of the century. Due to the changing regulations on radiation exposures and the growing concerns over uncertainty in our knowledge of atmospheric radiations, the NASA High Speed Research Project Office (HSRPO) commissioned a review of "Radiation Exposure and High-Altitude Flight" by the National Council on Radiation Protection and Measurements (NCRP). On the basis of their recommendations, the HSPRO funded a flight experiment to resolve the environmental uncertainty in the atmospheric ionizing radiation levels as a step in developing an approach to minimize the radiation impact on HSCT operations. To minimize costs in this project, an international investigator approach was taken to assure coverage with instrument sensitivity across the range of particle types and energies to allow unique characterization of the diverse radiation components. The present workshop is a result of the flight measurements made at the maximum intensity of the solar cycle modulated background radiation levels during the month of June 1997.

During the preparation of the proceedings from the workshop, it was decided to terminate the High Speed Research Program. Although the technology for the development of the HSCT had advanced greatly since the proposed SST the current state of the technology would not yet produce a cost effective high-speed commercial transport. Since subsequent workshops and flight measurements were not likely to occur, it was decided to postpone the publishing of the proceedings until the analysis of the June 1997 flight had matured. A sufficient level of maturity has now been reached for a report at this time. As a result the neutron spectrum is now well understood and only details on global variation are yet to be tested. A computational model has been identified for building the next generation *AIR* model. Flight measurements at times other than solar minimum are required to develop a philosophy for aircrew protection. A strong basis for health compensation of even subsonic aircrew is developing but requires more study of the health risks of US aircrew.

JWW

August 12, 2002

Contents

Chapter 1: Atmospheric Ionizing Radiation and the High Speed Civil Transport

D. L. Maiden*, J. W. Wilson*, I. W. Jones*, P. Goldhagen**

***NASA Langley Research Center, Hampton, VA 23681**
****DOE Environmental Measurements Laboratory, New York, NY 10014**

Atmospheric Ionizing Radiation and the High Speed Civil Transport

Preface

Atmospheric ionizing radiation is produced by extraterrestrial radiations incident on the Earth's atmosphere. These extraterrestrial radiations are of two sources: ever present galactic cosmic rays with origin outside the solar system and transient solar particle events that are at times very intense events associated with solar activity lasting several hours to a few days. Although the galactic radiation penetrating through the atmosphere to the ground is low in intensity, the intensity is more than two orders of magnitude greater at commercial aircraft altitudes. The radiation levels at the higher altitudes of the High Speed Civil Transport (HSCT) are an additional factor of two higher. Ionizing radiation produces chemically active radicals in biological tissues that alter the cell function or result in cell death. Protection standards against low levels of ionizing radiation are based on limitation of excess cancer mortality or limitation of developmental injury resulting in permanent damage to the offspring during pregnancy. The crews of commercial air transport operations are considered as radiation workers by the EPA, the FAA, and the International Commission on Radiological Protection (ICRP). The annual exposures of aircrews depend on the latitudes and altitudes of operation and flight time. Flight hours have significantly increased since deregulation of the airline industry in the 1980's. The FAA estimates annual subsonic aircrew exposures to range from 0.2 to 9.1 mSv compared to 0.5 mSv exposure of the average nuclear power plant worker in the nuclear industry. The commercial aircrews of the HSCT may receive exposures above recently recommended allowable limits for even radiation workers if flying their allowable number of flight hours. An adequate protection philosophy for background exposures in HSCT commercial airtraffic cannot be developed at this time due to current uncertainty in environmental levels. In addition, if a large solar particle event occurs during flight at HSCT altitudes then passengers and crew may greatly exceed allowable limits unless means are available to reduce exposures.

Introduction

The impact of ionizing radiation on the High Speed Civil Transport was not examined in High Speed Research Program Phase 1 where environmental issues were first addressed as it was not considered a first-priority environmental concern at that time. Although aircrews are recognized by the FAA, the EPA, the NCRP, and the ICRP as radiation workers (occupationally exposed), there are no US regulations for ionizing radiation exposures in commercial transports (unless they carry radioactive materials). Indeed, the concern over subsonic airtraffic commenced only after the latest report on greatly increased cancer risk coefficients and recommendations by national and international advisory bodies to significantly reduce the allowable exposure levels by factors of 2.5 to 5. There is an FAA Circular that recommends air carriers educate crewmembers on the hazards of ionizing radiation. The circular reports that pregnant crewmembers may run a risk as high as 1.3 per thousand births of severe illness to their children as a result of background radiation exposure. This has prompted a study of problems in early pregnancy of aircrews by the National Institute of Occupational Safety and Health (NIOSH).

The impetus to examine the impact of ionizing radiation stems from: (1) recent reductions in recommended radiation exposure limits by the ICRP and the National Council on Radiation Protection and Measurements (NCRP), and (2) recent scientific experimental results confirming the uncertainty in the amount of aircraft radiation exposure. The NCRP examined the state of knowledge of atmospheric radiation in high altitude flight and made recommendations on the need for improved information in order to develop a protection philosophy for high-altitude commercial flight operations. The HSR Environmental Impact radiation element developed the Atmospheric Ionizing Radiation (AIR) project to respond to the need for reduction of uncertainties in measurements applicable to HSCT based commercial operations after which an adequate protection philosophy can be developed.

Background

The Langley Research Center (LaRC) performed atmospheric radiation studies under the SST development program in which important ionizing radiation components were measured and extended by calculations to develop the existing atmospheric ionizing radiation (*AIR*) model. In that program the measured neutron spectrum was limited to less than 10 MeV by the available 1960-1970 instrumentation. Extension of the neutron spectrum to high energies was made using theoretical models. Furthermore, theoretical models of solar particle events showed that potentially high exposures may occur on important high latitude routes but acceptable levels of exposure could be obtained if timely descent to subsonic altitudes can be made. The principal concern was for pregnant occupants onboard the aircraft (Foelsche et al. 1974). As a result of these studies the FAA Advisory Committee on the Radiobiological Aspects of the SST (1975) recommended:

1. Crewmembers will have to be informed of their exposure levels
2. Maximum exposures on any flight to be limited to 5 mSv
3. Airborne radiation detection devices for total exposure and exposure rates
4. Satellite monitoring system to provide SST aircraft real-time information on atmospheric radiation levels for exposure mitigation
5. A solar forecasting system to warn flight operations of an impending solar event for flight scheduling and alert status.

These recommendations are a reasonable starting point to requirements for the HSCT with some modification reflecting new standards of protection as a result of changing risk coefficients.

One result of the SST studies was the realization that subsonic aircrew members are among the most highly occupationally exposed groups (Foelsche et al. 1974, Schaefer 1968) which prompted the FAA to develop methods to further study exposures resulting in the development of the CARI exposure estimation code (named after the Civil Aeronautical Research Institute) based on the LUIN transport code (developed by the Department of Energy (DOE) Environmental Measurements Laboratory) to generate the database (O'Brien and Friedberg 1994). The estimated risk of serious illness to the child of an aircrew member during pregnancy is on the order of 1.3 per thousand (Friedberg et al. 1992) and the FAA recommended that air carriers begin a program of training of their employees on the risks of in-flight subsonic exposures (White 1994). The dose rates at the HSCT altitudes are a

factor of 2-3 higher than for subsonic operations and the HSCT crew annual flight hours will have to be reduced by this same factor to maintain exposure levels comparable to the subsonic crews. One may assume that similar instruction of aircrew will be required for HSCT operations and restrictions on crew utilization of the HSCT will by necessity be different than on subsonic transports.

Regulations on exposure limitation are based mainly on the estimated cancer risk coefficients. These coefficients have increased significantly over the last decade, as solid tumor appearance is higher among the WW2 nuclear weapons survivors than initially anticipated (ICRP 1991). As a result, new recommendations for reducing regulatory limits have been made by national and international advisory bodies (ICRP 1991, NCRP 1993). Whereas subsonic crew exposures were well under the older regulatory limits, the substantial reductions (by factors of 2.5 to 5) in exposure limitations recommended by these advisory bodies resulted in the need to improve aircrew exposure estimates (Reitz et al. 1993). Hence, a workshop on Radiation Exposure of Civil Aircrew held in Luxembourg on June 25-27, 1991 was sponsored by the Commission of the European Communities Directorate General XI for Environmental Nuclear Safety and Civil Protection (Reitz et al. 1993). To be noted in the workshop is the closure of the gap between subsonic aircrew exposures and the newly recommended regulatory limits and in fact some concern that limits may be exceeded in some cases. Thus uncertainty in exposure estimates becomes a critical issue and emphasis on the numbers of and spectral content of high energy neutrons as well as the penetrating multiple charged ions were identified as a critical issue for subsonic flight crews. More recently Japanese flight crews have requested from their government, health benefits on the basis that their exposures are "far greater than the exposure of the average nuclear power plant worker" (Fiorino 1996). The issues for HSCT commercial air travel are compounded by the higher operating altitudes (higher exposure levels) and the possibility of exposures to a large solar event wherein annual exposure limits could be greatly exceeded on a single flight (Foelsche et al. 1974, Wilson et al. 1995).

Impact of *AIR* on HSCT environmental assessment

As a result of the higher expected exposures in high-altitude flight, the congressionally chartered federal advisory agency on radiation protection, NCRP, examined the data on atmospheric radiation and made recommendations (NCRP 1996) on the need for future studies. We summarize their recommendations as follows:

1. Additional measurements of atmospheric ionizing radiation components with special emphasis on high-energy neutrons
2. A survey of proton and neutron biological data on stochastic effects and developmental injury for evaluation of appropriate risk factors
3. Develop methods of avoidance of solar energetic particles, especially for flight above 60,000 ft
4. Develop an appropriate radiation protection philosophy and radiation protection guidelines for commercial flight transportation, especially at high altitudes of 50,000 to 80,000 ft

Clearly, these issues must be addressed before the HSCT goes into commercial service to ensure the safety of the crew and passengers. The current effort in this assessment is the development of an experimental flight package to reduce the uncertainty in AIR models in direct response to the NCRP recommendations.

Goals

The focused goal of this project is to develop an improved *AIR* model with uncertainties in the atmospheric radiation components reduced to twenty percent or less to allow improved estimation of the associated health risks to passengers and crew. Special emphasis will be given to the high-energy (10 to 1000 MeV) neutrons in the altitude range of 50,000 to 70,000 ft. The results will be expressed in terms of an environmental *AIR* model able to represent the ambient radiation components including important spectral and angular distributions that will allow evaluation of aircraft shielding properties and the geometry of the human body. The model must be capable of representing the atmospheric radiation levels globally as a function of solar modulation. The model must furthermore be capable of evaluating radiation levels during solar particle event increases in near real-time using data from available satellite systems to allow risk mitigation and flight planning in the case of a large solar event.

Following the development of the *AIR* model, studies of impact of radiation exposure limitations on crew utilization and impact on passengers (especially frequent flyers) will be made to assess the need of developing a specific philosophy to control exposures in HSCT operations. These will result in requirements for study of the economic impact on operations costs. For example, it has been suggested that the HSCT crew be utilized at one third to one half the number of block hours as now utilized by subsonic aircraft to minimize exposures, which requires more crews at increased cost. The other possibility is to rotate crews to less exposed routes for a portion of each year and especially during a declared pregnancy. The need for and the extent of such exposure control measures must await the improvement of the *AIR* model.

Current predictive methods and impact on HSCT operations

The first model developed for atmospheric ionizing radiation was empirically based on the global measurements program under the LaRC SST study (Foelsche et al. 1974). The instrumentation consisted of tissue equivalent ion chambers, fast neutron spectrometers, and nuclear emulsion. Limited flights were made with tissue equivalent proportional counters (TEPCs), Bonner spheres, and the Concorde prototype radiation-monitoring instrument. The flights were made over most of solar cycle 20 with altitude surveys, latitude surveys, and measurements during the solar particle event of March 1969. Unfortunately the program was terminated in the year prior to the largest solar event observed during solar cycle 20, the 4 August 1972 event. The data set was augmented by the decades of measurements of air ionization rates using argon filled steel-walled ion chambers. The high-energy neutrons were estimated using Monte Carlo calculations as an extension of the measured 1 to 10 MeV flux from the fast neutron spectrometers. These theoretical high-energy neutron flux calculations indicated that over half of the neutron dose is from neutrons of energy above 10 MeV and are quite uncertain in their spectral content and intensity as was noted in the LaRC study (Foelsche et al. 1974), concluded by the Luxembourg workshop (Reitz et al. 1993), and by the

NCRP (1995). The solar particle event predictions are based on Monte Carlo calculations using the Bertini nuclear model and the United Kingdom nuclear data files (Foelsche et al. 1974).

In a recent report by LaRC, a survey was made of measurements and calculations of the neutron flux spectra for which large uncertainties in the resulting neutron dose were estimated (Wilson et al. 1995). The effects of these uncertainties on subsonic and HSCT flight crews are shown in figure 1. The exposure limits recommended by the ICRP and NCRP as a result of the now known higher cancer risk coefficients and new standards for pregnancy (table 1 columns 3 and 4, note that foot note *b limits* the average annual exposure to about 10 mSv), leave subsonic flight a concern to aircrews throughout the world (Reitz et al. 1993, Fiorino 1996) and an emphasis on reducing the uncertainties for development of an adequate radiation protection philosophy is most appropriate (NCRP 1995).

This is especially true for the HSCT with its much higher exposure rates as shown. However, the concern for frequently flying passengers is more for the slower subsonic flights (fig. 2) than the HSCT unless there is a large solar event. Diplomatic and business couriers may be more exposed on subsonic flights if their number of trips is fixed but the HSCT exposures would be higher if their flight hours are fixed. Clearly any advice to be given on control of individual exposures to either crew/passengers is limited by the exposure uncertainties in figures 1 and 2.

A second model has appeared from the FAA using the LUIN transport code to generate the necessary database. Although the LUIN code was initially in poor agreement with the LaRC measurements (Friedberg and Neas 1980), the last several years have shown substantial improvements in the LUIN code to describe dose and dose equivalent rates. A recent examination of the LUIN model in comparison with more advanced transport codes is shown in figure 3. Shown are results of the FLUKA code, a Monte Carlo code (Merker) developed under the LaRC project, and the 1997-1998 version of the LUIN code. Note that the differences in the range from 10 to 1000 MeV are as large as an order of magnitude. Recall that the neutrons in this range contribute over half of the total neutron dose so that these differences are quite important to exposures. To better understand the meaning of these comparisons, a limited Bonner sphere measurement on Mount Zugspitze (Schraube et al. 1997) is shown in figure 4 with the FLUKA results and emphasizes the large uncertainty in the present radiation model used by the FAA.

An informal December 1995 report on "HSCT Radiation Exposure" by Steven L. Baughcum and James R. Gillis examined mission radiation exposures for four city-pairs. It is interesting to note that the same exposure was calculated with the Seattle to Tokyo route which traverses from 55 degrees N to 25 degrees N geomagnetic latitude and the Los Angeles to Tokyo route which traverses from about 40 degrees N to 25 degrees N, which is due to the differences in flight times. A northern route from New York to London indicated that the northern routes are more critical to high altitude radiation exposure. Baughcum and Gillis calculated 3.7 millirems for the 3-hour NYC to London trip. If this exposure is converted to millisieverts and scaled up for a maximum annual 900 block hour duty (actual duties could be less), the crewmember would have received 11.1 mSv (or 6.2 mSv for 500 block hours). Wilson et al (1995) indicate that the same 900 block hours should produce a minimum cumulative exposure of about 11.4 mSv (or 6.3 mSv for 500 block hours) at solar minimum but with current uncertainties that it could be as high as 21 mSv (or 11.7 mSv for 500 block hours). The ICRP 60 recommended exposure limit for

occupational exposures is 20 mSv per year and the new NCRP recommendation is for 10 mSv per annum for new designs to assure that lifetime exposures do not exceed 10 x age (mSv). The lower value calculated by the CARI code could be due to differences in solar modulation, in intensity/spectra of high-energy neutrons, in other radiation components, and in the dosimetric evaluations.

A route from Los Angles to London was examined [Friedberg letter] using CARI-2 by Dr. Wallace Friedberg at the FAA Civil Aeromedical Research Institute. His estimate was for a 6.3-hour mixed-Mach number flight that avoided supersonic flight over the landmass. He estimated the radiation dose for the HSCT flight to be 49 microSv. For 900 block hours this would accumulate to be approximately 7 mSv (or 3.9 mSv for 500 block hours). Baughcum and Gillis examined the same city pair for a similar 6.53-hour flight and came up with 5.5 mrem. Converting this to millisieverts and for 900 block hours this is approximately 7.59 mSv (or 4.2 mSv for 500 block hours). Wilson did not do a similar city pair estimate. Both of these estimates are within the ICRP 60 limit of 20 mSv per year, but push the new NCRP recommendation of 10 mSv per annum for new designs for those crew members which fly near their maximum allowable block hours. Numerous comparisons of the *AIR* model with other measurements and calculations are given elsewhere (Wilson et al. 1991).

AIR model development

The basic quantities of the present *AIR* model are the air ionization rate, the 1 to 10 MeV neutron flux, and the rate of nuclear star events in nuclear emulsion. These quantities were measured over a complete set of altitudes, geomagnetic latitudes, over the solar cycle, and scaled according to known procedures to allow a total time-dependent mapping of the global radiation field as a function of time. The limitations of the model concern the high-energy neutron spectrum, the quality factor of the ionic components, and the relative contribution of the nuclear stars.

The first step in improved model development is to add estimates of the proton and light ion flux using available transport models and databases. An international agreement with the Japan Atomic Energy Research Institute is being negotiated to provide computational support for adding improved results for the radiation-induced fields from the galactic cosmic ray protons. These results will be augmented by the light and heavier galactic cosmic ion components using the LaRC cosmic ray transport codes. Global fields as a function of time will be generated using the world wide vertical cutoff database and high-latitude neutron-monitor count rates. Model validation will require a definition of the mapping of the model field quantities to the ER-2 instruments. Although each investigator is responsible for the definition of their own instrument response functions, the LaRC team will assist in these definitions to the extent possible within funding and manpower limitations.

AIR flight measurements

An instrument package has been developed in accordance with the NCRP recommendations through an international guest investigator collaborative project to acquire the use of existing instruments to measure the many elements of the radiation spectra. Selection criteria was established which included: (a) the instruments had to fit into the cargo

bay areas of the ER-2 airplane and able to function in that environment (Some high-quality laboratory instruments were rejected because of their large size or inability to operate in the ER-2 environment.), (b) the instrument had to come at no-cost for use by the project to meet budget constraints, (c) the instrument must have a principal investigator which had their own resources to conduct data analysis, and (d) the array must include all significant radiation components for which the NCRP had made minimal requirements. The flight package must be operational and the first flight occur before or near the maximum in the galactic cosmic ray intensity (ca. spring/summer 1997) and extend through the next cosmic ray minimum (ca. June 2000 ± 13 months, Wilson et al. 1999).

The flight package developed uses all of the available space in the ER-2 cargo areas. The instrument layout is shown in Figure 5. The primary instruments in the package consist of neutron detectors, scintillation counters, and an ion chamber from the Environmental Measurements Laboratory of the Department of Energy and charged particle telescopes from Institute of Aerospace Medicine of Deutsche Forschungsanstalt fur Luft- und Raumfahrt (DLR), and Johnson Space Center. Ten other instruments from Germany, Italy, the United Kingdom, and Canada make up most of the remainder of the flight package. These include passive track detectors from Institute of Aerospace Medicine, DLR, and University of San Francisco; tissue equivalent proportional counters (TEPC) from Boeing and Defence Research Establishment Ottawa; and dosimeters from Boeing, Royal Military College of Canada in Ontario and National Radiological Protection Board (NRPB) in the UK. The existing primary instruments and data systems were modified for operation on the ER-2. A data acquisition system was incorporated to control operation of the entire instrument package, and to record data from the primary instruments during flight. Data from the other instruments are recorded separately by each instrument and recovered after a flight.

Status of regulatory process

The inherent assumption in regulating occupational exposures is that society and the individual worker obtains benefits from the execution of said occupation. The issue is the determination of the risks incurred by these occupations and the acceptability of those risks to both the individual worker and the society at large. The individual's decision to accept an at-risk occupation has to be made on a case by case basis with adequate information on the risks to be assumed (informed consent). At the same time it is a matter of law that the employer is to keep exposures as low as reasonably achievable (the ALARA principle) and is a function of the means at the employer's disposal. With respect to the general public, it is inherently assumed that these individuals are exposed without direct personal benefit and indeed without their consent. For this reason, the allowable exposures for the general public are normally set by regulators to be an order of magnitude lower than the exposure limits for the occupationally exposed.

The regulatory process is peculiar to each country. The process in the US is shown in figure 6. The ICRP is an international advisory body composed of members of various national advisory bodies among its committees. The NCRP is a congressionally chartered federal advisory council utilized by the national regulatory agencies in setting standards. The recommendations of the NCRP typically result in changes in US regulations about 5 to 7 years

later. The latest changes in recommendations on exposure limitations are contained in the ICRP report 60 (1991) and the report NCRP 116 (1993). Although there are no current regulations within the US governing aircrew exposures, the FAA has published an advisory circular recommending training of aircrews on radiation exposure risks (White 1994) and the ICRP has recommended that aircrews be recognized as an occupationally exposed group with the usual regulatory requirements (ICRP 1991).

The status of current US regulations on exposures is discussed elsewhere (Fed. Reg. 1991, OSHA 1996, EPA 1994) and in recently proposed changes to mainly cover pregnancy (Cool and Peterson 1991), and recent proposed exposure limitations (ICRP 1991, NCRP 1993) are shown in table 1. It is anticipated that US and foreign regulations will follow the NCRP 116 (1993) and ICRP 60 (1991) more closely by the end of the decade. Indeed, the FAA advisory circular on the training of aircrew refers exclusively to the ICRP 60 (1991) recommendations with obvious implications.

The European regulatory process is more complicated due to the inter-relation through the Commission of European Communities (CEC). The process in the UK is shown in figure 7 as compiled by C. K. Wilson (1993). The CEC has held a workshop on aircrew exposures (Reitz et al. 1993) which was a driving factor in the present project as well as in various international organizations (Three of whom are collaborators in the ER-2 flight project). It is anticipated that aircrew in Europe will be treated on the same level as other radiation workers and methods of exposure estimates are being explored. For example, the NRPB in figure 7 is a government agency in the UK developing dosimetric methods for use on commercial subsonic aircraft and a partner in the present ER-2 flight project.

At present we have no clear picture of the Japanese regulatory process but the Japanese Aircrew Unions have petitioned the government to treat their members on the same level as the other occupationally exposed workers within their country (Fiorino 1996).

The above statements apply to mainly subsonic airtraffic and are driven by the lowering of the ICRP recommended exposure limits as a result of the increased cancer risk estimates as determined from studies of the WW2 nuclear weapons survivors. The exposures at HSCT altitudes are substantially higher during ordinary days due to the higher operating altitudes and in addition may suffer from a solar particle event exposure in which high exposures may occur on a single flight, affecting not only the crew but also the passengers. For example, OSHA (1996) defines a "high radiation area" as one in which an hourly dose of 1 mSv is present (a level easily exceeded by a major solar event in an HSCT at high latitudes) and requires a "conspicuous sign" reading "Caution, High Radiation Area." The NCRP has cited a need for future studies to develop a radiation protection philosophy for risk mitigation and exposure control for which the present project is in direct response. A simplified listing of the NCRP recommendations is given in an earlier section of this report.

Relationship to other Government Entities

The most cost-effective means of performing this project was to utilize available equipment and personnel to make the necessary measurements and data analysis. This required us to look beyond the bounds of the US and the resulting team is international in character. The work will be accomplished under various interagency, national, and international agreements as follows:

United States

- DOE Environmental Measurements Laboratory
- DHHS National Institute of Occupational Health and Safety
- FAA Civil Aeromedical Institute
- NCRP National Council on Radiation Protection
- NASA Johnson Space Center
- Hampton University
- Prairie View A&M University
- Yale University

Canada

- Royal Military College
- Defence Research Establishment-Ottawa

Germany

- DLR Institute of Aerospace Medicine
- University of Kiel

United Kingdom

- National Radiological Protection Board

Italy

- University of Pisa
- Istituto Superiore di Sanita'

Japan

- Japan Atomic Energy Research Institute

Assessment of impact on HSCT

Studies have identified a substantial market for a future supersonic airliner--or High Speed Civil Transport-- to meet the rapidly growing demand for long haul travel, particularly around the Atlantic and Pacific rim. Over the period from 2005 to 2040, this market, without any environmental restrictions, could support over 1000 aircraft. The

current HSCT is designed to carry 300 passengers at Mach 2.4 on transoceanic routes over distances up to 5,000 nautical miles.

The current Mach 2.4 aircraft design will cruise at altitudes between 53,000 to 65,000 feet (16.8 to 19.2 km). Studies have indicated a utilization rate of at most 15 hours per day. If an average flight time of 4 hours is assumed, an HSCT will fly at most four flights per day or 1460 flights per year. If a down time of 10 percent for maintenance is assumed, the annual flights will be reduced to approximately 1314. For a load factor of 70 percent the number of passengers on board per flight will be 210 with an on board crew of about 12 (pilot, co-pilot, and 10 flight attendants). Therefore the number of person flights (passengers and crew) per HSCT per year is approximately 291,708. Assuming the crew flies 8 hours a week then the required crew size per aircraft consists of 168 members for which the majority are women of child bearing age (Reitz et al. 1993). One can further say that if there are 1000 units operating, the number of person flights per year would be 291,708,000 including the flights of the 168,000 crewmembers. Assuming a western distribution of ages, about 1 percent of the people flown will be pregnant, which totals 2,917,080 pregnant person flights including the flights of the 1,680 pregnant crew members. Of the 2.9 million pregnancies flown, 972,360 will be in the first trimester, the most critical time in the development of the fetus.

Background exposures of pregnant occupants- The FAA had estimated that subsonic crew exposures could result in as much as a 1.3 per thousand incidence rate of severe illness to the developing child by working during pregnancy (McMeekin 1990). This realization is in part the basis for the NIOSH/FAA study of pregnancy termination of women in the airline industry (Grajewski 1997). The background radiation levels at HSCT altitudes are a factor of 2 to 3 higher (Foelsche et al. 1974, Wilson et al. 1991) and incidence of severe illness could be as high as 3-4 per thousand assuming subsonic work patterns apply (McMeekin 1990). In this assessment we assume the crew will fly only one round trip per week so exposures are more comparable to subsonic exposures and the rate of severe illness is 1.3 per thousand. Assuming a western distribution of population (including children) among the 168,000 crew members which underestimates the pregnancy rate, one would anticipate 2 or more births with severe radiation induced developmental injury per year among the crewmembers. There is a clear need for development of a radiation protection philosophy and counseling of crewmembers on their personal exposures (NCRP 1995).

Solar particle event exposures- Assuming 15 hours of operation of 1000 aircraft with a 10 percent down time places 563 aircraft aloft at any time during the day. Utilization studies places 72 percent on high latitude routes with approximately 104,895 occupants. If a solar particle event occurs and assuming western population distributions, there could be as many as 1049 pregnancies on high latitude routes which could receive up to 10 to 20 mSv on a single flight unless means of controlling exposures is implemented. The number of individuals expected with serious health effects can be quite high if adequate precautions are not taken during large solar event. Clearly, some provision for protection of passengers and crew from such events needs to be developed (Reitz et al. 1993, NCRP 1995).

Exposures of the Crewmembers- The risk of health effects of greatest concern is excess fatal cancer. The excess risk of fatal cancer from background radiation among the crew (excepting pregnancy discussed in the preceding subsection) can be found by using the risk coefficient of 6.3 per 100,000 per mSv (White 1994). The annual exposure for flights from New York to London is as high as 21 mSv for 900 block hours (or 12 mSv for 500 block hours) which is a little over a factor of two higher than the subsonic exposures estimated by the FAA (9.1 mSv for 950 block hours). Assuming a 20-year career, the lifetime excess risk of fatal cancer for 500 block hours is 20 x 12 x 6.3 = 1512 per 100,000 which is comparable to risks of subsonic flight given by the FAA (White 1994) assuming 950 block hours per year. The expected number of excess cancer deaths among the 168,000 crewmembers is 2,540 compared to the normally expected number of naturally occurring cancer deaths of 36,960.

Exposures of the Frequent Flyer- For present purposes we have taken the frequent flyer to be an individual who makes ten round trips per year. Business and courier passengers may greatly exceed these values and would be treated as occupationally exposed, as is the crew. The health concerns (excepting pregnancy) of the frequent flyer are similar to the health concerns of the crew (fatal cancer) and depends strongly on the number of flights per year. The frequent flyer on an HSCT will incur significantly less risk than corresponding flights on subsonic carriers unless a large solar event occurs. The excess risk of fatal cancer from background radiation among the frequent flyers can be found by using the risk coefficient of 6.3 per 100,000 per mSv. The annual exposure for flights from New York to London is at most about 1 mSv for ten round trips which is almost a factor of two lower than the corresponding subsonic exposures. Assuming a 20 year career, the lifetime excess risk of fatal cancer is 20 x 1 x 6.3 = 126 per 100,000. We have no reliable estimates of the number of such travelers or their work patterns.

Be^7 as a maintenance hazard- Be^7 is a radioactive by-product of the interaction of cosmic rays with atmospheric constituents. It decays by electron capture with a half-life of 54.5 days emitting a 0.479 MeV gamma in 10 percent of the decays. The main source terms are in the stratospheric altitude range of 40,000 to 100,000 ft (Dutkiewicz and Husain 1985) and at high latitudes (above 55 degrees magnetic). The transport in the atmosphere is of considerable interest to atmospheric circulation studies and the DOE Environmental Measurements Laboratory has developed a database on Be^7 concentrations. The Be atom is an open electron shell structure and is expected to have a large sticking coefficient to surfaces. The rate of adherence (mainly to leading edge surfaces, Fishman et al. 1991) will depend on the atmospheric Be^7 concentration along the trajectory, air flow, and surface properties and reach a steady state in the 54.5 day time frame since the loss is mainly through decay to Li^7 which is not radioactive. It has been reported (A. Mortlock) that work crews on the Concorde wear radio-protective gear in servicing that aircraft. Given data on the Concorde contamination levels and the DOE/EML source database, one could scale to the HSCT flight conditions using a linear kinetics model.

Single Event Upsets- Single event upsets (SEU) from radiation found at high altitudes have been measured in present day avionics technologies based on microelectronic devices (Normand et al. 1994). Such electronic devices

are sensitive to the sudden introduction of charge into an active element of their circuits. The amount of such charge that is sufficient to change the state of a logic circuit is called the critical charge. As shown in figure 8, there is a rough relationship between critical charge Q_c and the device feature size L (note Q_c is proportional to L^2).

The critical charge also depends on chip design factors and operating voltage. The charge released in the device is proportional to the energy deposited by the particle (1 pico-coulomb of charge is released for every 22.5 eV deposited in silicon). The charge released is not the charge collected since ionization within charged particle tracks is very dense in the track center (Cucinotta et al. 1995) and recombination occurs on a very short time scale (Shinn et al. 1995). Single event upsets in the device are then dependent on the charge collected in comparison to the critical charge. The energy deposit depends linearly on the feature size while the critical charge depends on the feature size squared. Decreasing the feature size by a factor of 2 reduces the charge collected by a factor of 2 while the device sensitivity to upset increases by a factor of four. As the feature size decreases, new physical processes resulting in small energy deposition are able to upset the device. For cosmic ray heavy ions that are directly ionizing, the SEU rate is directly proportional to the cross sectional area of the sensitive region of each device (approximately proportional to L^2), and inversely proportional to the square of Qc (Qc^{-2}, therefore to L^{-4}); thus overall it is strongly inversely proportional to L. For protons and neutrons that ionize indirectly, through nuclear reactions with the device, the SEU rate may, very approximately, be taken to vary directly with the heavy ion SEU rate. Thus for protons and neutrons too, the SEU rate variation is strongly inversely proportional to feature size.

One example of the importance of this effect to aircraft is in avionics. Whereas older devices with feature sizes on the order of 4 microns were insensitive to nuclear reactions within the chip, smaller devices of <1 micron are sensitive to such effects. This is shown in figure 9 where the energy regions of various ion types to which a device upsets is shown in the figure along with the reaction products from high energy reactions in silicon. Note that the sensitive region lies to the right hand side of the indicated curve for each feature size. These types of upsets are caused by high-energy protons and neutrons (Normand et al. 1994). SEUs have been measured during flight by computers in conventional aircraft that were protected by error correction and detection (EDAC) circuitry (Tabor and Normand 1993).

These SEUs have been shown to be dominated by the atmospheric neutrons as shown in figure 10 (Normand 1996) since the altitude and latitude variations of the upsets correlate with the corresponding variations of the atmospheric neutron flux. For HSCT flight at higher altitudes, the SEU rate is still expected to be dominated by the neutrons, but protons and even primary cosmic rays, may also contribute very significantly to the SEU rate, especially in the polar regions.

The next generation of computers have feature sizes that are fractions of a micron feature size and are expected to be greatly more sensitive to these types of upsets than current technologies. Improved estimates of the intensity and spectral distribution of atmospheric neutrons and protons are important to evaluation of the expected upset rates which will be needed in the design of upset tolerant systems.

Materials Effects- The flight of the aircraft at 15 hours per day for 30 years will accumulate a dose of 164,250 x 1 mrad per hour = 164 rad = 1.64 Gy. Materials degradation effects in polymers from ionizing radiation thresholds are 10,000 Gy and no effects are anticipated. Metallic materials effect thresholds are even higher. Although the effects of the radiation on materials are expected to be negligible, the effects of construction materials on the radiation fields within the interior are measurable. For example, the measurements on board the RB-57F of 1-10 Mev neutrons were ten percent higher than on the balloon flights (Foelsche et al. 1974, Wilson et al. 1991). Measurements of variations in radiation levels on subsonic air transports of up to 30 percent have been observed (Wilson et al. 1994). The use of polymer composites especially those with neutron absorbing (carbon cored) boron fibers is expected to lower the interior environment below that for metallic construction. In addition to the basic wall materials, large metal structures (for example the wing box) may have a significant effect on the internal environment (amplification) and needs to be evaluated.

Recommendations and future plans

The progress needed to provide for the radiation safety of the HSCT and develop a radiation protection philosophy for future HSCT operations is given by the NCRP recommendations. Those recommendations embody in part the recommendations of the FAA Advisory Committee on the Radiobiological Aspects of the SST but go beyond those recommendations in recognition that the much higher fatal cancer risk coefficients found in recent analysis of the WW2 exposures needs to be addressed. To develop a comprehensive safety procedure it was recognized by the NCRP that improved estimates of the exposure levels need to be made. This is the main emphasis of the current task. In addition to this main task, the development of procedures for control of exposure levels on high latitude routes during a solar particle event is also to be addressed. This is being accomplished by implementing transport procedures to use GOES satellite data to provide real-time mappings of the solar particle event induced radiation levels to provide guidance in exposure avoidance. Important solar events of the past will be examined to test methods of reducing exposure through adjustments in the flight path. In support of these requirements we recommend the following steps.

Improvements of AIR model- The *AIR* flight package was flown during the peak galactic cosmic ray intensities in June 1997. The process of improvement and validation of the *AIR* model using this flight data needs to continue. The flights need to resume near the next galactic cosmic ray minimum (2000-2001).

The *AIR* model development should continue in parallel to the flight program and will utilize state of the art transport codes and databases to generate input data to the *AIR* model. The response functions of each instrument need to be modeled for validation of the *AIR* model by comparison with the flight data. The Bonner sphere, scintillation counters, particle telescopes, and nuclear track detectors will be used to improve the model spectral intensities.

To further utilize the results of the flight measurement program on the ER-2, a parallel effort to fly an SEU experiment should be considered. It would consist of an electronics board on which upsets would be detected,

corrected and recorded, allowing direct correlation with the detector and dosimetry data from the instruments on the ER-2.

Develop methods of evaluating solar particle induced radiation- A solar particle event routine will be developed for conversion of the GOES satellite data into atmospheric radiation levels. An interagency agreement should be established with NOAA Space Environmental Laboratory for integration of the AIR model and the satellite real-time data stream. A geomagnetic storm field model based on horizontal storm field component needs to be developed since geomagnetic storms may occur during particle event arrival.

The need for instrumentation to monitor the radiation levels will be met by some of the instruments included in the ER-2 flight package. Both passive and active dosimetric device candidates are being flown for comparison with the more detailed evaluations of the physical field measurements. The cross calibration of the several dosimetric devices flown with the actual environment will provide a basis for a future HSCT monitoring system.

Advocate solar particle event forecasting- Develop HSCT requirements for solar event forecasting. An advocacy package needs prepared for the Office of Space Sciences on needs for solar physics studies to meet HSCT requirements.

Develop Be^7 model from Concorde operational experience- The Concorde should have a database on Be^7 accumulation from flight operations. This data can then be scaled to HSCT altitudes and operation schedules using the DOE/EML source database on Be^7 concentrations and a linear kinetics model.

Reduce the biological uncertainties- The peculiarity of atmospheric ionizing radiation is that the exposure is dominated by heavily ionizing particles. The risk coefficients associated with such radiations are the main source of uncertainty especially for prenatal exposures. The NCRP should be funded to survey biological data for evaluation of risk factors for stochastic and developmental injury in neutron and proton exposures.

Develop a philosophy for radiation safety of the HSCT- With a validated *AIR* model and updated information on the associated risk coefficients and available instrumentation for solar forecasting and monitoring, the NCRP should be funded to develop a philosophy for radiation safety of high altitude commercial aircraft operations.

References

Biological Effects of Ionizing Radiations: Health Effects of Exposures to Low Levels of Ionizing Radiation: BEIR V. Natl. Acad. Press, 1990.

Cool, D. A., Peterson, H. T. Standards for Protection Against Radiation□10CFR part 20. NUREG-1446/BR-0117, US Nuclear Regulatory Commission. Oct. 1991.

Cucinotta, F. A. et al., Heavy ion track-structure calculations for radial dose in arbitrary materials. NASA TP-3497, 1995.

Dutkiewicz, V.A. and L. Husain, “Stratospheric and tropospheric components of Be-7 in air,” J. Geophys. Res. 90: 5783; 1985.

EPA, Federal Radiation Protection Guidance for Exposure of the General Public, Fed. Reg. 59 (246): 66414-66429: 1994.

FAA Advisory Committee on the Radiobiological Aspects of the Supersonic Transport, Cosmic radiation exposure in the Supersonic and subsonic flight. Aviat., Space & Environ. Med. 46:1170-1185; 1975

Fed. Regist., 10 CFR 20 Standards for Protection Against Radiation. Fed. Regist. Vol. 56, no. 98, May 21, 1991, pp. 23390-23470.

Fiorino, F. Airline outlook, Radiation Limits, Aviat. Week and Space Tech. p. 23, June 3, 1996.

Fishman, G., et al., “Observation of Be-7 on the surface of LDEF Spacecraft,” Nature, 349:678; 1991.

Foelsche, T., Mendell, R. B., Wilson, J. W., Adams, R. R. Measured and calculated neutron spectra and dose equivalent rates at high altitudes: Relevance to SST operations and space research. NASA TN D-7715, 1974

Friedberg W., Neas, B. R. eds., Cosmic radiation exposure during air travel, FAA-AM-80-2, Mar. 1980.

Friedberg, W., Snyder, L., Faulkner, D. N., Darden, E. D., O'Brien, K. Radiation Exposure of Aircrew Members II, Washington DC, DOT/FAA/AM-92/2, 1992.

Grajewski, B. The Working Women's Health Study: The NIOSH/FAA Study of Reproductive Disorders in Female Flight Attendants and Teachers, Status Report Q1 1997.

ICRP, Problems Involved in Developing an Index of Harm. ICRP Publ. 27, Pergamon Press, New York, 1977.

ICRP, Recommendations of the International Commission on Radiological Protection. ICRP Publ. 26, 1977

ICRP, 1990 recommendations of the International Commission on Radiological Protection, ICRP Publ. 60, Pergamon Press, 1991

McMeekin, R. F. Radiation Exposure of Air Carrier Crewmembers, FAA Advisory Circular AC 120-52, Mar 5, 1990.

NCRP, Limitation of exposure to ionizing radiation. NCRP Rep. No. 116, 1993.

NCRP, Radiation Exposure and High-Altitude Flight. NCRP Commentary No. 12, July 21, 1995.

Normand, E. et al., Single event upset and charge collection measurements using high energy protons and neutrons. IEEE Trans. on Nucl. Sci. 41:2203; 1994.

Normand, E. “Single Event Effects in Avionics,“ IEEE Trans. Nucl. Sci., 43, 461, (l996)

O'Brien, K., Friedberg, W. Atmospheric cosmic rays at aircraft altitudes. Environ. Intern. 20:645-663; 1994.

OSHA, 1910.1096 - Ionizing Radiation. OSHA, 1996.

Reitz, G., Schnuer, K., Shaw, K. (ed.), Radiation Exposure of civil Aircrew, Radiat. Prot. Dos. 48, no. 1, 1993.

Schaefer, H. J. Public health aspects of galactic radiation exposures at supersonic transport altitudes. Aerosp. Med. 39:1298-1303; 1968.

Schraube, H., Jakes, J., Sannikov, A., Weitzenegger, E., Roesler, S., Heinrich, W. The cosmic ray induced neutron spectrum on the top of the Zugspitze. Radiation Protection Dosimetry, to be published, 1997.

Shinn, J. L. et al. Effects of target fragmentation of LET spectra from space radiation in low-Earth orbit (LEO) environment: Impact on SEU predictions. IEEE Trans. Nucl Sci. 42: Dec. 1995.

Stather, J. W., et al., Health Effects Models Developed from the 1988 UNSCEAR Report. NRPB-R226, Chilton, Didcot, UK, 1988.

Taber, A., Normand, E. "Single Event Upset in Avionics." IEEE Trans. Nucl. Sci., NS-40, 120 (April, 1993)

United Nations Scientific Committee on Effects of Atomic Radiation, Gentic and Somatic Effects of Ionizing Radiation. United Nations, New York, 1986.

United Nations Scientific Committee Effects Atomic Radiation: Sources, Effects and Risks of Ionizing Radiation 1988 Report to the General Assembly, With Annexes. United Nations, 1988

White, W. J. Crewmember training on in-flight radiation exposure, FAA Advisory Circular, AC 120-61, May 19, 1994.

Wilson, C. K. The air transport of radioactive materials. Radiat. Prot. Dos. 48:129-133; 1993.

Wilson, J. W., et al., Transport Methods and Interactions for Space Radiations, NASA RP-1257, 1991.

Wilson, J. W., Nealy, J. E., Cucinotta, F. A., Shinn, J. L., Hajnal, F., Reginotto, M., Goldhagen, P. Radiation safety aspects of commercial high-speed flight transportation. NASA TP 3524, May 1995.

Wilson, O. J., et al., Cosmic radiation doses received by Australian Commercial flight crews and the implications of ICRP 60. Health Phys. 66: 493-502; 1994.

Table 1. Current and Projected Maximum Allowable Exposure Limits (Wilson et al 1995)

Exposure condition	Maximum allowable exposure, mSv			
	Present United States 10 CFR Part 20 (1991)	Proposed United States NUREG/BR-0117 (Cool and Peterson 1991)	Proposed NCRP Rep. 116 (1993)	Proposed ICRP Publ. 60 (1991)
Occupation:				
Annual	[a]50	50	50	20
Lifetime	[50 (Age - 18)]		[b]10 × Age	
Pregnancy (total)	5	5		[c]2
Pregnancy (monthly)			0.5	
Public:				
Annual, many years	[d]1	1	1	1
Annual, occasional		5	5	
Pregnancy (total)		5		[c]2
Pregnancy (monthly)			0.5	

[a]Not to exceed 30 mSv in any quarter year.

[b]Recommended limit for new designs in 10 mSv/yr.

[c]Abdomen surface for x-rays, 1 mSv in *utero*.

[d]5 mSv allowed with prior approval of NRC.

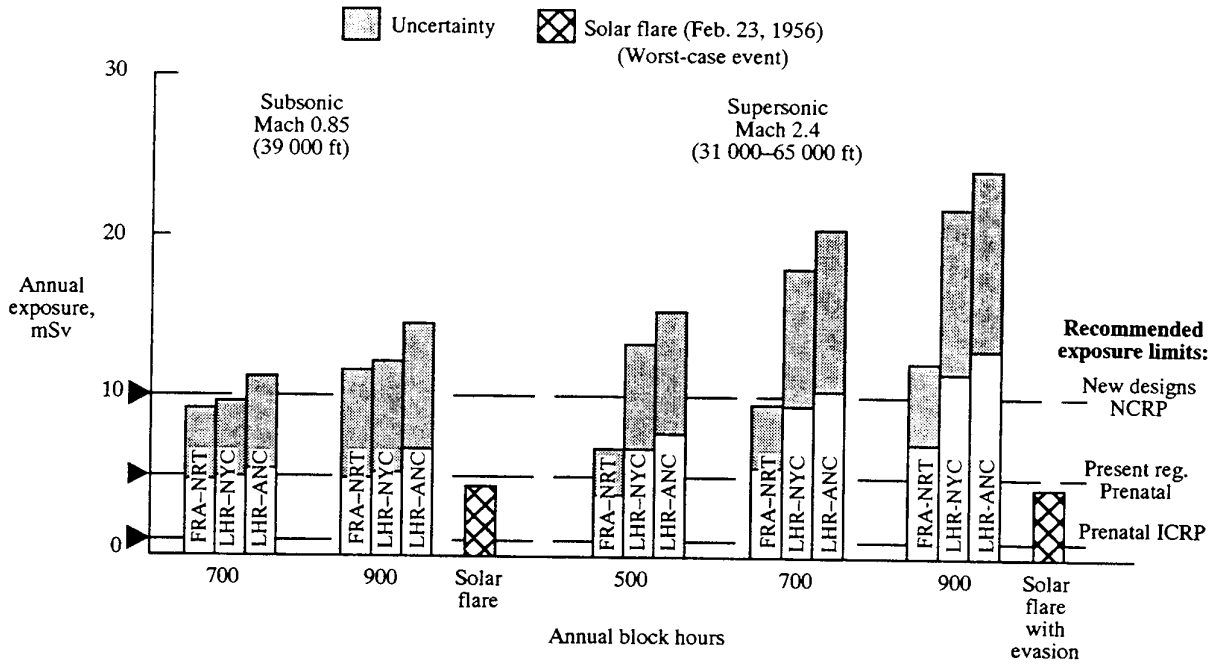

Figure 1.- Annual crew exposures of subsonic and Mach 2.4 flights along specific air routes for assumed number of block hours.

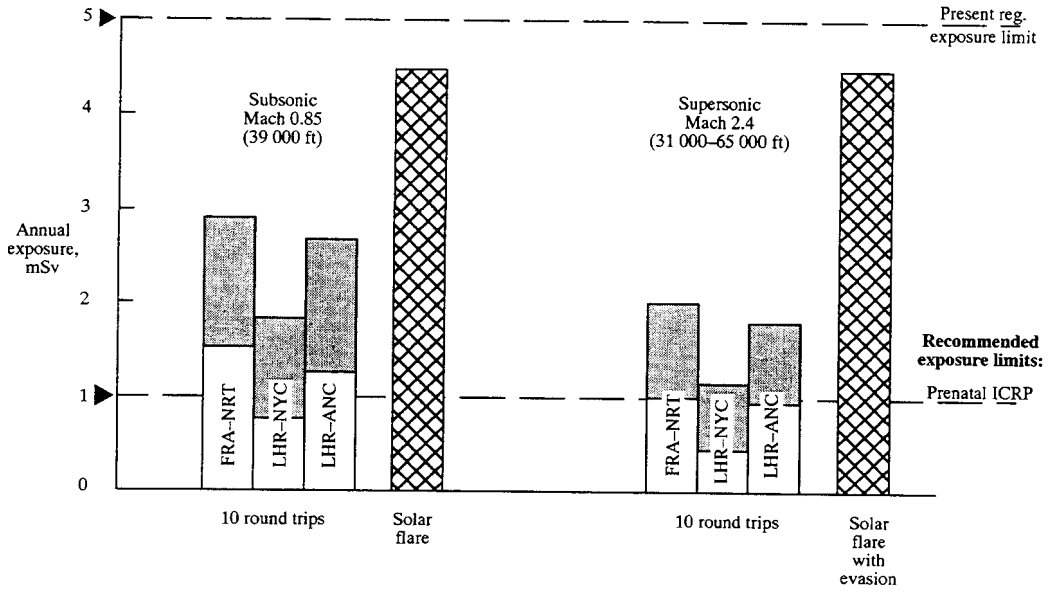

Figure 2.- Frequent Flyer annual exposure for subsonic and Mach 2.4 flights along specific air routes for 10 round trips.

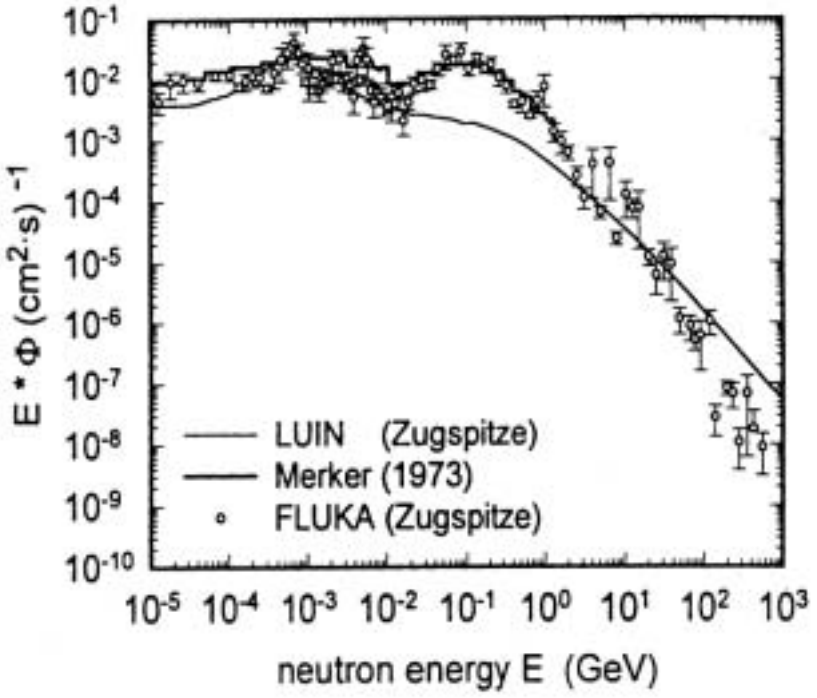

Figure 3.- The calculated cosmic ray neutron spectrum on the top of mount Zugspitze. (From Schraube et al. 1997)

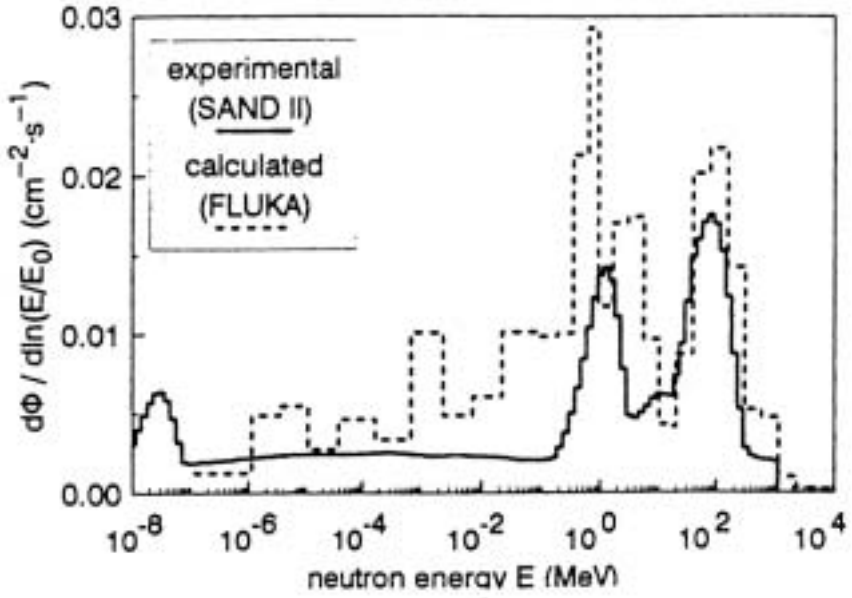

Figure 4.- The cosmic ray induced neutron spectrum on top of mount Zugspitze. (Schraubbe et al. 1997)

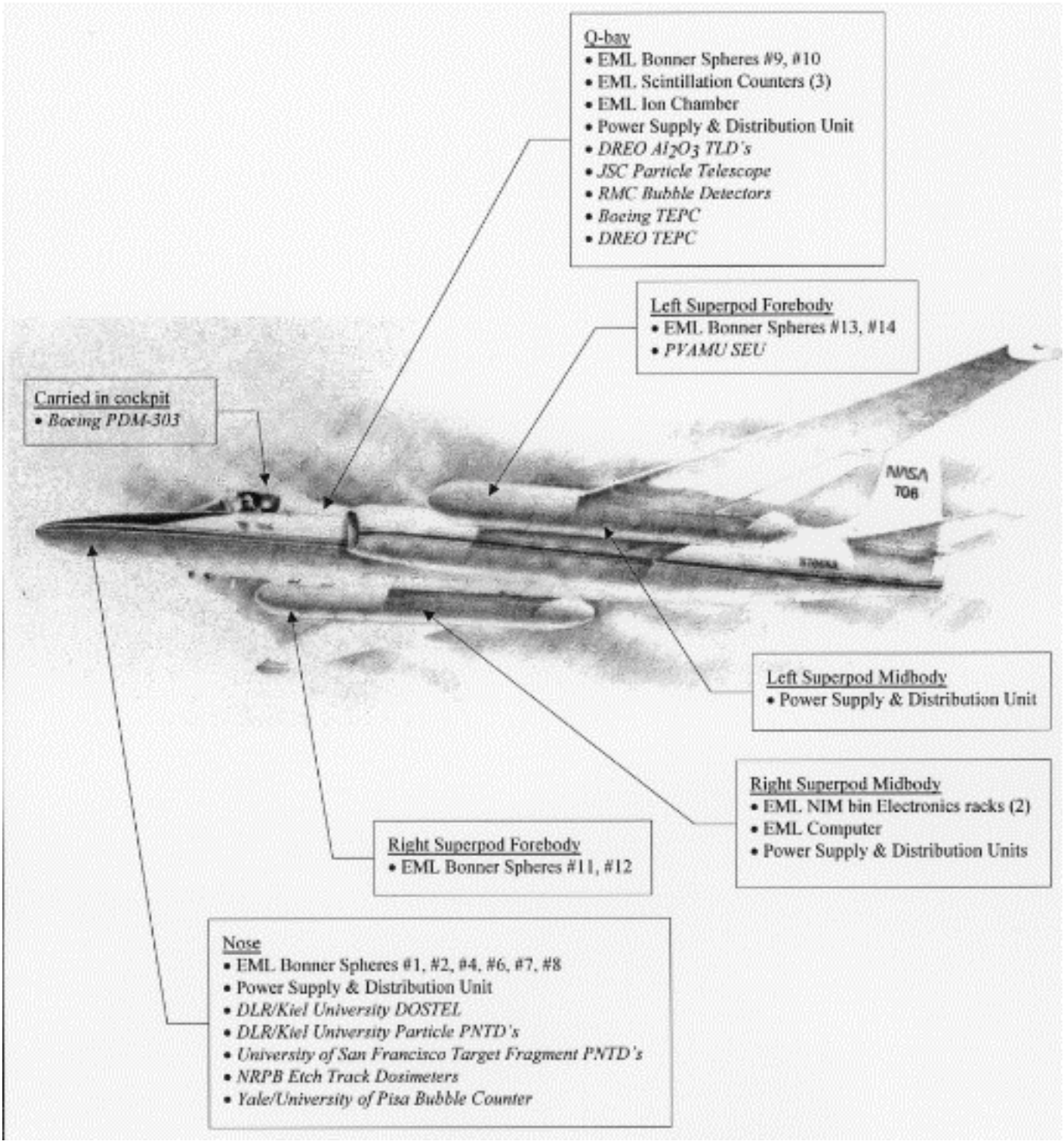

Figure 5.- Instrument Locations on the ER-2.

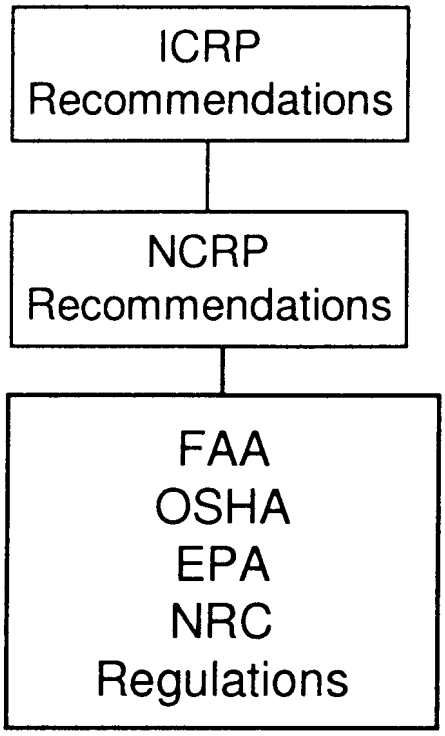

Figure 6. - US regulatory process

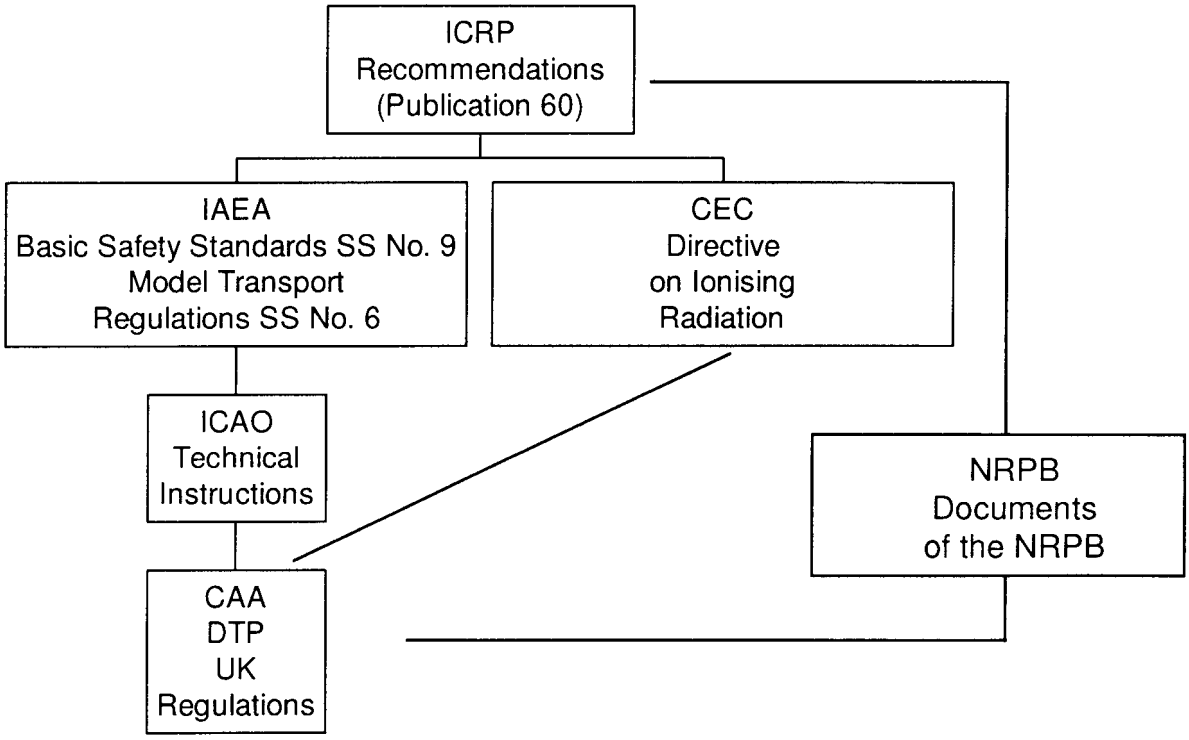

Figure 7. - Input to United Kingdom legislation

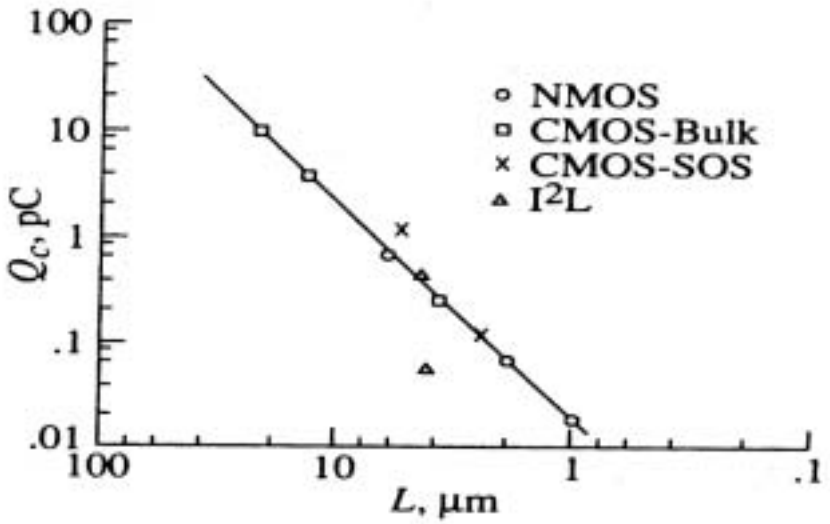

Figure 8.- Critical charge as a function of feature size in several device types.

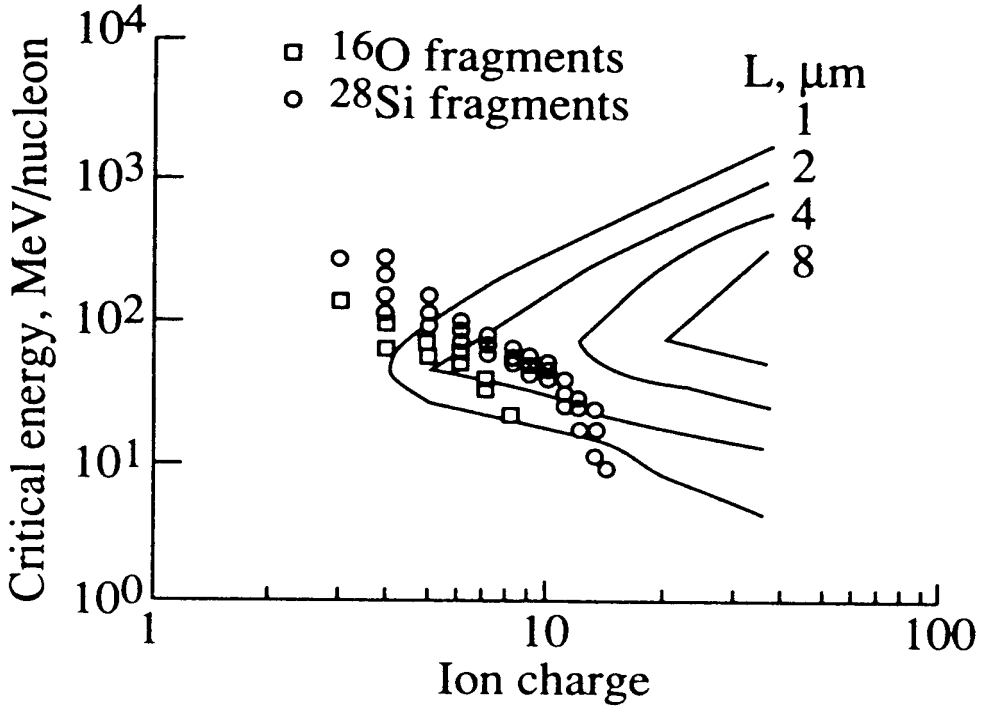

Figure 9.- Critical energy as a function of ion charge for several feature sizes. Average recoil energies of fragments of silicon and oxygen are superimposed.

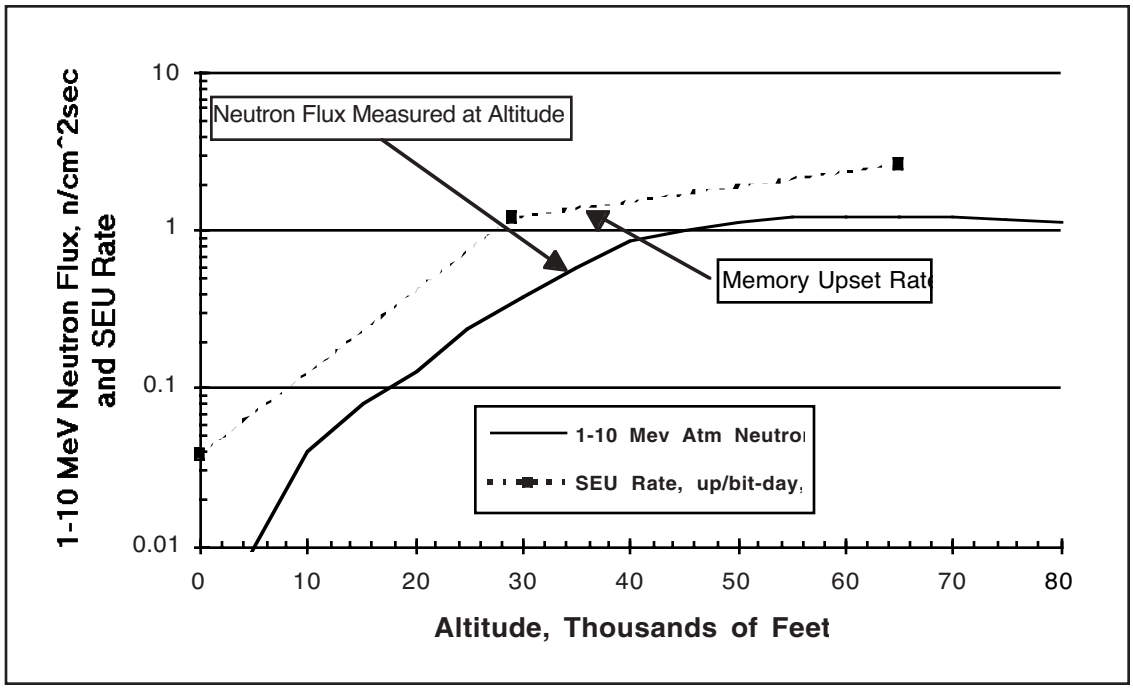

Figure 10.- Correlation of the inflight SEU rate in the IMS 1601 SRAM with atmospheric neutron flux as a function of altitude. The SRAM was operated at 2.5V (Normand 1994).

Chapter 2: Overview of Atmospheric Ionizing Radiation (*AIR*)

J. W. Wilson*, D. L. Maiden*, P. Goldhagen, H. Tai*, J. L. Shinn***

***NASA Langley Research Center, Hampton, VA 23681**
****DOE Environmental Measurements Laboratory, New York, NY 10014**

Overview of Atmospheric Ionizing Radiation (*AIR*)

Preface

The SuperSonic Transport (SST) development program within the US was based at the Langley Research Center as was the Apollo radiation testing facility (Space Radiation Effects Laboratory) with associated radiation research groups. It was natural for the issues of the SST to be first recognized by this unique combination of research programs. With a re-examination of the technologies for commercial supersonic flight and the possible development of a High Speed Civil Transport (HSCT), the remaining issues of the SST required resolution. It was the progress of SST radiation exposure research program founded by T. Foelsche at the Langley Research Center and the identified remaining issues after that project over twenty-five years ago which became the launch point of the current atmospheric ionizing radiation (*AIR*) research project. Added emphasis to the need for reassessment of atmospheric radiation resulted from the major lowering of the recommended occupational exposure limits, the inclusion of aircrew as radiation workers, and the recognition of civil aircrew as a major source of occupational exposures. Furthermore, the work of Ferenc Hajnal of the Environmental Measurements Laboratory brought greater focus to the uncertainties in the neutron flux at high altitudes. A re-examination of the issues involved was committed at the Langley Research Center and by the National Council on Radiation Protection (NCRP). As a result of the NCRP review, a new flight package was assembled and flown during solar minimum at which time the galactic cosmic radiation is at a maximum (June 1997). The present workshop is the initial analysis of the new data from that flight. The present paper is an overview of the status of knowledge of atmospheric ionizing radiations. We will re-examine the exposures of the world population and examine the context of aircrew exposures with implications for the results of the present research. A condensed version of this report was given at the 1998 Annual Meeting of the NCRP with proceedings published in the journal of *Health Physics* (Wilson 2000).

Introduction

Within a year of the discovery of X-rays comes reports of adverse biological consequences such as dermatitis, smarting of the eyes, and epilation followed by the first reported cancer within an X-ray produced ulcer (von Frieben 1903) and other adverse biological consequences (Upton 1989). As a result, various national and international commissions were established to provide protection guidelines against exposures to X-ray devices and radium (ICR 1928). These early recommendations were mainly to limit adverse consequences of acute exposures to individual workers and allowable limits remained high by today's standards. With the growing awareness of chronic exposure effects, the advent of nuclear technology, and the expansion of medical technology in the mid-twentieth century the recommended allowable limits of exposure were reduced dramatically (by 1/3 from 1934 to 1950 and a further factor of 3 by 1958, ICRP 1991). In the case of public exposures (non-occupational exposure) the judgement on acceptable limitations are based on the background levels experienced in ordinary life and great interest in understanding these exposures from natural radiation has developed over recent years. Furthermore, the largest contribution to exposure of human tissues is from the natural background since every living individual is

unavoidably exposed throughout their lifetime. The background exposures are important in assessing the natural radiation risks to the society at large for comparison with the added risks of a new process or technology (NCRP 1995). In addition to the development of nuclear and medical technologies, air and space travel result in elevated natural exposure levels, which have received greater attention in the last half of the twentieth century.

It had long been known that ions were present in the atmosphere since charged condensers (electrometers) would slowly discharge over a period of time. Furthermore the discharge rate was increased by the known radioactivity rays, cathode rays, and X-rays. Over most of the land mass approximately 10 to 20 ion pairs per cubic centimeter are formed every second. Assuming the Earth's natural radioactivity as the source, repeat of the experiments over bodies of water in fact reduced the electrometer discharge rate (Hess and Eugster 1949). The estimated attenuation of the most penetrating rays resulting from radioactivity in the atmosphere was 300 meters leading Th. Wulf, S.J. to compare discharge rates on the ground with those on top of the Eiffel Tower. He found the rate to be only half the ground level value and not a greatly reduced value as expected. Wulf rightly concluded that radiations must have been penetrating from the top of the atmosphere, although that interpretation was controversial. Balloon flight data was obtained by various investigators, but it was not until V. F. Hess developed an adequate electrometer experiment able to operate in the temperature and pressure extremes at balloon altitudes that conclusive evidence was found of radiations arriving at the top of the Earth's atmosphere. Hess's studies found the ionization rates to decrease with altitude up to 500 meters followed by a steady increase at higher altitudes to where the ground level rate is matched at 1500 meters. For this discovery, Hess would receive a Noble prize in physics (1936). Observations during a solar eclipse (incorrectly) brought the conclusion that the source was not the sun (solar cosmic rays arrive nearly isotropically) and probably came from deep space and the term "cosmic radiation" came into use in 1926 (Hess and Eugster 1949). Prior to this date the term "high altitude radiation" was in common use. J. Clay would discover that the ionization rates were smaller at lower latitudes in several voyages from Europe to the Dutch Indies in the period of 1927-1929 demonstrating that many of the rays are charged resulting in deflection in the geomagnetic field near the equator and allowing greater access in polar regions (Hess and Eugster 1949).

In the electrometer experiments, it was found that fresh air would result in faster discharge rates than older air (Hess and Eugster 1949). This is now understood to be due to short lived radon decay products and cosmogenic radioisotopes produced by the cosmic rays from atmospheric atoms. These are later recognized as important sources of human exposures.

That the cosmic rays consisted in part of charged particles was directly demonstrated by coincidence experiments using Geiger-Mueller tubes and resolving individual charged particle tracks within a Wilson cloud chamber. The cloud chamber lead to the discovery of the positron as part of the cosmic rays, followed by the discovery of the charged mesons, and further shed light on the important neutron component of the cosmic radiations in the atmosphere (Bethe et al. 1940). Worldwide surveys of cosmic ionization during the years 1931-1932 were made by several groups and Hess of Austria studied time variations associated with solar activity cycle on a mountaintop from 1931-1937. Global radiation levels correlated well with the expected effects of the geomagnetic deflection of cosmic radiations. A world wide network of stations began to develop leading to observed short term fluctuations

in the global ionization rates simultaneously in both the southern and northern hemispheres and correlated with solar disturbances (Hess and Eugster 1949). Observed large increases in the ionization rates would be attributed to particles coming directly from the solar events (figure 1) while more modest decreases over a few days as seen for the July-August 1946 event were attributed to disturbance of the local interplanetary medium by which approaching cosmic rays were excluded from the local Earth environment (Forbush decrease). It was now clear that extraterrestrial radiations from both the sun and the galaxy were contributing to the atmospheric ionization levels. The next-to-last piece of important evidence from a human exposure perspective was the discovery of heavy ion tracks by Phyllis Frier and coworkers (1948) using nuclear emulsion track detectors in high altitude balloon flight. Although the initial emphasis of this discovery was the ability to sample cosmic matter, attention would turn to the possibility of human exposure by these ions in high altitude aircraft and future space travel (Armstrong et al. 1949, Schaefer 1950).

E. Goldstein introduced the term "cathode rays" at the time (1876) of his discovery of the canal rays (positive ion beams, Hess and Eugster 1949). He suggested (incorrectly) that "cathode rays" from the sun were responsible for the observed aurora. C. Störmer (1955) studied the equations of charged particle motion in the geomagnetic field to understand the auroral patterns and found a general equation for the solutions that were open to asymptotic motion. He also found solutions which were bound with no asymptotic solution which he (incorrectly) recognized as not contributing to aurora but failed to suggest that these regions may be filled with trapped particles which are in fact the source of the aurora during conditions of extreme geomagnetic disturbance. The trapped radiations were directly observed by the first US satellite with a Geiger-Mueller tube (Van Allen et al. 1958) and are largely confined to the "forbidden" regions of Störmer's theory on the motion of charged particles in a magnetic dipole field (left hand proton contours in figure 2). The inner zone particles shown on the left of figure 2 consist of stable trapped radiations while the so-called outer zone particles on the right of figure 2 consist of a transient zone where particles of the solar wind are inserted into the magnetosphere through the geomagnetic tail and radially diffuse inward until they are depleted by precipitation into the Earth's atmosphere near the poles. It is these outer zone particles that mainly form the aurorae during geomagnetic disturbances.

Since the discovery of the magnetically trapped radiations, no new sources of natural radiations important to human exposure have been found (except of course those of the same classes in other planetary bodies). Even so, human activity has enhanced human exposures to natural radiations due to technological development. In what follows we will give a quantitative presentation of the various components of natural radiations and the extent of human exposures. Special attention will be given to the quality of the radiations involved as this also relates to the interpretation of the associated risks. Of particular interest will be the comparison of the level of exposures and the radiation quality of various groups of exposed individuals.

In the present chapter we will review the sources of atmospheric radiation exposure where most human exposures occur. This will include sources in the lower atmosphere dominated by natural radioactivity to the higher altitudes incountered by aircraft. There will be special emphasis on the most biologically effective components.

The Origin of Atmospheric Radiation

Terrestrial Atmospheric Radiation Sources

Ionization in the lower atmosphere is dominated by radionuclides in the Earth's crust. Over deep water, there are few dissolved radionuclides so that the ionization is dominated by radiation incident on the top of the atmosphere. The ionization over the landmass is complicated and depends on many physical and chemical factors.

Natural radioactivity. The radioactive elements remaining from the formation of the Earth are sustained by the unusually long lifetimes of U-235, U-238, Th-232, Rb-87, and K-40. They are chemically bound and found in various mineral formations either in quantity or as trace elements in the bulk. The decay of U-235, U-238, and Th-232 consists of a complex sequence of events terminating with stable nuclei (see tables 1-3). The Rb-87 and K-40 decay through simple beta emission directly into stable isotopes. The decay sequences are determined by the binding properties of neutrons and protons in nuclear matter. Nuclear instability is characterized by an excess of either protons or neutrons over what is required for a stable configuration. Heavy nuclei tend to have more neutrons than protons since the proton charge leads to large repulsive forces tending towards nuclear instability and is the source of nuclear fission. An important decay mode is alpha particle decay (emission of a He-4 nucleus, which is unusually tightly bound). Emission of beta particles (electrons of both charges, negatrons and positrons) to reduce the nuclear neutron excess (negatron emission) or the nuclear coulomb repulsion (positron emission). Angular momentum conservation requirements often result in an excited nuclear state that must be reduced in energy by gamma ray emission.

Although the decay energies of these various processes are similar, the differing types of decay particles have vastly differing penetration powers. The penetration of charged decay products is limited by the interaction with atomic electrons. The alpha particles have typical ranges in air of few to several centimeters but only tens of micrometers in condensed material. As an external source, alpha particle emitters are relatively harmless. If ingested or inhaled and thereby brought into contact with sensitive cells the alpha particle emissions can be most hazardous. The typical emitted electron has a range in air of tens of centimeters to meters but at most a few centimeters in condensed matter. The decay electrons pose a limited hazard as an external source since they do not penetrate deeply into the body. The stopping positrons undergo annihilation events with atomic electrons in which two energetic gamma rays (0.511 MeV) are emitted. The nuclear-decay gamma rays as well as the energetic annihilation gamma rays have no charge resulting in a slower attenuation rate penetrating even hundreds of meters of air and passing through large thickness of condensed matter. Gamma rays are the major source of external exposure and a contributor to atmospheric radiation from naturally occurring radioactivity.

The radioactive nuclei are chemically bound and reside as minerals of the Earth's crust. As such they are generally immobile and limited in human exposure except as an external source. Indeed only the upper 25-cm of the crust provides the escaping gamma rays for exposure. This is true for all except the radioisotopes of Radon (Rn) which appear in all three decay sequences. Radon has a closed electronic shell structure and is therefore chemically inert and normally in a gaseous state but is still limited in movement by its physical interactions. Although the U-235,

U-238, and Th-232 decay sequences all pass through this noble gas, the atom is trapped within the mineral matrix with little chance of escape depending on the materials porosity. Generally diffusion within minerals occurs mainly along the grain boundaries wherein escape to the atmosphere or to ground water is possible. The decay of Radium (Ra) by alpha emission results in nuclear recoil of the Radon atom which near grain boundaries allows escape from the mineral matrix. The lifetimes of Rn–219 and Rn-220 are short allowing little time for escape prior to decay into chemically active Polonium. Consequently most exposure to radioactive alpha emission is related to the single isotope Rn-222.

Distribution of terrestrial radioactive nuclei. The Earth's mantle is a relatively uniform mixture of molten minerals. The formation of the crust in cooling processes differentiates among mineral content. The early formation of silicate crystals is rich in iron and magnesium (dark colored mafic rocks). Later cooling results in silicates rich in silicon and aluminum (light colored salic rocks). Final cooling provides silicates rich in potassium and rubidium. Thorium and uranium are incompatible with the silicate crystal structure and appear only as trace elements within the silicate rocks and reside mainly as constituents of minor minerals in which they are the main or important constituents. The identification of specific igneous rock types is an indicator of radioactivity content (see table 4).

Physical and chemical processes collectively known as weathering further separate mineral types. Erosion by water, wind and ice mechanically breaks down the grain sizes and separates them into weather resistant and subjective mineral grains. Although only slightly soluble in water, leaching by dissolution into unsaturated running water transports mineral types to sedimentation points with mixing with other sedimentation products. Weather resistant mineral grains such as zircon and monazite leads to small mineral grains rich in thorium and uranium ultimately appearing as small dense grains in coarse sands and gravel in alluvium. Dissolved thorium and uranium minerals add to the clay deposits. Thus weathering the igneous rock leads to sands depleted in radioactivity, fine clays rich in radioactivity, and dense grains rich in thorium and uranium. In addition, decomposing organic materials produce organic acids that form complexes with uranium minerals to increase their mobility.

Water carries dissolved minerals and mechanically reduced particulates to places with a downward thrust to where sedimentation occurs. The buildup of successive layers of sedimentation forms an insulating layer against the outward transport of heat from the mantle and increased pressure in the lower layers. This heat and pressure causes phase transitions resulting in new segregation of mineral types. Within this same general process is the formation of coal, crude oil, and natural gas. Uranium has a particular affinity to these organic products. The radionuclide content is reasonably correlated with sedimentary rock type as noted in table 4. Eighty-five percent of the US population lives over sedimentary bedrock, as does a majority of other national populations (see for example, van Dongen and Stoute 1985 and Ibrahiem et al. 1993).

Activity of the soil is related first to the rock from which it is produced but altered by leaching, dilution by organic root systems and the associated changes in water content, and augmented by sorption and precipitation (NCRP 1987, Weng et al. 1991). Soil is transported laterally by water and wind. Modified by human activities as

erosion, topsoil transport, and fertilizers. Biochemical processes modify activity several ways. Root systems increase porosity and water content. Humic acids decompose rock into smaller fragments increasing water content and leaching action. The lower soil is changed from an oxidizing to a reducing medium. The overall effect of natural soil development is to reduce the radioactivity. The activity of a specific soil type depends on the local region and the specific processes in action as seen by comparing same soil types in tables 5 and 6. Although geological maps based on the uppermost bed rock is useful for a general characterization of activity, it is not a reliable guide to quantitative evaluation.

Plants selectively take up radionuclides dissolved in water. The reducing action of floodwater in paddy rice greatly reduces the Tc-95 activity of the rice grain compared to upland rice (Yanagisawa and Muramatsu 1995). Similar reducing environments reduce the mobility of uranium. Leafy vegetables tend to have high concentration compared to non-leaf vegetables (Yanagisawa and Muramatsu 1993). Similar metabolic differences are expected for other radionuclides. Field corn was found to expire Rn-222 at a rate several times higher than the soil on which the corn was growing (Pearson 1967).

External exposures from terrestrial radiation. The larger fraction of the earth's surface where people live and work has as natural cover the soil resulting from weathering processes. As noted, the lower atmospheric radiation and the associated external exposures are mainly from gamma rays emitted from the top 25 cm of the surface layer of the earth and the construction materials of the buildings. The buildings will reduce the exposure from the surface layer but may themselves be constructed from radioactive material that may add to the radiation exposure more than the shielding reduces it. The soil activity concentrations of China and the United States (UNSCEAR 1993) and the associated dose rate in air are given in table 7. There is a broad range of dose rates. The activity concentration and the associated dose rates for various building materials have been compiled by UNSCEAR (1993) and are given in table 8 dependent on the fraction of the materials in the specific building. Conversion of air kerma (assumed to be numerically equal to dose under equilibrium conditions) to effective dose depends on the geometry of the individual and values are given for adults, children, and infants in table 9.

Results from national surveys representing 60 percent of the world population of outdoor dose rates have been complied by UNSCEAR (1993). National average outdoor dose rates vary from 24 nGy/h for Canada to 120 nGy/h for Nambia. The population average is 57nGy/h. Many of the surveys included indoor and outdoor dose rates, which depends on construction materials used. The average indoor to outdoor dose rate ratio was 1.44 and varied from 0.80 (United States) to 2.02 (Netherlands). There are areas of exceptionally high dose rates associated with Th-232 and U-238 heavy minerals. Two such sites are Kerala, India with 200-4000 nGy/h (Sunta 1993) and the coast of Espirto Santo, Brazil with 100-4000 nGy/h (Pfeiffer et al. 1981). Unusually high dose rates have been reported in Kenya (12000 nGy/h, Paul et al. as reported in UNSCEAR 1993) and Ramsar, Iran (up to 30000 nGy/h, Schrabi as reported by UNSCEAR 1993). These radiation exposures decline with distance above the surface due to absorption by atmospheric constituents with an absorption length on the order of 300 m.

Extraterrestrial Atmospheric Radiation Sources

The ionization in the upper atmosphere results in part from the extraterrestrial particles incident on the top of the atmosphere. These particles are of two sources. A continuous stream of particles come from deep within the galaxy while a more intense but transient source is from our own sun.

Galactic cosmic rays. Cosmic rays originating in the galaxy by processes not entirely understood (Hall et al. 1996) upon entering the solar system interact with the outward propagating solar wind in which is embedded the solar magnetic field. A solution of the Fokker-Planck equation was found by Parker (1965) in which the inward diffusion of galactic cosmic rays is balanced by the outward convection by the solar wind. The density of cosmic ions within the solar system assuming spherical symmetry is then related to the external density as

$$\mu(r,R) = \mu_0(R)\ exp\ [\ -\ \int_r V(r')\ dr'/\ D(r',R)] \qquad (1)$$

where $\mu(r,R)$ is the ion density at radial distance r and rigidity R (particle momentum per unit charge), $\mu_0(R)$ is the density in interstellar space, $V(r)$ is the solar wind speed, and $D(r,R)$ is the diffusion coefficient (Balasubramanyan et al. 1967). The wind velocity and diffusion coefficient depend on the solar activity usually measured by the number of sunspots seen in the solar surface and there is a phase shift between sunspot number and modulation as the wind generated at the solar surface diffuses into the modulation cavity which extends far out into the solar system. The relation of sunspot number to the cosmic ray induced neutron monitor count rate in Deep River, Canada is shown in figure 3 during some of the more recent solar activity cycles. The inverse relation of solar activity and cosmic ray intensity is clearly seen in the figure. A simplified version of the diffusion model was implemented by Badhwar et al. (1994) in which the solar wind is held constant at 400 km/s and the diffusion coefficient is taken as a function of time and is correlated with the Mt. Washington neutron monitor count rate. The diffusion was found to be bimodal with unique dependence on the orientation of the solar magnetic dipole. Assuming an isotropic diffusion coefficient in which the diffusion coefficient generally increases with radial distance as $D(r,R) = D_0(R)\ r^s$ where s is on the order of 0 to 2. The above assumptions lead to

$$\mu(r,R) = \mu_0(R)\ exp\ \{ - V_0\ (r_0^{1-s}\ - r^{1-s})/[(1-s)D_0(R)]\} \qquad (2)$$

where V_0 ,r_0, and $D_0(R)$ are the wind speed, size of the modulation cavity (50 to 100 AU), and diffusion coefficient at 1 AU respectively. Equation (2) is used to scale the modulated flux at 1 AU to arbitrary distance. Modulation studies using various Pioneer, Voyager, and IMP spacecraft show variability of s with solar cycle for some restricted energy ranges but the gross behavior for all energies above 70 MeV is well represented by s = 0.5 (Fujii and McDonald 1997).

The GCR differential energy flux from the diffusion model is compared with measurements made in the near earth environment in figure 4 near minimum solar activity. The most prominent particles are in a broad energy range between 100 and 1,000 MeV per nucleon. These are very penetrating radiations able to penetrate deep into the atmosphere although only the most energetic particles produce effects at ground levels. The flux near solar

minimum or maximum depends on the degree of solar activity during the specific cycle as seen in the Deep River neutron monitor data. The "worst-case" observed flux is shown in figure 5 for which all other recent solar minima and maxima are expected to fall below the respective curves in the figure. A peculiarity of the GCR is the significant number of multiple charged ions as displayed in figure 6. The means by which they interact with the atmosphere and shield materials is still under active investigation as are the biological risk to such radiations (Schimmerling et al. 1998, Wilson 2000, Cucinotta et al. 2001).

Solar sources. Solar cosmic rays or solar particle events (SPEs) were first observed as sudden short-term increases in the ground level ionization rate (figure 1). The close correlation with solar flare events first identified them as originating in the solar surface plasma with eventual release into the solar system (Meyer et al. 1956). Thus it was assumed that the observation of solar surface phenomena would allow forecasting the possibility of such events (FAA 1975). Modern opinion considers the particle acceleration region not to be on the sun at all. Rather large coronal mass ejections from active regions of the solar surface propagate into the interplanetary environment carrying along with them the local solar surface magnetic field frozen into the ejected mass that is a good electrical conductor. There is a transition (shock) region between the normal sectored magnetic field structure of interplanetary space and the fields frozen into the ejected mass which forms a transition region (shock) in which the interplanetary gas is accelerated forming the solar particle event. The escape of the particles from the acceleration region is diffusion limited so that a maximum intensity is implied (Reames 1999). However, when the acceleration region passes the observation point the intensity is observed to increase by an order of magnitude to high levels in so-called shock events and no upper limit in intensity is known within the shock region. The SPE energies obtained in the acceleration process are related to the plasma density and velocity of propagation of the ejected mass. To understand the SPE is then to understand the release of coronal mass and its propagation into interplanetary space relative to the observation point.

The only solar particle events of interest to aircraft are those capable of ground level observations with ion chambers (figure 1) or neutron monitors. The rate of occurrence of such events (Shea and Smart 1993) is shown in figure 7. The ground level events vary greatly in intensity and only the most intense events are important to high-altitude aircraft protection. The largest ground level event yet observed occurred on Feb. 23, 1956 in which neutron monitor count rates rose to 3,600 percent above background levels (figure 8). No other events of this scale have been observed in over fifty years. The next largest ground level event (370 percent over background) was that of September 29, 1989 shown in figure 9 in comparison with a second series of events starting October 19, 1989. A list of particle intensities of the larger events is shown in table 10. The low-energy intensities for dates before November 1960 are most uncertain. The November 1960 event was probed by a series of sounding rockets using nuclear emulsion. SPE data of the 70's and 80's are supported by satellite measurements using active detectors and are most reliable.

It was found by Nymmik (1997) that the particle spectra tend to display a similar dependence above 30 MeV. From the model of Nymmik, the event-integrated proton fluence of the September 29, 1989 event above 30 MeV is given by

$$\int_{30}^{\infty} \phi(E)dE = 1.39 \times 10^9 \text{ protons/cm}^2 \tag{3}$$

where E is the kinetic energy and $\phi(E)$ is the differential fluence in protons/(cm^2-MeV). In this model, $\phi(E)$ is given as a power law above 30 MeV by

$$\phi(E)dE = \frac{C}{\beta} \times \left(\frac{P(E)}{P_{30}} \right)^{-4.5} dE \tag{4}$$

where, β is the proton speed relative to the speed of light, $p(E)$ is the momentum, p_{30} = 239.15 MeV/c is the momentum corresponding to a proton energy of 30 MeV. The coefficient C is given by

$$C = \frac{1.39 \times 10^9}{\int_{30}^{\infty} \left(\frac{239.15}{p(E)} \right)^{4.5} \frac{1}{\beta} dE} = 2.034 \times 10^7 \tag{5}$$

The differential fluence in protons/(cm^2-MeV) below 30 MeV is calculated by using an exponential distribution (Shea and Smart 1990), since there is a flattening of the spectra below that energy based upon observations of this event (Cleghorn and Badhwar 1997). This addition gives a very good empirical description of data below 30 MeV and the event-integrated fluence for protons of the entire measured energy range is well described as illustrated in figure 10.

Geomagnetic Effects. Charged particles arriving at some location within the geomagnetosphere are deflected by the Lorentz force $e\boldsymbol{v} \times \boldsymbol{B}$ which prevents penetration for some directions of incidence and some energies. Such phenomena were extensively studied by Störmer (1930) for a dipole magnetic field which provides the basis for classifying the orbital trajectories of charged particles arriving at some location within the field. As a part of Störmer's theory, allowed trajectories with no connection to asymptotic trajectories exist; these are now recognized as trapping regions associated with Van Allen radiation.

The geomagnetic field can be reasonably approximated by a tilted dipole with moment $M = r_e^3 31\,500$ nT displaced from the Earth's center by 430 km or $0.068r_e$, where r_e = 6378 km. The tilt angle is 11.7° at 69° W longitude. The magnetic quadrupole contributions are then about 10 percent at the surface and decrease to 5 percent at $2r_e$. Higher order moments are even smaller. The motion of charged particles in the geomagnetic field was studied extensively by Störmer. We outline his methods herein. In spherical coordinates, Störmer showed that the azimuth angle ϕ is an ignorable coordinate possessing an integral for the particle's trajectories such that

$$\cos\ \omega = \frac{\gamma}{m\upsilon r} - \left(\frac{ZeM}{m\upsilon r} \right) \frac{\sin\theta}{r^2} \tag{6}$$

where m is the mass of the particle, Ze is the charge, υ is the speed, c is the speed of light, r is radial distance from the center of the field, θ is magnetic colatitude, γ is an integration constant, and ω is the angle between the velocity vector and the azimuthal direction. The allowed Störmer regions consist of the space for which

$$|\cos\ \omega| \equiv \left| \frac{\gamma}{m\upsilon r\ \sin\ \theta} - \left(\frac{ZeM}{m\upsilon c} \right) \frac{\sin\theta}{r^2} \right| \leq 1 \tag{7}$$

Further analysis of the condition in equation (7) shows stable trapping regions as well as the Störmer main cone of transmission given for $\gamma = 2m\upsilon(ZeM / m\upsilon c)^{1/2}$. The Störmer main cone is represented (Kuhn, Schwamb, and Payne, 1965) by the solid angle element

$$\Omega = 2\pi(1 + \cos\omega) \tag{8}$$

which contains the allowed directions of arrival for particles of rigidity R (momentum per unit charge) given by

$$R = \frac{M}{c} \frac{\sin^4\theta}{r^2\left[1 + (1 - \sin^3\theta\cos\omega)^{1/2}\right]^2} \tag{9}$$

Henceforth we change variables from the magnetic colatitude θ to the magnetic latitude λ_m and note that Ω varies form 0 to 4π reaching its half-value at $\omega = \pi/2$ including angles up to the vertical direction. The vertical cutoff model is expressed as

$$\Omega \approx 4\pi\, U\left[R - R_C(\lambda_m)\right] \tag{10}$$

where the vertical cutoff rigidity from equation (9) is

$$R_C(\lambda_m) = \frac{M}{4cr^2} \cos^4\ \lambda_m \tag{11}$$

and U(x) is the unit step function.

Not included in the above formalism are those trajectories that are cut off by the shadow cast by the solid Earth. The fraction of the solid angle covered by the shadow of the Earth is estimated with the assumption that the curvature of the local trajectories is large compared with the radius of the Earth (Kuhn, Schwamb, and Payne, 1965). Then the solid angle fraction is

$$\frac{\Omega_{\text{sh}}}{4\pi} = \frac{1}{2}\left[1 + \cos\left(\sin^{-1}\frac{1}{r}\right)\right] \tag{12}$$

The corrected solid angle for the vertical cutoff model is then

$$\Omega = \Omega_{\text{sh}} U\left[R - R_C(\lambda_m)\right] \tag{13}$$

which leaves the local solid angle open to transmission of charged particles of rigidity R at altitude r and geomagnetic latitude λ_m.

During times of intense solar activity, the solar plasma emitted in solar flares and subflares advances outward and arrives at 1 AU from the Sun. If the Earth is locally present, the plasma interacts with the geomagnetic field in which the plasma pressure performs work on the local geomagnetic field. The initial impact produces hydromagnetic waves causing a general increase in geomagnetic intensity. As plasma flow is established, it generates large electric ring currents and a corresponding impressed magnetic storm field. In the initial phase (hydromagnetic wave), the storm field is parallel to the equatorial field after which the storm field reverses in the main phase of the storm caused by ring currents within the magnetopause and opposes the quiet field, causing a net decrease of the field strength. The main phase is followed by slow recovery to the quiet field conditions (Johnson, 1965).

The magnetic storm model used here assumes a uniform magnetic field impressed on the normal quiet field (Kuhn, Schwamb, and Payne, 1965). The storm field strength can be found from the change in the horizontal field component around the geomagnetic equator. We represent this field by H_{st}. Typical values of H_{st} in the main phase range from substorm values -10 nT to severe storms with -500 nT. On rare occasions, for very intense storms, the storm field exceeds -1000 nT.

Magnetic disturbances have been observed for many years, and various classification schemes for such disturbances have been proposed. The planetary magnetic index K_p is based on magnetometer measurements of 12 stations worldwide. The K_p index is related to a derived planetary index a_p and storm field strength by Bartels (Johnson, 1965) given in the table 11.

The vertical cutoff rigidity as given by equation (11) is further modified to approximate the effects of geomagnetic disturbances. It was shown by Kuhn, Schwamb, and Payne (1965) that the appropriate equation is

$$R_C(\lambda_m) = \frac{14.9}{r^2}\cos^4\lambda_m\left[1 + \frac{H_{\mathrm{st}}r^3}{M}\left(\frac{4}{\cos^6\lambda_m} - 1\right)\right] \tag{14}$$

This vertical cutoff replaces equation (11) and applies to storm conditions. Note the cutoff is zero whenever the result of equation (14) is negative. The geomagnetic field is in fact not a simple dipole. The vertical cutoff for the realistic field is shown in figure 11. Numerical solutions to the charged particle equations of motion in a more realistic geomagnetic field model were introduced by McCracken (1962) and further advanced by Shea and Smart (1983). The numerical work of Smart and Shea is indispensable in understanding extraterrestrial radiation in the Earth's atmosphere.

Atmospheric Interactions. The number of galactic cosmic rays incident on the Earth's atmosphere is modified first by the modulating effects of the solar wind and second by the deflections in the Earth's magnetic field as discussed in the prior sections. Upon entering the Earth's atmosphere, they collide through coulomb interaction with the air molecules delivering small amounts of energy to orbital electrons leaving behind an electron-ion pair. The ejected electron has sufficient energy to undergo similar additional ionizing events. The cosmic ions loose a small fraction

of their energy in these molecular collisions and must suffer many collisions before significantly slowing down. On rare occasions the cosmic ion will collide with the nucleus of an air atom in which large energies are exchanged and the ion and the nucleus are dramatically changed by the violence of the event. If the cosmic ion is a simple proton then the outcome of the reaction is limited compared to the more complex ions such as Si or Fe. The proton will under go collisions with constituents of the air atomic nucleus in which the constituents (neutrons, protons, and small nuclear clusters) are directly ejected from the air nucleus. The remnant of the air nucleus is highly disfigured and unstable emitting further air nuclear constituents in a cooling process similar to evaporation of water molecules from a water droplet and final decay through the usual radioactivity channels of gamma, beta, and electron conversion. Even protons and neutrons have unstable excited states that may emerge from the direct knockout process and subsequently decay by emitting mesons. The more complex ions may also lose particles through direct knockout with subsequent cooling adding decay products to the high-energy radiation field. As a result of nuclear reactions with air nuclei the already complex cosmic radiations increases in complexity as the atmosphere is penetrated. Even beyond the description above, the field further grows in complexity as a result of the mesons produced.

Most of the mesons produced are π-mesons or pions. The energy required to produce a pion depends on charge state and is about 135 MeV for neutral pions and 139.6 MeV for charged pions to which kinetic energy must be added. The pions are unstable particles appearing in three charge states (-1, 0, +1) with decay products depending on the charge. The decay process of charged pions is limited to so-called weak interactions as net charge must remain in the final products and the relatively long lifetime is 26 nanoseconds with the following decay scheme

$$\pi^{\pm} \rightarrow \mu^{\pm} + \nu \tag{15}$$

The $\mu^{\pm}$ (muon) decays with a relatively long lifetime of a 2.2 microseconds as

$$\mu^{\pm} \rightarrow e^{\pm} + \nu + \nu \tag{16}$$

where $e^{\pm}$ is a stable positive or negative electron and the neutrino ν are stable massless (or nearly massless) particles (actually there are at least two different neutrino's having opposite spin polarization states). The lifetimes are modified by the relativistic effect of time dilation depending on speed of the decaying particle. The neutrinos, having no charge, interact only weakly passing through the Earth with relative ease. The neutral pion, having no charge, decays quickly ($\approx 10^{-16}$ s) by electromagnetic processes into two very high-energy gamma rays

$$\pi^{0} \rightarrow \gamma + \gamma \tag{17}$$

It is the two gamma rays that add prolifically to the radiation field in a process known as the electromagnetic cascade. This process is initiated by collision of the gamma rays with air atoms (A) producing high-energy electron/positron pairs as

$$\gamma + A \rightarrow e^{+} + e^{-} + A \tag{18}$$

which in turn interact with air atoms to produce additional high-energy gamma rays as bremsstrahlung radiation

$$e^{\pm} + A \rightarrow \gamma + e^{\pm} + A \tag{19}$$

which in turn produce more electron/positron pairs. The positron also undergoes annihilation events

$$e^{+} + A \rightarrow \gamma + \gamma + A^{+} \tag{20}$$

resulting in energetic gamma rays adding to the cascade process and the resulting radiation field. Other mesons are produced in smaller number, as are antiprotons and antineutrons but are less important in human exposures because of their low frequency of occurrence.

The specification of the atmospheric radiation environment requires solution of the appropriate equations describing the above processes. The relevant transport equations are the linear Boltzmann equations for the flux density $\phi_j(\mathbf{x}, \mathbf{\Omega}, E)$ of type j particles given by

$$\mathbf{\Omega} \cdot \nabla\phi_j(\mathbf{x},\mathbf{\Omega},E) = \sum\int \sigma_{jk}(\mathbf{\Omega},\mathbf{\Omega}',E,E')\, \phi_k(\mathbf{x},\mathbf{\Omega}',E')\, d\mathbf{\Omega}'\, dE' - \{1/[v\tau_j(E)] + \sigma_j(E)\}\, \phi_j(\mathbf{x},\mathbf{\Omega},E) \tag{21}$$

where $\sigma_j(E)$ and $\sigma_{jk}(\mathbf{\Omega},\mathbf{\Omega}',E,E')$ are the media macroscopic cross sections, v is the particle speed, and $\tau_j(E)$ is the particle lifetime in the Earth's rest frame. The $\sigma_{jk}(\mathbf{\Omega},\mathbf{\Omega}',E,E')$ represent all those processes by which type k particles moving in direction $\mathbf{\Omega}'$ with energy E' produce a type j particle in direction $\mathbf{\Omega}$ with energy E. Note that there may be several reactions which produce a particular product, and the appropriate cross sections for equation (21) are the inclusive ones. The total cross section σ_j (E) with the medium for each particle type of energy E may be expanded as

$$\sigma_j\,(E) = \sigma_{j,at}\,(E) + \sigma_{j,el}\,(E) + \sigma_{j,r}\,(E) \tag{22}$$

where the first term refers to collision with atomic electrons, the second term is for elastic nuclear scattering, and the third term describes nuclear reactions. The microscopic cross sections and average energy transfer for most particles are ordered as follows:

$$\sigma_{j,at}\,(E) \sim 10^{-16}\ \text{cm}^2 \quad \text{for which } \Delta E_{at} \sim 10^2\ \text{eV} \tag{23}$$

$$\sigma_{j,el}\,(E) \sim 10^{-19}\ \text{cm}^2 \quad \text{for which } \Delta E_{el} \sim 10^6\ \text{eV} \tag{24}$$

$$\sigma_{j,r}\,(E) \sim 10^{-24}\ \text{cm}^2 \quad \text{for which } \Delta E_{r} \sim 10^8\ \text{eV} \tag{25}$$

This ordering allows flexibility in expanding solutions to the Boltzmann equation as a sequence of physical perturbative approximations. It is clear that many atomic collisions (~ 10^6) occur in a centimeter of ordinary matter, whereas ~ 10^3 nuclear coulomb elastic collisions occur per centimeter. In contrast, nuclear reactions are separated by a fraction to many centimeters depending on energy and particle type. Special problems arise in the perturbation approach for neutrons for which $\sigma_{j,at}\,(E) \sim 0$, and the nuclear elastic process appears as the first-order perturbation.

As noted in the development of equation (21), the cross sections appearing in the Boltzmann equation are the inclusive ones so that the time-independent fields contain no spatial (or time) correlations. However, space- and time-correlated events are functions of the fields themselves and may be evaluated once the fields are known (Wilson et al. 1991a, Cucinotta et al. 1996). Such correlations are important to the biological injury of living tissues. For example, the correlated release of target fragments in biological systems due to ion or neutron collisions have high probabilities of cell injury with low probability of repair, resulting in potentially large relative biological effectiveness (RBE) and quality factor (Shinn and Wilson 1991). Similarly, the passage of a single ion releases an abundance of low energy electrons from the medium resulting in intense fields of correlated electrons near the ion path. For example, electron tracks are visualized in nuclear emulsion in figure 12. The ions in the figure are cosmic ions of about 400 A MeV resulting in an energy deposit which is laterally spread from the ion path by distances which are large compared to a cell nucleus as seen in the figure (see also Cucinotta et al. 1998).

The solution of equation (21) involves hundreds of multi-dimensional integro-differential equations which are coupled together by thousands of cross terms and must be solved self-consistently subject to boundary conditions ultimately related to the environment at the boundary, the distribution and composition of the atmosphere, and the geometry of the person's body and/or a complex vehicle. In order to implement a solution one must have available the atomic and nuclear cross section data. The development of an atomic/nuclear database is a major task in code development.

The transport coefficients relate to the atomic/molecular and nuclear processes by which the particle fields are modified by the presence of a material medium. As such, basic atomic and nuclear theories as evaluated by critical experiments provide the input to the transport code database. It is through the nuclear processes that the particle fields of different radiation types are transformed from one type to another. The atomic/molecular interactions are the principal means by which the physical insult is delivered to biological systems in producing the chemical precursors to biological change within the cells. The temporal and spatial distributions of such precursors within the cell system govern the rates of diffusive and reactive processes leading to the ultimate biological effects.

The solution to equation (21) can be written in operational form as $\phi = G\ \phi_B$ where ϕ_B is the inbound flux at the boundary, and G is the Green's function which reduces to a unit operator on the boundary. A guiding principle in radiation-protection practice is that if errors are committed in risk estimates, they should be overestimates. The presence of strong scattering terms in equation (21) provides lateral diffusion along a given ray. Such diffusive processes result in leakage near boundaries. If ϕ_Γ is the solution of the Boltzmann equation for a source of particles on the boundary surface Γ, then the solution for the same source on Γ within a region enclosed by Γ_o denoted by $\phi_{\Gamma_o}(\Gamma)$ has the property

$$\phi_{\Gamma_o}(\Gamma) = \phi_\Gamma + \varepsilon_\Gamma \tag{26}$$

where ε_Γ is positive provided Γ_o completely encloses Γ. The most strongly scattered component is the neutron field, for which an 0.2 percent error results for infinite media in most practical problems (Wilson et al. 1991b). Standard practice in radiation protection replaces Γ as required at some point on the boundary and along a given ray by the corresponding Γ_N evaluated for normal incidence on a semi-infinite slab. The errors in this approximation are second order in the ratio of beam divergence and radius of curvature of the object, rarely exceed a few percent for space radiations as those incident on the top of the atmosphere, and are always conservative. The replacement of Γ by Γ_N as a highly accurate approximation for space radiation applications has the added advantages that Γ_N is the natural quantity for comparison with laboratory simulations and has the following properties: If Γ_N is known at a plane a distance x_o from the boundary (assumed at the origin), then the value of Γ_N at any plane $x \geq x_o$ is

$$G_N(x) = G_N(x - x_o)\, G_N(x_o) \tag{27}$$

Setting $x = x_o + h$, where h is small and of fixed-step size gives rise to the marching procedures such as those in the code HZETRN (Wilson et al. 1991b).

Estimates of the charged particle and nucleonic components (NCRP 1987) as a function of depth in the atmosphere are shown in figure 13. The neutron and pion components show a net increase (buildup) near the top of the atmosphere reaching a maximum at atmospheric depths of 50 to 100 g/cm^2 followed by an exponential decline. Protons show a steady decline in intensity. The decay of the charged mesons into charged muons causes a buildup of the muon component that shows little decline. The reason is that most of the nucleons undergo nuclear reactions, which accounts for their exponential decline while the charged pions are depleted by weak decay. Since most pions are produced near the top of the atmosphere where high-energy nuclear collisions are plentiful, the pions decline at greater depths. The muons from the pion decay are mainly produced in the upper atmosphere and have no nuclear reactions and are therefore little attenuated in reaching the larger depths. Furthermore, their long lifetime is effectively increased by relativistic time dilation, allowing many muons to reach the ground before they decay. The electrons are from the electromagnetic cascade driven by the high-energy gamma ray decay of the neutral pion, which are mainly produced in the upper atmosphere. The electron population declines as they loose energy through bremsstrahlung and atomic collisional processes. The relationship between atmospheric depth and altitude is given in figure 14.

Atmospheric radiations. The ionizing radiation within the earth's atmosphere has been studied by many groups, over many decades, and with various instruments. The observation over many decades with a common instrument allows the study of the time and latitude structure on a consistent basis. Such long-term studies are by necessity immune to modern detector development and their main value is the self-consistency of the resulting database. Two such detectors have played such a role: high-pressure ion chambers (Neher and Pickering 1962, Neher 1961, 1967, 1971, Neher and Anderson 1962) and Geiger-Mueller counters (Bazilevskaya and Svirzhevskaya 1998). A more limited study was made over most of solar cycle 20 (1965 to 1972) using tissue-equivalent ion chambers, nuclear

emulsion, and fast neutron spectrometers (Foelsche et al. 1974). The detectors give complementary information, the ion chamber relates directly to exposure (rate of ion formation in standard air), the Geiger-Mueller tube counts number of particles (insensitive to neutral particles), and the neutron spectrometer provides new data not available in the other two packages. The high-pressure ion chamber measures the ion current generated by the cosmic rays in the filling gas. The filling gas is usually argon within a steel walled chamber to maintain electron equilibrium at the gas/wall interface. It is relatively more sensitive to gamma radiation than the air molecules but the charged particles can be more directly related to air exposure rates. It is insensitive to neutrons. The Geiger-Mueller tube is nearly 100 percent efficient in counting charged particles and rather inefficient in counting uncharged particles such as gamma rays and neutrons. Only the neutron spectrometer allows clear identification of neutrons and their spectral properties.

The Geiger-Mueller counter has the advantage of being lightweight and compact allowing radiosound balloon studies that are relatively inexpensive as is necessary for long-term support. A remarkably detailed database on many of the small temporal details was obtained over the years of 1957 to 1997 in the studies of Bazilevskaya and Svirzhevskaya (1998). The cosmic ray flux is shown in figure 15 for low solar activity (February 1987) and high solar activity (September 1989) at two locations with differing geomagnetic cutoffs (R_c = 0.6 GV at Murmansk and R_c = 6.7 GV at Alma-Ata). The count rate increases with atmospheric depth as the multitude of secondary charged particles are added with deeper penetration into the atmosphere. The secondary particle generation process depends on the energy of the initiating cosmic particles at the top of the atmosphere; low energies are less deeply penetrating, with greater penetration depths at higher energies. The high latitude data (R_c = 0.6 GV) in figure 15 shows only a net modest increase in count rate with depth at the top of the atmosphere near solar minimum since the number of low energy particles present at the top of the atmosphere tend to dominate the GCR spectrum (see figure 5) at this time in the solar cycle. As solar maximum is approached, the low energy particles can no longer penetrate the solar modulation cavity (figure 5) and the resulting maximum atmospheric count rate moves deeper into the atmosphere as seen in figure 15. Note also the percent increase in the count rate is likewise much higher near solar maximum as one would expect. The low energy cosmic particles present at the top of the atmosphere are likewise removed by the geomagnetic field at lower latitudes as seen by comparing the Murmansk curves (triangles) with those measured at the lower latitudes at Alma-Ata (circles). Note that the count rates near the surface (~1,000 g/cm^2) are nearly independent of solar modulation and geomagnetic cutoff. This results from the fact that only the highest energies primary particles contribute significantly to the ground level radiation and are little affected by either factor (for example, see figure 5 for solar modulation effects).

Balloon flights during solar particle events (SPE) were likewise made by Bazilevskaya and Svirzhevskaya in which large perturbations in the atmospheric radiation was observed (figure 16). In this case, the observed particles are mainly protons since SPE are relatively low in energy for which meson production with their associated electromagnetic cascades is limited. The proton mean free path to nuclear absorption is on the order of several tens of g/cm^2 so that relatively few of the protons beyond 100 g/cm^2 depths are primary particles. There is a nucleonic cascade in which high-energy neutrons are in part responsible for carrying the radiation deep into the atmosphere

where they are converted into protons in nuclear reactions. The observations depicted in figure 16 show that the SPE can easily dominate the radiation fields at aircraft altitudes even when the ground level fields are only slightly affected as seen for the October 1989 event (compare figure 16 with figure 9). We anticipate that the much larger ground level events will have correspondingly large disturbances in aircraft radiations as will be addressed subsequently in this paper.

Observations were also made during large geomagnetic storms. In this case, the perturbations of the geomagnetic field during the storm main phase compresses the geomagnetic field increasing the loss of trapped electrons by increasing the rate of collision with the earth's atmosphere. It is those trapped particles that populate the trapped belts near the poles seen in figure 2 that are mainly lost to the atmosphere. These electrons were observed on May 1994 at high altitudes as seen in figure 17. As estimated by Foelsche et al. (1974), these particles pose no hazard to high altitude aircraft as can be judged by the results in the figure 17.

Although not a naturally occurring event, many of the balloon flights were made during the period of atmospheric nuclear testing. Measurements made in 1970 are shown in figure 18 in which high altitude radioactive pollution is clearly observed. The particles observed here are mainly gamma rays. The main concerns for these types of radiations is for aircraft surface contamination and intake into the cabin air circulation system (FAA 1975) followed by inhalation.

The Geiger-Mueller count rate is not sufficient to relate to human risks. Additional information on linear energy transfer (LET) is required as shown in figure 19 (Tobias 1952). In addition to the count rate is shown the average rate of energy loss that is nearly proportional to the average specific ionization. As the composition of the radiation changes through interaction with atmospheric constituents the energy loss rate of the radiation field is modified having important implications on radiation risks. Evaluation of risks requires specific knowledge of the particles and their corresponding energies present at the exposure.

Starting at the top of the atmosphere, a significant feature of GCR exposures is the presence of heavy ions which are potentially very damaging. A comparison of the solution of equation (21) with measurements of Webber and Ormes (1967) is shown in figure 20. The more massive ions attenuate more quickly in the atmosphere due to their larger nuclear cross sections. They fragment into smaller ions and neutrons producing mesons in the process. The fragmentation of the iron ions results in 120 different isotopes that need to be accounted (Kim et al. 1994). The data in the figure groups the isotopes by charge number to improve the statistics of the experiment. The fragmentation of the heavier ions result in contributions to the lightest ion group (Li, Be, B) which hardly changes at all over to relatively large penetration depths. Clearly, the composition of the GCR is undergoing large changes in the upper atmosphere. The penetrating component of the heavy ions poses some issues at high altitude commercial operations as one hit per gram tissue each month is anticipated for the crew in supersonic transport operations (Allkofer and Heinrich 1974).

It was generally regarded that although neutrons played an important role in understanding the trapped radiations and for the formation of many cosmogenic isotopes in the atmosphere, the role of neutrons in direct human exposure was believed to be very limited (ICRP 1966) and estimates of dose equivalent was largely taken as the air exposure (Wallace and Sondhaus 1978). However, when humans entered the space program the concern for space radiation led to the development of computational shield models that uncovered the important role of neutrons as secondary radiations. When the supersonic transport was first proposed, Foelsche proposed a number of concerns relating to neutrons as a potentially important component in atmospheric radiation (Foelsche 1961, Foelsche and Graul 1962). As a result a study of atmospheric radiations was made over most of solar cycle 20 in which neutrons and other biologically important components were the focus. The study consisted of over 300 airplane flights using the General Dynamics/Martin RB-57F, Lockheed U-2, and Boeing 707 aircraft and 25 high-altitude balloon flights as indicated in figure 21. The intent was to gain information on GCR background levels and attempt to make measurements during a SPE. A more detailed description is given by Foelsche et al. (1974) and Korff et al. (1979). The acquired data set was used to derive a parametric atmospheric ionizing radiation model (Wilson et al. 1991b).

Figure 22 shows measurements by the neutron spectrometer and tissue-equivalent ion chamber made on a high-altitude balloon flight near solar minimum (maximum GCR intensity) over Ft. Churchill, Canada (Rc = 0.2 GV). The instruments were only lightly shielded (less than 1 g/cm^2 fiberglass and foam). The features to be noted are the broad maximum in the neutron flux, with peak at 60 to 70 millibars (mbar) and a leveling off of the ion chamber dose rate above 50 mbar (1 mbar $\approx$ 1 g/cm^2). Also shown is the parametric environmental model (Wilson et al. 1991b). A second flight one month later above St. Paul, Minnesota (Rc = 1.3 GV) is shown in figure 23. The lower energies of cosmic rays are removed by deflection in the geomagnetic field which reduces the ion chamber dose rate considerably above 100 mbar and leaves the neutrons, produced mainly by higher energy cosmic rays, little affected. This conclusion applies only above the latitude knee and at high altitudes where low energy particles mainly contribute to the radiation field near solar minimum. As solar maximum is approached, the low energy particles are eliminated by the solar modulation and this effect is reduced as noted below. At lower altitudes and latitudes both ionization and neutron components result from high energy particles and the variations of ionization and the neutron fields are comparable (Hewitt et al. 1980, Goldhagen et al. these proceedings). A third flight about a week later over St. Paul shown in figure 24 includes the effects of a 15 cm thick tissue equivalent spherical phantom on the measurements in which the neutrons are dramatically reduced with little affect on the ion chamber dose rate. A reflight from Fort Churchill two years after solar minimum in figure 25 in which the neutron flux and ion chamber dose rate have decreased by about the same percentage. Also shown in the figure are the resulting model developed from the project (solid curve) and results of Monte Carlo calculations for the same time period (dashed curve). The Monte Carlo evaluated neutron spectra were used to estimate those neutrons not seen by the spectrometer as shown in figure 26. The conversion into dose and dose equivalent are shown in the figure. As can be seen, over half of the neutron dose and nearly half of the dose equivalent are from neutrons above 10 MeV. The contributions to dose equivalent from charged particle ionization, neutrons, and charged particle nuclear events in tissue are shown in figure 27. The data in the figure is for high latitudes and various times in the solar cycle. The

conversion to dose equivalent used the older quality factors which limit to 20 at 100 keV/micron and do not decrease at higher values of LET.

There is a lower level short-term structure in the atmospheric radiation levels, shown in figure 28, which has two sources. The diurnal variation is due to the relative tilt of the geomagnetic dipole to the solar wind direction during daily rotation. The amplitude depends on the temporal intensity of the local solar wind. The longer sidereal variation is related to solar rotation as the emitted coronal plasma depends on local features in the solar surface at the time of emission. The solar wind expands as an archimedean spiral that co-rotates with the solar surface (similar to a rotating water sprinkler) and long lived surface features will show a 28-day recurrence in the local cosmic ray intensities accounting for the longer-period structure in the figure. Such time variations, up to a few percent, should be taken into account in interpreting measured data such as that shown in figure 29. Figure 29 shows the model results for ionization in air and a flight measurement of relative values of ionization rate using a high-pressure ion chamber on an ER-2 aircraft on June 13, 1997. The model results in figure 29 do not yet include the short-term variations.

Background exposure levels. The data set obtained by Foelsche et al. had sufficient coverage that a parametric model by interpolation over geomagnetic cutoff, Deep River neutron monitor count rate, and altitude allowed a global model of atmospheric radiations for all times to be made. For example, the modeled 1 to 10 MeV neutron flux is shown in figure 30 in comparison to the flight data. The atmospheric ionization data was obtained from Neher (1961,1967, 1971) and Neher and Anderson (1962) as compiled by S. B. Curtis (Boeing 1969) in table 12 for solar minimum and table 13 for solar maximum and utilized by Wallace and Sondhaus (1978). The tissue equivalent ion chamber is taken as the conversion of air exposure rate to dose rate in tissue from all but the neutron dose rate which is related to the 1-10 MeV flux (figure 30) assuming the Monte Carlo extension of the neutron spectrum (figure 26). Added to this is a parametric representation of the nuclear stars in tissue estimated by the nuclear emulsion data after subtraction of the neutron-induced stars. The resulting dose equivalent per 1000 hours of operations (the maximum number of flight hours for crew members which does not include the "dead head times") is shown at solar minimum in figure 31. One can see that there is a high plateau in the Polar Regions where dose equivalent rates are maximum for any given altitude with a broad deep valley in equatorial regions. These are effects due to the geomagnetic field on the incident primary cosmic particles. The height of the polar plateau relative to the equatorial valley increases at the higher altitudes. The concentration of iso-dose equivalent contours in the intermediate latitudes is referred to as the knee of the latitude dependence. The irregularity of the contours relative to geographic coordinates is due to the tilt of the dipole field and presence of the quadrupole moments of the geomagnetic field. The north Atlantic flight corridor is one of the busiest in the world and is among the most highly exposed routes in aircraft operations. Much of European flight is near or below the latitude knee and somewhat lower exposures are expected. In distinction, flights over Canada are among the most exposed. The maximum solar modulation in solar cycle 20 is shown in figure 32. As expected, the effects of modulation show strong latitude and altitude dependence. Mainly those regions affected by the lower-energy particles show significant modulation effects.

Although most studies of atmospheric radiation are the result of concern for airline crew exposures, most individuals are exposed as a result of the ordinary circumstances of life (where they live and work). The populations of the world are located in large part on the coastal plains of the greater landmass. As a result, several studies of cosmic ray exposures from sea level to a few thousand meters have been made. Measurements of the associated environment require some care since the terrestrial radionuclide emissions are a confusing factor requiring some care in evaluation since the terrestrial radiations depend on local geological factors. In addition, even the cosmic radiations change character at ground level since interaction with the local terrain modifies the neutron fields above the surface. One can see from figure 13 that the near sea level environment is mainly composed of muons with smaller number of photons (not shown), electrons and neutrons which are produced high in the atmosphere by high-energy cosmic rays. As a consequence, the sea level ionization rate in a high-pressure ion chamber is closely related to both the absorbed dose and dose equivalent as the muons, photons, and electrons are minimum ionizing radiation (quality factor is unity) and the neutron absorbed dose is small. The difficulty in use of the ion chamber to study cosmic radiation near the surface is the confusion from the terrestrial radiation contributions that can be relatively large on the surface and decline with increasing altitude from the surface. From the earliest measurements of Wulf and Hess it was known that the atmospheric ionization rates declined with altitude followed by an increase at higher altitudes until the ground levels are achieved again at about 1,500 m.

The sea level cosmic ray ionization rate at middle to high latitudes was reviewed and consistently found to be in the range of 1.9 to 2.6 ion pairs/cm^3-s and the value of 2.1 ion pairs/cm^3-s has been consistently adopted since that evaluation (UNSCEAR 1982). Note that this is significantly lower than the value given by Wallace and Sondhaus in tables 12 and 13. Assuming the average energy for the formation of an ion pair in moist air is 33.7 eV, the absorbed dose rate corresponding to 2.1 ion pairs/cm^3-s is 32 nGy/h. Measurements near 15^o geomagnetic north in Taiwan by Weng and Chen (1987) on Mount Ali and by aircraft are shown in figure 33. The offset in dose rates on Mount Ali seen in the figure results from the terrestrial radionuclide emissions from the moutain. Extrapolation of the aircraft data to 100 m gives 34.5 nGy/h. Additional measurements over two deep water reservoirs and over South Bay yielded 31±6 nGy/h. Subtracting contributions of radionuclides in the air and water yields the cosmic ray contribution to be 26±7 nGy/h accounting for both uncertainty in Rn contributions in air and in the measurements. The value adopted by UNSCEAR (1982) is in the range of uncertainty of the Taiwanese measurements although lower values are indicated for the lower latitudes. Similar values were measured at Hong Kong (27-31 nGy/h at 6.5^o geomagnetic north) by Tsui et al. (1991) and Shenzen, China (28 nGy/h near 6.5^o geomagnetic north) by Yue and Jin (1987) indicating the ionization rates are lower by about 10-15 percent near the geomagnetic equator. The absorbed dose at high and low latitudes is given by Hewitt et al. (1980) shown in figure 34.

The neutron flux at sea level is estimated (Hajnal et al. 1971) at 50 degree geomagnetic North to be 0.008 neutrons/cm^2-s. The energy spectrum is very broad and difficult to measure so that dose equivalent estimates are still uncertain (Hajnal and Wilson 1991). Average effective dose equivalent was taken as 2.4 nSv/h by UNSCEAR (1988). With the changing quality factor (ICRP 1991) the dose equivalent is estimated to increase by about 50

percent (Wilson and Townsend 1988, Hughes 1993) for which UNSCEAR (1993) adopted the value of 3.6 nSv/h. The latitude dependence was further studied by Nakamura et al. (1987) using He-3 counters in a multi-sphere arrangement (six polyethylene spheres ranging from 5.1 cm to 45.2 cm) with results shown in figure 35 (older quality factors). Changes in quality factors would require increasing these results by about 50 percent. The altitude dependence over Japan was further studied using a high efficiency dose equivalent counter which was cross calibrated with the multi-sphere spectrometer as shown in figure 36. Again these results should be increased by about 50 percent for the changing quality factors.

The dose equivalent rate has been represented by the following functions. The direct ionization contribution is approximated as

$$H_I(z) = H_I(0)\,[0.205\,\exp(-1.649\,z) + 0.795\,\exp(0.4528\,z)] \tag{28}$$

where z is in km and $H_I(0)$ is 32 nSv/h. The corresponding neutron dose equivalent is approximated (Bouville and Lowder 1988) by

$$H_N(z) = H_N(0)\,\exp(1.04\,z) \tag{29}$$

for $z < 2$ km and

$$H_N(z) = H_N(0)\,[1.98\,\exp(0.698\,z)] \tag{30}$$

for $z > 2$ km where $H_N(0)$ is 3.6 nSv/h. The results are shown in figure 37. The neutron dose equivalent is small for altitudes less than 3 km and increases rapidly to be half of the total dose equivalent near 6 km.

Atmospheric SPE. It was clear from the observations in figure 16 that even a rather modest ground level SPE such as that which occurred in October 1989 could dominate the particle flux at aircraft altitudes, but their importance to human exposure needs to be explored. This requires measurements with instrumentation capable of distinguishing the biologically important components, such as that of Foelsche et al. (1974). Two such flights were achieved on March 30-31, 1969. The event was very modest as a ground level event but provides important information on exposures to high altitude aircraft (see figure 38). Assuming Nymmik's approximation is correct (see equation 4) then the high-energy fluence important to aircraft exposure would be nearly proportional to the ground level response. This relationship has been assumed to estimate the dose equivalent rate of other larger ground level events as indicated in the figure. An independent assessment using the estimated spectral flux of the February 23, 1956 event is shown in figure 39 and is in reasonable agreement with the estimate obtained from projecting the flight data.

The global distributions of dose equivalent rate during the February 23, 1956 event are shown in figure 40 at selected altitudes using the methods of Wilson et al. (1970). Again one sees a radiation plateau in the polar region and a broad valley at lower latitudes. Of particular note are the high rates over the north Atlantic as was the case for the background levels only the knee is sharper and at higher latitudes. The altitude dependence of the dose equivalent rate in the extreme north section of the usual US-to-Europe flight lanes is shown in figure 41. The accumulated dose equivalent on a flight during this event can be quite high even at subsonic altitudes. One should

keep in mind that this is the only event of this magnitude observed in over fifty years of observation and so is extremely rare. The next larger event is the September 29, 1989 event in which dose equivalent rates were an order of magnitude lower. The events of the magnitude of the September 29, 1989 are in fact rare with only one such event per decade on the average.

Cosmogenic radionuclides. Cosmogenic radionuclides are produced in the many nuclear reactions with the air atomic nuclei and to a lesser extent with the ground materials. The dominant isotopes are produced in reactions with the oxygen and nitrogen atoms and to a lesser extent with other trace gases as argon and carbon dioxide. Their importance in human exposure depends on the production rate, radionuclide lifetime, the chemical/physical processes of the atmosphere/terrain, and the body processing following ingestion and/or inhalation. There are only four such isotopes of importance to human exposure as given in table 14. The carbon-14 is mainly produced by neutron (n,p) events in nitrogen-14. The hydrogen-3 and berylium-7 are produced in high-energy interactions with nitrogen and oxygen nuclei. The sodium-22 is produced in high-energy interactions with argon. All of these radionuclides are mainly produced in the atmosphere in which residence times can be 1 year in the stratosphere before mixing with the troposphere. Residence times in the troposphere are only 30 days for nongaseous products. Carbon-14 undergoes oxidation soon after production to form carbon-14 dioxide. Not all of these radionuclides are accessible to human exposure. For example, about 90 percent of the carbon-14 is dissolved into deep ocean reservoirs or resides as ocean sediment with the remainder on the land surface (4 percent), in the upper mixed layers of the ocean (2.2 percent) and in the troposphere (1.6 percent). Carbon-14 enters the biosphere mainly through photosynthesis. Hydrogen-3 oxidizes and precipitates as rain water. The berylium-7 concentrations are unevenly distributed over the earth's surface being strongly effected by global precipitation patterns (NCRP 1987). The bioprocessing of sodium-22 is affected by the overlying canopy cover which serves as a filter to ground vegetation (Jenkins et al. 1972) and shows large variation in tissues of elk, deer, and caribou (Jenkins et al. 1972).

External exposures. Although most studies of atmospheric radiation have been the result of concern for airline crew exposures, most individuals are exposed as a result of the ordinary circumstances of life. Knowing the local galactic cosmic ray environment is the beginning of the problem but the effects of shielding of building structures and the human body are further modifying factors. It is usually assumed that the effective dose equivalent from the directly ionizing component is the same as the dose equivalent (28 to 32 nGy/h from equator to high latitudes). One must account then for modifications for building structures and occupancy factors. Indoor measurements in a 12-storey building showed a steady decline in cosmic ray exposures from the roof to the basement as shown in table 15. Additional studies by various groups are shown in table 16. The effective shielding factors vary by 30 percent depending on where the measurement is made within the building as shown by Fujitaka and Abe (1984a). Fujitaka and Abe (1984b) also show that the dose rate does not depend on the details of the building interior. However, the location of other buildings can have an effect on exposures on the lower floors but all such parameters will have only a 30 percent effect on the exposure. The single most important parameter is the floor material and structure (Fujitaka and Abe 1986). The neutron transmission factors are usually taken as unity (UNSCEAR 1988, 1993). The neutron spectrum must be better understood to improve on this estimate.

The distribution of effective dose equivalent was modeled by Bouville and Lowder (1988) and used to estimate the world population exposures based on terrain heights and population distributions. The annual effective dose equivalent was estimated from equations (28) to (30) in UNSCEAR (1988) with slightly different values of $H_I(0)$ and assuming a building shielding factor of 0.8 and an occupancy factor of 0.8. The distribution of collective dose in each altitude interval is shown in figure 42. About one half of the effective dose equivalent is received by people living at altitudes below 0.5 km and about 10 percent of those exposed are above 3 km. Thus, 90 percent of all exposures have less than 25 percent of the dose equivalent being contributed by neutrons (see figure 37). A small fraction of people living at high altitudes receive exposures for which 40 to 50 percent of the exposure is from neutrons. Some countries like the United States have large coastal regions where the population effective dose is near that at sea level. Other countries with large cities on elevated plateaux such as Mexico, Kenya, Ethiopia, and Islamic Republic of Iran have relatively high exposures (see table 17). For example, the cities of Bogata, Lhasa, and Quito receive annual effective dose equivalents from cosmic radiation in excess of 1 mSv (UNSCEAR 1988) of which 40 to 50 percent are from neutrons.

Passenger and crewmembers of commercial aircraft experience even higher dose equivalent rates of which 60 percent are from neutrons. The exposures are dependent on altitude, latitude, and time in the solar cycle. Most operating aircraft have optimum operating altitudes of 13 km but the many short flights operate at lower altitudes of 7-8 km at speeds of 600 km/h. For longer flights 11-12 km is typical. Estimates of human exposures were made by UNSCEAR (1993), assuming $3 \cdot 10^9$ passenger-hours aloft annually and 2.8 μSv/h at 8 km found 10,000 person Sv as the collective dose equivalent. Worldwide, this is an annual average effective dose of 2 μSv although in North America it is about 10 μSv. In any case, air travel is a small contribution to the annual worldwide average effective dose from cosmic rays of 380 μSv.

A small number of supersonic airplanes operate at cruise altitudes of 15-17 km. The average dose equivalent rate on the six French planes for the two years following July 1987 (from solar minimum through near solar maximum) was 12 μSv/h with monthly values up to 18 μSv/h (UNSCEAR 1993). During 1990 the average for the French planes was 11 μSv/h and the annual dose equivalent to the crew was about 3 mSv (Montagne et al 1993) while 2,000 flights of the British planes had an average of 9 mSv/h with a maximum of 44 mSv/h (Davies 1993). All of the dose equivalent estimates of the Concorde use older values of quality factor and revised estimates would be about 30 percent higher. The exposures to passengers on supersonic aircraft would be about the same as for the equivalent subsonic flight wherein the higher rate of exposure is nearly matched by the shorter supersonic flight time. Crew exposures can be substantially higher since time at altitude is about the same independent of speed. There is only a negligible contribution to the collective dose since the supersonic traveler and crew represent a small fraction of the airline industry.

Internal exposures. Cosmic rays produce a number of radionuclides of which the four most important are given in Table 14. The most significant exposures are for Carbon-14. The assessment of the exposures was made by UNSCEAR (1977) from the known specific activity of Carbon-14 of 230 Bq per kg of carbon leading to an annual effective dose of 12 μSv. The next most abundant of the radionuclides of Hydrogen-3, Berylium-7, and Sodium-22 in table 14 are totally negligible (UNSCEAR 1997). A concern for surface contamination by Be-7 for operations in the stratosphere has not yet been answered.

Neutron Exposure Issues

It is useful to understand exposures in aircraft in relation to other exposures. This is especially true in terms of neutron exposures for which the corresponding neutron exposure risk coefficients are uncertain. The main exposures to neutrons are either occupationally related and/or from the result of cosmic rays. Estimates of occupational neutron exposures within the US were given by the NCRP (1987) for the year 1980. These estimates are based on data gathered in the years 1977 to 1984 and are given in table 18. Studies by the Environmental Protection Agency indicate that such exposures had decreased by a factor of two in the years 1970 to 1980 due to improvement in protection practice (Klement et al. 1972, EPA 1984). Not included in the table are crew members of aircraft.

The cosmic ray dose equivalent rates were discussed in an earlier section. In that section the rates were evaluated on the basis of measurements made with various instruments. The ratio of the neutron dose equivalent rate to the total dose equivalent rate according to the parametric atmospheric radiation model is shown in figure 43. It is clear from the figure that 40 to 65 percent of the dose equivalent at ordinary aircraft altitudes are due to neutron exposures depending on latitude and longitude of the flight trajectory. The fraction of neutron exposure is altitude dependent but varies little over most aircraft operating altitudes. Since most commercial flights take place at relatively high latitudes, one can assume that about 60 percent of the dose equivalent is from neutrons in commercial airline operations.

Although a consistent data set over most of the geomagnetic latitudes and altitudes during most of solar cycle 20 has been measured, many of the individual components were not resolved due to instrument limitations at the time of measurement and the major portion of the neutron spectrum depends on theoretical calculations for proton interactions with the atmosphere (see figure 26). Prior measurements of the atmospheric neutron spectrum are shown in figure 44. Hess et al. (1959) estimated the neutron spectrum using moderated boron trifluoride counters and a bismuth fission chamber supplemented with a model spectrum. Korff et al. (1979) used a liquid scintillator spectrometer sensitive mainly to 1-10 MeV neutrons with analysis assuming a simple power law spectrum (note that the Korff et al. data in the figure is at a higher altitude). Hewitt et al. (1978) measured the neutron spectrum using a Bonner sphere setup at subsonic altitudes and analyzed the data assuming a simplified spectral analysis. The Hewitt et al. result confirms the importance of the high-energy neutrons but left the exact nature of the spectrum uncertain due to limitations of the analysis methods. Nakamura et al. (1987) used a Bonner sphere setup at much lower latitudes and his results are multiplied by 3X for comparison of spectral shape. Ferenc Hajnal of the US Department of Energy Environmental Measurements Laboratory developed new analysis techniques for unfolding

Bonner sphere neutron spectral data and found important structural features in Hewitt's data near 100 MeV (see figure 45) that have important implications for aircraft exposures (Hajnal and Wilson 1991, 1992).

A study of the atmospheric neutron spectrum lead by H. Schraube of GSF in Neuherberg has been funded by the Directorate General XII of the European Union. The experimental component consists of a Bonner sphere spectrometer with a ^{3}He proportional counter (Schraube et al. 1998) on a mountaintop (Zugspitze). The theory part of the study uses the FLUKA code at the University of Siegen and the known cosmic rays incident on the atmosphere (with the multiple charged ions assumed to be dissociated into constituents, Roesler et al. 1998). It is interesting to note that the structure expected from the analysis of Hajnal at 100 MeV (figure 45) appears in both the measurements and the FLUKA calculation (see figure 46). Note that this feature is absent in the results from the LUIN code (also shown in figure 46) which depended on the Hess spectrum for guidance as the LUIN code is not a fundamental calculation in that information outside the LUIN result is used to patch an answer into the final values (O'Brien and Friedberg 1994). The importance of the Schraube et al. study is that the neutron ambient dose equivalent is about a factor of two larger than that estimated using the LUIN code (Schraube et al. 1998) and the added contributions are from high-energy neutron interactions with tissue nuclei resulting in an array of high LET reaction products at each collision event (see figure 47 where LET spectra of a 1 GeV neutron event is compared to a typical alpha decay spectrum). Very little biological data exist on such radiation interactions (Baarli 1993, Wilson et al. 1990, 1995) and the important cancer risk coefficients are very uncertain.

Further studies were started at the NASA Langley Research Center. An instrument package was developed in accordance with the NCRP (1995) recommendations through an international guest investigator collaborative project, thereby ensuring the availability of the numerous instruments required to measure the many components of the radiation spectra. Selection criteria included: (a) the instruments had to fit within the cargo bay areas of the ER-2 airplane and be able to function in that environment, (b) each instrument must have a principal investigator with independent resources to conduct data analysis, and (c) the instrument array must be able to measure all significant radiation components for which the NCRP (1995) had established minimal requirements. Also, the flight package had to be operational and the first flight occur before or near the maximum in the galactic cosmic ray intensity (ca. spring/summer 1997). Flights of the ER-2 package were in June 1997 during the maximum of the galactic cosmic ray intensity (several months after sunspot minimum in September 1996, see figure 3). Preliminary results of these flights will be presented at this workshop.

Estimates of dose equivalent rates are available from a number of sources. Only a few give separate values for neutron contributions. Bagshaw et al. (1996) give average rates for long haul flignts from London to Tokyo as 3 μSv/hr for neutrons and an additional 3 μSv/hr for other components for a total of 6 μSv/hr. Schalch and Scharmann (1993) employed a proton recoil spectrometer to estimate the neutron dose equivalent arriving at 8 μSv/hr for neutrons and 11.5 μSv/hr total on Frankfort/New York routes and 9.5 μSv/hr for neutrons and 11.8 μSv/hr total on Dusseldorf/San Francisco routes. Altitude and latitude dependent results using a high-pressure ion chamber and spherical remmeter are given by Akatov (1993) in table 19. Although the quality of the ionization dose

is not given, it is seen that the neutron dose equivalent rate is on the order of half or more of the exposure. Since these measurements are made at solar minimum where the cosmic ray intensities are maximum, it can be concluded that a discrepancy appears between the Schalch and Scharmann result measured at much lower altitudes during elevated solar activity and the neutron dose equivalent rate given by Akatov at SST altitudes.

In addition to the flight routes used, the commercial aircraft crew exposures depend on the actual number of flight hours, which may be as many as 1,000 hours per year. Hughes and O'Riordan (1993) estimate that long haul crews are airborne 600 h/yr while short haul crews log only 400 h/yr and they used the average value of 500 h/yr. Bagshaw et al. (1996) quote for a mix of ultra long haul and long haul as 600 h/yr while exclusive ultra long haul crews fly up to 900 h/yr. Oksanen (1998) lists annual average cabin crew hour as 673 while the technical crew hours are 578. The range of hours given by Oksanen range from 293 to 906 hours per year. In addition to exposures in actual flight operations, added exposure is due to off duty flights in returning to a home base estimated by some to be twenty percent of the actual flight hours that are logged.

Hughes and O'Riordan (1993) estimate an average annual dose equivalent 3mSv/yr (≈ 1.8 mSv/yr neutron) for UK airlines with 6 mSv/yr (≈ 3.6 mSv/yr neutron) for near polar flights. Montagne et al. (1993) estimate and average for Air France long haul pilots of 2 – 3 mSv/yr (≈ 1.2 – 1.8 mSv/yr neutron). Wilson et al. (estimate during the years 1982 – 1983 that domestic crews in Australia received 1 – 1.8 mSv/yr (≈ 0.6 – 1.1 mSv/yr neutron) while international flights receive 3.8 mSv/yr (2.3 mSv/yr neutron). Preston (1985) gives average dose equivalent rates of 9.2 μSv/hr (≈ 5.5 μSv/hr neutron) in British Airways operations of the Concorde for the year of 1979 with a maximum observed rate of 38.1 μSv/hr (≈ 22 μSv/hr neutron). Observed technical crew exposures were on average 2.8 mSv/yr (1.7 mSv/yr neutron) and 2.2 mSv/yr (≈ 1.3 mSv/yr neutron) for the cabin crew (there are few flight hours for these crews). Similar differences (20 – 30 percent) between flight deck exposures and cabin exposures were observed by Wilson et al. (1994). Even differences between aircraft type (20 percent) were observed.

In estimating the collective dose equivalent we will follow the UNSCEAR (1993) who assumed $3 \bullet 10^9$ passenger-hours in flight during 1985 and an annual average rate of 2.8 μSv/hr (≈ 1.6 μSv/hr neutron) resulting in a collective dose equivalent of 8,400 person-Sv (5,040 person-Sv neutron). By 1997, air travel had grown to $4.3 \bullet 10^9$ passenger-hours in flight leading to a collective dose equivalent of 12,000 person-Sv (7,200 person-Sv neutron). The crew add little to the collective exposure due to their small number. If we assume that the worldwide occupational exposure to neutrons is five times that in the US and consider the exposures in the high cities we can construct the following table 20. The greatest collective dose equivalent of any group is the citizens of the high cities (12,280 person-Sv) with aircrew the largest occupationally exposed group (7,200 person-Sv). The nuclear workers are next largest with 338 person-Sv.

Concluding Remarks

In the present paper, we have given an overview of aircraft exposures and placed it in the context of world population exposures. It is clear that among occupational exposures that the aircrews are among the most consistently highly exposed individuals. In addition, a large fraction of these exposures are from high-energy

neutrons for which there is inadequate biological response data. It is also clear from table 20 that aircrew are among the highest exposed from neutrons as a result of their occupation. Still, the largest group exposures are those living in the high cities for which the present study is of great interest, especially in view of the uncertainty in the associated risk coefficients. The results of the present study for the development of the High Speed Civil Transport will reach beyond the objective of evaluation of the radiation safety of the associated operations to an improved understanding of the exposures of the world population which is of considerable interest (UNSCEAR 1993).

References

Akatov, Yu. A., Some results o dose measurements along civil airways in the USSR. Radiat. Prot. Dosimetry 48: 59-63; 1993.

Allkofer, O. C., Heinrich, W. (1974). "Measurement of galactic cosmic ray nuclei at supersonic transport altitudes and their dosimetric significance." Health Phys. 27, 543-551.

Armstrong, H., Haber, H., Strunghold, H. (1949), "Aero medical problems of space travel-panel meeting, School of Aviation Medicine," *J. Aviation Med.* **20**, 383-417.

Armstrong, T. W.; Chandler, K. C., Barish, J. (1973) "Calculation of neutron flux spectra induced in Earth's atmosphere by galactic cosmic rays." *J. Geophys. Res.* **78**, 2715.

Baarli, J. Radiological problems connected to exposure from cosmic radiation. Radiat. Prot. Dosimetry 48: 101-105; 1993.

Badhwar, G. D. (1997). Deep space radiation sources, models, and environmental uncertainties. In *Shield Strategies for Human Space Exploration,* J. W. Wilson, J. Miller, A. Konradi, and F. A. Cucinotta, eds. NASA CP-3360, pp.17-28, 1997.

Badhwar, G. D. , Cucinotta, F. A. , and O'Neill, P. M. (1994). An Analysis of Interplanetary Space Radiation Exposure for Various Solar Cycles, Radiat. Res. 138:201-208.

Bagshaw, M. Irvine, D., Davies, D. M., Exposure to cosmic radiation of British Airways flying crew on ultralonghaul routes. Occupational and Environmental Medicine **53**: 495-498; 1996.

Balasubramanyan, V. K., Bolt, E., Palmerira, R. A. R., Solar Modulation of Galactic Cosmic Rays, J. Geophys. Res. 72: 27-26; 1967.

Bazilevskaya, G.A., Svirzhevskaya, A. K. (1998). On the stratospheric measurements of cosmic rays. Space Sci. Rev. 85: 431-521.

Bethe, H. A., Korff, S. A., Placzek, G. (1940). "On the interpretation of neutron measurements in cosmic radiation," *Phys. Rev.* **57**, 573-587.

Bouville, A., Lowder, W.M. (1988) Human polulation exposure to cosmic radiation. Radiat. Prot. Dosim. 24: 293-299.

Cleghorn, T. F.; and Badhwar, G. D.(1997). Comparison of the SPE Model with Proton and Heavy Ion Data. *Impact of Solar Energetic Particle Events for Design of Human Missions Workshop*, September 9-11, 1997.

Cucinotta, F.A., Katz, R., Wilson, J.W. (1998) Radial distribution of electron spectra from high-energy ions. Radiat. Environ. Biophys. 37: 259-265.

Cucinotta, F.A., Katz, R., Wilson, J.W., Dubey, R.D., (1996) Radial dose distributions in the delta-ray theory of track structures. In: Proceedings of Two Center Effects in Ion-atom Collisions. AIP Conference Proceedings 362:245-265.

Cucinotta, F.A., W. Schimmerling, J.W., Wilson, L.E. Peterson, G.D. Badhwar, P. Saganti, J.F. Dicello, (2001) Space radiation cancer risks and uncertainties for Mars missions. *Radiat. Res*. **156**: 682-688.

Davies, D.M. (1993) Cosmic radiation in Concorde operations and the impact of new ICRP recommendations on commercial aviation. Radiat Prot. Dosim. 48: 121-124.

EPA (1984) Occupational Exposure to Ionizing Radiation in the United States: A Comprehensive Summary for the Year 1980 and a Summary of Trends for the years 1960-1985. EPA 520/1-84-005 (Environmental Protection Agency, Washington D.C.).

FAA Advisory Committee on the Radiobiological Aspects of the SST. "Cosmic radiation exposure in supersonic and subsonic flight." *Aviat., Space, & Environ. Med.* **46**: 1170-1185; 1975.

Fipov, R. A., Krisiuk, E.M. (1979) Radiation dose of the population of the Soviet Union from cosmic radiation. Atomnaja Energiya 47: 420-421.

Foelsche, T. (1961). Radiation Exposure in Supersonic Transports. NASA TN D-1383.

Foelsche, T., Mendell, R. B., Wilson, J. W., Adams, R. R. (1974). Measured and calculated neutron spectra and dose equivalent rates at high altitudes: relevance to SST operations and space research, NASA TN D-7715.

Fujii, Z., McDonald, F. B. Radial intensity gradients of galactic cosmic rays (1972-1995) in the heliosphere, J. Geophys. Res. 102(A11): 24,201-24,208; 1997.

Fujitaka, K., Abe, S. (1984a) Calculation on cosmic-ray muon exposure rate in non-walled concrete buildings. Radioisotopes 33: 350-356.

Fujitaka, K., Abe, S. (1984b) Modelling of cosmic-ray muon exposure in building's interior. Radioisotopes 33: 343-349.

Fujitaka, K., Abe, S. (1986) Effects of partition walls and neighboring buildings on the indoor exposure rate due to cosmic-ray muons. Health Phys. 51: 647-659.

Goldhagen, P., (2000) Overview of aircraft radiation exposure and recent ER-2 measurements. Proceedings No. *20 Cosmic Radiation Exposure of Airline Crews, Passengers, and Astronauts*. 1998 Annual Meeting of the NCRP, Washington, DC, March 30, 1998. Health Phys. **79**, 526-544.

Hajnal, F., Wilson, J. W. (1991). "High-altitude cosmic-ray neutrons: a significant contributor to the radiation exposures at aircraft altitudes." Seventh Symposium on Neutron Dosimetry, Berlin, October 14-18, 1991.

Hajnal, F., Wislon, J. W. (1992) High-altitude cosmic ray neutrons: probable source for the high energy protons at the earth's radiation belts. In Proc. 8th Congress Intl. Radiat. Prot. Ass. Montreal, p. 1620.

Hall, D. L., Duldig, M. L., Humble, J. E. (1996) Analysis of sidereal and solar anisotropies in cosmic rays, Space Sci. Rev. 17: 401-442.

Halliday, D. (1962). *Introductory Nuclear Physics*, Wiley and sons, New York, 1962.

Hess, V. F., And Eugster, J. (1949). *Cosmic Radiation and Its Biological Effects*, Fordham University Press, New York.

Hess, W. N., Canfield, E. H., Lingenfelter, R. E. (1961). "Cosmic-ray neutron demography." *J. Geophys. Res*. **66**, 665-667.

Hewitt, J. E., Hughes, J. B., McCaslin, et al. (1980) Exposure to cosmic-ray neutrons at commercial jet aircraft altitudes. Natural Radiation Environment III, Conf-780422, pp. 855-881.

Hughes, J. S., O'Riordan, M. C., Radiation Exposures of the UK Population-1993 Review. NRPB-R263, 1993.

Ibrahiem, N. M., Abd el Ghani, A. H., Shawky, S. M., Ashraf, E. M., Farouk, M. A. Measurement of radioactivity levels in soil in the Nile delta and Middle Egypt. Health Phys 64: 620-627; 1993.

ICAO, Annual Civil Aviation Report 1997. Available at www.icao.org/icao/en/jr/5306_ar3.htm, 1999.

ICRP (1991). *The 1990 Recommendations of the International Commission for Radiological Protection*, ICRP Report 60, Pergamon Press, Oxford, UK.

ICRP Task Group (1966). "Radiobiological aspects of the supersonic transport." Health Phys. 12, 209-226.

International Congress of Radiology, X-ray and Radium Protection, Br. J. Radiol. 1, 359-363: 1928.

Jenkins, C. E., Wogman, N. A., Rieck, H. G. (1972). "Radionuclide distributions in Olympic National Park, Wa." Water, Air, Soil Pollut. Vol. 1, p. 181.

Johnson, F. S. ed. (1965). *Satellite Environment Handbook*, Standford University Press.

Julius, H. W., van Dongen, R. (1985) Radaition doses to the population in the Netherlands, due to external natural sources. Sci. Total Environ. 45: 449-458.

Kim, M., Wilson, J. W., Kiefer, R. L., Thibeault, S. A. Effects of Isotope Selection on Solution Convergence in HZE Transport. NASA TP-3445, 1994.

Klement, A.W., Miller, C.R., Minx, R.P., Shleien, B. eds. (1972) Estimates of Ionizing Radiation Doses in the United States 1960-2000, ORP-CSD 72-1 (Environmental Protection Agency, Washington D.C.).

Kuhn, E., Schwamb, F. E., Payne, W. T. (1965) Solar Flare Haxard to Earth-Orbiting Vehicles. *Second Symposium on Protection Against Radiations in Space*, NASA SP-71, pp. 429-434.

Lal, D., Peters, B. (1967). "Cosmic ray produced radioactivity on the earth." Encyclopedia of Physics, Fluegge, S. and Sitte, K, Eds., vol. XLVI/2 on Cosmic Rays, Springer-Verlag, Berlin, p. 551.

Lauterbach, U., Kolb, W. (1978) Beitrag der kosmischen Strahlung zur naturlichen Strahlenbelastung in Wohnund Arbeitsraumen. Proceedings of the 12th Annual Meeting of the Fachverband fur Strahlenschutz e. V., in Radioaktivitat und Umwelt, II/993.

Mason, G. C., Radiation assessment of mineral sand and mining in Australia. Proceedings of the International Congress of International Radiation Protection Association (Vol. III), Pergamon Press, pp 1347-1350; 1988.

McCracken, K. G. (1962) The cosmic-ray flare effect. 1. Some new methods of analysis. J. Geophys. Res. 67:423-446.

McDonald, F. B., (1964). "Review of Galactic and Solar Cosmic Rays." *Second Symposium on Protection Against Radiations in Space,* Arthur Reetz , ed., NASA SP-71, 19-29.

Merker, M. (1973). "Contributions of galactic cosmic rays to atmospheric neutron maximum dose equivalent as function of neutron energy and altitude." *Health Phys*. **25**, 524.

Meyer, P., Parker, E. N., Simpson, J. A., Solar cosmic rays of February, 1956 and their propagation through interplanetary space. Phys. Rev. **104**: 768-781; 1956.

Miller, K.M., Beck, H.L. (1984) Indoor gamma and cosmic ray exposure rate measurements using a Ge spectrometer and pressurized ionization chamber. Radiat. Prot. Dosim. 7:185-189.

Montagne, C., Donne, J. P. Pelcot, D. et al. (1993) Inflight radiation measurements aboard French airliners. Radiat. Prot. Dosim. 48: 79-83.

Nakamura, T., Uwamino, Y., Ohkubo, T., Hara, A. (1987) Altitude variation of cosmic-ray neutrons. Health Phys. 53: 509-517.

NCRP (1987) Ionizing Radiation Exposure of the Population of the United States. Report No. 93.

NCRP (1987) Exposure of the population in the United States and Canada from Natural Background Radiation. Report No. 94.

NCRP (1995) Radiation Exposure and High Altitude Flight. NCRP Commentary No. 12.

National Council on Radiation Protection, Principles and Application of Collective Dose in Radiation Protection. NCRP Report 121, 1995.

NCRP, *Exposure of the Population in the United States and Canada from Natural Background Radiation*. NCRP Report No. 94, 1987.

Neher, H. V. (1961). "Cosmic-ray knee in 1958." J. Geophysical Res. 66, 4007-4012.

Neher, H. V. (1967). "Cosmic-ray particles that changed from 1954 to 1958 to 1965.", J. Geophys. Res. 72: 1527-1539.

Neher, H. V. (1971). "Cosmic rays at high latitudes and altitudes covering four solar maxima," J. Geophys. Res. 76: 1637-1851.

Neher, H. V., Anderson, H. R. (1962). "Cosmic rays at balloon altitudes and the solar cycle." J. Geophysical Res. 67, 1309-1315.

Neher, H. V., Pickering, W. H. (1942). "Results of a high altitude cosmic ray survey near the magnetic equator". Phys Rev. 61: 407-413.

Nymmik, R. A. (1997). Space environment (natural and artificial) – Probabilistic Model for Fluences and Peak Fluxes of Solar Cosmic Ray Particles. International Standard ISO WD 15391.

Oakley, D. T., Natural radiation exposures in the United States. USEPA Report ORP/SID-72-1; 1972.

O'Brien, K., Friedberg, W. (1994). "Atmospheric cosmic rays at aircraft altitudes." *Enviornment International* **20**, 645-663.

Parker, E. N. (1965).The Passage of Energetic Charged Particles Through Interplanetary Space, Planetary Space Sci. 13: 9-49.

Parker, J. F. West, V. R., eds. (1973) Bioastronautics Data Book, Second edition, NASA SP-3006.

Pearson, J. E., Natural Environmental Radioactivity from Radon-222, US Public Health Service Pub. 999-RH-26.

Pfeiffer, W. C., et al. Measurements of environmental radiation exposure dose rates at selected sites in Brazil, An. Acad. Bras. Cienc. 53: 683-691; 1981.

Preston, F. S., Eight years; experience of Concorde operations: medical aspects. *J. Royal Soc. Med.* **78**:193-196; 1985.

Reames, D.V., (1999) Particle accereration at the sun and in the heliosphere. Space Sci. Rev. 90: 417-491.

Roesler, S., Heinrich, W., Schraube, H. (1998). "Calculation of Radiation Fields in the Atmosphere and Comparison to Experimental Data." *Radiat. Res.* **149**, 87-97.

Schaefer, H. J. (1950). "Evaluation of present-day knowledge of cosmic radiation at extreme altitude in terms of the hazard to health," *J. Aviation Med.* **21**, 375-94.

Schaefer, H. J. (1959). "Radiation and man in space." *Adv. Space Res.* **1**, 267-339.

Schimmerling, W. , Wilson, J. W. , Cucinotta, F. A., Kim, M. Y. (1998). Evaluation of risks from space radiation with high-energy heavy ion beams, Physica Medica **14** (Suppl. 1): 29-38.

Schraube, H., Leuthold, G., Roesler, S., Heinrich, W. (1998). Neutron spectra at Flight Altitudes and Their Radiological Estimation." *Adv. in Space Res.* 21: 1727-1738; 1998.

Shea, M. A., Smart, D. F. (1993). "History of energetic solar protons for the past three solar cycles including cycle 22 update." *Biological Effects and Physics of Solar and Galactic Cosmic Radiation,* C. E. Swenberg, G. Horneck, G. Stassinopoulos, eds. Plenum Press, 37-71.

Shea, M. A.; and Smart, D. F. (1983). A world grid of calculated cosmic ray vertical cutoff rigidities for 1980.0. *18th International Cosmic Ray Conference-Conference Papers*, MG Sessions, Vol. 3, Tata Inst. Of Fundamental Research (Colaba, Bombay), 415-418.

Shea, M. A.; and Smart, D. F. (1990). A Summary of Major Solar Proton Events. Solar Physics, **127**, pp. 297-320.

Shinn, J.L., Wilson, J.W. (1991) Nuclear Reaction Effects in Use of Newly Recommended Quality Factor. Health Physics, 61: 415-419.

Simpson, J. A. (1983). Elemental and isotopic composition of the galactic cosmic rays. Annual Rev. of Nucl. and Part. Sci. 33: 323-381.

Störmer, C. (1955). *The Polar Aurora,* Oxford at the Clarendon Press.

Störmer, C. (1930). Periodische Elektronenbahen im Felde eines Elementarmagneten und ihre Anwendung auf Bruches Modellversuche und auf Eschenhagens Elementarwellen des Ermagnetismus. *Z. Astrophys.*, Bd. 1, pp. 237-274.

Sunta, C. M. A review of the studies of high background areas of the S-W coast of India. Proceedings of the International Conference on High Levels of Natural Radiation, Ramsar, IAEA, pp. 71-86; 1993.

Tobias, C. A. (1952). Radiation hazards in high altitude aviation. J. Aviat. Med. 23: 345-372.

Tsui, K. C., Wong, M. C. Lee, B. Y., (1991) Field estimation of cosmic contribution to total external gamma radiation in Hong Kong. Environmental Radiation Monitoring, Hong Kong, Technical Report No. 4.

UNSCEAR Ionizing Radiation: Sources and Biological Effects. UN publ. E.82.IX.8, 1982.

UNSCEAR, Sources, Effects, and Risks of Ionizing Radiation. UN publ. E.88.IX.7, 1988.

UNSCEAR Sources and Effects of Ionizing Radiation. UN publ E.94.IX.2, 1993.

Upton, A. C. (1989). *Radiobiology and Radiation Protection: The Past Century and Prospects for the Future*. NCRP Lecture No. 13, Bethesda.

Van Dongen, R., Stoute, J. R. D. Outdoor nautral background radiation in the Netherlands. Science of the Total Environ. 45: 381-388; 1985.

Von Frieben, A. (1903). "Hodenverauderungen bei tieren nach Rontgenstrahlung," *Muchen Med. Wuhnschi* **50**, 2295.

Wallace, R.G., Sondhaus, C. A. (1978). "Cosmic ray exposure in subsonic air transport." Aviation Space, & Environ. Med. 74, 6494-6496.

Webber, W. R., Ormes, J. F. (1967). "Cerenkof-scintillation counter measurements of nuclei heavier than helium in the primary cosmic radiation. 1. Charge composition and energy spectra between 200 MeV/nucleon and 5 beV/nucleon." J. Geophys. Res.--Space Phys. 72, 5957-5976.

Wehr, M. R., Richards, J. A. (1960). *Physics of the Atom*, Addison-Wesley Publ., Reading, MA.

Weng, P.-S., Chen, C.-F. (1987) Cosmic-ray ionization in the lower atmsophere. Health Phys. 52: 347-352.

Weng, P.-S., Chu, T.-C., Chen, C.-F., Natural radiation background in metropolitan Taipei, J. Radiat. Res. 32: 165-174; 1991.

Wilson, J. W., Lambiotte, J. J., Foelsche, T., Filippas, T. A. (1970). *Dose Response Functions in the Atmosphere Due to Incident High-energy Protons with Application to Solar Proton Events*. NASA TN D-6010.

Wilson, J. W., Denn, F. M. (1976). *Preliminary Analysis of the Implications of Natrural Radiations on Geostationary Operations*. NASA TN D-8290.

Wilson, J. W., Townsend, L. W. (1988) Radiation safety in commercial air traffic: a need for further study. Health Phys 55: 1001-1003 and Health Phys. 56: 973-974.

Wilson, J. W., Shinn, J. L., Townsend, L. W. (1990). "Nuclear reaction effects in conventional risk assessment for energetic ion exposures." *Health Phys*. **58**, 749-752.

Wilson, J. W., Townsend, L. W., Badavi, F. F. (1987). Galactic HZE propagation through the earth's atmosphere. Radiat. Res. 109:173-183.

Wilson, J.W., Cucinotta, F.A., Hajnal, F. (1991a)Analytical Relationships of Nuclear Fields and Microdosimetric Quantities for Target Fragmentation in Tissue Systems. Health Phys. 60, 559.

Wilson, J. W., Townsend, L. W., Schimmerling, W., Khandelwal, G. S., Khan, F., Nealy, J. E., Cucinotta, F. A., Simonsen, L. C., Shinn, J. L., Norbury, J. W. (1991b) Transport methods and interactions for space radiation. NASA RP-1257.

Wilson, J. W., Nealy, J. E., Cucinotta, F. A., Shinn, J. L., Hajnal, F., Reginatto, M., Goldhagen, P. (1995) Radiation safety aspects of commercial high-speed flight transportation. NASA TP-3524.

Wilson, J.W. (2000) Overview of radiation environments and human exposures. *Health Phys*. **79**: 470-494.

Wilson, O. J., Young, B. F., Richardson, C. K., Cosmic radiation doses received by asutralian commercial flight crews and the implications of ICRP 60. *Health Phys*. **66**: 493-502; 1994.

Yanagisawa, K. Muramatsu, Y. Transfer factors of technetium from soil to vegetables, Radiochimica Acta. 63: 83-86; 1993.

Yanagisaw, K. Muramatsu, Y., Transfer of technetium from soil to paddy and upland rice. J. Radiat. Res. 36: 171-178; 1995.

Yue, Q. Y., Jin, H. (1987) Measurement of ionization distribution in the lower atmosphere caused by cosmic ray. In Proceedings of Workshop on Occupational and Environmental Radiation Protection, Hong Kong.

Table 1. Principal nuclear decay sequence of Actinium Series (U-235).

Isotope	Lifetime	Decay mode(s)	Decay energy, MeV
U-235	7.1x10^8 yr	α	4.4
Th-231	25.5 h	-e	0.09 - 0.3
Pa-231	3.2x10^4 y	α	5.0
Ac-227	21.6 y	-e	0.05
Th-227	18.2 d	α	5.8 – 6.0
Ra-223	11.4 d	α	5.5-5.7
Rn-219	4.0 s	α	6.4-6.8
Po-215	1.8x10^-3 s	α	7.4
Pb-211	36.1 min	-e	1.4, 0.5
Bi-211	2.15 min	α	6.3, 6.6
Tl-207	4.79 min	-e	1.44
Pb-207	–	--	--

Table 2. Principal nuclear decay sequence of the Uranium Series (U-238).

Isotope	Lifetime	Decay mode(s)	Decay energy, MeV
U-238	4.5x10^9 yr	α	4.2
Th-234	24.1 d	-e	0.2, 0.1
Pa-234	1.17 min	-e	2.3
U-234	2.45x10^5 yr	α	4.7-4.8
Th-230	7.7x10^4 yr	α	4.6-4.7
Ra-226	1600 yr	α	4.8
Rn-222	3.82 d	α	5.5
Po-218	3.05 min	α	6.0
Pb-214	26.8 min	-e	0.7, 1.0
Bi-214	19.9 min	-e	0.4-3.3
Po-214	1.64x10^-4 s	α	7.7
Pb-210	22.3 yr	-e	~0.1
Bi-210	5.01 d	-e	1.2
Po-210	138 d	α	5.3
Pb-206	–	--	--

Table 3. Principal nuclear decay sequence of Thorium Series (Th-232).

Isotope	Lifetime	Decay mode(s)	Decay energy, MeV
Th-232	1.4x10^10 yr	α	4.0
Ra-228	5.75 yr	-e	~0.1
Ac-228	6.13 h	-e	0.4-2.2
Th-228	1.91 yr	α	5.3, 5.4
Ra-224	3.66 d	α	5.7
Rn-220	55.6 d	α	6.3
Po-216	0.15 s	α	6.8
Pb-212	10.6 h	-e	0.3, 0.6
Bi-212	60.6 min	-e (64%) a (36%)	2.2, 6.1
Tl-208	3.07 min	-e	1.0-1.8
Po-212	3.05x10^-7 s	α	8.8
Pb208	–	--	--

Table 4. Concentrations (Bq/kg) of radioactivity in major rock types and soils (NCRP 1987)

Rock type	K-40	Rb-87	Th-232	U-238
Igneous rocks				
Basalt (average)	300	30	10-15	7-10
Mafic	70-400	1-40	7-10	7-10
Salic	1100-1500	150-180	60-80	50-60……
Granite (average)	>1000	150-180	70	40
Sedimentary rocks				
Shale sandstones:	800	110	50	40
Clean quartz	<300	<40	<8	<10
Dirty quartz	400?	80?	10-25?	40?
Arkose	600-900	80	<8	10-25?
Beach sands (unconsolidated)	<300	<40	25	40
Carbonate rocks	70	8	8	25
Continental upper crust				
Average	850	100	44	36
Soils	400	50	37	66

Table 5. Concentrations (Bq/kg) of radioactivity in soil of Nordic countries (Christen et al 1990).

Soil type	K-40	Ra-226	Th-232
Sand and silt	600-1200	5-25	4-30
Clay	600-1300	20-120	25-80
Moraine	900-1300	20-80	20-80
Soils with Alum shale	600-1000	100-1000	20-80

Table 6. Mean concentrations (Bq/kg) of radioactivity in the Nile delta and middle Egypt (Ibrahiem et al. 1993).

Soil type	K-40	U-238	Th-232
Coastal sand (monazite, zirconium)	223.6	26.4	47.7
Sand	186.4	10.7	9.8
Sandy loam and sandy clay	288.6	14.8	15.5
Clay loam and silty loam	317.	15.5	17.9
Loam	377.5	19.6	19.1
Clay	340.7	15.5	17.9

Table 7. Concentrations of natural radionuclides and absorbed dose rates in air (UNSCEAR 1993).

Radionuclide	Concentration (Bq/kg)		Dose Coefficient (nGy/h per Bq/kg)	Dose rate (nGy/h)	
	Mean	Range		Mean	Range
China					
K-40	580 ± 200	12 - 2190	0.0414	24	0.5 - 90
Th-232 series	40 ± 28	1.5 - 440	0.623	31	0.9 - 270
U-238 series	40 ± 34	1.8 - 520	--	See Ra subseries	--
Ra-226 subseries	37 ± 22	2.4 - 430	0.461	17	1.1 - 200
Total				72	2 - 560
United States					
K-40	370	100 - 700	0.0414	15	4 - 29
Th-232 series	35	4 – 130	0.623	22	2 – 81
U-238 series	35	4 – 140	--	See Ra subseries	
Ra-226 subseries	40	8 – 160	0.461	18	4 – 74
Total				55	10 - 200

Table 8. Estimated absorbed dose rates in air within masonry dwellings (UNSCEAR 1993).

Material	Concentration (Bq/kg)			Activity utilization index[a]	Absorbed dose rate in air for indicated fractional mass of building material (nGy/h)			
	C_K	C_{Ra50}	C_{Th}		1.0	0.75	0.5	0.25
Typical masonry	500	50	50	1.0	80	60	40	20
Granite blocks	1200	90	80	1.9	140	105	70	35
Coal ash aggregate	400	150	150	2.4	180	135	90	45
Alum shale concrete	770	1300	67	9.0	670	500	390	170
Phosphogypsum	60	600	20	3.9	290	220	145	70
Natural gypsum	150	20	5	0.25	20	15	10	5

[a]Assuming full utilization of materials

Table 9. Conversion coefficients from air kerma to effective dose for terrestrial gamma rays (UNSCEAR 1993).

Radionuclides	Conversion coefficient (Sv per Gy)		
	Adults	Children	Infants
K-40	0.74	0.81	0.95
Th-232 series	0.72	0.81	0.92
U-238 series	0.69	0.78	0.91
Overall	0.72	0.80	0.93

Table 10. Fluence levels of solar events of cycle 19-22 associated with ground level events.

Date			Proton fluence (p/cm^2) at energies greater than--	
Month	Day(s)	Year	10 MeV	30 MeV
2	23	56	$2x10^9$	$1x10^9$
7	10-11	59	$5x10^9$	$1x10^9$
7	14-15	59	$8x10^9$	$1x10^9$
7	16-17	59	$3x10^9$	$9x10^8$
11	12-13	60)[a]	$8x10^9$	$2x10^9$
11	15	60	$3x10^9$	$7x10^8$
7	18	61	$1x10^9$	$3x10^8$
11	18	68	$1x10^9$	$2x10^8$
4	11-13	69	$2x10^9$	$2x10^8$
1	24-25	71	$2x10^9$	$4x10^8$
8	4-9	72)[b]	$2x10^{10}$	$8x10^9$
2	13-14	78	$2x10^9$	$1x10^8$
4	30	78	$2x10^9$	$3x10^8$
9	23-24	78	$3x10^9$	$4x10^8$
5	16	81	$1x10^9$	$1x10^9$
10	9-12	81	$2x10^9$	$4x10^8$
2	1-2	82	$1x10^9$	$2x10^8$
4	25-26	84	$1x10^9$	$4x10^8$
8-9	12-7	89	$8x10^9$	$2x10^8$
9-10	29-13	89	$4x10^9$	$1x10^9$
10-11	19-9	89	$2x10^{10}$	$4x10^9$
11-12	26-5	89	$2x10^9$	$1x10^8$

[a]Foelsche et al (1974)

[b]Wilson and Denn (1976)

Table 11. Relation of Magnetic Indices to Magnetic Storm Field Strength

K_p	a_p	$\lvert H_{st} \rvert$, nT
0	0	0
1	4	8
2	7	14
3	15	30
4	27	54
5	48	96
6	80	160
7	132	264
8	207	414
9	400	800

Table 12. Ionization Rates in Air Measured by Argon-Filled Chambers[a] at Solar Minimum (C = 98.3 in 1965)

R, GV	Ion pairs, cm^{-3}, for air depths, g/cm^2, of—													
	30	40	50	60	70	80	90	100	120	140	200	245	300	1034
0	445.0	430.0	414.0	399.0	383.0	366.0	349.0	332.0	298.0	266.0	181.0	136.0	95.0	11.4
.01	445.0	430.0	414.0	399.0	383.0	366.0	349.0	332.0	298.0	266.0	181.0	136.0	95.0	11.4
.16	444.0	430.0	414.0	399.0	383.0	366.0	349.0	332.0	298.0	266.0	181.0	136.0	95.0	11.4
.49	411.8	404.3	394.4	382.0	369.0	354.8	339.4	325.0	292.3	264.5	181.0	136.0	95.0	11.4
1.97	325.0	333.0	340.0	335.0	330.0	312.5	308.0	300.0	285.0	264.0	181.0	134.0	95.0	11.4
2.56	300.0	305.0	310.0	305.0	300.0	290.0	285.0	280.0	255.0	230.0	173.0	126.0	95.0	11.4
5.17	185.0	195.0	208.0	208.0	208.0	208.0	208.0	208.0	195.0	185.0	135.0	103.0	75.0	10.6
8.44	127.6	137.0	145.0	150.2	153.8	155.8	156.0	154.6	149.7	142.2	111.3	87.0	66.6	10.4
11.70	85.0	92.0	98.0	100.0	102.0	105.0	107.0	110.0	108.0	105.0	80.0	77.0	60.0	10.0
14.11	70.0	75.0	82.0	85.0	89.0	93.6	95.0	100.0	98.0	95.0	78.0	68.8	50.0	10.0
17.00	66.3	73.8	80.0	84.8	88.5	91.1	92.6	93.5	93.4	90.5	75.0	62.3	48.0	10.0

[a]Experimental data extrapolated to provide estimates of ionization rates over a wide range of altitudes and geomagnetic cutoffs.

Table 13. Ionization Rates in Air Measured by Argon-Filled Chambers[a] at Solar Maximum (C = 80 in 1958)

R, GV	Ion pairs, cm^{-3}, for air depths, g/cm^2, of—													
	30	40	50	60	70	80	90	100	120	140	200	245	300	1034
0	264.6	267.5	267.0	265.0	258.0	252.0	243.0	235.0	216.3	197.0	145.0	109.2	78.8	11.4
.01	264.6	267.8	267.0	265.0	258.0	251.0	243.0	235.0	216.3	197.0	145.0	109.2	78.8	11.4
.16	264.0	264.9	265.0	264.0	257.0	250.0	243.0	233.0	215.0	197.0	145.0	109.2	78.8	11.4
.49	264.0	264.9	265.0	262.0	256.0	249.0	242.0	231.0	213.2	197.0	145.0	109.2	78.8	11.4
1.97	264.0	265.0	265.0	262.0	252.0	245.0	241.0	231.0	212.5	197.0	145.0	107.8	78.8	11.4
2.56	235.0	237.5	240.0	240.0	239.0	238.0	237.0	230.0	209.0	197.0	145.0	101.6	78.8	11.4
5.17	162.5	168.0	179.0	182.0	178.0	175.2	174.0	173.8	170.0	160.0	159.0	88.3	65.0	10.6
8.44	95.0	103.5	112.0	118.0	118.0	119.0	120.0	122.0	118.0	117.0	100.6	78.7	60.2	10.4
11.70	78.2	85.0	90.7	92.7	94.8	98.0	100.0	103.1	101.2	98.4	75.0	72.2	56.2	10.0
14.11	65.7	70.7	77.5	80.5	84.3	89.0	90.5	95.5	93.5	90.9	74.0	65.9	47.9	10.0
17.0	63.0	70.3	76.4	81.4	84.8	87.5	89.1	90.2	90.1	87.4	72.6	60.3	46.5	10.0

[a]Experimental data extrapolated to provide estimates of ionization rates over a wide range of altitudes and geomagnetic cutoffs.

Table 14. Cosmogenic radionuclides contributing to human exposures (Lal and Peters 1967).

Radionuclide	Half-life	Main decay modes	Target nucleus	Global Inventory
Hydrogen-3	12.33 years	β 18.6 keV	N, O	3.5 kg
Berylium-7	53.3 days	Electron conversion, γ 477 keV	N, O	3.2 g
Carbon-14	5730 years	β 156 keV	N, O	68 mt
Sodium-22	2.60 years	β^+ 545, 1,820 keV; γ 1,275, 511 keV	Ar	1.9 kg

Table 15. Cosmic ray absorbed dose rate in the center of a 12 storey building in NY, NY (Miller and Beck 1984)

Level	Dose rate, nGy/h	Transmission factor
Roof	31.4	1
12	20.2	0.64
10	20.2	0.64
8	18.1	0.58
5	17.4	0.55
4	13.7	0.44
2	11.5	0.37
Basement	8.6	0.27

Table 16. Cosmic ray shielding factors in various dwellings

Dwelling	Sheilding factor	Reference
20 cm concrete	0.85	Lauterbach and Kolb 1978
Single homes, wood ceilings	0.82	Julius and van Dongen 1985
Row houses and office buildings, wood ceilings	0.76	Julius and van Dongen 1985
Dwellings with concrete ceilings and floors	0.50	Julius and van Dongen 1985
Apartment buildings	0.42	Julius and van Dongen 1985
Wooden houses	0.81-0.96	Fipov and Krisiuk 1979
Stone buildings	0.72-0.92	Fipov and Krisiuk 1979
Modern buildings	0.54-0.86	Fipov and Krisiuk 1979

Table 17. Average annual exposures to cosmic rays (UNSCEAR 1993)

Location	Population (millions)	Altitude (m)	Annual effective dose (μSv)		
			Ionizing	Neutron	Total
High-altitude cities					
La Paz, Bolivia	1.0	3,900	1,120	900	2,020
Lhasa, China	0.3	3,600	970	740	1,710
Quito, Ecuador	11.0	2,840	690	440	1,130
Mexico City, Mexico	17.3	2,240	530	290	820
Nairobe, Kenya	1.2	1,600	410	170	580
Denver, United States	1.6	1,610	400	170	570
Tehran, Iran	7.5	1,180	330	110	440
Sea level			240	30	270
World average			300	80	380

Table 18. *Neutron exposure estimates for radiation workers for the year 1980.* (NCRP 1987)

Occupational category	Number of exposed individuals	Average annual effective dose equivalent (mSv)	Collective effective dose equivalent (person- Sv)
US DOE contractors	25, 000	2.6	64
US Nuclear power	1,100	0.5	0.6
US Navy	12,000	0.24	2.9
Totals	38,100	1.8 (mean)	67.5

Table 19. Atmospheric dose equivalent rates measured onboard the TU-144 during March to June 1977 near Solar minimum (Akatov 1993).

	Radiation levels at latitudes of --					
	40°- 45° N		46°- 58° N		65°- 72° N	
Altitude, km	Ionising, μGy/hr	Neutron, μSv/hr	Ionising, μGy/hr	Neutron, μSv/hr	Ionising, μGy/hr	Neutron, μSv/hr
13	2.3	2.6	2.9	4.2	3.5	5.0
14	2.6	3.0	3.2	5.0	4.1	5.9
15	2.8	3.0	3.4	5.4	4.7	6.7
16	2.9	3.2	3.5	5.8	5.2	7.6
17	3.0	3.5	3.7	6.1	-	-
18	3.1	3.4	3.8	5.5	-	-

Table 20. Neutron collective dose equivalents for various exposed groups.

Category	Collective dose equivalent, person-Sv
Occupational worker	338
Commercial aircraft operations	7,200
High cities	12,280

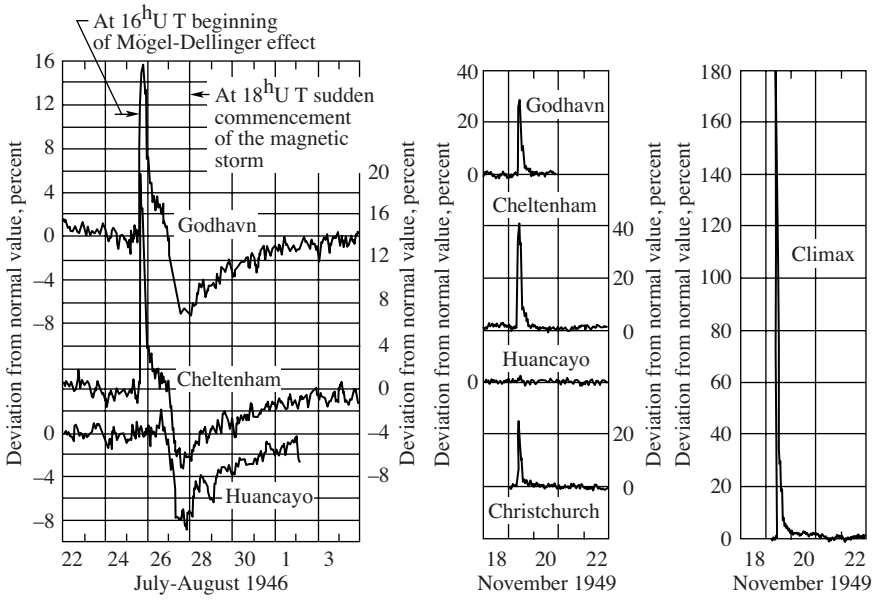

Figure 1. Ground level ion chamber observations of solar particle events of 1946 and 1949. (From Foelsche et al. 1974).

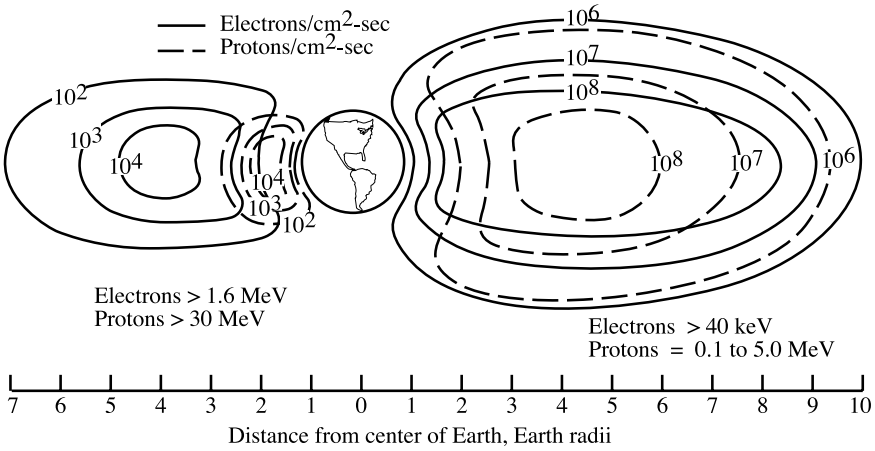

Figure 2. Near-Earth trapped radiation (Parker and West 1973).

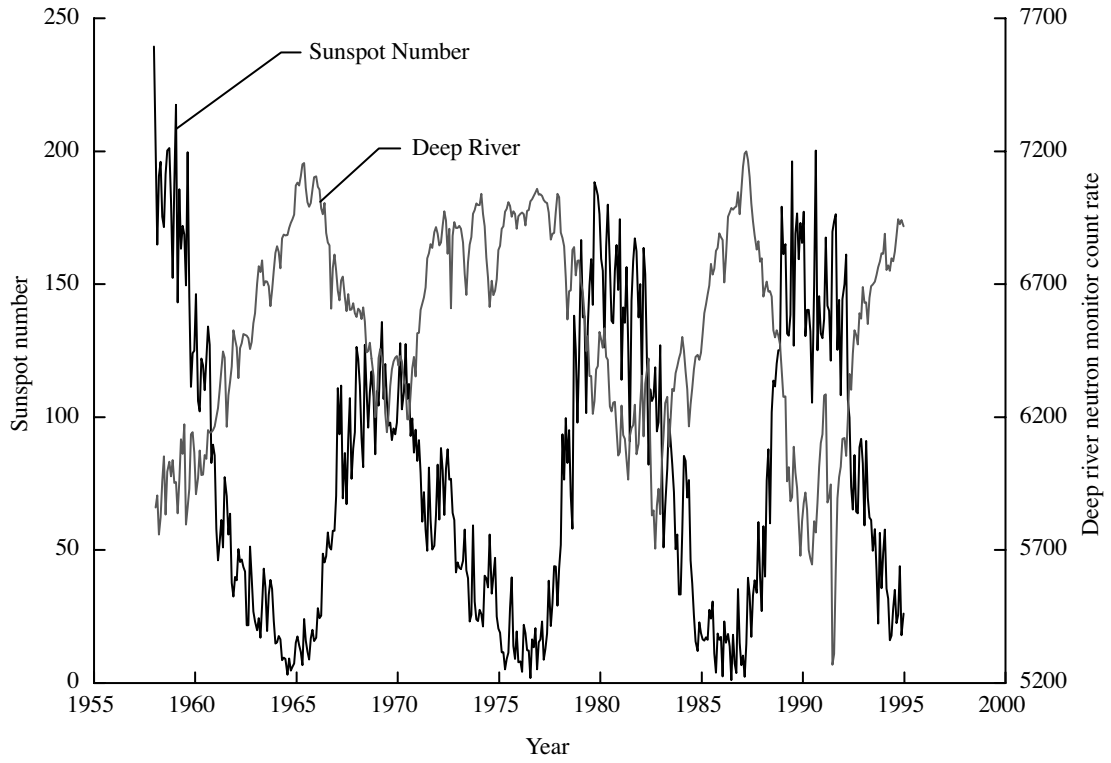

Figure 3. Sunspot number and Deep River neutron monitor count rate over the last few solar cycles.

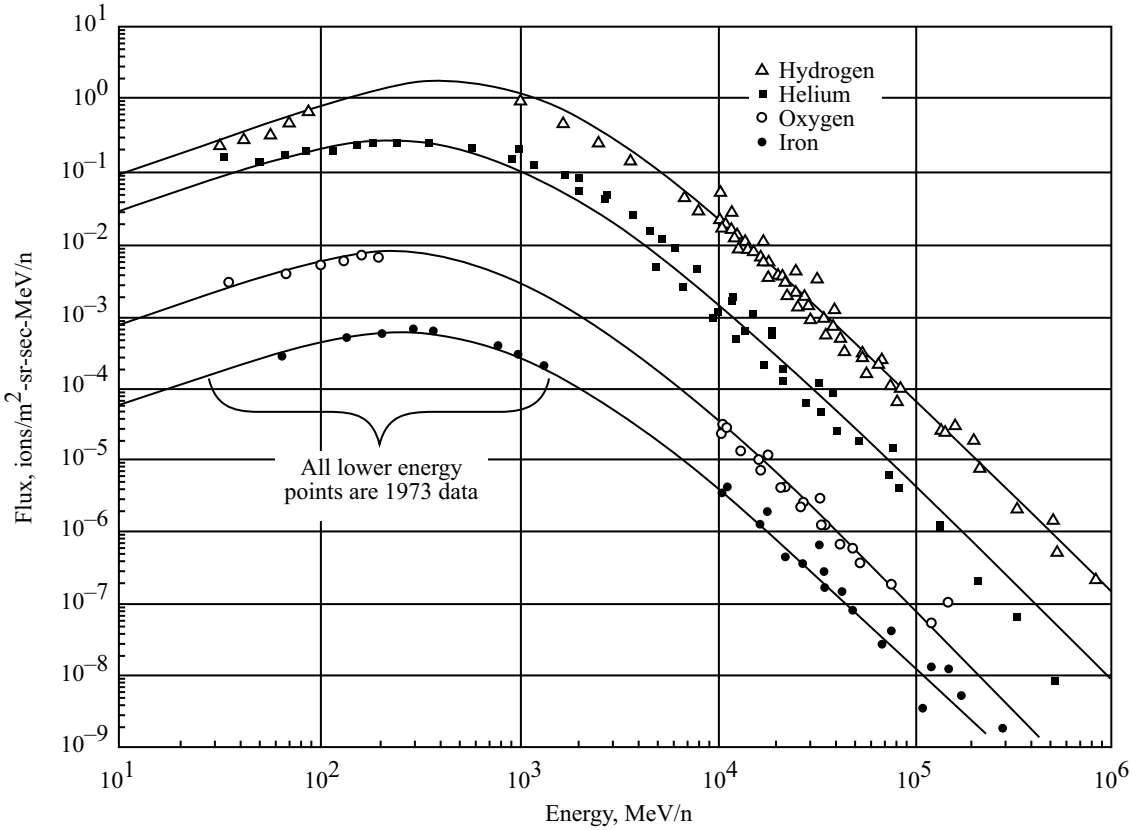

Figure 4. Fit the Fokker-Planck diffusion equation to 1973 differential energy spectra (Badhwar et al. 1994).

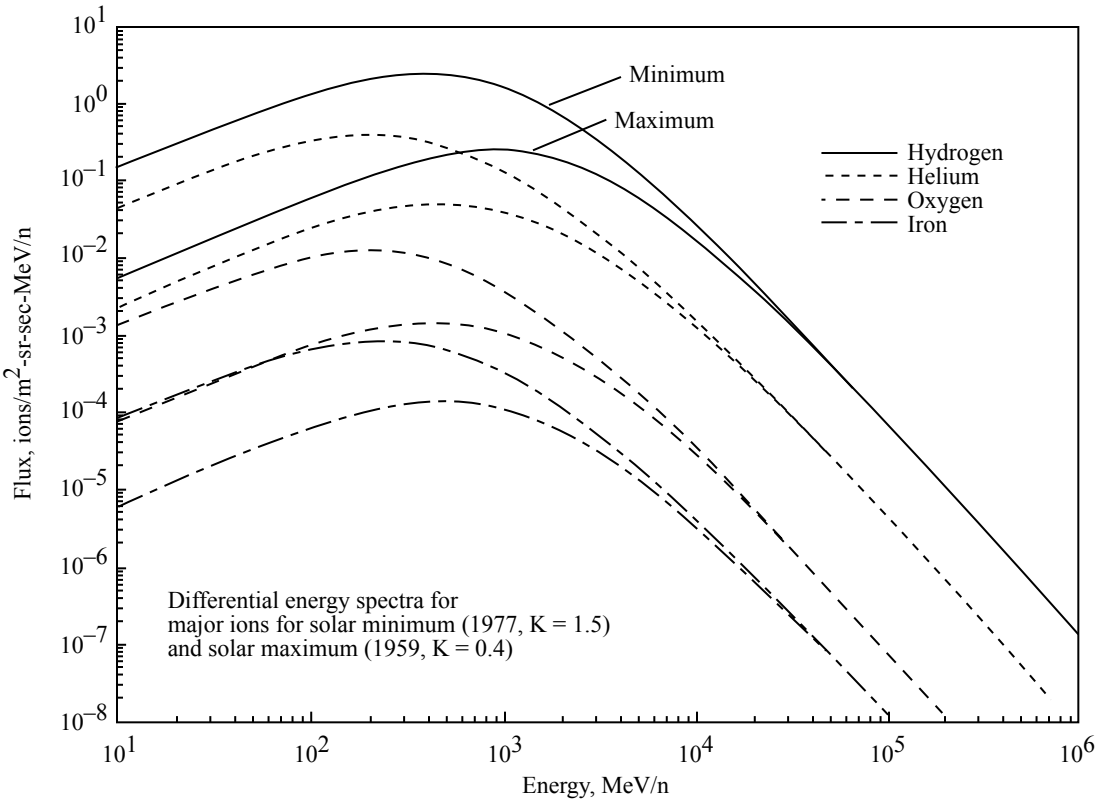

Figure 5. "Worst-case" differential energy spectra during solar minimum and solar maximum (Badhwar et al. 1994).

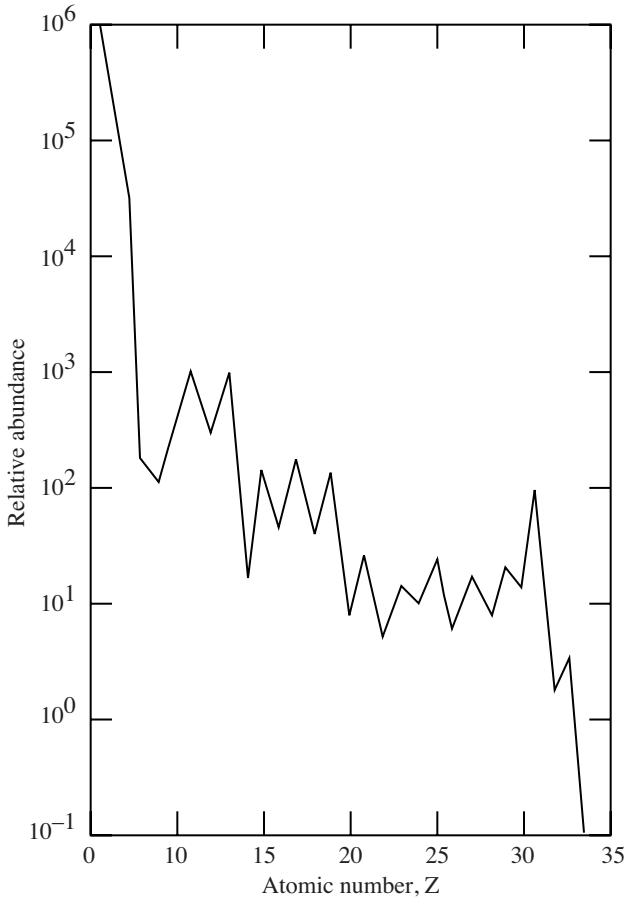

Figure 6. The charge distribution of GCR particles in atomic number (Simpson 1983).

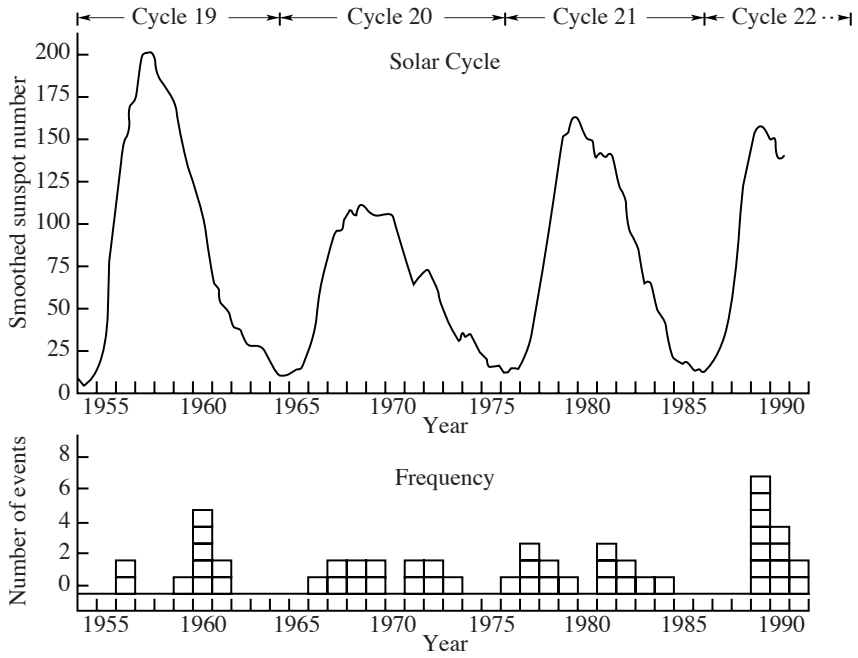

Figure 7. Temporal distribution of ground level solar particle events for the past 40 years. (Shea and Smart 1993).

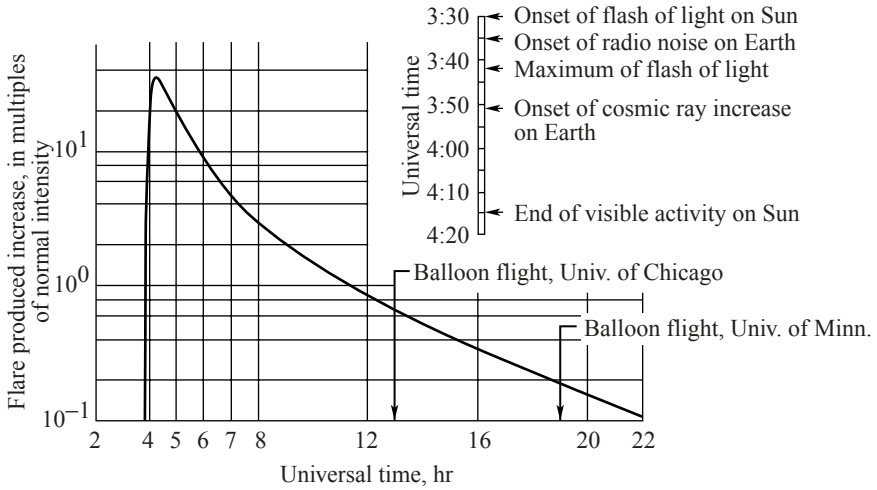

Figure 8. Ground level neutron monitor event seen at Durham, NH on Feb. 23, 1956. (Schaefer 1959).

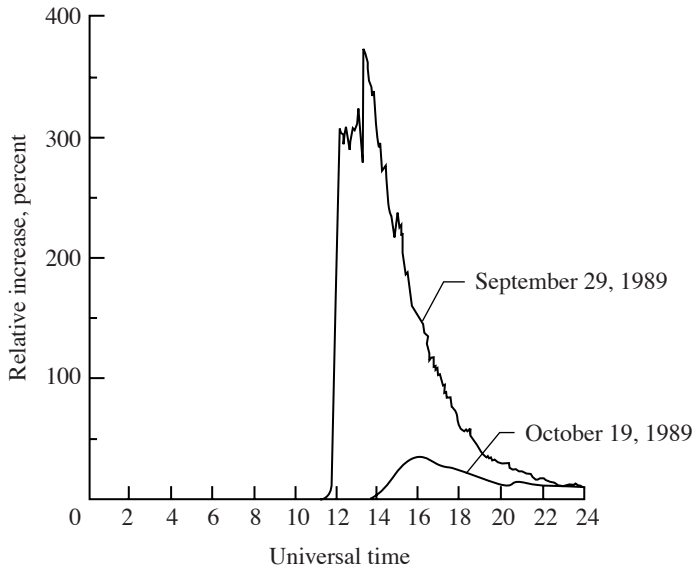

Figure 9. Deep River neutron monitor count rates during the solar particle events of October 19 and September 29 of 1989.

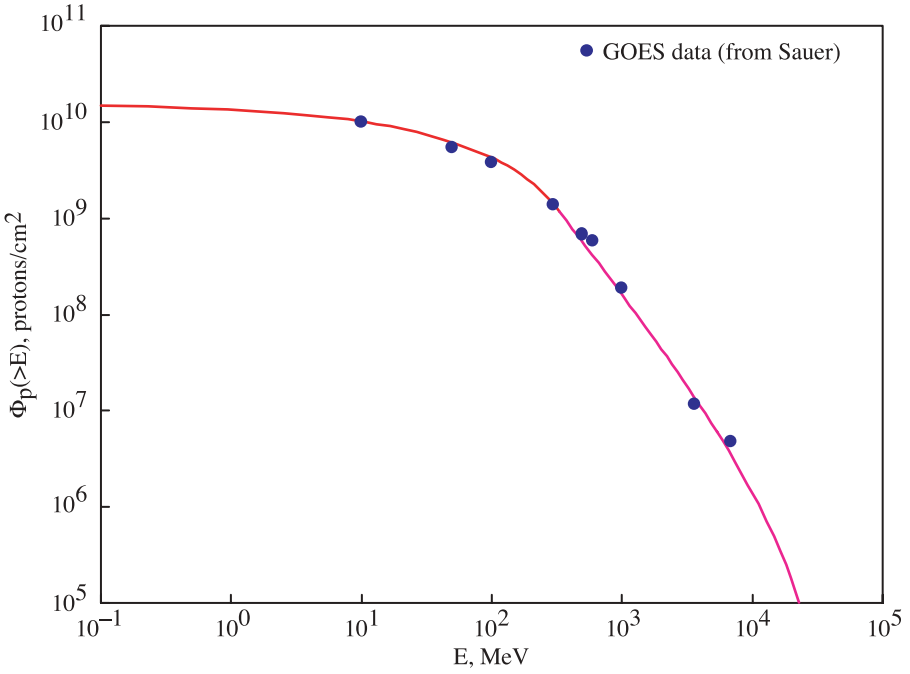

Figure 10. Solar particle event fluence spectra for the September 29, 1989 event.

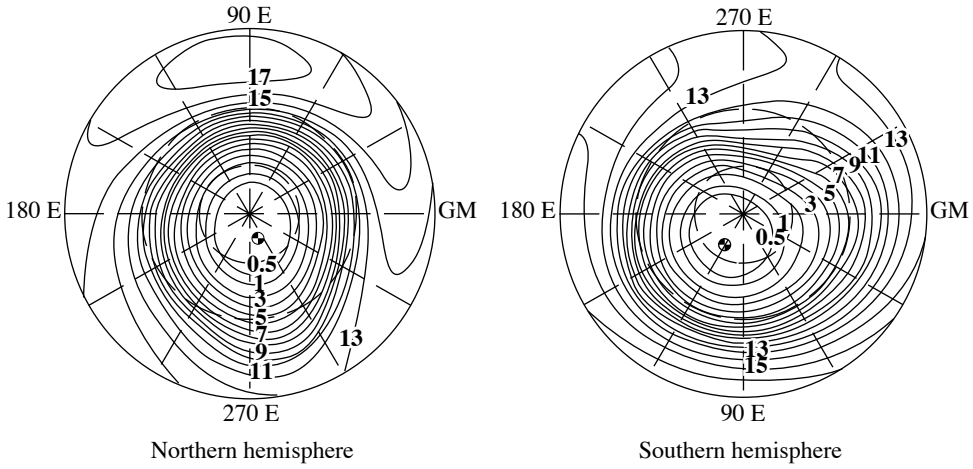

Figure 11. Contour of vertical geomagnetic cutoff values from data of Smart and Shea (1983). Contour increments are 1 GV except for the lowest (0.5 GV) contour. Magnetic pole locations are indicated.

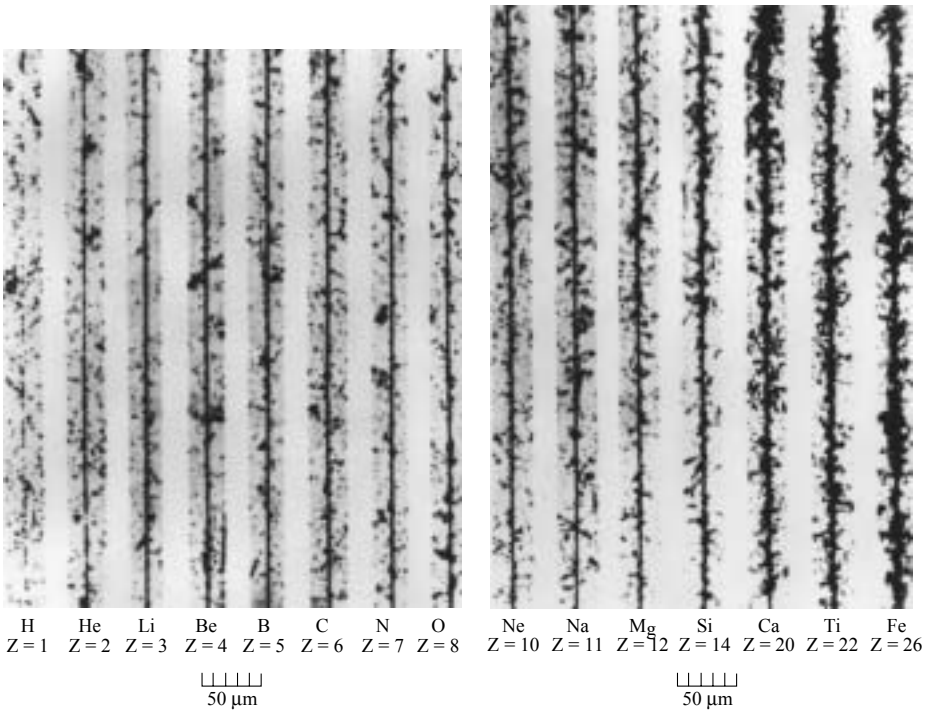

Figure 12. Cosmic-ray ion tracks in nuclear emulsion. (McDonald 1964).

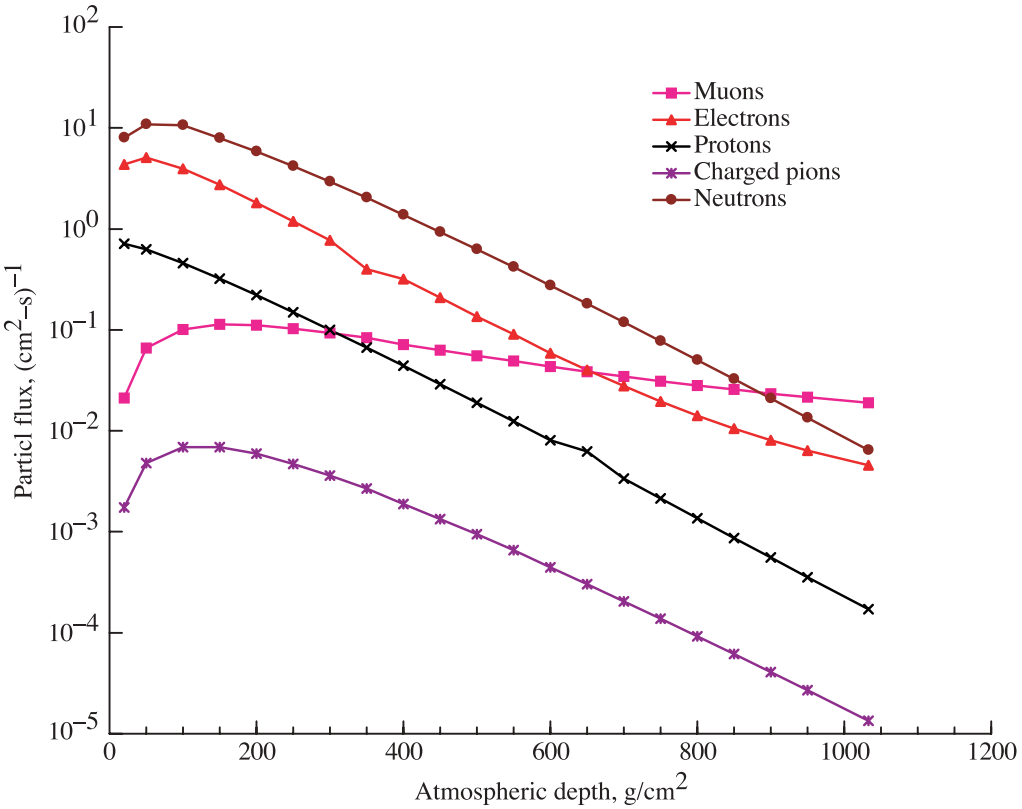

Figure 13. Calculated particle flux at 50° geomagnetic latitude as given by the NCRP (1987). Photon flux is not shown.

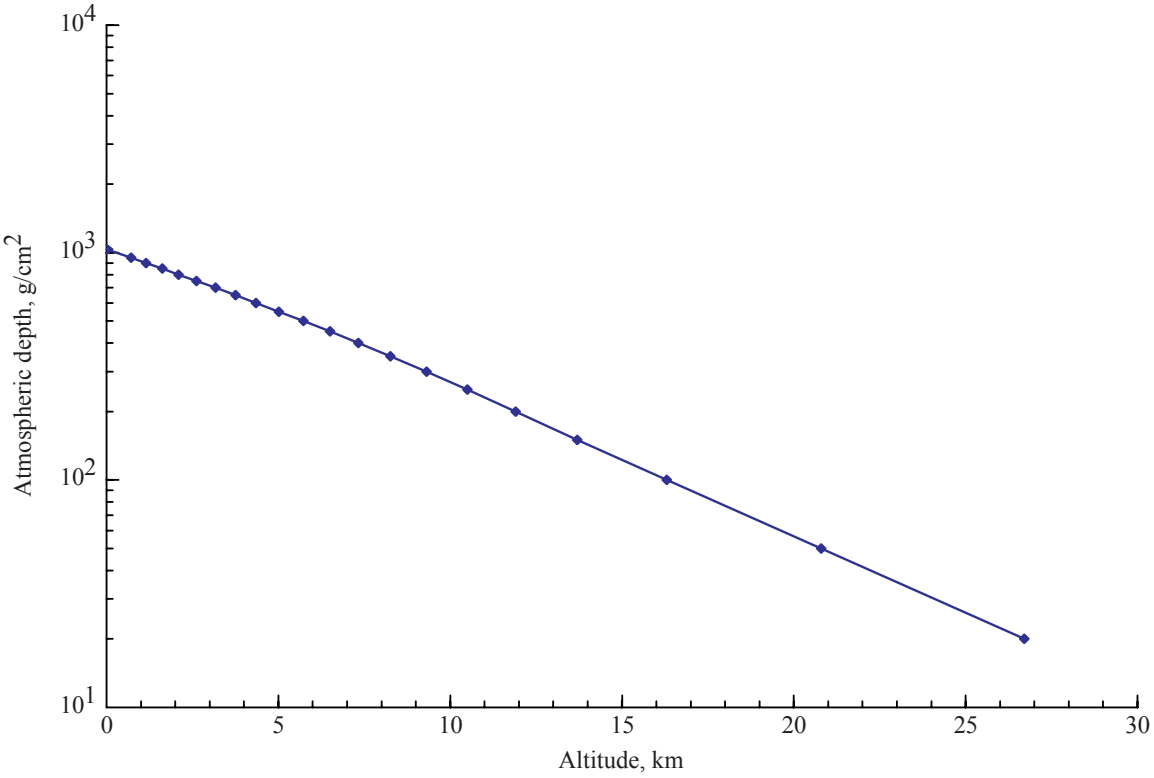

Figure 14. Atmospheric depth as a function of altitude as given by the NCRP (1987).

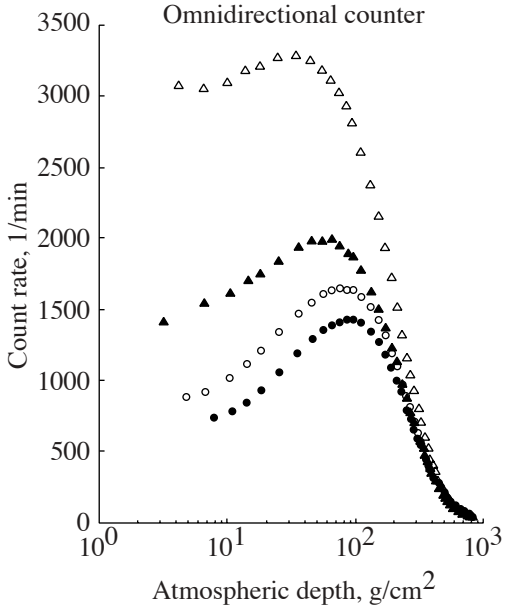

Figure 15. Atmospheric cosmic ray intensity at high latitude (triangles, Murmansk, R_c=0.6 GV) and intermediate latitude (circle, Alma-Ata, R_c = 6.7 GV) near solar minimum (open February 1987) and solar maximum (filled, September 1989). From Bazilevskaya and Svirzhevskaya (1998).

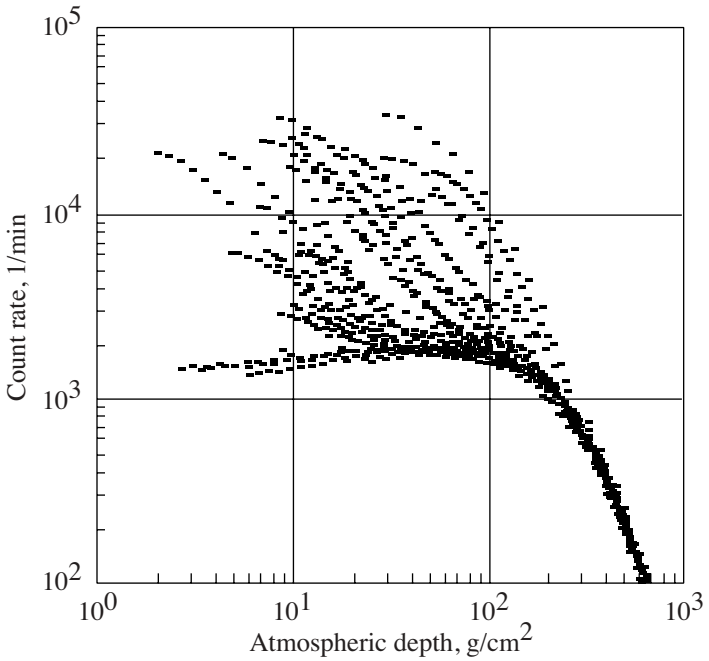

Figure 16. Atmospheric cosmic ray intensity during the October 1989 solar particle event (Bazilevskaya and Svirzhevskaya 1998).

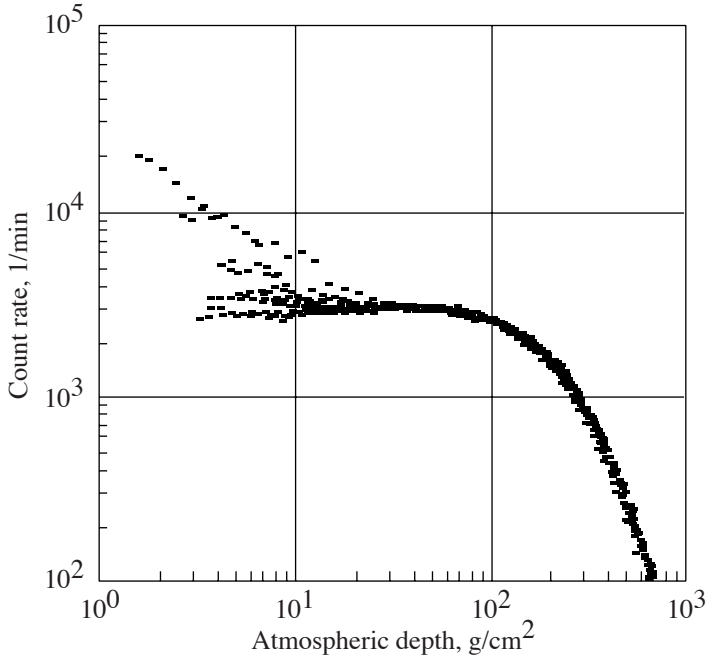

Figure 17. Magnetospheric electron precipitation event in May 1994 (Bazilevskaya and Svirzhevskaya 1998).

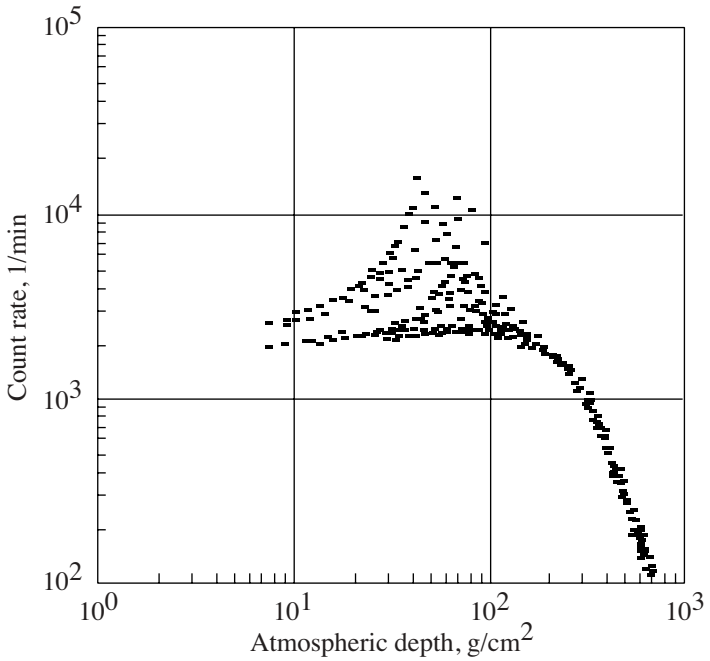

Figure 18. Atmospheric radioactivity following an atmospheric nuclear test in 1970 (Bazilevskaya and Svirzhevskaya 1998).

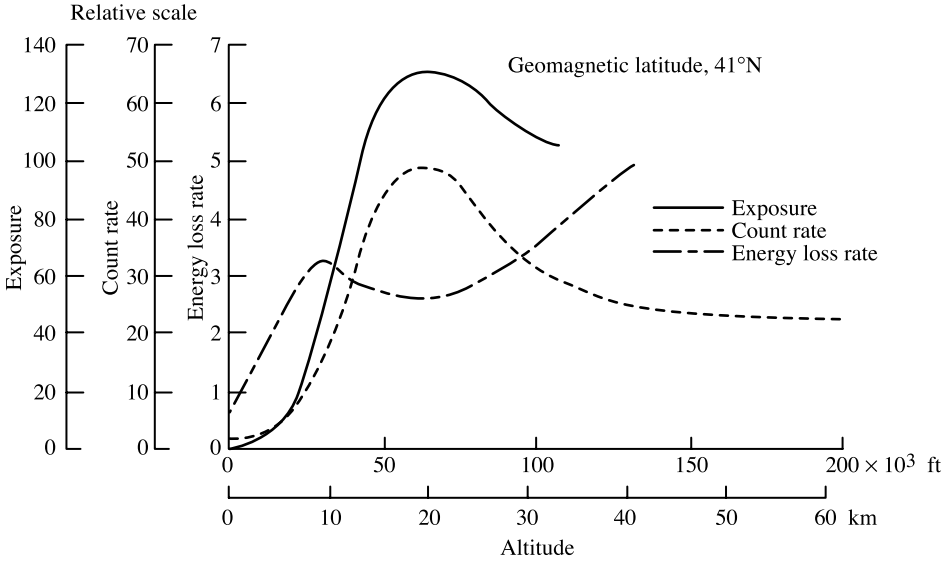

Figure 19. Ionization, counting rate, and average rate, and average rate of energy loss (proportional to specific ionization) (from Tobias, 1952).

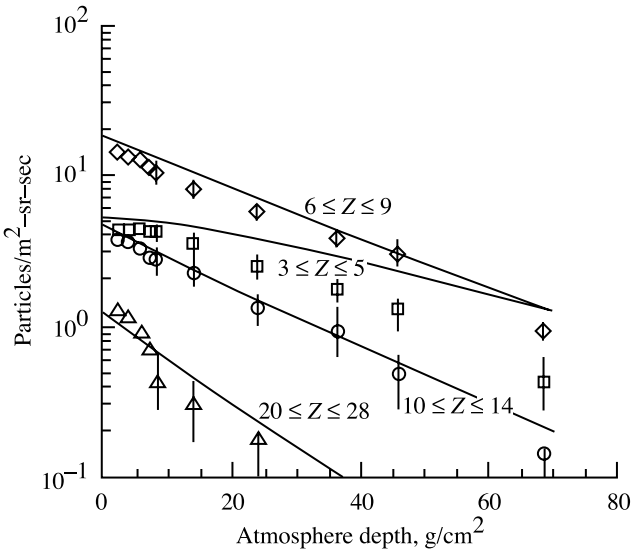

Figure 20. Vertical ion flux in upper atmosphere measured (symbols) by Webber and Ormes (1967) and calculated (lines) by Wilson et al. (1987).

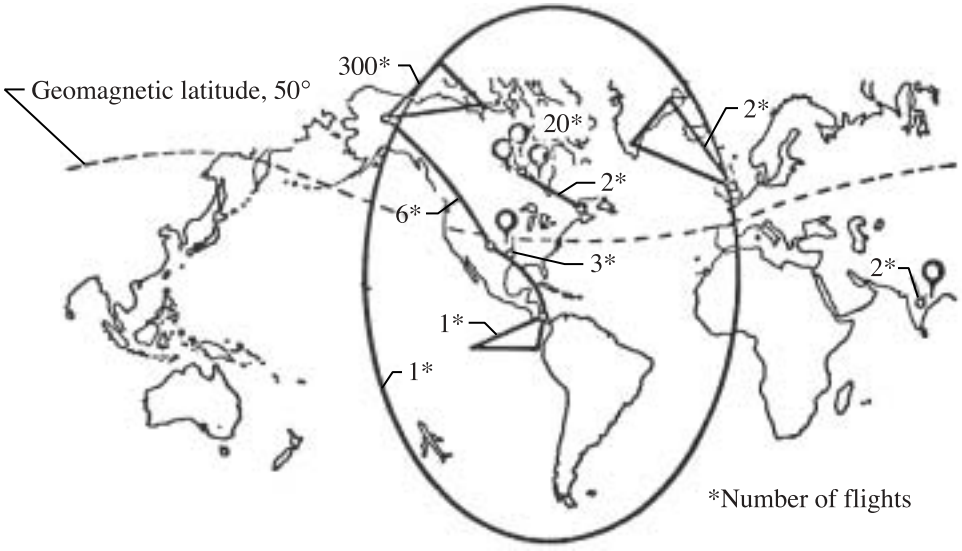

Figure 21. High-altitude radiation measurements made with neutron spectrometers and tissue equivalent ion chambers between 1965 and 1971 (Foelsche et al. 1974).

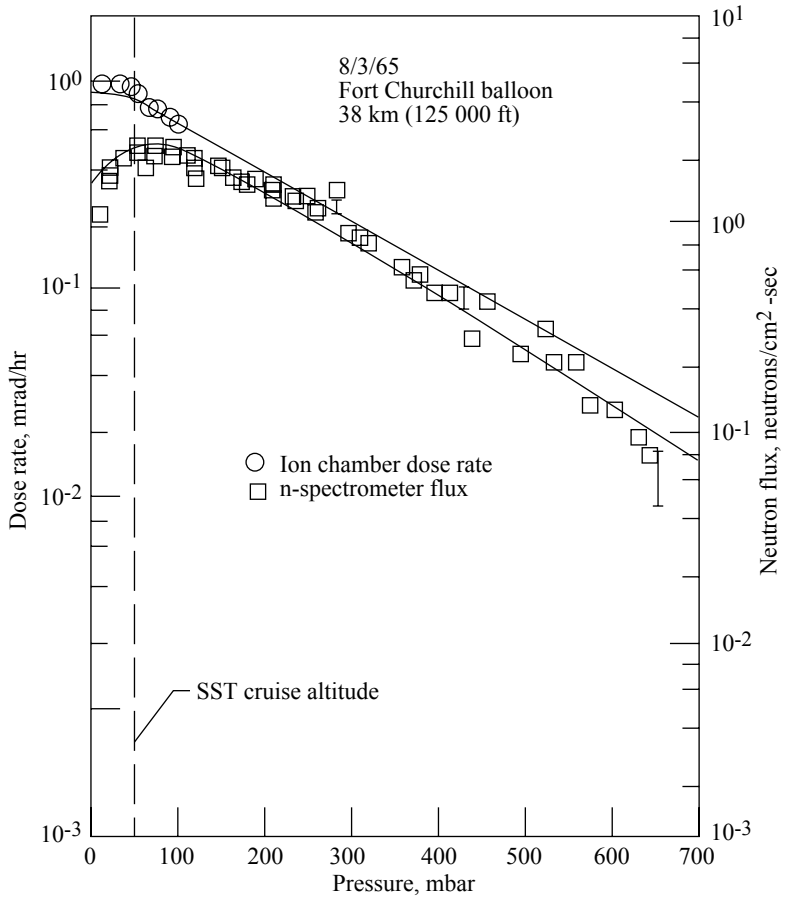

Figure 22. Galactic cosmic-ray maximum (August 3, 1965; 1 year after sunspot minimum: Fort Churchill, Canada; geomagnetic latitude ≈ 69º). Neutron flux from 1 to 10 MeV (right scale), and ion chamber dose rate (left scale) is a function of atmospheric depth (Foelsche et al. 1974). The solid lines are corresponding values from the AIR model (Wilson et al. 1991b).

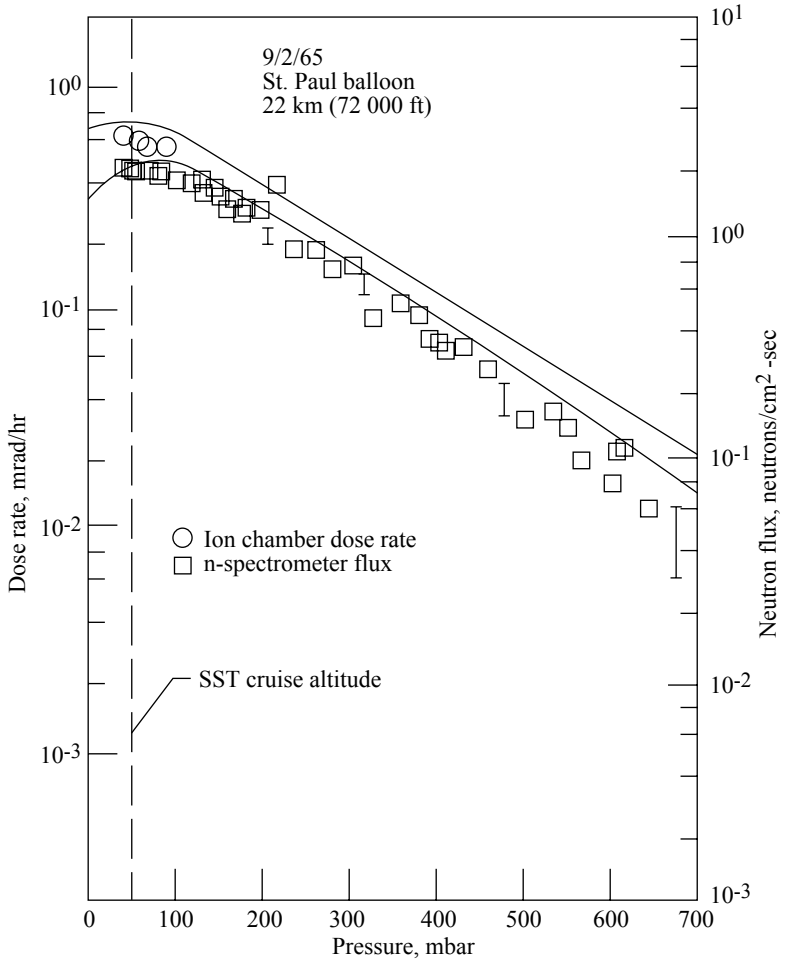

Figure 23. Galactic cosmic-ray maximum (September 2, 1965; St. Paul, Minnesota; geomagnetic latitude ≈ 55°). Neutron flux from 1 to 10 MeV (right scale), and ion chamber dose rate (left scale) is a function of atmospheric depth. Compare with data in figure 22 at higher latitude. (Foelsche et al. 1974) The solid lines are corresponding values from the AIR model (Wilson et al. 1991b).

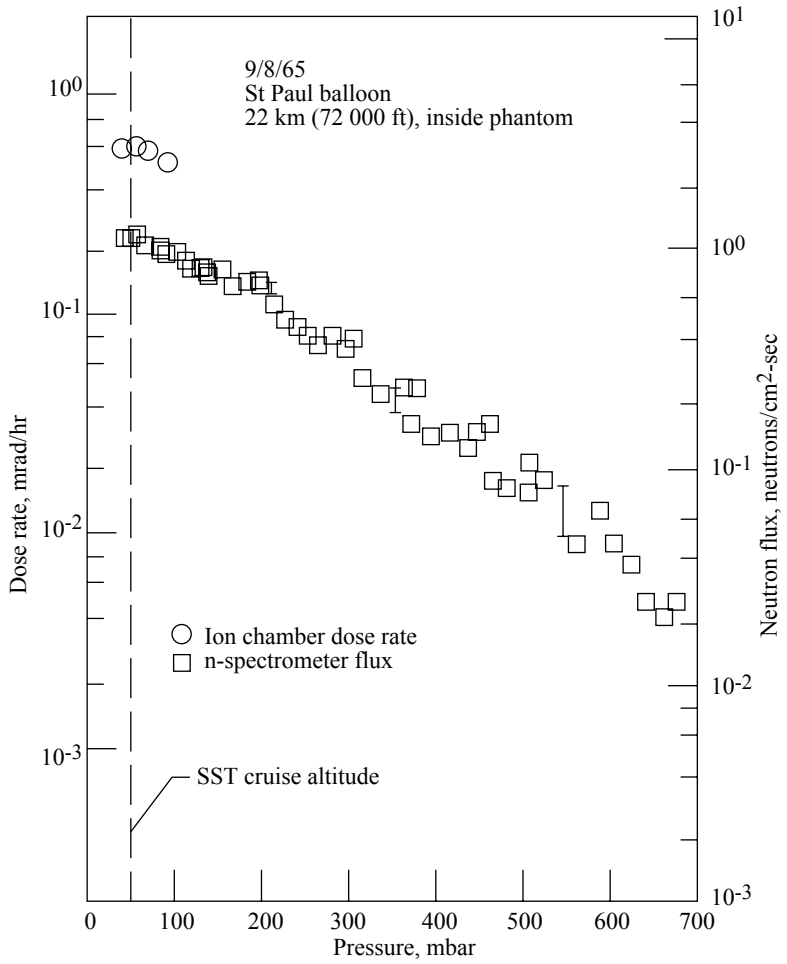

Figure 24. Galactic cosmic-ray maximum (September 8, 1965; St. Paul, Minnesota; geomagnetic latitude ≈ 55°). In flights of figures 22 and 23, the sensors were lightly shielded (less than 1 g/cm^2 of fiber glass and foam). In this flight, the sensors were surrounded by tissue equivalent material, including calcium, of about 15 g/cm^2 thickness to obtain an approximate measurement of the neutron fluxes and ion chamber dose rates in the center of the human body. (Foelsche et al. 1974)

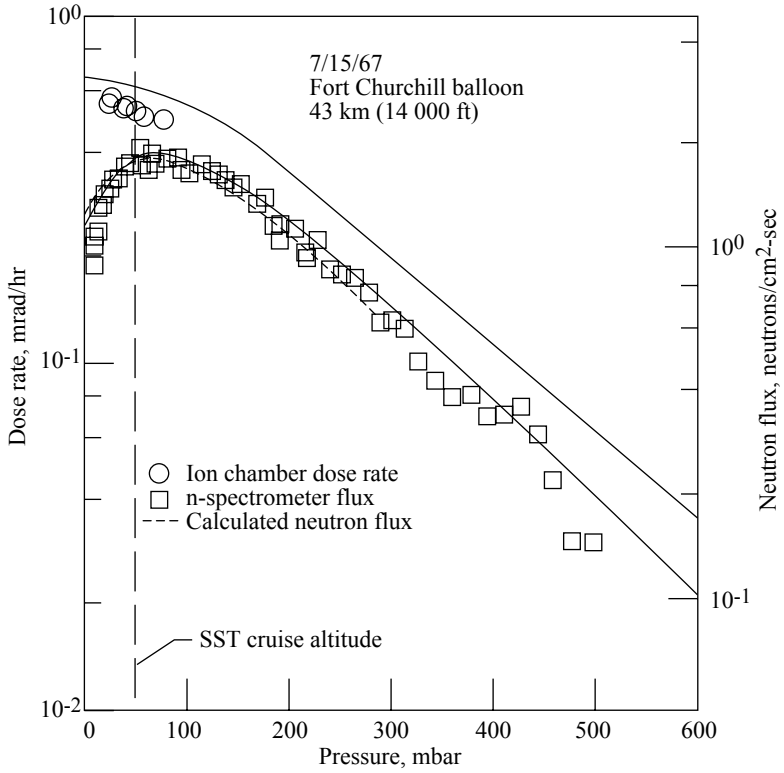

Figure 25. Galactic cosmic rays 2 years after galactic cosmic-ray maximum (July 15, 1967; Fort Churchill, Canada; geomagnetic latitude ≈ 69°). Compare with figure 22 for a flight at galactic cosmic-ray maximum. The neutron flux and ion chamber dose rate have both decreased about 25 to 30 percent at SST altitudes (solar modulation). The short-dashed line is the attitude dependence obtained by theory. (Foelsche et al. 1974) The solid lines are corresponding values from the AIR model (Wilson et al. 1991b).

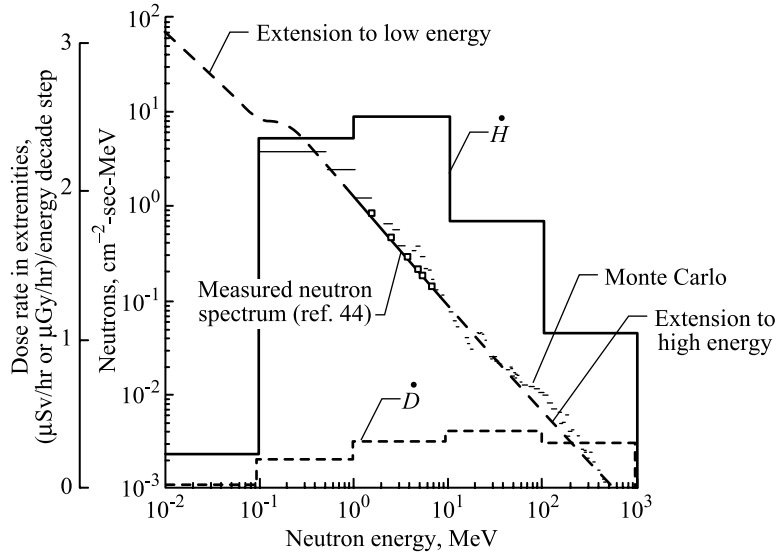

Figure 26. Neutron spectrum at 70,000 ft over Ft. Churchill on August 3, 1965. (Foelsche et al. 1974)

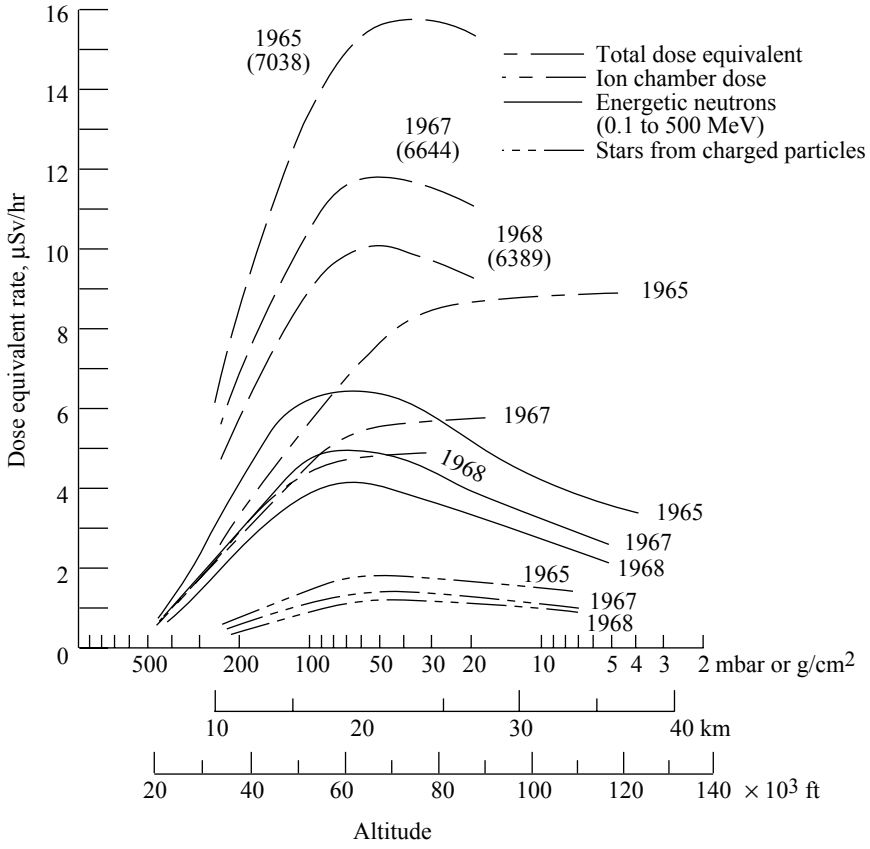

Figure 27. Galactic cosmic-ray dose equivalent rates for extremities (hands and feet) and approximately for eyes as a function of altitude at different phases of the solar cycle for high latitudes.

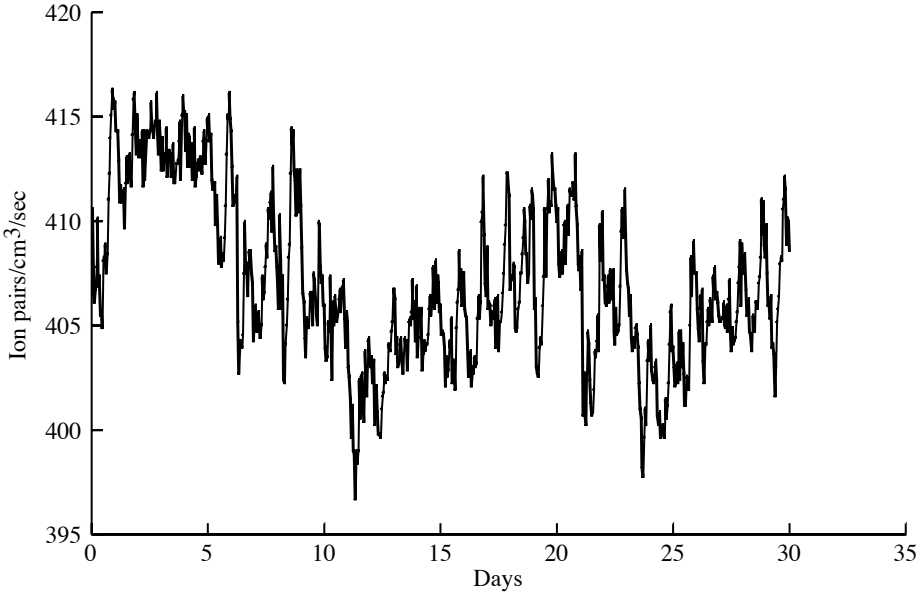

Figure 28. Ionization rate in the month of June, 1997, at 19.8 km near polar region. Atmospheric pressure is 55.2 mbar.

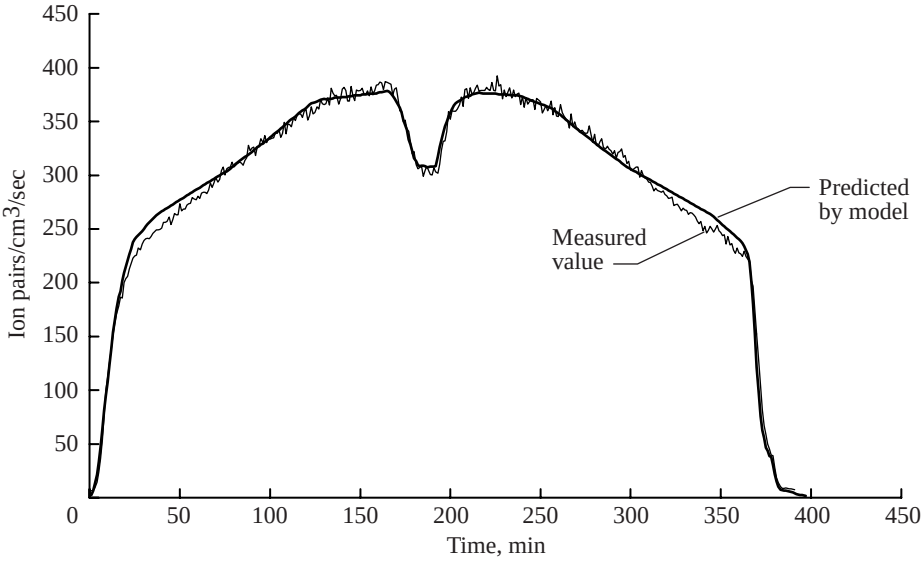

Figure 29. Predicted and measured (P. Goldhagen) values of air ionization rate as function of flight time for ER-2 flight on June 13, 1997. (See chapter 7).

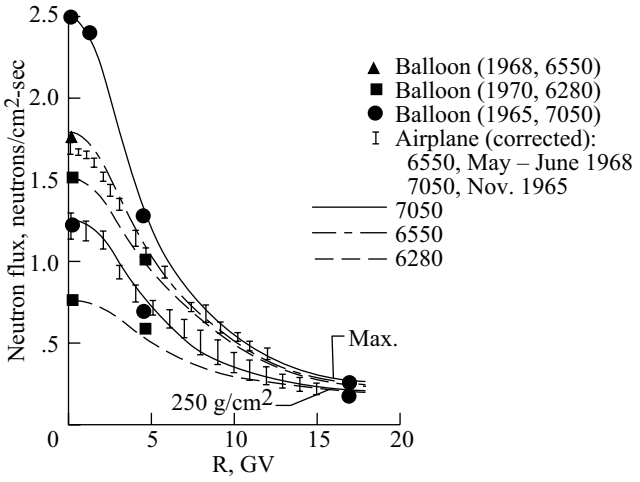

Figure 30. Fast neutron flux (in range from 1 to 10 MeV) at the transition maximum and 240-g/cm^2 depth as a function of vertical cutoff rigidity *R* for various times in the solar cycle and DRNM count rates.

H, mSv/1000 hr at 40 000 ft

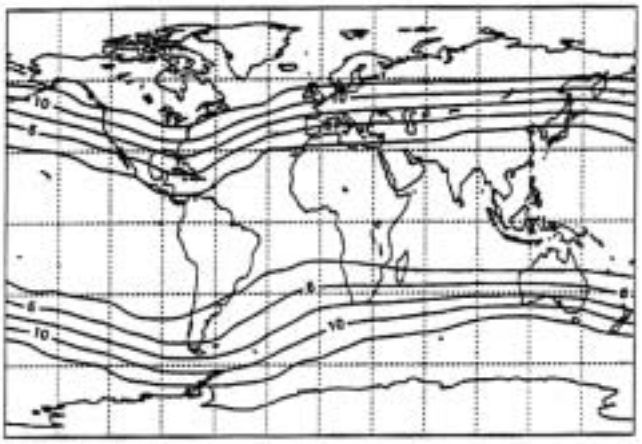

H, mSv/1000 hr at 50 000 ft

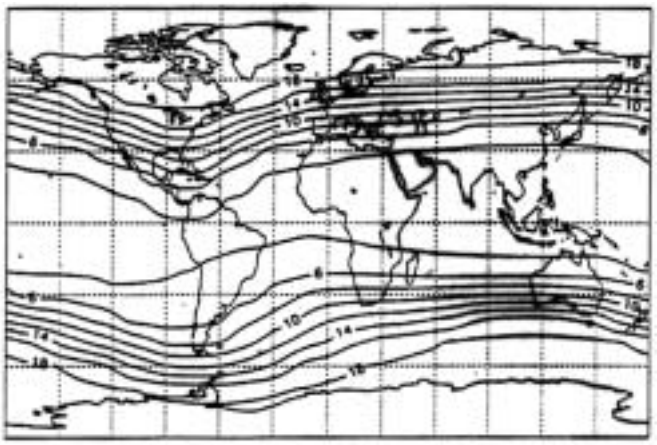

Figure 31. Background exposure levels in upper atmosphere at solar minimum (1965).

H, mSv/1000 hr at 65 000 ft

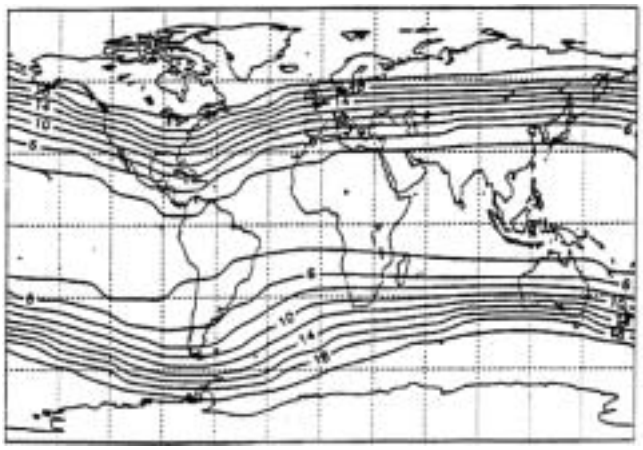

H, mSv/1000 hr at 73 000 ft

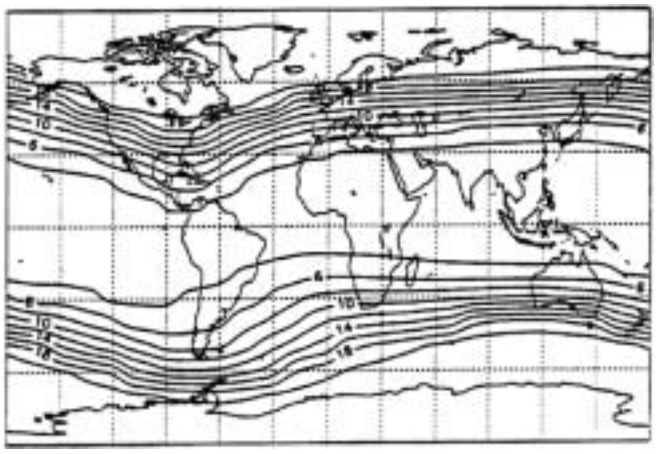

Figure 31. Concluded.

$(H_{sol})_{min}/(H_{sol})_{max}$ at 40 000 ft

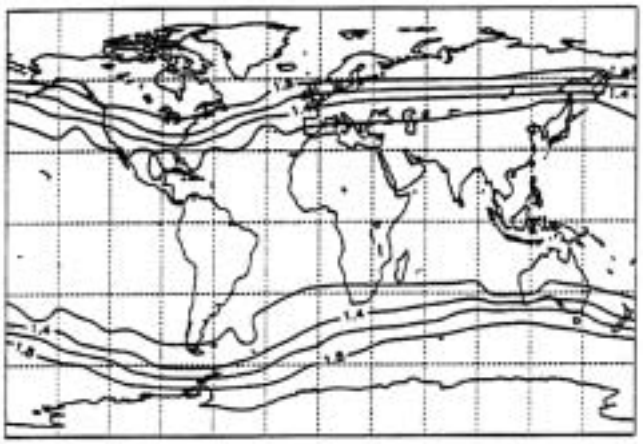

$(H_{sol})_{min}/(H_{sol})_{max}$ at 50 000 ft

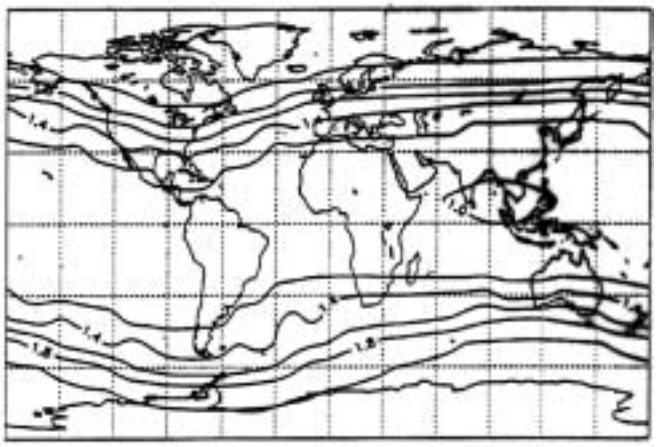

Figure 32. Maximum solar modulation ratio in atmospheric radiation levels.

$(H_{sol})_{min}/(H_{sol})_{max}$ at 65 000 ft

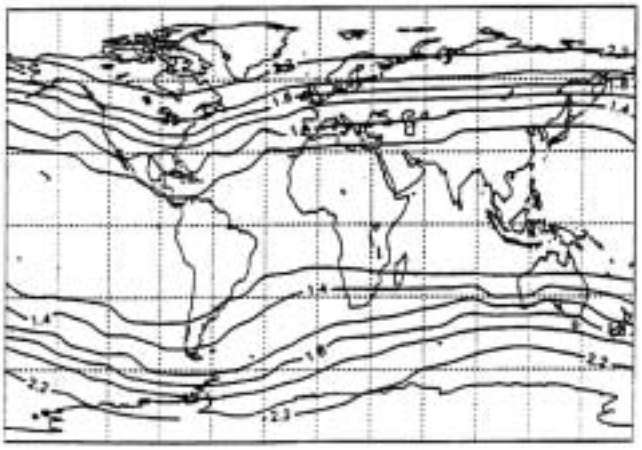

$(H_{sol})_{min}/(H_{sol})_{max}$ at 73 000 ft

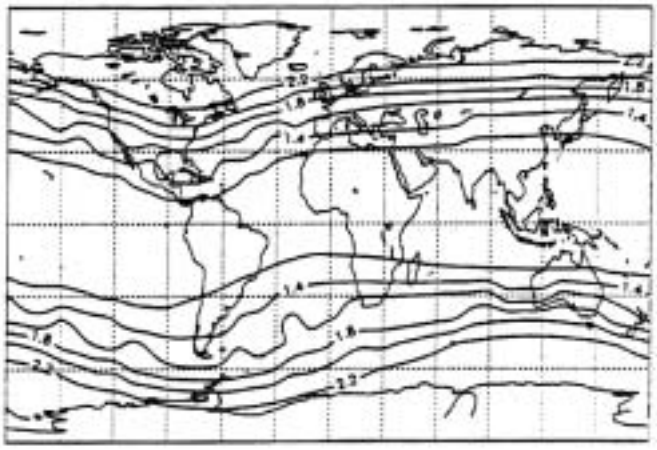

Figure 32. Concluded.

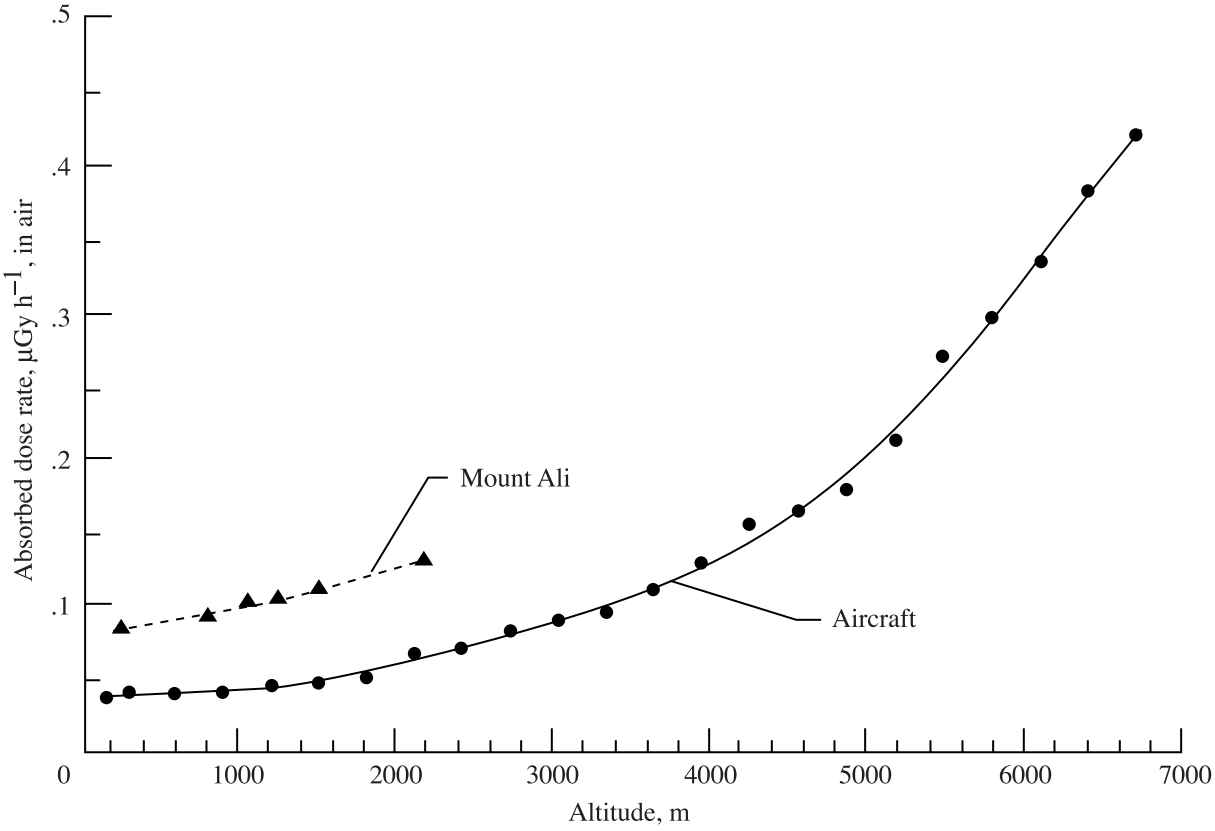

Figure 33. Measured absorbed dose rates on Mt Ali and in aircraft (Weng and Chen 1987).

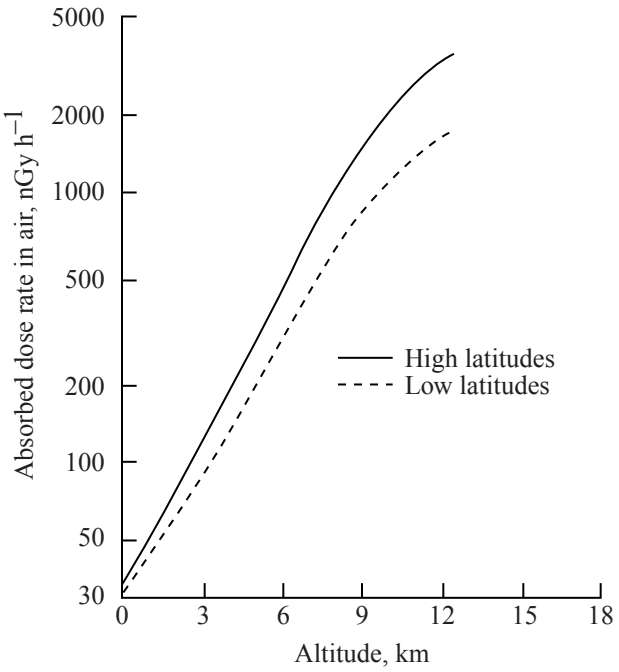

Figure 34. Absorbed dose rates in air as a function of altitude and geomagnetic latitude. (Hewitt et al. 1980)

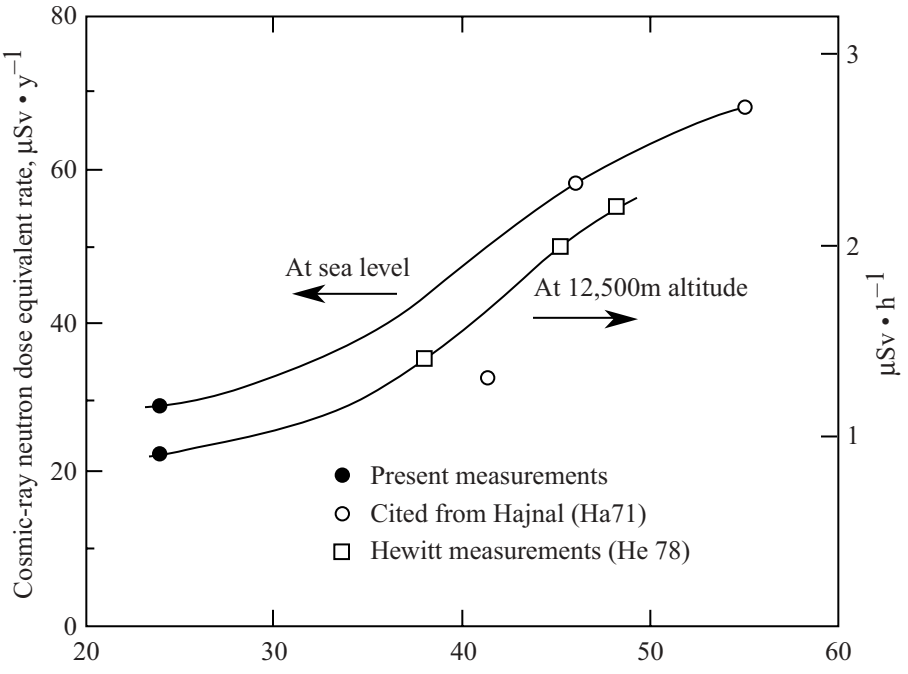

Figure 35. Measured neutron dose equivalent rate at various geomagnetic latitudes in the Northern Hemisphere. (Nakamura et al. 1987).

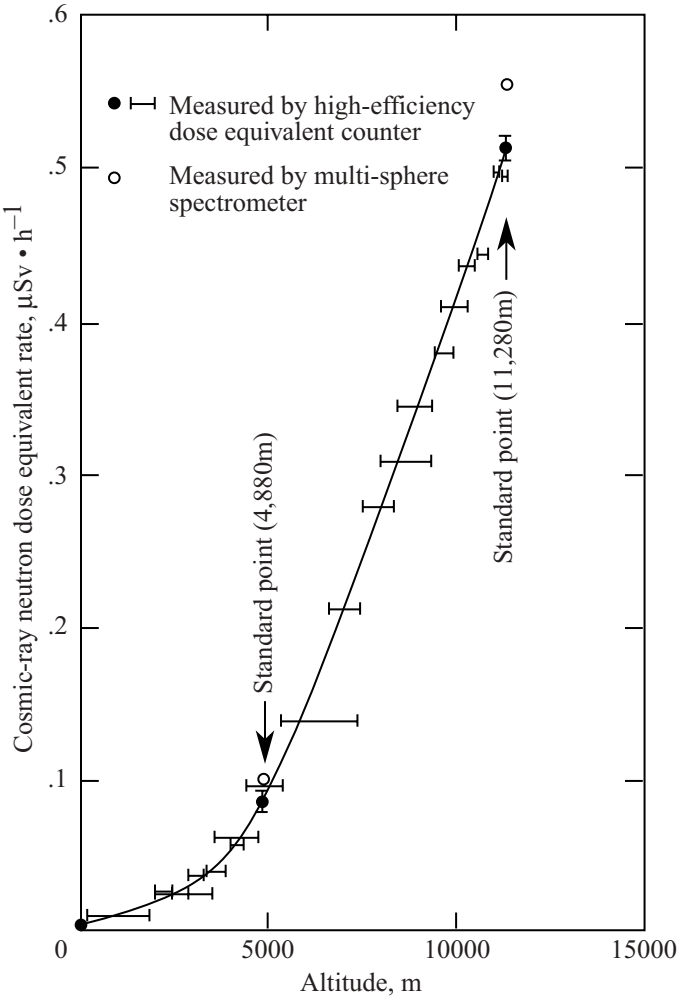

Figure 36. Altitude variation of neutron dose equivalent rates measure by the high-efficiency neutron dose equivalent counter. (Nakamura et al. 1987)

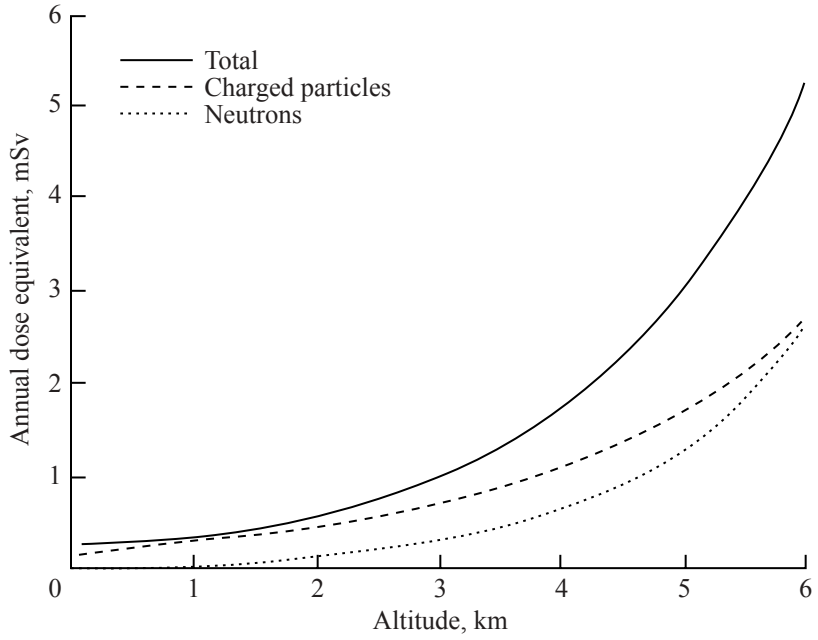

Figure 37. Variation of the annual effective dose equivalent from the Ionizing component and the neutron component of cosmic radiation as a function of altitude. (Bouville and Lowder 1988)

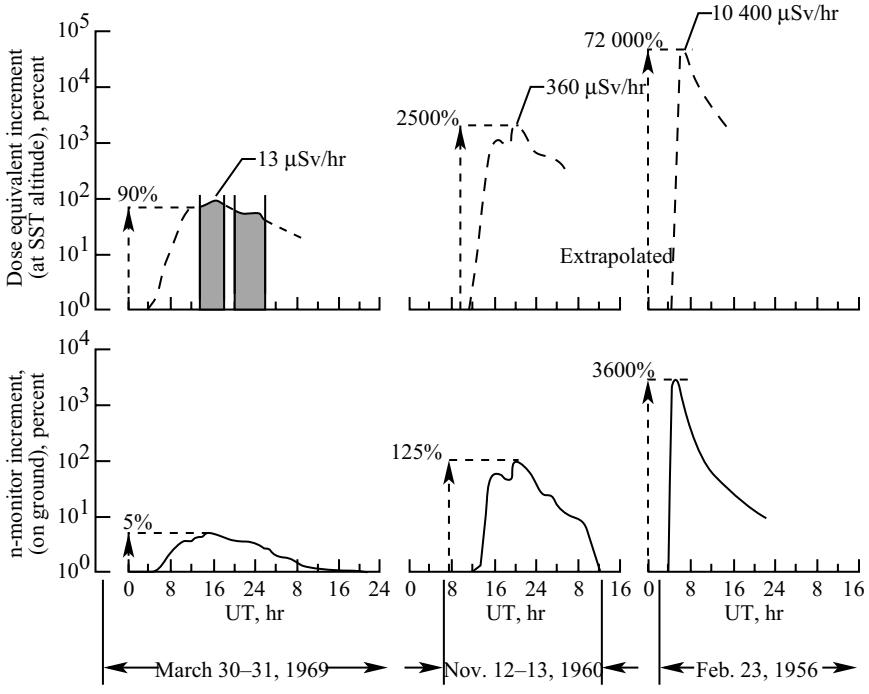

Figure 38. Energetic solar events measured on the ground and at SST altitude (Foelsche et al. 1974).

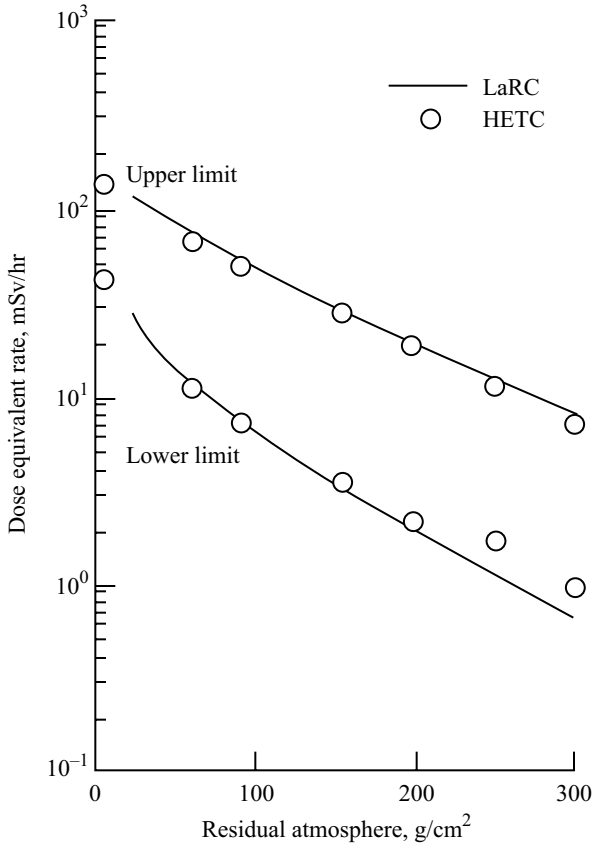

Figure 39. Calculated upper and lower limits for dose equivalent rate at high latitude for the Feb. 23, 1956 event (Foelsche et al. 1974).

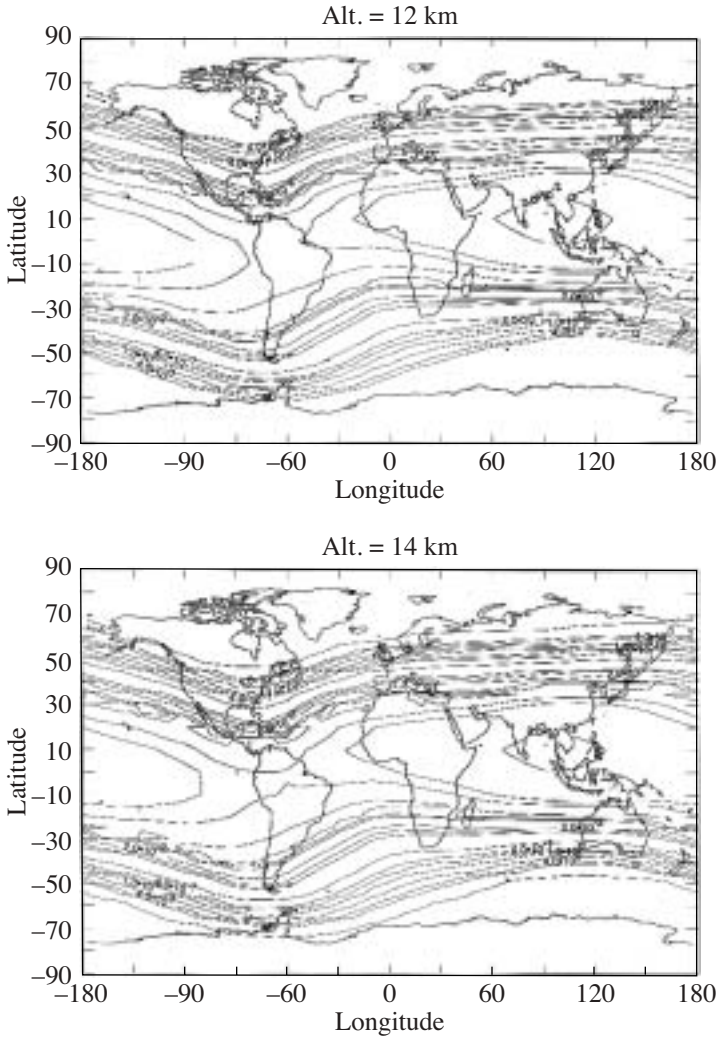

Figure 40. Global distribution of dose equivalent rate (mSv/h) at 0420 UT on Feb. 23, 1956 at various altitudes.

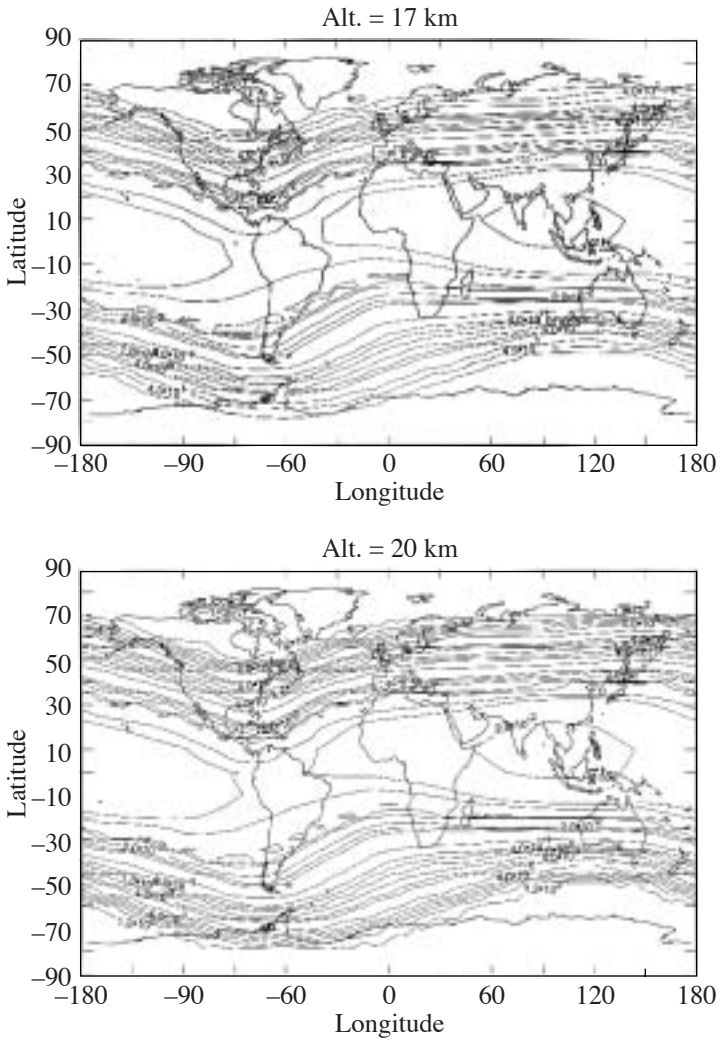

Figure 40 Concluded.

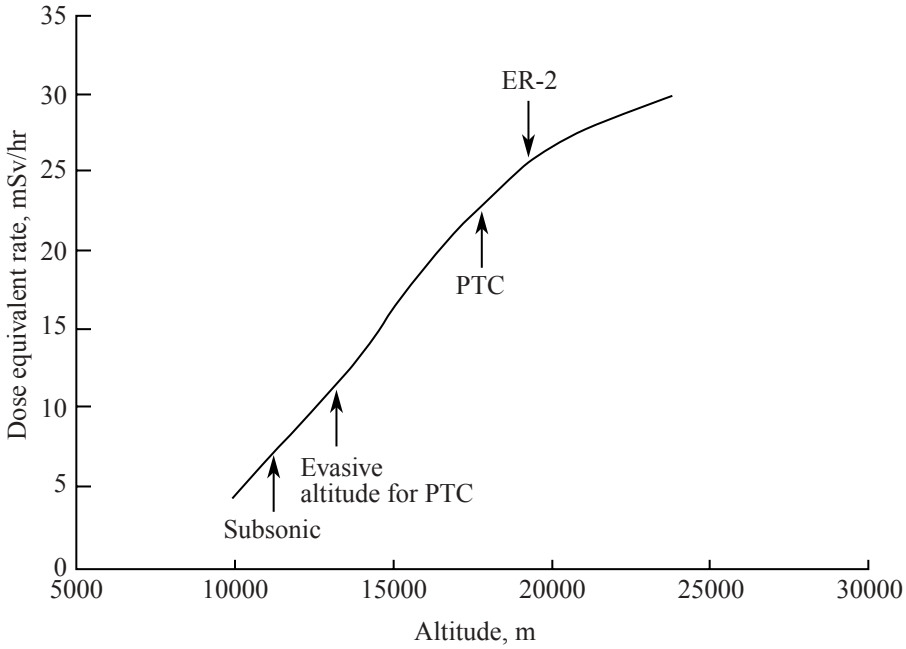

Figure 41. Dose equivalent rate at 55N 30W on Feb. 23, 1956 at 0410 UT.

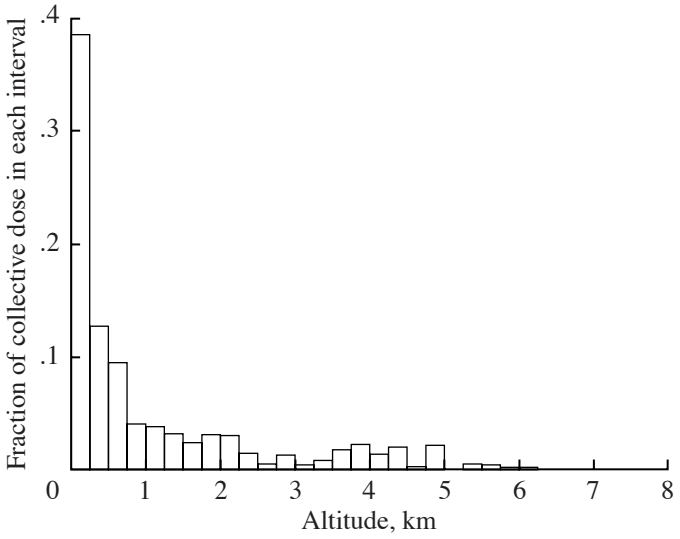

Figure 42. Distribution of the collective effective dose equivalent form cosmic radiation as a function of altitude (Bouville and Lowder 1988).

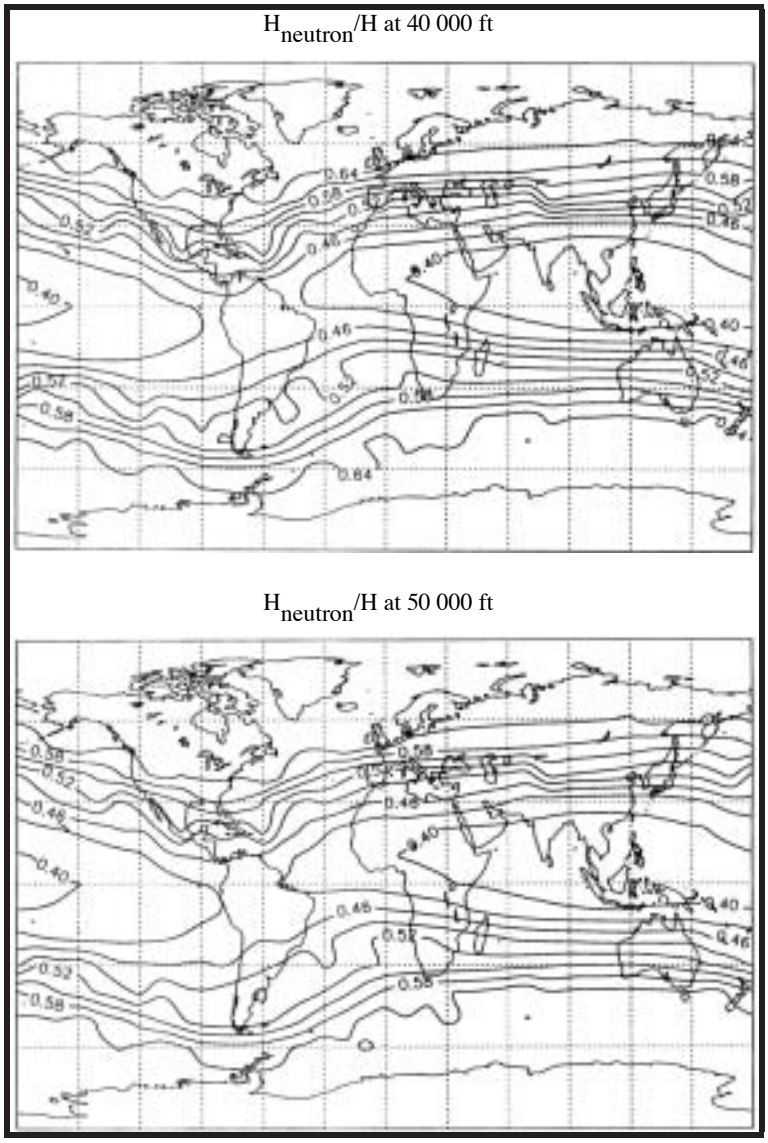

Figure 43. Fraction of dose equivalent due to neutrons at solar minimum (1965).

$H_{neutron}/H$ at 65 000 ft

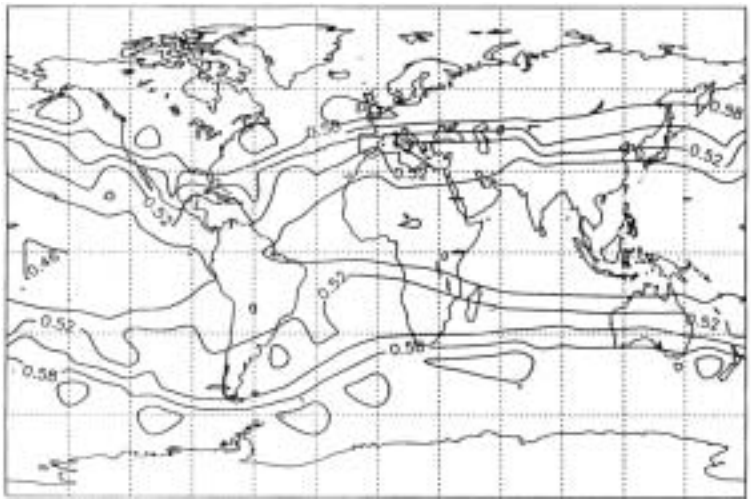

$H_{neutron}/H$ at 73 000 ft

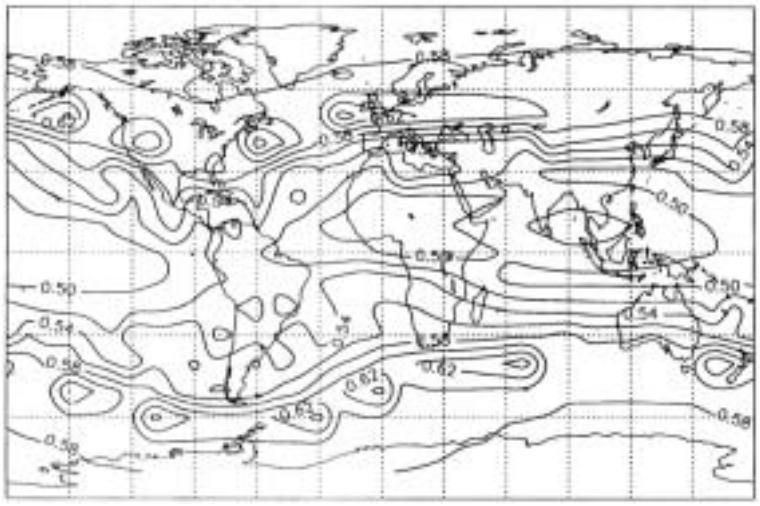

Figure 43. continued

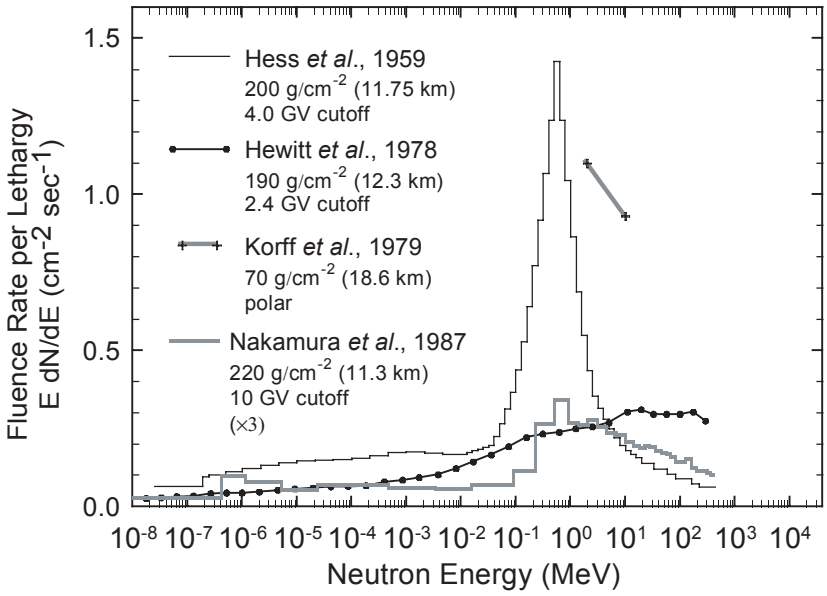

Figure 44. Cosmic-ray neutron spectra measured at jet airplane altitudes before 1997.

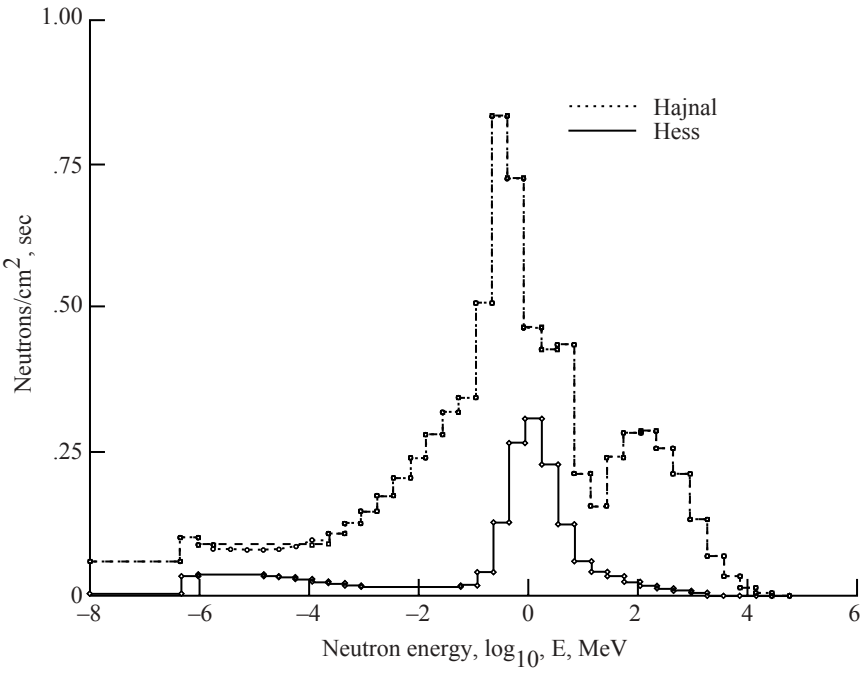

Figure 45. Hajnal unfolded neutron spectrum from Hewitt data measured at 17.46°N at 23.5 km compared to Hess spectrum.

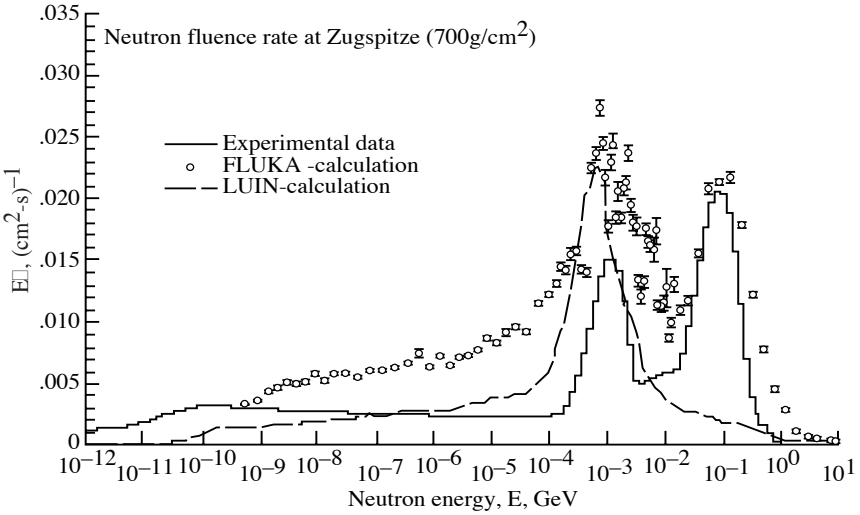

Figure 46. Spectral neutron fluence rate obtained by measurements and calculations on top of Zugspitze (by permission of Schraube et al. 1998).

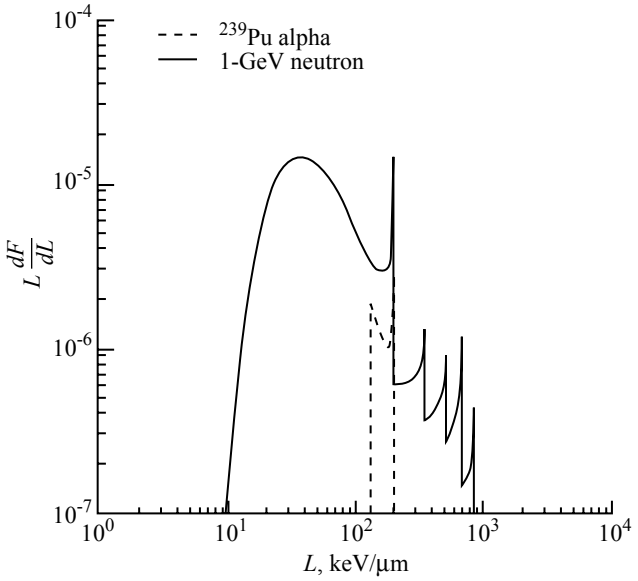

Figure 47. LET distribution porduced by 1-GeV neutron in tissue along with 239-Pu alpha decay spectrum.

Chapter 3: AIR Instrument Array

I. W. Jones*, J. W. Wilson*, D. L. Maiden*, P. Goldhagen, J. L. Shinn***
*NASA Langley Research Center
**DOE Environmental Measurements Laboratory

AIR Instrument Array

Preface

The large number of radiation types composing the atmospheric radiation requires a complicated combination of instrument types to fully characterize the environment. A completely satisfactory combination has not as yet been flown and would require a large capital outlay to develop. In that the funds of the current project were limited to essential integration costs, an international collaboration was formed with partners from six countries and fourteen different institutions with their own financial support for their participation. Instruments were chosen to cover sensitivity to all radiation types with enough differential sensitivity to separate individual components. Some instruments were chosen as important to specify the physical field component and other instruments were chosen on the basis that they could be useful in dosimetric evaluation. In the present paper we will discuss the final experimental flight package for the ER-2 flight campaign.

Instruments Provided

The environment consists of various energies of photons, electrons, muons, light ions, high-energy heavy ions, target nuclear fragments, and neutrons. The main emphasis of this study was on the nature of the neutron spectrum especially above 10 MeV. Several instruments were considered but only the DOE Environmental Measurements Laboratories multisphere (Bonner sphere) neutron spectrometer with its 3-He proportional counters had sufficient dynamic range, had sufficient sensitivity to minimize spectral statistical uncertainty, and could operate in the ER-2 environment. In addition, a high pressure ion chamber, scintillation counters with varying sensitivity to ions, muons and electrons, gamma rays, and total high-energy neutron flux, bubble detectors, charged particle telescopes, plastic nuclear track detectors, thermoluminescence detectors (TLD), and tissue equivalent proportional counters made up the experimental instrumentation. No single instrument gave an exclusive measurement of any individual component and requires some correction from the components emphasized by the other instruments. Some of the instruments were chosen for their good resolution of the physical fields while others were chosen as candidate dosimetric methods.

The instruments of the AIR flight are listed in table 1. The DLR/Kiel particle telescope is limited in charged particle information and cannot clearly separate the electrons and muons from other charged ions. The DLR/Kiel plastic track detector is used to identify and count multiple charged ions. The University of San Francisco particle track detectors will record LET spectra of nuclear star events. The NRPB nuclear etch track dosimeters will record nuclear recoil events. The Yale/University of Pisa Bubble counter will record the rate of high LET events. The DREO TLD's will record the total ionization during the flight. The JSC particle telescope will allow identification of charge particle type. The RMC Bubble detector will record the total high LET events on each flight. The DREO and the Boeing tissue equivalent proportional counters (TEPCs) will record the lineal energy spectra allowing an evaluation of dose and estimation of dose equivalent rate during the flight. The PVAMU

Single Event Upset experiment will record the events seen in a digital memory device. The Boeing PDM-303 is a solid-state neutron dosimeter device carried by the pilot. The DOE multisphere neutron spectrometer is the primary instrument on the ER-2 flights. The ion chamber and scintillation counters will allow information of specific charged components to be collected to make corrections to the neutron spectrum. The instrumentation and their particle detection characteristics are given in Table 2. A plus sign in the table indicates the primary sensitivity of the specific instrument that was targeted by the measurement and the minus sign indicates a lessor-confounding factor of the primary measurement.

Description of the Flight Package

The ER-2 has four pressurized and heated payload areas available: 1) The nose, where instruments are mounted to a removable rack that slides into the aircraft nose section. The nose area can support a payload weight of 650 lbs (294 kg) maximum, with a volume of 47.8 cubic feet (1.35 cubic meters) maximum. 2) The equipment bay, or Q-bay as it is called, where instruments are also mounted to racks that are attached to the aircraft structure. The maximum weight capacity of the Q-bay is 1300 lbs (590 kg) minus the nose payload weight. The volume available in the Q-bay is 64.6 cubic feet (1.83 cubic meters). 3) The left superpod has a removable nose section and a midbody section under the wing. The payload weight capacity of a superpod is 650 lbs (294 kg), and the volume available is 86 cubic feet (2.43 cubic meters). 4) The right superpod is identical to the left superpod. Each payload area is pressurized to an altitude equivalent to about 30,000 ft (9.1 km) when the aircraft is at 65,000 ft (19.8 km). The actual payload area internal pressure is 3.88 psi greater than the external pressure when the aircraft is above 18,300 ft (5.6 km). The temperature in each payload area during flight depends on the instrument heat generated in that area, and may be supplemented by aircraft heater/fan units. The instruments had to be packaged within these confines and the associated environmental factors resolved.

Placement of the *AIR* instrument components in the ER-2 was determined primarily by the requirement to separate the EML detectors as much as possible, to place the largest Bonner sphere detectors in a payload area away from the smallest Bonner sphere detectors, and to not place detectors under the ER-2 wing where fuel is carried. Lockheed (ER-2) Engineering also required that any detector containing flammable materials be placed inside a sealed container. This requirement applied to all of the EML detectors. In addition, the RMC Bubble Detector instrument, the University of Pisa Bubble Counter instrument, and the JSC Particle Telescope were placed inside sealed containers because they were designed to operate at sealevel pressure. The use of sealed containers greatly increased the complexity of the instrument array design. In addition, the EML detector signals had to be carried by the existing aircraft wiring from the other payload areas to the right superpod midbody section, where the control and data storage electronic modules were located. The final component locations in the ER-2 for all of the *AIR* detectors are shown in Figure 1. The *AIR* array filled nearly all of the available payload areas. Only the left superpod midbody section under the wing was left empty. The total weight of the *AIR* package was about 1800 lbs (818 kg), well under the maximum ER-2 capacity of 2600 lbs (1180 kg).

Physically, the *AIR* flight hardware consists of five aircraft racks and three electronics modules. The racks are mounted in the ER-2 nose, the Q-bay, and the left and right superpod nose sections. The electronics modules are mounted in the left and right superpod midbody sections. The *AIR* nose rack is shown in Photograph 1, on a ground support stand. The *AIR* components are mounted to a standard aircraft nose rack. Six cylinders attached directly to the rack contain EML Bonner spheres #1, #2, #4, #6, #7, and #8. The Bonner spheres are arranged consecutively from the smallest to the largest, starting at the forward end (left in the photograph). These cylinders are sealed on the ground and maintain one atmosphere pressure inside during flight. At the aft end of the rack, the two large boxes mounted above the cylinders are a Power Supply and Distribution Unit and a Bonner sphere amplifier box. Aircraft ballast weights are attached to the forward end of the rack, ahead of the first Bonner sphere cylinder. The long box on the forward end of the rack, mounted above the cylinders, contains the NRPB dosimeters. It is sealed on the ground and maintains one atmosphere pressure inside during flight. Immediately aft of the NRPB dosimeter box are the cylindrical pressure vessel for the Yale/University of Pisa Bubble Counter, and the flat plate pressure vessel for the DLR/Kiel plastic nuclear track detectors (barely visible behind the Bubble Counter cylinder in the photograph). The smaller rectangular box aft of the Yale/University of Pisa Bubble Counter cylinder contains the DLR/Kiel DOSTEL telescope. Photograph 2 shows the nose rack installed into the ER-2 nose cone. The view is of the aft end of the nose cone looking forward. The Q-bay rack is shown in Photograph 3, on a ground support stand. The *AIR* components are mounted to a modified aircraft Q-bay rack. At the forward end of the rack (left in the photograph) are the cylindrical JSC Particle telescope pressure vessel and a Bonner sphere amplifier box. Just aft of the JSC Particle Telescope is the EML Ion Chamber sealed cylinder. The tall cylinder in the middle of the rack is the sealed container for an EML scintillation counter. The cylinder visible at the aft end of the rack is another sealed container for EML scintillation counters. The EML Bonner Sphere sealed cylinders for detectors #9 and #10 are located on the far side of the rack in this view, as is the RMC Bubble Detector sealed cylinder. The Power Supply and Distribution Unit for the rack is located under the JSC Particle Telescope. Photograph 4 shows a view of the Q-bay rack installed in the ER-2. The row of cylinders visible in the foreground are the sealed containers for EML Bonner Sphere #9 (far right), the RMC Bubble Detectors (center), and EML Bonner Sphere #10 (far left). The rack holding TEPC units from DREO and from Boeing is visible on the far left, attached to the aft bulkhead of the ER-2 Q-bay. Photograph 5 shows a view of the Q-bay rack from under the ER-2 Q-bay (forward is to the right). The cylinders visible are for the EML Bonner Spheres, the EML Ion Chamber, and the EML scintillation counters. The two superpod nose racks are identical, and one is shown in Photograph 6, on a ground support stand. These racks each contain two sealed cylinders for the larger EML Bonner Spheres (#11, #12, #13, and #14). Photograph 7 shows the left superpod nose rack installation. The Power Supply and Distribution Unit and the amplifier box for each pod nose rack are mounted in the front of the superpod midbody section, just behind the nose racks. The EML computer components and the EML NIM bin assemblies are mounted in the midbody section of the right superpod. Photograph 8 shows a front view of the right midbody section, containing the nose rack Power Supply and Distribution Unit, the Bonner Sphere amplifier box, and components of the EML computer assembly. The EML NIM bin assemblies are shown in Photograph 9 being installed into the center section of the right superpod midbody. The forward end of the midbody section is to the left in this view.

Table 1. Atmospheric Ionizing Radiation *(AIR)* Measurements

Experiment	PI	Comments
1. DLR/Kiel University DOSTEL **[on nose rack]**	Dr. Guenter Reitz Dr. Rudolf Beaujean	Size: 140mm x 240mm x 10mm thick mounting plate. Unit is 150mm above mounting plate top. Wt.: not specified (<5 lbs) Power: ±12VDC, 30 ma each leg; +5VDC, 15 ma Connectors: LaRC supplies two 6-pin connectors to terminate power & data cables.
2. DLR/Kiel University Particle PNTD's **[on nose rack]**	Dr. Guenter Reitz Dr. Rudolf Beaujean	Size: 416mm x 260mm x 19mm high Wt.: <1 kg Power: none required
3. University of San Francisco Target Fragment PNTD's **[on nose rack]**	Dr. Eugene Benton	Size: 2.5" x 2.5" x 2.5" Wt.: 0.4 lbs Power: none required Requires pressurized container.
4. NRPB Etch Track Dosimeters **[on nose rack]**	Dr. David Bartlett	Size: CR39's are 4cm x 4cm x 0.5cm each. TLD's are 5cm x 6cm x 1cm each. Wt.: very light, each unit Power: none required Want to fly as many of each type as possible - prefer 50 each.
5. Yale/University of Pisa Bubble Counter **[on nose rack]**	Dr. Francesco d'Errico	Size: 17 cm diam. x 16 cm tall cylinder Wt.: 3 kg Power: 10 watts peak, 28VDC (ER-2 power) Connectors: LaRC supplies U. of Pisa with an 8-10 pin connector to terminate power cable.
6. DREO Al_2O_3 TLD's **[on Q-bay lower rack]**	Dr. Thomas Cousins	Size: few millimeters on a side for each TLD Wt.: <1 lb Power: none required Want to fly 6 TLD's. Mount near EML ion chamber.
7. JSC Particle Telescope **[on Q-bay lower rack]**	Dr. Gautam Badhwar	Size: 9.25" dia. x 21" high Wt.: 45 lbs Power: 28VDC, 45 watts (ER-2 power) Connector: PT07H-20-16P in base.
8. RMC Bubble Detectors **[on Q-bay lower rack]**	Dr. L.G.I. Bennett	Size: 8.5" dia. x 16.5" tall cylinder Wt.: 15 lbs Power: 20 watts, 115VAC, 400Hz (ER-2 power) Connector: MS3449H10C6P connector in base plate.

Experiment	PI	Comments
9. Boeing TEPC **[on Q-bay vertical rack]**	Dr. Alexander Chee	Size: 7.25" dia. x 20" long cylinder with 9" square top flange. Wt.: 22 lbs Power: 28VDC, max at startup 2 amps (ER-2 power) Connector: MS3449H10C6P connector in top flange.
10. DREO TEPC **[on Q-bay vertical rack]**	Dr. Thomas Cousins	Size: 7.25" dia. x 20" long cylinder with 9" square top flange. Wt.: 22 lbs Power: 28VDC, max at startup 2 amps (ER-2 power) Connector: MS3449H10C6P connector in top flange.
11. Single event upset **[on left superpod rack]**	Dr. Tom Fogarty	Size: 17" x 17" x 6" high Wt.: unspecified, approx. 15 lbs Power: 115VAC, 400Hz, 1 amp (ER-2 power) LaRC supply external box & connectors. PVAMU supply internal hardware.
12. Boeing PDM-303 **[carried in cockpit]**	Dr. Eugene Normand	Size: 5" x 0.38" x 1" Wt.: few oz. Power: none required
13. DOE Multisphere Neutron Spectrometer **[various locations]**	Dr. Paul Goldhagen	Size: various (14) spheres 1.3" to15" diameter Wt.: 1190 lbs Power: 500 watts
14. DOE Ionization Chamber **[on Q-bay rack]**	Dr. Paul Goldhagen	Size: 12" x 12" x 17" Wt.: 30 lbs Power:
15. DOE BGO/Plastic Scintillation Counters **[on Q-bay rack]**	Dr. Paul Goldhagen	Size: 20" x 10" x 29" Wt.: 30 lbs Power:
16. DOE NaI Scintillation Counter **[on Q-bay rack]**	Dr. Paul Goldhagen	Size: 20" x 10" x 29" Wt.: 30 lbs Power:

Table 2. AIR Instrument Array and Sensitivity to Environmental Components

Instrument	Photons	Leptons	Neutrons	Light ions	HZE ions	Target fragments
Bonner spheres			+	-	-	
Ion telescope		-		+	+	
Neutron telescope			+			
Ion chamber	+	+		+	+	+
TEPC	+	+	+	+	+	+
PNTD			+	-	+	+
BGO scintillator	-	-	+	-	-	-
NaI scintillator	+	+		+	+	-
Organic scintillator	-	+	-	+	+	-
Bubble detectors			+		-	-

+ indicates prime measurement, - indicates confounding factor

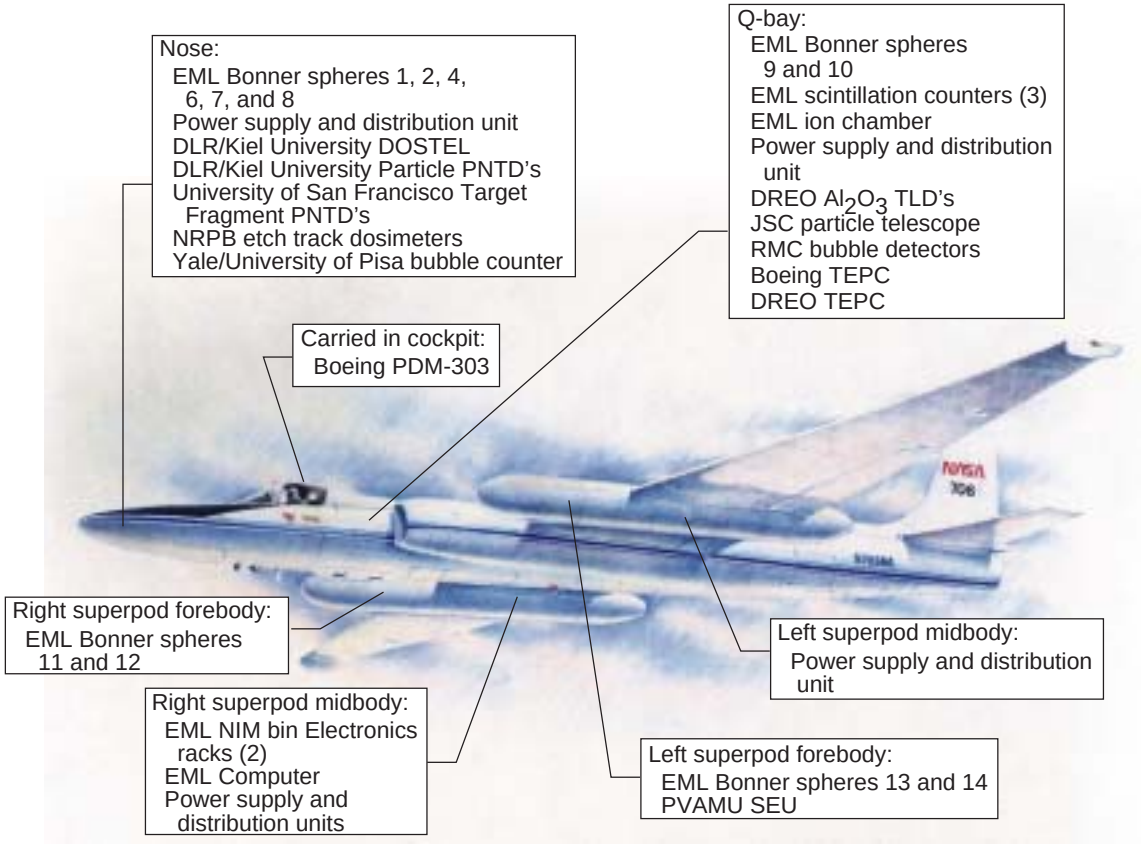

Figure 1. Instrument Locations on the ER-2

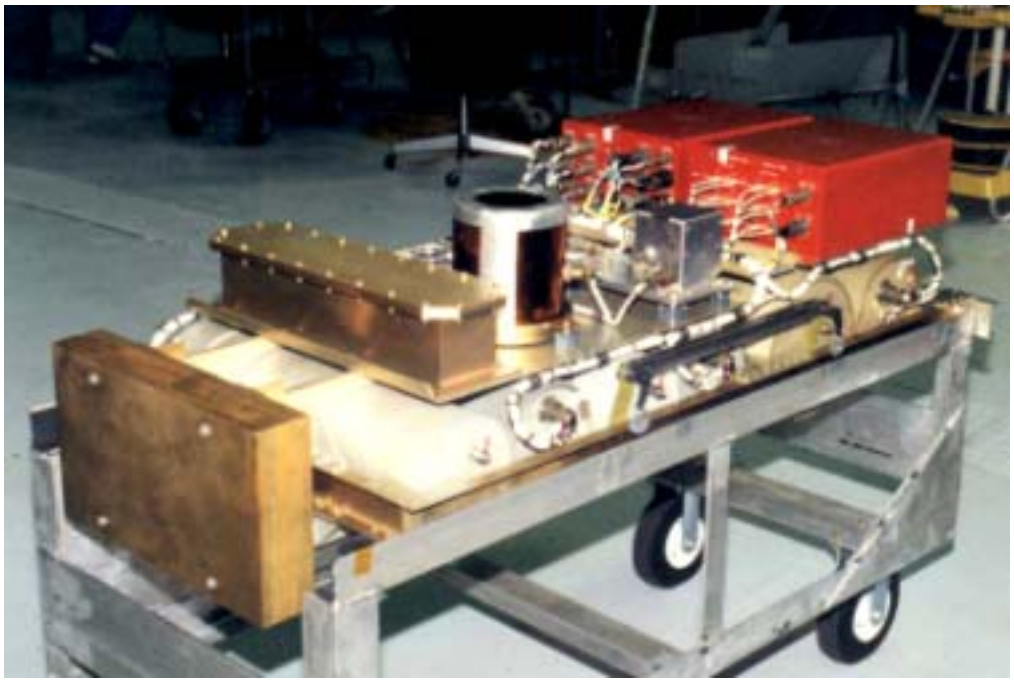

Photograph 1. Nose Rack on Ground Support Stand

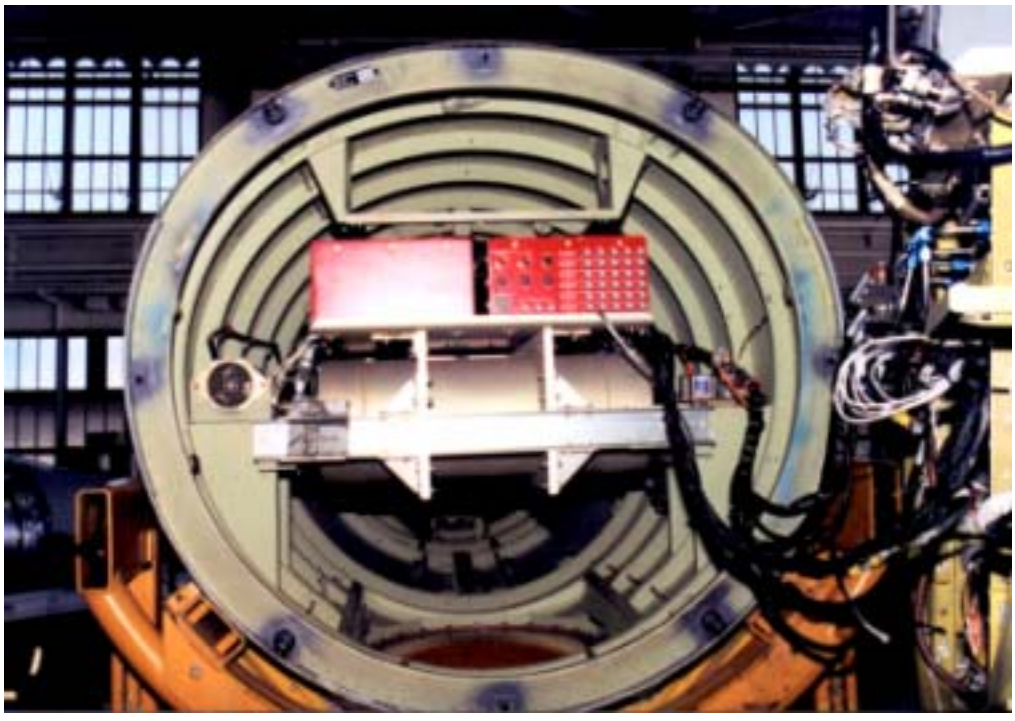

Photograph 2. Nose Rack Installed in the ER-2

Photograph 3. Q-Bay Rack on Ground Support Stand

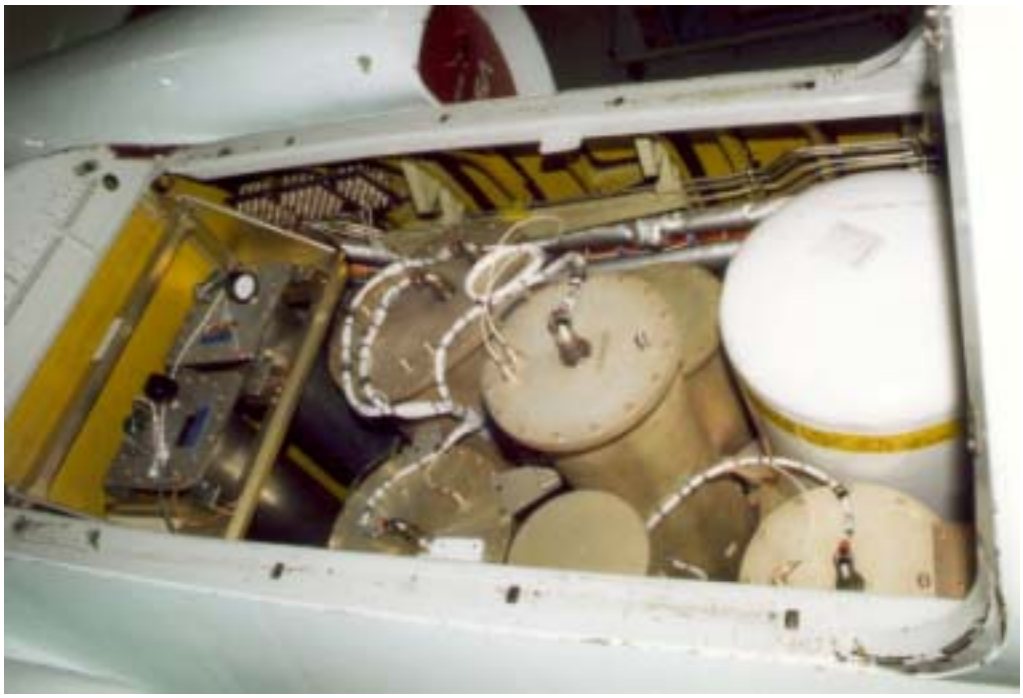

Photograph 4. Q-Bay Rack Installed in the ER-2 (Top View)

Photograph 5. Q-Bay Rack Installed in the ER-2 (Bottom View)

Photograph 6. Pod Rack on Ground Support Stand

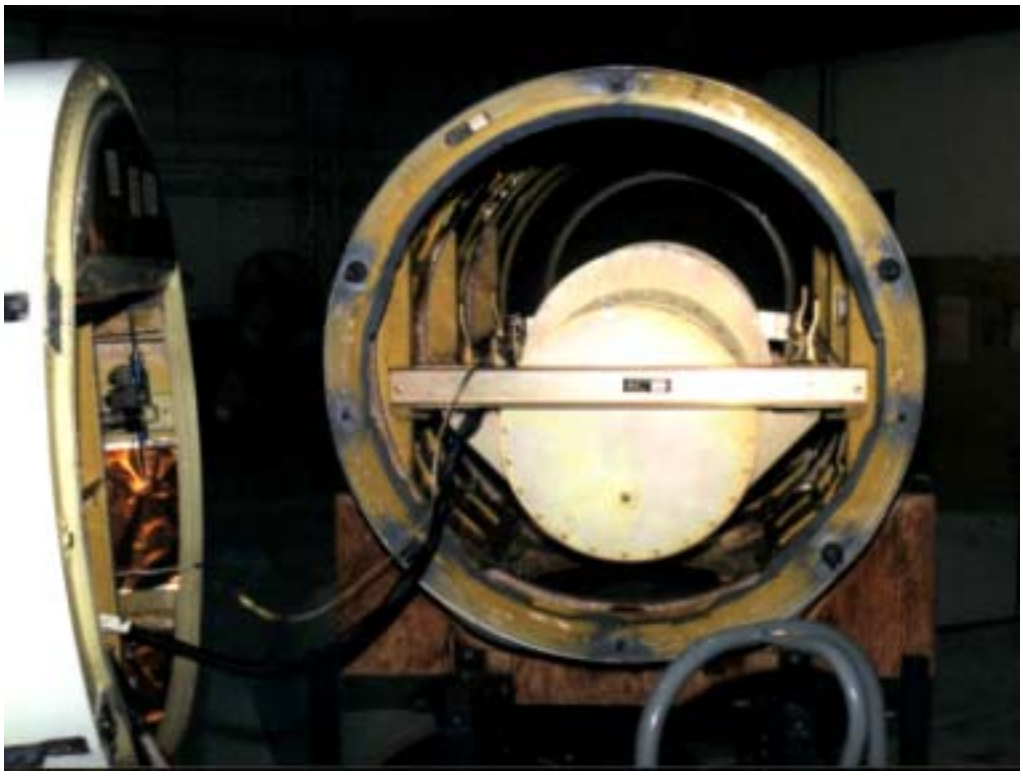

Photograph 7. Pod Rack Installed in the ER-2

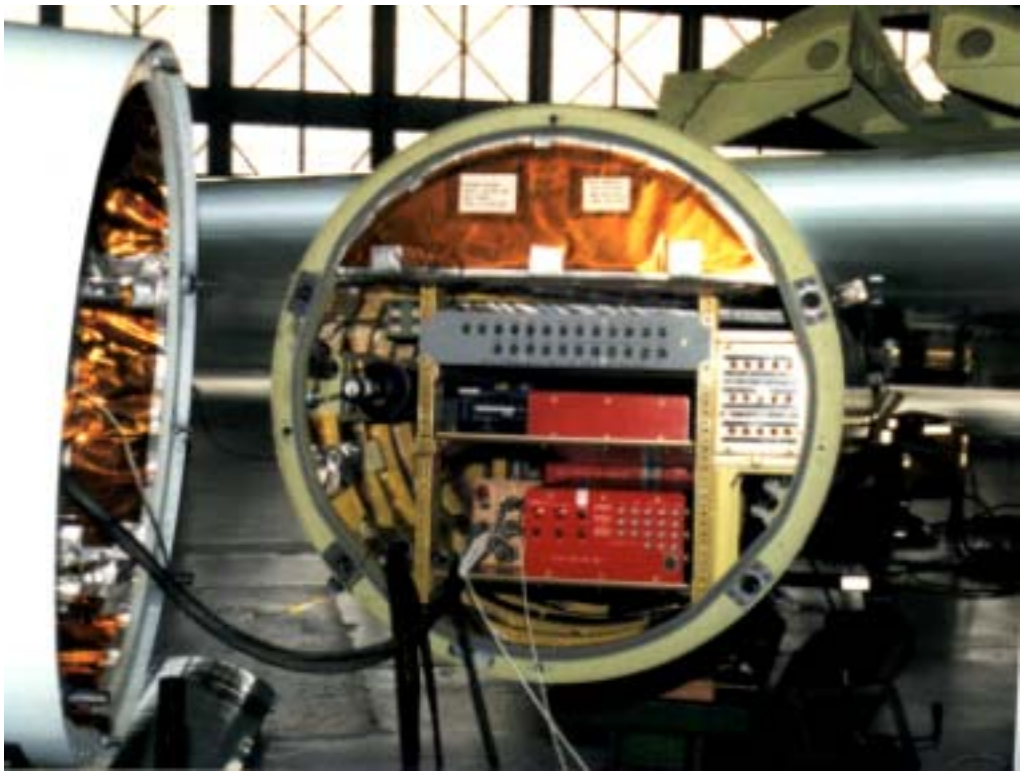

Photograph 8. Pod Rack Electronics Installed in the ER-2

Photograph 9. Right Pod Mid-Body Electronics Installed in the ER-2

Chapter 4: *AIR* Model Preflight Analysis

H. Tai, J. W. Wilson, D. L. Maiden
NASA Langley Research Center

AIR Model Preflight Analysis

Preface

Atmospheric ionizing radiation (*AIR*) produces chemically active radicals in biological tissues that alter the cell function or result in cell death. The *AIR* ER-2 flight measurements will enable scientists to study the radiation risk associated with the high-altitude operation of a commercial supersonic transport. The ER-2 radiation measurement flights will follow predetermined, carefully chosen courses to provide an appropriate database matrix that will enable the evaluation of predictive modeling techniques over a large dynamic range. Explicit scientific results such as dose rate, dose equivalent rate, magnetic cutoff, neutron flux, and air ionization rate associated with these flights are predicted by using the AIR model. Through these flight experiments, we will further increase our knowledge and understanding of the AIR environment and our ability to assess the risk from the associated hazard.

Introduction

The broad aim of the atmospheric ionizing radiation (*AIR*) ER-2 flight measurement campaign is to improve our understanding of the ionizing radiation environment, for example, composition, spectral distribution, and corresponding intensities in the upper troposphere and lower stratosphere where people flying future supersonic transports will spend the majority of their flight time. These radiation measurements will enable radiobiologists to improve our understanding of the health risks associated with this exposure to high-altitude flight. The impetus to examine the impact of ionizing radiation stems from (1) recent reductions in recommended radiation exposure limits by the International Commission on Radiological Protection (ICRP 1991) and the National Council on Radiation Protection and Measurements (NCRP 1993), and (2) recent experimental results showing that an uncertainty in aircraft radiation exposure exists. The NCRP examined the state of knowledge of atmospheric radiation in high-altitude flight and made recommendations on the need for improved information to develop a protection philosophy for high-altitude commercial operations. The High-Speed Research (HSR) Environmental Impact Radiation group developed the *AIR* project to reduce the uncertainties of radiation measurements applicable to the high-altitude flight program of the High-Speed Civil Transport (HSCT). Once these uncertainties are reduced, an adequate protection philosophy can be developed.

Langley Research Center (LaRC) performed atmospheric radiation studies under the Supersonic Transport (SST) development program in which important ionizing radiation components were measured and extended by calculation to develop the existing *AIR* model. In that program, the measured neutron energy spectrum was limited to an upper value of 10 MeV by the instrumentation of that era. Extension of the neutron spectrum to higher energies was made by using theoretical models. Subsequent evaluation of solar particle events showed that

high exposures will occur on important high-latitude routes, but acceptable levels of exposure can be obtained if a timely descent to subsonic altitudes is made. The principal concern was for pregnant occupants onboard the aircraft (Foelsche et al. 1974). As a result of these studies, the Federal Aviation Administration (FAA) Advisory Committee on the Radiobiological Aspects of the SST recommended (FAA 1975) the following:

1. Crewmembers will have to be informed of their exposure levels.

2. Maximum exposures on any flight should be limited to 5 mSv.

3. Airborne radiation detection devices for total exposure and exposure rates will be provided.

4. A satellite monitoring system should provide SST aircraft real-time information on atmospheric radiation levels for exposure mitigation.

5. A solar forecasting system will warn flight operations of an impending solar event for flight scheduling and alert status.

These recommendations are a reasonable starting point for requirements of the HSCT with some modification reflecting new standards of protection as a result of changing risk coefficients.

One result of the SST studies was the realization that subsonic aircrews are among the most highly exposed occupational groups (Foelsche et al. 1974, Schaefer 1968). This study prompted the FAA to develop the CARI (Civil Aeronautical Research Institute) exposure estimation code based on the LUIN transport code (developed by the Department of Energy (DOE) Environmental Measurements Laboratory) to further study these air crews (O'Brien and Friedberg 1994). The estimated risk of serious illness to the child of an air crew member during pregnancy is on the order of 1.3 per thousand in excess of the general population risk rate of 1.15 per thousand (Friedberg et al. 1992), including all types of cancer and mental retardation among children. Hence, the FAA recommended that air carriers begin to train their employees on the risks of in-flight subsonic exposure (White 1994). The dose rates at the HSCT altitudes are a factor of 2 to 3 higher than for subsonic operations, and the HSCT crew's annual flight hours will have to be reduced by this same factor to maintain exposure levels comparable to those of the subsonic crews. One may assume that similar instruction for aircrews will be required for HSCT operations and that restriction on crew usage of the HSCT will, by necessity, be different from those on subsonic transports.

Regulations for exposure limits are based primarily on the estimated cancer risk coefficients. These coefficients have increased significantly over the last decade because solid tumor appearance is higher among the World War II nuclear weapons survivors than was initially anticipated (ICRP 1977, BEIR 1990, UNSCEAR 1988, ICRP 1991). As a result, new recommendations for reducing regulatory limits have been made by national and international advisory bodies (ICRP 1991, NCRP 1993). Whereas subsonic crew exposures are well under the current regulatory limits, the substantial reductions (by factors of 2.5 to 5) in the recommended limits will result in the need to improve aircrew exposure estimates (Reitz et al 1993, Fiorino 1996). Hence, a workshop on

Radiation Exposure of Civil Air Crews held in Luxembourg on June 25 to 27, 1991 was sponsored by the Commission of the European Communities Directorate General XI for Environmental Nuclear Safety and Civil Protection (Reitz et al. 1993). The workshop noted the closure of the gap between subsonic aircrew exposures and the newly recommended regulatory limits and, in fact, was concerned that limits may be exceeded in some cases. Therefore, uncertainty in exposure estimates becomes a critical issue, and emphases on the number and spectral content of high-energy neutrons, as well as the penetrating multiple charged ions, were identified as a critical issue for subsonic flight crews. The issues for HSCT commercial air travel are compounded by the higher operating altitudes (higher exposure levels) and the possibility of exposures to a large solar event, wherein annual exposure limits could be greatly exceeded on a single flight (Foelsche et al. 1974, Wilson et al. 1995). Because of the higher expected exposures in high-altitude flight, the congressionally chartered Federal Advisory Agency on Radiation Protection (NCRP) examined the data on atmospheric radiation and made recommendations (NCRP 1995) on the need for future studies as follows:

1. Make additional measurements of atmospheric ionizing radiation components with special emphasis on high-energy neutrons.

2. Conduct a survey of proton and neutron biological data on stochastic effects and developmental injury for evaluation of appropriate risk factors.

3. Develop methods to avoid solar energetic particles, especially for flight above 60 000 ft.

4. Develop an appropriate radiation protection philosophy and radiation protection guidelines for commercial flight transportation, especially at high altitudes of 50 000 to 80 000 ft.

Clearly, these issues must be addressed before the HSCT goes into commercial operation to ensure the safety of the crew and passengers. In direct response to the NCRP recommendations, development of an experimental flight package to reduce the uncertainty in *AIR* models is being readied. The focused goal of this project is to develop an improved *AIR* model with uncertainties in the atmospheric radiation components of 20 percent or less to allow improved estimation of the associated health risks to passengers and crew. Special emphasis will be given to the high-energy (10 to 1000 MeV) neutrons in the altitude range of 50 000 to 70 000 ft.

The results will be expressed in terms of an environmental *AIR* model able to represent the ambient radiation components, including important spectral components with angular distributions, which will allow evaluation of aircraft shielding properties and the geometry of the human body. The model also must be capable of representing the atmospheric radiation levels globally, as a function of solar modulation and of evaluating radiation levels during solar particle event increases. Following the development of the *AIR* model, impact studies on radiation exposure limits for crew usage and passengers (especially frequent flyers) will be performed to assess the need of developing a specific philosophy to control exposures in HSCT operations. Using data from available satellite systems, new real-time software, based on the new *AIR* model, will allow risk mitigation and flight planning in the case of a large solar event.

These studies will result in requirements for studying the economic impact on operations costs. For example, it has been suggested that the HSCT crew be used at one-third to one-half the number of block hours now used by subsonic aircraft to minimize exposure. This reduction in hours will require more crews at increased cost. The other possibility is to rotate crews through less exposed routes for a portion of each year, especially during a declared pregnancy among the crew. The need for and the extent of such exposure control measures must await the improvement of the *AIR* model.

ER-2 Measurement and Instrumentation

An instrument package is being developed in accordance with the NCRP recommendations through an international guest investigator collaborative project to acquire the use of existing instruments to measure the many elements of the radiation spectra. Instrument selection criteria were established which include the following: (1) instruments must fit into the cargo bay areas of the ER-2 airplane and be able to function in that environment (some high-quality laboratory instruments were rejected because of their large size or inability to operate in the ER-2 environment), (2) instruments must be free for the project to meet budget constraints, (3) instruments must have a principal investigator with his or her own resources to conduct data analysis, and (4) the instrument array must include all significant radiation components for which the NCRP made minimal requirements. The flight package must be operational, and the first flight must occur before or near the maximum in the galactic cosmic ray intensity (circa spring-summer 1997) and extend through the next cosmic ray minimum (circa June 2000).

The flight package developed used all available space in the ER-2 cargo areas. The instrument layout is shown in figure 1. The primary instruments in the package consisted of neutron spectrometer detectors, scintillation counters, an ion chamber from the Environmental Measurements Laboratory (EML) of the Department of Energy, and charged-particle telescopes from the Institute of Aerospace Medicine of Deutsche Forschungsanstalt fur Luft- und Raumfahrt (DLR), and Johnson Space Flight Center. Ten other instruments from Germany, Italy, the United Kingdom (UK), and Canada made up most of the remainder of the flight package. These included passive track detectors from the Institute of Aerospace Medicine, DLR, and the University of San Francisco; tissue equivalent proportional counters (TEPC's) from Boeing and the Defence Research Establishment in Ontario, Canada; and dosimeters from Boeing, the Royal Military Academy in Ontario, Canada, and the National Radiological Protection Board (NRPB) in the UK. The existing primary instruments and the data systems were modified for operation on the ER-2. A data acquisition system was incorporated to control operation of the entire instrument package, and to record data from the primary instruments during flight. Data from the other instruments were recorded separately by each instrument and were recovered after a flight. The first flights were in June 1997 near solar minimum and need to be continued through solar maximum, which is expected on June 2000 ± 13 months.

AIR Model Development

The basic quantities of the present *AIR* model are the air ionization rate, the 1 to 10 MeV neutron flux, and the rate of nuclear star events in nuclear emulsion. These quantities were measured over a complete set of altitudes, geomagnetic latitudes, and over the solar cycle and were scaled according to known procedures to allow a total time-dependent mapping of the global radiation field (Wilson et al. 1991). The limitations of the model concern the high-energy neutron spectrum, the quality factor of the ionic components, and the relative contribution of the nuclear stars. The first step in improved model development is to add estimates of the proton and light ion flux by using available transport models and databases. An international agreement with the Japan Atomic Energy Research Institute is being negotiated to provide computational support for adding improved results for the radiation-induced fields from the galactic cosmic ray protons. These results will be augmented by the light and heavier galactic cosmic ion components by using the LaRC cosmic ray transport codes. Global fields, as a function of time, will be generated by using the worldwide vertical cutoff database and high-latitude neutron monitor count rates. Model validation will require a definition of the mapping of the model field quantities to the ER-2 instruments. Although all investigators are responsible for defining their own instrument response functions, the LaRC team will assist in these definitions to every extent possible within funding and manpower limitations. The first model developed for atmospheric ionizing radiation was empirically based on the global measurements program under the LaRC SST study (ref. 1). The instrumentation consisted of tissue equivalent ion chambers, fast neutron spectrometers, and nuclear emulsion. Limited flights were made with tissue equivalent proportional counters (TEPC's), Bonner spheres, and the Concorde prototype radiation-monitoring instrument. The flights were made over most of solar cycle 20 with altitude surveys, latitude surveys, and measurements during the solar flare of March 1969. Unfortunately, the program was terminated in the year prior to the largest recorded solar event that was observed during solar cycle 20, the 4 August 1972 event. The data set was augmented by the decades of measurements of air ionization rates using argon filled steel-walled ion chambers. The high-energy neutrons were estimated by using Monte Carlo calculations as an extension of the measured 1 to 10 MeV flux from the fast neutron spectrometers. These theoretical high-energy neutron flux calculations indicate that over half the neutron dose is from neutrons of energy above 10 MeV and are quite uncertain in their spectral content and intensity, as was noted in the LaRC study (Foelsche et al. 1974), concluded by the Luxembourg workshop (Reitz et al. 1993) and by the NCRP (1995). The solar particle event predictions are based on Monte Carlo calculations using the Bertini nuclear model and the United Kingdom nuclear data files (Foelsche et al. 1974).

The *AIR* model development should continue to parallel that of the flight program and should use state-of-the-art transport codes and databases to generate input data to the AIR model. The response functions of each instrument need to be modeled for validation of the *AIR* model by comparison with the flight data. The Bonner sphere, scintillation counters, particle telescopes, and nuclear track detectors will be used to improve the model spectral intensities.

Flight Trajectory

All flights originate from Moffett Field, California, the current home base of the NASA ER-2 aircraft. The ground track of the scheduled flights (flights 2, 3, 5, 6, and 7) are shown in figure 2 with radiation contours of the *AIR* model.

Flight 1 will be approximately a 2-hr engineering flight required by the ER-2 operations office with pilot's choice of flight path (assumed to be a racetrack around the home base). The aim is to check aircraft operational characteristics and all aircraft and experimental instrumentation to ensure that everything is operating satisfactorily prior to the acquisition of science measurements.

Flight 2 will be approximately a 6.5-hr flight on prescribed northern and easterly headings and will return to home base over the reverse flight path. The aim for this flight is to determine whether radiation measurements are being affected by the shielding characteristics of onboard aviation fuel, to determine the consistency of instrument readings, and to take science data as a function of altitude along a constant-radiation, geomagnetic latitude line. The flight plan for flight 2 is as follows:

- (37° 24' N, 122 ° 6' W) Take off and climb from Moffett Field.
- (39 ° 19'49" N, 121 ° 27' W) Turn easterly and continue climb.
- (38 ° 30' N, 117 ° W) Begin 20-min altitude hold (assumed to be near Wine Glass at 63 000 ft); then climb back to an altitude at which climb at constant Mach number can be attained along the prescribed easterly heading.
- (37 ° 30' N, 112 ° W) Correct course to maintain constant cutoff.
- (35 ° 54' N, 105 ° W) Correct course to maintain constant cutoff. Begin to maintain constant altitude for 10 min before reaching point F.
- (34 ° 39' N, 100 ° W) Execute 180 ° turn and make slow descent (500 ft/min) (Amarillo) to 52 000 ft. Maintain 52 000 ft for 10 min and then climb to normal cruise altitude along the prescribed flight path, repeating the ground track on the return to Wine Glass.
- (35 ° 54' N, 105 ° W) Correct course to maintain constant cutoff.
- (37 ° 30' N, 112 ° W) Correct course to maintain constant cutoff.
- Before returning to Wine Glass, descend to the same altitude as on the outbound leg over Wine Glass (assumed to be 63 000 ft) and maintain that altitude for about 20 min.
- (38 ° 30' N, 117 ° W) Wine Glass, start descent in preparation of ending mission.

- (39 ^{o} 19'49" N, 121 ^{o} 27' W) Turn south and continue descent.

- (37 ^{o} 24' N, 122 ^{o} 6' W) Land at Moffett Field.

Flight 3 will be approximately an 8-hr flight on prescribed northern, western, and southern headings. The aim is to obtain radiation measurements as a function of geomagnetic latitude as far north as possible with an altitude excursion along a constant-radiation, geomagnetic latitude line at the extreme northern latitude location. The flight plan for flight 3 is as follows:

- (37 ^{o} 24' N, 122 ^{o} 6' W) Take off and climb from Moffett Field and ascend to cruise altitude. Cruise to point G.

- (59 ^{o} 00' N, 116 ^{o} 00' W) Turn west toward point H. Hold altitude fixed for 5 min (Ft. Nelson) after west turn; then execute a medium-rate descent (750 ft/min) to 52 000 ft. Maintain 52 000 ft for 5 min.

- (60 ^{o} 00' N, 123 ^{o} 40' W) Turn southerly (toward Moffett Field) and ascend to cruise altitude. Cruise to Moffett Field.

- (37 ^{o} 24' N, 122 ^{o} 6' W) Descend and land.

Flight 4 will be an engineering flight of approximately 2 hr after instrumentation additions-changes with pilot's choice of flight path (assumed to be a racetrack around home base). The aim is to allow time in flight schedule to check aircraft operational characteristics and all aircraft and experimental instrumentation to ensure everything is operating satisfactorily prior to the acquisition of additional science measurements. This flight will be used only if necessary.

Flight 5 will be approximately a 6.5-hr flight on a prescribed southerly heading over the North Pacific Ocean. At the position Latitude 17 deg N, longitude 127 deg 28 min W, execute a 180 ^{o} turn and return to base. The aim of the mission is to obtain radiation measurements as a function of geomagnetic latitude to as far south as reasonably possible.

Flight 6 will be approximately a 6.5-hr flight on prescribed northern, western, and southern headings. The aim is to obtain radiation measurements as a function of geomagnetic latitude as far north as possible with altitude excursions along a constant-radiation, geomagnetic latitude line near Edmonton, Canada. The flight plan for flight 6 is as follows:

- (37 ^{o} 24' N, 122 ^{o} 6' W) Take off and climb from Moffett Field, ascend to cruise altitude, and cruise to point J.

- (54 ^{o} 48' N, 116 ^{o} 48' W). Turn west toward point K. Hold altitude fixed for 5 min after west turn; then execute a medium-rate descent (750 ft/min) to 52 000 ft and maintain 52 000 ft for 5 min.

- (56 ^{o} 00' N, 125 ^{o} W) Turn south, ascend to cruise altitude and cruise toward Moffett Field.

- (37 ^{o} 24' N, 122 ^{o} 6' W) Descend and land.

Flight 7 is a repeat of flight 5. The aim of flight 7 is to check data measurement repeatability.

Flight 8a will be approximately a 3-hr flight; however, this flight must be combined with flight 8b with a 12-hr interval between the flights. Science requirements dictate that flight 8a should be launched about 11:00 a.m. Immediately after takeoff, climb to maximum altitude, cruise for about 30 min, and hold constant altitude for about 10 min. Initiate descent about 12:00 noon and descend at about 500 ft/min (slow rate) to 52 000 ft; then continue descent at the standard rate of descent to landing. The aim of this flight is to acquire daylight data for comparison with nighttime data to determine diurnal variation of radiation.

Flight 8b will be approximately a 3-hr flight after dark (with takeoff after about 11:00 p.m.) with a flight path similar to flight 8a (assumed to be a racetrack around the home base). Climb to maximum altitude, cruise for about 30 min, and hold a constant altitude for about 10 min. Initiate descent at 12:00 midnight and descend at about 500 ft/min (slow rate) to 52 000 ft; then continue descent at the standard rate of descent to landing. The aim of this flight is to acquire nighttime data for comparison with daylight data to determine diurnal variation of radiation.

The total flight hours for these missions is 44 hr. We currently budgeted for 46 hr; an additional 2 hr (as reserve) are recommended in case we need extra engineering flights.

Expectation from *AIR* Model

Computer simulations are made for flights 2, 3, 5, and 6. For each flight, the ground track is depicted in figure 2. The ground track is taken as great circular routes between the navigation points in the figure. The flight path, the location of the flight path, the latitude, the longitude, as well as the altitude profile as a function of time, are obtained. The flight path for flight 2 is shown in figures 3(a) to 3(c). The scientific quantities such as magnetic cutoff, dose equivalent rate, dose rate, neutron flux, and air ionization rate are predicted as a function of flight time, expressed in minutes. The results for flights 2, 3, 5, and 6 are presented in figures 3(a) to 20. For example, figures 3(a) and 3(b) show the coordinates of the flight path in which the pilot tries to maintain a constant geomagnetic cutoff. Because flight 2 has the prescribed northern and easterly heading and return to home base over the reverse flight path, the coordinates clearly show all the locations as a function of time. Figure 3(c) shows the altitude profile that the airplane is to execute, which also serves as the input data in the AIR model. Figures 3(d) to 7 are the predictions from the AIR model. Because flight 2 is designed to fly parallel to geomagnetic latitude for the major leg (easterly heading and reverse), clearly figure 3(d) shows that the magnetic cutoff value is a horizontal straight line about 4 GV. Figures 4 and 5 show the predictions for dose equivalent rate and dose

rate from the AIR model. Keep in mind that those rate values are a complicated function of flight coordinates as well as the altitude and other factors. Based on the figures, clearly the altitude factor alone suggests that the rate can change from 12 to ~15 percent from 16 km to 20 km altitude. The *AIR* model predicts the neutron flux whose energy range is about 1 to 10 MeV in figure 6 and air ionization rate in figure 7 along the flight path for flight 2. That is, the AIR model predicts an altitude variation in the 1 to 10 MeV neutron flux of about 12 percent and in the air ionization rate of 11 percent at the 4 GV cutoff.

Figures 8(a) to 12 show similar quantities for flight 3, that is, the 8-hr flight on prescribed northern, western, and southern headings. As we mentioned earlier, the purpose for this flight is to obtain radiation measurements as a function of geomagnetic latitude to as far north as possible, with an altitude excursion along a constant-radiation, geomagnetic latitude line at the extreme northern latitude location. Figure 8(b) shows that at the extreme northern latitude, the magnetic cutoff value registers with 0.5 GV were achieved where the altitude survey was performed. Compare figures 9 to 12 with figures 3(c) through 5 for the flight 3 route; the AIR model predicts much higher radiation values than does the flight 2 route. In other words, flight 3, from a radiation safety point of view, flies in a less safe route than flight 2, as was expected. The altitude survey at 0.5 GV shows a variation on the order of 11 percent in 1 to 10 MeV neutron flux and 23 percent for the air ionization rate. Because the prime purpose of flight 3 is to perform a latitude survey, we see that the high-altitude variation in the environment during the cruise portion of the flight, along the northern path, is 32 percent in the 1 to 10 MeV neutron flux and 33 percent in the air ionization rate.

Flight 5 will examine the latitude dependence of the high-altitude environment south of the ER-2 base at Ames Research Center. The model predicted a variation of only a few percent in the radiation levels in a possible altitude survey, and such a survey was eliminated from the flight plan because it was to take place over the Atlantic Ocean and was considered an unnecessary hazard to the pilot. The cutoff reached is predicted to be over 12 GV, giving a latitude survey in conjunction with flight 3 a factor of 24 in cutoff variation. It is clear from figures 14 and 15 that a valley in exposure rates is being approached as we fly into equatorial regions.

Flight 6 is a shorter northern flight to the edge of the northern plateau of the exposures, while repeating the latitude dependence measurements up to 0.8 GV. The maximum environmental quantities are lower, but the altitude variation is a somewhat smaller excursion.

Concluding Remarks

The atmospheric ionizing radiation (*AIR*) ER-2 preflight analysis, one of the first attempts to obtain a relatively complete measurement set of the high-altitude radiation level environment, is described in this paper. The primary thrust is to characterize the atmospheric radiation and to define dose levels at high-altitude flight. A secondary thrust is to develop and validate dosimetric techniques and monitoring devices for protecting aircrews. With a few chosen routes, we can measure the experimental results and validate the AIR model predictions. Eventually, as more measurements are made, we gain more understanding about the hazardous radiation environment and acquire more confidence in the prediction models.

References

Biological Effects of Ionizing Radiations; Board on Radiation Effects Research Commission on Life Sciences; and National Research Council: *Health Effects of Exposure to Low Levels of Ionizing Radiation—BEIR V*. National Academy Press, 1990.

FAA Advisory Committee on the Radiobiological Aspects of the Supersonic Transport. Cosmic Radiation Exposure in Supersonic and Subsonic Flight. *Aviat., Space, & Environ. Med*., vol. 46, Sept. 1975, pp. 1170–1185.

Fiorino, Francis, compl.; Airline Outlook. *Aviat. Week & Space Technol*., June 3, 1996.

Foelsche, T.; Mendell, R. B.; Wilson, J. W.; and Adams, R. R.: Measured and Calculated Neutron Spectra and Dose Equivalent Rates at High Altitudes: Relevance to SST Operations and Space Research. NASA TN D-7715, 1974.

Friedberg, W.; Snyder, L.; Faulkner, D. N.; Darden, E. B.; and O'Brien, K.: *Radiation Exposure of Air Carrier Crewmembers II*. DOT/FAA-AM-92/2, FAA, 1992.

ICRP *Recommendations of the International Commission on Radiological Protection*. ICRP Publ. 26, Pergamon Press, 1977.

ICRP *Recommendations of the International Commission on Radiological Protection*. ICRP Publ. 60, Pergamon, 1991.

NCRP *Limitation of Exposure to Ionizing Radiation*. NCRP Rep. No. 116, Mar. 1993.

NCRP *Radiation Exposure and High-Altitude Flight*. NCRP Commentary No. 12, July 1995.

O'Brien, K.; and Friedberg, W.: Atmospheric Cosmic Rays at Aircraft Altitudes. *Environ. Int.*, vol. 20, no. 5, 1994, pp. 645–663.

Reitz, G.; Schnuer, K.; and Shaw, K.: Editorial—Workshop on Radiation Exposure of Civil Aircrew. *Radiat. Prot. Dosim*., vol. 48, no. 1, 1993, p. 3.

Schaefer, H. J.: Public Health Aspects of Galactic Radiation Exposure at Supersonic Transport Altitudes. *Aerosp. Med.,* vol. 29, 1968, pp. 1298–1303.

UNSCEAR Sources, Effects and Risks of Ionizing Radiation—United Nations Scientific Committee on the Effects of Atomic Radiation 1988 Report to the General Assembly, With Annexes. United Nations, 1988.

White, W. J.: *Crewmember Training on In-Flight Radiation Exposure*. Advisory Circular No. 120-61, FAA, May 19, 1994.

Wilson, J. W., Townsend, L. W., Schimmerling, W., Khandelwal, G. S., Khan, F., Nealy, J. E., Cucinotta, F. A., Simonsen, L. C., Shinn, J. L., Norbury, J. W. Transport methods and interactions for space radiation. NASA RP-1257, 1991.

Wilson, John W.; Nealy, John E.; Cucinotta, Francis A.; Shinn, Judy L.; Hajnal, Ferenc; Reginatto, Marcel; and Goldhagen, Paul: *Radiation Safety Aspects of Commercial High-Speed Flight Transportation*. NASA TP-3524, 1995.

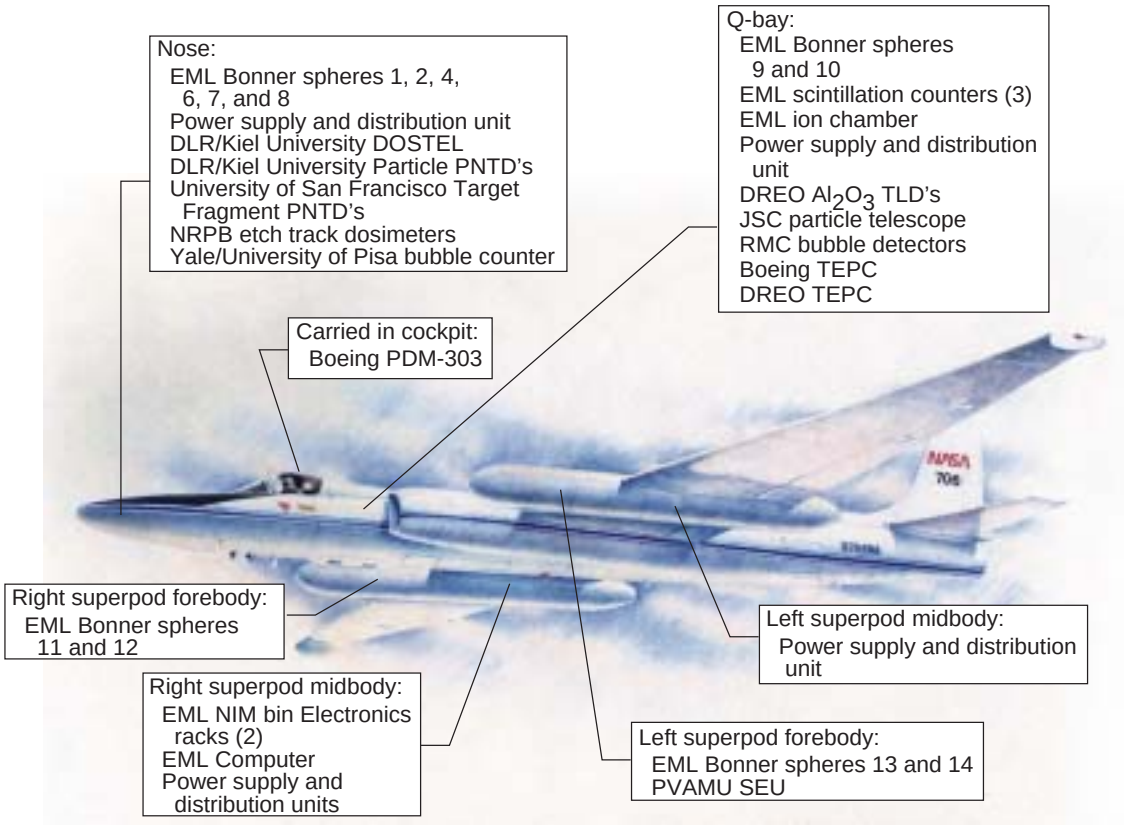

Figure 1. Instrument locations on the ER-2.

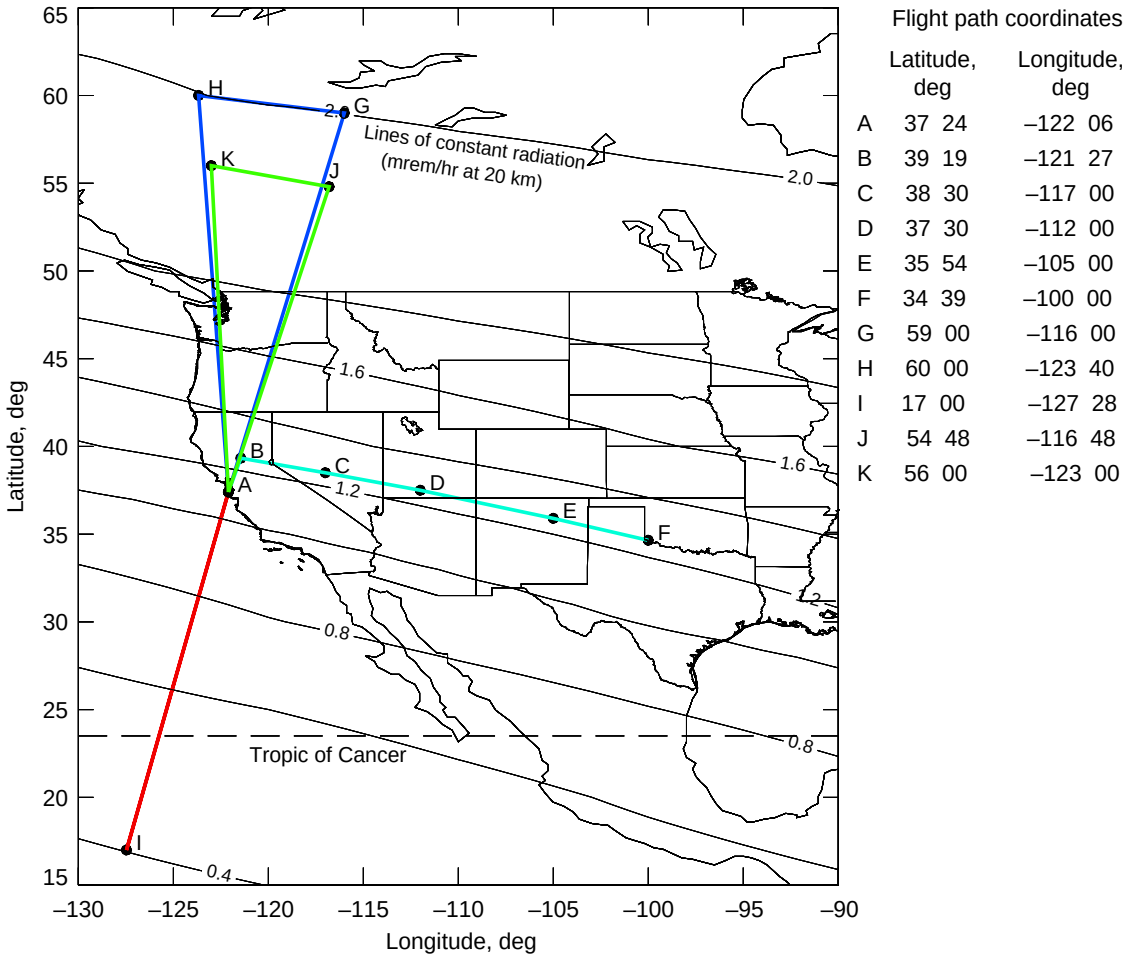

Figure 2. AIR/ER-2 ground tracks.

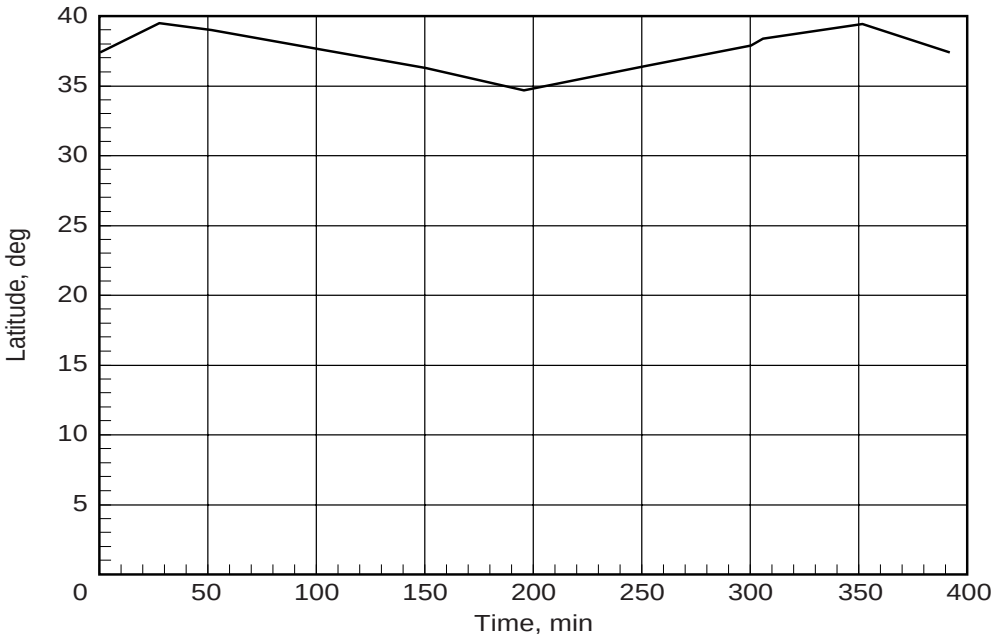

(a) Latitude.

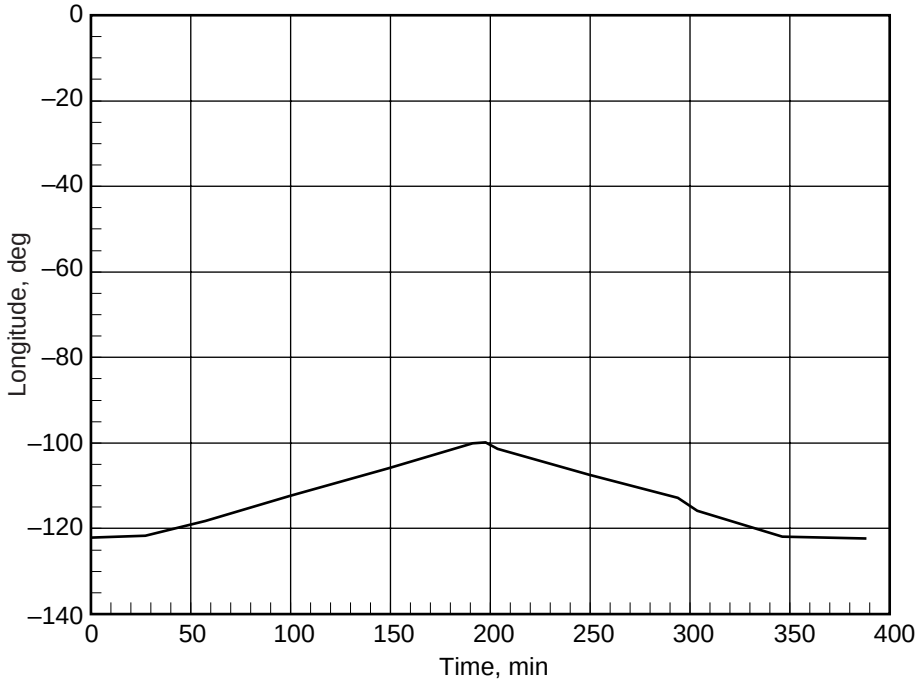

(b) Longitude.

Figure 3. Latitude and longitude of flight path as function of time for flight 2.

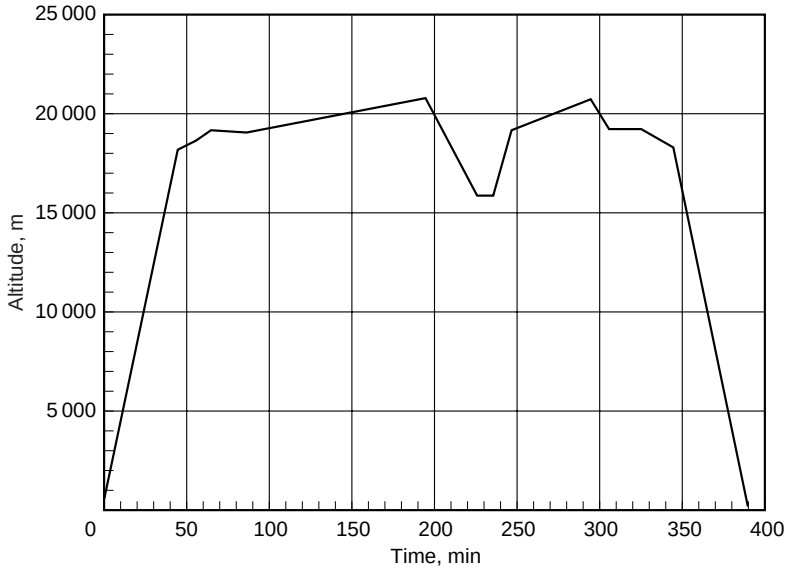

(c) Altitude.

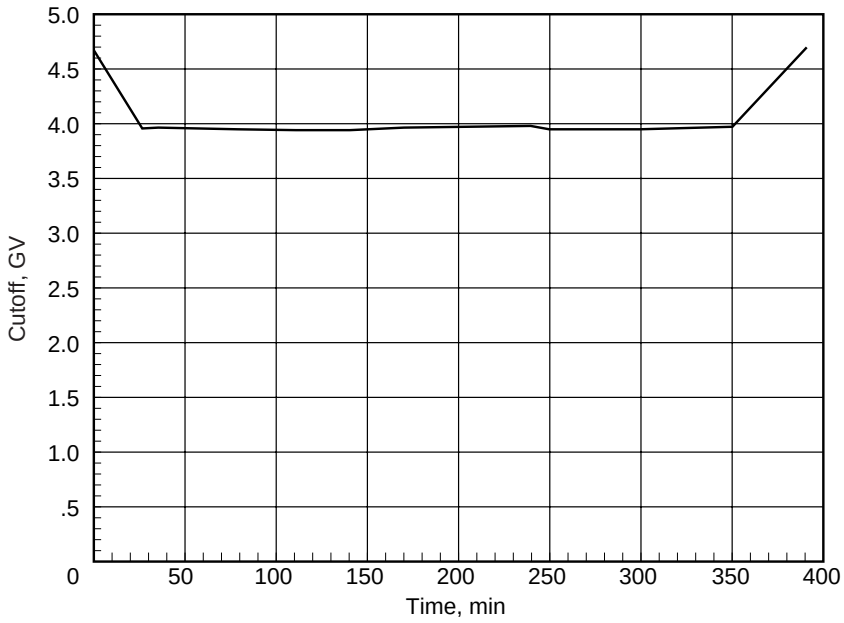

(d) Magnetic cutoff.

Figure 3. Concluded.

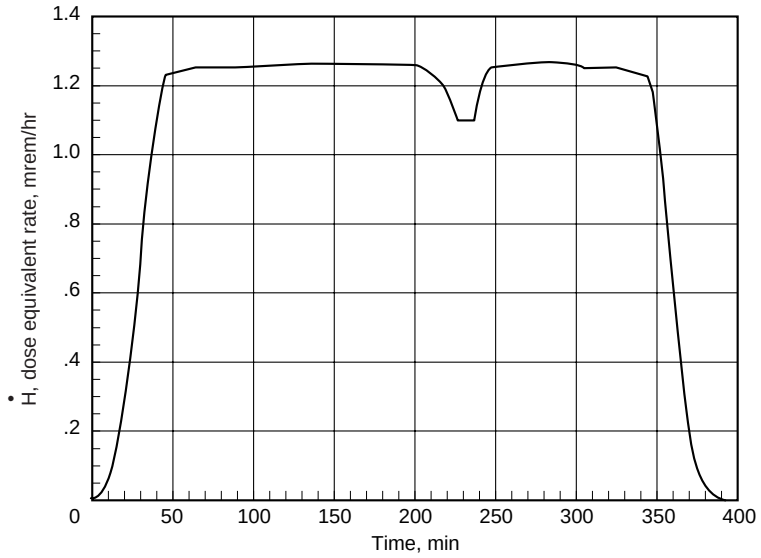

Figure 4. Dose equivalent rate as function of time for flight 2.

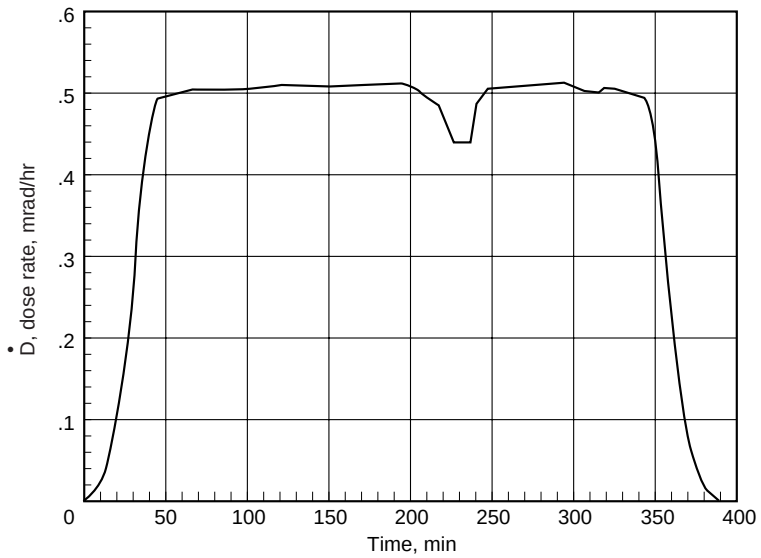

Figure 5. Dose rate as function of time for flight 2.

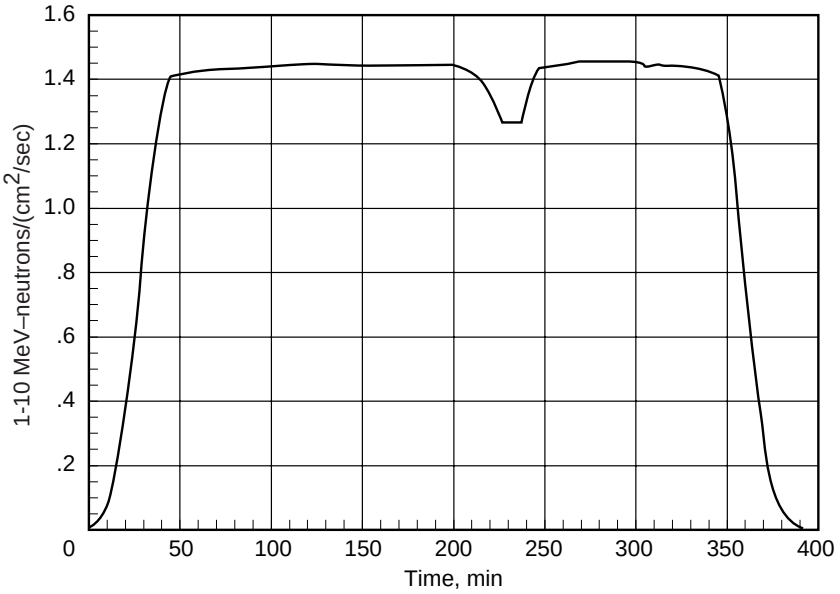

Figure 6. Neutron flux as function of time for flight 2.

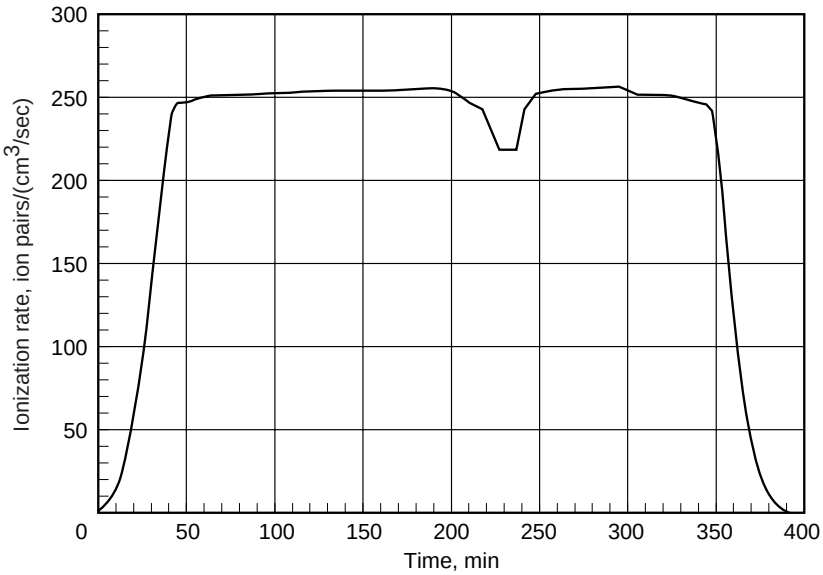

Figure 7. Air ionization rate as function of time for flight 2.

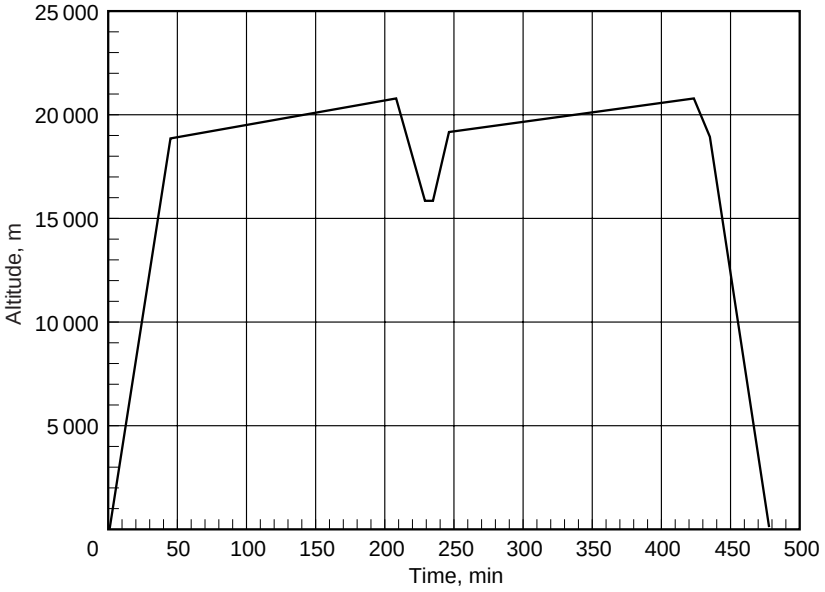

(a) Altitude.

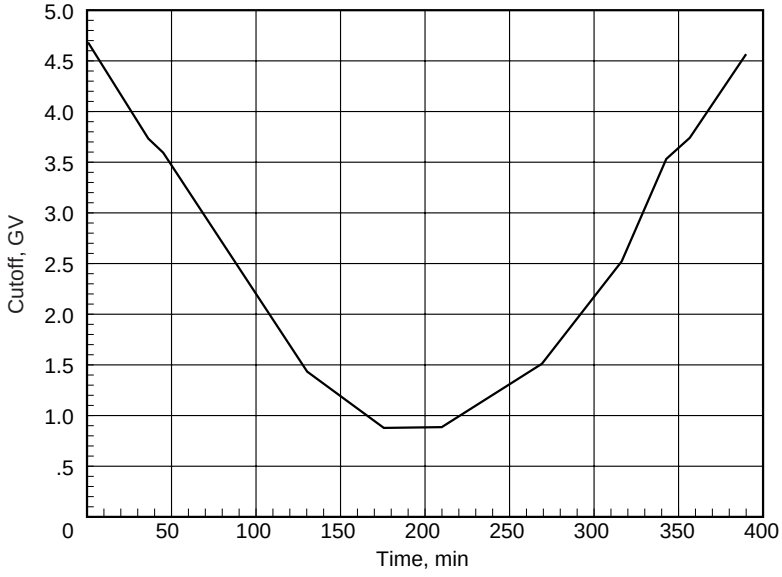

(b) Magnetic cutoff.

Figure 8. Flight path as function of time for flight 3.

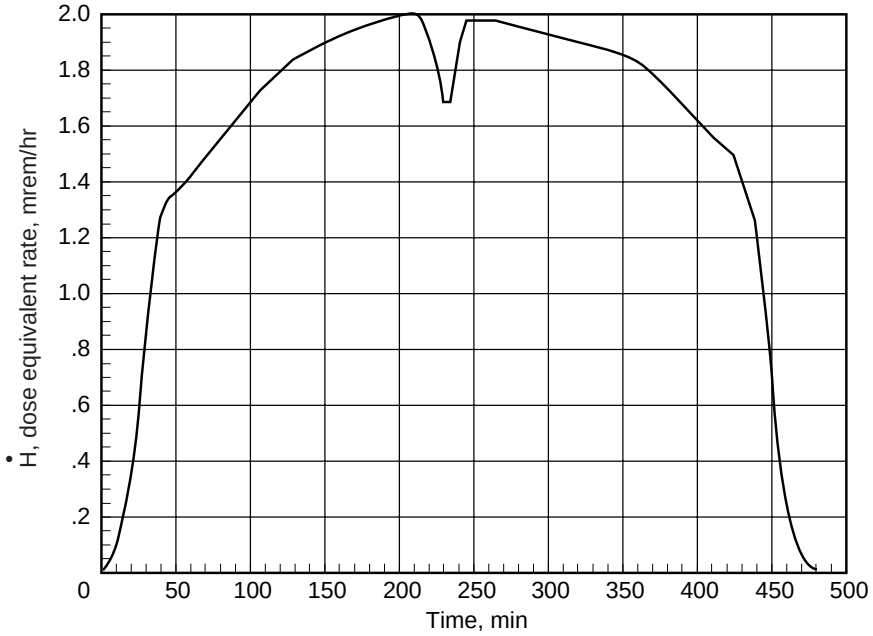

Figure 9. Dose equivalent rate as function of time for flight 3.

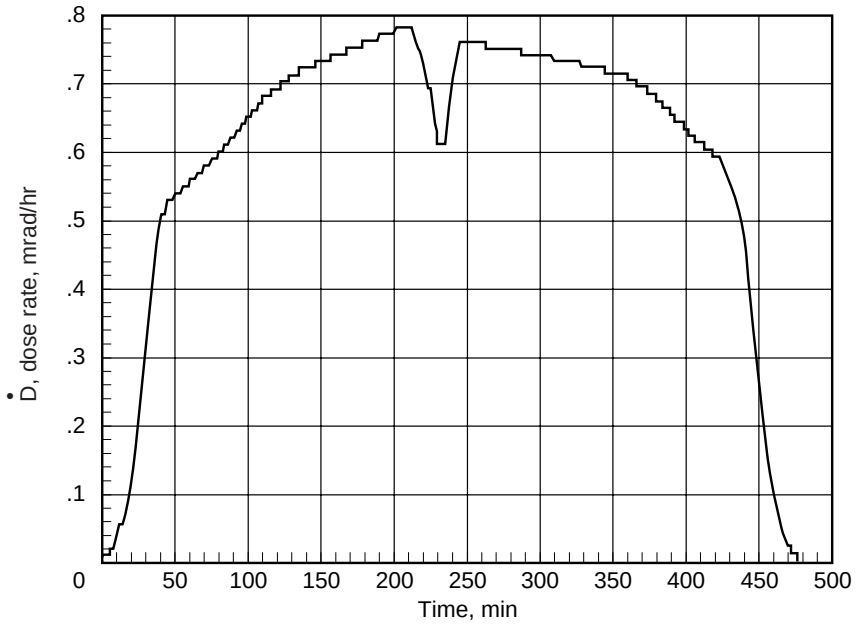

Figure 10. Dose rate as function of time for flight 3.

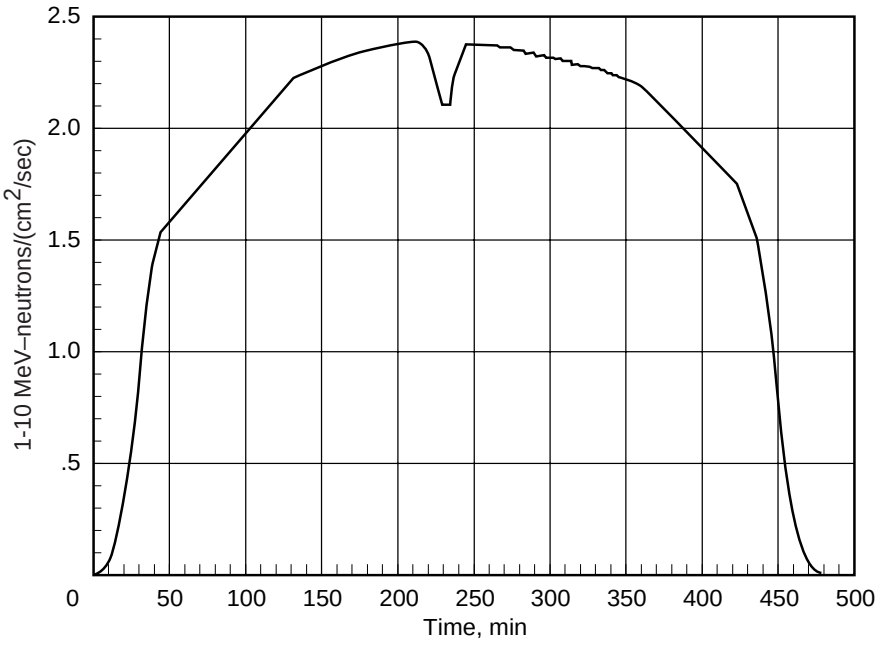

Figure 11. Neutron flux as function of time for flight 3.

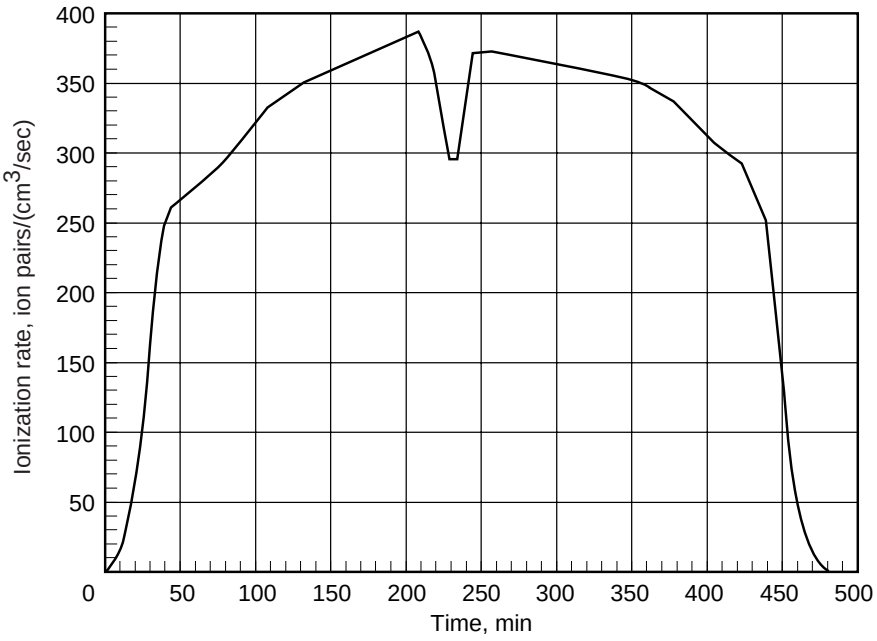

Figure 12. Air ionization rate as function of time for flight 3.

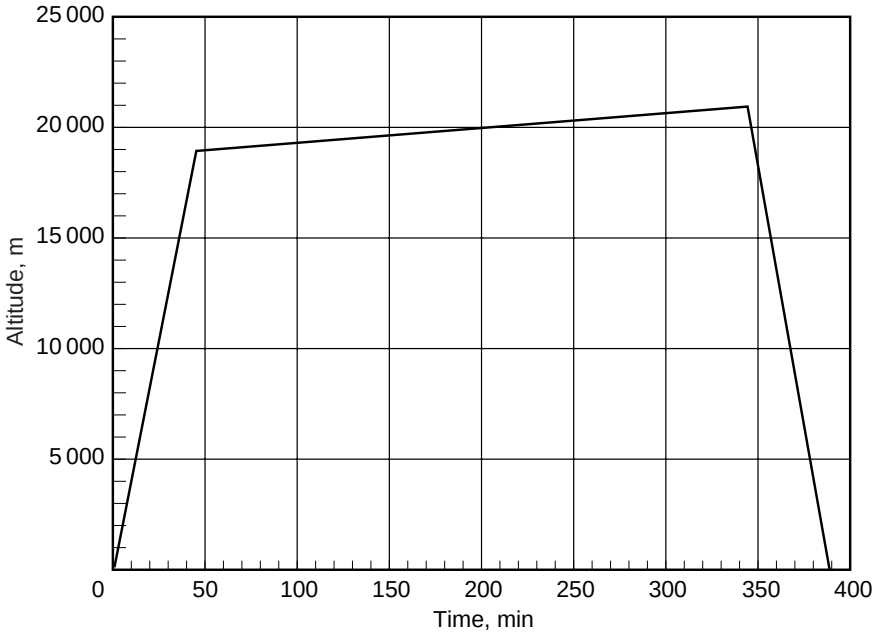

(a) Altitude.

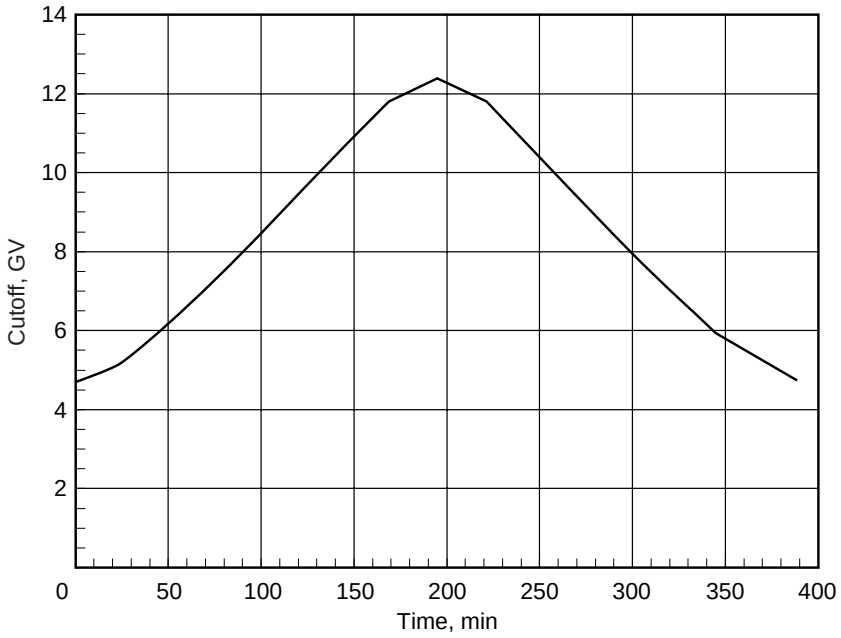

(b) Magnetic cutoff.

Figure 13. Flight path as function of time for flight 5.

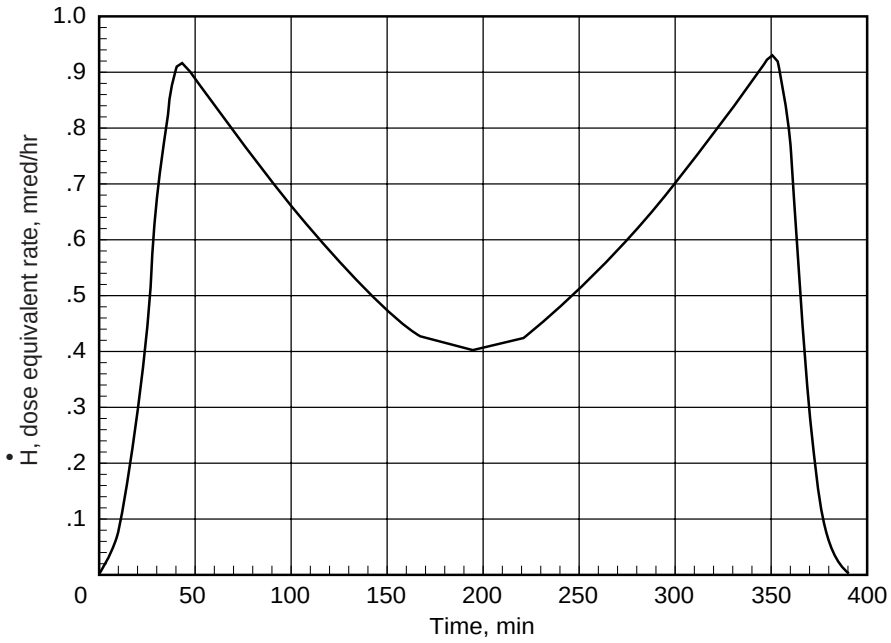

Figure 14. Dose equivalent rate as function of time for flight 5.

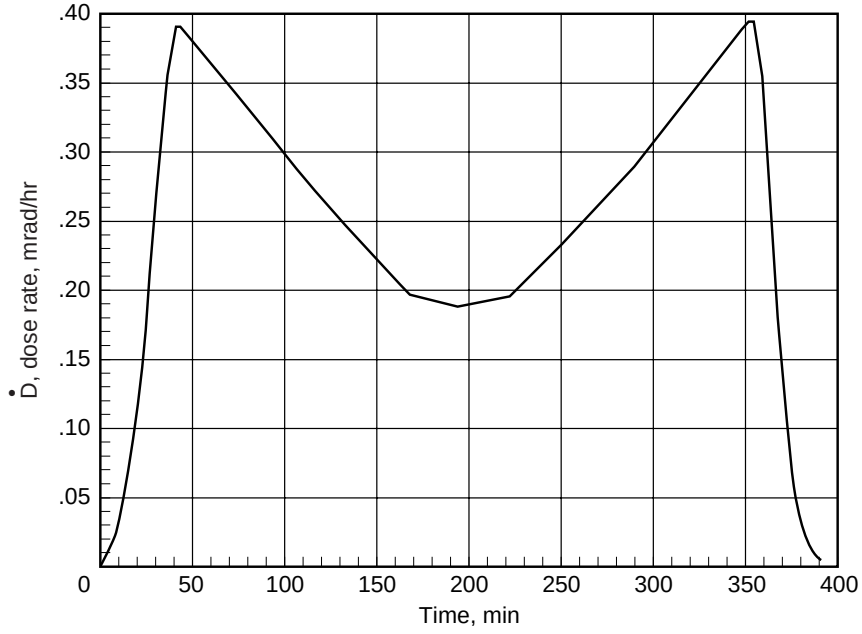

Figure 15. Dose rate as function of time for flight 5.

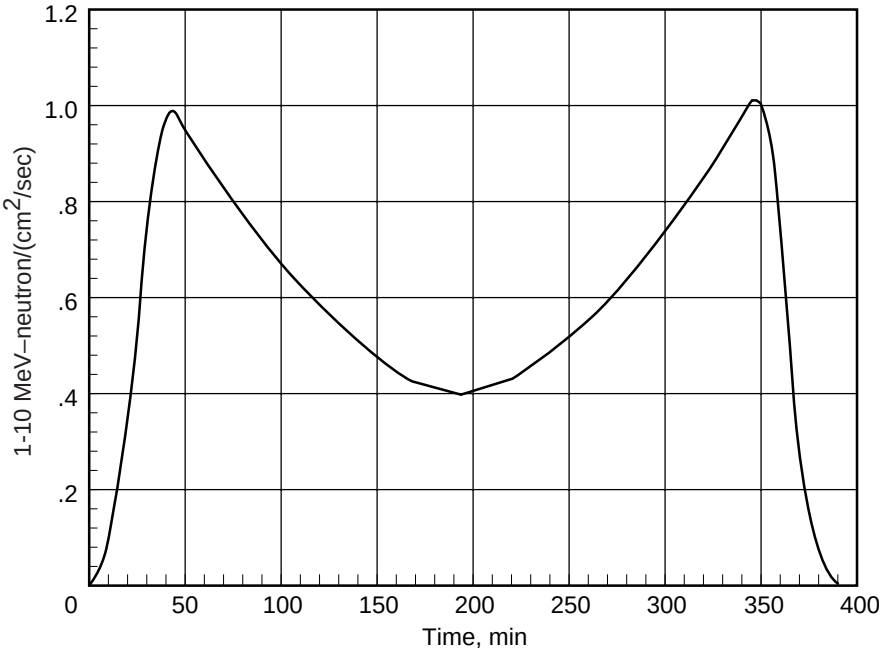

Figure 16. Neutron flux as function of time for flight 5.

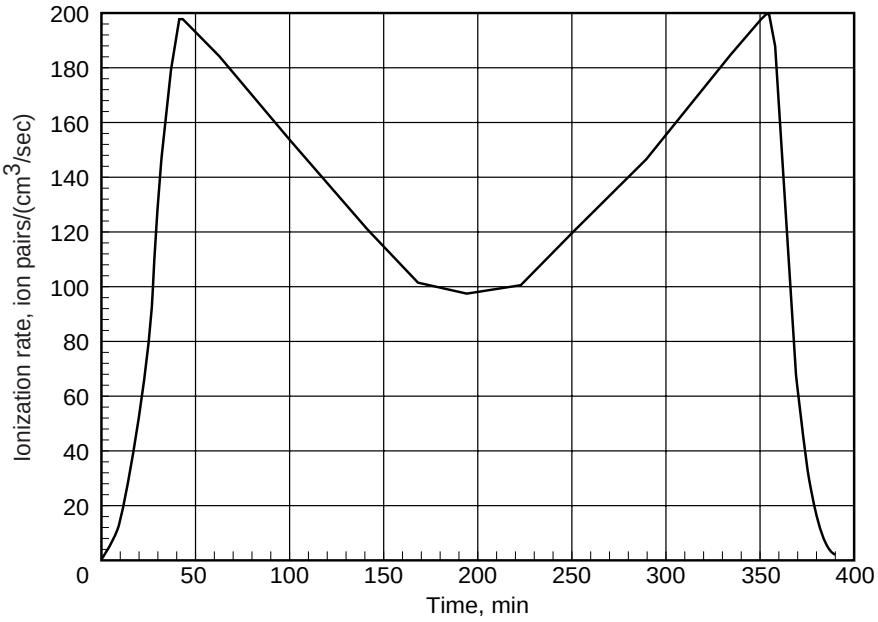

Figure 17. Air ionization rate as a function of time for flight 5.

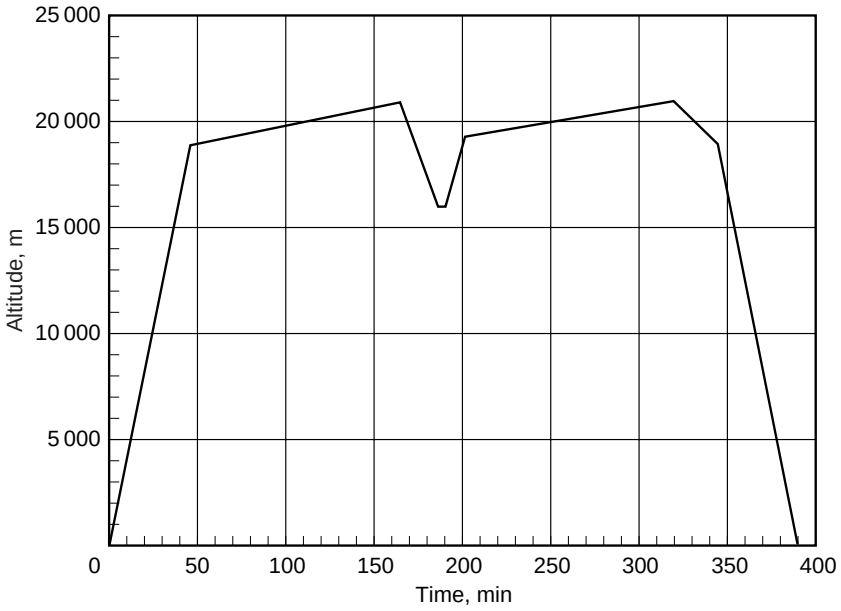

(a) Altitude.

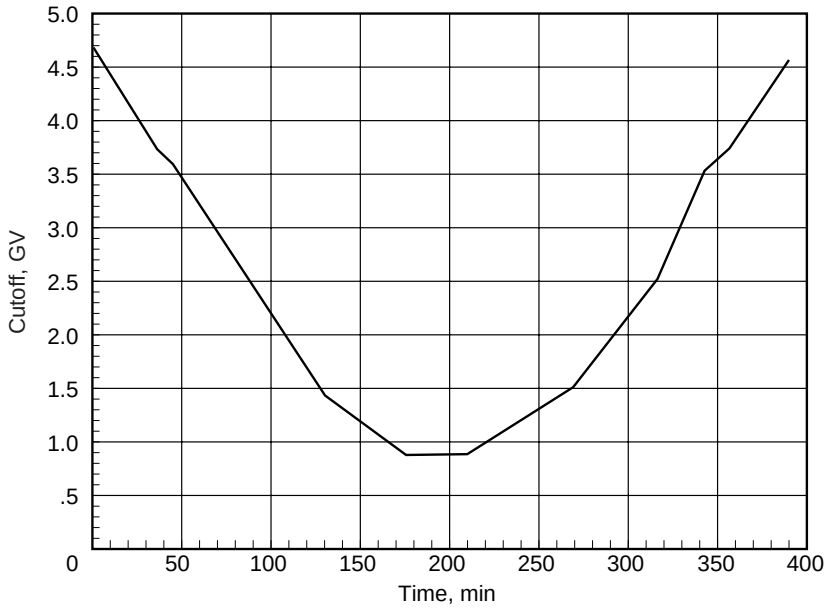

(b) Magnetic cutoff.

Figure 18. Flight path as function of time for flight 6.

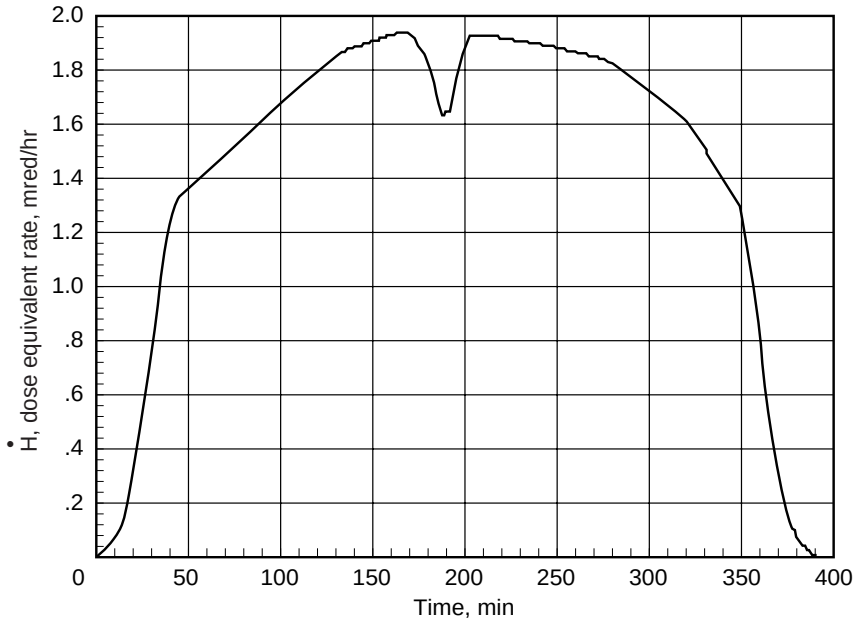

Figure 19. Dose equivalent rate as function of time for flight 6.

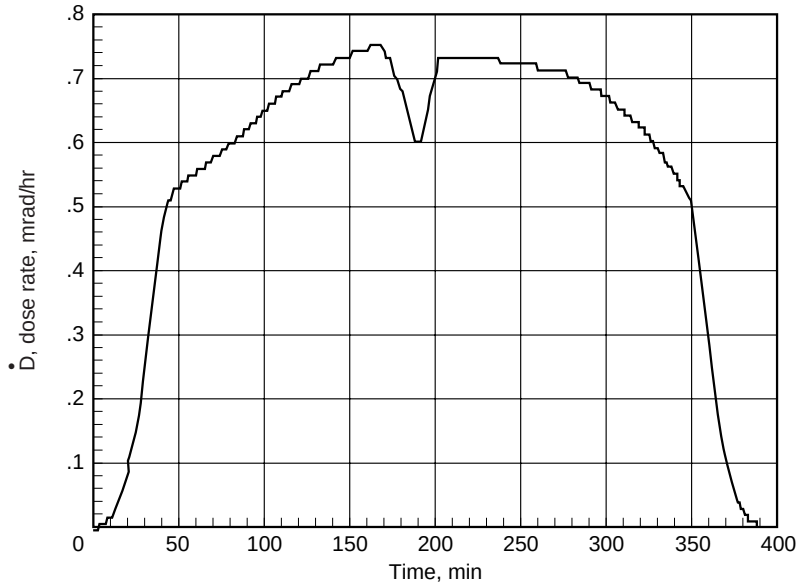

Figure 20. Dose rate as function of time for flight 6.

Chapter 5: June 1997 ER-2 Flight Measurements

Irby W. Jones
NASA Langley Research Center

June 1997 ER-2 Flight Measurements

Preface

Within our current understanding of the atmospheric ionizing radiation, the ER-2 flight package was designed to provide a complete characterization of the physical fields and evaluate various dosimetric techniques for routine monitoring. A flight plan was developed to sample the full dynamic range of the atmospheric environment especially at altitudes relevant to the development of the High Speed Civil Transport. The flight of the instruments occurred in June of 1997 where predictive models indicated a maximum in the high altitude radiation environment occurring approximately nine months after the minimum in the solar sunspot cycle. The flights originated at Moffett field at the Ames Research Center on ER-2 aircraft designated as 706. The equipment was shipped mid-May 1997 for unpacking and checkout, size fitting, systems functional test, and preflight testing on aircraft power with flight readiness achieved on May 30, 1997. The equipment was qualified on its first engineering flight on June 2, 1997 and the subsequent science gathering flights followed during the period of June 5 – 15, 1997. Herein we give an account of the flight operations.

Introduction

The NASA Earth Resources (ER)-2 is a civilian version of the Air Force's TR-2 aerial reconnaissance aircraft. Both of these aircraft are the direct descendents of the old Lockheed U-2 which carried cameras on spy missions starting in the mid 1950s. The AIR/ER-2 flights were launched from Moffett Field, CA, and were precisely flown by the pilots along coordinates provided by the AIR Project as discussed in Chapter 4. The operations of the ER-2 aircraft were conducted under the management of the High Altitude Missions Branch at the Ames Research Center.

The AIR Project is an international collaboration devised by scientists at the NASA Langley Research Center and the DOE Environmental Measurements Laboratory with more than 12 domestic and foreign laboratories to make measurements and calculations of the stratospheric radiation field due to galactic cosmic rays. The first series of ER-2 flights for the AIR Measurement Project were successfully completed on schedule at the peak of the galactic cosmic radiation in June 1997.

The measurement part of the AIR Project involved placing 15 instruments on multiple flights of the NASA ER-2 aircraft. The instrument layout is shown in Figure 1. Payload integration of the international instrument array with the ER-2 was done by Langley Research Center and Lockheed Skunk works personnel in a very short time and on a constrained budget and fixed launch window. The first series of flights took place June 2-15, 1997 from the NASA Ames Research Center in California, covering altitudes from 52,000 to 70,000 feet and latitudes from 18 to 60 degrees N. The six flights are listed in Table 1. Data from these measurements are being used to benchmark an improved Langley model of the radiation environment which can be used to calculate radiation exposures that will be incurred in future high-speed civil transport (HSCT) commercial operations.

May 15-June 15, 1997 *AIR* Missions Plan: Sortie Definitions

All flights originate from Moffett Field, CA, the home base of the NASA ER-2 aircraft. The priority order of flights could change due to unexpected delays and the fixed June 15, 1997 end date for the campaign. The science flights in order of priority are 2,3,6,7,8,4 and 5.

Flight 1: This will be approximately a two-hour engineering-flight required by the ER-2 operations office with pilot's choice of flight path (assumed to be a racetrack around the home base). The aim is to check aircraft operational characteristics, and all aircraft and experimental instrumentation to assure everything is operating satisfactorily prior to the acquisition of science measurements.

> **Abort Criteria:** Red light condition - Computer is not recording measurement data. Turn switch off, wait two minutes and then turn switch back on. If red light is still on, repeat off/on procedure once more. If red light persists, return to base.
>
> **Success criteria:** All systems go for measurements.

Flight 2: This will be approximately a **six & one-half hour** flight on prescribed northern and easterly headings and return to home base over the reverse flight path. In the vicinity of Wine Glass (lat 38 deg 30 min N, long 117 deg W) maintain the current, standard-climb altitude (assumed to be about 63,000 ft) for about 20 minutes and then climb back to an altitude at which climb at constant Mach number can be attained along the prescribed easterly heading,. In the vicinity east of Amarillo, Texas (lat 34 deg 39 min N, long 100 deg.W), execute a 180 degree turn and descend to 52,000 feet at about 500 feet per minute (slow descent). Maintain 52,000 feet for 10 minutes and then climb to maximum altitude along the prescribed flight path repeating the ground track on the return to Wine Glass. Before returning to Wine Glass descend to the same altitude as on the outbound leg over Wine Glass (assumed to be 63,000 ft) and maintain that altitude for about 20 minutes. The aim for this flight is to determine if radiation measurements are being affected by the shielding characteristics of on-board aviation fuel, determine consistency of instrument readings, and take science data as a function of altitude along a constant-radiation, geomagnetic latitude line.

> **Abort Criteria:** Constant red light condition after two restart attempts - Computer is not recording measurement data.
>
> **Success criteria:** Seventy percent of instruments functioning and sufficient data as required to determine any possible effects from aviation fuel shielding.

Flight 3: This will be approximately an **eight hour** flight on prescribed northern, western and southern headings. In the vicinity east of Fort Nelson, CANADA (lat 58 deg, 30 min N, lon- 1 18 deg, W), execute a turn to the west and descend to 52,000 feet at a descent rate of about 750 feet per minute (moderately slow descent rate). Maintain 52,000 feet for about 5 minutes and then climb at constant Mach number. In the vicinity west of Fort Nelson (lat 60 deg, 30 min N, lon 60 deg 30 min W) execute a turn to the south and climb to cruise altitude and return to home base. The aim is to obtain radiation measurements as a function of geomagnetic latitude to as far north as

possible with an altitude excursion along a constant-radiation, geomagnetic latitude line at the extreme northern latitude location.

Abort Criteria: Constant red light condition after two restart attempts - Computer is not recording measurement data.

Success criteria: Seventy percent of instruments functioning and data acquired.

Flight 4: This will be an engineering flight of approximately **three hours** after instrumentation additions with pilot's choice of flight path (assumed to a racetrack around home base). If this flight is combined with flight 5 on the same day there should be a 12hour interval between the flights which would dictate that flight 4 should be launched about 10:00 am. After engineering flight objectives are obtained for flight 4, continue to acquire science data by climbing to maximum altitude and hold for about 10 minutes. Initiate descent about 12:00 noon and descend at about 500 feet per minute (slow rate) to 52,000 feet and then continue descent at the standard rate of descent to landing. The aim of this flight is to acquire daylight data for comparison with night time data to determine diurnal variation of radiation.

Abort Criteria: Constant red light condition after two restart attempts Computer is not recording measurement data.

Success criteria: All systems go for measurements.

Flight 5: This will be approximately a **three hour** flight after dark (with take-off after about 10:00 PM) with a flight path similar to Flight 4 (assumed to be a race track around the home base). Climb to maximum altitude, cruise for about 30 minutes and hold a constant altitude for about 10 minutes. Initiate descent at 12:00 midnight and descend at about 500 feet per minute (slow rate) to 52,000 feet and then continue descent at the standard rate of descent to landing. The aim of this flight is to acquire night-time data for comparison with daylight data to determine diurnal variation of radiation.

Abort Criteria: Constant red light condition after two restart attempts - Computer is not recording measurement data.

Success criteria: Seventy percent of instruments functioning and data acquired.

Flight 6: This will be approximately a **six & one-half hour** flight on a prescribed southerly heading, over the North Pacific ocean. At the position Latitude 17 deg N, lon 127 deg 28 min W, execute a 180 degree turn and return to base. The aim of the mission is to obtain radiation measurements as a function of geomagnetic latitude to as far south as reasonably possible. An altitude variation at the extreme south was not attempted since less than on percent variation is expected and there is a danger of flame out.

Abort Criteria: Constant red light condition after two restart attempts - Computer is not recording measurement data.

Success criteria: Seventy percent of instruments functioning and data acquired.

Flight 7: This will be approximately a **six and one-half hour** flight on prescribed northern, western, and southern headings. In the vicinity of Edmonton, CANADA (lat 53 deg 43 min N, lon 1 19 deg 48 min W), execute a turn to the west and descend to 52,000 feet at a descent rate of about 750 feet per minute (moderately slow descent). Maintain 52,000 feet for about 5 minutes. In the vicinity east of Fort St. John, Canada (lat 56 deg 33 min N, lon 125 deg W), execute a turn to the south and return to base climbing to the highest altitude. The aim is to obtain radiation measurements as a function of geomagnetic latitude to as far north as possible with altitude excursions along a constant radiation, geomagnetic latitude line near Edmonton, CANADA.

> **Abort Criteria:** Constant red light condition after two restart attempts - Computer is not recording measurement data.
>
> **Success criteria:** Seventy percent of instruments functioning and data acquired.

Flight 8: This is a repeat of flight #6. The aim of this flight is to check data measurement repeatability.

> **Abort Criteria:** Constant red light condition after two restart attempts - Computer is not recording measurement data.
>
> **Success criteria:** Seventy percent of instruments functioning and data acquired.

The total flight hours for these missions is 42 hours. We currently are budgeted for 46 hours. The 4 extra hours is held as reserve in case we need additional engineering flights for unknown reasons.

Results of the June 1997 Campaign

Flight #1 (N97-104, Engineering Test)

The first flight was an Ames/Lockheed-required two hour duration engineering flight. The Ames flight number was N97-104. Its purpose was to verify compatibility of the instrument array with all of the ER-2 systems, including aircraft flight handling. All instruments in the array were fully operational, and gathered data during the flight, except as noted below. The pilot reported no interference with ER-2 systems, and the instrument array was certified by Ames/Lockheed for flying on the ER-2. The flight ground track is shown in Figure 2 and consisted of a race track path around Ames. Figure 3 shows the altitude profile.

Ten of the fourteen EML detectors functioned properly during the flight. Post flight review of the EML data showed that the high voltage power supplies for four detectors cut off during the flight: in the nose bonner sphere #2 and in the Q-bay bonner sphere #9, bonner sphere #10, and the ion chamber. Science data from these detectors ended when the high voltage was lost. Two of the EML detector cutoffs were caused by a leak in the pressure containers surrounding the detectors. Faulty pressure fittings on these containers were found and replaced. All of the EML pressure containers functioned properly for the remainder of the flights. The other 2 EML detector cutoffs were the continuation of a intermittent problem discovered earlier during all-up system operation, and was not resolved.

After this flight, the JSC Particle Telescope flight data was retrieved from the unit and sent to JSC for analysis. They reported back that the unit was not reading data from 8 of the 10 detector channels, effectively making its data useless. A quick look inside the unit revealed a malfunctioning connector, but fixing it did not cure the problem. Because of budgetary and time constraints, JSC elected not to fix the problem at that time. The Particle Telescope was left in place on the ER-2 rack, and operated on subsequent flights, but did not produce meaningful data.

The ER-2 system that records the high altitude (above 10 km) ambient pressure also failed during this flight, making it impossible to read both the high altitude pressure and the low altitude pressure at the same time. The pressure readings at high altitude were considered most important, so the system was configured to record only the high altitude ambient pressure for subsequent flights. In spite of a few issues concerning a few detectors and the altimeter, the overall mission reached the threshold of success as defined in the planning document.

Flight #2 (N97-105, Easterly)

The second flight was to be a six and one-half hour flight on a prescribed northern and easterly path and return over the reverse path. Leaving Moffett Field the craft headed on a northerly path to the vicinity of Wine Glass (38^{o} 30"N, 117^{o} W) and then followed an easterly line of constant magnetic latitude to Amarillo, Texas. The altitude continuously increased as the ER-2 "cruise climbed" until Wine Glass where a constant altitude was maintained for 20 minutes. Normal cruise climb then resumed to Amarillo. An altitude dip was performed shortly after turnaround. After turnaround, the pilot retraced the previous path back to Ames. Just before leaving the constant magnetic latitude path, the pilot descended to match his altitude at the same location during the outward bound leg. He held this altitude for 20 minutes to allow a comparison of the measured data at two distinct fuel loads at the identical locations in the radiation fields. The Ames flight number was N97-105. All instruments in the array were fully operational, and gathered data during the flight, except as noted below. The flight ground track is shown in Figure 4 where a storm over northern New Mexico was avoided. Figure 5 shows the altitude profile.

Twelve of the fourteen EML detectors functioned properly during this flight. Post flight review of the EML data showed that again the high voltage power supplies for two detectors were cut off by the computer system: bonner sphere #2 in the nose and bonner sphere #10 in the Q-bay. Science data from these detectors ended when the high voltage was shut off. The detector shutdowns were again caused by the same problem that showed up on the previous flights, and was not yet resolved.

The JSC Particle Telescope was operated, and the flight data was left onboard the unit.

Flight #3 (N97-106, North-1):

The third flight path headed north as far north as the ER-2 could fly in an extended 8 hour mission, turned west along a constant geomagnetic latitude line, and then returned directly to Ames. An altitude dip was executed along a constant magnetic latitude line at the northern extremity of the path. The Ames flight number was N97-106. All instruments in the array were fully operational, and gathered data during the flight, except as noted below. The flight ground track is shown in Figure 6. Figure 7 shows the altitude profile.

Eleven of the fourteen EML detectors functioned properly during this flight. Post flight review of the EML data showed that the high voltage power supplies for three detectors cut out during the flight: bonner sphere #2 in the nose; bonner sphere #10 in the Q-bay; and bonner sphere #12 in the right superpod. Science data from these detectors ended when the high voltage was lost. The three detector cutoffs were the continuation of the same problem that showed up on the previous flights, and was not yet resolved.

Flight #4 (N97-107, South-1):

The fourth flight path was south, following a path nearly perpendicular to the geomagnetic latitude lines down to about 18° latitude, and then back along the same path to Ames. The Ames flight number was N97-107. The ER-2 was allowed to cruise climb in altitude the entire flight. All instruments in the array were fully operational, and gathered data during the flight. The flight ground track is shown in Figure 8. Figure 9 shows the altitude profile.

All of the EML detectors functioned properly during this flight. Software changes installed prior to this flight apparently stopped the high voltage shutdown problem.

The JSC Particle Telescope was operated again, and the flight data was left onboard the unit.

Flight #5 (N97-108, North-2):

The fifth flight path was essentially a repeat of the first northerly flight. The outbound and return legs were shortened to allow a 6.5 hour flight time. An altitude dip was again executed during the westerly, constant geomagnetic latitude at the northern extreme. The Ames flight number was N97-108. All instruments in the array were fully operational, and gathered data during the flight, except as noted below. The flight ground track is shown in Figure 10. Figure 11 shows the altitude profile.

All of the EML detectors functioned properly during this flight. The JSC Particle Telescope was operated, and the flight data was left onboard the unit.

Flight #6 (N97-109, South-2):

The sixth flight path was a repeat of the first southerly flight #4. The Ames flight number was N97-109. All instruments in the array were fully operational, and gathered data during the flight. The flight ground track is shown in Figure 12. Figure 13 shows the altitude profile.

All of the EML detectors functioned properly during this flight. The JSC Particle Telescope was operated, and the flight data was left onboard the unit.

Postmortem

The loss of high voltage on the early flights was software/hardware interaction problem and change in software parameters allowed reliable operation in successive flights. The JSC telescope ran without fault although some of the data failed to record rendering the data unusable. The inability to down load data without disassembling the

device would have allowed the determination of the continued problem and a possible fix between flights. The DOSTEL instrument operated properly, but analysis of the flight data months after the flight series has shown an interference on some of the data. The source of the interference appears to be an ER-2 navigation transmitter (TACAN). Although the DOSTEL data shows noise in a middle spectral range the spectrum can still be constructed by interpolation with a loss in accuracy. The BGO and plastic scintillation counters were never completely integrated into the system and data from them was not obtained. The NaI scintillation counter did obtain data and although noise appears in the lower spectral channels the real data range appears not to have been effected.

Conclusions:

In spite of the low funding and the fast track to meet the June 1997 flight date, the overall performance of the flight package was well over the threshold required for success and the flight team received an award for the "Outstanding planning, coordination and implementation of a complex Atmospheric Ionizing Radiation ER-2 flight measurements campaign in support of the Environmental Impact element of the HSR Program." Members of the team are listed in an appendix at the end of these proceedings.

Table 1 - *AIR* flights at Ames - June, 1997

Flight Designation	Date	Duration	AIR Flight No.	Ames Flight No.	Start Time	End Time
Engineering	6/2/97	2 hrs	101	N97104	20:00 GMT	22:00 GMT
East	6/5/97	6.5 hrs	102	N97105	16:00 GMT	22:33 GMT
North 1	6/8/97	8 hrs	103	N97106	16:00 GMT	23:47 GMT
South 1	6/11/97	6.5 hrs	104	N97107	16:00 GMT	22:30 GMT
North 2	6/13/97	6.5 hrs	105	N97108	16:00 GMT	22:37 GMT
South 2	6/15/97	6.5 hrs	106	N97109	18:00 GMT	00:24 GMT

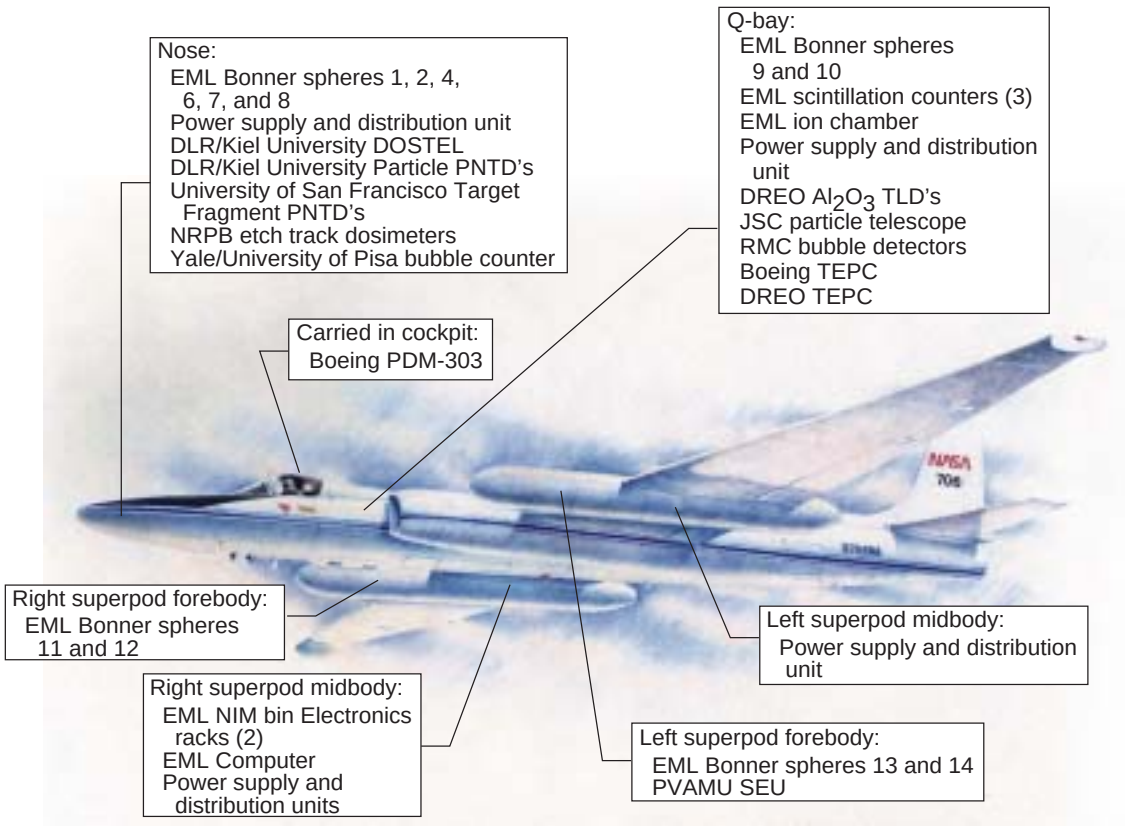

Figure 1.- Instrument Locations on the ER-2.

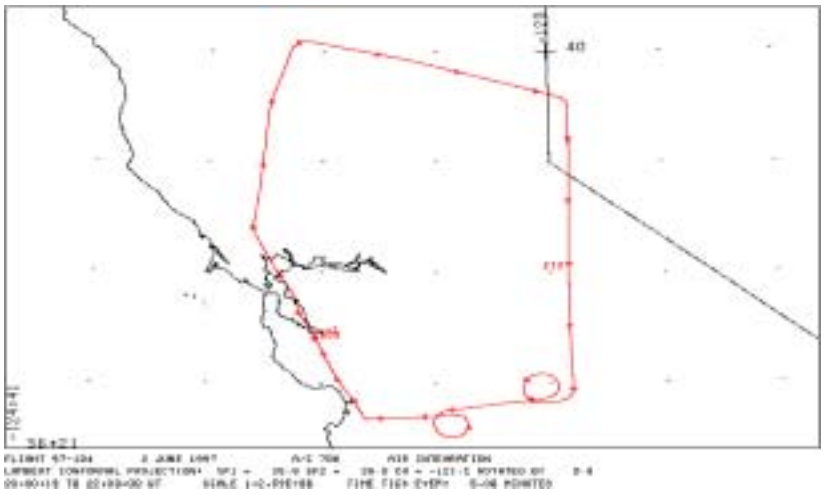

Figure 2 - Engineering Flight Ground Track

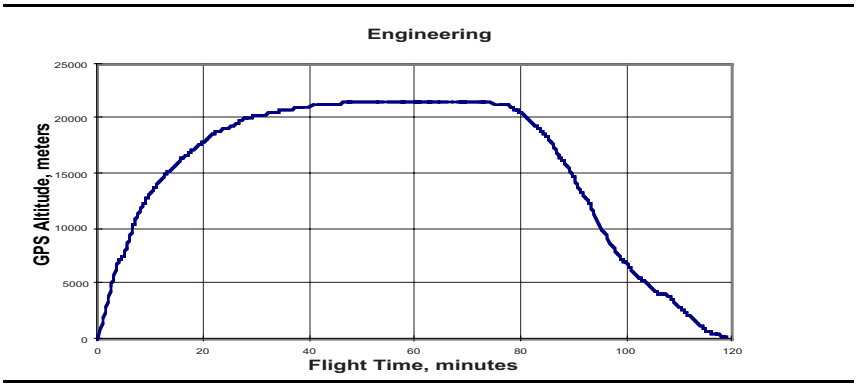

Figure 3 - Engineering Flight Altitude Profile

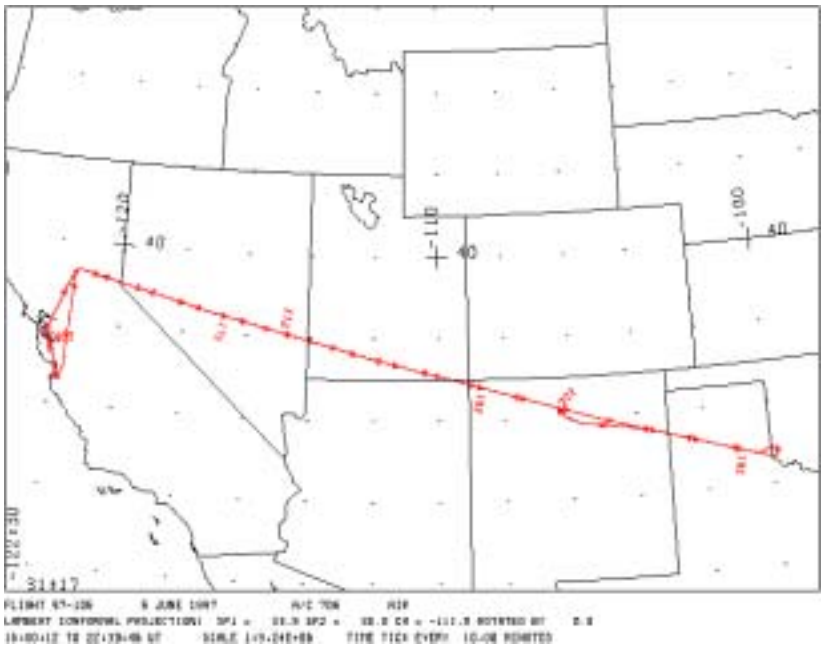

Figure 4 - East Flight Ground track

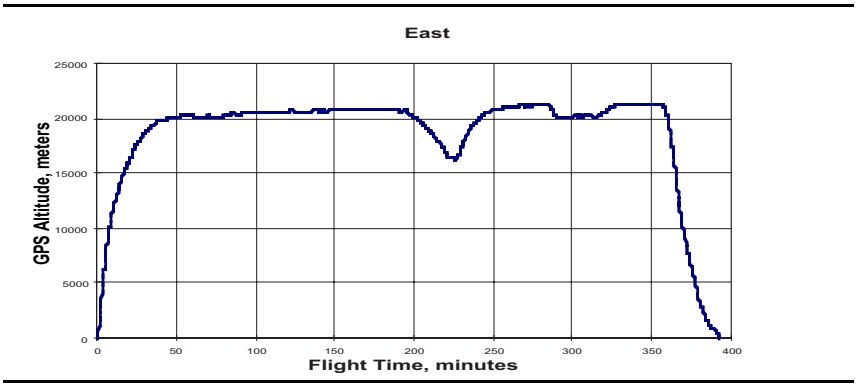

Figure 5 - East Flight Altitude Profile

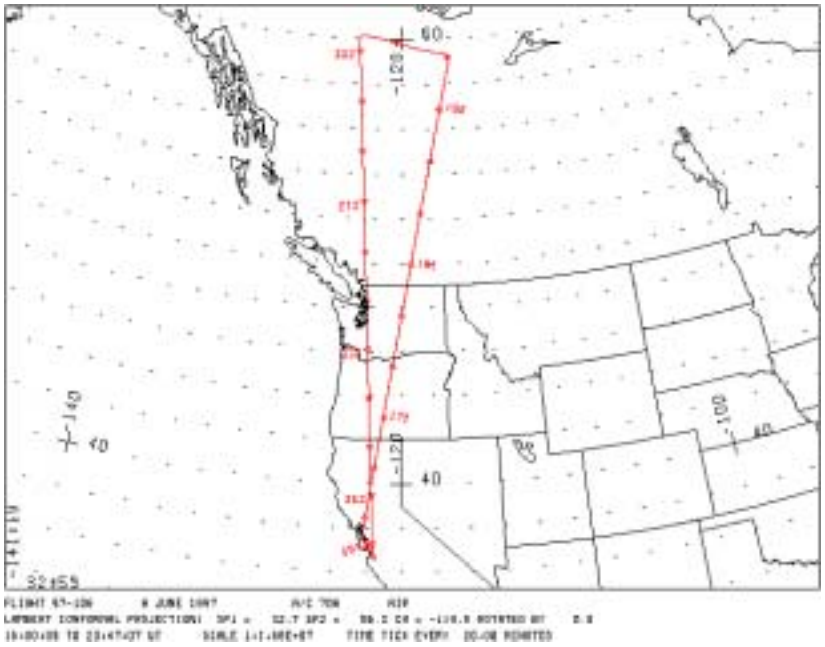

Figure 6 - North-1 Ground Track

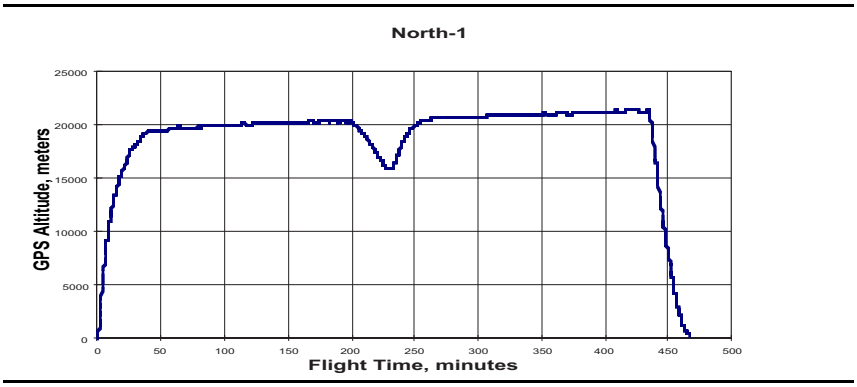

Figure 7 - North-1 Altitude Profile

Figure 8 - South-1 Ground Track

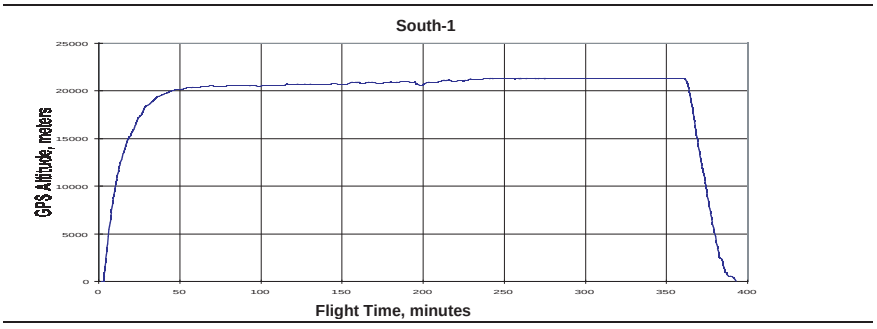

Figure 9 - South-1 Altitude Profile

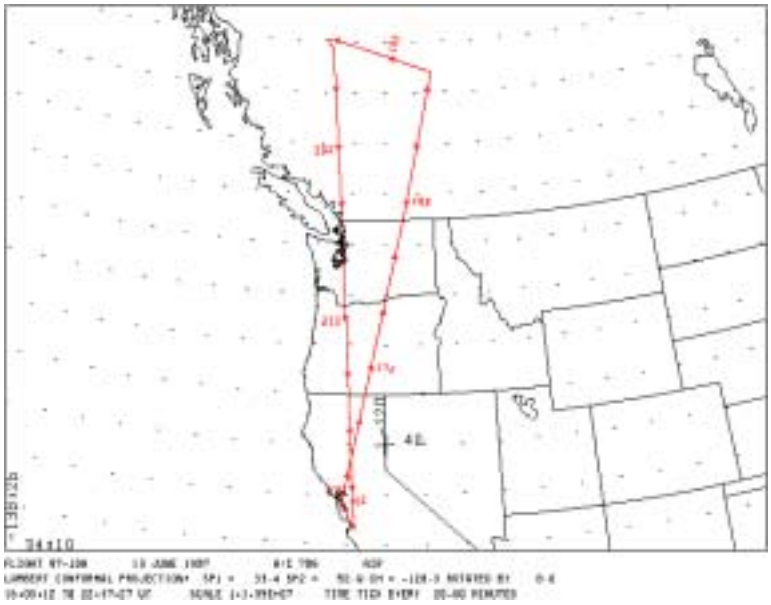

Figure 10 - North-2 Ground Track

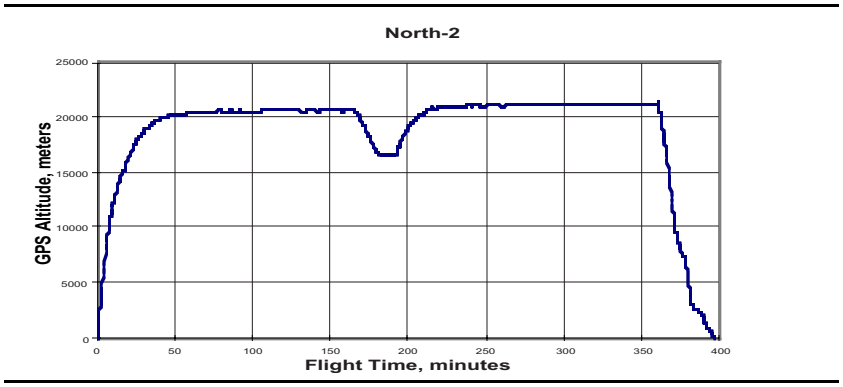

Figure 11 - North-2 Altitude Profile

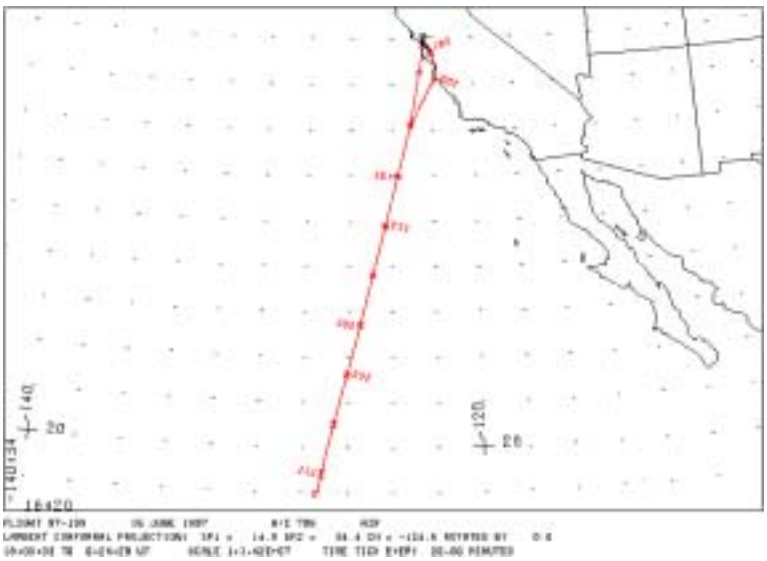

Figure 12 - South-2 Ground Track

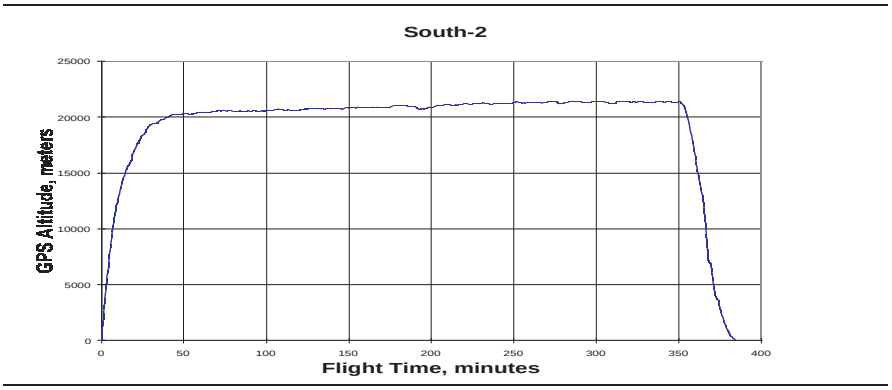

Figure 13 - South-2 Altitude Profile

Chapter 6: Preliminary Analysis of the Multisphere Neutron Spectrometer

P. Goldhagen,[1] T. Kniss,[2] J. W. Wilson,[3] R. C. Singleterry,[3] I. W. Jones,[3]
W. Van Steveninck[1]

[1]Environmental Measurements Laboratory, U. S. Department of Energy, New York, NY, 10014-4811
[2]Keithley Instruments, Inc., 28775 Aurora Road ,Cleveland, OH, 44139
[3]NASA Langley Research Center, Hampton, VA 23681-0001

Preliminary Analysis of the Multisphere Neutron Spectrometer

Abstract

Crews working on present-day jet aircraft are a large occupationally exposed group with a relatively high average effective dose from galactic cosmic radiation. Crews of future high-speed commercial aircraft flying at higher altitudes would be even more exposed. To help reduce the significant uncertainties in calculations of such exposures, the Atmospheric Ionizing Radiation (AIR) Project, an international collaboration of 15 laboratories, made simultaneous radiation measurements with 14 instruments on five flights of a NASA ER-2 high-altitude aircraft. The primary AIR instrument was a highly sensitive extended-energy multisphere neutron spectrometer with lead and steel shells placed within the moderators of two of its 14 detectors to enhance response at high energies. Detector responses were calculated for neutrons and charged hadrons at energies up to 100 GeV using MCNPX. Neutron spectra were unfolded from the measured count rates using the new MAXED code. We have measured the cosmic-ray neutron spectrum (thermal to >10 GeV), total neutron fluence rate, and neutron effective dose and dose equivalent rates and their dependence on altitude and geomagnetic cutoff. The measured cosmic-ray neutron spectra have almost no thermal neutrons, a large "evaporation" peak near 1 MeV and a second broad peak near 100 MeV which contributes about 69% of the neutron effective dose. At high altitude, geomagnetic latitude has very little effect on the shape of the spectrum, but it is the dominant variable affecting neutron fluence rate, which was 8 times higher at the northernmost measurement location than it was at the southernmost. The shape of the spectrum varied only slightly with altitude from 21 km down to 12 km (56 - 201 g cm^{-2} atmospheric depth), but was significantly different on the ground. In all cases, ambient dose equivalent was greater than effective dose for cosmic-ray neutrons.

Introduction

The earth is continually bathed in high-energy particles that come from outside the solar system, known as galactic cosmic rays. When these particles penetrate the magnetic fields of the solar system and the Earth and reach the Earth's atmosphere, they collide with atomic nuclei in air and create cascades of secondary radiation of every kind (Reitz 1993). The intensity of the different particles making up atmospheric cosmic radiation, their energy distribution, and their potential biological effect on aircraft occupants vary with altitude, location in the geomagnetic field, and time in the sun's magnetic activity cycle (Reitz 1993, Wilson 2000, Heinrich et al. 1999). The atmosphere provides shielding, which at a given altitude is determined by the mass thickness of the air above that altitude, called atmospheric depth. The geomagnetic field provides a different kind of shielding, by deflecting low-momentum charged particles back into space. The minimum momentum per unit charge (magnetic rigidity) a vertically incident particle can have and still reach a given location above the earth is called the geomagnetic vertical cutoff rigidity (or

simply cutoff) for that point. (Values of geomagnetic cutoff as a function of geographic location used in this paper are the ones used by recent versions of the CARI and LUIN codes, O'Brien et al. 1992, O'Brien 1999, Reitz et al. 1993.)

Over the past 10 years, there has been increasing concern about the exposure of air crews to atmospheric cosmic radiation (O'Brien et al. 1992, Reitz et al. 1993, Goldhagen 2000). At aviation altitudes, the neutron component of the secondary cosmic radiation contributes about half of the dose equivalent, but until recently it has been difficult to accurately calculate or measure the cosmic-ray neutron spectrum in the atmosphere to determine accurate dosimetry (Goldhagen 2000, Wilson et al. 1995, Roesler et al. 1998, Kurochkin et al 1999, Roesler et al. 2001). Dose rates from atmospheric cosmic radiation at commercial aviation altitudes are such that crews working on present-day jet aircraft are an occupationally exposed group with a relatively high average effective dose (Wilson 2000, O'Brien et al. 1992, Goldhagen 2000). Crews of future high-speed commercial aircraft flying at higher altitudes would be even more exposed (Wilson 2000).

The Atmospheric Ionizing Radiation (AIR) Project Measurements

To help reduce the significant uncertainties in calculations of such exposures, the Atmospheric Ionizing Radiation (AIR) Project, an international collaboration of 15 laboratories organized by the NASA Langley Research Center, made simultaneous radiation measurements with 14 instruments on a NASA ER-2 high-altitude aircraft (Goldhagen 2000). Of the many AIR measurements, this paper discusses only the neutron spectrometry.

The AIR ER-2 flights were scheduled for June 1997, a time of maximum galactic cosmic radiation (solar minimum), and were designed to cover as wide a range of latitude and altitude as possible within the operational capabilities of the ER-2. There were five measurement flights. Their four paths (there were two identical South flights) are shown on a map in Fig. 1. All flights originated at the NASA Ames Research Center (37.4° N, 122° W) in California and started with a northward climb. The East flight provided a long period of nearly constant radiation level by flying at constant geomagnetic cutoff. The rest of the flights measured the effects of latitude and of altitude at low geomagnetic cutoffs. The East and the two North flights included an altitude dip while flying magnetic west at constant geomagnetic cutoff, allowing measurements at altitudes from 21.3 km (70,000 ft) down to 16 km (52,500 ft). Fig. 2 shows graphs of altitude as a function of time after takeoff for three of the flights. Overall, the flights covered latitudes from 18° to 60°N, corresponding to geomagnetic vertical cutoff rigidities from 12 GV to 0.4 GV, and atmospheric depths from 50 to 110 g cm^{-2}, not including initial climb and final descent, which yield some data at lower altitudes for one latitude. Neutron spectrometry measurements were also made on the ground.

The High-Energy Multisphere Neutron Spectrometer

The primary AIR instrument was a highly sensitive extended-energy multisphere (Bonner sphere) neutron spectrometer (MNS, Thomas and Alvera 2001) designed specifically for cosmic-ray measurements (Goldhagen and Van Steveninck 1995, Tume et al. 1996). Its 14 detectors are spherical 5.08 cm-diameter ^{3}He-filled proportional

counters, with one unshielded, one surrounded with a layer of cadmium, and the rest surrounded with high-density polyethylene spheres with diameters ranging from 6.7 to 38 cm. Moderator diameters and masses for all the detectors are given in Table 1. The large cross-sectional area of the ^{3}He proportional counters and simultaneous measurement with all the detectors gives the spectrometer high sensitivity. To reduce response to thermal neutrons, all but the largest moderator spheres are surrounded with thin cadmium shells. To meet the safety requirements for flight on the ER-2, each detector, together with its high-voltage supply and preamplifier, was enclosed in a cylindrical aluminum container sealed at atmospheric pressure. Detectors were placed in all four major payload bays of the ER-2. Due to space constraints, detectors 3 and 5 were not flown.

The signal processing and data acquisition electronics and methods were similar to those described for previous MNS measurements (Goldhagen and Van Steveninck 1995, Harver and Hajnal 1993, Goldhagen et al. 1996). After passing through a preamplifier and a purpose-built amplifier (Goldhagen and Van Steveninck 1995), signals from each proportional counter were routed through one of a pair of 8-channel multiplexers to an analog to digital converter and the pulse height stored in a computer-card multichannel analyzer. Pulse-height spectra were recorded on the computer's magneto-optical disk every 60 s throughout each flight. Pulses as small as 5% of the peak pulse-height from ^{3}He(n,p)^{3}H thermal-neutron capture were recorded. During analysis, neutron capture pulses were cleanly separated from electronic noise and pulses from minimum ionizing particles by setting a software threshold at 24% of the peak pulse-height channel. The average in-flight cosmic-ray neutron count rate in the detectors was about 4 to 32 per s, allowing statistically sound spectra to be collected in a few minutes.

Even very large Bonner spheres with standard all-plastic moderators have responses that drop to low values as the energy increases from about 15 MeV to several hundred MeV (see Fig. 3, curves 8 - 12), so standard MNSs cannot be used to measure the shape of neutron spectra at energies much above 20 MeV. Following suggestions of Hsu et al. (1994) based on work by Birattari et al. (1990), the Environmental Measurements Laboratory developed high-energy detectors incorporating 1.65 cm thick metal shells within their polyethylene moderators. Detectors 13 and 14 have the same diameter moderators (30 and 38 cm) as detectors 11 and 12, but detector 13 has a 25-kg lead shell embedded in its moderator, and 14 has an 18-kg steel shell. High-energy neutrons striking the nuclei of atoms with high atomic number cause hadronic showers with easily detected secondary neutrons, creating a rising response with increasing energy (see Fig. 3, curves 13 - 14).

Detector responses as a function of energy (see Figures 3 and 4) were calculated for neutrons at energies up to 150 MeV using MCNP (version 4b, Briesmeister 1997) and MCNPX (version 2.1.5, 19-Mar-2000, Hughes et al. 1997, Waters 1999) with evaluated cross sections (Briesmeister 1997, Chadwick et al. 1997) and for neutrons, protons and charged pions from 10 MeV to 100 GeV using MCNPX with cross sections from nuclear models (see Fig. 5). The methods used with MCNP have been described previously (Goldhagen et al. 1996, Kniss 1996) and are similar to those used by Mares et al. (1991, 1997). We used a continuous distribution of incident energy, with the results grouped into 20 equal-log(E)-width bins per energy decade. The dips in response at neutron energies between 10^{-4} and 10^{-1} MeV come from nuclear resonances in the cadmium shells and aluminum surrounding the spheres. Of

the high-energy nuclear models currently available in MCNPX, we chose the Bertini model with preequilibrium from 150 MeV to 3.5 GeV and the "scaled Bertini" model above 3.5 GeV. We did not use the "Fluka model" in MCNPX because it is from an early version of the FLUKA code (Aarnio et al. 1990) which gives very different answers (Preal 1999) from more recent versions. From 10 to 150 MeV, we had a choice of results for our neutron response functions. For detectors 1-13, we chose the results from MCNPX with evaluated cross sections. For detector 14, with its steel shell, we used the results from the Bertini model starting at 70 MeV because above that energy the evaluated cross sections for iron give evaporation neutron yields higher than experimental data (fig. 24a of Mares et al. 1991). Recently, we learned of an experiment (Zucker et al. 1998) showing that the Bertini model with preequilibrium overestimates the yield of moderatable neutrons from protons on lead by about 13% at incident energies from 0.5 to 1.4 GeV. This means our response function for detector 13 may be too high by a similar amount in this energy region. The effects of the various materials surrounding each detector were included in the response calculations by modeling the entire assembly of AIR apparatus in each ER-2 payload bay. Fig. 4 shows the neutron response functions of three of the detectors with and without including the effects of nearby materials. Response decreased at low energies because of shielding effects and increased at high energies because of hadron showers in surrounding metals. We have verified our response calculations at fission energies to within 4% using measurements of a calibrated ^{252}Cf neutron source (Kniss 1996). An experiment to verify the calculated responses in the energy range 150-700 MeV has been performed at the Los Alamos Neutron Science Center, but has not yet been analyzed.

For all the larger detectors, the raw count rates must be corrected for counts caused by high-energy cosmic-ray protons and pions, which produce neutrons by nuclear interactions with the metals and carbon in the detectors and their surroundings. This requires calculating response functions for these particles as well as for neutrons and knowing their (approximate) cosmic-ray spectra. Fig. 5 compares calculated neutron, proton and charged pion response functions for detectors 9 and 13. Surrounding materials were included in the calculations. At present, the only available calculation of proton and pion cosmic ray spectra for all locations in the atmosphere is from the LUIN code (O'Brien 1999, 1978). This analytic radiation transport code relies on several approximations which are valid only above several hundred MeV, but it is still widely used (within the CARI code, O'Brien et al. 1997) for aircraft route dose calculations. There is also a recent Monte Carlo calculation of cosmic radiation in the atmosphere (Kurochkin et al. 1999) that includes proton and pion spectra at one location (at 200 g cm^{-2} above Braunschweig, Germany). We calculated the count rates that would occur in our detectors at this location assuming the charged hadron fluence spectra calculated by Kurochkin et al. and by using LUIN-99 (O'Brien 1999), and found the former to be 1.22 times the latter. To estimate the charged-hadron count rates present in the AIR MNS measurements, we used 1.11 times the proton plus pion counts predicted by the LUIN spectra at each measurement location folded with our calculated proton and pion response functions. This charged-hadron count rate was subtracted from the raw count rate to get the neutron count rate.

Once the neutron count rates and response functions of the MNS detectors are known, a deconvolution (unfolding) computer code is applied to determine the neutron spectrum. The deconvolution process is not straightforward because information in addition to the measurement and the response functions must be applied to obtain a unique

solution. We use the unfolding code MAXED (Reginatto and Goldhagen 1998, 1999, 2001), which takes into account the individual uncertainties in the detector count rates and allows for the inclusion of *a priori* information in a well defined and mathematically consistent way. The *a priori* information is in the form of an initial (default) spectrum that represents knowledge about the spectrum before the measurement is made (Reginatto and Goldhagen 1998). Since MAXED applies no smoothing, it preserves any structure in the default spectrum that is finer than the resolution of the spectrometer.

Measured Cosmic-Ray Neutron Spectra

As initial spectra for unfolding our measurements and for comparison with them, we examined available calculated cosmic-ray neutron spectra. Fig. 6a shows graphs of three calculated cosmic-ray neutron spectra for different locations in the atmosphere made by different groups (Roesler et al. 1998, Kurochkin et al. 1999, Armstrong et al. 1973) using different Monte Carlo radiation transport codes. Neutron fluence rate (neutrons cm^{-2} s^{-1}) per lethargy (the natural logarithm of energy) is plotted on the vertical axis versus neutron energy in MeV with a logarithmic scale on the horizontal axis. (Fluence rate per lethargy is equivalent to $E(d\phi/dE)$, where E is particle energy and ϕ is fluence rate.) The calculated spectra have been scaled to fit one of our measurements (see below), so they overlap and their shape can be compared. The calculated spectra all have a large "evaporation" peak centered at 1 or 2 MeV, a smaller peak at about 100 MeV, and detectable numbers of neutrons up to about 10 GeV (10^4 MeV). The spectrum of Roesler et al. (1998), calculated for 200 g cm^{-2} at 4.3 GV cutoff, shows fine structure from nuclear resonances in the nitrogen and oxygen of the atmosphere. It also has a larger ratio of high-energy neutrons to evaporation neutrons than the calculations by Kurochkin at al. (1999, 200 g cm^{-2}, 2.9 GV cutoff) and by Armstrong et al. (1973, 50 g cm^{-2}, 4.6 GV cutoff). Only the Armstrong calculation included thermal energies.

Fig. 6b shows cosmic ray neutron spectra unfolded from our MNS measurements at one location using each of the calculated spectra in Fig. 6a as the default spectrum. (The Armstrong thermal tail was attached to the other two calculated spectra before unfolding.) Except for their bin structure, the three unfolded spectra are practically identical, and we can refer to any of them as the measured spectrum. The measured spectrum is generally similar to the calculated spectra, but it has a taller evaporation-neutron peak and is lower from 10^{-4} to 0.2 MeV. The measured spectrum has a smaller 100-MeV peak than the Roesler spectrum, a wider valley between the two peaks than the Kurochkin spectrum, and almost no thermal neutrons.

When the calculated spectra are scaled (without changing their shapes, as in Fig. 6a) to fit the measured neutron count rates, the Roesler and Kurochkin spectra fit better than the Armstrong spectrum (reduced χ^2 = 9.8, 10.6, and 18.2, respectively). In the rest of the figures in this paper, we show measured spectra unfolded using the Kurochkin rather than the Roesler spectrum as the default spectrum only because the former's simpler structure facilitates visual comparisons.

The data unfolded in Fig. 6b were taken on the shorter North flight near the northern extreme of its outbound leg (54°N, 117°W, cutoff = 0.8 GV) at an atmospheric depth of 56 g cm^{-2} (20 km (65,600 ft) altitude). Over 2×10^5 neutron counts were recorded in 10 minutes. Fig. 7 shows the same measured spectrum together with a spectrum measured for 24 minutes near the southern extreme of the South 1 flight (18.7°N, 127°W, 12 GV cutoff) at almost the same atmospheric depth (53.5 g cm^{-2}, 20.3 km). The total neutron fluence rate at the northern location was 8 times the fluence rate at the southern location; the southern spectrum is shown multiplied by 8. The spectra have almost the same shape. What difference there is may be due to the lower statistics of the southern measurement and the relatively large uncertainty of the correction for charged hadrons when applied to two locations with such different geomagnetic cutoffs.

Figure 8 shows cosmic-ray neutron spectra measured at three different altitudes on the ER-2 and on the ground. The locations, atmospheric depths, and altitudes of the measurements are given in Table 2. The measurement at 56 g cm^{-2} (dotted line) is the same northern spectrum shown in Figs. 7 and 6b. At 101 g cm^{-2}, the atmospheric depth is 1.8 times greater, but the total neutron fluence rate decreased by less than 3%. The small difference between the spectral shapes at 56 g cm^{-2} and 101 g cm^{-2} is large enough to affect the ratio of dosimetric quantities to total neutron fluence. The difference is probably real, because the two measurements were taken on the same flight with nearly the same total counts and count rate at nearly the same cutoff. The difference between the spectrum measured at 201 g cm^{-2} (11.9 km, 39,000 ft) and the spectra at higher altitudes may be within our uncertainties. The measurement at 201 g cm^{-2} was taken by combining 2 minutes of data from each of 4 flights as the ER-2 rapidly climbed through normal commercial aviation altitudes shortly after takeoff (see Fig. 2). About 54,000 neutron counts were recorded in those 8 minutes. The cosmic-ray neutron spectrum measured on the ground shows a distinctly different shape, because soil reflects neutrons differently than air does. As expected, a significant number of thermal neutrons is produced in the ground. Normalized to the same total fluence rate as the in-flight measurements, the ground spectrum is lower from 10^{-6} to 2 MeV and enhanced or the same at higher energies. The data for the ground measurement shown were collected for a week and had about 2.1×10^5 neutron counts.

Dosimetric Results and Discussion

Total fluence, effective dose, and ambient dose equivalent (H*(10)) rates have been determined from the cosmic-ray neutron spectra measured at the five locations analyzed so far. The results for these integral quantities are shown in Table 2. These values are the mean of the two values obtained from measured spectra unfolded using the Roesler and Kurochkin calculated spectra as default spectra, although no integral quantity differed by more than 3.3% between the two unfolded spectra. We used the neutron fluence to effective dose (isotropic irradiation) and H*(10) conversion factors from ICRU Report 57 (1998) up to 20 and 201 MeV, respectively, and from Ferrari and colleagues (1997, 1998) above those energies. Ambient dose equivalent was always greater than effective dose. For the high-altitude spectra, neutrons with energies >10 MeV made up 24% of the total fluence rate and contributed 38-

39% of H*(10) and 68-70% of the effective dose rates. The high-energy fractions were slightly lower at 201 g cm^{-2} (22%, 36%, 66%) and higher on the ground (25%, 44%, 72%).

Ours are the first MNS measurements of cosmic-ray neutrons to make a correction for response to associated charged hadrons. Fig. 9 shows the measured neutron spectrum at 56 g cm^{-2} with and without the correction for protons and pions. The proton spectrum used for the correction is also shown. The total fluence rate of the uncorrected neutron spectrum is too high by 7%. Since all of the excess is at high energy, the uncorrected H*(10) and effective dose rates are too high by 11% and 51%. Clearly, the effect of charged hadrons should not be ignored in measurements of this kind. Since our correction for charged hadrons is based on LUIN and a calculation at one location that differs from it by 22%, the estimated uncertainty in our correction is roughly ±20%, and the propagated uncertainties in H*(10) and effective dose are ±2% and ±10%. New calculations by Roesler et al. (2001) should soon provide us with better atmospheric cosmic-ray particle spectra at several locations, which we can use for default neutron spectra in our unfolding as well as improved charged-hadron correction.

When comparing our measured cosmic-ray neutron spectra to similar measurements by others ,e.g. (Schaube et al. 1997), note that if the unfolding is cut off much below 10 GeV, especially if the effect of charged hadrons is ignored, the high-energy neutron peak can be surprisingly enlarged. Figure 9 shows a spectrum unfolded from our uncorrected data while limiting the energy to <1 GeV.

Summary and Conclusions

We summarize our results at the five locations analyzed so far as follows. At high altitude, geomagnetic latitude has very little effect on the shape of the spectrum, but it is the dominant variable affecting neutron fluence rate, which was 8 times higher at the northernmost measurement location than it was at the southernmost. The shape of the cosmic ray neutron spectrum varies only slightly with altitude from 21 km down to 12 km (56 - 201 g cm^{-2} atmospheric depth), but is significantly different on the ground. In all cases, ambient dose equivalent was greater than effective dose for cosmic-ray neutrons. These are very encouraging results for those who are modeling and measuring air crew doses. They strongly suggest that the shape of the neutron spectrum is constant everywhere commercial aircraft now fly and allow the use of relatively simple measurements of H*(10) as a conservative estimator of neutron effective dose.

Only a small sample of the AIR MNS data have yet been analyzed. With further analysis, we will have a database of cosmic-ray neutron spectra and associated dosimetric quantities at solar minimum for a wide range of latitudes at high altitude, one latitude at commercial aviation altitudes, and for several times in the solar cycle at several latitudes and altitudes on the ground. The results can be used to verify, and if necessary, correct cosmic-ray transport calculations used to determine air crew doses. In addition, the results have applications in radiation effects on microelectronics, in determining source terms for cosmogenic nuclides used for atmospheric tracers and geological dating, and in evaluation of the background radiation exposure of the world population.

Acknowledgments

This work was supported by the High Speed Research Projects Office (HSRPO) of the NASA Langley Research Center, with additional support from the U. S. Dept. of Energy. We thank D. Maiden and the rest of the HSRPO, the NASA technicians and engineers, and the ER-2 pilots, ground crew, and liaison staff for making the flights possible and successful. We thank H. Tai, J. L. Shinn, F. Hajnal, M. Sims and L. Waters and the MCNPX development team. We thank T. Armstrong, K. Copeland, W. Friedberg, V. Mares, K. O'Brien, R. Prael, S. Roesler, B. Wiegel and H. Beck for results of their calculations and valuable discussions.

References

Aarnio, P.A., et al., "FLUKA89," CERN informal report (January 2, 1990).

Armstrong, T.W., K.C. Chandler, J. Barish, J. Geophysical Res. 78 (1973) 2715.USA, 1998).

Birattari, C., A. Ferrari, C. Nuccetelli, M. Pelliccioni, M. Silari, Nucl. Instr. and Meth. A 297 (1990) 250.

Briesmeister, J.F., (Ed.) Los Alamos National Laboratory Report LA-12625-M, Los Alamos, NM, USA, 1997.

Chadwick, M.B., P.G. Young, S. Chiba, S.C. Frankle, G.M. Hale, H.G. Hughes, A.J. Koning, R.C. Little, R.E. MacFarlane, R.E. Prael, L.S. Waters, Nucl. Sci. Eng. 131 (1999) 293.

Ferrari, A., M. Pellicioni, M. Pillon, Radiat. Prot. Dosim. 71 (1997) 165.

Ferrari, A., M. Pellicioni, Radiat. Prot. Dosim. 76 (1998) 215.

Goldhagen, P., W. Van Steveninck, in: Environmental Measurements Laboratory Annual Report – Calendar Year 1994, USDOE Report EML-571, New York, NY, USA, (1995), p. 30.

Goldhagen, P., M. Reginatto, F. Hajnal, in: Proc. American Nuclear Society 1996 Topical Meeting, Radiation Protection and Shielding, North Falmouth, MA, USA, 21-25 April 1996 (American Nuclear Society, La Grange Park, IL, USA, 1996) p. 139.

Goldhagen, P., Health Phys. 78 (2000) 526.

Harvey, W.F., F. Hajnal, Radiat. Prot. Dosim. 50 (1993) 13.

Heinrich,W., S. Roesler, H. Schraube, Radiat. Prot. Dosim. 86 (1999) 253.

Hsu, H.H., K.R. Alvar, D.G. Vasilik, IEEE Trans. Nucl. Sci. 41, 4 part 1 (1994) 938.

Hughes, H.G., R.E. Prael, R.C. Little, Los Alamos National Laboratory Report XTM-RN(U)97-012, Los Alamos, NM, USA (1997).

International Commission on Radiation Units and Measurements, ICRU Report 57, (ICRU, Bethesda, Maryland,

Kurochkin, A., B. Wiegel, B.R.L. Siebert, Radiat. Prot. Dosim. 83 (1999) 281.

Kniss, T.A., Thesis, University of Akron, Akron, Ohio, USA (1996).

Mares, V., G. Schraube, H. Schraube, Nucl. Instr. and Meth. A307 (1991) 398.

Mares, V., A. Sannikov, H. Schraube, in: Proc. Third Specialist Meeting on Shielding Aspects of Accelerators, Targets and Irradiation Facilities, 12-13 May, 1997, Sendai, Japan (OECD Nuclear Energy Agency, 1997).

O'Brien, K., F. Friedberg, F.E. Duke, L. Snyder, E.B. Darden, H.H. Sauer, Radiat. Prot. Dosim. 45 (1992) 145. CARI is available at http://www.cami.jccbi.gov/AAM-600/600Radio.html

O'Brien, K., LUIN-99 code, private communication.

O'Brien, K., USDOE EML-338, update of HASL-275, New York, NY, USA (1978), available from: National Technical Information Service, Springfield, VA, USA.

Prael, R.E., private communication, 1999.

Reginatto, M., P. Goldhagen, USDOE Report EML-595, New York, NY, USA (1998). Available at http://www.eml.doe.gov/publications/reports/.

Reginatto, M., P. Goldhagen, Health Phys. 77 (1999) 579.

Reginatto, M., P. Goldhagen, S. Neumann, Nucl. Instr. and Meth. A (these proceedings) (2001).

Reitz, G., Radiat. Prot. Dosim. 48 (1993) 5.

Reitz, G., K. Schnuer, K. Shaw, eds. Proc. Workshop on Radiation Exposure of Civil Aircrew, Luxembourg, June 25-27, 1991, Radiat. Prot. Dosim. 48 (1993).

Roesler, S., W. Heinrich, H. Schraube, Radiat. Res. 149 (1998) 87.

Roesler, S., W. Heinrich, H. Schraube, Radiat. Prot. Dosim. 98 (2002) 367.

Schraube, H., A. Jakes, A.. Sannikov, E. Weitzenegger, S. Roesler, W. Heinrich, Radiat. Prot. Dosim. 70 (1997) 405.

Thomas, D.J., A.V. Alevra, Nucl. Instr. and Meth. A (these proceedings) (2001).

Tume, P., and 14 others, Proc. Amer. Nucl. Soc. 1996 Topical Meeting, Radiation Protection and Shielding, North Falmouth, MA, USA, 21-25 April 1996 (American Nuclear Society, La Grange Park, IL, USA, 1996) 68.

Waters, L.S., (Ed.) Los Alamos National Laboratory Report LA-UR 99-6058, Los Alamos, NM, USA, http://mcnpx.lanl.gov/, "MCNPX User's Manual" (1999).

Wilson, J.W., J.E Nealy, F.A. Cucinotta, J.L. Shinn, F. Hajnal, M. Reginatto, P. Goldhagen, NASA Technical Paper 3524 (1995) (National Technical Information Service, Springfield, Virginia).

Wilson, J.W., Health Phys. 78 (2000) 470.

Zucker, M.S., N. Tsoupas, P.E. Vanier, U. von Wimmersperg, S.F. Mughabghab, E. Schmidt, Nucl. Sci. Engineering 129 (1998) 180.

Table 1. Detector Moderator Diameters and Masses

Detector No.	Outside Diameter (in.)	Outside Diameter (cm)	Mass of Polyethylene (kg)	Mass of Converter Shell (kg)
1 (bare)	-	-	-	-
2 (Cd)	-	-	-	-
3[a]	2.620	6.66	0.0773	-
4	3.234	8.21	0.2021	-
5[a]	3.849	9.78	0.3893	-
6	4.626	11.75	0.7306	-
7	5.626	14.29	1.3845	-
8	6.814	17.31	2.521	-
9	8.232	20.91	4.478	-
10	9.830	24.97	7.680	-
11	11.846	30.09	13.481	-
12	14.974	38.03	27.305	-
13	11.848	30.09	11.262	25.225 Pb
14	15.030	38.18	25.395	17.917 Fe

[a]Not flown because of ER-2 space constraints.

Table 2. Neutron Integral Quantities Measured at Various Locations

Geographic Location	Cutoff (GV)	Atmospheric Depth (g cm^{-2})	Altitude (km)	Altitude (ft)	Neutron Fluence Rate (cm^{-2} s^{-1})	Effective Dose Rate (μSv h^{-1})	H*(10) Rate (μSv h^{-1})
19°N, 127°W	12	53.5	20.3	66,500	1.28	0.91	1.06
54°N, 117°W	0.8	56	20.0	65,600	10.2	6.9	8.5
56°N, 121°W	0.7	101	16.2	53,300	10.0	6.2	7.8
38°N, 122°W	4.5	201	11.9	39,000	3.4	2.1	2.7
37°N, 76°W	2.7	1030	0	0	0.0122	0.0083	0.0093

Fig. 1. Flight paths of the AIR measurement ER-2 flights.

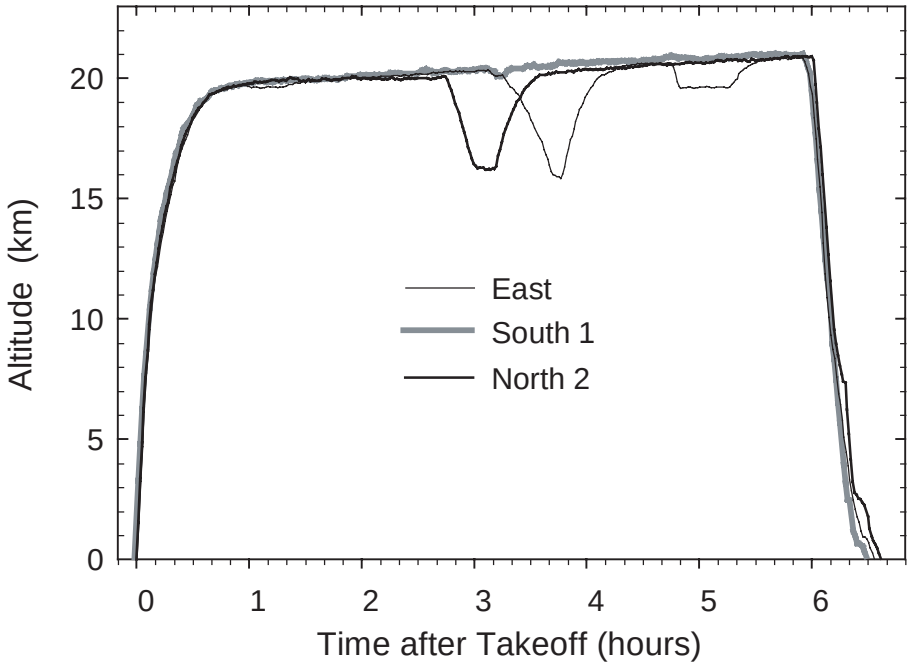

Fig. 2. Altitude as a function of time during three of the flights.

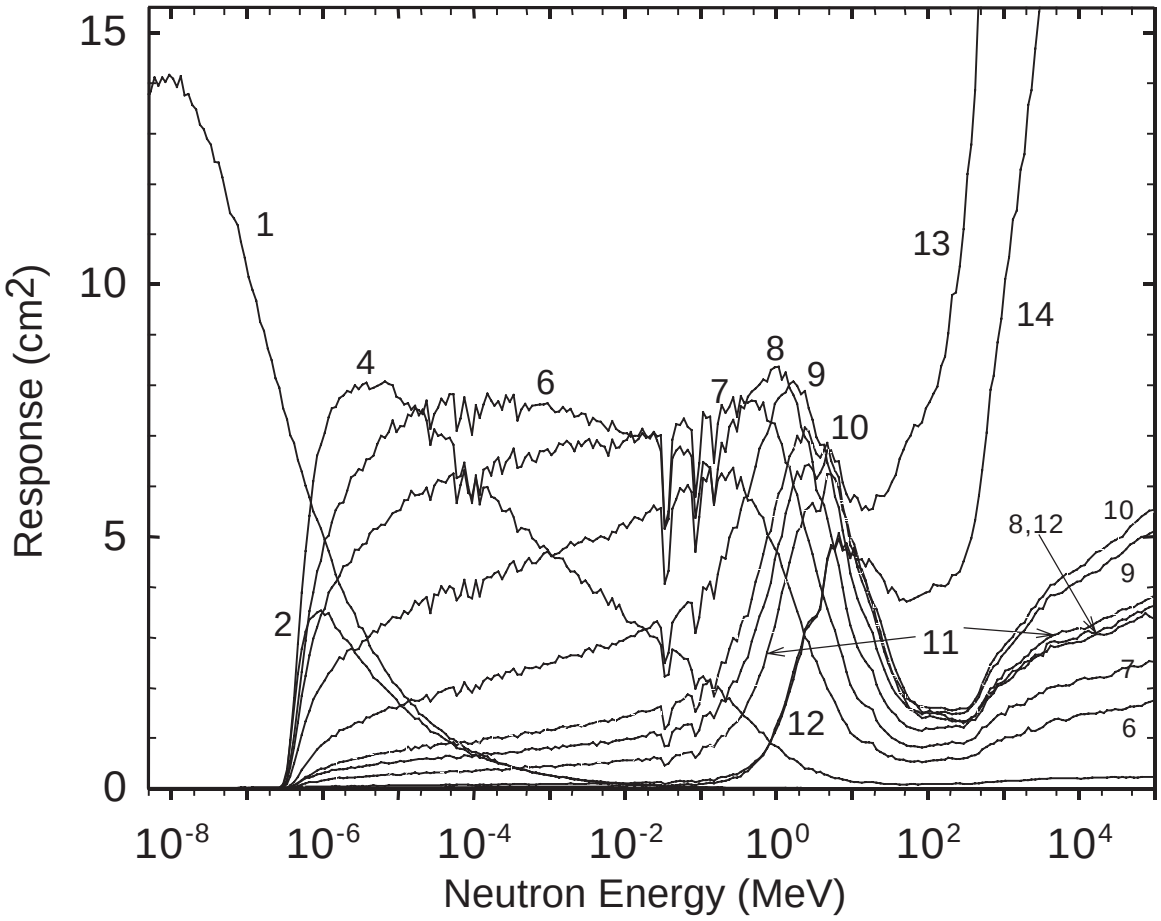

Fig. 3. Calculated neutron response functions for each of the detectors of the EML high-energy multisphere spectrometer. The curves for detectors number 10 and 11 are dashed only to help visually distinguish them from nearby curves.

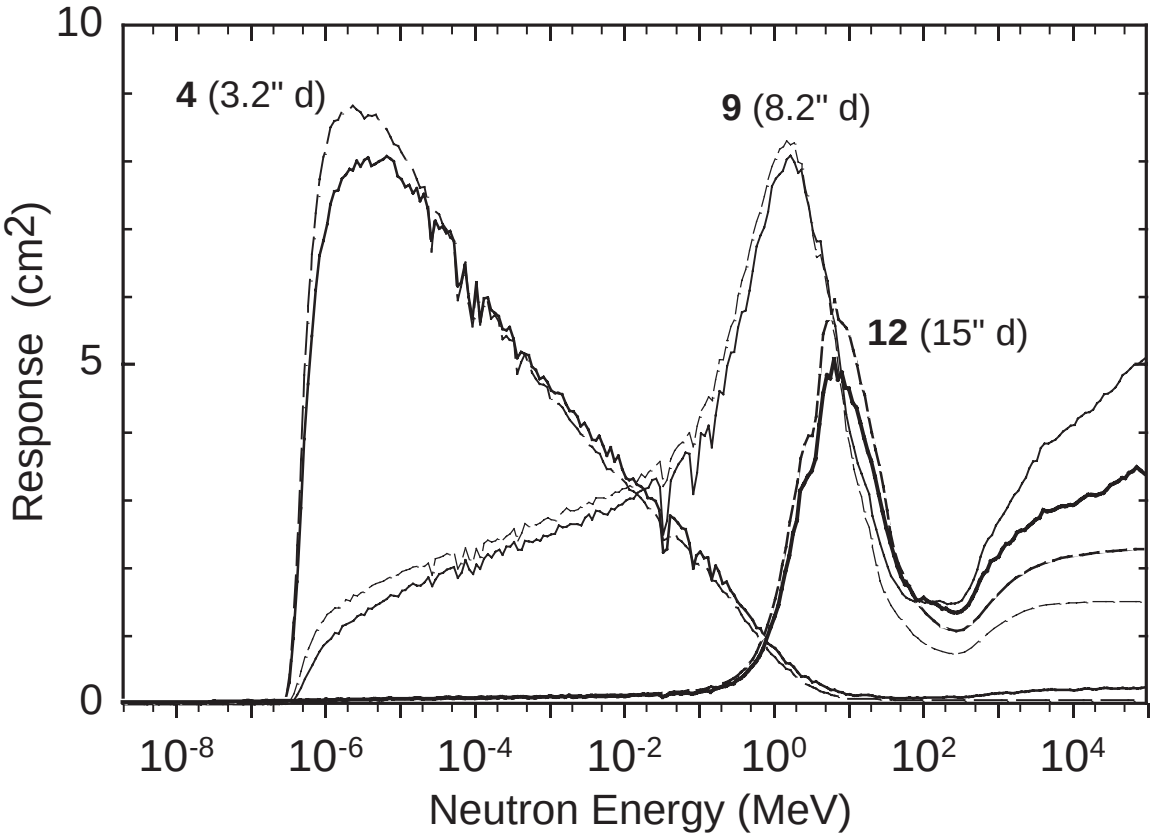

Fig. 4. Calculated neutron response functions for a small, medium and large detector of the MNS with (solid curves) and without (dashed curves) including the containers, other detectors and surrounding materials in the response calculation.

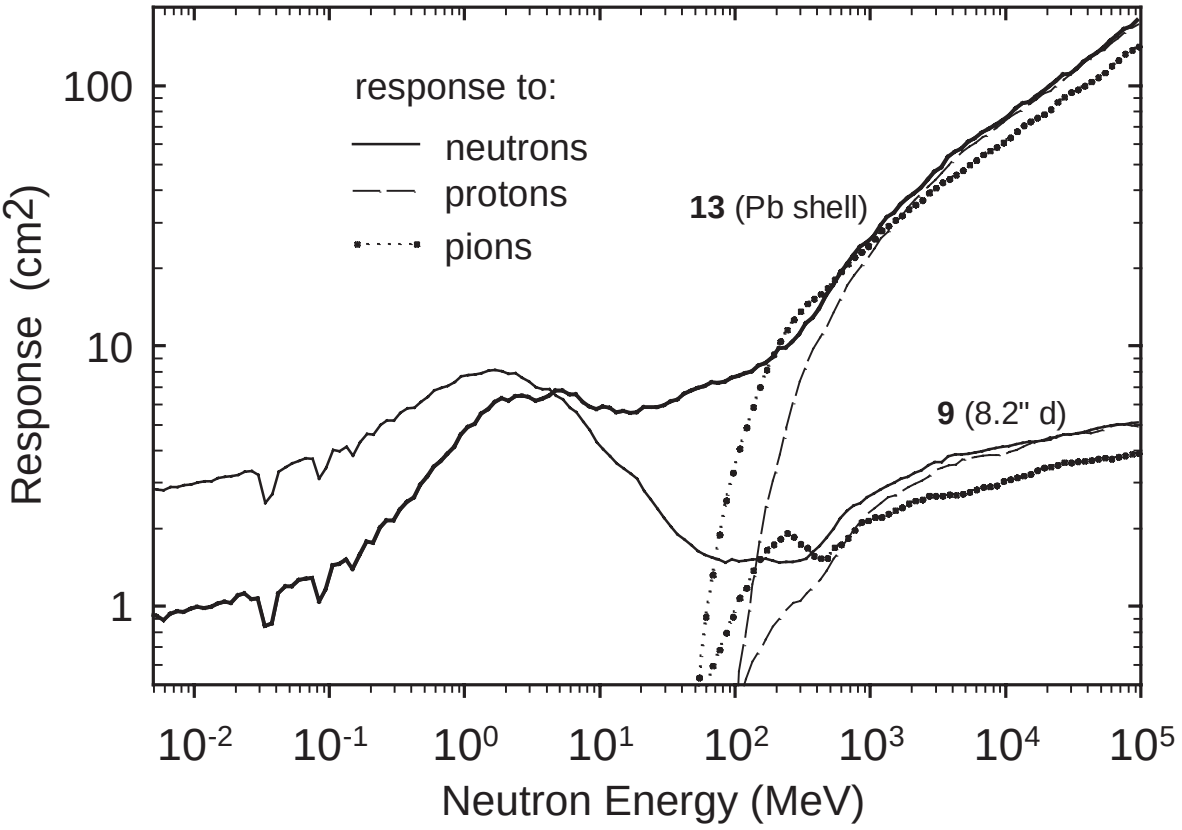

Fig. 5. Calculated neutron, proton and charged pion response functions for detectors 9 (8.2” diameter moderator) and 13 (11.8” moderator with 25 kg embedded lead shell). Surrounding materials were included in the calculations.

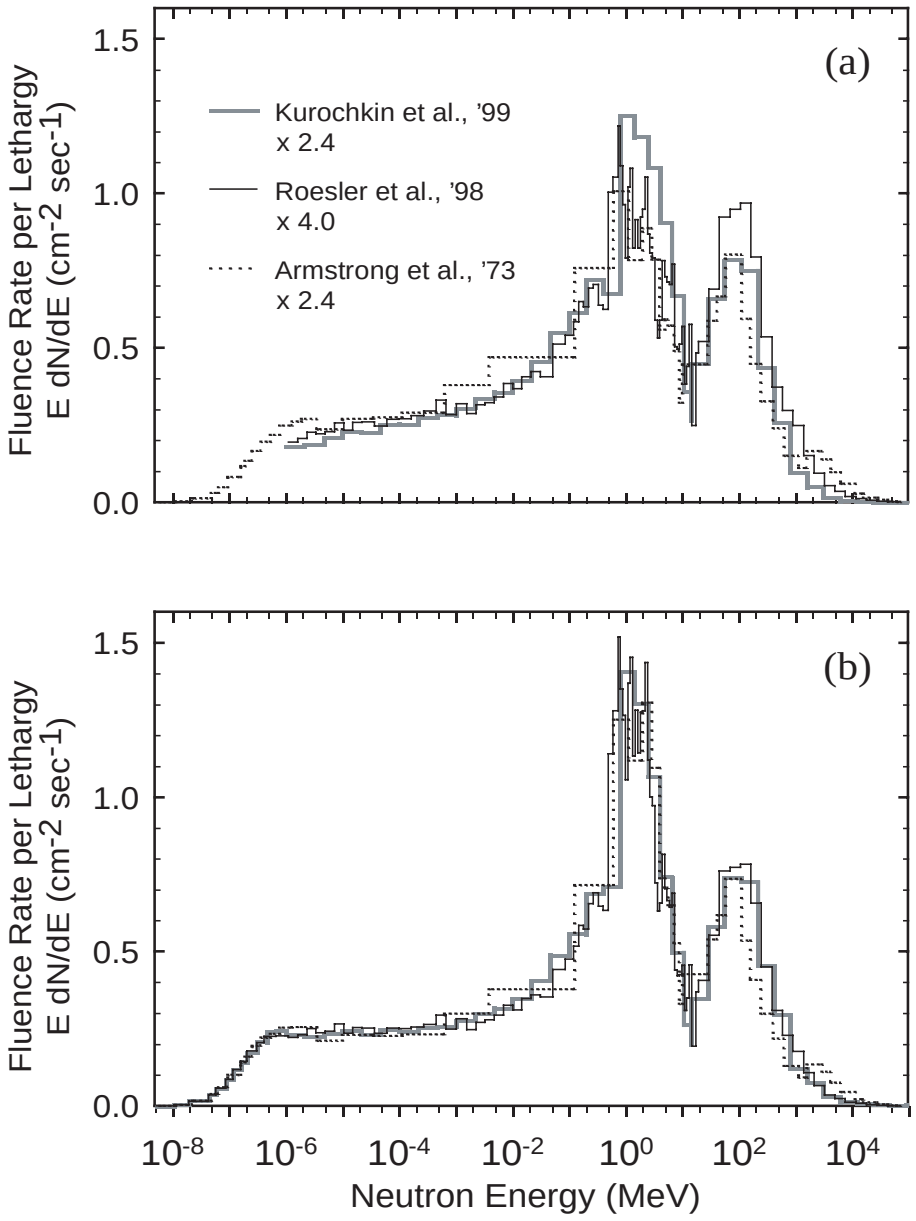

Fig. 6. (a) Three calculated cosmic ray neutron spectra [9-10, 33] used as default spectra in unfolding the measured spectra. The calculated spectra are shown scaled to give the best fit to the data used to unfold the spectra in (b). (b) Cosmic ray neutron spectra unfolded from measurements at high altitude and high northern latitude (56 g cm^{-2} atmospheric depth, 20 km altitude; 54°N, 117°W, 0.8 GV geomagnetic cutoff) using each of the calculated spectra in (a) as the default spectrum.

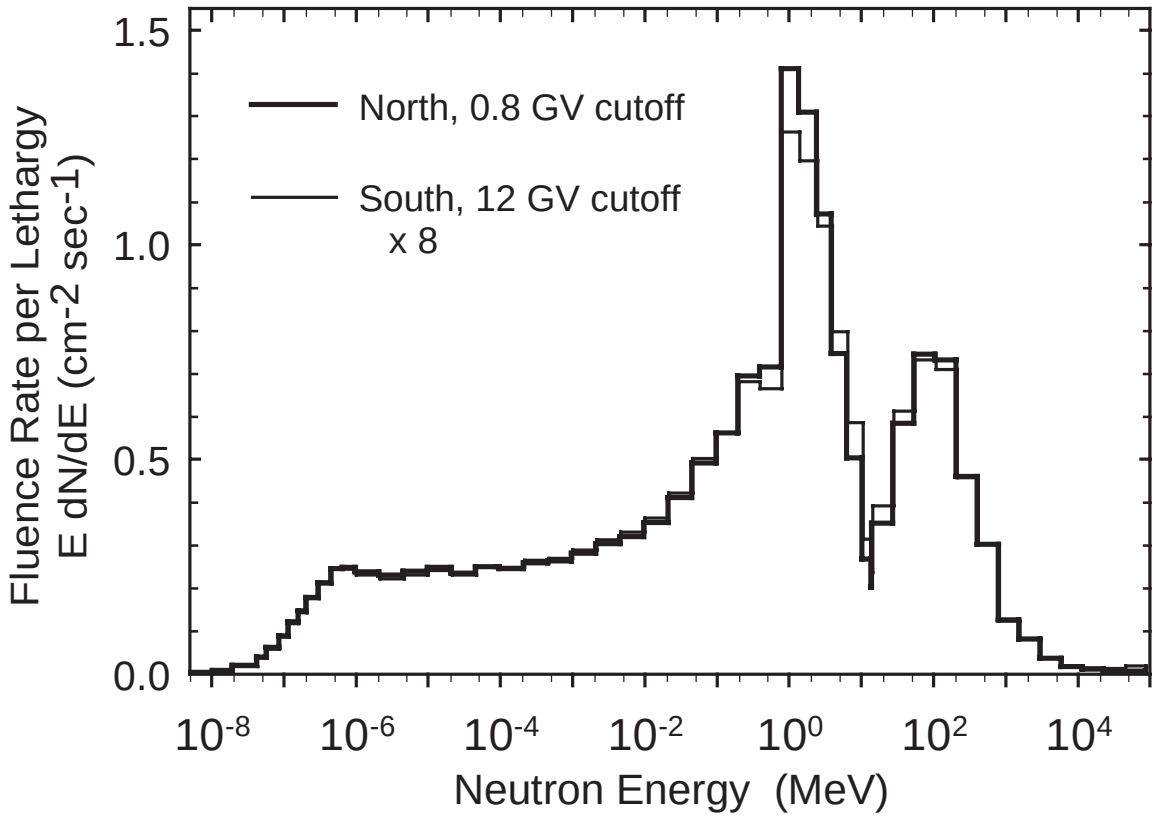

Fig. 7. Cosmic-ray neutron spectra measured at the same northern location as in Fig. 6b and at the south end of the South-1 flight (19°N, 127°W, 12 GV cutoff; 54 g cm^{-2} atmospheric depth). The south spectrum is shown multiplied by 8.

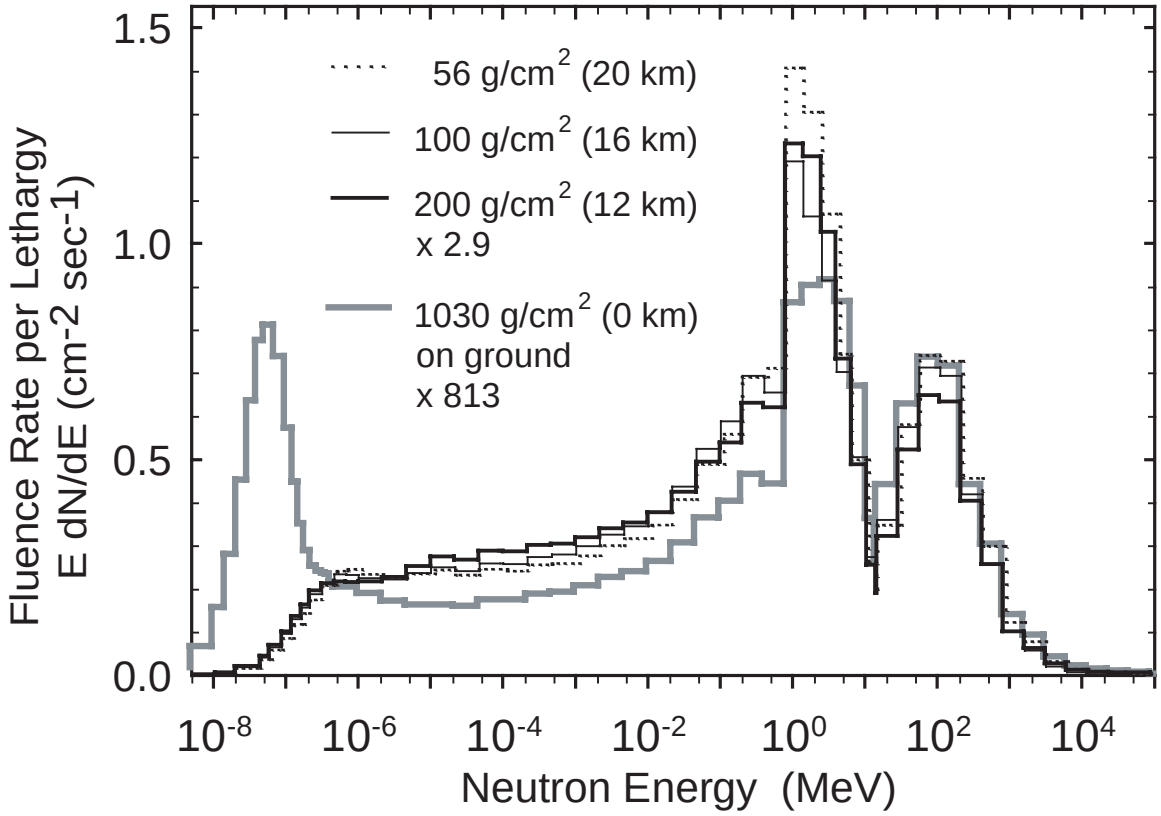

Fig. 8. Comparison of cosmic-ray neutron spectra measured at different atmospheric depths (altitudes) during the ER-2 flights and on the ground at sea level.

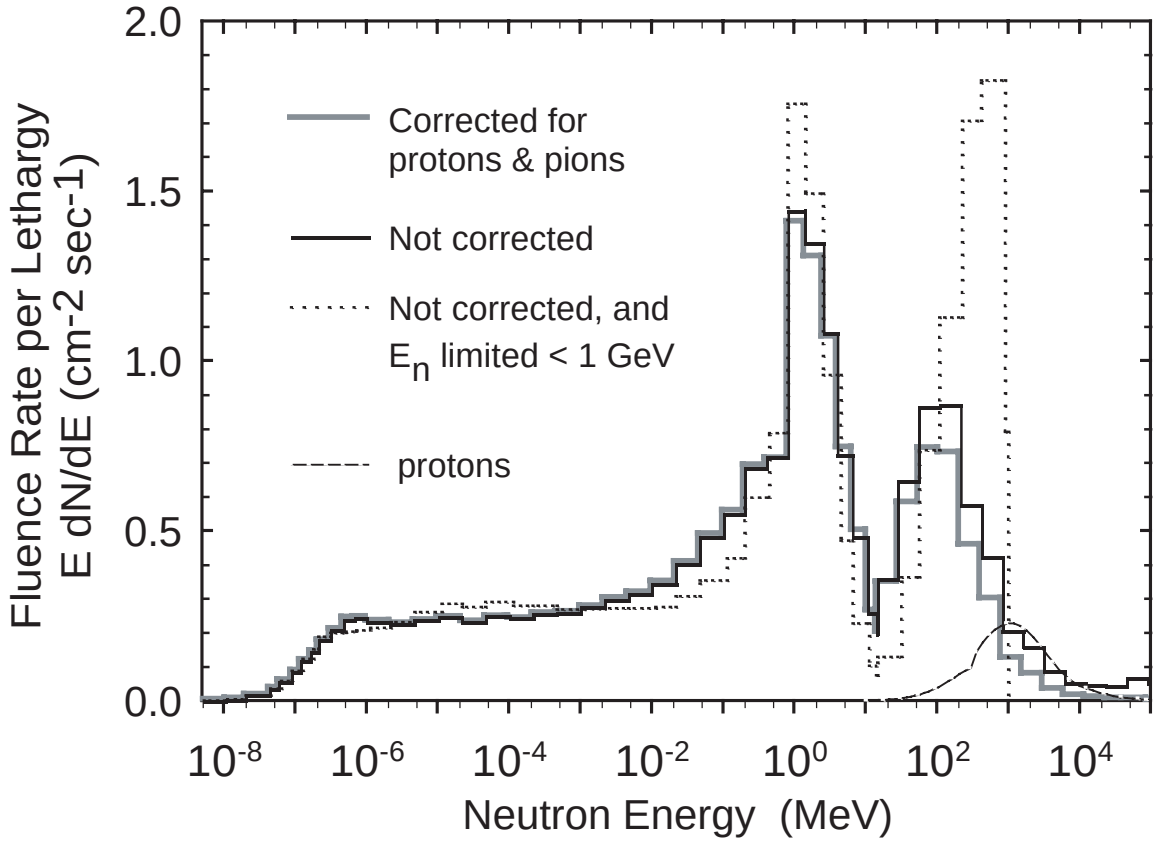

Fig. 9. Measured cosmic ray neutron spectra before and after making the correction for counts caused by protons and pions. The proton spectrum used to make the correction is also shown, as is the effect of limiting the maximum neutron energy to 1 GeV.

Chapter 7: Post-flight Analysis of the Argon Filled Ion Chamber

H. Tai*, P. Goldhagen, I. W. Jones*, J. W. Wilson*, D. L. Maiden*, J. L. Shinn***

***NASA Langley Research Center, Hampton, Virginia 23681-0001**

****DOE Environmental Measurements Laboratory, New York, NY 20014**

Atmospheric Ionizing Radiation (AIR) ER-2 Stratospheric Measurements Post-flight Analysis: The Argon Filled Ion Chamber

Preface

Atmospheric ionizing radiation is a complex mixture of primary galactic and solar cosmic rays and a multitude of secondary particles produced in collision with air nuclei. The first series of Atmospheric Ionizing Radiation (AIR) measurement flights on the NASA research aircraft ER-2 took place in June 1997. The ER-2 flight package consisted of fifteen instruments from six countries and were chosen to provide varying sensitivity to specific components. These AIR ER-2 flight measurements are to characterize the AIR environment during solar minimum to allow the continued development of environmental models of this complex mixture of ionizing radiation. This will enable scientists to study the ionizing radiation health hazard associated with the high-altitude operation of a commercial supersonic transport and to allow estimates of single event upsets for advanced avionics systems design. The argon filled ion chamber representing about 40 percent of the contributions to radiation risks are analyzed herein and model discrepancies for solar minimum environment are on the order of 5 percent and less. Other biologically significant components remain to be analyzed.

Introduction

The AIR ER-2 flight measurements are part of a program established by the High-Speed Research (HSR) program to study the radiation risk associated with the high-altitude flight operation of a commercial supersonic transport (Foelsche et al. 1974, FAA 1975, Schaefer 1968). This program also includes the development of an AIR predictive code, and a national assessment of the radiation health hazard associated with high altitude flight. The High Speed Research Project Office (HSRPO) at the Langley Research Center has been delegated the responsibility by NASA Headquarters, Washington DC, to develop key technologies to enable the development of an economically viable and environmentally acceptable High Speed Civil Transport (HSCT, a supersonic airliner) by the year 2005. The leading candidates for the new HSCT supersonic transport is a Mach 2.4 configuration which will cruise efficiently at altitudes between 18 to 20 kilometers. Marketing networks show about 60% of HSCT operations will occur at northern geomagnetic latitudes. Because of the high-altitude at cruise and predominately northern-latitude operating networks, the aircraft is less protected from the natural environment of galactic and solar cosmic rays. Thus arises the need to access the possible high-altitude radiation health hazard to which the HSCT crew and passengers will be subjected (O'Brien and Friedberg 1994). The National Council on Radiation Protection and Measurements (NCRP) recommended that a program be established to reduce the uncertainties in risk estimates for high altitude flight to levels comparable with those of ground based occupational exposure risks (1993, 1995).

Hazardous radiation comes in two forms: non-ionizing, (ultraviolet, infrared and microwave) and ionizing, (gamma, x-rays, and subatomic particles). Both types are dangerous because of their adverse biological effects when they pass through body tissue. At flight altitudes, cosmic radiation consists of high-energy subatomic particles, originating for the most part outside the solar system, which collide with and disrupt atoms of nitrogen, oxygen, and other constituents of the atmosphere. Additional subatomic particles are produced from these collisions. The particles from beyond the solar system and their secondary particles produced in the atmosphere are referred to collectively as galactic cosmic radiation. Another source of in-flight ionizing radiation is solar cosmic radiation, which arises primarily from solar particle events (resulting from coronal mass ejection). Although charged particles are continuously being ejected from the sun, they are usually too low in energy to contribute to the radiation level at flight altitudes. However, on infrequent and unpredictable occasions, the numbers and energies of ejected solar particles are high enough to increase substantially the dose rate at these altitudes. The understanding of such complex radiation environment at high altitudes requires a diverse array of instruments that are not available at any one laboratory. A national and international collaboration has been devised to ensure that the environmental components are adequately covered within a reasonable budget with existing instrumentation and within the payload requirements of the NASA ER-2 aircraft. The (AIR) ER-2 flight measurements took place from June 2 to June 15, 1997. There were a total of five science mission flights (ER-2 Sortie 97-105 to 97-109) and one engineering flight (flight 97-104) flown. A total of 37.2 hours of airtime were logged. Instruments on board were selected based the recommendations by the National Council on Radiation and Protection (NCRP) (1995) to help provide a basis for radiation monitoring during high altitude operations of the ER-2 aircraft. This whole airborne campaign is coordinated by the National Aeronautics and Space Administration Langley Research Center (NASA/LaRC) in collaboration with the US Department of Energy (DOE), Environmental Measurements Laboratory (EML); the NASA Johnson Space Center; the German Aerospace Research Establishment (DLR); Canadian Royal Military College (RMC); Canadian Defense Research Establishment Ottawa (DREO); UK National Radiological Protection Board (NRPB); the Boeing Company; the University of Pisa, Italy; the University of San Francisco, California; the National Institute of Occupation and Health (NIOSH); and the Federal Aviation Agency (FAA), Civil Aeromedical Institute. The flight package placement on the ER-2 aircraft is shown in figure 1.

AIR Model Version 0

The AIR model version 0 is the parametric fit to data gathered by the Langley Research Center studies of the radiation at SST altitudes in the years 1965 to 1971 covering the rise and decline of solar cycle 20. Scaling of the data with respect to geomagnetic cutoff, altitude, and modulation of the Deep River Neutron Monitor was found to allow mapping of the environment to all locations at all times resulting in an empirically based model named AIR model Version 0 (Wilson et al. 1991). The basic data consisted of tissue equivalent ion chamber rates, fast neutron spectrometer, and nuclear emulsion detection of nuclear reaction products in amino acids (gel). The model was based on global surveys with airplane and balloons.

The latitude surveys by balloons and aircraft are shown for the transition maximum in figure 2. The curves in the figure are our approximation to the data and given by

$$\phi(x,R,C) = f(R,C) \exp(-x/\lambda) - F(R,C) \exp(-x/\Lambda) \quad (1)$$

where

$$f(R,C) = \exp(250/\lambda)\ \phi_s\ (R,C) \quad (2)$$

$$F(R,C) = (\Lambda/\ \lambda)\ f(R,C) \exp(x_m/\ \Lambda - x_m/\ \lambda) \quad (3)$$

and

$$\Lambda = \lambda\ [\ 1 - \phi_m(R,C) \exp(x_m/\lambda)/f(R,C)] \quad (4)$$

where the transition maximum altitude x_m corresponds to

$$x_m = 50 + \ln\{2000 + \exp[-2(C-100)]\} \quad (5)$$

$$\phi_s\ (R,C) = 0.17 + [0.787 + 0.035\ (C - 100)] \exp(-R^2/25)$$
$$+ \{-0.107 - 0.0265\ (C-100)$$
$$+ 0.612 \exp[(C - 100)/3.73]\}\exp(-R^2/139.2) \quad (6)$$

$$\phi_m(R,C) = 0.23 + [1.1 + 0.167\ (C-100)] \exp(-R^2/81)$$
$$+ \{0.991 + 0.0501\ (C - 100)$$
$$+ 0.4 \exp[(C - 100)/3.73]\}\ \exp(-R^2/12.96) \quad (7)$$

In the above equations, R is the local cutoff rigidity (in units of GV) and C is the high-latitude neutron monitor count rate in percent of maximum. At depths below 250 g/cm^2, the neutrons attenuate with attenuation length (g/cm^2) given by

$$\lambda = 160+ 2\ R \quad (8)$$

The neutron environment model is shown in figure 2 in comparison to experimental measurements. The flux from 1-10 MeV is converted to dose equivalent and dose rates using 3.14 μSv-(cm^2/s)/hr and 0.5 μGy-(cm^2/s)/hr respectively. They are based on older dosimetric relations as described in Foelsche et al. (1974) using the ICRP 26 quality factor. The use of the ICRP 60 quality factor would increase the neutron dose equivalent by about 55 percent.

Unfortunately not all ion chamber data or all nuclear emulsion data were reduced. For our purpose we use the argon-filled ion chamber data to represent the altitude, latitude and solar cycle dependence of dose from all components except neutrons and use the available tissue equivalent ion chamber data as a guide. The ion chamber data of Neher and Anderson compiled by Curtis et al at the 1965 solar minimum (C = 98.3) in table 1 and the 1958 solar maximum (C = 80) in table 2. We have augmented the table with data from the work of Neher and Anderson. We note that the low-energy GCR had not fully recovered in the summer of 1965 with the result that the high-latitude ionization at high altitude is about 10 percent lower than that in 1954. Furthermore, the 1958 measurements near solar maximum covered only mid to high latitudes, and the low-latitude data in table 2 are likely to be about 10 percent too high at high altitudes. The ionization rates in tables 1 and 2 are the rates in air per atmosphere of pressure (directly related to the exposure unit Roentgen). The atmospheric ionization rates are interpolated in altitude, geomagnetic cutoff, and solar modulation and directly converted to exposure units and absorbed dose in tissue. The comparison with the tissue equivalent ion chamber requires the addition of the neutron absorbed dose rates and good consistency between this method and the tissue equivalent ion chamber has been demonstrated. Dose equivalent estimates require an estimate of the high LET components associated with charged particles and are found from the measurements in nuclear emulsion as shown in elsewhere. The corresponding average quality factor for the argon ion chamber dose is found to be

$$Q = 1+ 0.35 \exp(-x/416) - 0.194 \exp (-x/65) \quad (9)$$

This quality factor is to be applied only to the dose component derived from the argon ion chamber only. The approximate average quality factor (9) was fit to data at high latitudes and high altitudes and is a source of uncertainty elsewhere in the atmosphere.

Flight Trajectory and AIR Model Predictions

All ER-2 flights originated from Moffett Field, CA. In Fig. 3, a map of the ground track of the scheduled flights (flights code ER2 Sortie 97-105 to 97-109) are shown superimposed with radiation contours predicted by the AIR model.

Aside from the scientific data recorded by the instruments aboard the ER-2 plane that may take some time to get analyzed, the portion of navigation data, however are readily available. This important navigational information was recorded by on-board ER-2 instruments every second during the whole length of flight. This information consists of position (latitude and longitude), altitude (actually the atmospheric depth), pressure, heading, yaw and rolling angle, and ambient temperature. For analysis we need only selected data at every minute. What we have done is either choose the middle value or take the averaged value over the whole minute. They are not expected to differ significantly. In the following tables and graphs, average values are used. The science flight trajectory data and the corresponding AIR model values are given in an appendix.

Flight 97-104: This was approximately a two-hour, engineering flight required by the ER-2 operations office with pilot's choice of flight path (typically a race track around the home base). The aim is to check aircraft operational characteristics, and all aircraft and experimental instrumentation to assure everything is operating satisfactorily prior to the acquisition of science measurements.

Flight 97-105: This was approximately a six & one-half hour flight starting on June 5 at 15:50 on prescribed northern and easterly headings and return to home base over the reverse flight path. The aim for this flight was to determine if radiation measurements are being affected by the shielding characteristics of on-board aviation fuel, determine consistency of instrument readings, and take science data as a function of altitude along a constant-radiation, geomagnetic latitude line. The flight began at (37°24' N, 122°6' W) with a climb out of Moffett Field to the location (39°19'49" N, 121°27' W) where a easterly turn was executed (fig. 4 to 6) and continue to climb to cruise altitude near Wine Glass where the altitude was held constant at 20 km for about 20 minutes (fig. 6). Minor midcourse corrections were made to maintain a constant geomagnetic cutoff trajectory as shown in figure 7. A U-turn was made at (34 ° 39' N, 100 ° W) followed by a slow descent (500 ft/min) near Amarillo to 52,000 ft. which was maintained for 10 minutes. The pilot then climbed to normal cruise altitude along the prescribed flight path repeating the ground track on the return to Wine Glass making necessary course corrections to maintain constant geomagnetic cutoff. There was a thunder storm over north central New Mexico which had to be avoided on the return trip as seen in figure 3. Before reaching Wine Glass the pilot descended to the 20 km altitude as on the outbound trip and maintained that altitude for about 30 minutes. This was followed by return to cruise altitude and ending the flight by decent to Moffett Field. The model geomagnetic cutoff, dose equivalent, dose, 1-10 MeV neutron fluence rates are shown in figures 7 to 11.

Since the flight 97-105 was designed to fly parallel to geomagnetic latitude for the major leg (easterly heading and reverse), Fig. 7 shows the magnetic cut-off value was a horizontal straight line about 3.92-3.95 GV. Fig. 8 and 9 show the predictions for dose equivalent rate and dose rate from AIR model. Keep in mind that those rate values are a complicated function of flight coordinates as well as the altitude and other factors. Based on the figures, clearly the altitude factor alone suggests that the rate can change 12~15% from 16 km to 20 km in altitude. The AIR model predicts the neutron flux whose energy range is 1-10 MeV in Fig. 10 and air ionization rate in Fig. 11 along the flight path for this flight. That is, the AIR model predicts an altitude variation in the 1-10 MeV neutron flux of about 12 percent and in the air ionization rate of 11 percent at the approximate 3.935 GV cutoff.

Flight 97-106: This was approximately an eight hour flight on June 8 beginning at 15:52 on prescribed northern, western and southern headings. The aim was to obtain radiation measurements as a function of geomagnetic latitude to as far north as possible with an altitude excursion along a constant-radiation, geomagnetic latitude line at the extreme northern latitude location. The flight (fig. 3) began at (37 ° 24' N, 122 ° 6' W) with a climb out of Moffett Field and ascent to cruise altitude (fig. 12 to 14). Cruise to point near Ft. Nelson (59 ° 00' N, 116 ° 00' W) and turned west along constant geomagnetic cutoff trajectory (fig.

15) held altitude fixed (fig. 14) for 5 minutes after the west turn then executed a medium-rate descent (750 ft/min) to 52,000 ft. and maintained that altitude for 5 minutes (fig. 14). At location (60 ^{o} 00' N, 123 ^{o} 40' W) the aircraft turned south (toward Moffett Field) and ascended to cruise altitude until the decent at Moffett Field. The model geomagnetic cutoff, dose equivalent, dose, 1-10 MeV neutron fluence rates are shown in figures 15 to 19.

The purpose for this flight was to obtain radiation measurements as a function of geomagnetic latitude to as far north as possible with an altitude excursion along a constant-radiation, geomagnetic latitude line at the extreme northern latitude location. Fig. 13 shows that at the extreme northern latitude, magnetic cut-off values of 0.42-0.44 GV were achieved where the altitude survey was performed. Comparing Fig. 14-16 with Fig. 6-9, for the flight 97-106 route, the AIR model predicts much higher radiation values than for the flight 97-105 route. In other words, Flight 97-106, in a sense from the radiation safety point of view, flies a less safe route than flight 97-105 which was expected. The altitude survey at approximately 0.43 GV shows a variation on the order of 11 percent in 1-10 MeV neutron flux and 23 percent for the air ionization rate. Since the primary purpose of flight 97-106 was to perform a latitude survey, we see that the high altitude variation in the environment during the cruise portion of the flight along the northern path is 32 percent in the 1-10 MeV neutron flux and 33 percent in the air ionization rate reflecting the nearly factor of ten variation in geomagnetic cutoff during the flight.

Flight 97-107: This was approximately a six & one-half hour flight starting on June 11 at 15:53 on a prescribed southerly heading over the North Pacific ocean (fig. 3). The trajectory was chosen to be approximately normal to the lines of constant geomagnetic cutoffs to maximize the dynamic range of the radiation variation. At the position Latitude 17 deg N, longitude 127 deg 28 min W, the pilot executed a 180 degree turn and returned to base (fig. 20 to 22). The aim of the mission was to obtain radiation measurements as a function of geomagnetic latitude to as far south as reasonably possible and geomagnetic cutoffs of 4.5 to 12.2 GV were obtained (fig. 23). Once altitude was achieved, the environmental quantities declined to nadir at the southern most latitudes as seen in figures 24 to 27. An altitude survey was not attempted since model predictions estimated only a few percent variation in decent to 52,000 ft.

Flight 97-108: This was approximately a six and one-half hour flight starting June 13 at 15:52 on prescribed northern, western, and southern headings similar to flight 105 (fig. 3). The aim was to approximately repeat the radiation measurements as a function of geomagnetic latitude to as far north as possible with altitude excursions along a constant-radiation, geomagnetic latitude line near Edmonton, Canada. The flight (fig. 28 to 30) started at (37 ^{o} 24' N, 122 ^{o} 6' W) with a climb out of Moffett Field. And ascended to cruise altitude and cruised to (54 ^{o} 48' N, 116 ^{o} 48' W). This was followed by a turn west toward (56 ^{o} 00' N, 125 ^{o} W) holding altitude fixed for 5 minutes after the west turn, then executed a medium-rate descent (750 ft/min) to 52,000 ft and maintained at 52,000 ft for 10 minutes (fig.30). At (56 ^{o} 00' N, 125 ^{o} W) the aircraft turned south and ascended to cruise altitude and cruise toward Moffett Field where the flight was ended. The model geomagnetic cutoff, dose equivalent, dose, 1-10 MeV neutron

fluence rates are shown in figures 31 to 35. The northern most geomagnetic cutoff achieved is 0.86 GV compared with 0.43 GV of flight 97-106. It appears that neither the neutron flux nor the ionization rate has reached a plateau as shown in figures 34 and 35.

Flight 97-109: This was a repeat of the first southerly flight 97-107. The aim of this flight was to check data measurement repeatability. There is little difference in the flight trajectory of flight 97-107 with nearly identical model results (fig. 36 to 43).

Comparison to the ion chamber measurement

Since the majority of measured data are being analyzed by each individual laboratory, it may take months or years to obtain the complete results; however one piece of important information; the air ionization rate is readily available. Although the absolute comparison is still not available yet, since the exact dimension, composition of the ion chambers provided by EML and the computer driven data lagging require calibration, the only relation we could establish is the correlation between prediction by AIR model and the measurement and the derivation of an empirical conversion factor from ion chamber output to air ionization rate. The following procedure is adopted. Suppose the predicted set of data is denoted as a_i , the measured bias a function of time measured in minute. Taking ratio

$$c_i = a_i / b_i \tag{10}$$

where a_i is the model air ionization rate and b_i is the ion chamber output we define the average conversion factor as

$$\langle c \rangle = \Sigma\, c_i / N \tag{11}$$

where N is the total number of data points. The resulting estimate of the air ionization rate d_i is then given as

$$d_i = \langle c \rangle\, b_i \tag{12}$$

The actual conversion factor depends on the specific components resulting in ionization and must await a detailed evaluation. Still the present analysis represents a useful preliminary analysis of the flight data. The comparisons of model values a_i with the converted flight data d_i using equation (12) are shown in figures 44 to 48.

Results from flight 97-105 are shown in figure 44. It is seen that the model ionization rates overestimate the air ionization rate by about 3 or 4 percent at these altitudes and geomagnetic cutoffs (R of about 4 GV). A similar overestimate is seen in the first hour of flight 97-106 where the model shows improved agreement for the remainder of the northern leg of the flight. There is a progressive overestimate in the altitude survey at the northern most latitude as seen in figure 45. The return trip shows an underestimate

on the southern leg of less than 5 percent and may reflect irregularities in the geomagnetic field or a temporal fluctuation in the radiation levels. The ion chamber data was stopped abruptly at 400 minutes in the flight. The southern flight (fig. 46) shows the same overestimate near the 4 GV cutoff which extends to lower latitudes followed by an underestimate at the southern terminus of the flight. Again differences are on the order of 5 percent. The second northern flight 97-108 shows the same overestimate near 4 GV with reasonable agreement elsewhere even on the return leg (fig. 47). This would indicate that the underestimate on the southern leg of flight 97-106 is probably not a problem with the geomagnetic cutoff but may be an intensity fluctuation in solar modulation. These issues need to be further studied. The results of flight 97-109 in fig. 49 are almost an exact repeat of flight 97-107. It is clear that the air ionization within the AIR model version 0 is probably accurate to better than 5 percent and could be improved. There is evidence of a temporal fluctuation on the order of a few percent that will be pursued in a latter analysis.

Concluding Remark

The AIR ER-2 flight measurements is a one of the first attempts to a relatively complete measurement of the high altitude radiation level environment. The primary thrust is to characterize the atmospheric radiation components and to later define risk levels at high altitude flight. A secondary thrust is to develop and validate dosimetric techniques and monitoring devices for protecting aircrews. The present analysis of the AIR ion chamber represents about 40 percent of the health risk. We are quite pleased that preliminary results are rather encouraging that the measured physical quantities and our model predicted values do agree well. As more measured values are revealed, we will gain more understanding about our harzadous radiation environment and acquire more confidence in our prediction models.

References

FAA Advisory Committee on the Radiobiological Aspects of the Supersonic Transport, Cosmic radiation exposure in the Supersonic and subsonic flight. Aviat., Space & Environ. Med. 46:1170-1185; 1975

Foelsche, T., Mendell, R.B., Wilson, J.W., Adams, R.R., Measured and calculated neutron spectra and dose equivalent rates at high altitudes: Relevance to SST operations and space research. NASA TN D-7715, 1974

NCRP, Limitation of exposure to ionizing radiation. NCRP Rep. No. 116, 1993.

NCRP, Radiation Exposure and High-Altitude Flight. NCRP Commentary No. 12, July 21, 1995.

O'Brien ,K., Friedberg, W., Atmospheric cosmic rays at aircraft altitudes. Environ. Intern. 20:645-663; 1994.

Schaefer, H.J., Public health aspects of galactic radiation exposures at supersonic transport altitudes. Aerosp. Med. 39:1298-1303; 1968.

Wilson, J. W., et al., Transport Methods and Interactions for Space Radiation, NASA RP-1257, 1991.

Table 1. Ionization Rates in Air Measured by Argon-Filled Chambers[1]
at Solar Minimum (C = 98.3 in 1965)

Ion pairs, cm-3_sec-1, for air depths, g/cm2, of

R, GV	30	40	50	60	70	80	90	100	120	140	200	245	300	1034
0	445.0	430.0	414.0	399.0	383.0	366.0	349.0	332.0	298.0	266.0	181.0	136.0	95.0	11.4
.01	445.0	430.0	414.0	399.0	383.0	366.0	349.0	332.0	298.0	266.0	181.0	136.0	95.0	11.4
.16	444.0	430.0	414.0	399.0	383.0	366.0	349.0	332.0	298.0	266.0	181.0	136.0	95.0	11.4
.49	411.8	404.3	394.4	382.0	369.0	354.8	339.4	325.0	292.3	264.5	181.0	136.0	95.0	11.4
1.31	390.0	385.0	380.0	370.0	365.0	350.0	335.0	320.0	290.0	264.0	181.0	135.0	95.0	11.4
1.97	325.0	333.0	340.0	335.0	330.0	312.5	308.0	300.0	285.0	264.0	181.0	134.0	95.0	11.4
2.56	300.0	305.0	310.0	305.0	300.0	290.0	285.0	280.0	255.0	230.0	173.0	126.0	95.0	11.4
5.17	185.0	195.0	208.0	208.0	208.0	208.0	208.0	208.0	195.0	185.0	135.0	103.0	75.0	10.6
8.44	127.6	137.0	145.0	150.2	153.8	155.8	156.0	154.6	149.7	142.2	111.3	87.0	66.6	10.4
11.70	85.0	92.0	98.0	100.0	102.0	105.0	107.0	110.0	108.0	105.0	80.0	77.0	60.0	10.0
14.11	70.0	75.0	82.0	85.0	89.0	93.6	95.0	100.0	98.0	95.0	78.0	68.8	50.0	10.0
17.00	66.3	73.8	80.0	84.8	88.5	91.1	92.6	93.5	93.4	90.5	75.0	62.3	48.0	10.0

[1]Experimental data extrapolated to provide estimates of ionization rates over a wide range of altitudes and geomagnetic cutoffs.

Table 2. Ionization Rates in Air Measured by Argon-Filled Chambers[1]
at Solar Maximum (C = 80 in 1958)

Ion pairs, cm-3_sec-1, for air depths, g/cm2, of

R, GV	30	40	50	60	70	80	90	100	120	40	00	45	300	1034
0	264.6	267.5	267.0	265.0	258.0	252.0	243.0	235.0	216.3	197.0	145.0	109.2	78.8	11.4
.01	264.6	267.8	267.0	265.0	258.0	251.0	243.0	235.0	216.3	197.0	145.0	109.2	78.8	11.4
.16	264.0	264.9	265.0	264.0	257.0	250.0	243.0	233.0	215.0	197.0	145.0	109.2	78.8	11.4
.49	264.0	264.9	265.0	262.0	256.0	249.0	242.0	231.0	213.2	197.0	145.0	109.2	78.8	11.4
1.31	264.0	265.0	265.0	262.0	253.0	247.0	241.0	231.0	213.0	197.0	145.0	108.0	78.8	11.4
1.97	264.0	265.0	265.0	262.0	252.0	245.0	241.0	231.0	212.5	197.0	145.0	107.8	78.8	11.4
2.56	235.0	237.5	240.0	240.0	239.0	238.0	237.0	230.0	209.0	197.0	145.0	101.6	78.8	11.4
5.17	162.5	168.0	179.0	182.0	178.0	175.2	174.0	173.8	170.0	160.0	159.0	88.3	65.0	10.6
8.44	95.0	103.5	112.0	118.0	118.0	119.0	120.0	122.0	118.0	117.0	100.6	78.7	60.2	10.4
11.70	78.2	85.0	90.7	92.7	94.8	98.0	100.0	103.1	101.2	98.4	75.0	72.2	56.2	10.0
14.11	65.7	70.7	77.5	80.5	84.3	89.0	90.5	95.3	93.5	90.9	74.0	65.9	47.9	10.0
17.0	63.0	70.3	76.4	81.1	84.8	87.5	89.1	90.2	90.1	87.4	72.6	60.3	46.5	10.0

[1]Experimental data extrapolated to provide estimates of ionization rates over a wide range of altitudes and geomagnetic cutoffs.

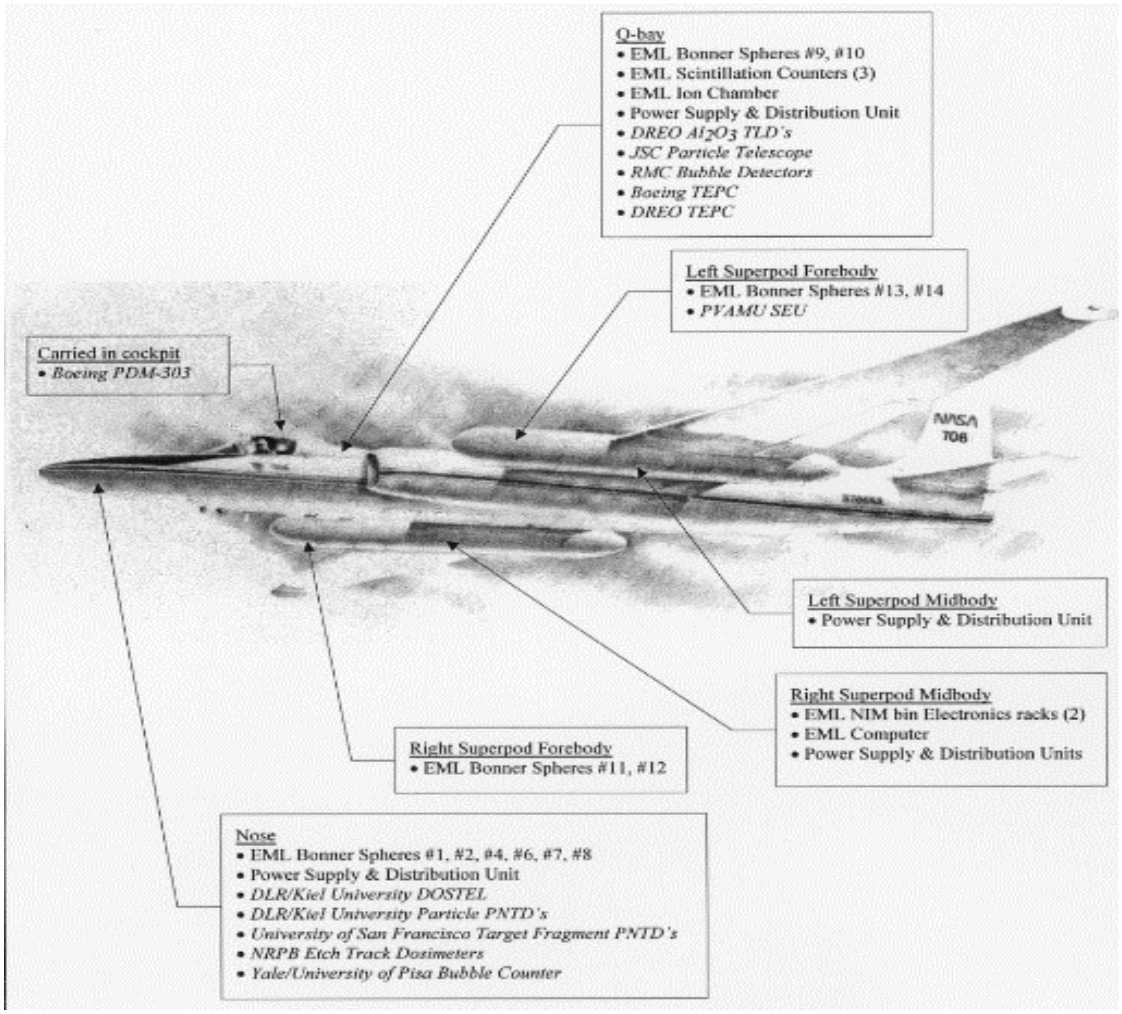

Figure 1.- Instrument Locations on the ER-2.

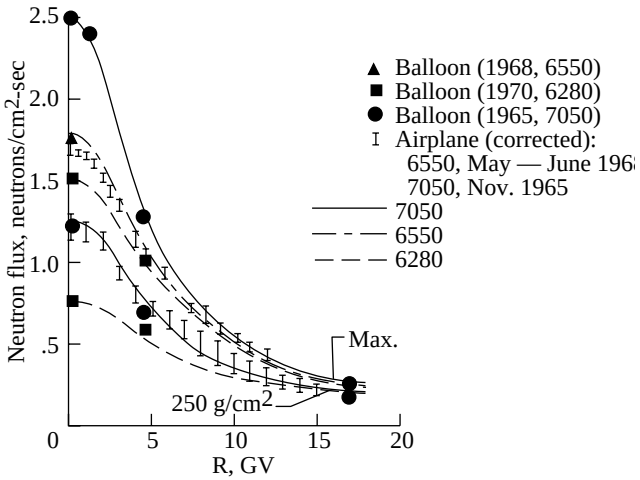

Figure 2. Fast neutron flux (in range from 1 to 10 MeV) at the transition maximum an 240-g/cm^2 depth as a function of vertical cutoff rigidity *R* for various times in the solacycle and DRNM count rates.

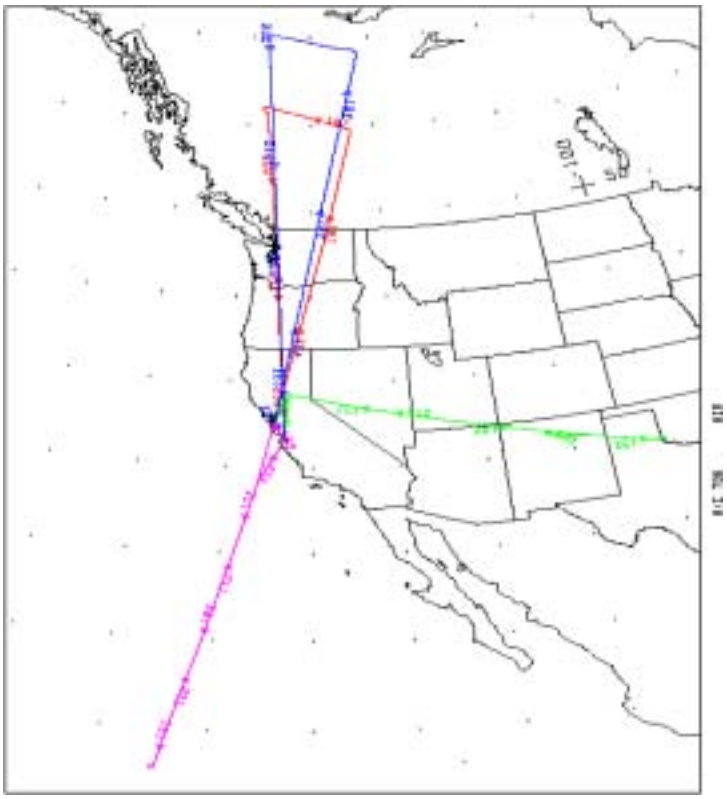

Figure 3. Ground tracks of flights 97-105 to 97-109.

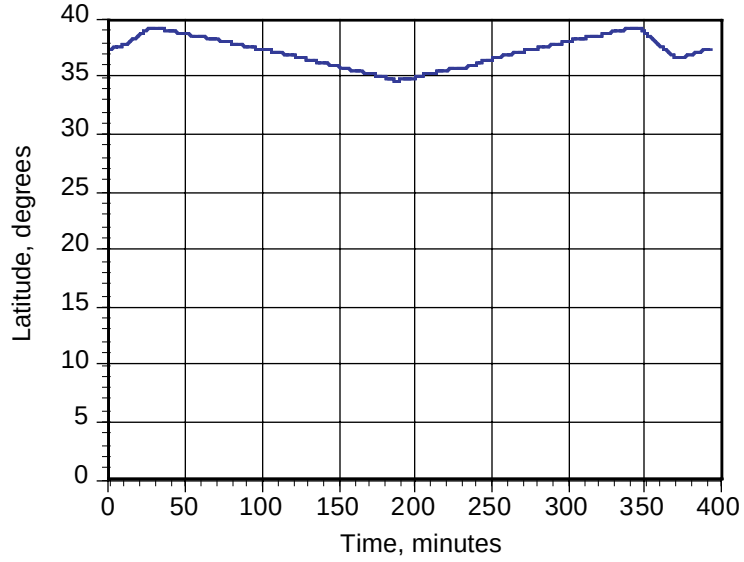

Fig. 4 Latitude of flight path as function of Time for Flight 97-105

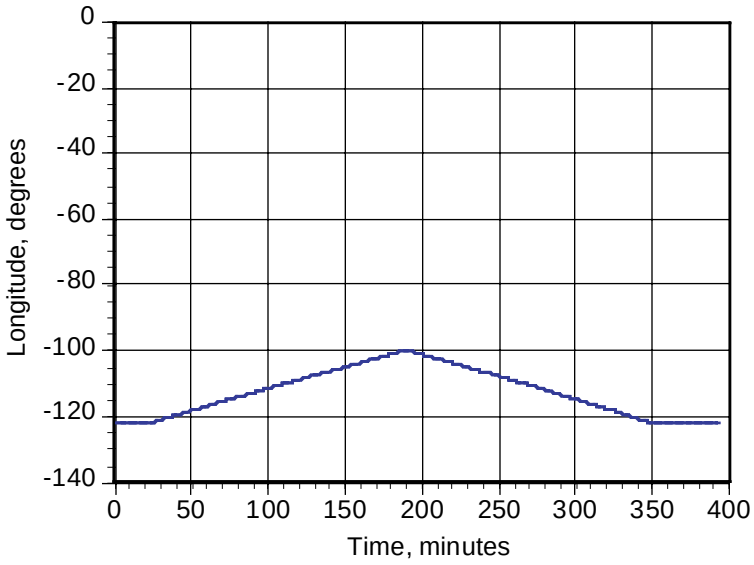

Fig. 5 Longitude of flight path as function of time for Flight 97-105

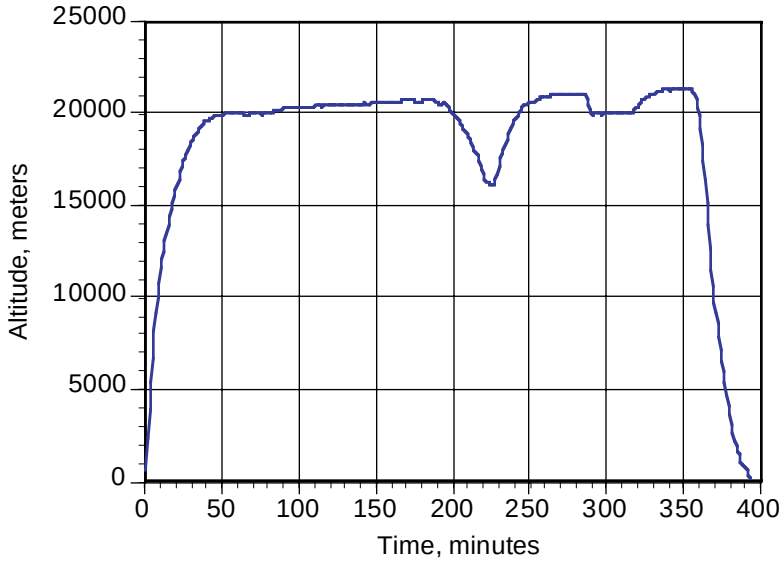

Fig. 6 Altitude of flight path as function of time for Flight 97-105

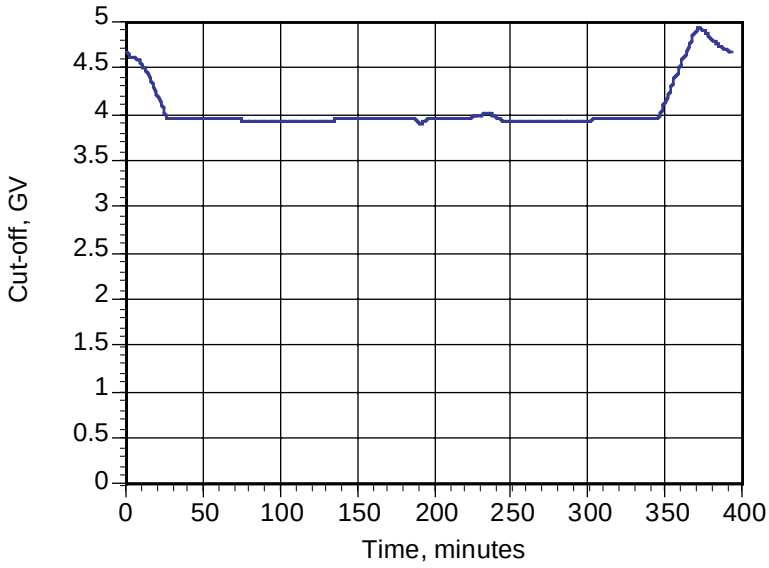

Fig. 7 Magnetic cut-off of flight path as function of time for Flight 97-105

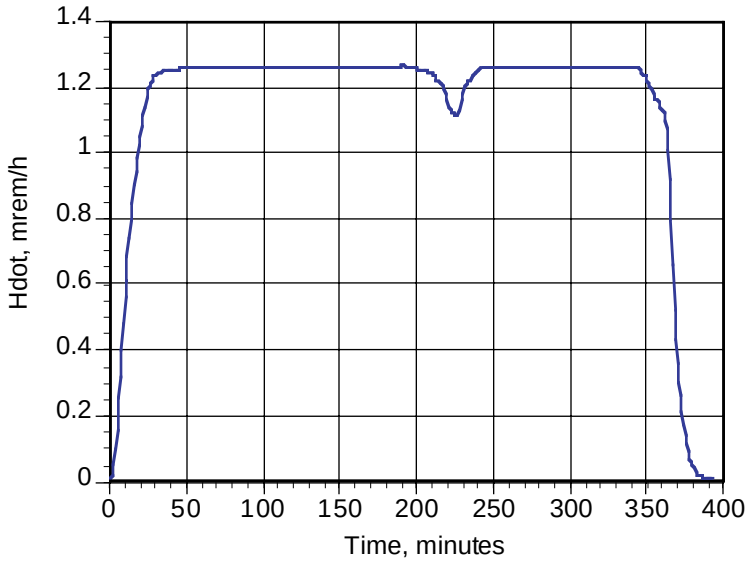

Fig. 8 Dose Equivalent Rate as function of time for Flight 97-105

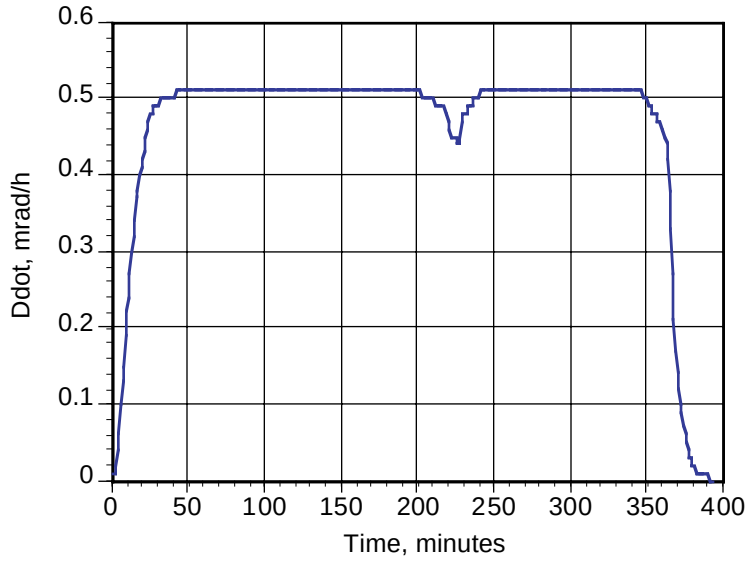

Fig. 9 Dose Rate as function of time for Flight 97-105

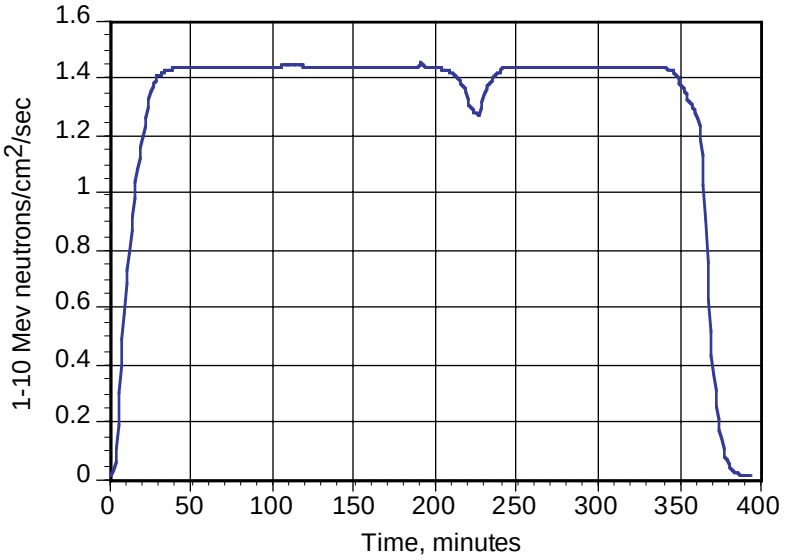

Fig. 10 Neutron Flux as function of time for Flight 97-105

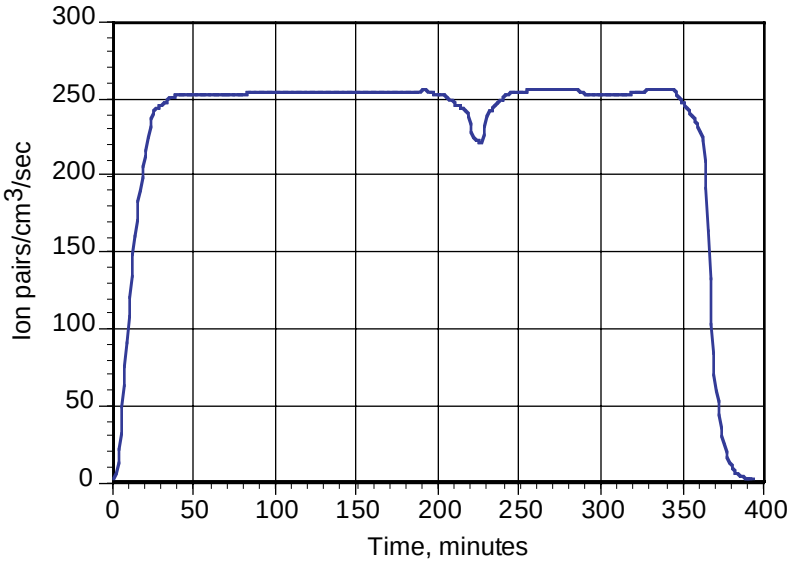

Fig. 11 Air Ionization Rate as function of time for Flight 97-105

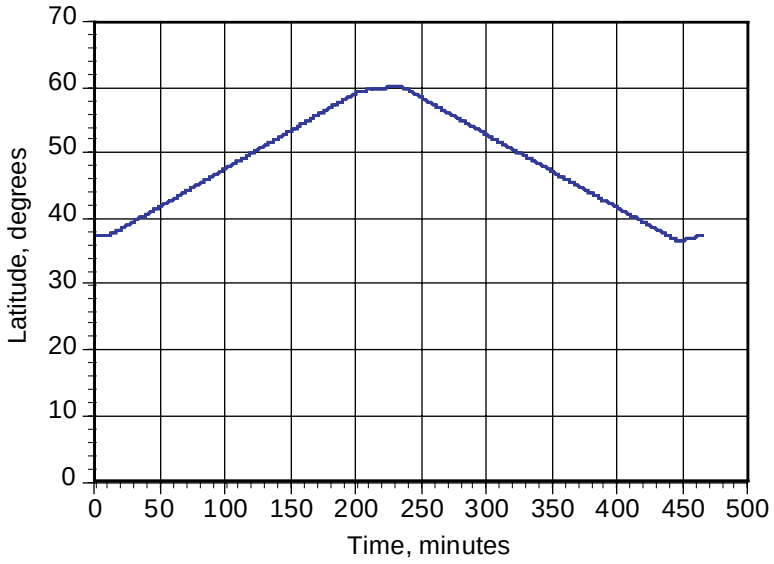

Fig. 12 Latitude of flight path as function of time for Flight 97-106

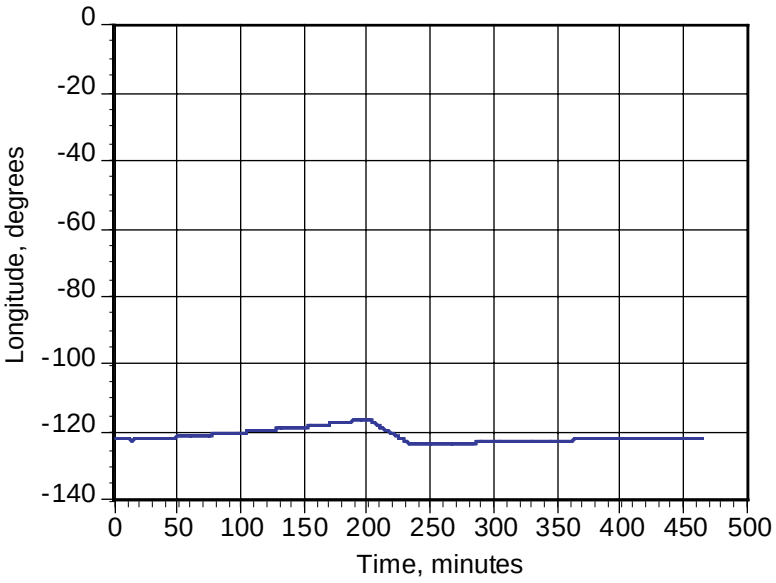

Fig. 13 Longitude of flight path as function of time for Flight 97-106

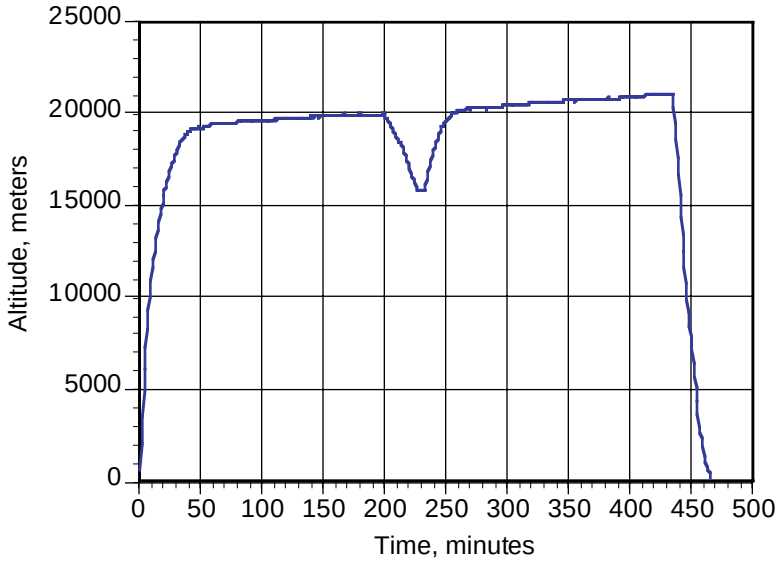

Fig. 14 Altitude of flight path as function of time for Flight 97-106

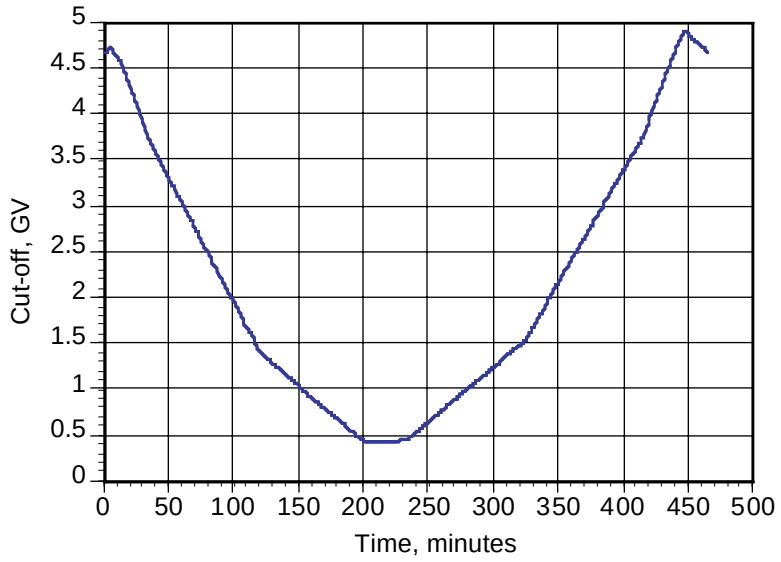

Fig. 15 Magnetic cut-off of flight path as function of time for Flight 97-106

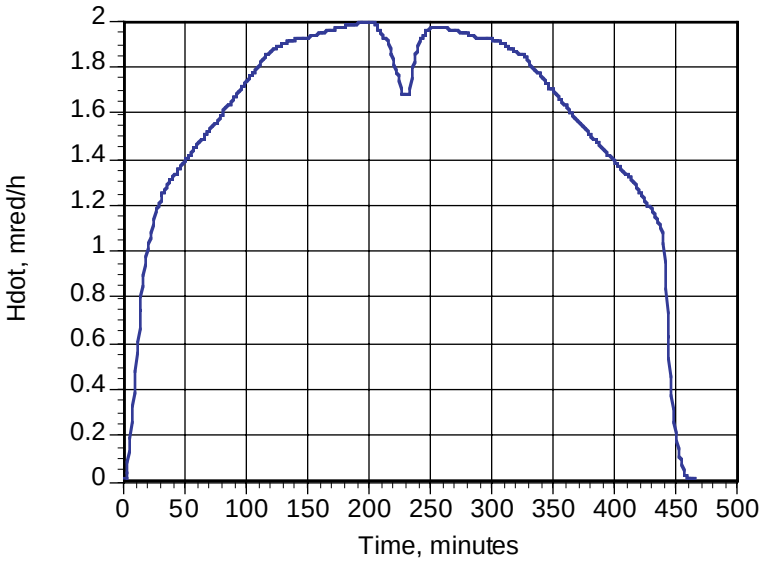

Fig.16 Dose Equivalent Rate as function of time for Flight 97-106

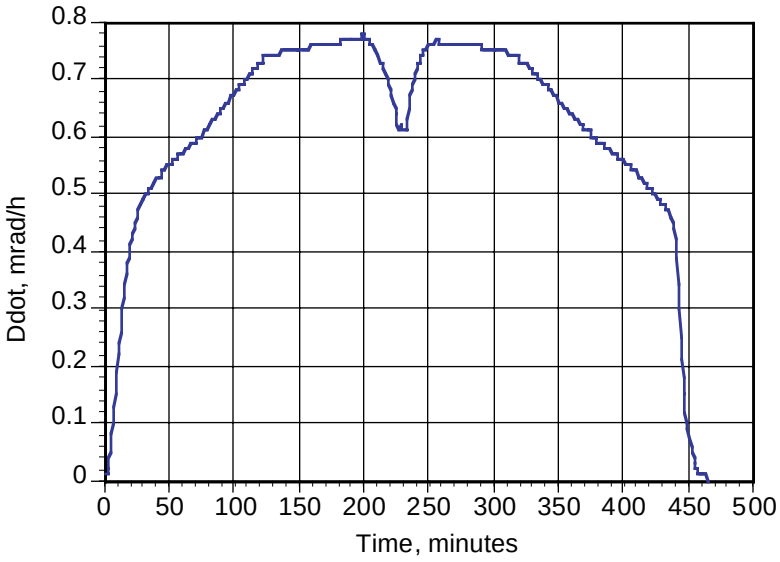

Fig.17 Dose Rate as function of time for Flight 97-106

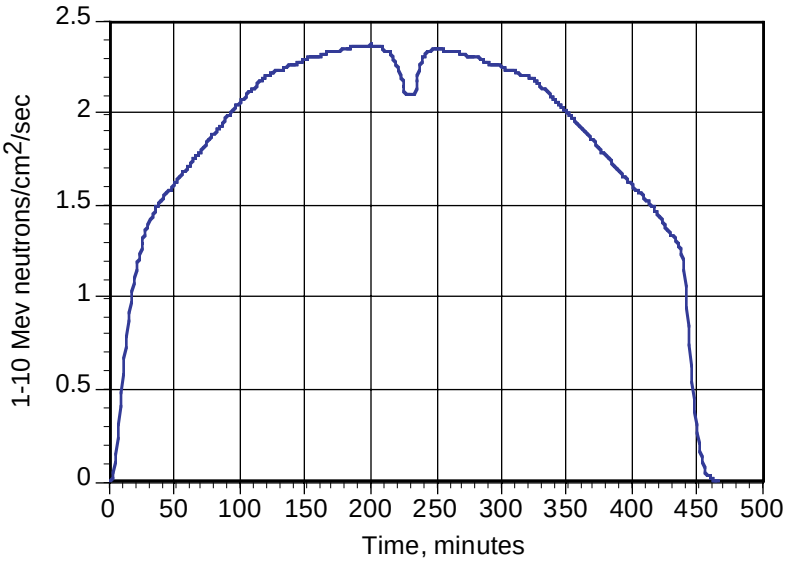

Fig.18 Neutron Flux as function of time for Flight 97-106

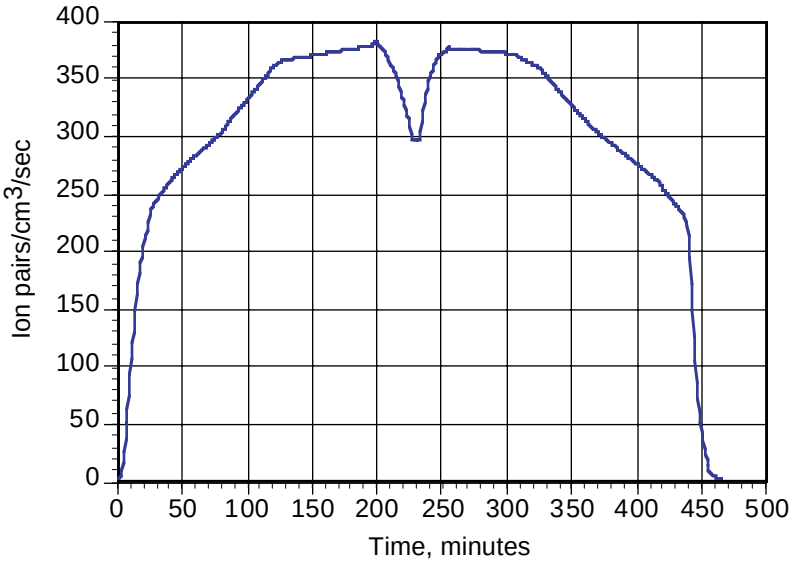

Fig.19 Air Ionization Rate as function of time for Flight 97-106

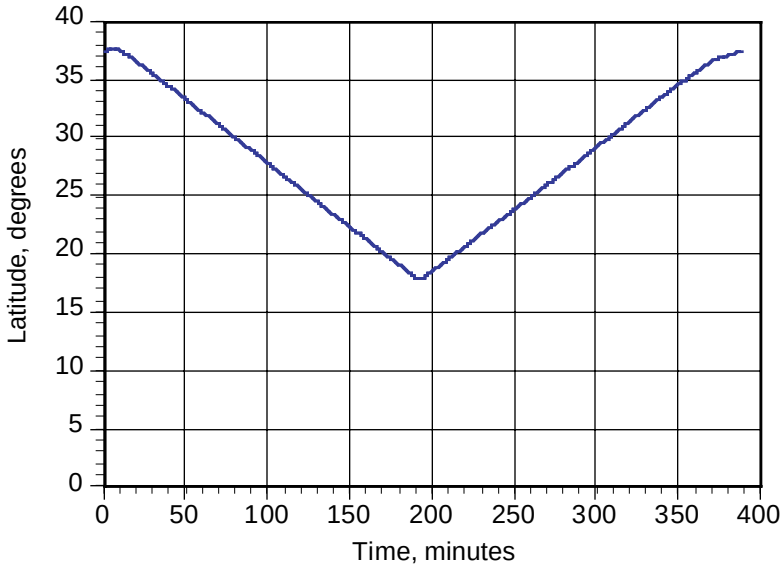

Fig. 20 Latitude of flight path as function of time for Flight 97-107

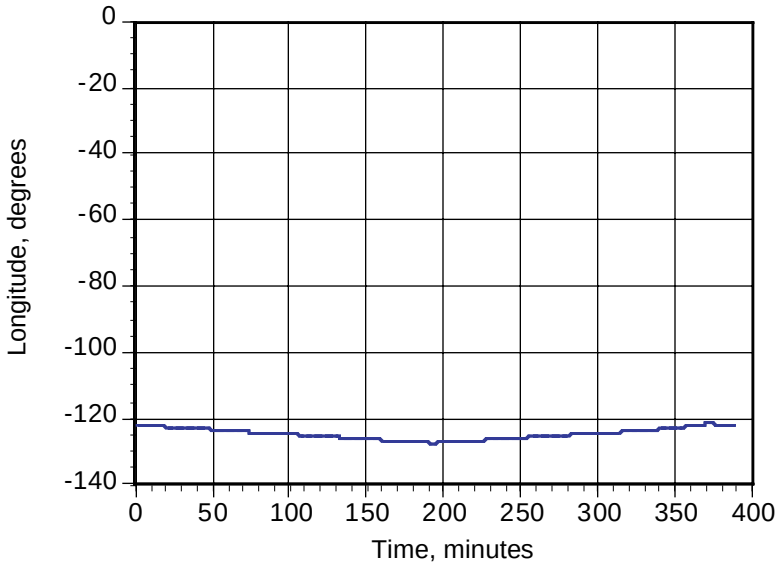

Fig. 21 Longitude of flight path as function of time for Flight 97-107

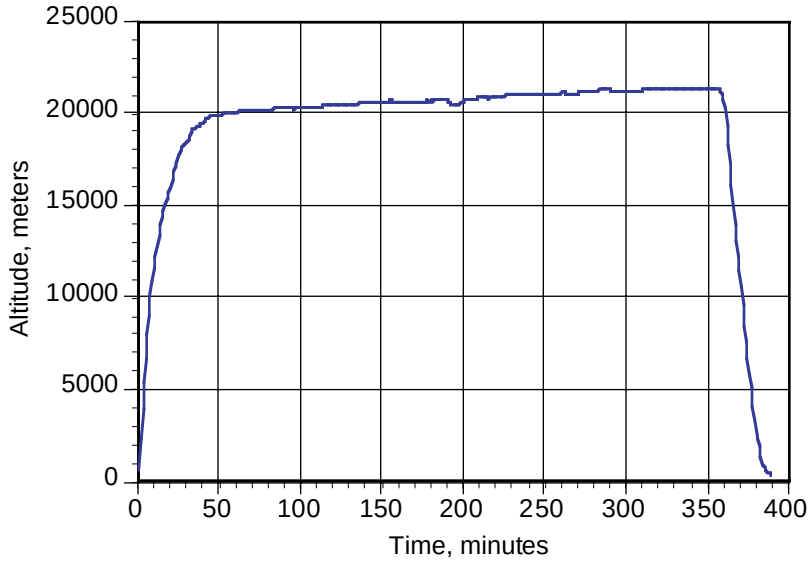

Fig. 22 Altitude of flight path as function of time for Flight 97-107

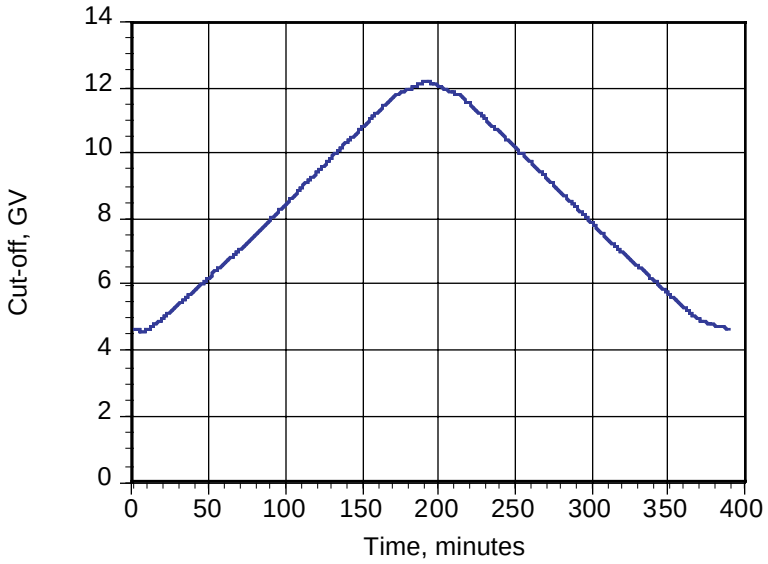

Fig. 23 Magnetic cut-off of flight path as function of time for Flight 97-107

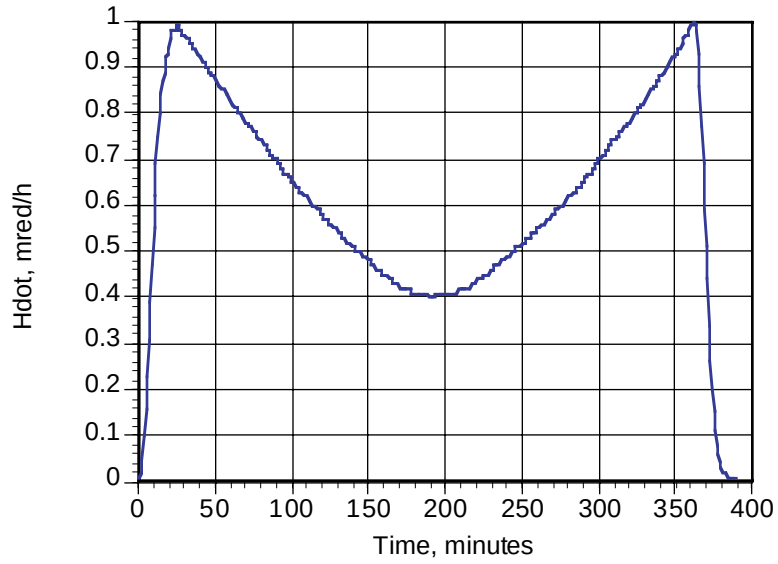

Fig.24 Dose Equivalent Rate as function of time for Flight 97-107

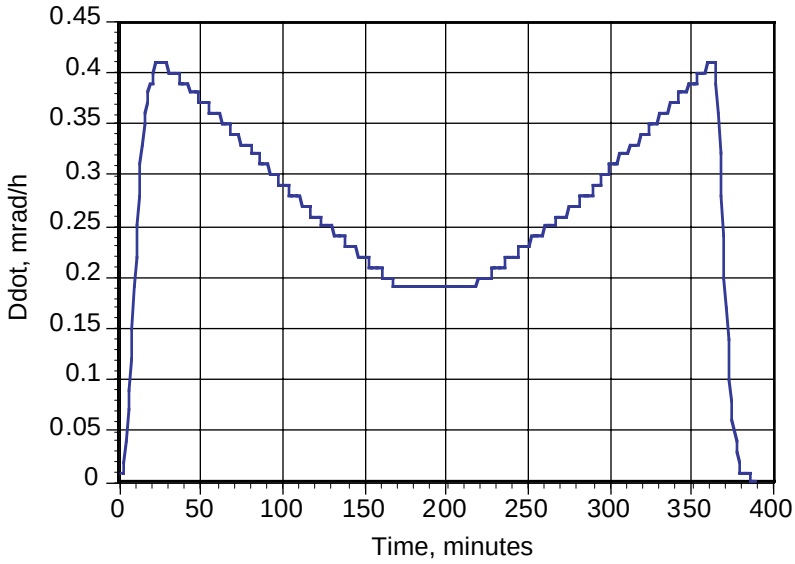

Fig.25 Dose Rate as function of time for Flight 97-107

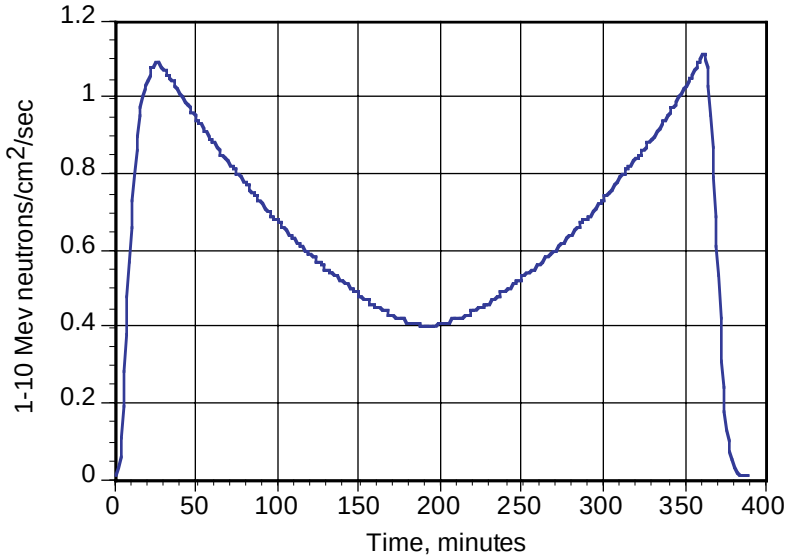

Fig. 26 Neutron Flux as function of time for Flight 97-107

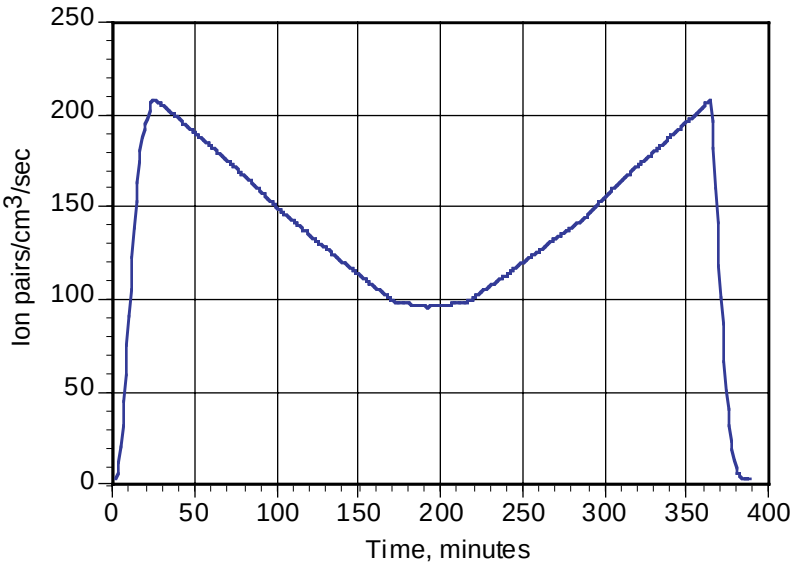

Fig.27 Air Ionization Rate as function of time for Flight 97-107

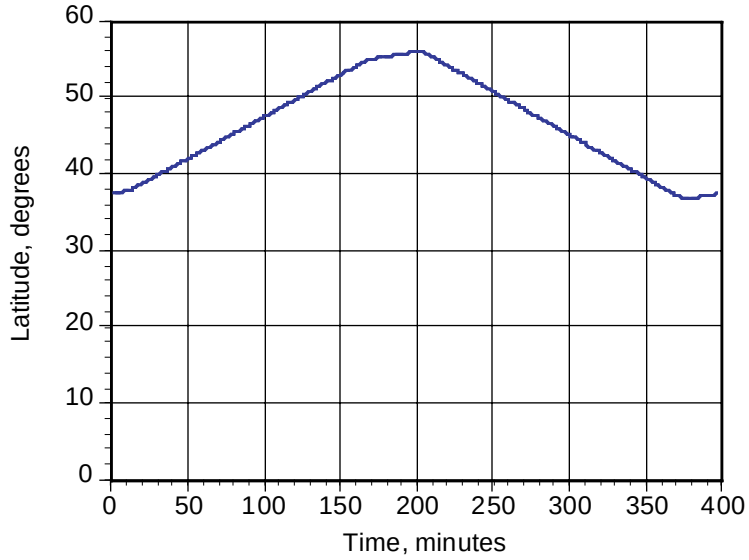

Fig. 28 Latitude of flight path as function of time for Flight 97-108

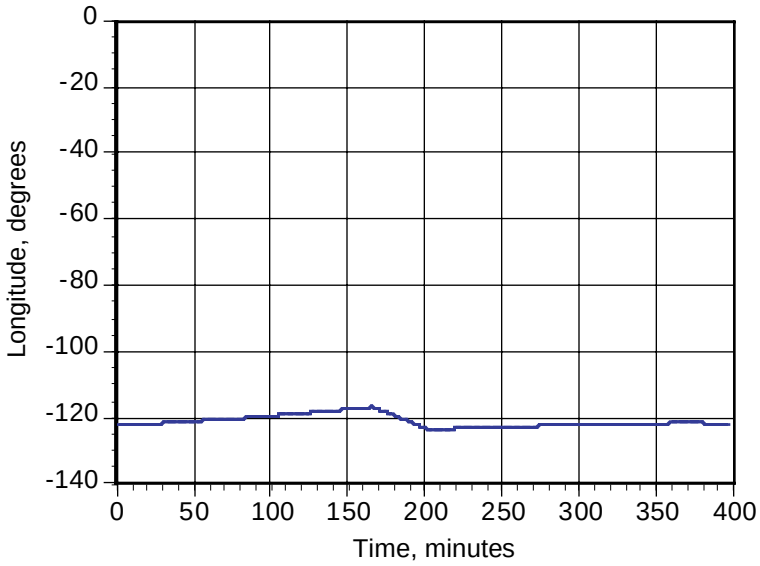

Fig. 29 Longitude of flight path as function of time for Flight 97-108

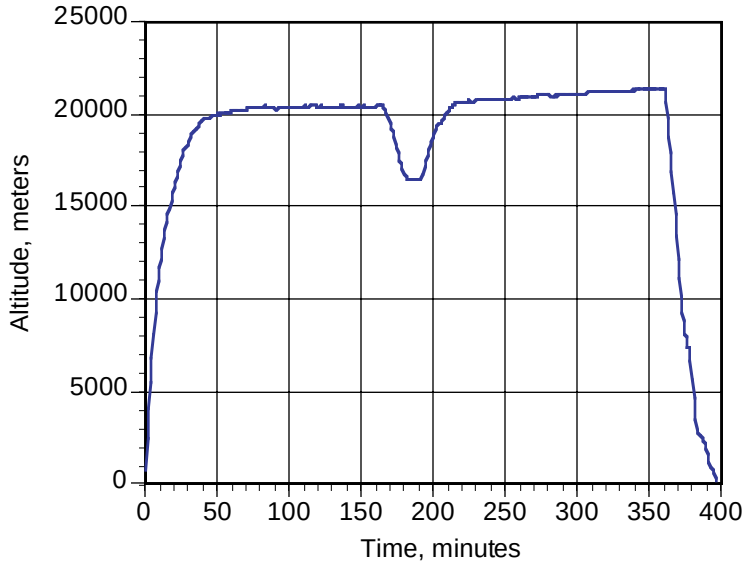

Fig. 30 Altitude of flight path as function of time for Flight 97-108

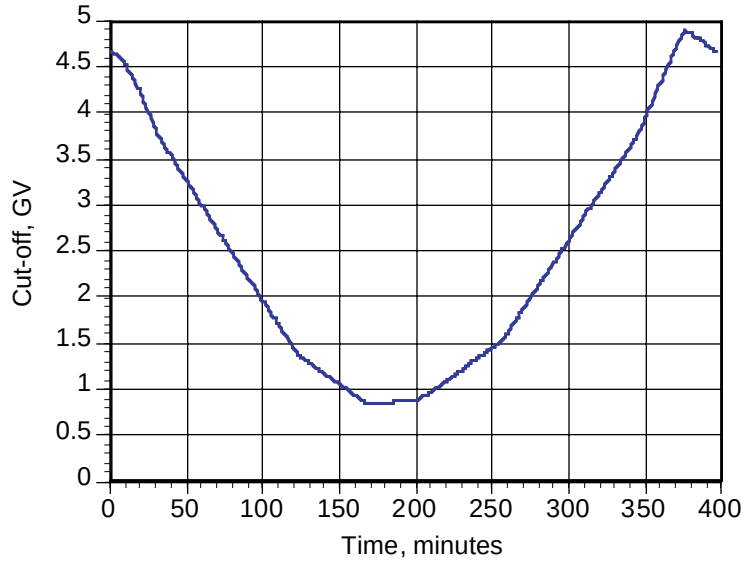

Fig. 31 Magnetic cut-off of flight path as function of time for Flight 97-108

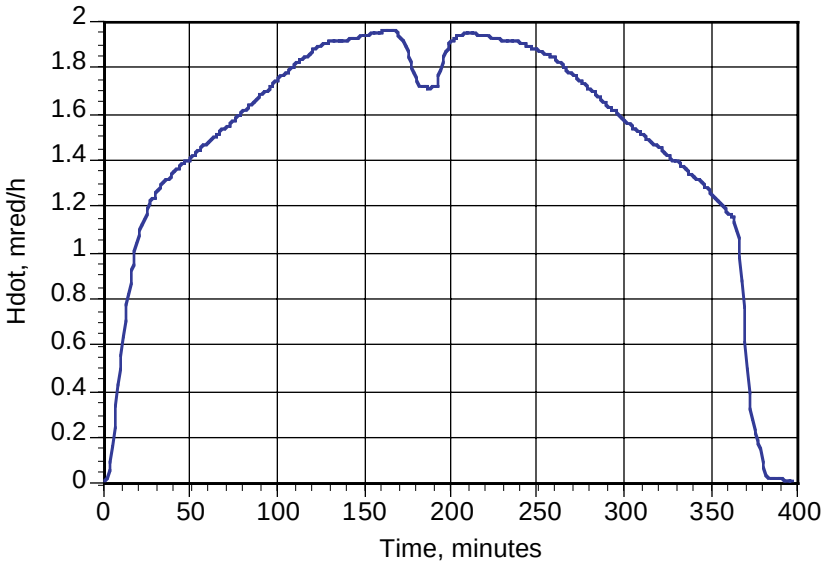

Fig.32 Dose Equivalent Rate as function of time for Flight 97-108

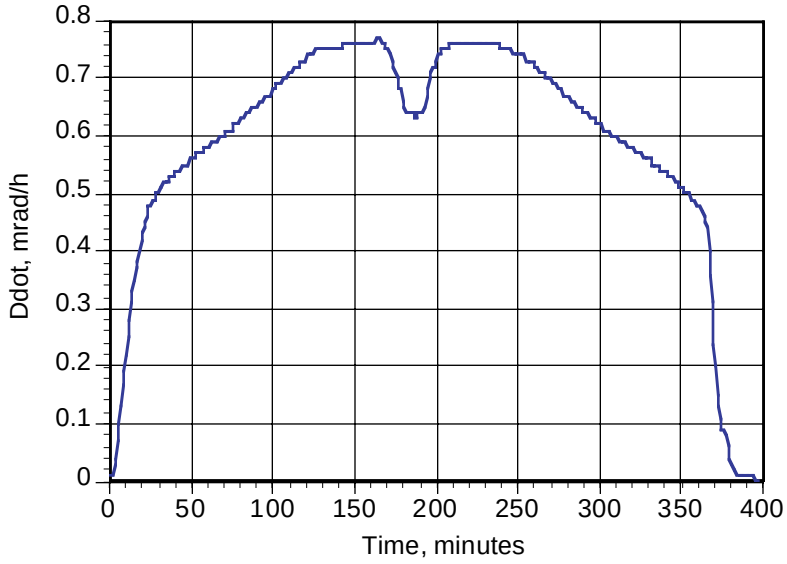

Fig.33 Dose Rate as function of time for Flight 97-108

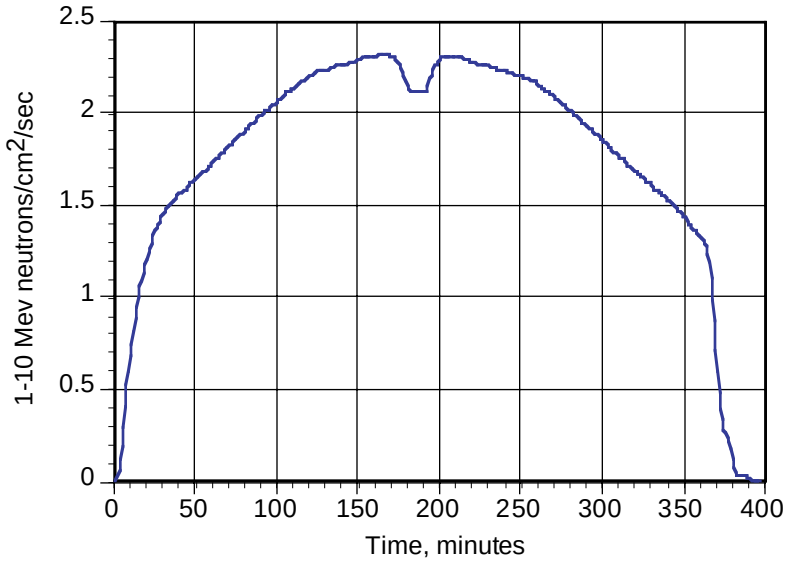

Fig.34 Neutron Flux as function of time for Flight 97-108

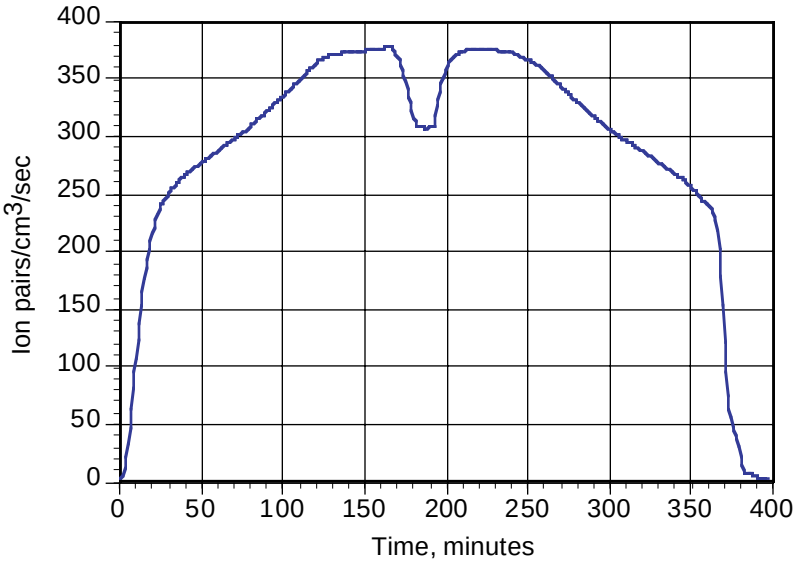

Fig. 35 Air Ionization Rate as function of time for Flight 97-108

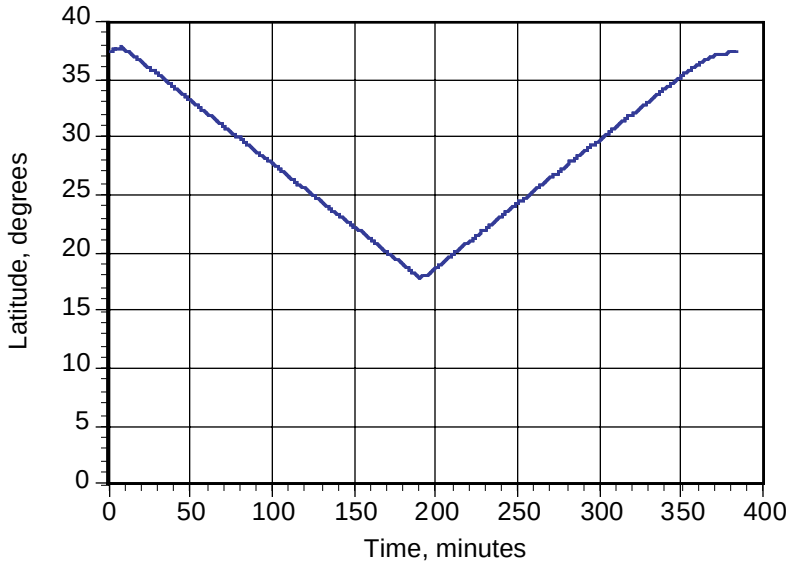

Fig. 36 Latitude of flight path as function of time for Flight 97-109

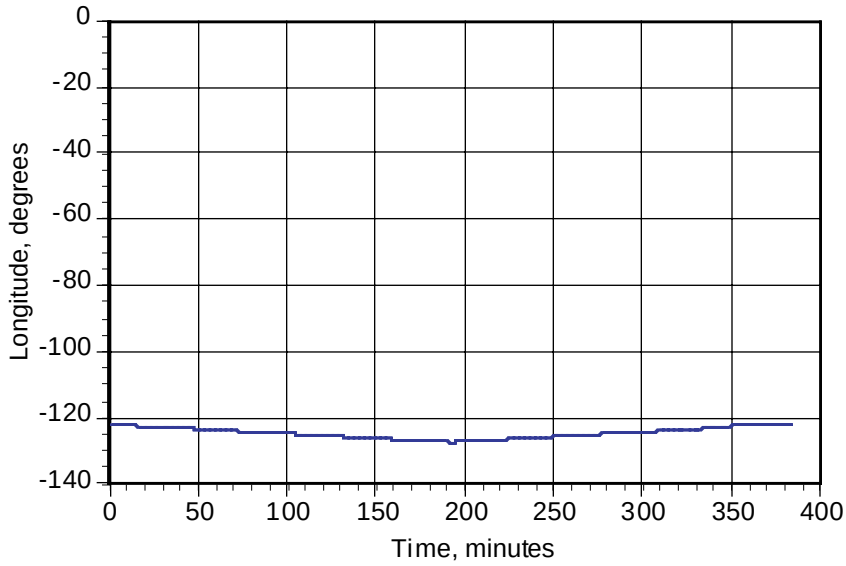

Fig. 37 Longitude of flight path as function of time for Flight 97-109

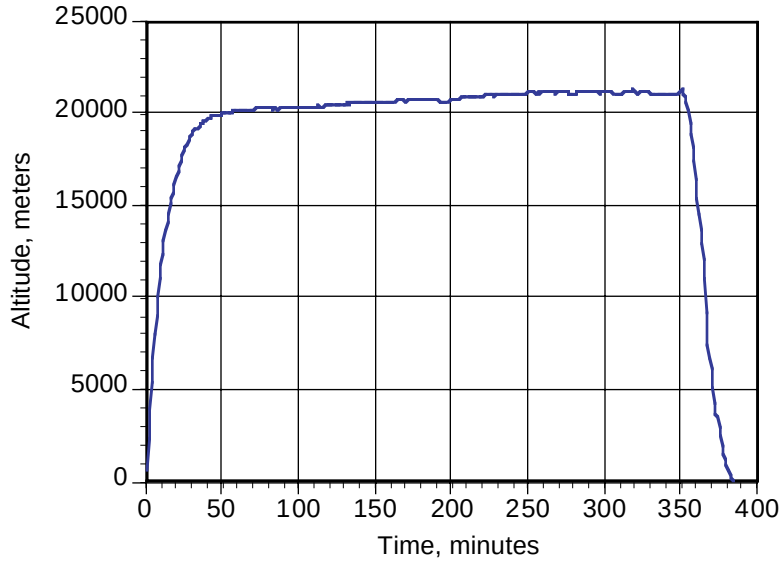

Fig. 38 Altitude of flight path as function of time for Flight 97-109

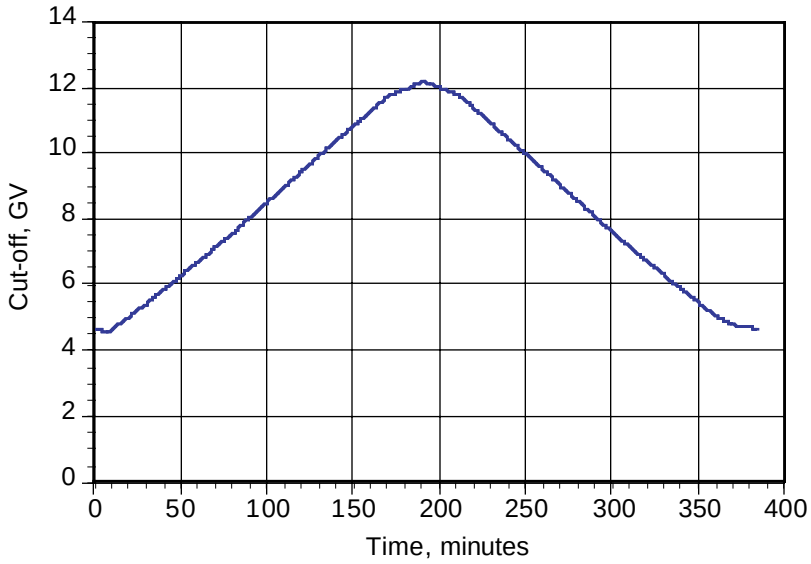

Fig. 39 Magnetic cut-off of flight path as function of time for Flight 97-109

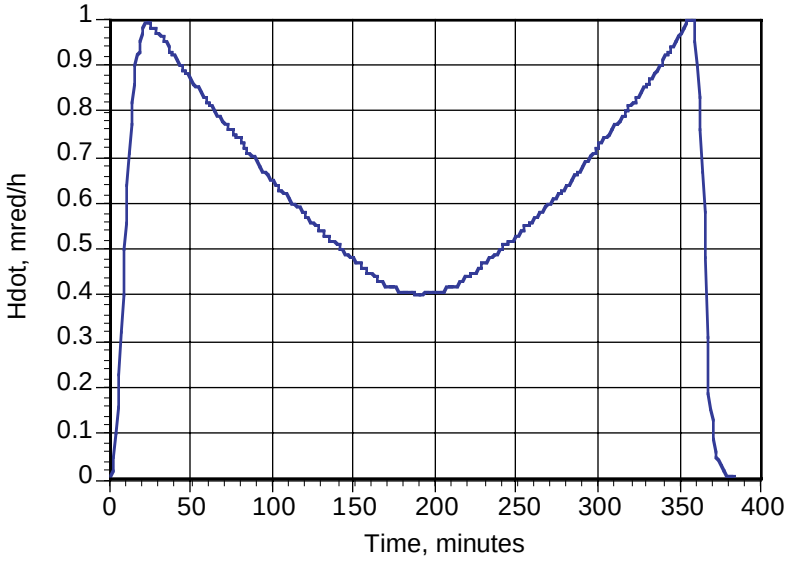

Fig.40 Dose Equivalent Rate as function of time for Flight 97-109

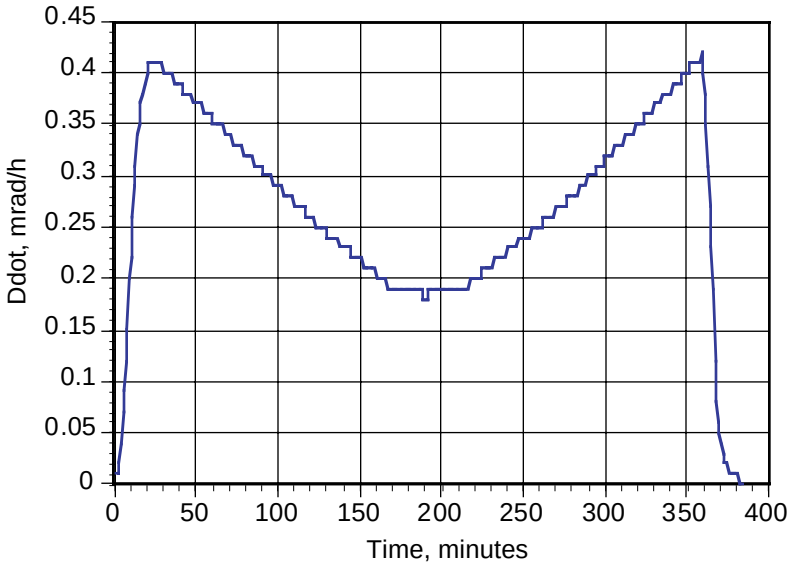

Fig.41 Dose Rate as function of time for Flight 97-109

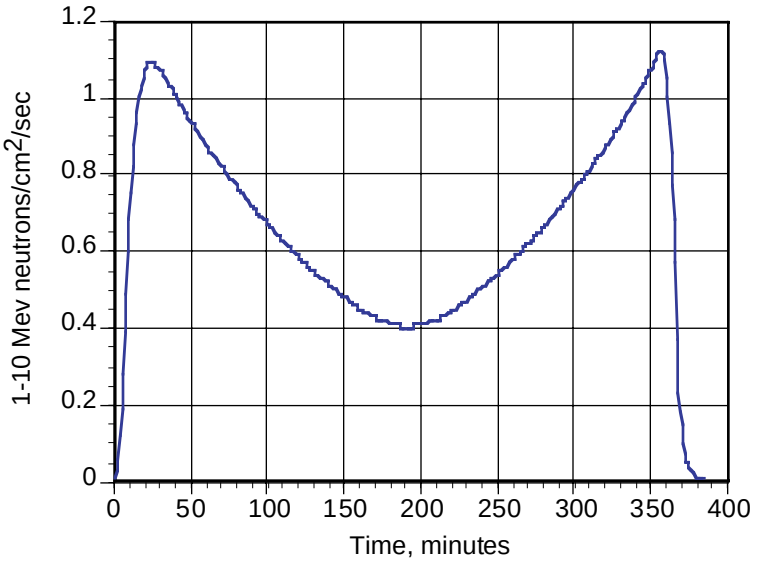

Fig.42 Neutron Flux as function of time for Flight 97-109

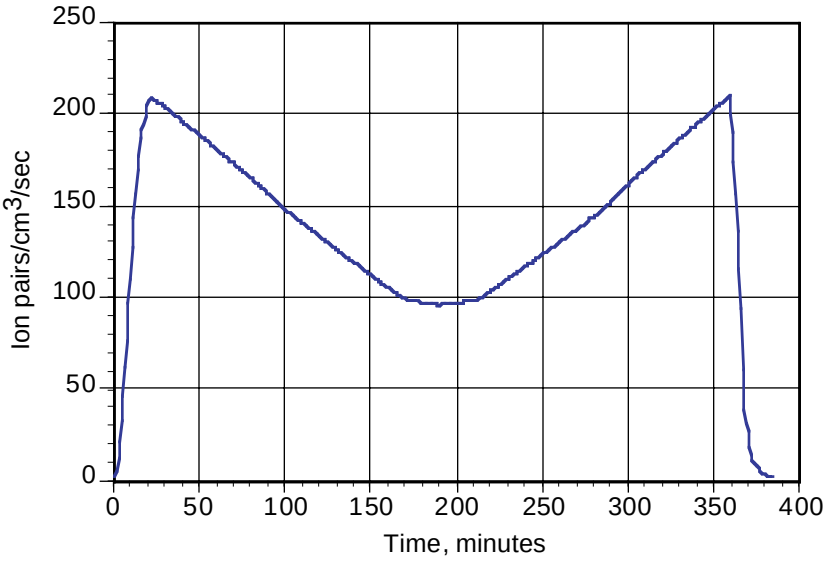

Fig.43 Air Ionization Rate as function of time for Flight 97-109

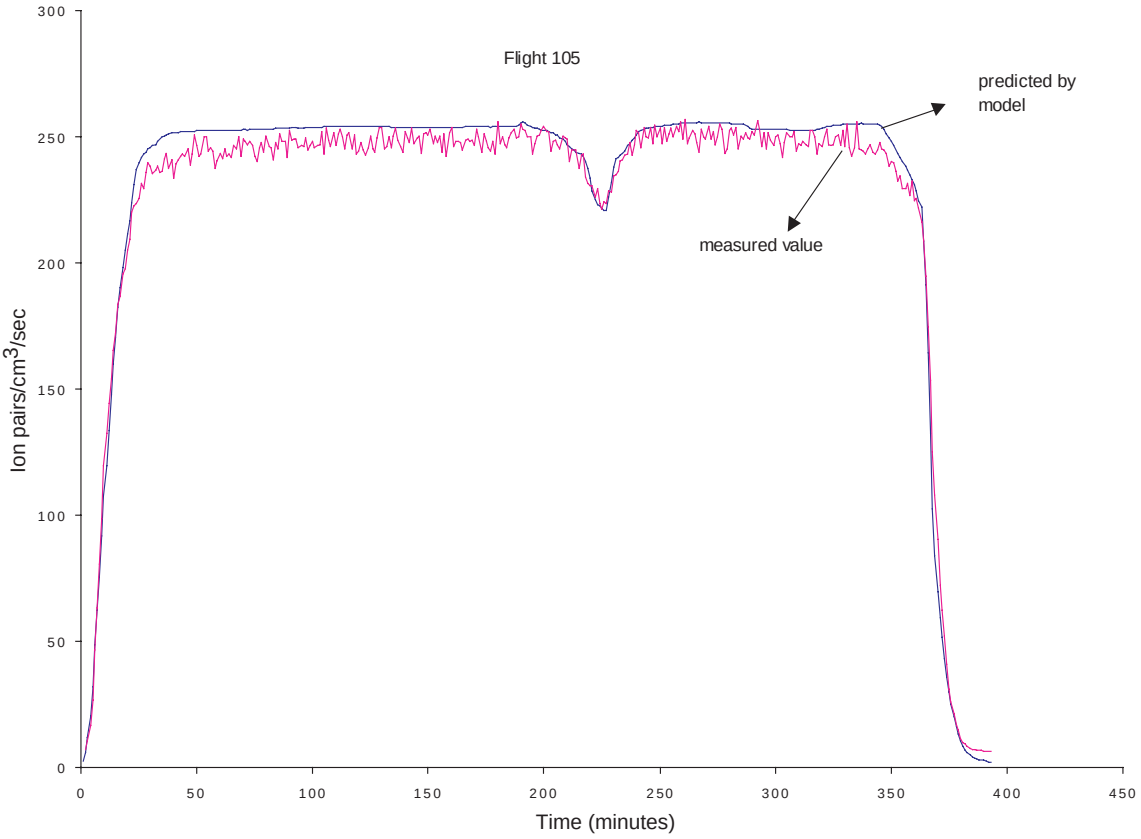

Fig. 44 Predicted and measured value of Air Ionization Rate as function of time for Flight 97-105

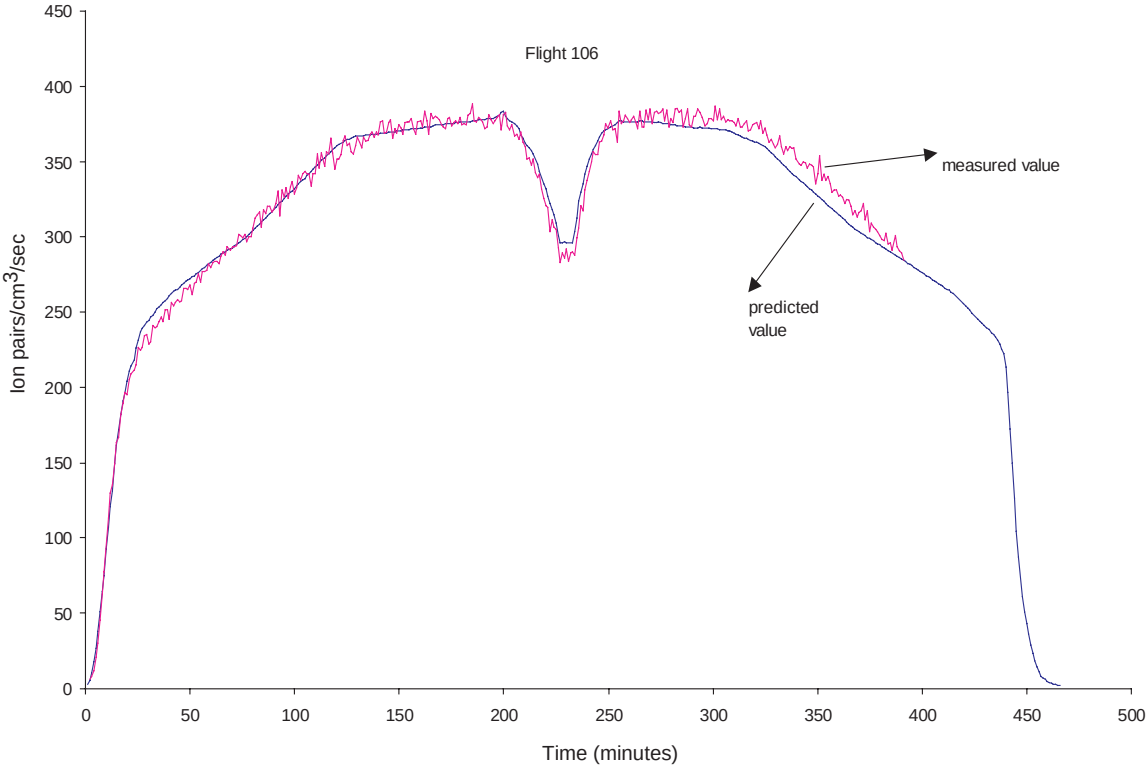

Fig. 45 Predicted and measured value of Air Ionization Rate as function of time for Flight 97-106

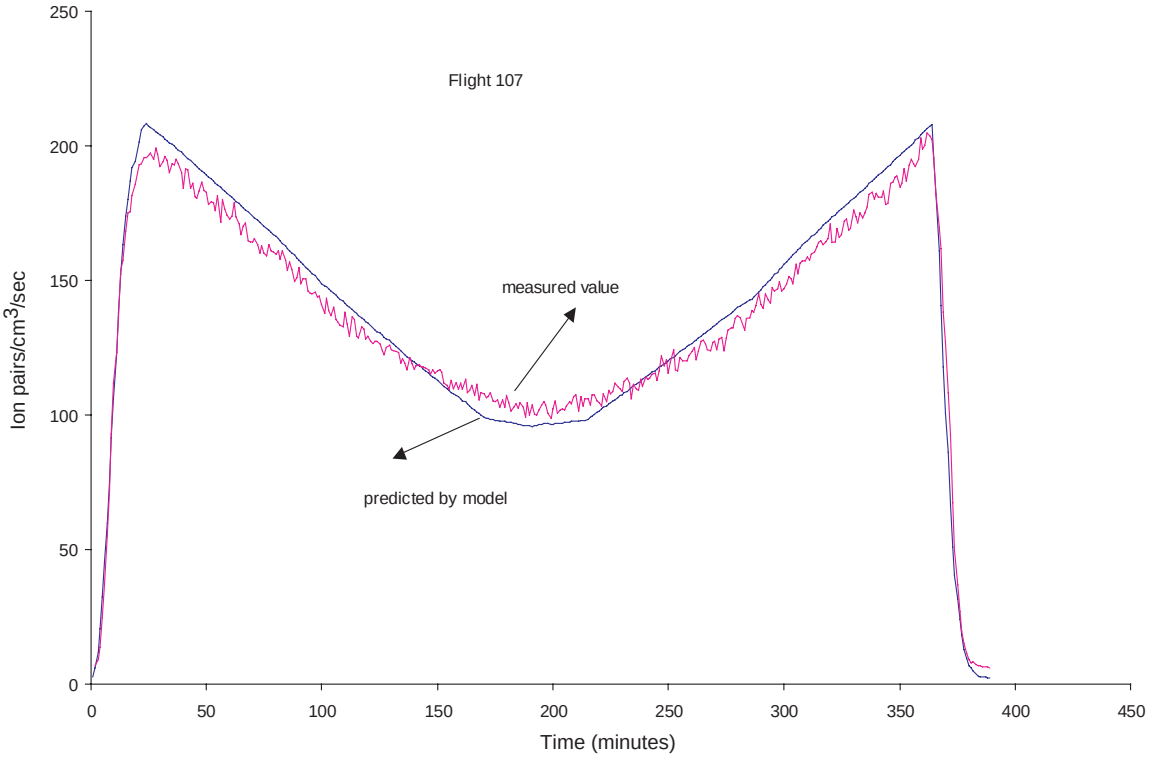

Fig. 46 Predicted and measured value of Air Ionization Rate as function of time for Flight 97-107

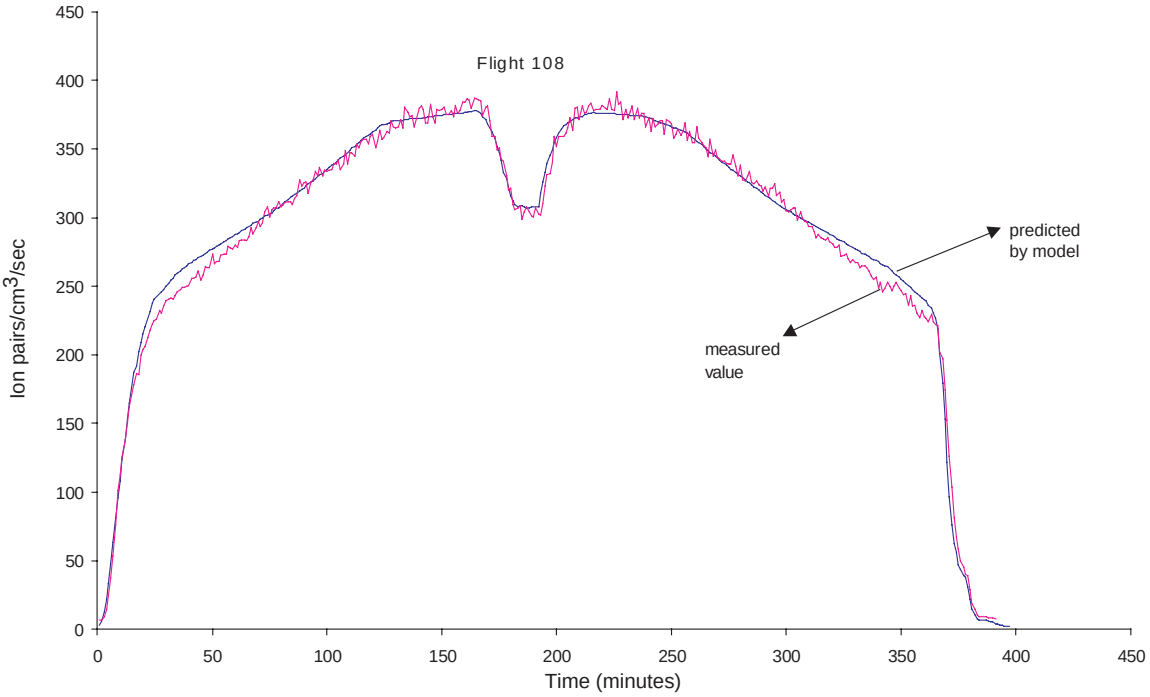

Fig 47 Predicted and measured value of Air Ionization Rate as function of time for Flight 97-108

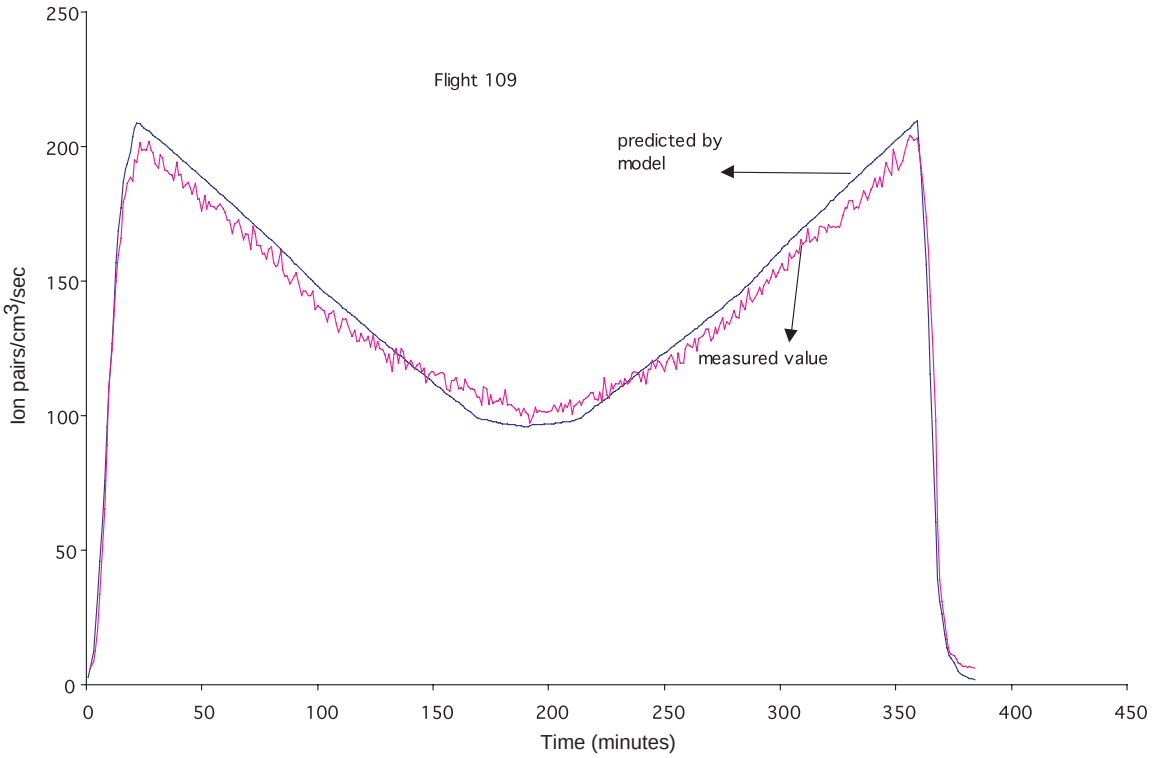

Fig. 48 Predicted and measured value of Air Ionization Rate as function of time for Flight 97-109.

Chapter 8: Radiation Dose in Silicon Detectors on ER-2 Flights

R. Beaujean[1], J. Kopp[1], G. Reitz[2]

[1]Universität Kiel, Experimentelle und Angewandte Physik, Extraterrestrik, D-24118 Kiel
[2]DLR, Institut für Luft- und Raumfahrtmedizin, Abteilung Strahlenbiologie, D-51140 Köln

Radiation Dose in Silicon Detectors on ER-2 Flights

Abstract

Based on two silicon detectors of 315 μm thickness, the DOSTEL active dosemeter measured count and dose rates as well as LET spectra on ER-2 flights. The instrument was located close to the TACAN transmitter which induced noise background to the instrument except on the two southbound flights. These two flights showed periods of undisturbed measurements with valid data for the dose rate and the LET spectra. Using the effective quality factor of 1.9 deduced from the LET specta and the conversion factor of 1.2 from LET in silicon to LET in water the mean dose equivalent rate arrives at 3.7 μSv/h for the low latitude flights.

Introduction

For the radiation risk assessment of future supersonic air transport systems, NASA initiated the AIR project using the ER-2 aircraft for a survey of the radiation environment in the atmosphere at about 20 km altitude at different magnetic latitudes and longitudes over North America. The complex radiation field in the atmosphere requires different instruments to measure dose and dose equivalent values induced by charged particles, neutrons and photons. Our group joined the investigation with the active dosemeter DOSTEL and passive devices consisting of TLDs and plastic nuclear track detectors. This report contains results from the active instrument DOSTEL during the first set of ER-2 flights in 1997.

Instrument description

Based on two identical passivated implanted planar Silicon (PIPS) detectors (Canberra Semiconductors) the instrument DOSTEL is designed to measure the energy deposit of charged particles. Both detectors have a thickness of 315 μm and a sensitive area of 693 mm^2 (Burger 1996). They are mounted at a distance of 15 mm forming a telescope with a geometric factor of 823.8 mm^2 sr.

Each detector is connected to an independent analogue signal section consisting of a charge sensitive amplifier (Amptek A250) followed by a two-step pulse amplifier (1 μs pulse shaping time constant) and two peak detectors. Together with a multiplexed 8-bit ADC this design allows a pulse height analysis of the detector signals with 255 channels of about 15keV width for low energy deposits up to 3.9 MeV and 255 channels of about 300 keV width for high energy deposits up to 77 MeV.

Main components of the digital signal section are the 8-bit CPU 68HC711, the 1Mb flash memory E28F008SA and the timer 68HC68T1. The clock starts after the initial power-on reset and provides an internal time scale. The use of a 0.1 F electrolyte capacitor as a power backup for the timer allows the internal clock to continue up to 6 hours in the event of a power loss.

The instrument was originally designed for space flights on the NASA shuttle. It is housed in an aluminum container of size 7x7x10 cm^3 and has passed vibration and EMC tests according to NASA specification. The total mass is 0.57 kg, the total power consumption is 0.7 W from ±10 Vdc and +5Vdc.

The energy deposit response is calibrated with α-particles from Am241.

Data Processing

Measured data are processed in real time to yield count and dose rates for the individual detectors in the single detector mode as well as Linear Energy Transfer (LET) spectra for events with a coincidence in both detectors. All data are stored in the internal flash memory for postflight analysis. In order to cover the whole first set of ER-2 flights without a memory overflow, time intervals of 30 s and 20 min were selected for dose rate (and count rate) measurement and the LET spectra accumulation, respectively. Neither energy deposit nor arrival time of individual events were recorded. Every 20 minutes housekeeping data (test pulses, temperature, voltages etc.) were sampled and stored.

For the computation of the LET spectra only coincidence events are selected. For penetrating particles this insures a restricted pathlength in the planar detectors by the telescope geometry. For isotropic arrival directions the mean pathlength for the telescope geometry is 364 μm and this value is used for all events to calculate the LET from the measured energy deposit. However, this LET computation is not correct for stopping particles and for short range secondaries. In these cases the deduced LET underestimates the correct value.

Measurements

On all flights of the AIR project DOSTEL was installed in the nose compartment of the ER-2 aircraft. When the data were checked at the end of the flight series, serious noise background was observed on all flight data except from the two southbound flights and short periods of one northbound flight. Postflight investigation indicated the aircraft TACAN system as the probable source of this interference for the following reasons: a) the instrument was installed close to the transmitter in the nose compartment, b) the TACAN system was shut down on the two southbound flights when the aircraft position was far offshore over the ocean (these time periods show undisturbed data).

Dose and count rates during noise affected periods of the flights can not be analysed.

Results

In the two southbound flights during the time interval 70-320 minutes after activation the measurement reflects the valid data. Fig. 1 shows the count and dose rates (in silicon) during this time period on flight South 1 in more detail. The mean dose rate in silicon for this period is 1.64 μGy/h. Using the periods of undisturbed measurements on the two southbound flights the LET spectra of Fig. 2 were deduced. The two curves combine data from both flights for two latitude regions. In addition one spectra from a Northbound flight is shown. The disturbances by the TACAN system occurred in a LET range between 1 and 20 kev/μm. This LET-range is approximated in Fig. 3 by a straight line.

Discussion

The LET spectra were calculated from the energy deposit distribution in the silicon detector #1 (top) using a mean pathlength of 364 μm and a stopping power conversion factor 1.2 from silicon to water. With quality factors of ICRP 60 (1991) an effective Q-factor of 1.9 was deduced from the LET spectra. Applying both factors the mean dose equivalent rate arrives at 3.7 μSv/h. In the North spectra more particle counts can be noted. The slopes of the North and South spectra are nearly the same, except for high LET values where the slope for the South spectrum becomes more flat.

DOSTEL as a silicon detector based instrument is not tissue equivalent. It was developed to measure ionizing particles and underestimates the high LET contribution induced by neutron interactions compared to a tissue equivalent proportional counter (TEPC). The slope of DOSTEL measurements for civil airflight altitudes in 10 to 13 kmt (Beaujean et al. 1999) agree very well with the slope of the TEPC measurements for both high and low latitude regions (Schrewe 2000). Comparison of DOSTEL with TEPC yield that for this flight altitudes the DOSTEL measurements miss about 21 % of the dose equivalent. Since the neutron contribution in the flight altitude of 20 km is decreased which holds especially for evaporation neutrons, the dose equivalent portion DOSTEL misses should be in the range of 10 % to 15%.

References

Beaujean R, Kopp J, **Reitz G** Radiation exposure in civil aircraft, Rad.Prot. Dos , Vol. 85, Nos 1-4, pp 287-290; 1999.

Burger, P., (Canberra Semiconductors), private communication (1996)

ICRP, 1990 Recommendation of ICRP, Report 60, Oxford, Pergamon Press (1991)

Schrewe, U., ACREM, Rad. Prot. Dos., Vol. 91, No. 4, pp.347-364; 2000

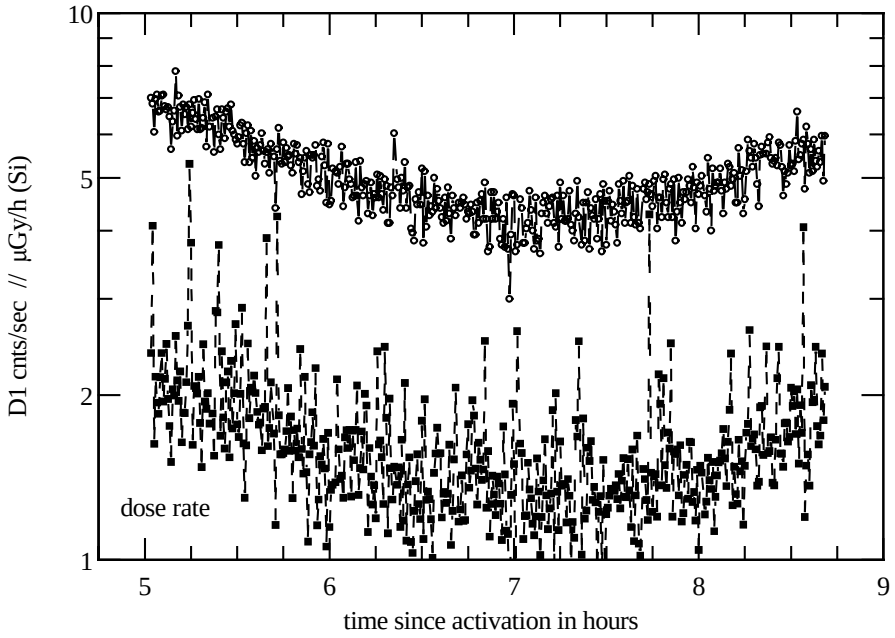

Fig. 1: Undisturbed count and dose rates of flight South #1

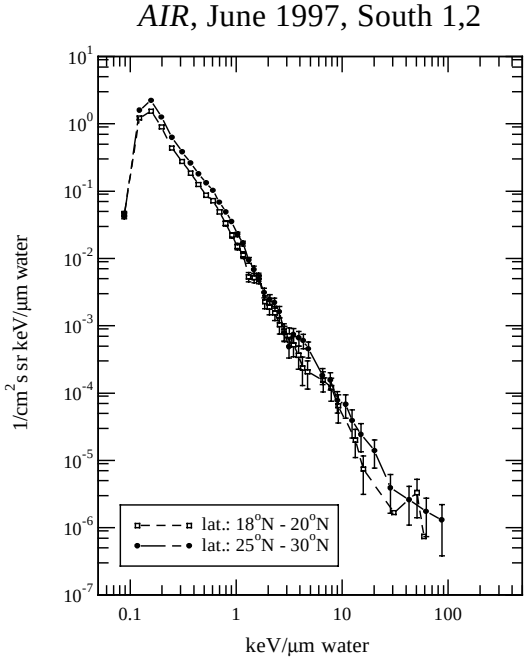

Fig. 2: LET spectra of flights South #1+#2 combined for two latitude regions

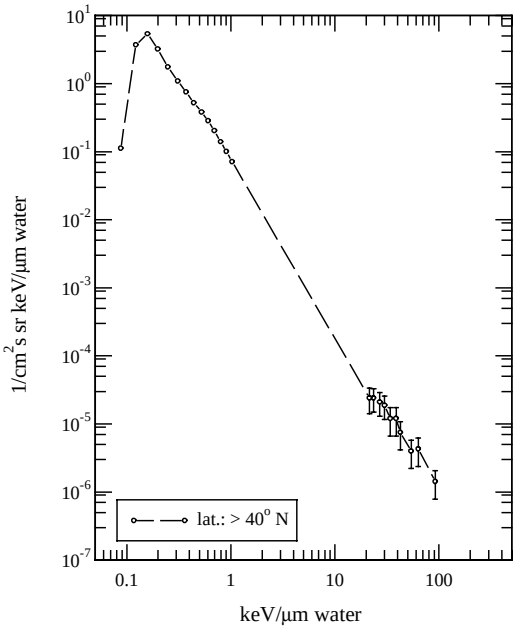

Fig. 3: LET spectra of North#1+#2. Noise effected parts in the LET spectrum are extrapolated by a straight line.

Chapter 9: JSC Particle Telescope

G. D. Badhwar*
***NASA Johnson Space Center, Houston, TX 77058**

JSC Particle Telescope

PHIDE Instrument Description

Figure 1 is a schematic of the telescope geometry. It consists of two 1 mm thick lithium-drifted silicon detectors A1 and A2 that define the geometry of the telescope to be 35° opening angle. These two detectors are followed by four 5 mm thick lithium-drifted detectors (B1 to B4), a 1 mm thick lithium-drifted detector A3 and a sapphire Cerenkov detector, C, which is view by a photomultiplier tube. The whole telescope is surrounded by an NE 102 plastic scintillator mantle, D, that is view by 3/4" diameter photomultiplier tubes. The output of the two opposite tubes is summed and thus there are two independent measurements D1 and D2 from this anti-coincidence detector. Figure 2 is very simplified block diagram of the electronics. The basic trigger of this telescope is A1, A2 and require an incident proton energy > 13 MeV. If this trigger is satisfied, then each of the detectors Al, A2, B1, ... B4, A3, C, and D1 and D2 are pulse height analyzed into 4096 channel analog to digital converter (ADC). In addition, counting rates in each of these detectors is monitored every 10 s, as are the coincidence rates. The linearity and calibration of detector electronics is checked every 4 h using a precision pulse generator. The flight data is recorded on two 20 MB hard disks.

The detector telescope operates in three data modes. Only particles that do not trigger the anti-coincidence scintillator D are analyzed. If the particle stops in any of the detectors then the telescope acts as a double dE/dx x E detector system. For such particles, plot of energy loss ΔE versus total residual energy, E, are hyperbolas corresponding individual isotopes.

$$\Delta E \times E \alpha M^{n-1} Z^2$$

The mass M, charge Z, and energy per nucleon can be calculated using the range-energy relationship, $R (E/M) = (Z^c/M) K E^n$. The constant K and n are obtained by least square fit to the standard range-energy tables for silicon (sapphire). The area-solid angle product ($A\Omega$) varies from 6.23 to 12 CM^2 sr, for an isotropic incident particle flux, depending upon where the particle stops in the detector stack.

If the particle passes through A3, triggers C ($A\Omega = 6.23$ CM^2 sr) without stopping, and gives signal in excess of the scintillation signal, the telescope is the double dE/dx x C mode. In

this case particles with threshold (β_0) energy of > 200 MeV/n. With at least two measurements of ΔE from A1 and A2 (Z^2/β^2) and $C = K_2 Z^2 [1- (\beta_0/\beta)^2]$, one can calculate the charge Z and

velocity of energy/nucleon.

In the intermediate energy range where the particles did not stop in the detector stack or produce a Cerenkov signal, the particles are now known to have energy in the range of ~ 100 -200 MeV/n. In this case, one compares the measurements of energy loss in all seven solid-state detectors Al, A2..... A3, with calculated energy losses in silicon for particle with energy between 100 -200 MeV/n. The energy that gives the best fit to the seven measurements is the incident particle energy. This is done by minimizing the chi-square, χ^2,

$$\chi^2 = \sum [\Delta E_i^{\text{obs}} - \Delta E_i^{\text{meas}}]^2$$

Flight Experience

The system was designed to take data serially with minimal attendance, and the pressure-tight housing had to be opened in order to download the data for analysis. After the engineering flight, the housing was opened, data downloaded, the housing reassembled, and PHIDE placed back in the ER-2. Analysis of the data later showed that the detectors were not receiving power. A subsequent disassembly showed that the main connector had a bent pin that shorted the power and damaged the instrument. No useful data was collected during the first flight series. For the next flight series, provision will be made for downloading data without opening the housing.

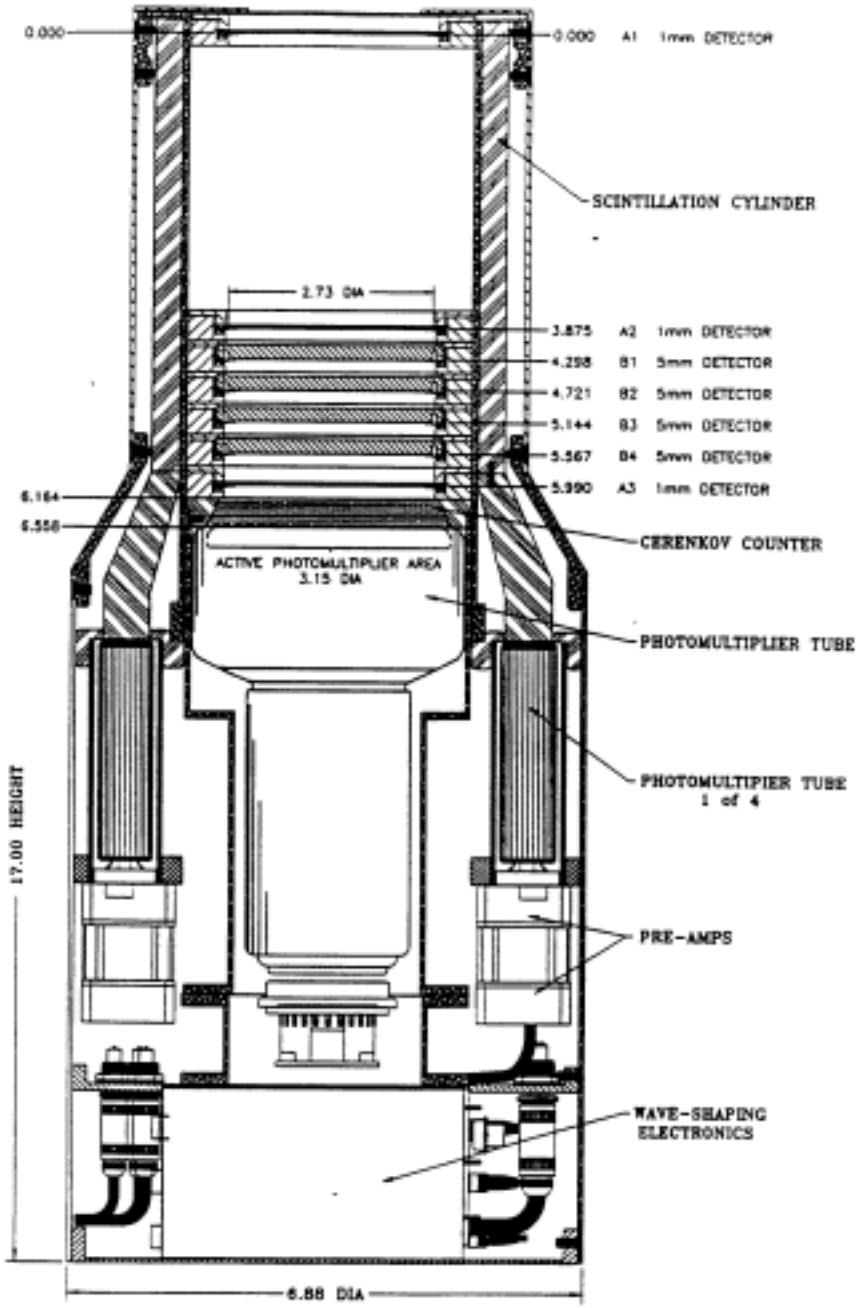

Fig. 1. A schematic diagram of the detector telescope.

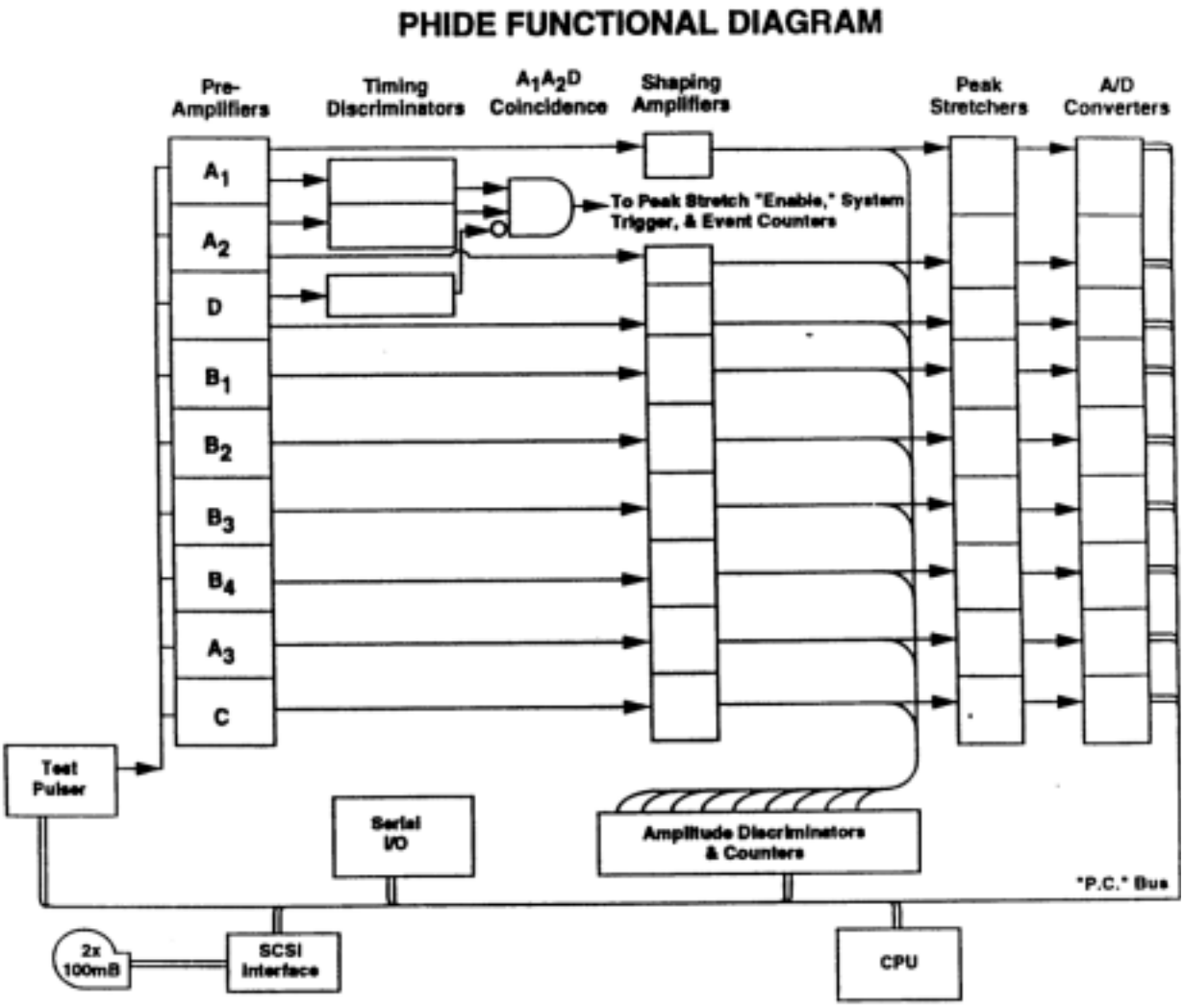

Fig. 2. An electronic block diagram of the detector telescope.

Chapter 10: TEPC Response Functions

J. L. Shinn and J. W. Wilson
NASA Langley Research Center, Hampton, VA 23681-0001

TEPC Response Function

Preface

The tissue equivalent proportional counter had the purpose of providing the energy absorbed from a radiation field and an estimate of the corresponding linear energy transfer (LET) for evaluation of radiation quality to convert to dose equivalent. It was the recognition of the limitations in estimating LET which lead to a new approach to dosimetry, microdosimetry, and the corresponding emphasis on energy deposit in a small tissue volume as the driver of biological response with the defined quantity of lineal energy. In many circumstances, the average of the lineal energy and LET are closely related and has provided a basis for estimating dose equivalent. Still in many cases the lineal is poorly related to LET and brings into question the usefulness as a general purpose device. These relationships are examined in this paper.

Introduction

The energy deposited within a gas from ionizing radiation consists of discrete events with energy partitioning among excitation and ionization processes. As a result, the gas proportional counter allows a measure of the energy deposited in the gas by these discrete ionization events and an accounting of the number of such events. These instruments were first utilized in galactic cosmic ray studies of the bimodal attenuation in the atmosphere of these radiations. This bimodal attenuation consists of, as interpreted by McClure and Pomerantz (1950), a fast attenuating high charge and energy component discovered only a few years earlier (Frier et al. 1948) and a more slowly attenuating component associated with light ion induced nuclear disintegration events. It was only after the introduction of Linear Energy Transfer (LET) as an explanation of radiation quality (Lea 1946, Zirkle et al. 1952) that the use of gas proportional counters were developed as a means of measuring LET for dosimetric purposes (Rossi and Rosenzweig 1955). It was in the difficulties of interpreting the LET results so measured that the randomness of the deposition events became understood and the realization that LET itself was possibly less meaningful than the uncorrected data of the energy deposit spectrum (Rossi 1959, Kellerer 1996). It has been suggested that the usual LET dependent quality factor, Q, be replaced by a microdosimetric (lineal energy) dependent quality factor (ICRU 1986) for use in protection practice.

One of the recognized difficulties of implementing a lineal energy dependent quality factor is limitation in estimating the lineal energy spectra in computational shield design practice (ICRU 1986). In spite of great advances in understanding the physical processes associated with microdosimetry (ICRU 1983), a simplified system of estimation using a triangular lineal energy response model with its many limitations was suggested (ICRU 1986). It was the decision of the ICRP (1991) not to implement such a system although a re-evaluation of the LET dependent quality factor was given. Still, the microdosimeter has been very useful as a dosimetric tool as an indicator of spectral distribution of radiation components of different LET quality. However, the use of such an

instrument to evaluate the degree to which the environment is understood is limited by lack of knowledge of the relation of the radiation fields to the microdosimeter response except under restricted field conditions (Kellerer and Chmelevsky 1975). It is noted by Kellerer and Chmelevsky (1975) that LET is only one of the many factors which determines energy deposition in microscopic sensitive site. Other factors are ion range, energy loss straggling, and energy dissipation by delta-arys. Various regions influenced by these different factors have been plotted (Kelleree and Chmelevsky, 1975) as a function of site diameters and particle energies and there is a narrow region for which the energy deposit can be approximately equated to the value of LET.

Tissue equivalent proportional counters (TEPC) are widely used in both ground and flight measurements of radiation quality. For example, Badhwar et al. (1994) estimated dose equivalent and the derived quality factors at various locations inside the Space Shuttle using onboard TEPCs which are accurate over a wide range of LET. The results reveal that the Q value is higher due to GCR than to Earth's trapped radiation for the Shuttle orbits. The derived quality factors using ICRP-26 (ICRP, 1977) and ICRP-60 (ICRP, 1991) were obtained assuming the measured TEPC lineal energy (y) spectrum to be the LET spectrum (Badhwar et al. 1994). This assumption was necessary since it is difficult to convert a lineal energy spectrum to an LET spectrum, especially for radiation sources as complex as GCR. This is also true for the complex radiation fields existing at the proposed HSCT altitudes. On the other hand, the lineal energy spectra can be obtained when the energy and charge of incident particles are given, by using Monte Carlo method (Zaider et al. 1983, Wilson and Paretzke 1981) which is often time-consuming or, alternatively, by using analytic methods (Wilson and Paretzke 1994, Olko and Booz 1990) for limited ion species and energies. Recently, a generalized analytic model was developed to calculate energy deposition of direct ion events in a micron-size detector for incident ions of arbitrary species and energy (Xapsos et al. 1996). This model is used for the TEPC response calculations made in this study. In the following, a brief description of the analytical model (Xapsos et al.,1996) and its validation are given. The uncertainties related to the use of a TEPC in measuring radiation quality is examined by applying the analytical model.

TEPC Response Model

As an ion traverses a detector volume of micron size, the amount of ionization in the volume will depend on the actual path length of the ion in the volume, the energy transported by delta rays out of the volume, and the energy partitioning between ionization and inelastic excitations. Ions which do not traverse the volume but pass by close enough may also deposit some of their energy by injecting delta rays into the volume. The latter case is usually referred to as indirect events (Kellerer, 1971) or "touchers" (ICRU-36, 1983) and the former as direct events (Kellerer, 1971) or "crossers" (ICRU-36, 1983). The analytical approach developed by Xapsos *et al*. (1996; 1994) to obtain a solution for the ionization spectrum produced in a small volume by the passage of monoenergetic ions is currently limited to the direct events. Herein we will briefly describe the approach for use in the estimate of instrument response and resulting Q values.

As the detector (or target) size becomes smaller, the randomness of energy deposition processes become increasingly important. The relative variance for the single event, V derived by Kellerer (1968) is

$$V = V_L + V_s + V_L \cdot V_s + V_{str} + V_F \quad (1)$$

where V_L is the relative variance of the LET distribution of incident particles, V_s is the relative variance of the particle's path length distribution through the volume, V_{str} is the relative variance of energy-loss straggling and V_F is the relative variance of Fano fluctuations related to the energy partitioning. For monoenergetic particles, V_L is zero and equation (1) reduces to

$$V = V_s + V_{str} + V_F \quad (2)$$

Equation (2) indicates that the probability distribution function for ionization produced by the random traversal of an ion through the volume requires the knowledge of the path length distribution and the energy-loss straggling including the Fano fluctuation. The probability distribution function for the ion's path length can be easily obtained from the chord length distribution of the detector (target) volume assuming that the ion is energetic enough to travel in straight lines through the volume. The energy-loss straggling approximates a lognormal distribution (Xapsos et al.1996). This results because with each collision, the ion loses some random fraction of its energy that is proportional to its energy before the collision. This observation is consistent with the application of the lognormal distribution to the related problem of energy deposition distributions (Wilson and Paretzke, 1994; Condon and Breit, 1935; Lepson, 1976; Burke, 1975). Given $p_s(x, E_j)$ as the probability density distribution function for the lognormal process to produce x number of ionizations related to a path length s of an incident ion j with energy E_j, the overall probability density distribution is then

$$f(x,E_j) = \int_s p_s(x,E_j)\ c(s)\ ds \quad (3)$$

where c(s) is the chord length density distribution function. If the representation of the lognormal process is given as

$$p_s\left(x, E_j\right) = \frac{1}{\sqrt{2\pi}\sigma_s x}\ e^{-\frac{1}{2}\left(\frac{\ln x - \mu_s}{\sigma_s}\right)^2} \quad (4)$$

then the parameters of the lognormal distribution are related to the mean and relative variance of the number of ionizations as follows (Aitchison and Brown, 1957)

$$\mu_s = \ln(\bar{x}) - 0.5\sigma_s^2 \tag{5}$$

and

$$\sigma_s^2 = \ln(1 + V_x) \tag{6}$$

where V_x is the sum of V_{str} and V_F for x number of ionizations.

Unlike the earlier work of Wilson and Paretzke (1994) and Olko and Booz (1990), the evaluation of parameters μ_s and σ_s needed in calculating energy-loss straggling, equation (4), does not rely on curve fitting from existing Monte Carlo results. The parameters are strongly dependent on the detector medium and size, particle types and energy values. The approach here is to obtain an analytical expression for the relative variance V_x so that equation (3) is readily soluble for any given size of detector exposed to an arbitrary ion field .

The relative variance of energy-loss straggling is

$$V_{str} = \delta_2 / \varepsilon \tag{7}$$

where δ_2 is the energy-weighted mean of the energy deposited per ion-electron collision in the site and ε is the average energy deposited in the site by a single ion track (see equation 4 in Xapsos et al. 1996). For a micron size volume of tissue traversed by an ion with energy greater than 3 MeV/A or so, the track width will be large enough to allow some of its deposited energy carried away from the volume by the delta rays. The fraction of such energy loss is treated analytically (Xapsos 1992) and is included in the evaluation of ε. An approximate form for δ_2 is also available from the work of Vail and Burke (1984) for use in evaluation of V_{str}. It is also easy to evaluate the relative variance of Fano fluctuation which is given as (Kellerer 1968)

$$V_F = F\frac{W}{\varepsilon} \tag{8}$$

where F is the Fano factor (Fano 1947) and W is the average energy required to produce an ion pair by the incident radiation. The values for W in various media are widely available from the literature.

The ionization spectrum detected by a TEPC due to random passage of ion j with differential energy flux $\phi_j(E_j)$ is then

$$\Phi_j(x) = \int \phi_j\left(E_j\right)\ f\left(x, E_j\right)\ dE_j \qquad (9)$$

Φ_j (x) can be easily converted to a lineal energy differential spectrum, ψ_j (y), through the relation $y = x\,W/\bar{c}$, where $\bar{c}$ is the average chord length and y is lineal energy. The derived quality factor is then given by

$$Q_j(y)_{TEPC} = \frac{\int y\,Q(y)\ \psi_j(y)\ dy}{\int y\,\psi_j(y)\ dy} \qquad (10)$$

where Q(y) is assumed (Badhwar et al. 1994) to be the ICRP quality factor, Q(LET).

Model Validation

Monte Carlo: The validity of Xapsos model was demonstrated previously by Xapsos et al. (1996) showing good agreement with Monte Carlo results of Olko and Booz (1990). The comparison was for the probability density distribution as a function of ionization produced by a 1 MeV proton randomly incident on a 100 nm diameter water sphere. Also presented (Xapsos et al., 1996) were analytical results for a 1 MeV proton randomly incident on 1 micron and 10 nm diameter spheres of silicon where it is illustrated that the distribution for 1 micron diameter is less affected by energy straggling than that for a nm diameter sphere. As the diameter increases the distribution approaches the microscopic limit resembling more closely the chord length distribution of the sphere which is a right triangle. This is in agreement with the trend presented in the graphs by Kellerer and Chmelevsky (1975) delineating regions of site diameters and energies influenced by various factors other than LET. Here we further present results to illustrate the differences in the distribution due to the varying ion energy. Figure 1 shows the probability distribution as a function of lineal energy *y* for a one-micron diameter water sphere irradiated randomly by a single proton of various energies (from 0.3 to 5 MeV). The results for all the energies are generally in good agreement with the Monte Carlo histograms (Olko and Booz, 1990) showing the same general trend in straggling effect that is less important for the lower proton energies as evidenced by the changing shape of distributions. Although there is a noticeable discrepancy for the lowest energy (0.3 MeV), it has been verified (Shinn et al., 1999) that there is no error in the results calculated using the current model.

Shuttle Flight Experiments: Space qualified instruments are usually small and of light weight with no exception for the TEPCs used in monitoring radiation health of astronauts in Shuttle flights. The detector head used in the Shuttle simulates a 2-micron tissue site which is of cylindrical shape with equal diameter and height (Badhwar et al., 1994). The associated chord-length distribution contains a sharp peak occurring at the chord length equal to the diameter (also the height) with a low flat background. This right circular cylindrical shape allows a better resolution in the measured LET spectral components since many particles traverse near the diameter or through the end surfaces (Badhwar et al., 1992). However, the overall measured lineal energy distribution of GCR fluences for the Shuttle flights show very little resolution due to the overriding effect of energy loss straggling as seen in figure 2 for STS-56. The calculated LET spectrum is obtained using a new version of the HZETRN code (Shinn and Wilson, 1992;

Wilson et al., 1995) to account for the particle-field change as the GCR particles penetrate and interact with the Shuttle structural materials. The figure indicates existing spikes in calculated LET spectrum disappear as the HZETRN results were post-processed with the TEPC response function, in agreement with the measured results. The lower prediction by HZETRN at lineal energy below 2 keV/micron is likely due to the neglect of pions, kaons, and electromagnetic cascade in HZETRN (Shinn et al. 1998) although the response model needs further improvement such as including indirect delta-ray events and wall effects (Rademacher et al., 1998).

Laboratory Experiments: The response model used in the HZETRN post processing has been validated with Monte Carlo comparisons for relatively low energy proton beams. Further validation of the model for high energy particles relevant to space radiations as related to HZETRN code are accomplished by comparing with existing ground-based experimental results. Figure 3 shows dose distributions obtained for the 3.9 GeV nitrogen beam at the Princeton Particle Accelerator (Rodgers et al., 1973). The experimental results are for a 2-micron diameter wall-less counter of spherical shape situated behind a 2-cm thick water column. The present calculation is seen to agree well with the experiment except for the low y (below 10 keV/micron) region for which contributions from indirect delta ray events are not yet considered in the current model. For the same reason, the calculated peak tends to be slightly higher because of normalization. Preliminary results of an extended model (Xapsos, 1999) to include indirect delta ray effect is shown (figure 4) to yield a very good comparison with the data. Other example of validating the model with high energy laboratory data obtained by using 160 MeV proton beam on a 1-micron wall-ess counter at the platteau location of water column (Kliauga et al., 1978) is given in figure 5. The agreement between present calculation and experimental results is reasonably good except for the region above 2 keV/micron. This discrepancy is due to the fact that the present caluclation assumes only slowing down of the proton beam through water column without considering nuclear fragments which are of high LET.

Implications

In the comparison with Monte Carlo calculations and laboratory experiments, it has been illustrated how energy-loss staggling influences lineal energy distribution measured by a spherically shaped detector. Since cylindrically shaped TEPCs are advantageous in spectral resolution and often used in the modern days as in the case of Shuttle experiments, it is of importance to examine the effect of some of the above mentioned factors (Kellerer and Chmelevsky, 1975) on these detectors using the existing response model (direct delta rays only). Figure 6 shows results for the Shuttle TEPC randomly irradiated by protons of various (low) energies. As the energy increases the peak becomes less sharp due to the increase in energy-loss straggling. Moreover, the location of the peaks do not correspond well with the LET values [see inserted table in figure 6] of the monoenergetic protons incident on the gas volume and tends to be located at higher values for all the cases except the lowest energy (0.075 MeV) protons whose range is shorter than some of the detector chord lengths. Very low energy protons as well as short range heavy ions are important contributors to the risk estimate for GCR exposure due to their high LET values although they are less abundent (Cucinotta et al. 1996). It is not clear from the results given in Fig. 6 that a consistent estimate of radiation quality will result from the TEPC measurement.

The effect of the microdosimetric distribution on the estimates of radiation quality can be best seen from the ratio of derived quality factor (see equation 10) over the nominal value as defined by the ICRP for each GCR ion of varying LET and ion charge. For all the results given in the following the LET values correspond to the ion energies above the Bragg peak. Figs. 7 and 8 show such ratio for ICRP-26 and ICRP-60, respectively, with the instrument-derived quality factor being predicted by the analytic model. In general, the deviation from unity is surprisingly large and appears to be greater for ICRP-60 than ICRP-26. This can be explained by the fact the quality factor which is used in equation (10) as a multiplier to the microdosimetric distribution varies less smoothly over the entire LET range for ICRP-60. For example, the peak of predicted lineal energy spectrum for monoenergetic alpha particles of 50 keV/μm in LET is near 72 keV/μm, as shown in Fig. 9. The maximum of the ICRP-60 quality factor is closer to this peak value than that of ICRP-26. As a result, the ratio for ion charge Z = 2 at 50 keV/μm is higher for ICRP-60 (Fig. 8) than for ICRP-26 (Fig. 7). Also, no systematic trend is seen in the predicted ratio across various ion charges nor across varying LET values. For a constant LET of 100 keV/μm, the ratio for ICRP-60 stays at a nearly constant value of 0.81 for all the ions but the ratio for ICRP-26 decreases from 1.1 for light ions to 0.95 for heavy ions. This decrease can be understood by comparing (see Fig. 10) the TEPC lineal energy spectra for alpha particle and titanium, both having an LET of 100 keV/μm. The distribution for titanium tends to weigh more in the region below 100 KeV/μm where the quality factor for ICRP-26 decreases sharply. Note that the difference in the location of these distribution peaks is due to the fact that the track structure for the high-energy titanium ion is wider than the detector site and a substantial fraction of delta rays carrying energy lost by the ion in fact escapes the site.

As mentioned earlier, the model currently used in estimating microdosimetric distribution does not include indirect delta-ray events (except for figure 4) and wall effects; nonetheless, the characteristics of these results probably would not change significantly once these effects were added. The indirect delta-ray events will add very small energy events that result in insignificant dose equivalent contribution and will have minimal effect on the calculated ratio. On the other hand, the wall effect will tend to contribute at the high lineal energy tails of spectra that may slightly increase the ratio depending on the LET of the ion.

Concluding Remarks

Although microdosimeters are useful dosimetric tools to indicate spectral distribution of radiation components of different quality, relating the measured spectrum to knowledge of the environment requires understanding of the detector response functions. The dose equivalent resulting from the measurement may be inaccurate by as much as a factor of two depending on the ion field. For this reason, “measured” dose equivalent may be of limited usefulness in environmental characterization in some applications.

References

Aitchison, J.; Brown, J. A. C. The log normal distribution. Cambridge University Press, Cambridge, U.K.; 1957

Badhwar, G. D.; Konradi, A.; Hardy A.; Braby, L. A. Active dosimetric measurements on Shuttle flights. Nucl. Tracks. Radiat. Meas. 20:12-20; 1992.

Badhwar, G. D.; Cucinotta, F. A.; Braby, L. A.; Knoradi, A. Measurements on the shuttle of the LET spectra of galactic cosmic radiation and comparison with the radiation transport model. Rad. Res. 139:344-351; 1994

Burke, E. A. Ionizing events in small devise structure. IEEE Trans. Nucl. Sci. 22:2543-2548; 1975.

Condon, E. U.; Breit, G. The energy distribution of neutrons slowed by elastic impacts. Phys. Rev. 49:229-231; 1935.

Cucinotta, F. A.; Wilson, J. W.; Shinn, J. L.; Badavi, F. F.; Badhwar, G. D. Effects of target fragmentation on evaluation of LET spectra from space radiations: Implications for space radiation protection studies. Radiat. Meas. 26:923-934; 1996.

Fano, U. Ionization yields of radiations. II. The fluctuations of the number of ions. Phys. Rev. 72:26-29; 1947.

Frier, P.; Lofgren, E. J.; Ney, E. P.; Oppenheimer, F. The heavy component of primary cosmic rays. Phys. Rev. 74:1818-1827; 1948.

International Commission on Radiological Protection. Recommendations of the International Commission on Radiological Protection. Oxford: Pergamon Press; ICRP Publication 26, Ann. ICRP **1**(3); 1977.

International Commission on Radiological Protection. The 1990 recommendations of the International Commission on Radiological Protection. Oxford: Pergamon Press; ICRP Publication 60, Ann. ICRP **21**(1-3); 1991.

International Commission on Radiological Units and Measurements. Microdosimetry. Bethesda, MD: ICRU; Report 36; 1983.

International Commission on Radiological Units and Measurements. The quality factor in radiation protection. Bethesda, MD: ICRU; Report 40; 1986.

Kellerer, A. M. Microdosimetry and the theory of straggling. In biophysical aspects of radiation quality. Second Panel Report, International Atomic Energy Agency, Vienna; 1968.

Kellerer, A. M. An assessment of wall effects in microdosimetric measurements. Radiat. Res. 47:377-386; 1971.

Kellerer, A. M. and Chmelevsky, D. Criteria for the applicability of LET. Radiat. Res. 63:226-234;1975.

Kellerer, A. M. Radiobiological challenges posed by microdosimetry. Health Phys. 70:832-836; 1996.

Kliauga, P. J., Colvett, R. D., Lam, Y. P. and Rossi, H. H. The relative biological effectiveness of 160 MeV protons. Int. J. Radiat. Oncology Biol. Phys. 4: 1001-1008; 1978.

Lea, D. E. Action of radiation on living cells. Cambridge University Press, London and Macmillan, New York: 1946.

Lepson, B. Statistical fluctuations of energy losses of charged particles passing through matter. Adv. Appl. Prob. 8:233-234; 1976.

McClure, G. W.; Pomerantz, M. A. Ionization chamber bursts at very high altitudes. Phys. Rev. 79:911-912; 1950.

National Academy of Science/National Research Council. Radiation hazards to crews of interplanetary missions: Biological issues and research strategies. National Academy Press, Washington, D.C.; 1996.

National Council on Radiation Protection and Measurements. Guidance on radiation received in space activities. Bethesda, MD: NCRP; Report No. 98; 1989

Olko, P. and Booz, J. Energy deposition by protons and alpha particles in spherical sites of nanometer to micrometer. Radiat. Environ. Biophys. 28:1-17; 1990.

Rademacher, S. E., Borak, T. B., Zeitlin, C., Heilbronn, L. and Miller, J.: Wall effects observed in tissue-equivalent proportional counters from 1.05 GeV/nucleon ^{56}FE particles. Radiat. Res., 149: 387-395, 1998.

Rodgers, R. C., Dicello, J. F. and Gross, W. The biophysical properties of 3.9-GeV nitrogen ions. II. Microdosimetry. Radiat. Res. 54: 12-23; 1973.

Rossi, H. H.; Rosenzweig, W. Measurements of neutron dose as a function of linear energy transfer. Radiat. Res. 2:417-425; 1955.

Rossi, H. H. Specification of radiation quality. Radiat. Res. 10:522-531; 1959.

Schimmerling, W.; Wilson, J. W.; Nealy, J. E.; Thibeault, S. A.; Cucinotta, F. A.; Shinn, J. L.; Kim, M.; Kiefer, R. Shielding against galactic cosmic rays. Adv. Space Res. 17: (2)31-(2)36; 1996.

Shinn, J. L. and Wilson, J. W. An efficient HZETRN (A galactic cosmic ray transport code. NASA-TP-3147; 1992. Washington, D.C.

Shinn, J. L.; Badhwar, G. D.; Xapsos, M. A.; Cucinotta, F. A.; Wilson, J. W. An analysis of energy deposition in a tissue equivalent proportional counter onboard the Space Shuttle. Radiat. Meas.; 1999.

Vail, P. J.; Burke, E. A. Fundamental limits imposed by gamma dose fluctuations in scaled mos gate insulators. IEEE Trans. Nucl. Sci. 31:1411-1416; 1984.

Wilson, W. E.; Paretzke, H. G. Calculation of distributions for energy imparted and ionization by fast protons in nanometer sites. Radiat. Res. 87:521-527; 1981.

Wilson, W. E. and Paretzke, H. G. A stochastic model of ion track structure. Radiat. Protect. Dosimetry 52:249-253, 1994.

Wilson, J. W., Badvi, F. F., Cucinotta, F. A., Shinn, J. L., Badhwar, G. D., Silberberg, R., Tsao, C. H., Townsend, L. W. and Tripathi, R. K. HZETRN: Description of a free-space transport and shielding program. NASA TP-3495; 1995 Washington, D.C.

Xapsos, M. A. A spatially restricted linear energy transfer equation. Radiat. Res. 132:282-287; 1992.

Xapsos, M. A.; Burke, E. A.; Shapiro, P.; Summers, G. P. Energy deposition and ionization fluctuations induced by ions in small sites: An analytical approach. Radiat. Res. 137:152-161; 1994.

Xapsos, M. A., Burke, E. A. Shapiro, P.; Summers, G. P. Probability distributions of energy deposition and ionization in sub-micrometer sites of condensed media. Radiat. Meas. 26:1-9; 1996.

Xapsos, M. A. private communication; 1999.

Zaider, M.; Brenner, D. J.; Wilson, W. E. The applications of track calculations to radiobiology. I. Monte Carlo simulations of protons tracks. Radiat. Res. 95:231-247; 1983.

Zirkle, R. E.; Marchbank, D. F.; and Kuck, K. D. Exponential and sigmoid survival curves resulting from alpha and z-irradiation of Aspergillus spores. J. Cell. Comp. Physiol. 39 (Suppl. 1): 75-85; 1952.

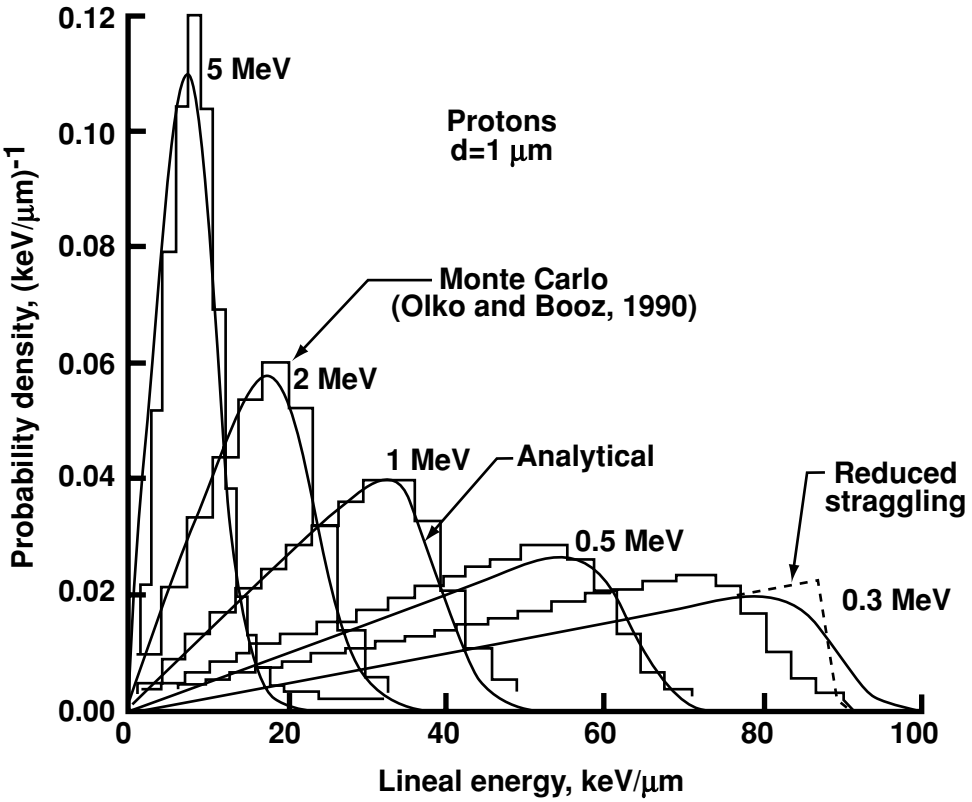

Figure 1. Probability density distributions of lineal energy for a 1-μm diameter water sphere irradiated by a single randomly incident proton of various energies.

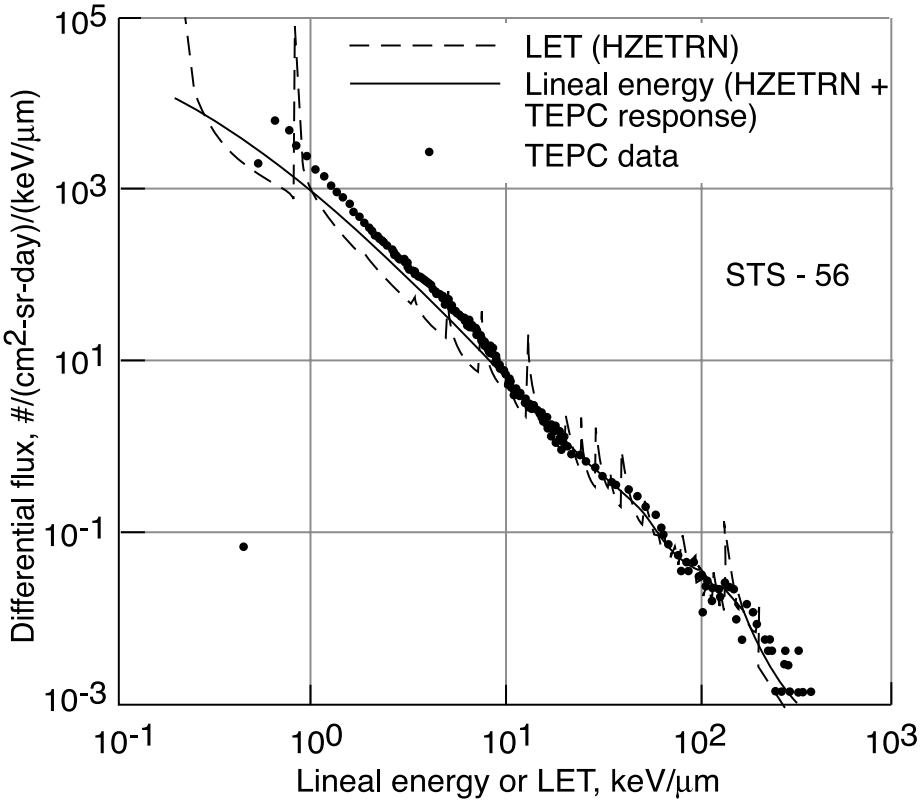

Figure 2. GCR differential LET or lineal energy spectra, in comparison with TEPC data for a 57 degree Shuttle flight.

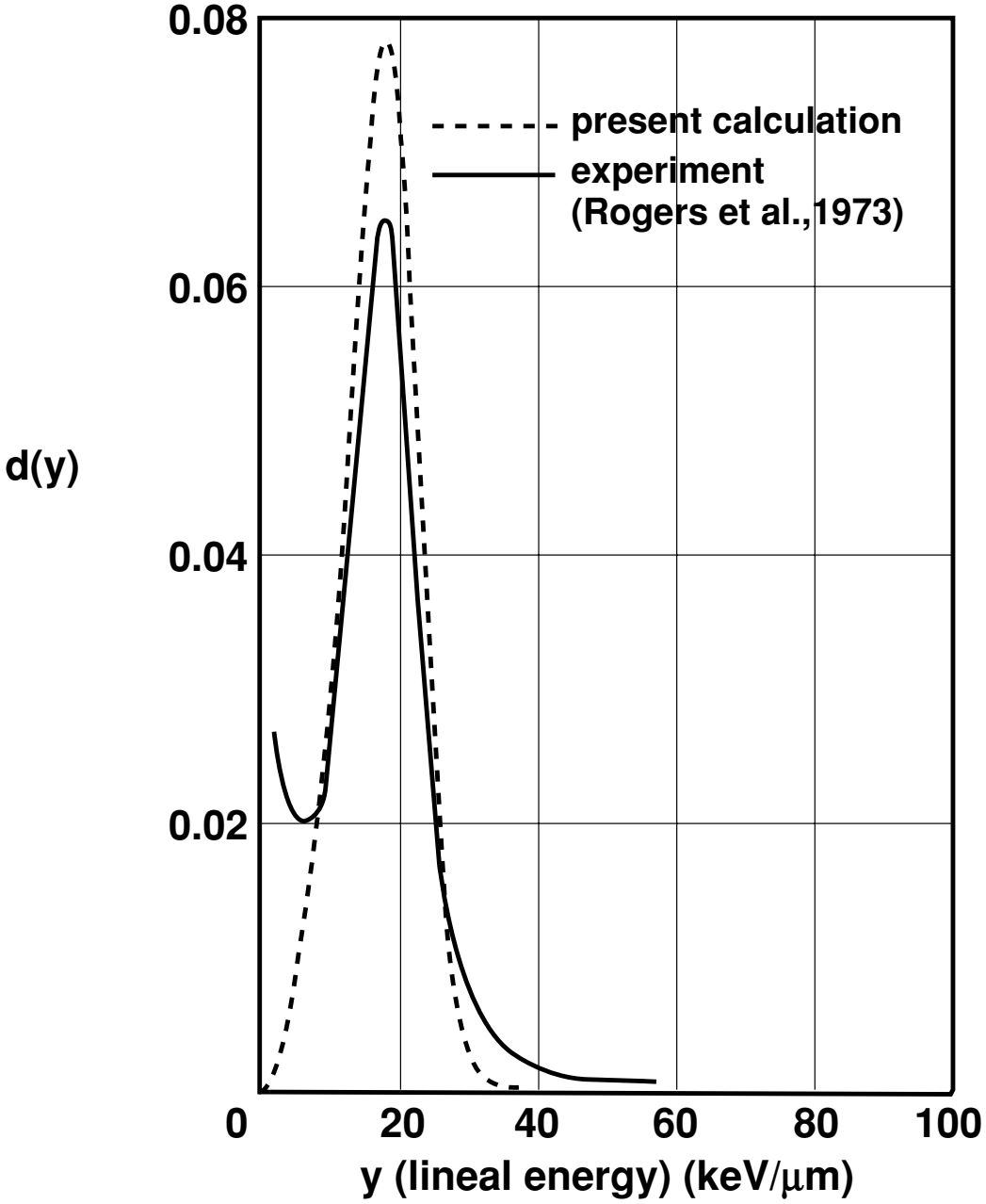

Figure 3. Dose distributions measured by a 2-μm diameter spherical, wall-less TEPC 2-μm depth in a water column irradiated by 3.9-GeV nitrogen ion beam.

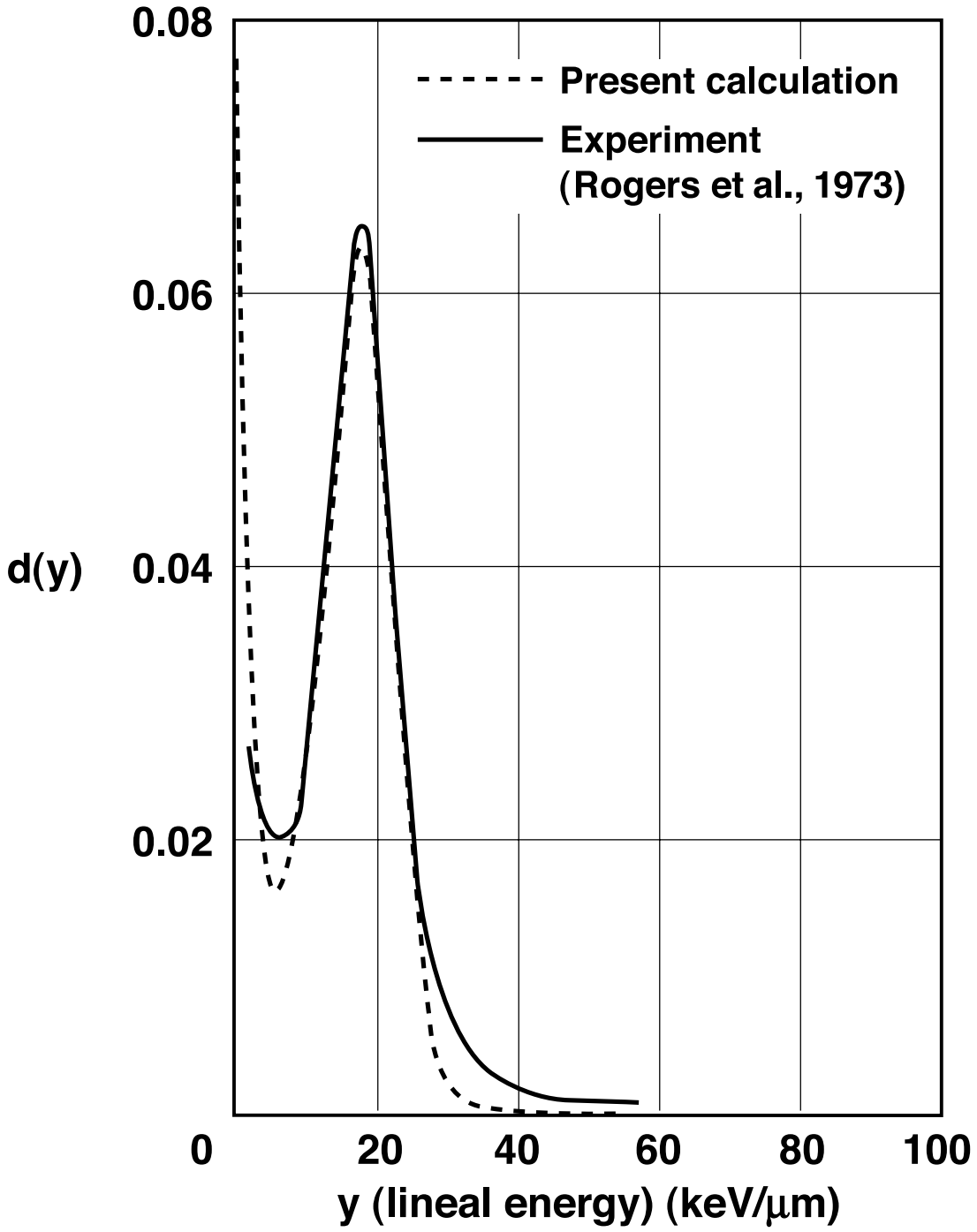

Figure 4. Dose distribution measured by a 2-micron diameter spherical, wall-less TEPC 2-micron depth in a water column erradiated by 3.9-GeV nitrogen ion beam. Calculation includes indirect delta ray effect.

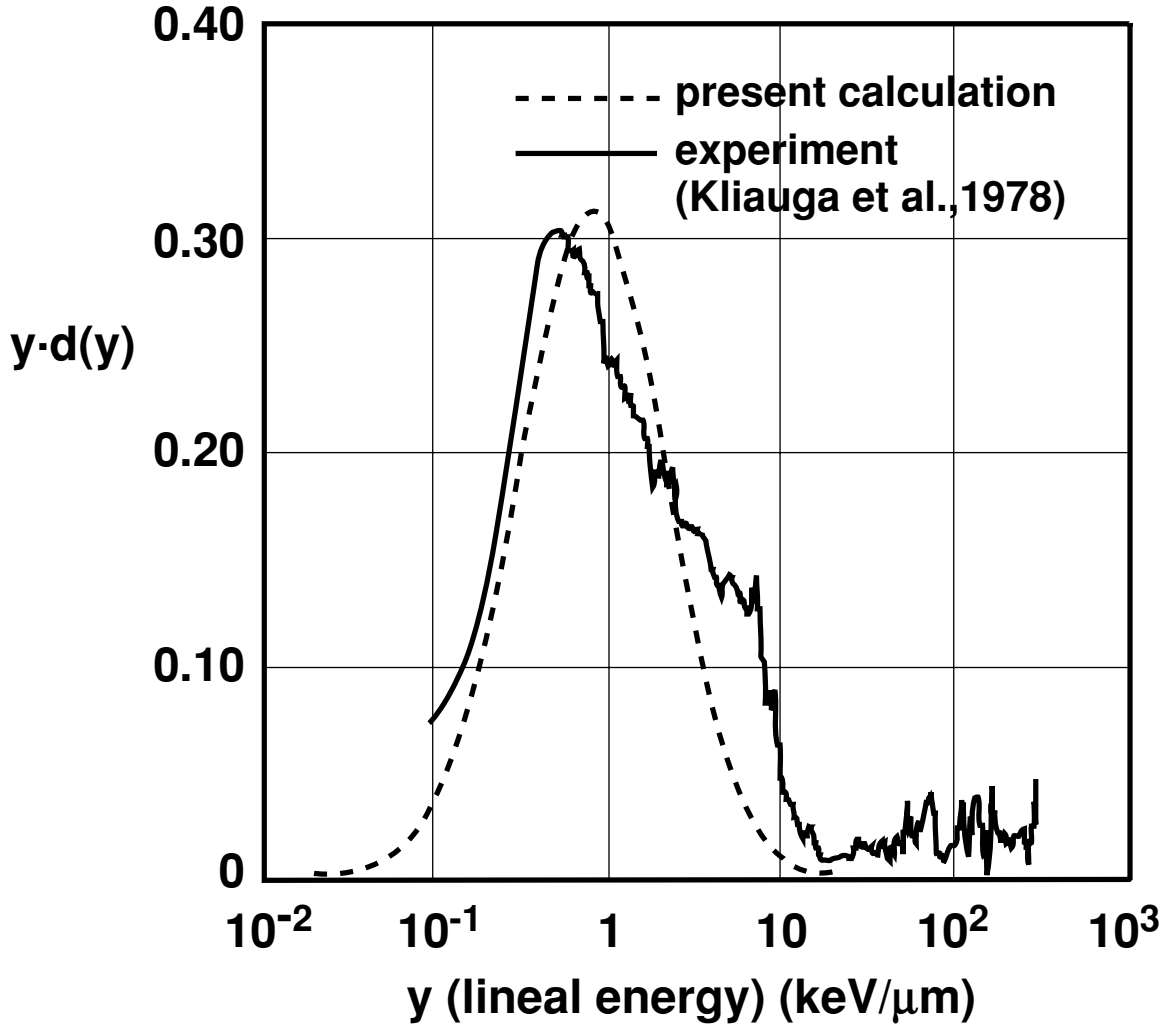

Figure 5. Microdosimetric spectra (dose times lineal energy,y) as a function of y, at 1.9 cm depth (plateau location) in water column irradiated by 160 MeV proton beam, as measured by a wall-less, 1-μm diameter spherical TEPC.

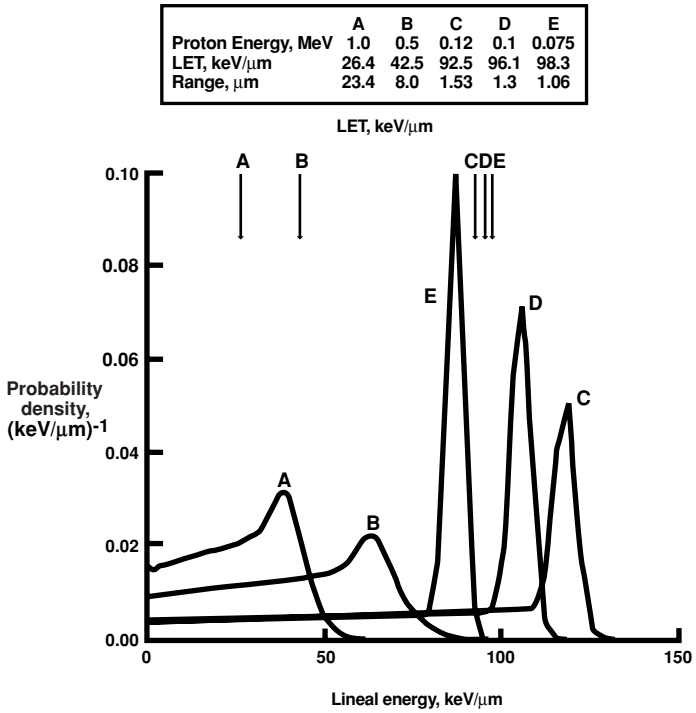

Fig. 6. Probability density distributions of lineal energy for a cylindrical TEPC irradiated by a single randomly incident proton of various energies. The TEPC has equal dimension of a diameter and height which is 1.8 μm in water.

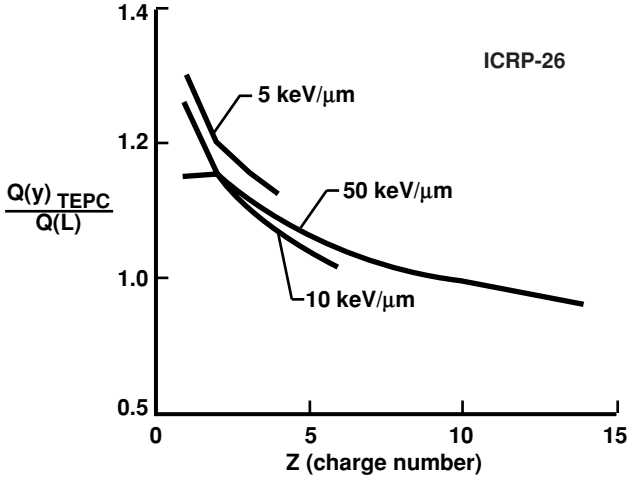

Fig. 7(a). LET < 100 keV/μm

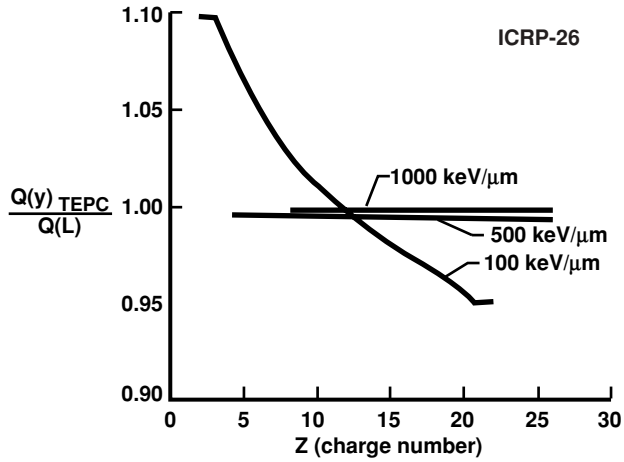

Figure 7(b) LET > 100 keV/μm.

Fig. 7. Ratio of TEPC-derived quality factor over the nominal value for various charged ions of varying LET. ICRP-26 quality factor is used in the calculation.

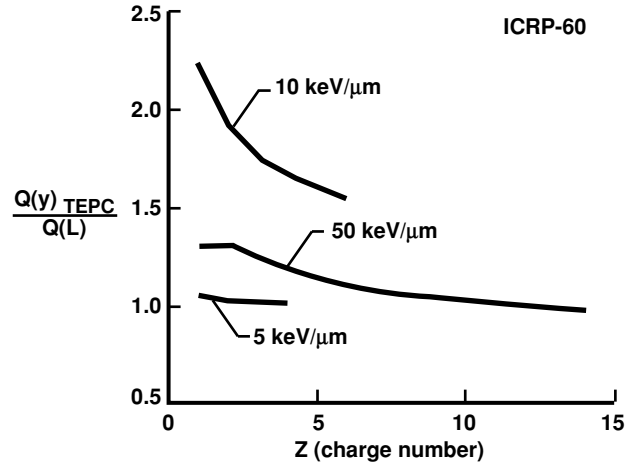

Fig. 8(a). LET < 100 keV/μm.

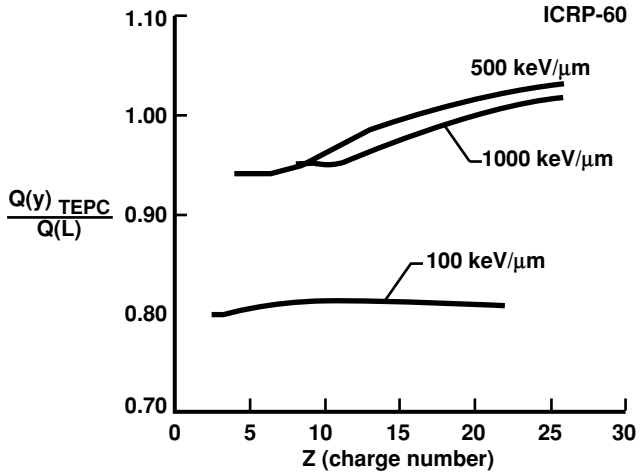

Figure 8(b) LET ≥ 100 keV/μm.

Fig. 8. Ratio of TEPC-derived quality factor over the norminal value for various charged ions of varying LET. ICRP-60 quality factor is used in the calculation.

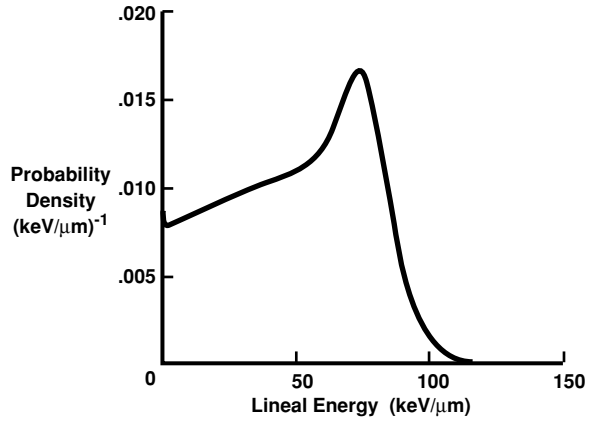

Fig. 9. Probability density distribution of lineal energy for a cylindrical TEPC irradiated by a single randomly incident alpha-particle of 50 keV/μm in LET. The TEPC has the same dimensions as in Fig. 6.

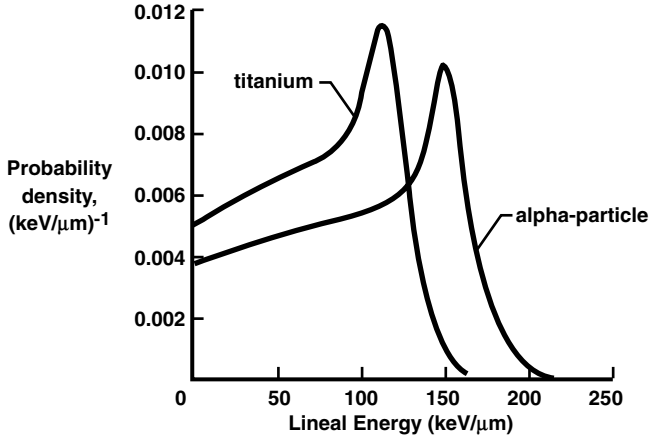

Fig. 10. Probability density distribution of lineal energy for a cylindrical TEPC irradiated by a single randomly incident alpha-particle or titanium ion of 100 keV/μm in LET. The TEPC has the same dimensions as in Fig. 6.

Chapter 11: TEPC Measurements of High Altitude Radiation

Alexander Chee
The Boeing Company, Seattle, Washington

TEPC Measurements of High Altitude Radiation

Preface

The Tissue Equivalent Proportional Counter (TEPC) that was flown by the Boeing Company was built by Battelle Pacific Northwest Laboratories and incorporates a special 5" detector built by Far West Technology, Inc. The overall construction of the TEPC is similar to those originally designed by P. W. Benjamin and associates (Benjamin et al. 1998). The detector was filled with a mixture of gases and pressurized to simulate a cavity of about two microns. The specifications of the TEPC are given in Table 1.

Radiation Measurements

Radiation data was recorded by the TEPC in two sections, each being an energy spectrum of 256 channels. There is a high gain spectrum that covers the range 0 to 25.5 keV/µm in 0.1 keV/µm increments, and there is a low gain spectrum that covers the range 0 to 1280 keV/µm in 5 keV/µm increments. Data, as the number of counts in each energy increment, was recorded at one minute intervals. Absorbed dose was calculated from the counts and, by applying the quality factor from ICRP 60 (1991) and substituting lineal energy for LET, the dose equivalent in each energy increment was calculated. The summation of the individual channels' dose equivalent, gave the overall dose equivalent. Figure 1 shows the absorbed dose data for South flight 1, East flight, and North flight 2. The absorbed dose graphs clearly show the effect of latitude change on the dose rate. For the South flight 1 the absorbed dose rate at Ames was about 125 nGy/min and decreased as the aircraft flew south, reaching 75 nGy/min at the turn around point. On the East flight the absorbed dose rate fluctuated around 125 nGy/min throughout the flight except where it fell to 100 nGy/min when the aircraft dipped in altitude near the midpoint of the flight. On the North 2 flight, the absorbed dose rate went from 125 nGy/min at Ames to 200 nGy/min at the northern most point. Where the aircraft made a dip, it fell to 150 nGy/min. Generally, within the latitude range of the flights, there was an approximately 3 nGy/min increase per degree latitude north of Ames and a similar 3 nGy/min decrease per degree latitude south of Ames. At the altitude where most of the measurements were made, 20 km, a 9.6 nGy/min increase per 1000 m increase in the aircraft altitude was estimated at 55 degrees north. This decreased to 6.35 nGy/min per 1000 m at 37 degrees north, and to 2.5 nGy/min per 1000 m at 17 degrees north.

Figure 2 shows the ten minute running average overall dose equivalent for the South 1 and North 2 flights. The ten minute running averages were calculated in order to reduce the statistical fluctuations that occur due to the small number of interactions that produce these low doses. The dose equivalents around Ames (latitude 37 degrees north), were about 200 nSv/min. Flying south, the dose equivalent fell to 80 nSv/min

and going north, the value rose to about 500 nSv/min. The mid flight dip in altitude for the north flight is also recorded in the dose equivalent tracing. The highly variable nature of the dose equivalent would suggest that a large portion of the dose equivalent is due to a small number of high LET (and therefore high quality factor value) events.

Overall Quality Factor

For each minute of data, the dose equivalent divided by the absorbed dose were computed to produce an overall quality factor. A 10-minute running average was then computed. Figure 3 shows the variation in the overall quality factor for the South 1 flight. The quality factor decreases slightly towards the south but for the whole flight, the quality factor for South 1 flight was about 1.75, with a value of 1.6 at the turn around point. The overall quality factors for the east flight and the north flights showed similar tracings, the overall quality factors being about 2.2 for the east flight and about 2.5 for the north flights.

Quality Factor for Events >10 keV/µm

Analysis of the lineal energy spectrum above 10 keV/µm will give information on high LET radiation. Figure 4 shows the quality factor for events >10 keV/µm, 10 minute running average, for South 1 flight. At the farthest point south, the value was 11. For the east flight and near Ames, the value ranged from 13 to 13.7. At the north end of the north flights the quality factor for events >10 keV/µm was about 13.9.

Percent Dose Equivalent > 10 keV/µm

Calculations were made to determine the fraction of the dose equivalent that came from events > 10 keV/µm. The percentage of the dose equivalent >10 keV/µm for South 1 flight is shown in Figure 5. The percentage varies from about 50% at Ames to 34% at the south turn around point. For the east flight, the percentage stayed at about 55% throughout the flight. And for the north flights, the percentage dose equivalent > 10 keV/µm rose to 62%.

Variation of Radiation Energy Spectrum with Latitude

The values of overall quality factors, quality factors for events >10 keV/µm, and percent dose equivalent from events > 10 keV/µm for various points along the flight paths are given in Figure 6. These three parameters are given as triplets alongside the portion of the flight path with which they are associated. Because the aircraft flew at roughly the same altitude, the values shown are for an altitude of 65,000 ft to 70,000 ft except for the westerly portion of the north flights where the aircraft made an altitude dip to about 53,000 ft. The values at the dip were not noticeably different from those at the other locations. This suggests that at high latitudes and altitudes, the energy spectrum does not change much with altitude.

Comparing the values of the mid and south latitude parameters with the north, it is observed that the overall quality factor decreases slightly at mid latitude but falls significantly at the south (to 65% of the

north value. These results indicate that the change in the profile of the high linear energy transfer (LET) portion of the spectrum was not as great as the change in the overall profile. Thus, going from north to south, the energy distribution within the high LET portion of the spectrum changed only a little but the energy distribution of the overall radiation spectrum shifted significantly to the low LET end.

The percentage absorbed dose from events >10 keV/mm varies from 10.3 percent in the north to 5.3 percent in the south. This further indicates that the high LET portion of the spectrum decreased much faster than the low LET portion. Previous studies have reported the dose equivalent from high and low LET components of the radiation field at 10.1 km., using a quality factor of 6.5 (Hewitt et al. 1980). In Table 2 the dose equivalents from Hewitt et al. are divided by 6.5 to yield absorbed dose values. The table then compares the percent absorbed dose from high LET radiation at two altitudes. At 20 km, going from 55 degrees north to 20 degrees north the contribution of high LET radiation fell by 50%. At 10 km, the drop was even more drastic, at 80%.

Energy Distribution of Ionization Events

Plots of the number distribution of dose versus log of lineal energy were generated from the North 1, East, and South 1 flights. In each case, 51 minutes of data were taken from as far north, as far south, and a portion of East flight. The altitude was kept between 65,000 ft and 70,000 ft. In each plot the cross over point between data from the high and low gain spectra can be clearly seen at 1.4 (log 25.5 keV/μm). Below this point, counts were accumulated in 0.1 keV/μm increments and above this point, counts were accumulated in 5 keV/μm increments. The plots are shown in Figures 7, 8, and 9.

For each plot we compare the low LET portion (where log energy approximately equals 0.5) and the high energy portion (where log energy lies between 1.5 and 2) immediately below and above the ICRP's cutoff point for high and low LET, 10 keV/μm. For North1, the ratio between the low and high LET number distribution of dose was 4.6. For East flight the ratio was 5.5 and for South 1, it was 10. The ratios are given in Table 3. Going from north to south, the low/high LET ratios of y^2 n(y) change slightly at mid latitudes but increase sharply at the south.

Conclusion

At 60,000 to 70,000 ft a relatively small number of High LET events contributed to most of the dose equivalent. At high altitudes, the high energy spectrum changes little with latitude but overall, going from north to south, the spectrum shifts toward low energy end.

REFERENCES

Benjamin, P.W., Kemshall,C.D., and Redfern, J. "A High Resolution Spherical Proportional Counter", Personal communication (preprint) 1998.

Hewitt, J.E., et al. (1980) "Exposure to Cosmic Ray Neutrons at Commercial Jet Aircraft Altitude". Natural Radiation Environment III, CONF-780422, Vol.2 pp.855-881 Washington, D.C., USA.

ICRP (1990). International Commission on Radiological Protection, Publication 60, p.82, T A-2.

Table 1. Boeing Tissue Equivalent Proportional Counter

Detector diameter	5 inches (12.7 cm)
Wall thickness	0.09 inches (0.229 cm)
Wall Material	A-150 tissue equivalent plastic
Simulated sit size	Two microns

Table 2. Percent Absorbed Dose From High LET Radiation

Degrees North Latitude	10 km*	20 km**
55	4.3	10.3
35	3.2	9.1
20	0.9	5.3
% change 55-20 degrees	-80	-50

* From Hewitt(1980); recalculated using q.f. = 6.5
**TEPC measurements, absorbed dose

Table 3. y^2 n(y) for Low and High LET Radiation; North, East, and South Flights*

	North	East	South
Degrees North	52-58	36-38	18-21
Low LET	800,000	500,00	220,000
High LET	175,000	90,000	20,000
Low/High Ratio	4.6	5.5	10

* at 65,000 ft to 70,000 ft

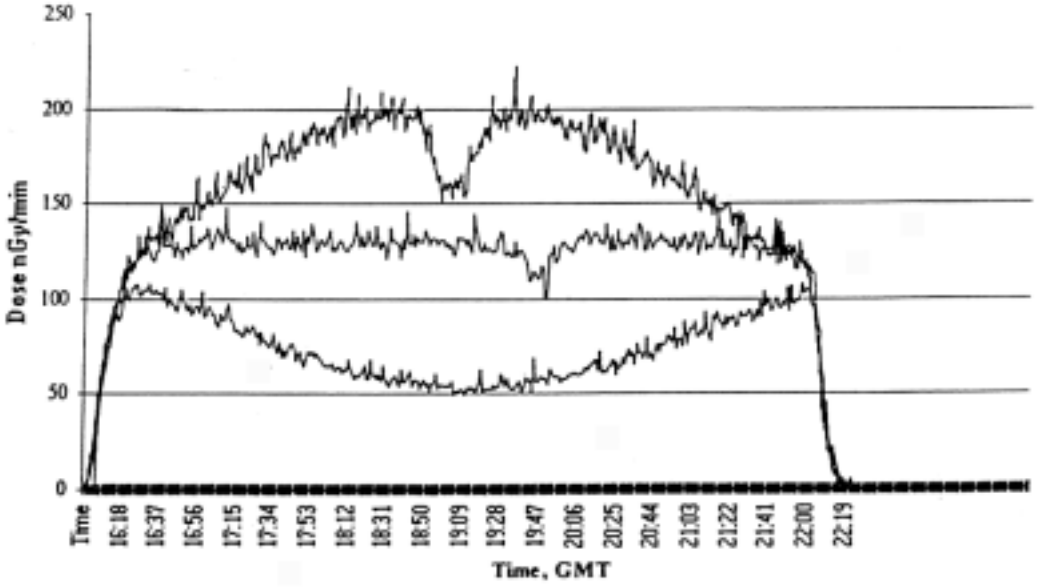

Figure 1. Absorbed Dose During ER-2 Flights; South 1 (lowest graph), East, and North 2 (top graph).

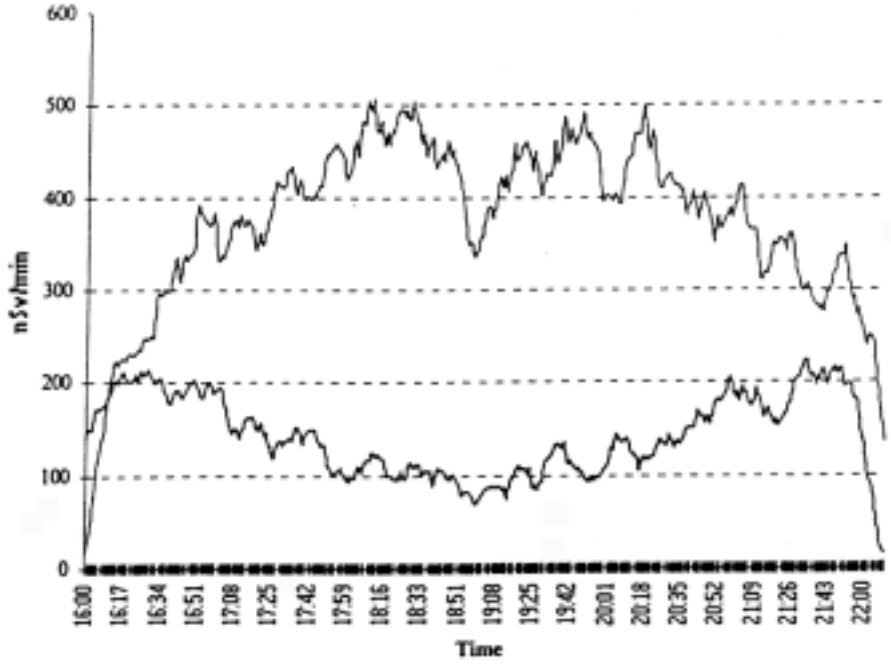

Figure 2. Dose Equivalent, 10 min Running Average; North 2 (top graph) and South 1 Flights.

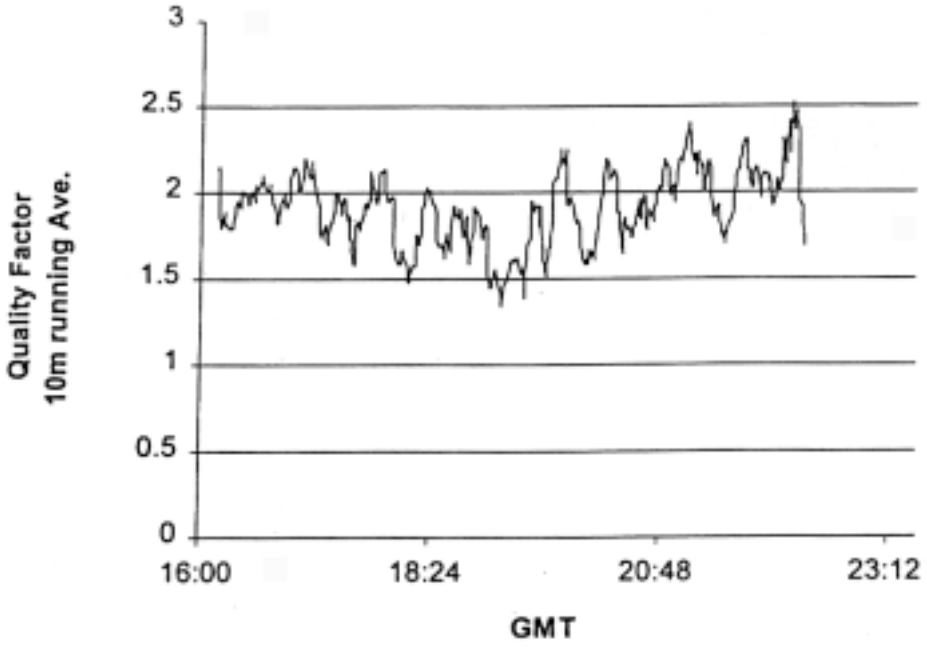

Figure 3. Overall Quality Factor for South 1 Flight.

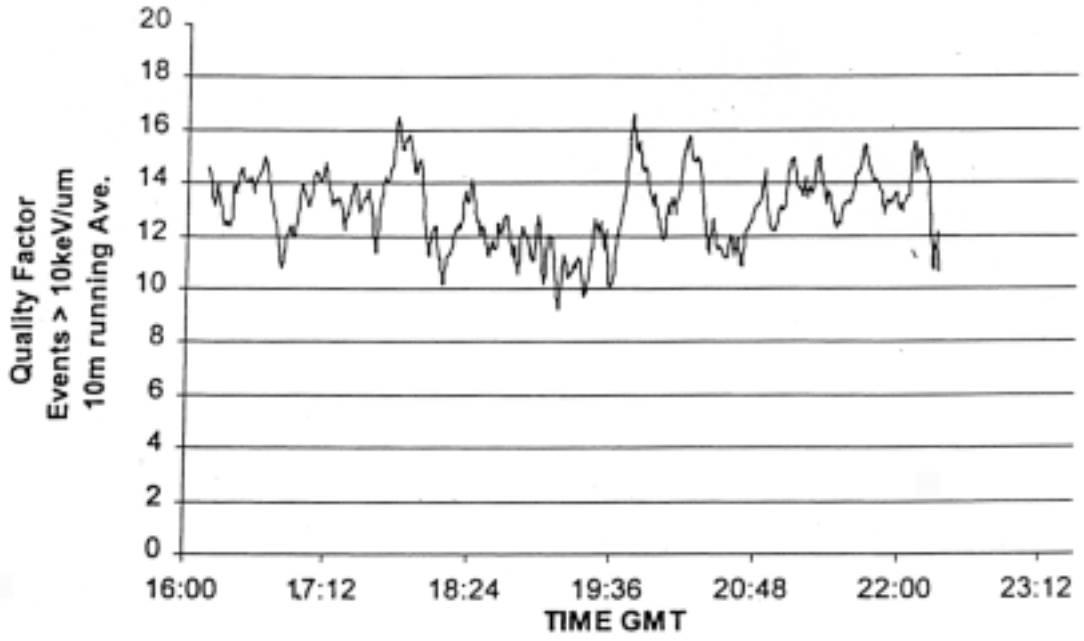

Figure 4. Quality Factor for Events > 10 KeV/μm, South 1 Flight.

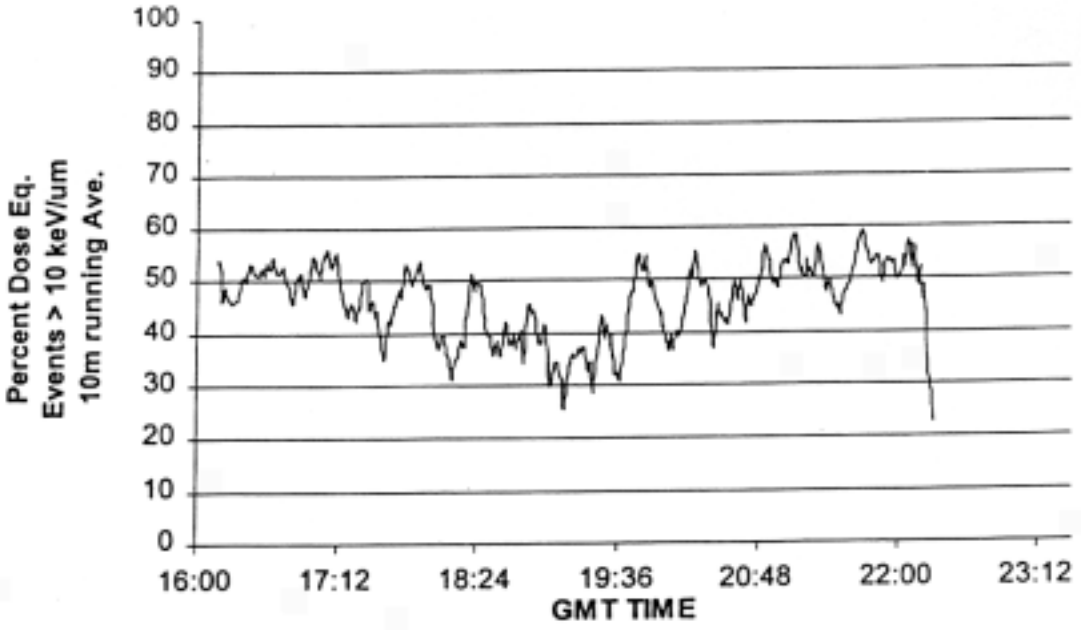

Figure 5. Percent Dose Equivalent from Events > 10 KeV/μm, South 1.

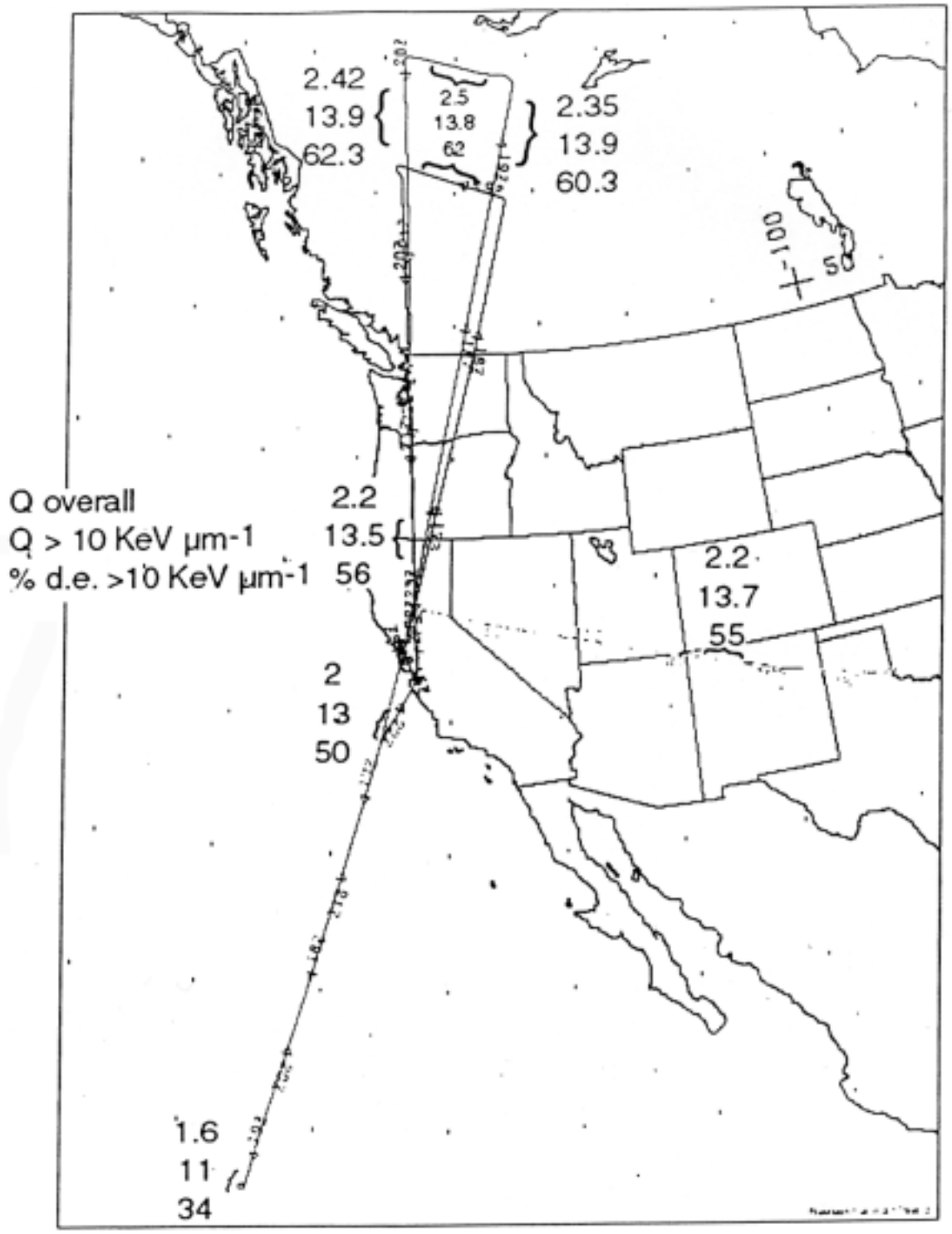

Figure 6. Values of Q Overall, Q > 10 KeV μm^{-1} Particles, and Percent Dose eq > 10 KeV μm^{-1} Along Flight Paths.

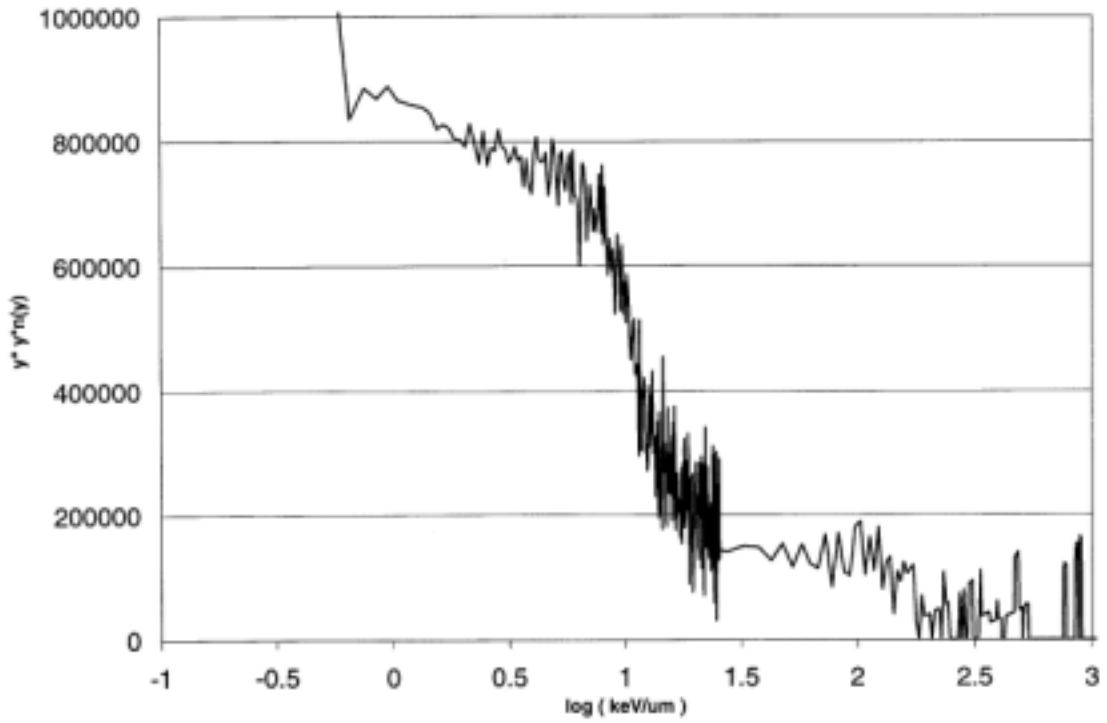

Figure 7. North Spectrum 51min.

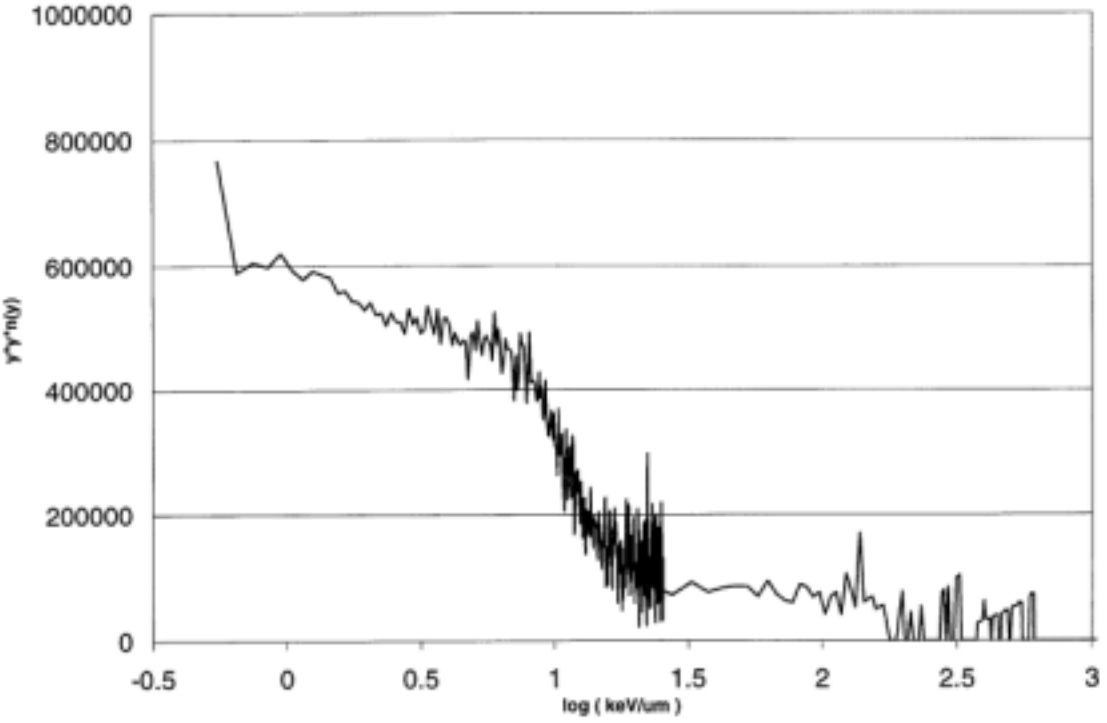

Figure 8. East Spectrum 51min.

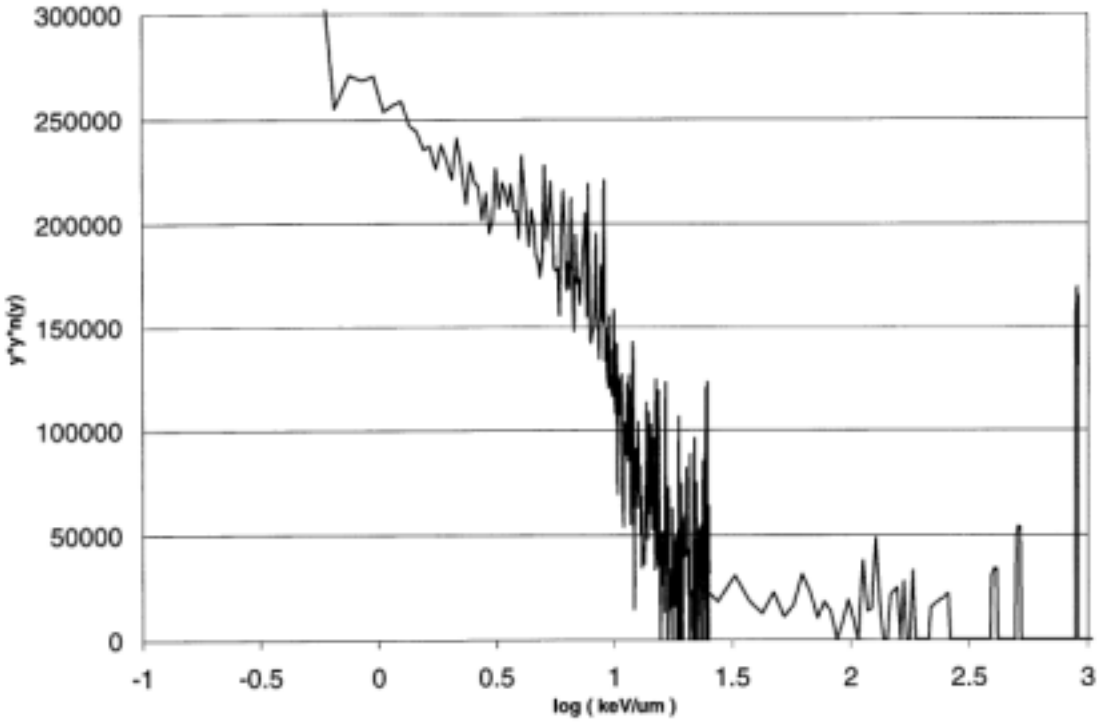

Figure 9. South Spectrum 51min.

Chapter 12: Assessment of High-Altitude Cosmic Radiation Exposure Using Tissue Equivalent Proportional Counters and Bubble Detectors

P. Tume, B.J. Lewis, L.G.I. Bennett and M. Pierre
Royal Military College of Canada, P.O. Box 17000 Stn Forces, Kingston, Ontario, Canada, K7K 7B4

T. Cousins, B.E. Hoffarth, T.A. Jones and J.R. Brisson
Defence Research Establishment Ottawa, Ottawa, Ontario, Canada, K1A 0Z4

Assessment of High-Altitude Cosmic Radiation Exposure Using Tissue Equivalent Proportional Counters and Bubble Detectors

Introduction

In 1995, the National Council on Radiation Protection and Measurements recommended that a program be established to reduce the health risks associated with high-altitude transport so as to be comparable with those of ground-based workers (NCRP 1995). Consequently, NASA Langley Research Center initiated the Atmospheric Ionizing Radiation (AIR) Mission with the specific objectives to: (i) understand the composition, intensity and spectral distribution of the natural radiation field at high altitudes (50 000 to 70 000 ft), and (ii) improve the understanding of health risk estimates. The results from these flights will be used to validate a transport computer code. Ultimately, this information will be used to develop a risk management philosophy, and its supporting technology, for personal in-flight exposures.

To support this task, NASA has organized an international effort to instrument an ER-2 aircraft with a variety of radiation detectors, spectroscopy and dosimeter systems. Sponsored by the Department of National Defence, the Canadian instrument package consists of a tissue equivalent proportional counter (TEPC) and neutron sensitive bubble detectors (BDs). This paper documents the analysis of the TEPC and BD results and summarizes these measurements with respect to the ER-2 flight parameters. The present results are also compared to those recently obtained on Northern subsonic flights using the same equipment.

Equipment

Tissue Equivalent Proportional Counter A 5-inch diameter detector built by Far West Technologies was used to measure the total ionization (produced by all types of radiation) in a simulated ~2 μm (i.e., 1 x 10^{-6}m) tissue volume. By design, the TEPC walls are sufficiently thin so that they do not attenuate the incident radiation, but are thick enough to establish secondary particle equilibrium. By sampling a portion of the charged track left from the passage of the radiation, the measured (lineal) energy spectrum can be related to the absorbed dose and dose equivalent for in-flight measurement. The calculation of dose equivalent depends on the choice of the quality factor (Q), which can be a function of either the LET or lineal energy (y) (see Section 2.3) (ICRP 1991, ICRU 1986). The analysis software developed for the TEPC implicitly uses a Q versus LET relationship, as recently recommended by the ICRP-60 (1991).

The TEPC cannot specifically distinguish between all types of particles due to an overlap of spectral contributions, although certain lineal energy regions are commonly associated with a specific particle type. For instance, ionizing events due to electrons (produced by primary and secondary photons) have lineal energies that are less than 10 keV/μm, recoil protons occur in the range of 5-100 keV/μm, and heavy ions lie in the region of 100-1000 keV/μm. Cosmogenic neutrons, which are produced as secondary particles due to primary proton interaction with atmospheric

nuclei, typically have an LET greater than 10 keV/μm. Thus, an estimate of the high-LET component of the in-flight radiation field (of which neutrons are a major component) can be crudely estimated. Unfortunately, the neutron energy spectrum is not specifically available in this type of measurement.

Bubble Detectors The bubble detector (BD) consists of a polycarbonate tube filled with an elastic polymer gel in which micrometer-sized superheated droplets of detector liquid have been homogeneously dispersed. Although BDs are sensitive to temperature variations, a temperature-compensated model has been chosen for the present investigation. The BD-PND model has a liquid overlay above the gel to provide an operating region between 17 to 40°C where the sensitivity of each detector is known to within 25%. The detector is activated by relieving pressure above the superheat matrix by unscrewing a piston adjacent to a rubber diaphragm. The linear energy transfer from recoil protons, produced from neutron interaction with the detector medium, boils the superheated liquid to form gas bubbles. The polymer matrix traps these bubbles, after which they can be counted for a given flight leg. Since the BD-PND has been characterized for a cosmogenic neutron spectrum (see Section 2.4), it is possible to convert the count to an ambient dose equivalent (in ICRP-60 units) for a given flight.

Because of the possibility of significant temperature variation in the present experiment, a temperature-controlled instrument package was developed. This package consists of a hermetically sealed aluminum outer cylinder and bottom mounting plate (see Figures 1(a) and 1(b)). Inside the inner cylinder are up to 18 bubble detectors, a temperature control circuit, a pressure transducer and a data logger to record real-time temperature and pressure data. Temperature control was maintained with flexible heating strips and a thermostat control, by employing a thermocouple inside the gel of an inactive BD. The pressure transducer was used to confirm that the internal pressure of the package remained at the sealing pressure of one atmosphere. The BD package was located in the Q bay of the ER-2 aircraft.

Microdosimetry Theory Energy deposition in the TEPC ionizes the detection gas and produces an electronic signal that is collected at the detector anode. A multichannel analyzer (MCA), which measures the pulse size received by the counter, processes the signal. The pulse heights are assigned to a lineal energy bin from which an event frequency distribution may be obtained. Processing of the TEPC data is a non-trivial process, which is briefly explained below to aid in the data interpretation in Section 4.2.1 (Gerdung et al. 1995, Rossi and Zaider 1996, Walker 1995).

The lineal energy, y, is the quotient of the quantity of energy imparted to matter in a volume of interest (by the passage of radiation) to the mean chord length in the volume. For a spherical gas cavity, the pulse height calibration relationship is:

$$y = h \frac{\delta \varepsilon_c}{h_c} \frac{3}{2d} G_r \qquad (1)$$

where h is the measured pulse height, $\delta\varepsilon_c$ is the energy loss of the calibration source, h_c is the pulse height of the calibration point, d is the cavity diameter and G_r is the ratio of the gain with respect to the analog-to-digital converter.

From the TEPC counts, a cumulative distribution function, F(y), can be developed for the probability that the lineal energy is equal to or less than y:

$$F(y) = \frac{\sum_{Channel=0}^{Channel\ of\ energy\ y} Counts}{\sum_{Channel=0}^{All\ Channels} Counts} \tag{2}$$

The probability density function, f(y), follows:

$$f(y) = \frac{dF(y)}{dy} \approx \frac{\Delta F(y)}{\Delta y} \tag{3}$$

where the bin width Δy is defined for a given instrument gain. For the present measurement series, the high-gain region was 0 to 22 keV/μm, with a bin width of 0.092 keV/μm. This bin width provided an increased resolution for the high-count bins compared to the low-gain region which covers the remaining channels up to 1273 keV/μm with a bin-width of 5 keV/μm.

Mean quantities can be calculated from the microdosimetric distributions. Here, the first moment of f(y) is the frequency mean lineal energy as defined by:

$$\bar{y}_F = \sum_{y=0}^{y=1272.5} yf(y)\Delta y \tag{4}$$

and the dose mean lineal energy is given by:

$$\bar{y}_D = \frac{1}{\bar{y}_F} \sum_{y=0}^{y=1272.5} y^2 f(y)\Delta y \tag{5}$$

Equation (5) specifically gives the average value of the lineal energy for the absorbed dose distribution. Finally, the absorbed dose distribution is defined as:

$$d(y) = \frac{y}{\bar{y}_F} f(y) \tag{6}$$

The calculation of the integral absorbed dose, D, is somewhat complex and must take into account several factors including: the pulse height at each lineal energy, the frequency distribution, the conversion from lineal energy into

specific energy (i.e., microscopic absorbed dose) and the detector calibration and dimensions. The total dose equivalent, H, is then given by:

$$H = D\overline{Q} \tag{7}$$

where the average quality factor is determined from:

$$\overline{Q} = \int Q(y)d(y)dy \tag{8}$$

In summary, the output of the TEPC provides the number of counts as a function of the lineal energy (y) which, in turn, is converted into a probability density function for both the absorbed dose, d(y), or similarly the dose equivalent, i.e., h(y) =d(y)Q(y). The quality factor Q(y) can be related directly to the lineal energy, as described by the International Commission on Radiation Units (ICRU 1986) (publication 40), or estimated by replacing y with LET and following the standard ICRP-60 recommendation (Appendix A).

Bubble Detector Calibration The number of bubbles (N_B) accumulated over the various high-altitude flights were recorded. From these measurements, the neutron dose equivalent (DE_n) was evaluated from:

$$DE_n = \frac{N_B}{RD} \tag{9}$$

The calibration factor for the BD is given by the response-to-dose equivalent (Tume et al. 1999):

$$RD = \frac{\int \frac{RF(E)\phi(E)}{h(E)} dE}{\int \phi(E)\, dE} \tag{10}$$

Here RF(E) is the energy response function of the detector (as determined from high-energy accelerator experiments), ϕ(E) is the cosmic-ray neutron-energy spectrum, and h(E) is the ambient dose equivalent-to-neutron conversion function. For the original calibration, the manufacturer used an AmBe neutron spectrum in combination with a known RF(E) up to 20 MeV and a referenced function h(E) that predates the current ICRP recommendation units. This approach is acceptable for most terrestrial applications where the shape of the spectrum typically extends to approximately 12 MeV. However, for aircrew applications, the cosmic-ray neutron spectrum must be used.

Prior to this work, the response function, RF(E), was known to 20 MeV, but has been extended in this study to 500 MeV (Figure 2). To calibrate the BDs, experimental measurements of the response-to-dose equivalent (RD) were made at the TRI-University Meson Facility (TRIUMF). This facility was chosen since the neutron spectrum generated at the Thermal Neutron Facility (TNF) at TRIUMF simulates the neutron spectrum encountered (up to 500 MeV in energy) by aircrew at jet aircraft altitudes (Figure 3) (Hess et al. 1959, Hess et al. 1961). The 100 MeV feature in the TRIUMF spectrum is also thought to exist in the neutron spectrum encountered by aircrew. However, this feature was not observed by Hess et al. owing to the resolution capability of the instrumentation and the

unfolding procedures used when the spectrum was proposed some forty years ago. This is more clearly seen in the lethargy plot of Figure 4 which compares Monte Carlo calculations based on the FLUKA code (at a depth of 700 g cm^{-2}) (Roesler et al. 1998) with the TRIUMF and Hess spectral shapes.

The RD factor in Eq. (10) must be referenced to a specified system of dose conversion units. Several modelling reference systems exist for various irradiation conditions and geometry. In this work, the absolute calibration factor for the BD-PND was based on a combined h(E) function using the H*(10) operational units of Schuhmacher et al. (at a 10 mm depth inside an ICRU sphere and below 20 MeV) and Sanikov et al. (at a 10 mm depth on a slab and above 20 MeV) (see Figure 5) (Schuhmacher and Siebert 1992, Sanikov and Savitskaya 1997). In both cases, the authors use a plain, parallel incident neutron beam and ICRP-60 units. Sanikov and Savitskaya have argued that this choice of model geometry best represents the equilibrium irradiation conditions for high-energy neutron exposure behind accelerator shielding. By inference, this argument can also be applied to aircrew in which there is atmospheric shielding and a constant source of incident high-energy radiation.

Using Eq. (10) with the respective curves for RF(E) in Figure 2, the TRIUMF spectrum in Figure 3, and the stated dose equivalent conversion function h(E) in Figure 5, an integral value of RD = 4 ± 1 bubbles μSv^{-1} is calculated (for a lower integration limit of 1×10^{-8} MeV and an upper integration limit of 500 MeV). This conversion factor is applicable to a detector with a given sensitivity of 6 bubble μSv^{-1} as calibrated by the manufacturer in an AmBe neutron spectrum. This integral value is in good agreement with that measured at TRIUMF (i.e., 5 ± 1 bubble μSv^{-1}). Similarly, the TRIUMF spectrum can be replaced by the actual Hess cosmogenic neutron spectrum of Figure 3, yielding a final RD value of 4 ± 1 bubble μSv^{-1}.

Clearly, the feature at 100 MeV present in the TRIUMF spectrum (see Figure 3 or 4) does not contribute significantly to the value of RD because of the overall lower neutron flux at this energy. The "actual" shape of the cosmogenic neutron spectrum is expected to be close to that calculated with the FLUKA code (Roesler et al. 1998). Since the shape of the lethargy plot of the FLUKA spectrum falls somewhere between that of Hess and TRIUMF in Figure 4, the calibration factor will be bounded between the two values of 4 and 5 bubble μSv^{-1}, as determined previously for the Hess and TRIUMF spectra, respectively. An RD = 4 ± 1 bubble μSv^{-1} is selected in the present analysis (i.e., until a better spectral measurement becomes available) since this lower-bound value will yield a more conservative calculation for DE_n in Eq. (9). Since each detector has a unique sensitivity, the calibration factor can be suitably scaled to reflect the given sensitivity. Having properly calibrated the BD, this simple (passive) device can be used routinely for in-flight measurement of the neutron dose equivalent.

Experimental Results

ER-2 Flight Series Description In accordance with NASA scheduling, Flight series A consisted of 5 flights from June 2-15, 1997. While all of the flights originated and terminated at the AMES flight center in California (see Table

1), the flight routes spanned 19 to 56° North latitude. For example, the flight profiles for the East, North 2 and South 2 flights are shown in Figures 6 (a), (b) and (c), respectively.

Table 1: AIR Flights at Ames in June 1997

Flight	Date	Duration (h)	AIR #	Ames Sortie #	Start Time	End Time
Engineering Test	2 June	2	101	N97104	1:00pm PDT 20:00 GMT	3:00pm PDT 22:00 GMT
East	5 June	6.5	102	N97105	9:00am PDT 16:00 GMT	3:33pm PDT 22:33 GMT
North 1	8 June	8	103	N97106	9:00am PDT 16:00 GMT	4:47pm PDT 23:47 GMT
South 1	11 June	6.5	104	N97107	9:00am PDT 16:00 GMT	3:30pm PDT 22:30 GMT
North 2	13 June	6.5	105	N97108	9:00am PDT 16:00 GMT	3:37pm PDT 22:37 GMT
South 2	15 June	6.5	106	N97109	11:00am PDT 18:00 GMT	5:24pm PDT 00:24 GMT

Tissue Equivalent Proportional Counter Using Equation (6), the absorbed dose can be best represented as a yd(y) versus log(y) plot (see Figure 7). In this type of plot, equal areas under the curve represent equal amounts of dose.

The absorbed dose distribution obtained from both the DREO and Boeing TEPCs are consistent for both the North-2 (N97108) and South-2 flights (N97109) (see Figures 7 and 8), except for an anomalous spike in the DREO data near 9 keV/μm for the North-2 flight. This spike is thought to be attributed to noise. The spike event affects the total spectrum (as per the discussion in Section 2.3) and results in a somewhat skewed yd(y)-distribution in Figure 7 (i.e., compared with Figure 8), where the DREO data fall below the Boeing data. Spectral structure similar to Figure 8 was observed on the East flight, where both the DREO and Boeing units were in agreement.

The absorbed dose distribution for the North-2 flight from the Boeing TEPC is again reproduced in Figure 9. As expected, most of the absorbed dose distribution is observed below 10 keV/μm. This result is consistent with previous measurements made on a First Air flight on May 6, 1997 aboard a Boeing 727 at an altitude of approximately 35 000 ft over Northern Canada. The latter flight consisted of 5 flight legs (total flight time of 10 h) which spanned 68 ^{o}N to 74 ^{o}N latitude from Ottawa, ON (YOW) to Iqaluit (YFB), Iqaluit to Resolute Bay (YRB), Resolute Bay to Nanisivik (YSR), Nanisivik to Iqaluit and Iqaluit to Ottawa. Interestingly, the higher altitude ER-2 flight shows a flatter and more extended low-LET contribution below about 7 keV/μm. There is also a slightly greater high-LET contribution for this ER-2 flight.

As indicated in Figure 10, the dose mean lineal energy (see Eq. (5)) appears to double with increasing latitude from 19 to 56° North for the same altitude. The plateau near 56° North is an artifact of the slight decrease in altitude during the turn around on the North-2 flight. Since the dose mean lineal energy is the integral of yd(y) (see Eqs. (5)

and (6)), it is not surprising that both TEPCs exhibit the same trend. The East flight has a mean lineal energy that is consistent with the values in Figure 10 between 37° to 40° North.

As discussed in Section 2.3 and described in Appendix A, there is some concern that the choice of quality factor may influence the measured total dose equivalent. As shown in Figure 11, the choice of quality factor has only a slight effect on the dose equivalent, i.e., the total dose equivalent only varies by a few percent with the two different quality factors (see discussion below).

The distribution of the dose equivalent is similar to that obtained on the First Air flight at roughly half the altitude of the North-2 flight (see Figure 12). In both cases, the dose equivalent above 10 keV/μm maximizes at about 100 keV/μm (i.e., near the so-called "proton edge", Walker 1995) and diminishes with a very high-LET tail that represents a small fraction of the total dose equivalent distribution (~10%). Although scatter occurs at the high-LET end of the spectrum (>300keV/μm), these data are real and represent the production of high-LET particles due to fragmentation of atmospheric nuclei with high-energy protons. The scatter is principally due to statistics associated with fewer counts in the high energy bins.

The total dose equivalent, as measured with both the Boeing and DREO TEPC, is summarized in Figure 13 for all flights. As shown, the change in quality factor has a negligible effect on the TEPC measurements

Bubble Detector The measured neutron dose equivalent for the various flights, for the bubble detector measurements, using Eq. (9) with the calibration factor in Section 2.4, is given in Table 2. As expected, the integrated neutron dose equivalent (and dose-equivalent rates) appear to increase with increasing latitude (i.e., both quantities are greater for the northern flights than the southern ones). As shown in Figure 13, the neutron dose equivalent from the bubble detector measurements follow the trend of the integrated total dose equivalent from both the DREO and Boeing TEPCs. This trending indicates that the neutron bubble detector is monitoring the major (dose-equivalent) component of the radiation field (i.e., the high-LET component above 10 keV/μm as seen, for example, in Figure 12).

Table 2: Measured Neutron Dose Equivalent from BD

Flight	Ames #	Neutron Dose Equivalent (μSv)	Flight Neutron Dose Equivalent Rate (μSv/h)	Neutron Fraction (BD/TEPC)	High-LET Fraction
East	N97105	39	6.5	0.34	0.65
North 1	N97106	59	7.4	0.30	0.64
South 1	N97107	14	2.2	0.22	0.54
North 2	N97108	56	8.6	0.39	0.63
South2	N97109	21	3.2	0.35	0.58
First Air (North)	n/a	29	3	0.42	

For instance, using an arbitrary cut-off of 10 keV/μm, the round-trip total dose equivalent was divided into a low- and high-LET component. For comparison purposes, the fraction of the high-LET TEPC component was calculated and compared to the BD neutron fraction (i.e., the BD neutron dose equivalent divided by the total dose equivalent from the TEPC) (see Table 2 and Figure 14). These data indicate that the high-LET fraction is ~60% of the total dose equivalent, which is roughly twice that determined from the BD measurements (Table 2). This discrepancy is not surprising since there is significant overlap (i.e., "tails") between the low- and high-LET components where the use of a single value of 10 keV/μm is somewhat arbitrary. This can be further illustrated in Figure 10 where the dose mean lineal energy ($\bar{y}_D$) varies between 10 to 20 keV/μm as a function of latitude.

The BD neutron fractions on the low-altitude First Air flights (~35-42%) were comparable to those observed on the ER-2 northbound routes in Figure 14 (~ 30 to 40%). In terms of the neutron dose equivalent rate, the ER-2 northern flights were almost 3 times greater than that of the First Air flights (see Table 2). This result is consistent with the total dose equivalent rate, as measured with the TEPC, where the northern ER-2 flights were roughly a factor of 4 times greater than that of First Air (i.e., ~5 versus 22 μSv/h) (from Table 1 and Figure 13). These two results are principally due to an altitude effect since the First Air flight was conducted at higher latitudes.

Summary

TEPC and neutron bubble detector measurements have been made in support of the NASA-Langley AIR mission. The TEPC data have been processed with quality factors from both ICRU-40 and ICRP-60, yielding little difference in the dose equivalent. Microdosimetric spectra from the DREO and Boeing TEPCs are consistent. The ER-2 results have also been compared to low-altitude measurements from First Air (using the same instrumentation); an increase in the low-LET component is observed at high-altitude.

A calibration factor for the bubble detector has been developed for a Hess neutron spectrum at commercial aircraft altitude, which can be updated as more neutron spectral information become available. The neutron dose equivalent as measured with the bubble detectors followed the same trend as the TEPC total dose equivalent, indicating the importance of the high-LET (i.e., neutron) contribution to the radiation field.

References

Gerdung, S., Pihlet, P., Grindborg, J. E., Roos, H., Schrewe U. J., Schuhmacher, H., "Operation and Application of Tissue-Equivalent Proportional Counters", Radiat. Protect. Dosim. 61 (4), p. 381 (1995).

Hess, W.N., Patterson, H.W., Wallace, R., Chupp, E.L., "Cosmic-Ray Neutron Energy Spectrum," Phys. Rev.116 (2), 445 (1959).

Hess, W.N., Canfield E.H., Lingenfelter, R.E., "Cosmic-Ray Neutron Demography," J. Geo. Phys. Res. 66 (3), 665 (1961).

ICRP, International Commission on Radiological Protection, 1990 Recommendations of the International Commission on Radiological Protection, ICRP Publications 60, Pergamon Press, Oxford (1991).

ICRU, International Commission on Radiation Units and Measurements, The Quality Factor in Radiation Protection, ICRU Publication 40, Bethesda, Maryland, U.S.A., April (1986).

NCRP, National Council on Radiation Protection and Measurements, Radiation Exposure and High-Altitude Flight, NCRP Commentary No. 12, NCRP Publications, 21 July, 1995.

Roesler, S., Heinrich W.W., Schraube, H., "Calculation of Radiation Fields in the Atmosphere and Comparison to Experimental Data," Radiat. Res. 149, 87 (1998).

Rossi, H. H., Zaider, M., Microdosimetry and Its Applications, Springer-Verlag Berlin Heidelberg, New York (1996).

Sanikov, A., Savitskaya E.N., , "Ambient Dose Equivalent Conversion Factors for High Energy Neutrons Based on the ICRP-60 Recommendations," Radiat. Prot. Dosim. 70 (1-4) 383 (1997).

Schuhmacher, H., Siebert, B.R.L., "Quality Factors and Ambient Dose Equivalent for Neutrons Based on the New ICRP Recommendations," Radiat. Prot. Dosim. 40 (2) 85 (1992).

Tume, P., Lewis, B.J., Bennett L.G.I., Cousins, T., "Characterisation of Neutron-Sensitive Bubble Detectors for Application in the Measurement of Jet Aircrew Exposure to Natural Background Radiation.," Nucl. Instr. Meth. A., in press.

Waker, A. J., "Principles of Experimental Microdosimetry," Radiat. Protect. Dosim. 61 (4), p. 297 (1995).

Appendix A: Quality Factor

The concept of relative biological effectiveness, RBE, was developed to account for the biological effects from radiation exposure. The RBE of a given absorbed dose depends on the microscopic energy distribution, which is determined by the nature and energy of the radiation. The concept of linear energy transfer (LET) has been traditionally used to relate the type of radiation to the biological response of the system to an irradiation of 250 keV X-rays. In turn, this concept gave rise to the use of a quality factor (Q) as an approximation to the experimental RBE value with respect to either lineal energy (y) in a micron-sized spherical tissue volume or LET in water (see Figure A.1).

The relationship between quality factor and lineal energy, as defined by the International Commission on Radiation Units (ICRU-40 1986) is:

$$Q(y) = \frac{a_1}{y}[1 - \exp(-a_2 y^2 - a_3 y^3)] \qquad \text{(A.1)}$$

where a_1 = 5510 keV μm^{-1}, a_2 = 5 x 10^{-5} μm^2 keV^{-2} and a_3 = 2 x 10^{-7} μm^3 keV^{-3}. The quality factor as a function of LET is given in Table A.1 by the International Commission on Radiological Protection (ICRP-60).

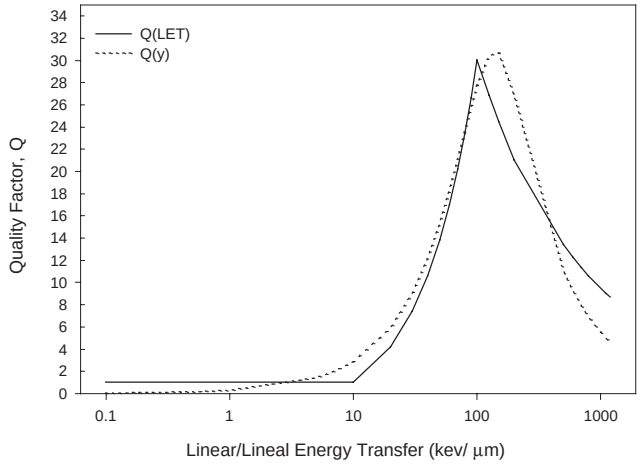

Figure A.1. Quality factor as a function of linear energy transfer (LET) and lineal energy (y).

The curves in Figure A.1 are derived from Equation (A.1) and Table A.1. More recently, the ICRP-60 have also defined the concept of weighting factors (w_R) that are specific to the type and energy of the particle(s) as an alternative to using quality factors. The direct relationship between the Q (LET) (Table A.1) and the weighting factor methodology is unclear.

Table A.1: Quality Factor (ICRP 1991) as a Function of Linear Energy Transfer (LET)

LET, keV/µm	Q (LET)
<10	1
10-100	0.32*LET-2.2
<100	300/√LET

It is worthwhile to note that these concepts are applied to radiation protection in fields typically consisting of one type of radiation (e.g., X-rays), with energies lower than that of cosmic rays. Furthermore, the bodies of evidence for radiation risk factors (and hence weighting factors) are derived from the Hiroshima and Nagasaki bomb data that are applicable for only fast neutrons (< 20 MeV) and gamma rays. Consequently, there are possible complications in extrapolating weighting factors to very high-energy particles (e.g., 100 MeV neutrons) and mixed-radiation environments, where there is limited experimental evidence of biological consequence.

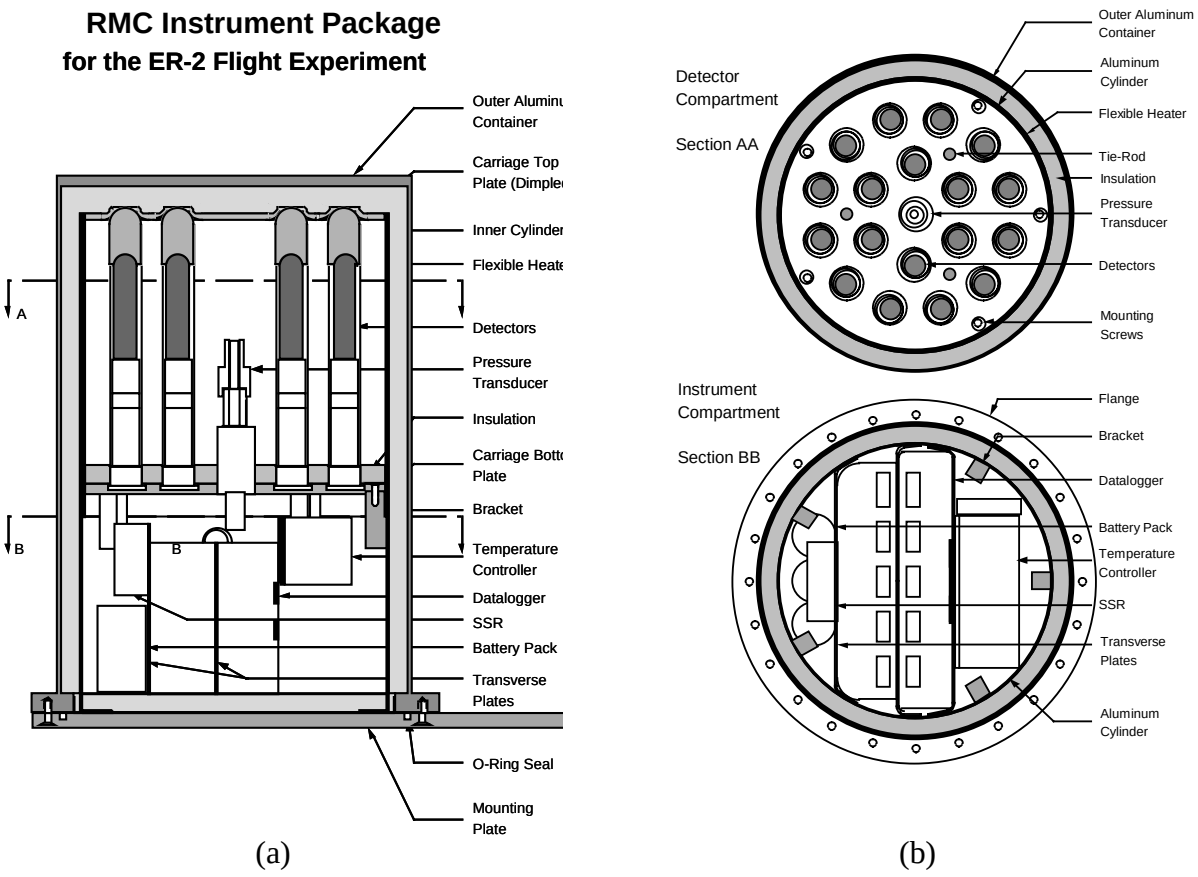

Figure 1.(a) RMC instrument package for the ER-2 flight experiment.
(b) Sectioned views of the RMC instrument package.

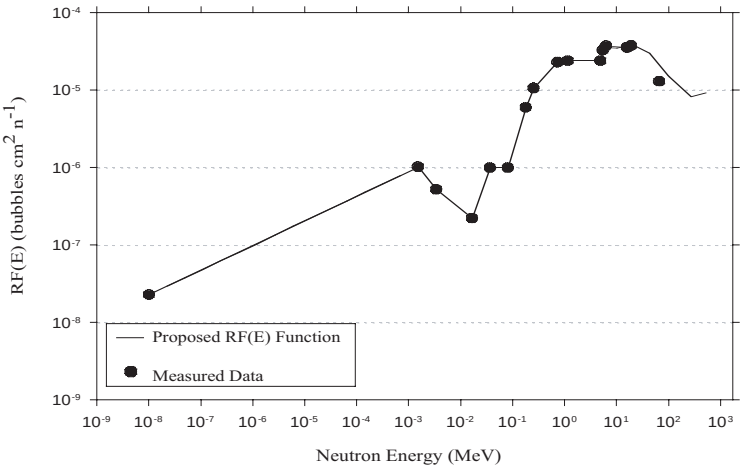

Figure 2. Response-to-fluence function, RF(E) (at 20 ^{0}C).

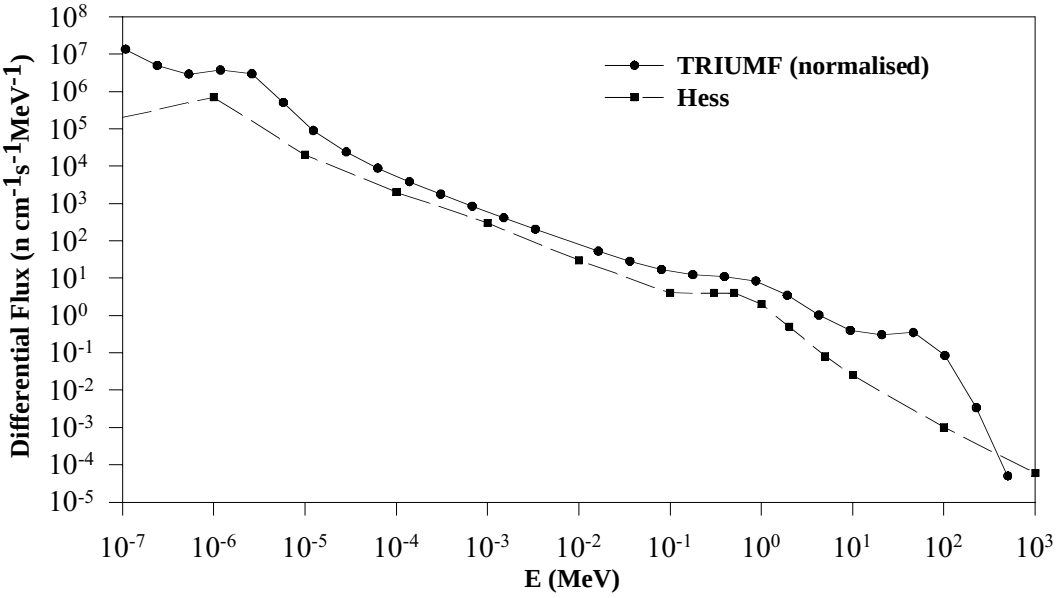

Figure 3. Comparison of the TRIUMF and Hess neutron spectra. The TRIUMF spectrum is normalised to 100 μA of accelerator beam current.

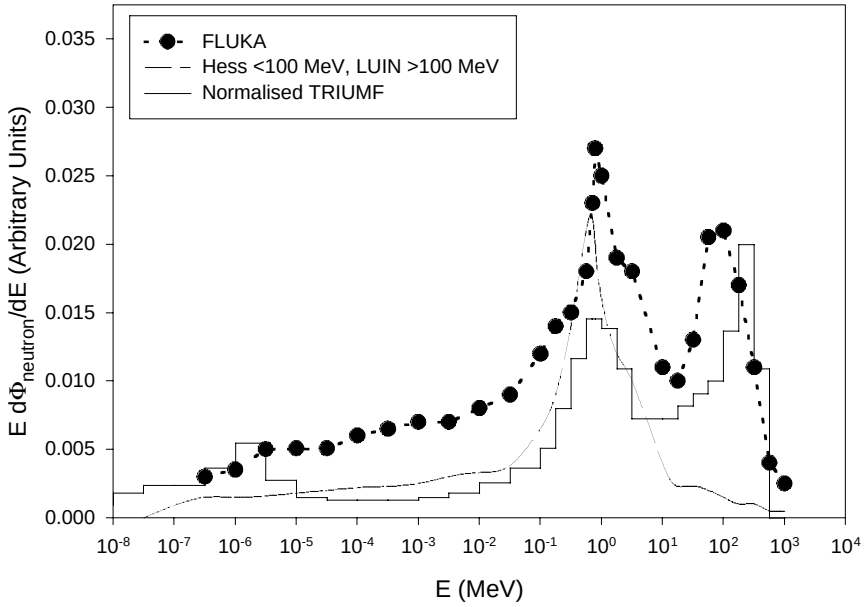

Figure 4. Lethargy plot of neutron spectra from FLUKA and LUIN calculations with measurements by Hess et al. and at TRIUMF.

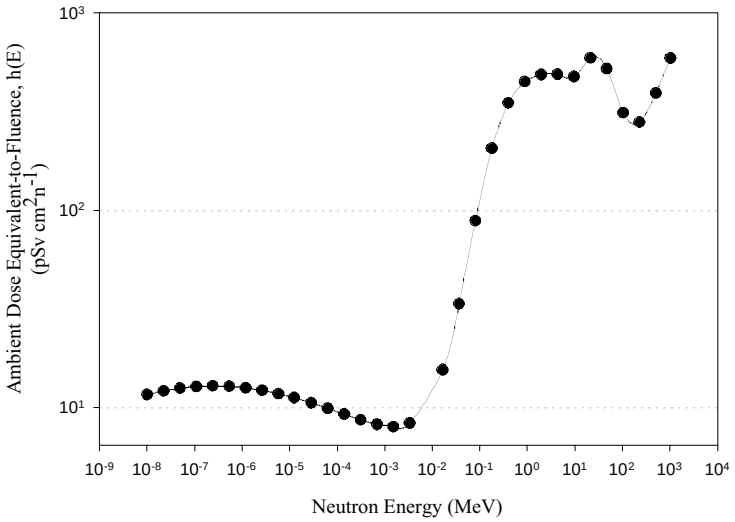

Figure 5. Ambient dose equivalent-to-fluence, h(E), as a function of neutron energy for ICRP-60 recommendations, with a plain parallel beam incident on an ICRU sphere (E<20 MeV) and a slab phantom (E>20 MeV).

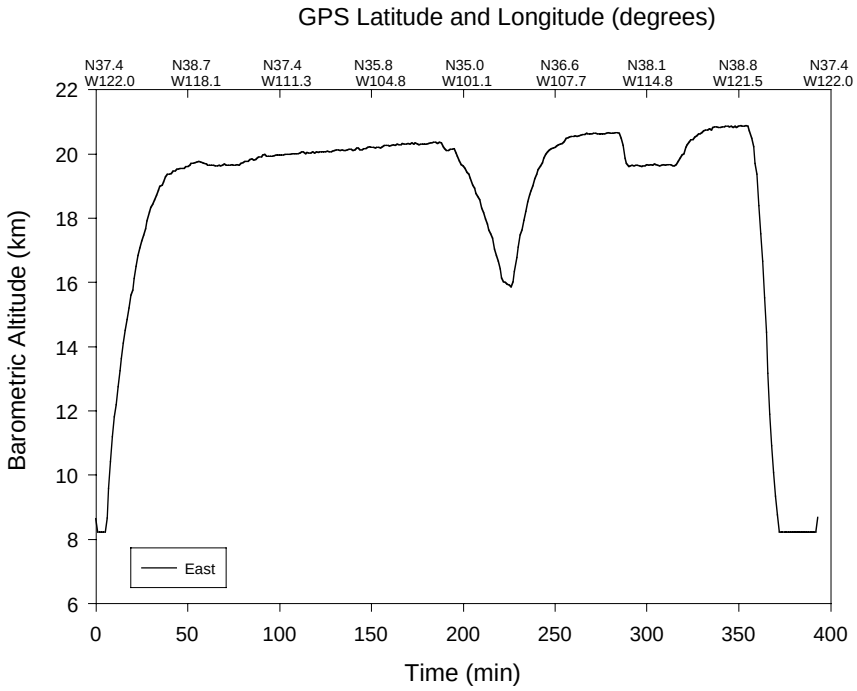

Figure 6 (a). Flight profile for the East flight.

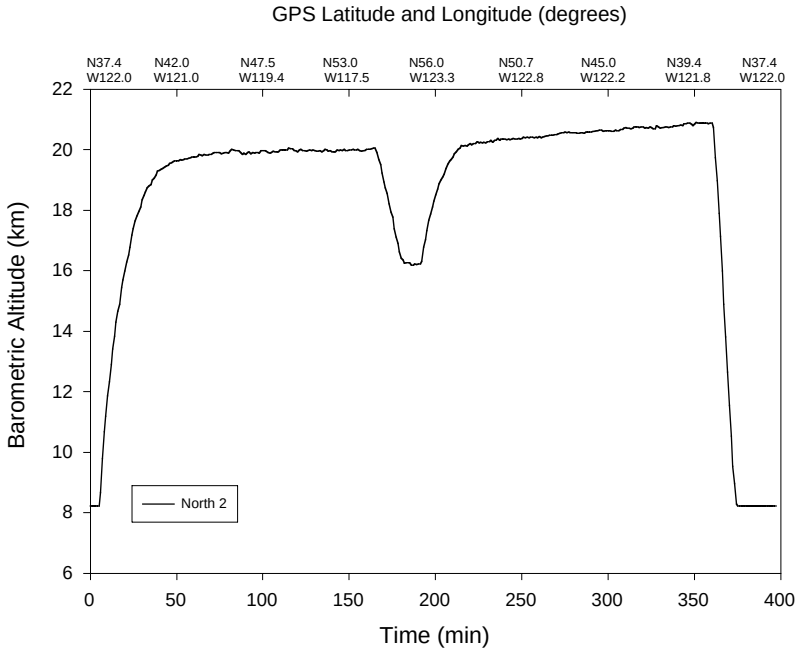

Figure 6 (b). Flight profile for the North-2 flight.

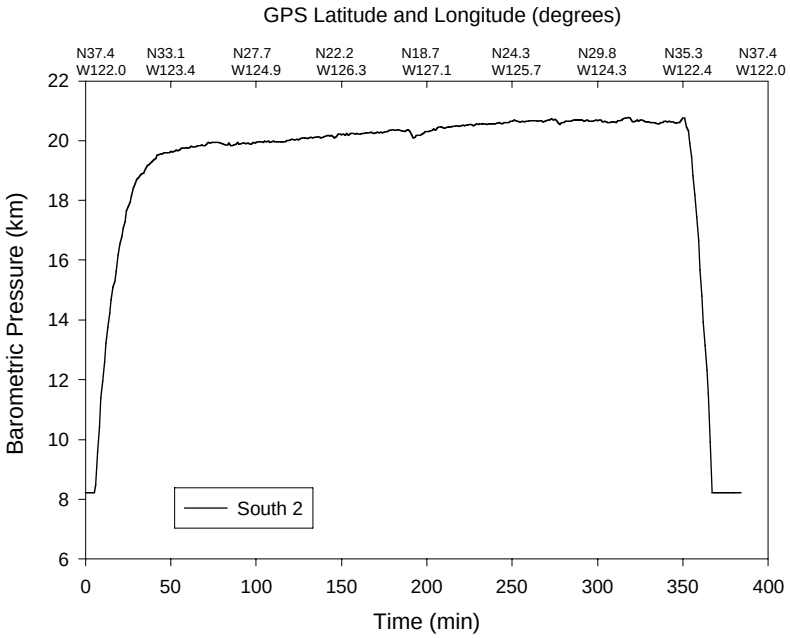

Figure 6 (c). Flight profile for the South-2 flight.

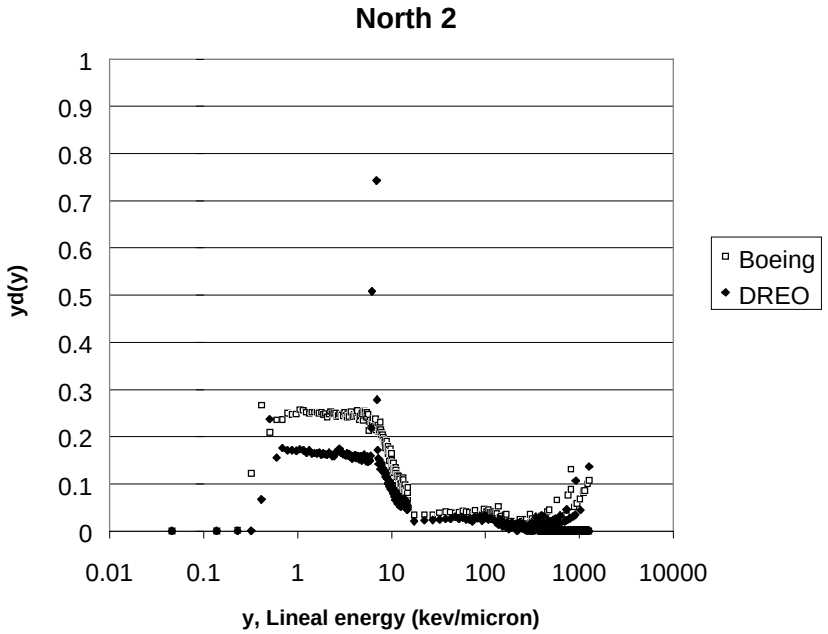

Figure 7. Absorbed dose distribution for the Boeing and DREO TEPCs for the North-2 flight (Ames sortie number N97108).

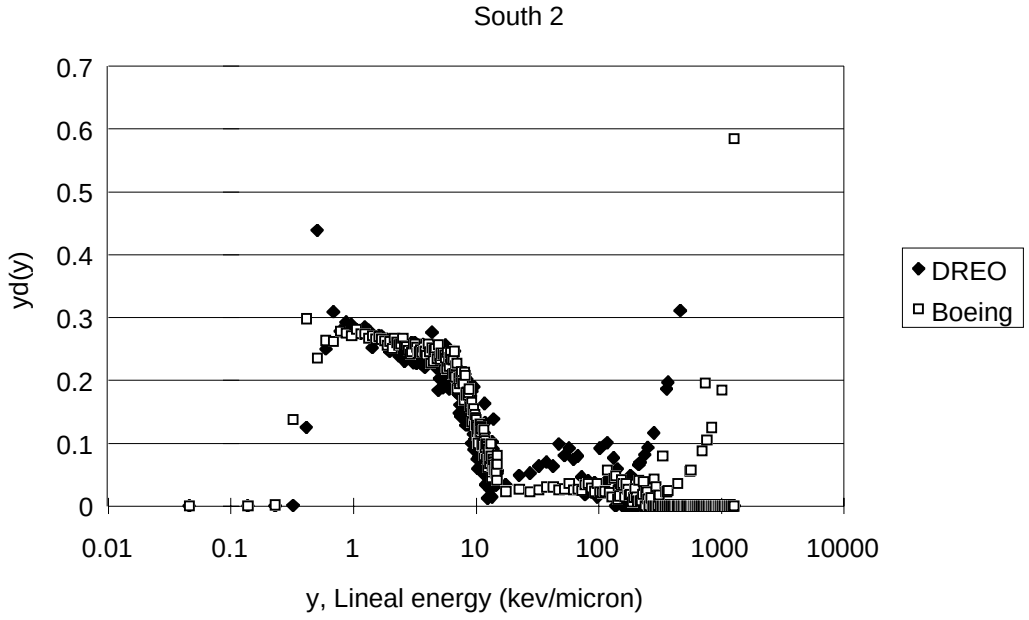

Figure 8. Absorbed dose distribution for the Boeing and DREO TEPCs for the South-2 flight (Ames sortie number N97109).

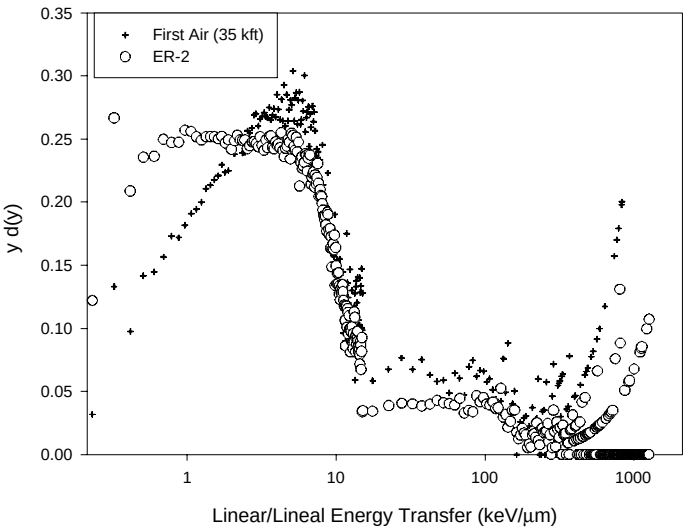

Figure 9. Absorbed dose distribution from the ER-2 North-2 and First Air flights.

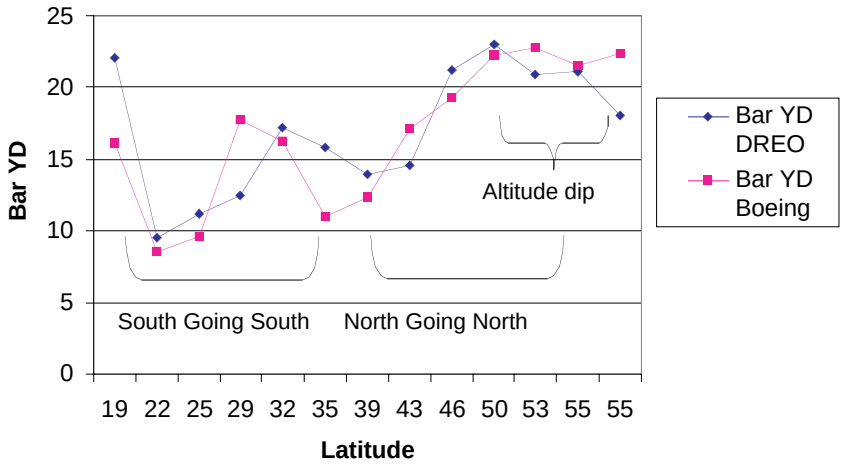

Figure 10. Dose-mean lineal energy as a function of latitude for the DREO and Boeing TEPCs.

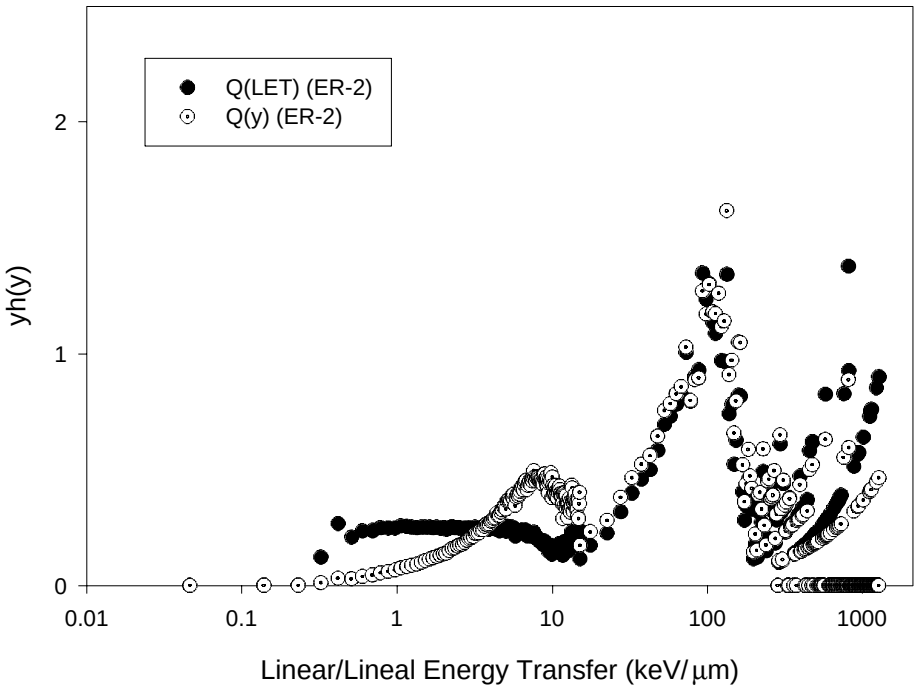

Figure 11. Dose equivalent distribution for the round-trip North-2 flight comparing the choice of quality factor, i.e., Q(LET) (ICRP-60) versus Q(y) (ICRU-40).

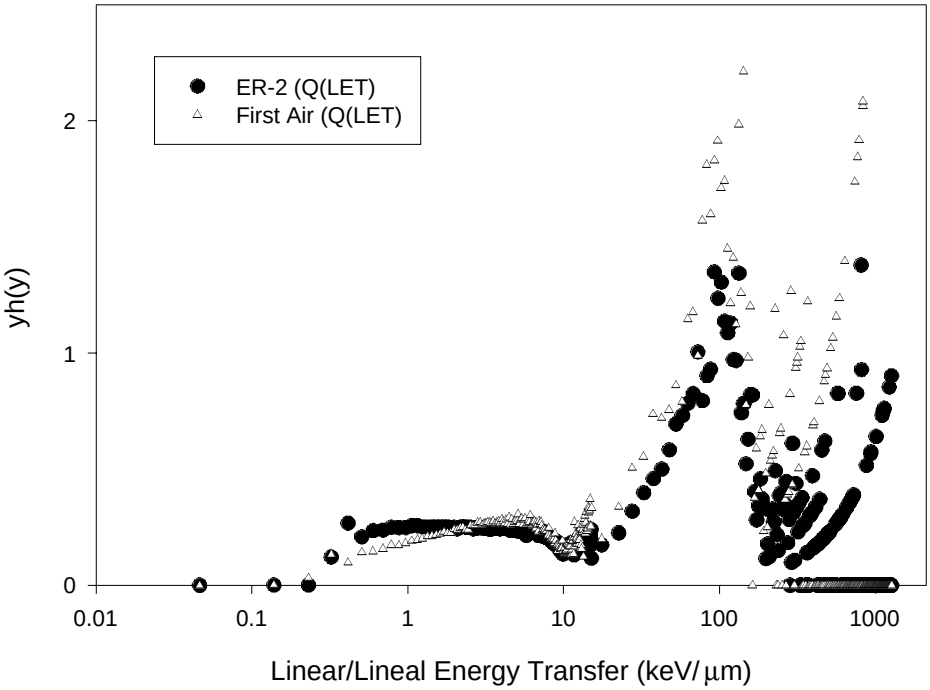

Figure 12. Dose equivalent distribution for the round-trip North-2 flight as compared to the First Air data using the conventional Q(LET) relationship.

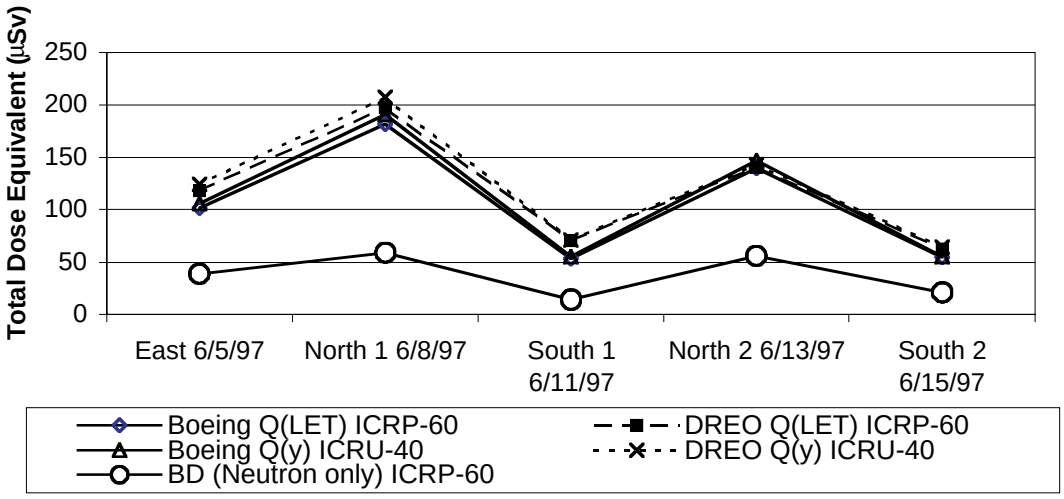

Figure 13. Comparison of the neutron dose equivalent (measured with BDs) with the integrated total dose equivalent (from the DREO and Boeing TEPCs) for the various flight series in Table 1.

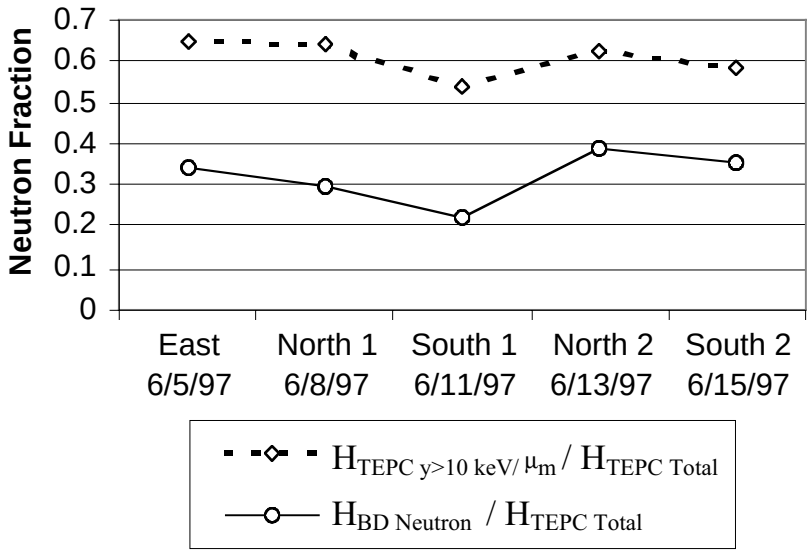

Figure 14. Neutron fraction derived from the ratio of the bubble detector measurements, or the TEPC data above 10 keV/μm, to the TEPC total dose equivalent. The TEPC data are based on average values from the DREO and Boeing instruments.

Chapter 13: Cosmic Radiation Measurements with Superheated Drop Detectors

Francesco d'Errico, Robert Apfel
Yale University, Department of Mechanical Engineering, 9 Hillhouse Avenue, New Haven CT 06520 USA.

Giorgio Curzio
Dipartimento di Ingegneria Meccanica, Nucleare e della Produzione (DIMNP), Università degli Studi di Pisa, Via Diotisalvi 2, I-56126 Pisa, Italy.

Ravinder Nath
Yale University School of Medicine, Department of Therapeutic Radiology, Division of Radiological Physics, 333 Cedar Street, New Haven CT 06510 USA.

Cosmic Radiation Measurements with Superheated Drop Detectors

Introduction

The NASA-DOE AIR project took advantage of the complementary properties of a large array of radiation detection instruments to investigate the radiation field encountered on high-altitude flights. A highly sensitive extended-energy multisphere spectrometer was the primary neutron measuring device, while fourteen other radiation detectors provided additional information. Among these, active and passive devices based on superheated emulsions (superheated drop detectors and bubble damage detectors) were included for their ability to measure neutron dose equivalent while discriminating the sparsely ionizing components of the radiation field. With the assistance of the NASA Langley Research Center, Yale University and the Università degli Studi di Pisa (Italy) developed for these measurements a compact active monitor based on superheated drop detectors. The device was especially designed to operate in the nose rack of the NASA ER-2 aircraft, at low levels of temperature and pressure. It was successfully flown on all the AIR sorties carried out in June 1997. The measurements were analyzed on the basis of extensive investigations of the superheated drop detector response to high energy neutrons. The fluence response of the detector was determined up to 134 MeV performing calibrations in quasi-monoenergetic neutron beams available at various radiation metrology and research centers. The calibration factor converting number of bubbles to neutron ambient dose equivalent was determined at CERN using a reference field which reproduces the neutron spectra encountered in the stratosphere. While the count rate of the device was too for a dose rate determination, total neutron ambient dose equivalent values were determined with an estimated uncertainty of less than 30% and agree with the values determined using etched track dosimeters and tissue equivalent proportional counters.

Superheated Drop Detector Instrumentation

Superheated emulsions (denomination adopted by ICRU and ISO for superheated drop detectors [1], bubble damage detectors [2], and all similar detectors) consist of uniform dispersions of over-expanded halocarbon and/or hydrocarbon droplets suspended in a compliant material such as a polymeric or an aqueous gel. These detectors operate like the bubble chamber [3], long used in high energy particle physics: charged particles liberated by radiation interactions nucleate the phase transition of the superheated liquid and generate detectable bubbles (Figure 1). Bubble chambers utilize a pressurized homogeneous liquid that is suddenly and briefly brought to a transient superheated state by dropping the pressure. Conversely, superheated emulsions are continuously sensitive since the liquid is kept in steady-state superheated conditions.

The superheated drop detector (SDD) instrument developed for the AIR project (Figure 2) comprised: (1) a neutron sensor consisting of an emulsion of superheated dichlorodifluoromethane droplets; (2) an electronic device recording the bubble formation events occurring in the sensor; (3) a sealed and insulated container maintaining the instrumentation at atmospheric pressure and at a temperature close to 31.5 °C. These three main components of the instrumentation are separately described hereafter.

The neutron sensors employed in the AIR measurements were 4 ml SDD vials containing about 20,000 droplets of 100±10 μm diameter of dichlorodifluoromethane (CCl_2F_2, commercially denominated Freon-12™). This halocarbon is used in superheated drop detectors for neutron dosimetry since it responds to fast neutrons, *via* the charged particles from scattering interactions, and also to thermal and intermediate neutrons, *via* the products of their exothermic (*n,p*) capture reaction on ^{35}Cl. An optimal dosimetric performance is achieved when Freon-12 detectors are kept at a temperature of 31.5°C, in which case their response closely matches ICRP recommended fluence-to-ambient-dose-equivalent conversion coefficients [4].

An electronic device was used for the real time registration of bubble formation occurring in the superheated drop detector. This device records the acoustic pulses associated with the rapid expansion of the vaporizing superheated droplets. These are oscillating pressure pulses, of about 10 ms duration, which can be easily detected by means of piezoelectric transducers. The instrument developed for the AIR project was based on the ASM™ monitor earlier manufactured and commercialized by Apfel Enterprises, Inc. (New Haven, CT USA). This compact device (4.5 cm x 8 cm x 13 cm, weight ~300 g) records detector pulses and external noise using two piezo-electric transducers and performs a comparative pulse-shape analysis. The signals are amplified and fed to analog circuitry for rectification and low-pass filtering, followed by analog-to-digital conversion and sampling (Figure 3). The microprocessor of the ASM then evaluates shape and amplitude of the signals, and if these satisfy the acceptance criteria of a real bubble-formation event, a pulse is counted. Vaporization events are distinguished from spurious noise both by anti-coincidence and by pulse shape analysis. In addition, vibration-dampers de-couple the vial from the monitor-case, thus improving the noise discrimination. This allows operation with noise ambient levels up to 110 dB.

When the ER-2 aircraft flies at 65,000 ft (19.8 km), the pressure inside the payload sections drops to about 0.3 atmospheres while the temperature depends on the heat generated by the various instruments and may fall well below 0 °C. Therefore, to ensure an optimal operation of the superheated drop detectors, the instrumentation was placed inside a sealed and insulated container whose internal pressure was set at one atmosphere while the temperature was kept close to 31.5°C. The container was a right cylindrical vessel built at NASA Langley Research Center from a single piece of aluminum. The container had a total height of 17 cm, a diameter of 16 cm and a weight of 3 kg. The cylinder was sealed by a flange connected to the nose rack of the ER-2 by means of shock absorbers. The temperature of the instrumentation inside the container was regulated using two temperature controllers (Heaterstat CT198, Minco Products, Inc., Minneapolis MN USA). These compact solid-state devices use etched-foil heaters to control and also measure the temperature. Brief current pulses are sent each second to measure the resistance of the high-temperature-coefficient heater foils and thus acquire a temperature reading. If the temperature is below the set-point, the heater foils are powered for periods of 1-2 seconds (with a peak electric

power consumption of about 10 W), until the set-point is regained. The heater foils chosen for the AIR SDD device measured 5.1 cm x 10.2 cm and were held in contact with the two larger faces of the instrument, measuring 8 cm x 13 cm, by a molded holder built from NASA-supplied insulating material. An 8-10 pin sealed connector allowed us to power the heaters using the 28 VDC supply of the ER-2 aircraft and also to connect the instrument to a computer and download the data recorded during each flight.

Response of superheated drop detectors to high energy neutrons

Superheated emulsions of dichlorodifluoromethane present an excellent dose equivalent response in the neutron fields encountered in conventional radiation protection practice. However, when neutron energies exceed ~10 MeV, the dose equivalent response decreases due to the declining interaction cross sections between neutrons and detector elements. The response of superheated emulsions to high energy neutrons has been extensively investigated for almost a decade [4,5,6,7]. These studies were motivated by growing concerns about occupational neutron exposures at nuclear research accelerators, at radiotherapy installations using particle beams and during commercial high-altitude flights and space missions[8,9,10,11,12]. Until recently, however, only response data for broad-spectrum fields or semi-empirical calculations were reported, while detailed response function determinations were not available.

Prior to this investigation, measurements of the fluence response of dichlorodifluoromethane emulsions had been performed with ISO standard monoenergetic beams up to 19 MeV [13]. In order to analyze the results of the AIR project, high-energy response measurements were performed in the quasi-monoenergetic neutron beams of the Université Catholique de Louvain (UCL), in Louvain la Neuve, Belgium and of The Svedberg Laboratory (TSL), in Uppsala, Sweden [14,15]. Generated using the ^{7}Li(*p,n*) reaction, these beams present high energy peaks in the 46-134 MeV range, comprising 30-40% of the spectral fluence, and a lower energy continuum [16,17]. In order to resolve the detector responses corresponding to the peak neutron energies of the beams, some theoretical response functions above 19 MeV were first modeled after the cross sections for the production of heavy charged particles in the detector. These responses were folded over the UCL and TSL spectral fluence distributions, producing the following convolution integrals:

$$\frac{\int_{0.1\,MeV}^{19\,MeV} R_{\Phi}\Phi_E dE + \int_{19\,MeV}^{46\,MeV} R_{\Phi}\Phi_E dE}{\int_{0.1\,MeV}^{46\,MeV} \Phi_E dE}, \quad \frac{\int_{0.1\,MeV}^{46\,MeV} R_{\Phi}\Phi_E dE + \int_{46\,MeV}^{62\,MeV} R_{\Phi}\Phi_E dE}{\int_{0.1\,MeV}^{62\,MeV} \Phi_E dE}, \quad \frac{\int_{0.1\,MeV}^{62\,MeV} R_{\Phi}\Phi_E dE + \int_{62\,MeV}^{134\,MeV} R_{\Phi}\Phi_E dE}{\int_{0.1\,MeV}^{134\,MeV} \Phi_E dE}$$

Only minor adjustments to the model response functions were necessary to achieve an agreement within 20% between convolution integrals and measured data. This degree of agreement was considered quite satisfactory, considering that experimental data were affected by total uncertainties (at 1σ level) of at least 12% for the UCL

measurements and 32% for the TSL measurements. These were derived by quadratic summation of the uncertainties on detector batch uniformity (5%), bubble counting statistics (7%), temperature fluctuations (2%) and total fluence estimates (7% at UCL and ~30% at TSL).

The cross sections necessary to model the response functions were those for the production of heavy charged particles from neutron-induced nuclear reactions on fluorine and chlorine (present in the superheated droplets), on carbon (present in the droplets and in the emulsifier gel surrounding them), and on oxygen (present in the gel). Cross sections for oxygen and carbon were drawn from the recent LA150 Library [18], whereas data for fluorine and chlorine in the 20-180 MeV range were generated with the Monte Carlo high-energy transport code HADRON [19], which is based on the cascade and exciton models of nuclear interactions and has been extensively validated against reference double-differential cross section data.

The complete fluence response functions of dichlorodifluoromethane (Freon-12™) emulsions at 25 and 31.5 °C are shown in Figure 4, including data points for the resolved peak neutron energies of the UCL and TSL beams. An operating temperature of 31.5 °C was the design goal for the AIR SDD instrument. In fact, this temperature corresponds to an optimal dosimeter response to thermal neutrons as well as to fast neutrons between about 0.1 and 10 MeV. This is illustrated in Figure 4 by a comparison with the ICRP74/ICRU57 fluence-to-ambient-dose-equivalent conversion coefficients [20]. It may be observed that the emulsions under-read ambient dose equivalent for epithermal up to about 100 keV neutrons and for high energy neutrons, especially above 40 MeV. Spectra normally encountered in radiation protection practice typically present a relatively scarce "1/E" neutron population in the epithermal and intermediate energy region, so that the detector's under-reading may not be a serious deficiency. Conversely, the divergence from the conversion coefficients above 10 MeV leads to an underestimate of dose equivalent which had to be accounted for in the AIR measurements.

The calibration factor used to derive neutron ambient dose equivalent from the number of bubbles recorded on the AIR flights was determined at CERN using a high-energy reference calibration field [21]. This field is generated by bombarding a 0.5 meter copper target with a beam of 120 GeV/c protons and pions. A well characterized neutron transmission field is available at a reference position termed CT6 above the concrete slabs used to shield the nuclear interaction products. The spectrum of this field resembles that of cosmic neutrons encountered in the lower stratosphere as shown in Figure 5 by a comparison between the CERN field and the spectrum acquired during the AIR campaign at an altitude of 20 km above the coordinates 53.9N, 117.2 [22]. The CERN experiments indicated that the calibration factor of 250 nSv per bubble, previously determined with Am-Be irradiations, had to be increased by 35% for the AIR measurements. This was also found to be consistent with the results of earlier measurements carried out on commercial flights [23] and at a neutron therapy facility [12], which had shown under-responses ranging between 30 and 50%.

Superheated emulsions of Freon-12 at temperatures between 25 and 30°C become sensitive to low energy protons at the end of their range, which reach a linear energy transfer (LET) of 69 keV/μm and sustain it over about 0.5 μm across their Bragg peak. In addition, the detectors respond to highly charged and energetic (HZE) particles

when their LET is again greater than about 70 keV/μm [24]. However, the fluence of low energy protons and of HZE particles is relatively low [25], and it is considered that the CERN calibration permits estimates of the neutron dose equivalent within a systematic uncertainty of 20-30%.

Results of the superheated drop detector device

Data acquired during the ER-2 sorties were downloaded to a computer immediately after the landing of the aircraft. The information recorded as a function of time included number of bubbles, temperature of the detector (measured by a digital thermistor next to the vial), and spurious noise events. The latter were rare and did not interfere with the correct registration of the bubbles. The temperature profiles revealed that the detector was at the desired set point of 31.5 °C only during the first two hours of the flights, afterwards the temperature gradually decreased until it stabilized at 23-24 °C. Accordingly, the results were corrected for the temperature dependence of the response using a factor of 1.03 $°C^{-1}$ measured at TSL and UCL with high energy neutrons. Results were also corrected for the non-linearity of the response deriving from the progressive depletion of superheated drops in the detector. This correction was minimal since the initial number of drops was about 20,000 while the highest number of bubbles recorded during any single flight was 245 (North 1 sortie). The pulse analysis performed by the ASM electronic bubble counter requires a relatively long 80 ms, however, no dead time correction was necessary because of the low count rate during the flights. The adjusted number of bubbles was finally converted to neutron ambient dose equivalent using the previously discussed CERN calibration factor.

The analyzed results of the AIR superheated drop detector device are summarized in Table 1 and illustrated in Figure 6, where neutron ambient dose equivalent profiles are plotted as a function of flight time. Due to the low sensitivity of the detectors, the count rate during the flights was too low for an accurate determination of the dose rate as a function of flight time. However, the dose profiles were clearly consistent and indicate higher dose rates along the two Northerly routes, lower rates along the Southerly ones and an intermediate level during the Easterly flight. The total neutron ambient dose equivalent values are within 20 % of those determined using etched track dosimeters [25] and tissue equivalent proportional counters [26]. Overall, the AIR measurements with superheated drop detectors were considered highly successful and the experience that was gained lead to the development of instruments with higher sensitivity and an improved energy dependence of the response [14].

Table 1. Results of the AIR measurements with superheated drop detectors.

Sortie	Flight duration (hours)	Farthermost point*	Neutron ambient dose equivalent (μSv)
East	6.5	34.7 N, 99.8 W	45
North 1	7.8	60.1 N, 123.4 W	101
South 1	6.5	17.8 N, 127.4 W	20
North 2	6.5	56.1 N, 123.6 W	85
South 2	6.4	17.8 N, 127.4 W	25

* from NASA Ames Research Center (37.4 N, 122.0 W)

References

1 Apfel, R.E. *The Superheated Drop Detector*. Nucl. Instrum. Methods **162**, 603-608 (1979).

2 Ing, H. and Birnboim, H.C. *A Bubble-Damage Polymer Detector for Neutrons*. Nucl. Tracks Radiat. Meas. **8**(1-4), 285-288 (1984).

3 Glaser, D.A. *Some effects of ionizing radiation on the formation of bubbles in liquids*, Phys. Rev. **87**, 665 (1952).

4 d'Errico, F. and Alberts, W.G. *Superheated Drop (Bubble) Detectors and Their Compliance with ICRP 60*. Radiat. Prot. Dosim. **54**(3-4) 357-360 (1994).

5 d'Errico, F., Alberts, W.G., Dietz, E., Gualdrini, G.F., Kurkdjian, J., Noccioni, P. and Siebert, B.R.L. *Neutron Ambient Dosimetry with Superheated Drop Detectors*. Radiat. Prot. Dosim. **65**(1-4), 397-400 (1996).

6 Spurny, F. and Votockova, I. *The Response of Bubble Damage Neutron Detectors in Reference Neutron Fields*. Radiat. Prot. Dosim. **65**(1-4) 393-396 (1996).

7 Spurny, F. *Individual dosimetry for high energy radiation fields* Radiat. Prot. Dosim. **85**(1-4) 15-20 (1999).

8 Apfel, R.E. *Exposure to neutron radiation in commercial flights.* Radiat. Prot. Dosim. **47**(1-4) 551-554 (1993)

9 d'Errico, F. and Egger, E. *Proton Beam Dosimetry with Superheated Drop (Bubble) Detectors*. In: Hadrontherapy in Oncology. Eds U. Amaldi and B. Larsson. Excerpta Medica, Int. Congr. Series 1077, pp.488-494 (Amsterdam: Elsevier Science, 1994).

10 Lewis, B.J., Kosierb, R., Cousins, T., Hudson, D.F. and Guery, G. *Measurement of neutron radiation exposure of commercial airline pilots using bubble detectors.* Nucl. Techn. **106**(3) 373-383 (1994).

11 Ing, H. and Mortimer, A. *Space Radiation Dosimetry Using Bubble Detectors*. Adv. Space Res.**14**, 73 (1994).

12 Benck, S., d'Errico, F., Denis, J.M., Meulders, J.P., Nath, R. and Pitcher, E.J. *In-Phantom Spectra and Dose Distributions from a High-Energy Neutron Therapy Beam*. Nucl. Instr. Methods **A476**(1-2) 127-131 (2002).

13 d'Errico, F., Alberts, W.G., Curzio, G., Guldbakke, S., Kluge, H. and Matzke, M. *Active Neutron Spectrometry with Superheated Drop Detectors*. Rad. Prot. Dosim. **61**(1-3) 159-162 (1995).

14 d'Errico, F., Agosteo, S., Sannikov, A.V. and Silari, M.*High Energy Neutron Dosimetry with Superheated Emulsions.* Radiat. Prot. Dosim. **100**(1-4) 529-532 (2002).

15 d'Errico, F., Prokofiev, A., Sannikov, A.V., Schuhmacher, H. *High-energy neutron detection and spectrometry with superheated emulsions.* Nucl. Instr. Methods. in press (2003)

16 Schuhmacher, H., Brede, H.J., Dangendorf, V., Kuhfuß, M., Meulders, J.P., Newhauser, W.D., Nolte, R. *Quasi-monoenergetic neutron beams with energies from 25 to 70 MeV.* Nucl. Instrum. Methods **A421** 284-295 (1999).

17 Condé, H., Hultqvist, S., Olsson, N., Rönnqvist, T.,. Zorro, R, Blomgren, J., Tibell, G., Håkansson, A., Jonsson, O., Lindholm, A., Nilsson, L., Renberg, P.-U., Brockstedt, A., Ekström, P., Österlund, M., Brady, F.P., and Szeflinski, Z. *A facility for studies of neutron-induced reactions in the 50-200 MeV range* Nucl. Instrum. Methods **A292** (1) 121-128 (1990).

18 Chadwick, M.B., Hughes, H.G., Little R.C., Pitcher E.J. and Young P.G. *Nuclear Data for Accelerator-Driven Systems*. Prog. Nucl. Energy **38**(1-2) 179-219 (2001).

19 Sannikov, A.V., Savitskaya, E.N. *Physics of the HADRON code: recent status and comparison with experiment*. Nucl. Instrum. Methods **A450**(1) 127-137 (2000).

20 *Conversion coefficients for use in radiological protection against external radiation.* ICRP Publication 74 (Oxford, UK: Pergamon Press, 1997).

21 Ferrari, A., Mitaroff, A., Silari, M. *A reference radiation facility for dosimetry at flight altitude and in space*. Physica Medica. 17 (Suppl. 1) 115-18 (2001).

22 Goldhagen, P., J.M. Clem, J.W. Wilson, *Recent results on measurements of the energy spectrum of cosmic-ray neutrons aboard a ER-2 airplane and on the ground.* Adv. Space Res. in press (2003).

23 d'Errico, F. *Measurements with Superheated Drop Detectors*. In: ACREM Air Crew Radiation Exposure Monitoring. Eds P.Beck, U. Schrewe, K. O'Brien, and P. Ambrosi, ARC Report OEFZS-G—0008, pp. 99-101 (Seibersdorf: Austrian Research Centers, 1999).

24 d'Errico, F. *Radiation Dosimetry and Spectrometry with Superheated Emulsions.* Nucl. Instr. Methods **B184**(1-2) 229-254 (2001).

25 Bartlett, D.T.,Hager, L.G.,Tanner, R.J.,Steele, J.D. *Measurements of the high energy neutron component of cosmic radiation fields in aircraft using etched track dosemeters*. Radiat. Measurements **33**, 243–253 (2001).

26 Normand, E. *Correlation of Inflight Neutron Dosimeter and SEU Measurements With Atmospheric Neutron Model*. IEEE Trans. Nucl. Sci. **48**(6) 1996-2003 (2001)

Figure 1. Superheated drop detectors before and after irradiation.

Figure 2. AIR superheated drop detector instrument.

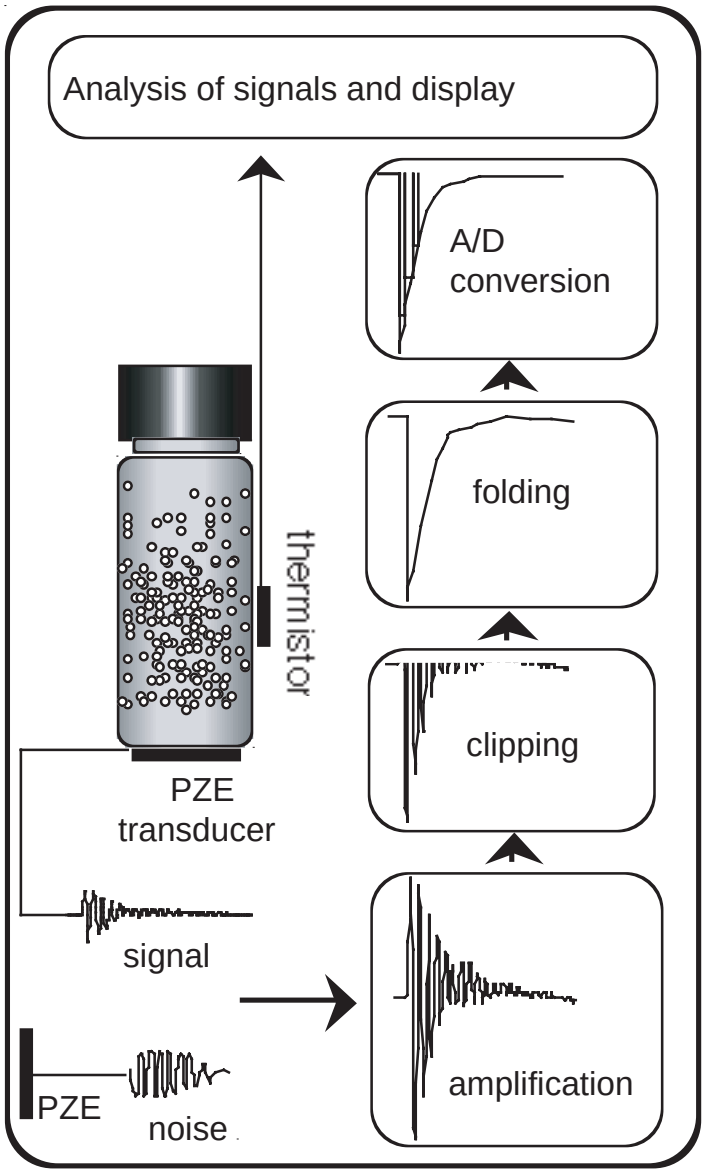

Figure 3. Schematic of electronics of superheated drop detector instrument.

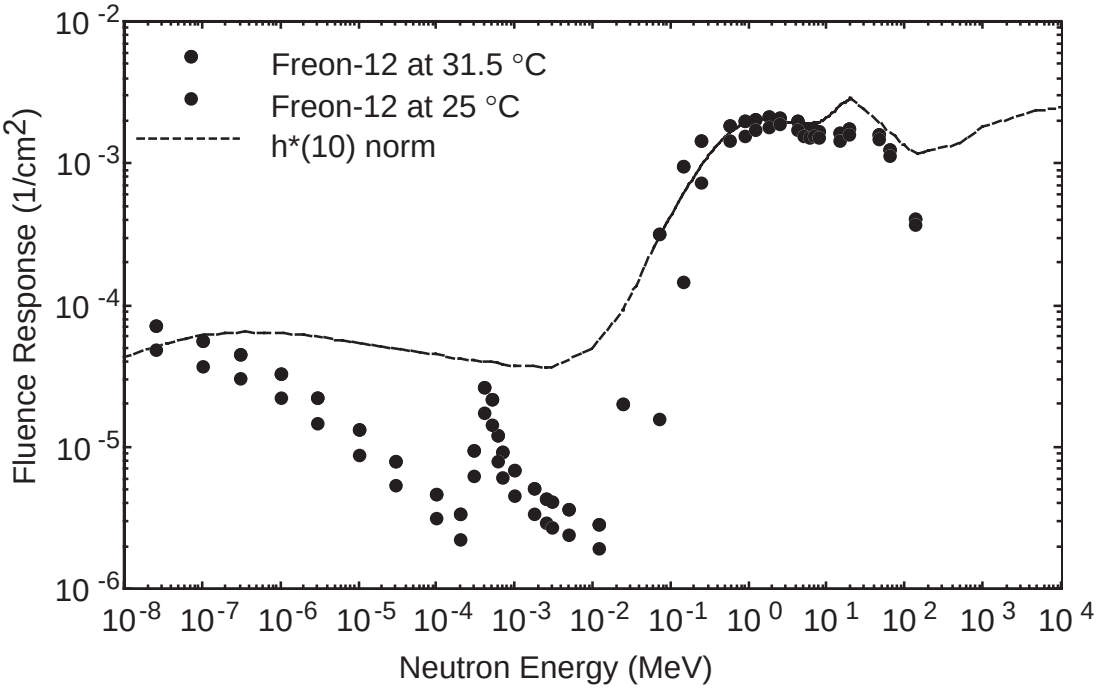

Figure 4. Fluence response of superheated emulsions of Freon-12 at 25 and 31.5 °C.

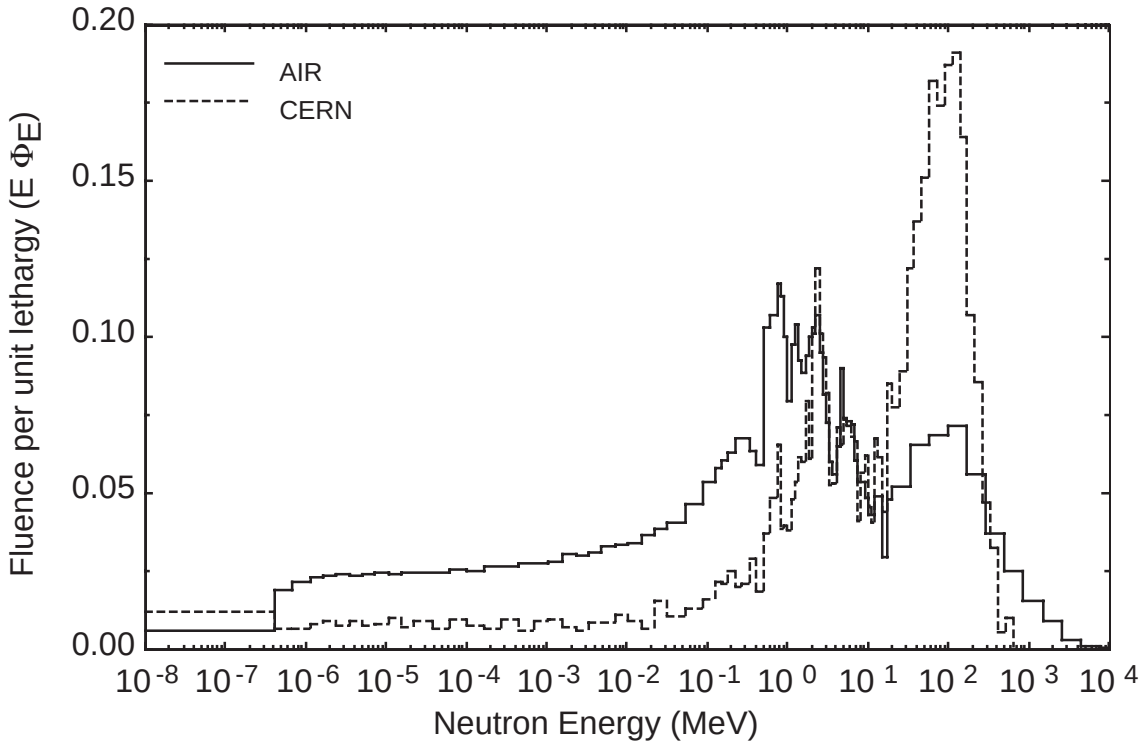

Figure 5. Comparison between AIR spectrum and CERN calibration field.

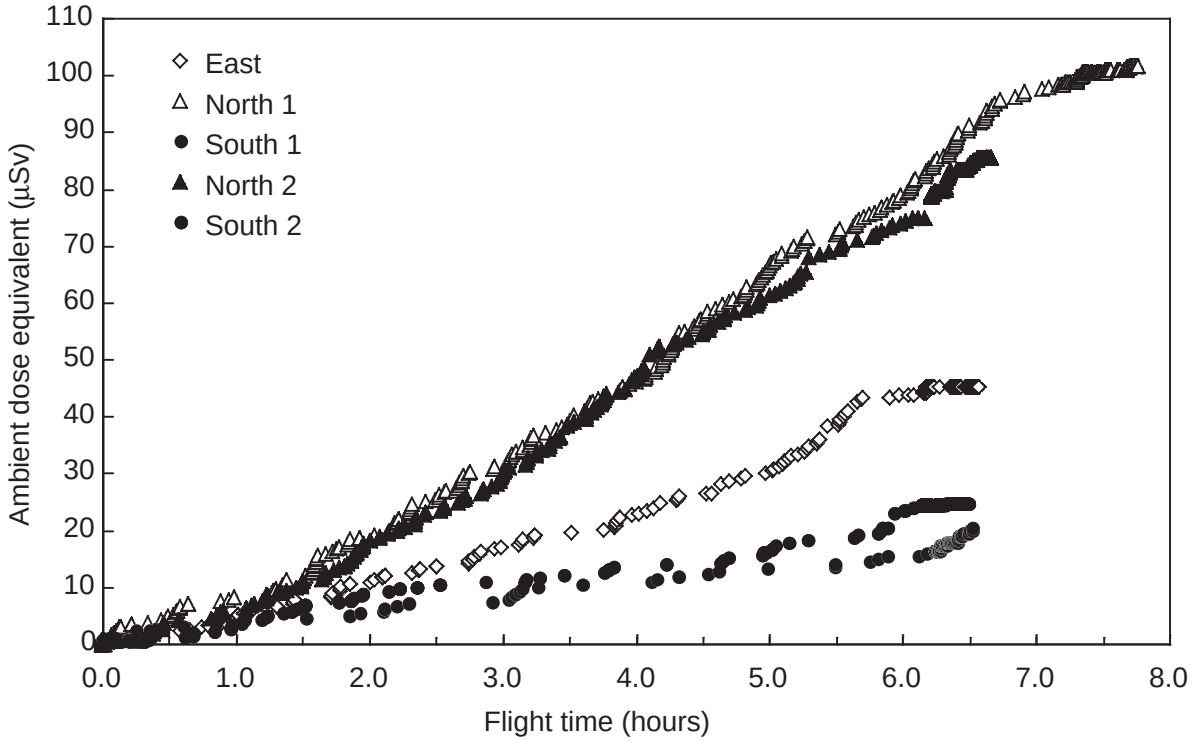

Figure 6. Results of the AIR superheated drop detector instrument.

Chapter 14: Assessment of High Altitude Cosmic Radiation Exposures Using a Simple Electronic Neutron Dosimeter, the PDM-303

Eugene Normand
Boeing Information Space and Defense Systems, Seattle, WA 98124

Assessment of High Altitude Cosmic Radiation Exposures Using a Simple Electronic Neutron Dosimeter, the PDM-303

Introduction

The Boeing Radiation Effects Laboratory (BREL) has been using the electronic neutron dosimeter PDM-303 to monitor high-energy neutrons for several years. The response of the PDM-303 is given in dose equivalent units, mSv, via electronic readout. Although this response varies with neutron energy (from ~ 0.5-3 for E > 1 MeV), its ease of use and ability to be calibrated, make it suitable for monitoring neutron exposures during high altitude flights. Thus, the dosimeter was used as one of the monitors in the ER-2 flight measurements program during June, l997.

Because the unit is self-powered (by a coin-sized lithium battery), it was worn by the pilot in his shin pocket on all the five scientific flights, as well as the engineering checkout flight. Its readout was taken once the airplane landed, and gave the pilot an immediate sense of the radiation dose that he received during each flight.

We compare the PDM-303 readings against two other ways of characterizing the neutron dose equivalent measurements: 1) by a much more sophisticated monitor, Boeing's TEPC, and 2) the 1-10 MeV neutron fluence for each flight as given by the NASA-Langley atmospheric neutron model, AIR. In both cases there is good agreement between the dose equivalent readings of the simple PDM-303 neutron dosimeter and the TEPC measurements, as well as with the AIR model neutron fluences.

Equipment

PDM-303 Dosimeter

The PDM-303 neutron dosimeter is manufactured by the Japanese company Aloka. It is designed to be worn on the person monitored and gives a digital readout in mSv, with the lowest response being 0.01 mSv. The dosimeter itself is very small and lightweight (~ 5.5" long x 1" wide and weighs ~0.15 lb.). To comply with ER-2 safety concerns that the dosimeter be shown to operate normally at low-pressure conditions, the unit was tested for 6 hours at a moderate vacuum (80-100 torr) in one of BREL's vacuum chambers without a problem.

Calibration of Dose Equivalent Response

The manufacturer provides a curve of the dose response of the PDM-303 as a function of neutron energy over a limited neutron energy range: thermal (0.025 eV) and 0.1-14 MeV (Aloka Co.). Similar but much more complete dose response data was taken by workers at PTB in Germany (Alberts et al. 1994) and at CERN (Aroua and Hofert 1996). The resulting curve of the relative dose equivalent response of the PDM-

303, over about 10 orders of magnitude of neutron energy, is shown in Figure 1. The relative dose response of the dosimeter is clearly too high in the intermediate region of 10^{-6} –10^{-2} MeV by as much as a factor of 80, although the relative response is much better than this for higher energies, ranging from ~ 0.5-3 for E > 0.1 MeV. For the atmospheric neutron spectrum, as calculated by Armstrong et al. (1973) or as measured by Hewitt et al. (1978), the fraction of neutrons in the range of 10^{-6} –10^{-2} MeV is still small. Based on our calculations for the Armstrong and Hewitt spectra, using the curve fit for the relative response shown in Fig. 1, neutrons in the 10^{-6} –10^{-2} MeV range contribute about 2% of the total dose equivalent, but about 30% of the total dose equivalent response of the PDM-303. Thus, the over response of the PDM-303 to neutrons in the intermediate energy range has a noticeable, but nevertheless relatively small effect on the overall response of the PDM-303 to the entire atmospheric neutron spectrum.

Another limitation of the dose response curve is that it does not go high enough in energy, i.e., there is no data above 55 MeV and so the best we could do was to assume it remained constant at ~ 2.5 for E > 55 MeV. Alternatively, we could calibrate the dosimeter in a neutron field similar to that of the atmospheric neutrons, comparing the response of the PDM-303 against that of other dosimeter systems.

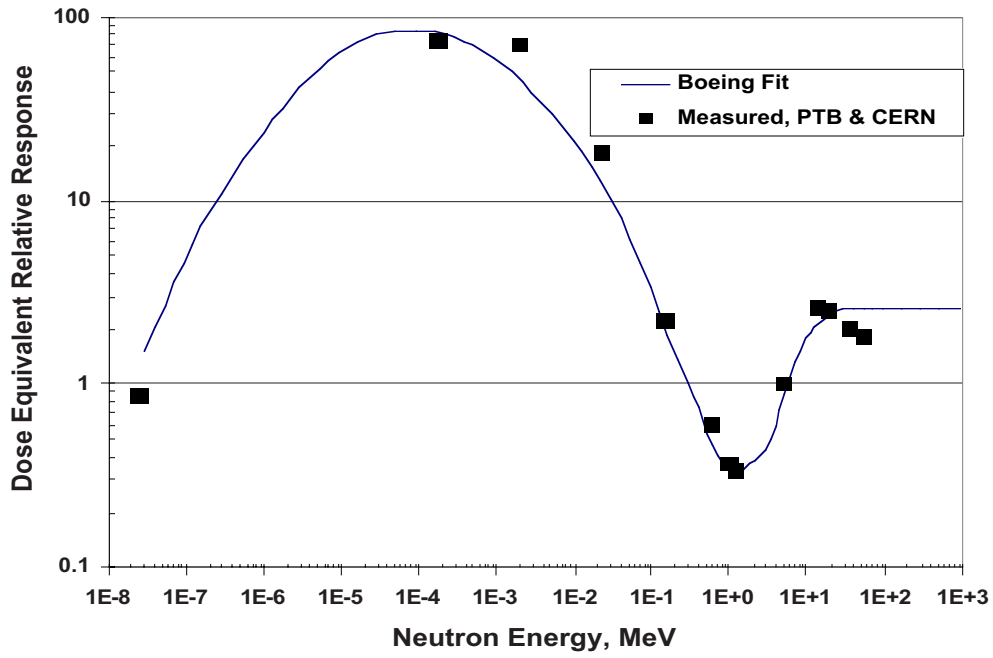

Figure 1 Dose Equivalent Relative Response Curve for the PDM-303 Based on Measurements at PTB (Alberts et al. 1994) and CERN (Aroua and Hofert 1996).

Three sets of such calibration data are available: 1) measurements made at the Weapons Neutron Research (WNR) facility at Los Alamos National Lab, 2) measurements at the High-Energy Reference Field of the Commission of European Communities (CEC) at CERN and 3) measurements made aboard aircraft. The WNR high-energy neutron beam is created by bombarding 800 MeV protons into a tungsten target and

collimating the resulting neutron beams. Thus, for energies up to ~ 600 MeV, the neutron spectrum is very similar to that of the atmospheric neutrons, only more intense [1 hour in the beam is equivalent to ~2.5E5 hours of neutron fluence at 40,000 ft. (Normand et al. 1994)]. Based on our own BREL measurements and those by Los Alamos (Casson et al. 1995), the PDM-303 over-responds to the neutrons by about a factor of 2.5.

Researchers at CERN (Aroua and Hofert 1996) have used the PDM-303 in the CEC reference field and compared its neutron dose equivalent response to that of other neutron dosimeters. The CERN neutron reference field is a section of a high-energy proton accelerator with a reduced amount of shielding surrounding the beam (205 GeV protons onto a copper target, shielded by 80 cm of concrete). Based on a comparison of the dose equivalent as measured by other types of neutron dosimeters, the response of the PDM-303 is about a factor of 5 too high (Aroua and Hofert 1996) for that radiation field. Similarly Bartlett of the British National Radiation Protection Board (NRPB), has taken the PDM-303 aboard a number of commercial aircraft flights that also included a number of other neutron dosimeters, such as track detectors which had been calibrated at the CERN reference field. Based on these in-flight measurements, the PDM-303 over responds by a factor of 5 (Bartlett, personal communication).

The major difference between the WNR beam and radiation fields at the other two locations (CERN reference field and inside an airplane), is that the WNR beam contains only neutrons, whereas the other two radiation fields have high-energy secondary protons, along with the neutrons. The WNR beam purposely filters out the secondary protons. Furthermore, it appears that the neutron response in the PDM-303 is indirect via neutron reactions in a converter material to produce charged particles that can be measured by a PIN diode. Originally, we had thought that the converter was plastic, leading to the production of proton recoils, however it appears that the actual converter is made of lithium (Aroua and Hofert 1996). Neutrons of all energies will react with the Li-6 producing an alpha particle and a triton. However, in addition, Li-7 will react with energetic protons to produce neutrons and Be-7. Furthermore, protons of certain energies may also be capable of depositing enough energy directly into the diode for the PDM-303 to respond (secondary protons with energies > 700 MeV have ranges greater than 100 cm in concrete and thus are present at the reference field). Thus the presence of energetic protons along with cosmic ray neutrons will complicate the response of the PDM-303, and there are no measurements we are aware of how the PDM-303 responds to beams of pure protons of different energies.

Thus, in contrast to the WNR beam, the highly energetic secondary protons created by the cosmic rays in the atmosphere and by the CERN beam passing through the concrete shielding are likely to cause the PDM-303 to respond, either by direct or indirect ionization. We have two calibration factors, 2.5 based on Boeing and LANL measurements in the WNR beam, and 5 based on measurements at CERN and on aircraft. For purposes of the ER-2 measurements we will use the calibration factor of 5 as the more accurate way of correcting the PDM-303 readings to obtain the dose equivalent delivered by the atmospheric neutrons.

Experimental Results

ER-2 Flight Description

The E-2 flight program consisted of five scientific flights and a preliminary engineering test flight, all originating out of NASA-Ames, Moffet Field, CA. Two flights went south, two north and one east. Table 1 summarizes the flights and their routes.

Table 1 AIR Flights From NASA-Ames, June 1997

Flight	Date	Duration	Ames Sortie	Start Time	End Time
Engineering Test	June 2, 1997	2 hr.	N97104	1:00pm PDT	3:00pm PDT
East	June 5	6.5 hr.	N97105	9:00 am PDT	3:33 PM PDT
North 1	June 8	7.5 hr.	N97106	9:00 am PDT	4:47 PM PDT
South 1	June 11	6.5 hr.	N97107	9:00 am PDT	3:30 PM PDT
North 2	June 13	6.5 hr.	N97108	9:00 am PDT	3:37 PM PDT
South 2	June 15	6.5 hr.	N97109	11:00 am PDT	5:24 PM PDT

PDM-303 Measurements

The recorded neutron dose equivalent for each of the flights is given in Table 2. The raw PDM-303 readings are given first in the third column, followed by two columns with corrected readings, one based on the calibration factor of 2.5 (Boeing and LANL measurements) and the second based on the calibration factor of 5 (CERN and NRPB measurements). The sixth column contains the dose equivalent measurements obtained using the Boeing TEPC (Chee 1998), and in the last column, we list the ratio of the corrected PDM reading (CERN/NRPB) to the TEPC reading. From the Ratio column it is clear that with the CERN/NRPB calibration factor, the PDM-303 dose equivalent readings are in excellent agreement with those from the TEPC. Here we are using the TEPC dose equivalent contribution from high LET particles (neutrons and protons), defined as having y (lineal energy transfer) > 10 keV/μm

PDM-303 Results Compared with 1-10 MeV Neutron Fluence

Although many additional comparisons will be made after all of the measurements from the various instruments flown on ER-2 are published, a relative comparison can be made at this time among the various routes. Furthermore, we also make a similar comparison based on the NASA-Langley 1-10 MeV neutron distribution model developed by Wilson and Nealy (Wilson and Nealy 1992). This model extrapolates and interpolates neutron fluxes measured during dedicated flights in the 1960s and early 70s based on three parameters: 1) the air column density (in gm/cm^2, related to the altitude) 2) the vertical rigidity cutoff (related to the latitude and longitude and 3) a parameter indicative of the cosmic ray intensity. The model has been revised recently and is now called the AIR model (Wilson et al. 1998).

Table 2 Comparison of PDM-303 and TEPC Measurements on AIR Flights

Sortie	Route	Raw PDM Reading, mSv	Corrected PDM Dose Equiv.,* mSv	Preferred Corrected PDM Dose Equiv., mSv‡	TEPC Dose Equiv., mSv†	Ratio, PDM/ TEPC Dose Equiv.
97-104	San Francisco Bay Area	0.04	0.016	0.008	0.011#	0.73
97-105	East	0.26	0.104	0.052	0.06	0.87
97-106	North 1	0.57	0.228	0.114	0.113	1.01
97-107	South 1	0.14	0.056	0.028	0.028	1.00
97-108	North 2	0.37	0.148	0.074	0.084	0.88
97-109	South 2	0.12	0.048	0.024	0.027	0.89

- *Calibration factor of 1/(2.5) obtained from calibrations of PDM-303 with WNR neutron beam by LANL and Boeing
- ‡ Calibration factor of 1/5 obtained from calibrations of PDM-303 by CERN and NRPB in neutron/proton environments
  † Response of Boeing TEPC on ER-2 for LET > 10 keV/μm
  # Based on averaging first 30 minutes of TEPC responses for East and South 1 routes, then multiplying by 4 to obtain 2 hour response

The neutron dose equivalent for a given flight is proportional to the neutron fluence for that flight. Most of the neutrons lie in the energy range of 1-1000 MeV. Thus the fluence of 1-10 MeV neutrons should be proportional to and representative of the entire neutron fluence over all energies for all flights, and so it should also be proportional to the neutron dose equivalent for all flights. For each route we estimated the 1-10 MeV neutron fluence using the Wilson-Nealy model to calculate the flux. The flux multiplied by the corresponding flight duration gave the fluence.

All ER-2 flights were assumed to be at 65,000 ft. altitude (56 gm/cm^2), and the latitude-longitude variation was accounted for by using five locations along each route. Thus, we used the Wilson-Nealy model to calculate the flux at the five locations and used the average flux value to obtain the fluence. This was done for the East and South routes which were essentially identical on the outbound and inbound legs. For the northern routes, there was a 1-hour east-west segment at the northernmost part of the routes. Thus two characteristic fluxes were used, one for the north-south portion and the higher one for the east-west portion. Table 3 contains the 1-10 MeV fluxes and fluences for the ER-2 routes.

The eastern flight was chosen as the base case, and the two types of data, PDM-303 readings and route 1-10 MeV neutron fluences, were normalized relative to the east flight data point. As seen in the last two columns of Table 3, there is excellent agreement between the normalized fluences and normalized PDM-303 readings for both southern flights and the north 2 flight. For the longer north 1 flight, the normalized PDM-303 ratio is higher than the normalized 1-10 MeV fluence ratio by about 35%. We believe that the reason for this is that the percentage of protons relative to neutrons in the atmosphere is higher at the higher latitudes than at more southerly latitudes (Bui Van et al. 1993). In addition, at the highest latitude,

we speculate that other cosmic ray primaries besides protons ($Z \geq 2$) are present in more significant proportions compared to lower latitude locations. Thus, the protons, and possibly other cosmic ray primaries, contribute proportionally more to the PDM-303 reading for the north 1 flight than for all the other flights.

Table 3 Comparison of PDM-303 Data For Various Flights Against 1-10 MeV Neutron Fluence, Based on Wilson-Nealy Neutron Flux Distribution Model

Flight #	Route	Raw PDM Read, mSv	1-10 MeV Neutron Flux (Wilson-Nealy)*, $n/cm^2 sec$	Route 1-10 MeV Neutron Fluence (Wilson-Nealy), n/cm^2	Ratio PDM Rdgs, Route/ East Route	Ratio 1-10 MeV Neut Fluence, Route/ East Route
97-105	East	0.26	1.48	3.46E+04	1.00	1.00
97-106	North 1	0.57	2.03/2.46	5.64E+04	2.19	1.63
97-107	South 1	0.14	0.75	1.76E+04	0.54	0.51
97-108	North 2	0.37	2.03/2.46	4.91E+04	1.42	1.42
97-109	South 2	0.12	0.75	1.76E+04	0.46	0.51
-	Sea-NYC	0.12	1.15	1.99E+04	0.46	0.57
-	Seattle-Minnea-polis	0.05	1.09	1.10E+04	0.19	0.32
-	Los Alamos	0.017	0.03	6.54E+03	0.07	0.19

Table 3 also contains PDM-303 readings for two commercial jet routes and for one high altitude ground level location, Los Alamos, New Mexico (7200 ft.). The relevant times over which the readings were made for each of these are: Seattle-NYC, 4.8 hours, Seattle-Minneapolis, 2.8 hours and Los Alamos, 64 hours. The same normalizations were carried out for the PDM-303 readings and for the 1-10 MeV neutron fluence.

For these three cases, unrelated to the ER-2 flights, the 1-10 MeV neutron fluence ratios were always higher than the PDM-303 ratios. There could be two reasons for this. First, at lower altitudes, the percentage of protons relative to neutrons appears to be lower compared to that at higher altitudes (Bui Van et al. 1993). Secondly, the PDM-303 readings for Los Alamos and the Seattle-Minneapolis flight are based on many fewer counts (each 0.01 mSv increase being equivalent to one count) compared to the ER-2 flights, so the statistical uncertainty [taken as $(counts)^{1/2}$] is much larger. For the Seattle-NYC flight, for which the PDM-303 reading is quite similar to those on some of the ER-2 flights, the agreement is much better. For the Seattle-NYC flight, the statistical uncertainty is smaller, and the agreement between the normalized PDM-303 readings and the normalized 1-10 MeV neutron fluences is very similar to that for the ER-2 flights.

Summary

A simple electronic neutron dosimeter, the PDM-303 was flown on all of the ER-2 flights in the shin pocket of the pilot's suit. The raw PDM-303 readings were corrected for the cosmic ray neutron/proton spectrum using the calibration factor of 1/5 from CERN and NRPB to obtain the true dose equivalent due to the neutrons. The corrected PDM-303 neutron dose equivalent values were in excellent agreement with the flight dose equivalent due to neutrons as measured by the Boeing TEPC. A comparison of the PDM-303 neutron dose equivalent readings was also made against the total neutron fluence for the flights as represented by the 1-10 MeV neutron fluence calculated by the early version of the AIR model (Wilson-Nealy model). For this comparison, all ER-2 flights were normalized relative to the east flight. For the two southern flights and north 2 flight, the normalized ratios of PDM-303 readings and 1-10 MeV neutron fluence were in excellent agreement. For the north 1 flight, the PDM-303 over responded compared to the 1-10 MeV neutron fluence. This was the only flight that went to latitudes beyond 60^{o} north. The discrepancy is explained as being caused by a higher percentage of protons and higher Z primary cosmic rays in the atmosphere at the high latitude portion of this flight compared to that for the other flights. Only at such high latitudes, where the geomagnetic field is very weak, can cosmic ray primaries penetrate.

References

Alberts, W.G., et al, "Response of An Electronic Personal Neutron Dosemeter", Radiat. Prot. Dosim. 51, 207, (1994)

Aloka Co., Electronic Pocket Dosimeter MYDOSE Model PDM-303 Instruction Manual, Aloka Company, Ltd., Mitaka-Shi, Tokyo

Armstrong, T.W., et al, "Calculation of Neutron Flux Spectra in the Earth's Atmosphere by Galactic Cosmic Rays ", ",J. Geophys. Res., 78, 2715 (1973)

Aroua, A., Hofert, M., "Investigation of the PDM-303 Neutron Pocket Dosemeter in Various Neutron Fields," Nucl. Instrum. Methods, 372A, 318 (1996)

Bartlett, D., personal communication

Bui Van, N.A., et al, "Secondary Protons in the Atmosphere at Different Latitudes," Il Nuovo Cimento, 16C, No. 2, 179, (1993)

Casson, W.H., Devine, R.T., Staples, P.A., Walker, L.S., "The Response of an Electronic Neutron Dosimeter in Neutron Fields with Energies Extending up to 600 MeV", Health Physics, 68, #6 Supplement, S22, (1995)

Chee, A., "TEPC Measurements of High Altitude Radiation," paper presented at the Atmospheric Ionizing Radiation (AIR) Investigators' Workshop: Preliminary Results and Lessons Learned from the June 1997 ER-2 Flights, March, 1998

Hewitt, J.E., et al., "Ames Collaborative Study of Cosmic Ray Neutrons: Mid-Latitude Flights", Health Physics, 34, 375, (1978)

Normand, N., et al, "Single Event Upset and Charge Collection Measurements Using High Energy Protons and Neutrons," IEEE Trans. Nucl. Sci., 41, 2203 (l994)

Wilson J.W., Nealy, J.E., "Model and Data Base for Background Radiation Exposure of High Altitude Aircraft," Proceedings of the Topical Meeting on New Horizons in Radiation Protection and Shielding, American Nuclear Society, 1992

Wilson, J.W., et al "AIR Model Development and Preflight Analysis," paper presented at the Atmospheric Ionizing Radiation (AIR) Investigators' Workshop: Preliminary Results and Lessons Learned from the June 1997 ER-2 Flights, March, 1998

Chapter 15: The Determination Using Passive Dosemeters of Aircraft Crew Dose

David T. Bartlett, Luke G. Hager, Richard J. Tanner
National Radiological Protection Board, Chilton, Oxon, OX11 0RQ, United Kingdom

The Determination Using Passive Dosemeters of Aircraft Crew Dose

Introduction

In the course of their work, aircraft crew and frequent flyers are exposed to elevated levels of cosmic radiation of galactic and solar origin and secondary radiation produced in the atmosphere, aircraft structure, etc. This has been recognised for some time and estimates of the exposure of aircraft crew have been made previously and included in, for example, UNSCEAR (United Nations Scientific Committee on the Effects of Atomic Radiation 1993) publications. The recent increased interest has been brought about by several factors – the consideration that the relative biological effectiveness of the neutron component was being underestimated; the trend towards higher cruising altitudes for subsonic commercial aircraft and business jet aircraft; and most importantly, the recommendations of the International Commission on Radiological Protection (ICRP 1991) in Publication 60, and the revision of the Euratom Basic Safety Standards Directive (BSS 1996).

The calculation of the complex radiation fields is difficult, and so is the measurement. No one device, active or passive, can entirely satisfactorily measure the whole range of particle types and energies. A tissue equivalent proportional counter (TEPC) measures absorbed dose and, to a first approximation, dose equivalent to a small volume of tissue (1 or 2 μm diameter unit density equivalent) from all radiation components (Lindborg et al 1995). However there are practical difficulties of sensitivity (for a typical active volume of 15 to 20 cm diameter) and robustness. Progress is being made with such devices. A large number of passive and active devices have been used to measure the dose in aircraft and a summary of the results obtained and the characteristics of the devices are given in a EURADOS report (1996). Detailed information on the radiation field components is necessary to fully interpret and relate instrument readings to radiological protection quantities of interest. This procedure is easier for the non-neutron components: most of the difficulties of measurement relate to neutron dose equivalent (as does the main difference between computer codes for dose calculation). However the neutron component is the most variable (with altitude, latitude and the magnitude of the magnetic field) and is the dominant component for altitudes above 10 km at higher latitudes. The high energy response characteristics of dosemeters and instruments are not sufficiently well known, nor are the neutron spectra which must be measured. One approach to overcome this problem, is to calibrate neutron measuring devices in a radiation field which simulates (within current knowledge) the neutron fields in aircraft. Mixed high energy particle fields have been recently set up at the super proton synchroton (SPS) at CERN (Hofert and Stevenson 1994). These stray radiation fields are created by beams of high energy protons and pions. The target area is surrounded by massive shielding and the calibration fields are located outside the shielding. The investigations of the CERN reference fields started in 1992. Since 1993, these fields have been available for testing and calibration of detectors and equipment from other European laboratories, and various measurements have already been performed on the initiative of the CERN radiation protection group and the European Commission.

APPROACH

For aircraft crew whose dose is unlikely to exceed 1 mSv per year, the BSS Directive does not require dose assessment. Dose assessments may be made for crew (and possibly frequent flyers) for whom it is necessary by folding staff roster data with average route doses obtained from sample measurements, or from calculations validated by measurements. Alternatively, instruments might be carried on board to measure doses on each flight. The issue of personal dosemeters to individual crew members would not be necessary.

The European Commission, Directorate-General XII (Science, Research and Development, Radiation Protection Research Action) has provided funding for research on aircraft crew dosimetry, in particular under a contract entitled 'Study of Radiation Fields and Dosimetry at Aviation Altitudes'. As part of this study, NRPB has developed a 'passive survey meter' to determine route effective dose. The 'passive survey meter' consists of two sets of routine issue personal dosemeters. Thermoluminescent detectors (TLDs) are used to assess the photon and directly ionising component, the non-neutron component, of the radiation field. Poly allyl diglycol carbonate (PADC) track etch detectors are used to estimate the neutron component. 30 TLDs and 40 PADC dosemeters are used to obtain sufficient precision (Bartlett et al. 1997). The 15% determination limit (that is the effective dose for which the coefficient of variation is 15%) is about 100 μSv.

The TLDs with ^{7}LiF : Mg, Ti as the thermoluminescent detector are calibrated in terms of tissue kerma in a ^{137}Cs field. The results of calculations of O'Brien (1972) of the radiation field in the atmosphere at aircraft altitudes indicate that the depth-dose profile in tissue is not pronounced. From these data, it is concluded that tissue dose for the non-neutron component may be equated to average absorbed dose in the human body, with a systematic error of no more than 10%. Using the photon interaction coefficients calculated by Hubbell and Seltzer (1995), the ICRU tabulations of electron (ICRU 1984) and proton (ICRU 1993) stopping powers and data on muon stopping powers (O'Brien 1978, Stevenson 1983, Hofert 1987), it is concluded that using a ^{137}Cs field calibration the TLDs will give a valid estimation of tissue dose equivalent for the radiation field in Concorde within 5%. (For photons up to 10 MeV: < 5% overestimate; for electrons up to 50 MeV: within 2%; for protons up to 1 GeV: within 2%; for cosmic radiation muon spectrum: 5% underestimate). It has been assumed in these calculations that the light conversion efficiencies for energy deposition by these radiations in ^{7}LiF, remains close to unity.

The ^{7}LiF detectors will have some response to the neutron component of the radiation field. Energy deposition from direct nuclear interactions in the detectors and heavy recoils and low energy recoil protons from interactions in the dosemeter holder will be about 33% of total neutron kerma, but will have low light conversion efficiency, of the order of 10% of that to energy deposition for the calibration field. The energy transfer from neutrons to energetic recoil protons will be approximately 66% of the total neutron kerma in the material of the passive survey meter (Savitskaya and Sannikov 1995), the total kerma being similar to that for soft tissue. For energy deposition by the resultant secondary proton energy spectrum, a light conversion efficiency in the region of 50% may be assumed (Jahnert 1971). The neutron component of the radiation field is in the range 10-20% of the total in terms of

absorbed dose depending on altitude and latitude (O'Brien 1972, 1997). Thus the contribution from the neutron component to the response of the TLDs is of the order of 5%.

The proton component of the radiation field, depending on altitude and latitude, is in the range 15 to 35% of the non-neutron component of total dose. Tissue dose for this component will be estimated, for the calibration used, within a few percent. In ICRP Publication 60 (1991) it is recommended that a radiation weighting factor of 5 should be applied when calculating effective dose, and the EU Directive (1996) follows this recommendation. In the USA the National Council on Radiation Protection and Measurements (NCRP) has recommended a value for the proton radiation weighting factor, w_R of 2 for protons up to 100 MeV and of 1 for higher energies (NCRP 1993). Were a proton weighting factor of unity applied, the value of the non-neutron component of tissue dose estimated from the TLD measurements may simply be equated to effective dose with an overall error of no more than 20%. To incorporate the proton weighting factor of 5, the multiplying factor to be applied to the measured value of the non-neutron component of absorbed dose to obtain effective dose is, taking into account the 5-10% overestimate of absorbed dose by our measurement technique: 0.95 times (1+4x) where x is the fraction of total non-neutron dose which is deposited by incident protons. Using O'Brien's results for LUIN97, x = 0.18, 0.27, 0.35 for 12, 18 and 21 km respectively. (At the present time the O'Brien data are the only available data). The non-neutron component is increased by 70% and the total effective dose by about 20% to 25% for a cruising altitude of 10 to 12 km.

The PADC neutron dosemeters respond to thermal and epithermal neutrons and fast neutrons above an energy of about 100 keV. The effective dose (or personal dose equivalent) response characteristic is energy dependent. The response characteristic is well established up to 14 MeV. Above this energy, response data have been obtained for neutron spectra with peak energies of 44 and 66 MeV in the irradiation facilities at the Paul Scherrer Institute (PSI) (Tanner et al. 1995) and 160 MeV at the The Svedberg Laboratory, Uppsala (Bartlett et al. 1997). These high energy neutron fields have large lower energy components, typically 50% of the total neutron fluence, of uncertain spectrum, as a result of which there is a large uncertainty associated with these high energy response data. Nevertheless the data are self-consistent and are in broad agreement with the results of Spurny (1995) where a flat dose equivalent response characteristic for energies greater than about 100 MeV is indicated. With the reservations as to the correctness of the high energy response data, the PADC response characteristics have been folded with the calculated neutron spectrum for a depth in the atmosphere of 200 g/cm^2, corresponding to an altitude of 12 km (39,000 ft) by Roesler et al. (1997) using the Monte Carlo code FLUKA (Fasso et al. 1994a, 1994b), and for the concrete shielded high energy stray field at CERN, the CERN/European Commission Reference Field (CERF) (Hofert and Stevenson et al. 1994b) by Rancati and Ferrari (1996, Bartlett et al. 1996), also using FLUKA. The calculated fluence spectra are also folded with conversion coefficients for E(ISO) (Ferrai et al. 1997) and the results are shown in Table 1 together with experimentally determined dosemeter response data for CERF. The calculated neutron spectra are compared in Figure 1 (fluence) and Figure 2 (E(ISO)). The good agreement between the calculated and measured dosemeter response in the CERF spectrum gives confidence to the use of the measured PADC dosemeter response characteristic and to the correctness of the FLUKA calculations for CERF. Whilst being aware of the remaining uncertainty as to the neutron spectrum within an aircraft and its variation with altitude, the broad similarities between the CERF spectrum and calculated neutron spectra in the atmosphere are considered to

justify the direct calibration in CERF, of the neutron dosemeter set of the passive survey meter. In additional, PADC sheet normalisation factors (determined for ^{252}Cf neutrons) are applied.

The PADC dosemeters will have some response to the proton component of the radiation field in aircraft. The PADC detector responds directly to protons, but only of energy less than about 2 MeV. The proton energy spectrum at each detector will be modified from that incident on the outside of the passive survey meter by slowing down and other interactions. However, if to a first approximation it is assumed that there is partial radiation equilibrium (the survey meter is about 6 g/cm^2 thick), the proton spectrum at a detector will have little fluence below 2 MeV. Accordingly, the use of the CERF calibration is considered to give a good estimate, within 20 or 30%, of effective dose.

RESULTS

The details of the flight profiles for the NASA ER-2 high altitude flights from NASA Ames Research Center made during 1997 are given elsewhere in the meeting. The results obtained with the passive survey meter are estimates of total effective dose obtained using the approach given above. The results are shown below in Table 2 for the northerly, easterly and southerly flights. Effective dose is estimated using proton weighting factors of 1 and 5. Estimates of ambient dose equivalent (using the neutron conversion coefficients of Sannikov and Savitskaya, 1995) are also given for comparison.

DISCUSSION

The results which have been reported here are shown in Figure 3 with other results obtained by the same approach for London-Tokyo flights (Bagshaw et al. 1996) and London-New York by Concorde, and the results reviewed by EURADOS (1996). The route doses obtained using the passive survey meter have been converted to a mean dose rate over the range of cruising altitudes. The results are in broad agreement.

Given the difficulties of measuring and determining dose equivalent quantities to the complex radiation field in aircraft at altitude, agreement of measured and calculated values to within 20-30% must be considered satisfactory. For many circumstances in routine radiation protection, in the nuclear industry for example, agreement this close would be found to be most acceptable. However, meaningful comparison of, and understanding of the results shown here and elsewhere can only be made if what is being measured is well defined and where the response characteristics of the device are well known. For the results we have reported, there are various aspects which require further investigation. One is the degree of confidence in the CERF neutron spectrum. At the moment the results of the FLUKA calculations have been accepted without reservation. There are supporting data showing agreement of measured and calculated instrument readings, and there are measurements of the spectrum, all of which may need to be re-evaluated. The second is the validity of using the CERF neutron spectrum as a calibration spectrum. How well does it correspond to the spectrum in aircraft at cruising altitudes? How much does the spectrum in aircraft vary? The third is the variability of the measurement system. The fourth is the uncertainty in

the relative magnitude of the proton component of the non-neutron doses needed to separate the proton component in order to apply the ICRP radiation weighting factor. Effort is being devoted to these matters.

Acknowledgements This work was partly funded by the European Commission, Directorate-General XII, under contract F14P-CT95-0011. The authors are grateful for many valuable discussions with colleagues, particularly with other contractors, with Professor O'Brien, and with Drs Stevenson, Silari and Höfert at CERN, and for the assistance and cooperation of staff at British Airways.

References

Bagshaw, M., Irvine, D. Davies, D.M.: 'Exposure to Cosmic Radiation of British Airways Flying Crew on Ultra Long Haul Routes'. *Occup. Environ. Med*., **53**, pp. 495–498, (1996).

Bartlett, D.T., Hager, L.G., Rancati, T., Ferrari, A., Silari, M., Otto, T.: 'Neutron Radiation Fields at the CERN/EC Reference Field Facility : December 1996 Interim Report'. NRPB Technical Memorandum 25/96, 1996.

Bartlett, D.T., Hager, L.G., Tanner, R.J.: Unpublished results, 1997.

Bartlett, D.T., Tanner, R.J., Hager, L.G., Lavelle, J.: 'The Measurement Using Passive Dosemeters of the Neutron Component of Aircraft Crew Dose'. *Radiat. Meas*., **28** (1–6), pp. 519–524, 1997.

Council Directive 96/29/EURATOM of 13 May 1996 Laying Down the Basic Safety Standards for Protection of the Health of Workers and the General Public Against the Dangers Arising from Ionising Radiation. Official Journal of the European Communities 39, L159, 29 June 1996.

EURADOS, European Radiation Dosimetry Group; Exposure of Air Crew to Cosmic Radiation, a report of EURADOS Working Group 11, EURADOS Report 1996-01, European Commission Report, Radiation Protection 85, Eds: I. R. McAulay, D. T. Bartlett, G. Dietze, H. G. Menzel, K. Schnuer, U. J. Schrewe, ((European Commission, Luxembourg), 1996.

Fassó, A. Ferrari, A., Ranft, J., Sala, P.R.: 'FLUKA : Present Status and Future Developments'. Proc. IVth Int. Conference on Calorimetry in High Energy Physics, La Biodola, Italy, 1993, p493, (World Scientific: Singapore), 1994.

Fassó, A. Ferrari, A., Ranft, J., Sala, P.R.: 'FLUKA : Performances and Applications in the Intermediate Energy Range'. Proc. 1st Specialists' Meeting on Shielding Aspects of Accelerators, Targets and Irradiation Facilities, Arlington, USA, 1994, p287, (OECD NEA: Paris), 1994.

Ferrari, A., Pelliconi, M. Pillon, M.: 'Fluence to Effective Dose Conversion Coefficients for Neutrons up to 10 TeV', *Radiat. Prot. Dosim*., **71**, pp.165–173, 1997.

Höfert, M.: 'Dosemeter Response to Muons'. *Radiat. Prot. Dosim*., **20**, pp.149–154, 1987.

Hófert, M., Stevenson, G.R.: 'The CERN-CEC Reference Field Facility'. Proc. American Nuclear Society 8th Int. Conference on Radiation Shielding, Arlington, USA, 1994, European Laboratory for Particle Physics Report CERN/TIS-RP/94-2/CF, 1994.

Höfert, M., Stevenson, G.R.: The CERN-CEC High-Energy Reference Field Facility, European Laboratory for Particle Physics, Report CERN/TIS-RP/94-02/FC, 1994.

Hubbell, J.H., Seltzer, S.M.: 'Tables of X-ray Mass Attenuation Coefficients and Mass Energy-Absorption Coefficients, 1 keV to 20 MeV for Elements Z = 1 to 92 and 48 Additional Substances of Dosimetric Interest' National Institute of Standards and Technology Report NISTIR 5632, (US Dept of Commerce: Gaithersburg), 1995.

International Commission on Radiological Protection. 1990 Recommendations of the International Commission on Radiological Protection. ICRP Publication 60 (Oxford: Pergamon Press), 1991.

ICRU, International Commission on Radiation Units and Measurements. ICRU Report 37 'Stopping Powers for Electrons and Positrons', (ICRU: Bethesda), 1984.

ICRU, International Commission on Radiation Units and Measurements. ICRU Report 49 'Stopping Powers and Ranges for Protons and Alpha Particles', (ICRU: Bethesda), 1993.

Jahnert, B.: 'Thermoluminescent Research of Protons and Alpha Particles with LiF (TLD-700)'. Proc. 3rd Int. Conf. Luminescence Dosimetry, Risø, 1971. Risø Report 249, pp.1031-1039 (Risø: Denmark), 1971.

Lindborg, L., Grindborg, J.E., Gullberg, O., Nilsson, U., Samuelson, G., Uotila, P.: 1995: TEPC Measurements with the Variance-Covariance Method on Board Aircraft. *Radiat. Prot. Dosim*., **61** (1–3), pp. 119–124, 1995.

NCRP, National Council on Radiation Protection and Measurements. NCRP Report 116 'Limitation of Exposure to Ionizing Radiation' (NCRP: Bethesda), 1993.

O'Brien, K.: 'The Cosmic Ray Field at Ground Level'. Proc. 2nd Int. Conference on Natural Radiation Environment, August 1972, Honiton, USA. Report Conf-720805-PC, pp.15–54, (US Dept of Commerce: Gaithersburg), 1972.

O'Brien, K.: 'The Response of LiF Thermoluminescence Dosimeters to the Ground-Level Cosmic-Ray Background'. *Int. J. Appl. Radiot. Isotop*., **29**, pp.735–739, 1978.

O'Brien, K.: LUIN97 - unpublished results. Private Communication, 1997.

Rancati, T., Ferrari, A.: Private Communication, 1996.

Roesler, S., Heinrich, W.W., Schraube, H.: 'Calculation of Radiation Fields in the Atmosphere and Comparison to Experimental Data', (in press), 1997.

Sannikov, A.V., Savitskaya, E.N.: 'Ambient Dose Equivalent Conversion Factors for the High Energy Neutrons Based on the New ICRP Recommendations'. State Research Center of Russia, Institute for High Energy Physics Report IHEP95-98, 1995.

Savitskaya, E.N., Sannikov, A.V.: 'High Energy Neutron and Proton Kerma Factors for Different Elements'. *Radiat. Prot. Dosim*., **60**, pp.135–146, 1995.

Spurny, F.: 'Dosimetry of Neutrons and High Energy Particles with Nuclear Track Detectors'. *Radiat. Meas*., **25**, pp.429–436, 1995.

Stevenson, G.R.: 'Dose and Dose Equivalent From Muons'. European Laboratory for Particle Physics, CERN/TIS-RP/099, 1983.

Tanner, R.J., Bartlett, D.T., Turner, D.J.: 'Results for the NRPB PADC Neutron Personal Dosemeter' in EURADOS Report 1995-01 'Fast and High-Energy Neutron Detection with Nuclear Track Detectors : Results of the European Joint Experiments 1992/3', Eds, H. Schraube, W. G. Alberts, A. R. Weeks. GSF-Bericht 15/95, 1995.

United Nations Scientific Committee on the Effects of Atomic Radiation. Sources, Effects and Risks of Ionising Radiation. UNSCEAR 1993. Report to the UN General Assembly with Scientific Annexes. New York: United Nations, 1993.

Table 1
Neutron Spectra and PADC Response

Calculated neutron spectrum		E(ISO) weighted conversion coefficient (pSv cm^2)	PADC Reading per unit fluence		PADC Reading per unit E(ISO)	
			calculated	measured	calculated	measured
			(tracks cm^2 10^{-6})		(tracks mSv^{-1})	
Roesler 200 g/cm^2	FLUKA	220	20.7	27.8[a] ± 2.8	94.1	113 ± 11
Ferrari CERF†	FLUKA	245	26.6	27.9[b] ± 1.7	108	114 ± 7

† concrete shielded, position T3 (a) 1996 calibration (b) 1997 calibration

Table 2

NASA ER-2 High Altitude Flights from Ames, California

(with statistical uncertainties only ± 1 SEM)

	Proton $w_R = 1$	Proton $w_R = 5$	H*(10)new
Northerly Flights			
Total estimated effective dose:	161 µSv ± 19	241 µSv ± 20	169 µSv ± 21
comprising non-neutron component:	57 µSv ± 2.3	137 µSv ± 5.8	57 µSv ± 2.3
neutron component:	104 µSv ± 19	104 µSv ± 19	112 µSv ± 21
Easterly Flights			
Total estimated effective dose:	40 µSv ± 10	61 µSv ± 11	42 µSv ± 11
comprising non-neutron component:	15 µSv ± 1.8	36 µSv ± 4.3	15 µSv ± 1.8
neutron component:	25 µSv ± 10	25 µSv ± 10	27 µSv ± 11
Southerly Flights			
Total estimated effective dose:	42 µSv ± 15	74 µSv ± 16	44 µSv ± 16
comprising non-neutron component:	23 µSv ± 1.7	55 µSv ± 4.1	23 µSv ± 1.7
neutron component:	19 µSv ± 15	19 µSv ± 15	21 µSv ± 16

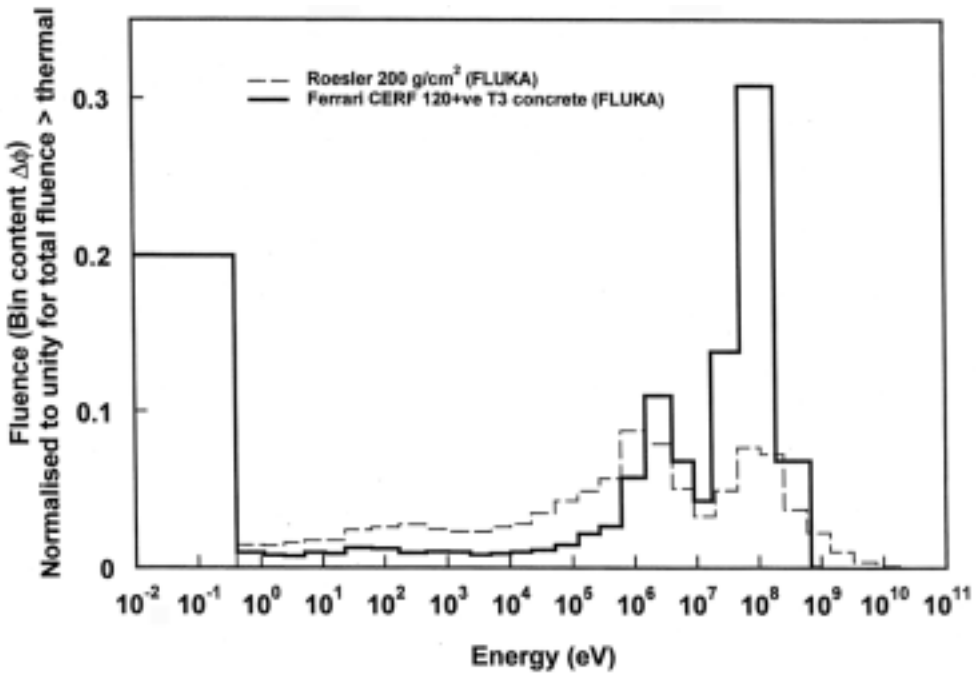

Figure 1. Calculated Neutron spectra.

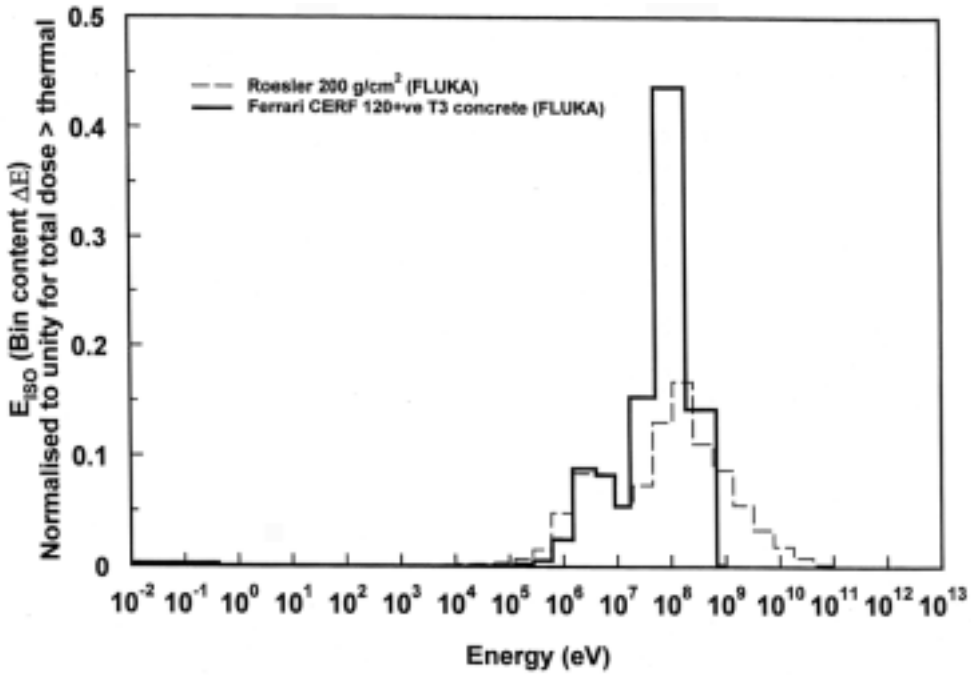

Figure 2. Calculated Neutron spectra.

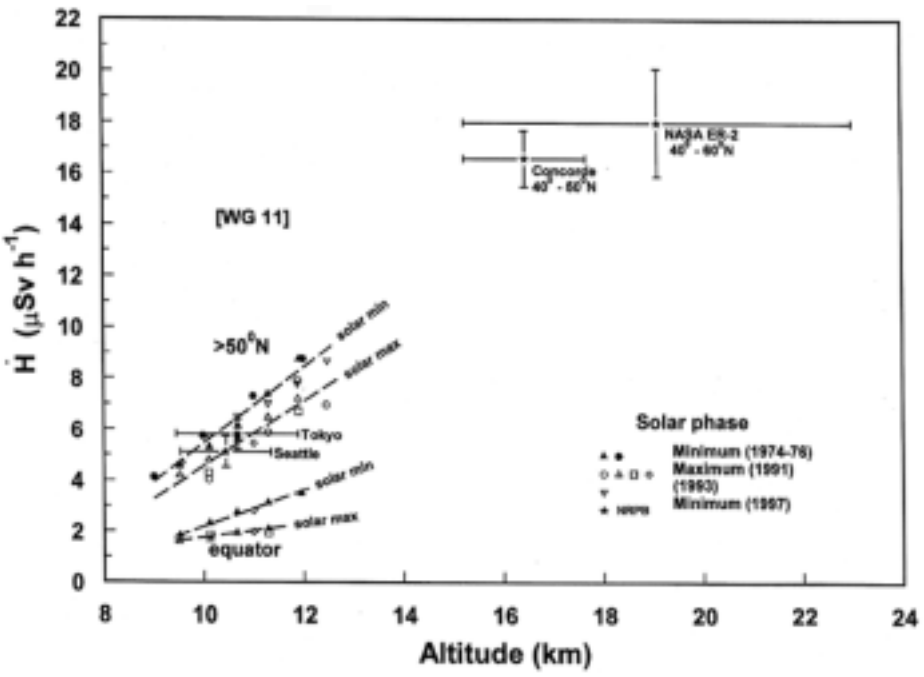

Figure 3. Measurements in Aircraft.

Chapter 16: Results of Passive Radiation Detector Exposures at High-Altitude

E. R. Benton, E. V. Benton, and A. L. Frank
Eril Research, Inc., P.O. Box 150788, San Rafael, CA 94915-0788

Results of Passive Radiation Detector Exposures at High-Altitude

Preface

A two element passive radiation detector, consisting of thermoluminscent detectors (TLDs) and CR-39 plastic nuclear track detectors (PNTDs), was exposed aboard a NASA ER-2 high-altitude research aircraft during the June 1997 AIR Campaign. Dose rates of 7.8 and 7.2 μGy/hr were measured using ^{7}LiF TLD (TLD-700) on the East-West (constant latitude) and Northbound flights, respectively, while a dose rate of 1.5 μGy/hr was measured using ^{7}LiF TLD for the Southbound flight. Despite extensive efforts to analyze the CR-39 PNTDs, the short duration of the exposures, e.g. ~12 hours for the Northbound flights, did not provide sufficient signal above background to yield a meaningful measurement. Results from two additional high-altitude exposures carried out by ERI are reviewed.

Introduction

In June 1997 the High Speed Research (HSR) program at NASA's Langley Research Center sponsored an extensive effort to measure the radiation environment at ~70,000 ft. using NASA's ER-2 high-altitude research aircraft and a suite of both active and passive instruments. A separate passive radiation detector provided by Eril Research, Inc. (ERI) was exposed on each of the three ER-2 flight paths: East-West at constant latitude, Northbound from NASA Ames Research Center (ARC) to Northern Canada and return, and Southbound from NASA ARC to Baja California and return. The ERI detector packages contained two types of passive detectors: ^{7}LiF TLD (TLD-700) to measure total absorbed dose and CR-39 plastic nuclear track detector (PNTD) to measure the LET spectrum ≥5 keV/μm. This detector combination, in the form of the Crew Passive Dosimeter (CPD) was originally developed for use by NASA astronauts in low Earth orbit and has been worn by crew members on every mission of the Space Shuttle since STS-1 in 1981. With the aid of an empirically-derived dose response function for TLD-700, dose from TLDs and the LET spectrum from PNTDs can be combined to yield corrected total dose and total dose equivalent.

Thermoluminscent Detectors

TLDs are one of the most commonly used detectors for radiation dosimetry. They are completely passive in mode of operation and record absorbed dose. TLDs are sensitive to ionizing radiation covering the entire LET spectrum. As LET increases above ~10 keV/μm, the efficiency of dose measured in TLD decreases due to saturation of the electron traps. However for the major fraction of directly ionizing radiation encountered at aircraft altitudes—protons, electrons and positrons, muons, pions, and γ-radiation—TLDs function with 100% efficiency. Because TLDs only record the total accumulated dose, it is not possible to

obtain any spectral data. Following exposure, readout of the TLDs is carried out using one of a number of commercially produced TLD readers. TLDs have a low dose threshold in the μGy range and thus are ideally suited for the low levels of radiation encountered during high-altitude flight. ERI has considerable experience using TLD-700 (^{7}LiF) aboard spacecraft and have measured the high-LET efficiency of TLD-700 using heavy-ion beams at a variety of ground-based accelerators.

Following exposure the TLDs were returned to the laboratory for processing and readout. The TLDs were read out with a Harshaw Model 4000 reader. Flight TLDs were read out along with calibration and background TLDs from the same manufactured batch. The calibrations were performed using a standard ^{137}Cs source. Absorbed doses accumulated during the flights were generated from the readout values. Dose rate results from the ERI TLDs exposed on the June 1997 ER-2 flights are summarized in Table 1. While on the South-bound missions an average dose rate of only 1.5 μGy/hr was measured, on the East-West and North-bound flights an average dose rate of ~7.5 μGy/hr was obtained. The uncertainty in each measurement is quite large due to the short amount of time the aircraft was at high altitude (>60,000 ft) during each measurement. ERI conducted the read out of TLDs provided by Reitz, DLR, Germany for the AIR Campaign and these results are also provided in Table 1. Dose measurements from the DLR TLDs are consistent with those of ERI.

Table 1. Doses and mean dose rates measured with TLDs during the June 1997 AIR Campaign aboard a NASA ER-2 Aircraft.

Dosimeter	Absorbed Dose (μGy)*	Mean Dose Rate (μGy/hr)	Mission
ER-2-1	43 ± 12	6.6 ± 1.8	East-West Flight (6/5/97)
ER-2-2	88 ± 17	6.1 ± 1.2	First (6/8/97) and Second (6/13/97) North-bound Flights
ER-2-3	16 ± 15	1.2 ± 1.1	First (6/11/97) and Second (6/15/97) South-bound Flights
Reitz-1	121 ± 47	4.3 ± 1.3	All Flights
Reitz-2	123 ± 50	3.4 ± 1.4	All Flights

*Background doses for TLDs were ~250 μGy.

CR-39 Plastic Nuclear Track Detectors

ERI has been using CR-39 plastic nuclear track detectors (PNTDs) to measure the LET spectra above 5 keV/μm aboard low Earth orbit (LEO) spacecraft like the NASA Space Shuttle and the Russian Mir Space Station for many years. The near tissue-equivalent composition of the CR-39 polymer and its ability to record tracks from both primary HZE (high charge and kinetic energy) particles and high-LET, short-range recoil secondaries makes it an ideal complement to TLDs in measuring total dose and dose equivalent

exposures of astronauts in LEO. ERI also has experience in flying this type of detector aboard both high-altitude aircraft and research balloons.

CR-39 PNTDs were included in the ERI dosimetry packages flown aboard a NASA ER-2 during the June 1997 AIR campaign. At altitudes of ~70,000 feet, there are few primary GCR and nearly all the high-LET particles are secondaries. These include knock-on protons (tracks from elastic neutron-proton and proton-proton collisions) and, to a lesser degree, short-range target fragment tracks from inelastic interactions between atmospheric neutrons and protons and the oxygen and carbon nuclei of the CR-39 detector.

Following the conclusion of the 1997 AIR Campaign, CR-39 PNTD layers from the detectors were disassembled and processed in 6.25 *N* NaOH solution at 50° C. Processing times were 36 hr and 7 d. The 36 hr processing is optimal for measurement of short range, high LET particle tracks including secondaries with $Z \geq 2$. The 7 d processing is optimal for tracks of lower LET and greater ranges. The tracks were located and measured using a microscope with controlled stage and an automated image analysis system. The major and minor diameters of the elliptical track openings in the surfaces of the PNTDs were measured for the detected tracks. These values, along with the PNTD bulk etch (the thickness of material removed from the PNTD surface during processing) allow an LET value to be determined for each particle track. Layers of CR-39 PNTD from the same manufactured batch and which served as ground-controls during the AIR exposures were also analyzed and a background subtraction of the flight detector data was made. Our plan was to generate a separate LET spectra for the 36 hr and 7 d detectors. The two LET spectra would then be combined into single spectrum covering the total applicable range of LET for the PNTDs (5 - 1250 keV μm^{-1}). Flux, dose rate and dose equivalent rate spectra would then be generated. Considerable effort was expended in the analysis the CR-39 PNTDs of June 1997 exposures. Unfortunately due to the short duration of the exposures (~12 hours for the North-bound flights) few tracks were formed in the detector and it was not possible to measure any appreciable signal above background. An area of 4 cm^2 was scanned on the flight detector and only ~120 tracks were located. Of these, ~60% were eliminated by the background correction. These tracks were mostly stopping α-particles from the decay of natural radon and its daughters.

Previous High-Altitude Dosimetric Measurements

In1989 ERI participated in the Cosmic Ray Upset Experiment (CRUX) sponsored by IBM to investigate single event upsets (SEU) in DRAM produced by cosmic rays in the upper atmosphere. ERI detectors were flown on two flights of NASA's ER-2, one at polar latitudes out of Norway, and one at a constant latitude of 36°N. A third set of exposures was made aboard a commercial airliner flying out of Seattle. ERI detector packages included CR-39 PNTDs to measure the LET spectra > 5 keV/μm, ^{6}LiF/CR-39/Gd thermal and resonance neutron detectors, and two types of TLDs—^{7}LiF (TLD-700) and CaF (TLD-200). Of particular

interest was the ER-2 flight at Arctic latitudes. Total exposure time was 124.7 hours of which 94.3 were at polar latitudes.

Table 2 shows doses and dose rates measured by the two types of TLDs aboard the 1989 Arctic flight. The ^{7}LiF measurements are somewhat higher than the CaF measurements, indicating some difference in response to the high-altitude radiation environment relative to the standard ^{137}Cs γ-ray source used for calibration.

Table 2. Doses and Dose rates measured by ^{7}LiF and CaF TLDs during the 1989 ER-2 Arctic flights.

Detector	TLD Type	Tissue Absorbed Dose (μGy)	Dose Rate (μGy/hr.)
F2	CaF	554 ± 18	4.5
	^{7}LiF	627 ± 29	5.0
F3	CaF	568 ± 24	4.5
	^{7}LiF	635 ± 29	5.1
Control	CaF	79 ± 4	
	^{7}LiF	74 ± 7	

The integral LET flux spectra ≥5 keV/μm measured in CR-39 for the 1989 Arctic ER-2 flight is shown in Figure 1. The analysis of these CR-39 detectors was carried out before development of the short-range track measurement technique and the shortest range particles measurable were on the order of 80 μm, compared to the 8 μm minimum range we are now capable of measuring. Nevertheless track selection criteria was used to separate particle events that left tracks on two adjacent surfaces of CR-39 from particle events formed on four adjacent surfaces of CR-39. The long range events (≥1200 μm) are assumed to be primary galactic cosmic rays (GCR). The shorter range events (~80 μm) are assumed to be secondary particle tracks. The long range charged particle component is negligible, the vast majority of events being produced by short-range secondary particles. The measured LET spectrum doesn't extend much beyond 100 keV/μm indicating that most of the tracks are from stopping protons produced in neutron–proton elastic scattering. The highest LET for a stopping proton is ~100 keV/μm. The density of tracks in the CR-39 detectors flown on the 36° ER-2 missions and the subsonic commercial flights was too low to be accurately counted and no LET spectra could be measured from these detectors. The shorter duration of the exposures as well as the latitude, and altitude in the case of the subsonic flight, is principally responsible for the negligible track density in the CR-39 detectors. The flux, dose rate and dose equivalent rate ≥5 keV/μm is presented in Table 3.

Table 3. Flux, dose rate and dose equivalent rate ≥5 keV/μm measured in CR-39 PNTDs exposed aboard the 1989 Arctic ER-2 flights. Total exposure time in the Arctic was 94.3 hours.

Particle Type	Flux ($cm^{-2}s^{-1}sr^{-1}$)	Dose Rate (μGy/hr)	Dose Equivalent Rate (μSv/hr)
Total	1.33×10^{-4}	0.14	0.88
GCR	7.7×10^{-6}	0.01	0.04
Secondaries	1.26×10^{-4}	0.14	0.84

Dose equivalents from thermal and resonance neutrons measured using ^{6}LiF/CR-39/Gd detectors on the 1989 Arctic ER-2 flights are listed in Table 4. Thermal neutron energy is taken to be ≤0.2 eV while resonance neutron energy is defined by 0.2 eV ≤ E_n ≤ 1MeV. The quality factor Q for thermal neutrons was taken to be 2 and for resonance neutrons a Q of 6.4 was used. Results from the three types of detectors were combined to obtain total dose equivalents. Total dose equivalents from the three flight paths are listed in Table 5.

Table 4. Neutron measurements made using ^{6}LiF/CR-39/Gd detectors on the 1989 Arctic ER-2 flights.

Detector	Neutron Fluence (cm^{-2})	Dose Equivalent (μSv)	Dose Equivalent Rate (μSv/hr)
Flight			
Thermal	$1.0 \pm 0.8 \times 10^{4}$	0.1 ± 0.08	8.3×10^{-4}
Resonance	$6.4 \pm 0.9 \times 10^{5}$	31 ± 4	0.25
Ground Control			
Thermal	$<6 \times 10^{3}$	<0.06	
Resonance	$1.2 \pm 0.4 \times 10^{5}$	6 ± 2	

Table 5. Dose Equivalent rates measured by the three ERI passive detector packages during the IBM CRUX experiment.

Mission	Altitude (ft.)	Dose Equivalent Rate (μSv/hr)			
		TLD (LET <5 keV/μm)	CR-39 (LET ≥5 keV/μm)	^{6}LiF/CR-39/Gd (E_n <1 MeV)	Total
ER-2 Arctic	~70,000	5.0	0.88	0.28	6.2
ER-2 36°	~70,000	3.7	negligible	0.19	3.9
Subsonic	~35,000	0.6	negligible	0.3	1.0

CR-39 PNTDs have been exposed on a number of other high-altitude missions by ERI. Figure 2 shows the integral LET flux spectrum measured aboard an Arctic balloon mission in 1994 and the LET spectrum

measured aboard the 1989 Arctic ER-2 flights. There is a significant contribution from primary GCR HZE particles in the balloon exposure which took place at an average altitude of 117,000 ft. At ~70,000 ft, where the ER-2 exposures were made, the primary GCR is almost completely attenuated and the dominant fraction of tracks come from neutron-induced proton knock-on events. The cross section for elastic neutron-proton collisions is much greater than that for neutron–induced target fragmentation. Consequently nearly all the track recorded in the detector are from protons. Since protons can have a maximum LET of ~100 keV/μm in CR-39, the LET spectrum does not extend much beyond this value. In addition, the 1989 Arctic ER-2 detectors were read out using an older analysis technique that required only conical tracks with well-defined tips be accepted. This excluded stopping particles and particles with short range (< 80 μm) including the heavy recoil nuclei from neutron- and proton-induced target fragmentation events.

Conclusions

ERI measurements of doses aboard high altitude aircraft (>60,000 ft) have yielded dose rates up to ~6 μGy/hr and dose equivalent rates up to ~8 μSv/hr. The highest rates were measured in the polar regions and a strong decline in radiation levels with declining latitude was found. Particles of high LET (≥10 keV/μm) were found in significant numbers only in the polar regions and particles of LET >100 keV/μm were found only at high altitudes in the polar region (>110,000 ft).

An important fraction of dose equivalent missing from all the measurements is that due to fast neutrons (>1 MeV). The measurement of fast neutrons will result in a substantial increase in total dose equivalent rates. This is the single most important problem yet to be solved in determining radiation exposures to aircraft crew.

Acknowledgements: The authors would like to thank John Wilson, Don Maiden, and Irby Jones of the NASA Langley Research Center, Hampton, VA, and Paul Goldhagen of the DOE Environmental Measurements Laboratory, New York, NY for the opportunity to participate in the Atmospheric Ionizing Radiation program.

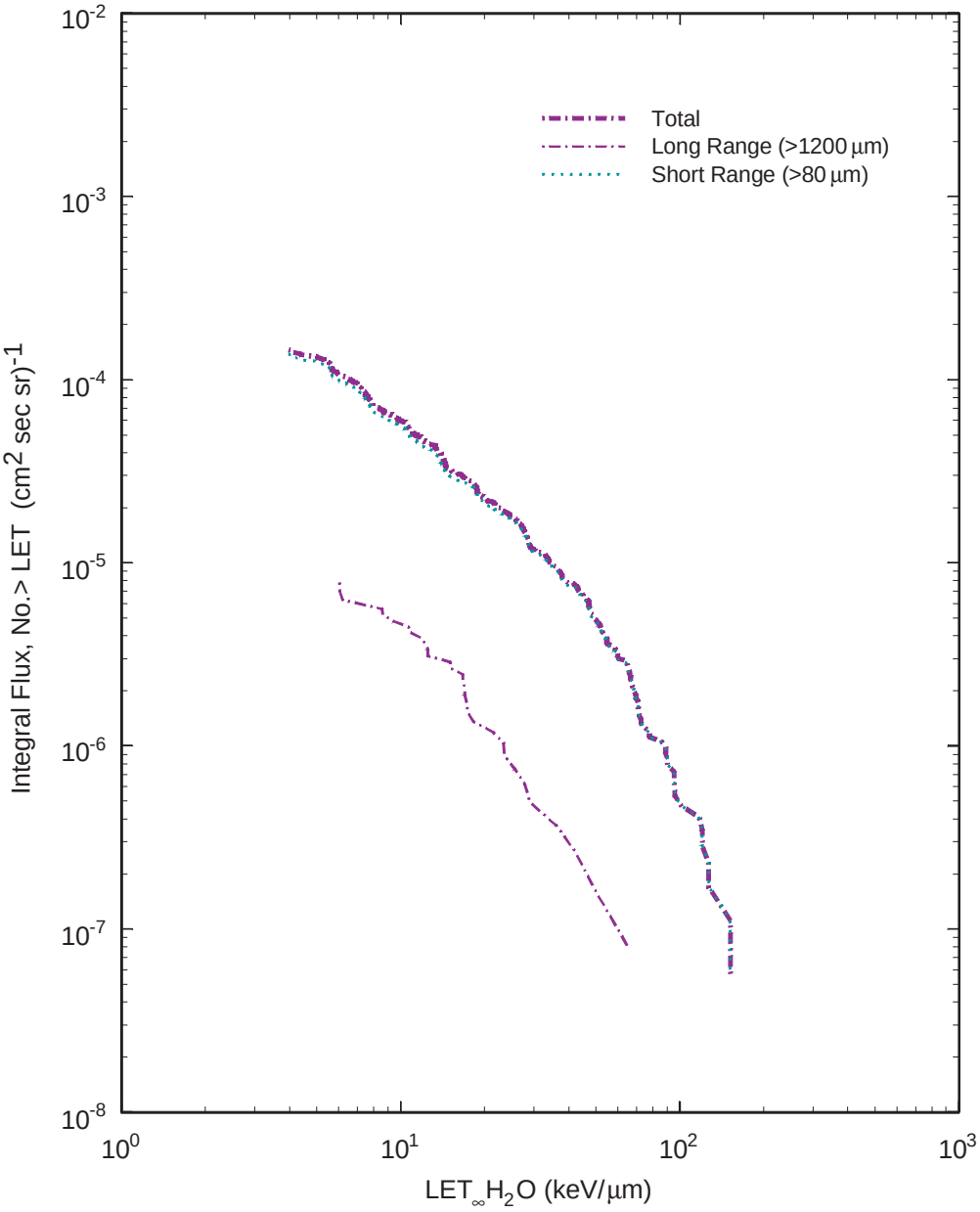

Figure 1. Integral LET flux spectra measured in CR-39 PNTDs exposed on the 1989 Arctic ER-2 flights.

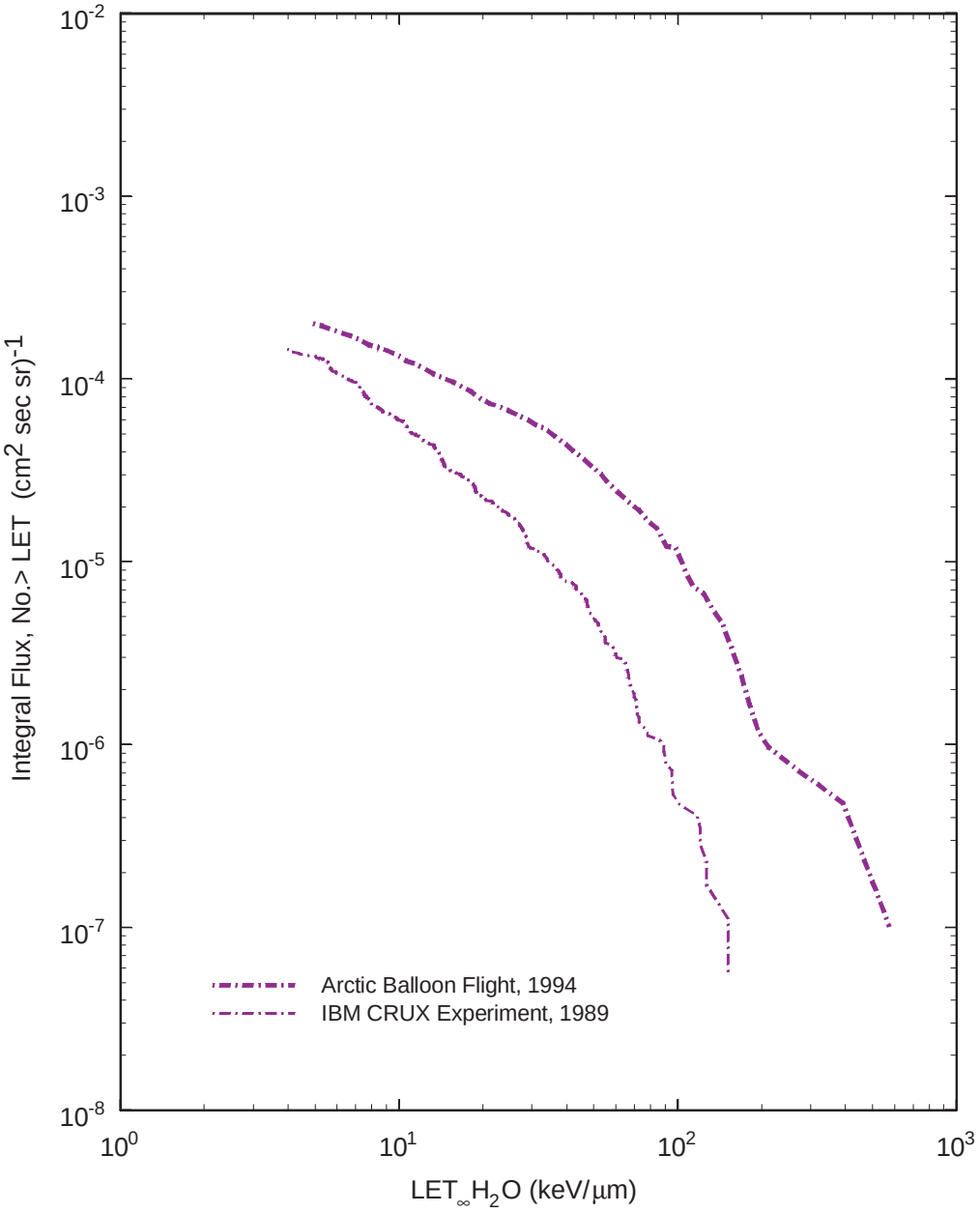

Figure 2. Integral LET Flux Spectrum measured aboard an Arctic Balloon at 117,000 ft. in 1994 and aboard a NASA ER-2 flying out of Norway at ~70,000 ft. in 1989.

Chapter 17: Capabilities of the WNR High Energy Neutron Beam at LANSCE

S. A. Wender, L. S. Walker, J. L. Ullmann,
Los Alamos National Laboratory

Capabilities of the WNR High Energy Neutron Beam at LANSCE

Preface

The Weapon Neutron Research facility (WNR) located at the Los Alamos Neutron Scattering Center (LANSCE) is the only facility in the USA with the capability of providing a Time-of-Flight (TOF) measured, un-moderated white neutron spectra from 800 MeV protons on a thin tungsten target. Current beam spot size is limited 10 cm x 10 cm however, the 30 degree right or left flight paths can be modified to provide up to a 100 cm diameter beam spot 30 meters from the target. The LANSCE accelerator also has the capability of using at energies as low as ~256 MeV with five different energies per 100 MeV up to 800 MeV. At each different energy, the WNR facility can then bombard a lithium target and produce quasi-mono energetic neutrons thus producing a very wide range of energies. The WNR facility has flight paths at various angles from the tungsten target. These flight paths range from 900 to 15'. The more forward flight paths have much harder spectra. The white spectra in these flight paths can then be modified using absorbers to harden the neutron spectra even further. Examples of how the WNR facility can be used to complete health physics measurements will be presented.

Introduction:

WNR is located at the Los Alamos Neutron Scattering Center (LANSCE) (Figure 1.), formerly called the Los Alamos Meson Physics Facility (LAMPF). WNR (Figure 2.) is a parasite target area of the LANSCE 800 MeV proton accelerator. The WNR beam is produce and accelerated as H- beam from the LANSCE injectors. It is then kicked out of line A and into line D using a master timer and a kicker magnet. Beam intensity is reduced with another kicker magnet in line D just prior to the proton storage ring and converted to p+ using a stripper foil near the entry to the blue room. Beam current to the WNR area is limited to 0.5 micro-amps in the Blue room and 3 micro-amps in target 4. (Target 4 can be operated with proton currents up to 10 micro-amps if needed but cannot be operated at the same time the blue room is in operation).

High energy neutron experiments make use of both the Blue Room (target 2) and target 4. Target 4 is a thin (7.5 cm long by 3 cm diameter) tungsten target in which the 800 MeV protons spallate to produce a white neutron spectrum. When target 4 was designed, the beam lines were arrayed from the center of the target in IS to 30 degree increments out to 90 degrees in both directions. Flight paths available for experiments include: Flight Path 1 S' Right (FP 15R), FPL30R, FPL60R, FP90R, flight path 150 left (FP15L), FP30L, and FP90L (Figure 2). The average neutron spectral energy becomes higher in the more forward directed flight paths. Poly filtration is used to harden

the neutron spectrum by filtering out the lower energy neutrons. Examples of the spallation neutron spectra and poly filtered spectra from flight paths FP60R and PF 15 L are displayed in Figure 3.

The experimental potentials of target 2 are very broad. Health Physics experiments in the blue room utilize proton interactions with very low Z targets to produce a neutron spectra in which approximately one third of the neutrons are emitted in the forward direction (p,n reaction) with energies around the maximumal beam energy, while the remainder of the spectrum is a very broad peak centered about 300 MeV below the beam energy and produced from proton delta resonance reactions in the nucleus. The spectrum from 800 MeV protons on lithium (used in a qualitative measurement completed in the fall of 1995) is displayed in figure 4. Beam time for blue room experiments is greatly limited since only one WNR experiment can be conducted at a time and target 4 cannot be used while target 2 is in use. However, the proton beam can be tuned to a wide array of energies from 250 MeV up to 800 MeV. When target 2 is used at a different energy, it takes approximately 8 hours to tune and deliver the proton beam and an additional 8 hours to re-tune the 800 MeV proton beam when the differential energy experiment is complete. In addition, proton beam tuned to a different energy is advantageous only in target 2. Thus, beam time becomes very expensive and time is limited because all the other targets must be turned off.

Experimental Setup:

The time of flight (TOF) measurements used to benchmark neutron dose and neutron spectra are completed by measuring the time it takes a pulse of protons to be converted to neutrons and travel to a flight path detector shed where they are detected in a fission chamber. Most of the neutrons generated by the proton pulse will arrive at the fission chamber prior to the arrival of the next pulse of neutrons. On the longer flight paths, the low energy neutrons generated by the pulse of protons don't arrive in the detector prior to the next pulse of neutrons, thus the pulses overlap or "wrap around." Subtracting the wrap around requires further measurements with the fission chamber.

Currently, health physics experiments at WNR are limited by a 10 cm x 10 cm square or 10 cm diameter beam spot. Therefore, the experiments with bonner spheres and other large detector systems which require full immersion in the beam are limited. Flight paths 30 degrees left and right can be altered by removing columnation to create 100 cm diameter beam spots. The monetary investment to complete this modification is not substantial (< $30,000).

The dose rate can be changed by moving the equipment closer or further from the target, by changing the micro pulse structure with a chopper or by changing the macro pulse rate (Hz). The dose rate can be measured on a per pulse basis using the time of flight data from fission chambers. A per pulse analysis allows the user to determine very closely the dose given to a dosimeter, detector, etc. Pulsed neutron fields are only measurable with passive detectors, detectors with small RC time constants or detectors with no RC time constants.

The proton beam has the following characteristics:

Macro Pulse Spacing: 40 to 120 HZ

Micro Pulse Spacing:	1.8 to 10 micro-seconds
Micro Pulse Size:	3x 108protons/pulse
Micro Pulse Width	~ 250 micro seconds
Beam Current	Up to 10 micro amps

WNR High Energy Neutron Experiments:

Personnel at Los Alamos National Laboratory started high energy neutron experiments in 1993 by measuring of the response of a Health Physics Instruments model 2080 neutron dose rate survey meter and the response of Bonner Spheres to high energy neutron beam in FP60R[1]. The following year (1994) we again used FP60R with 5 different thicknesses of poly filtration (0, 2.54, 5.08, 10.16 and 20.32 cm) to measure the response of: 1) A wide variety of neutron detectors: PN-3, Bubble, CR-39, TLD, ALOKA® and NTA[2,3,4]. 2) A set of Bonner spheres, a bismuth fission chamber and a carbon scintillator. 3) Another HPI 2080 neutron dose rate instrument. In 1995 we moved the experiments to a forward directed flight path (FP 15 L) for one experimental set and a second experiment on the zero degree flight path with a lithium target in the blue room. The 1995 experimental setup utilized a series of repeated measurements with six filtered beams (0, 2.54, 5.08, 10.16, 20.32, and 40.64 cm). Experimental results: 1) Established the limitation of Bonner sphere response to high energy neutron beams, and the precision of the measurement. 2) Proved the viability of the PN-3 badge as a high energy neutron dosimeter and measured both direct response and angular response in a neutron field[7]. 3) Finished describing energy dependence of the HPI 2080 neutron survey meter[8]. Proposed experiments in coming years will focus on the new techniques of neutron spectrum measurement and the statistical reproducibility of the PN-3 badge.

Conclusions:

WNR is the only facility in the world where high energy neutron dosimetry and spectroscopy measurements in the range between 250 and 800 MeV can be completed and the only facility where these beams are well characterized with time of flight measurements. With small modifications on flight paths 30 left or right 4 the neutron beam can be enlarged to handle any size detector currently in use. Environmental Safety and Health(ESH-1&4) and Physics division (P- 23) personnel from Los Alamos National Laboratory have completed a series of high energy neutron dosimetry and spectral measurements at WNR during the past three years. These measurements have proven the viability of the PN-3 badge and added significantly to the knowledge of high energy neutron dosimetry as well as defining the limitations and providing new ideas for the advancement of high energy neutron spectroscopy. Personnel from Los Alamos National Laboratory who are participating in these experiments would welcome collaboration from personnel at other accelerators.

References:

Since space is limited in this publication, references are avialable from the author at: L. S. Walker, Mail Stop H815, LANL, Los Alamos, NM 87545

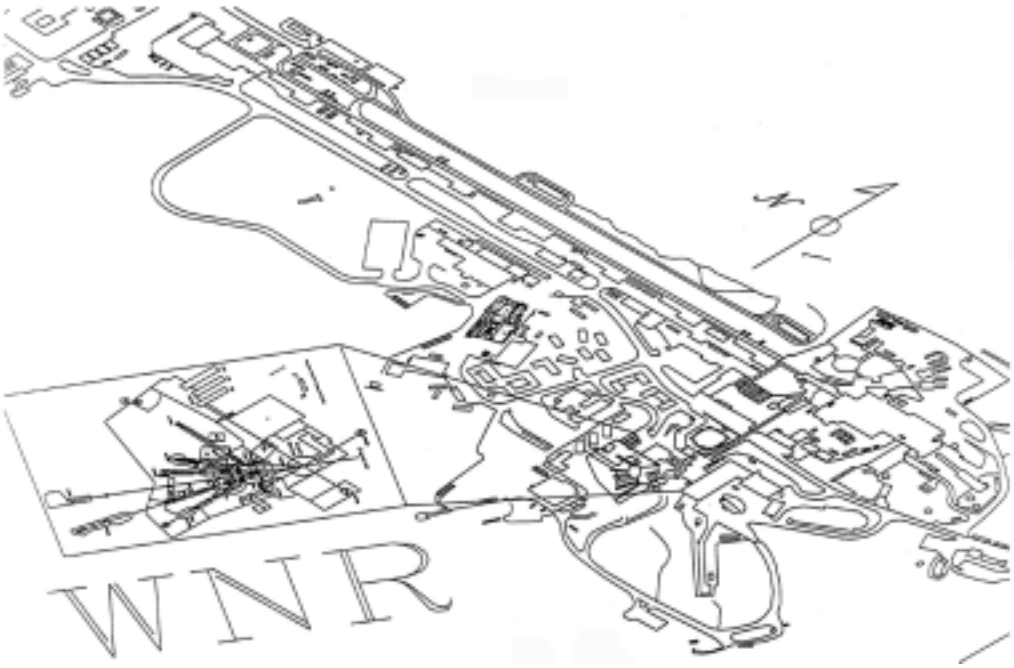

Figure 1. Map of Weapon Neutron Research facility (WNR) located at Los Alamos Meson Physics Facility (LAMPF).

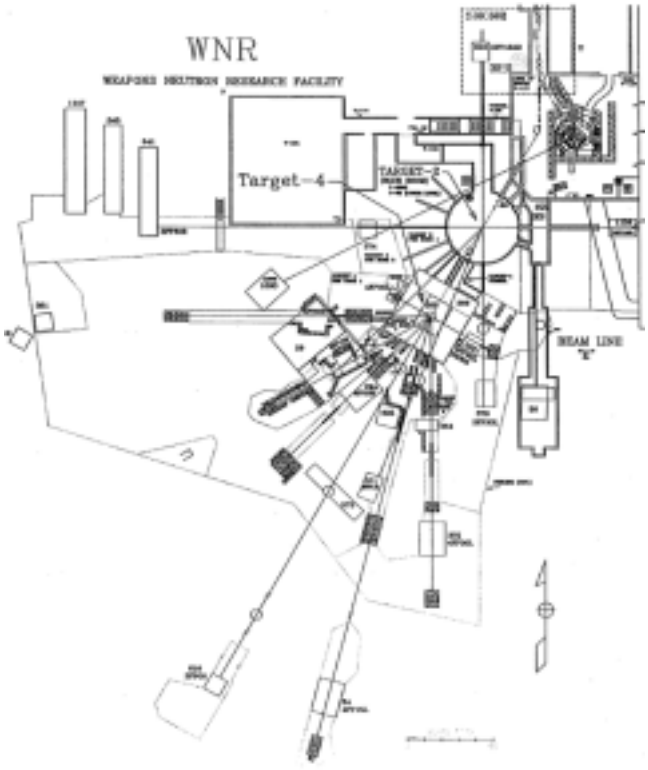

Figure 2. Enlarged detail map of WNR.

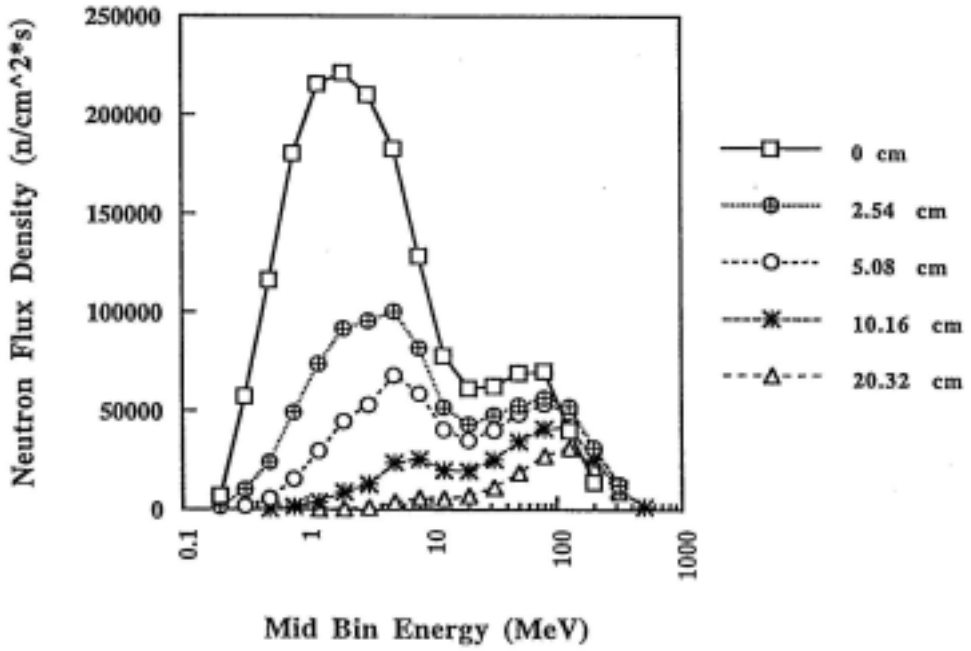

Figure 3. 1994 Time of Flight Data Neutron Flex Density vs. Energy (MeV) as a Function of Poly Filtration (cm) (WNR Flight Path 60R).

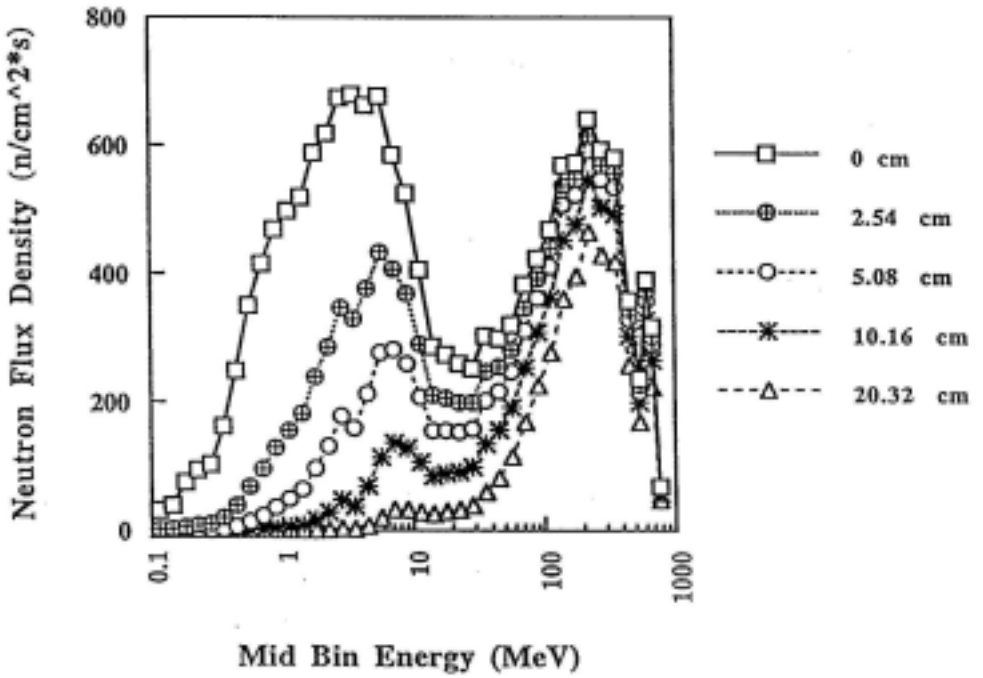

Figure 4. 1995 LAHET Calculated Neutron Flux Density vs. Energy (MeV) as a Function of Poly Filtration (cm) (WNR Flight Path 15L).

Chapter 18: Radiation-Related Risk Analysis for Atmospheric Flight Civil Aviation Flight Personnel

G. De Angelis[1,2,3] and J.W. Wilson[2]

[1]Old Dominion University, Norfolk, VA 23508, USA
[2]NASA Langley Research Center, Hampton, VA 23681, USA
[3]LEB, Istituto Superiore di Sanità, Viale Regina Elena 299, 00161 Rome (Italy)

Radiation-Related Risk Analysis for Atmospheric Flight Civil Aviation Flight Personnel

Preface

Human data on low dose rate radiation exposure and consequent effects are not readily available, and this fact generates groundtruth concerns for all risk assessment techniques for possible health effects induced by the space radiation environment, especially for long term missions like those foreseen now and in the near future. A large amount of such data may be obtained through civil aviation flight personnel cohorts, in the form of epidemiological studies on delayed health effects induced by the cosmic-ray generated atmospheric radiation environment, a high-LET low dose and low dose rate ionizing radiation with its typical neutron component, to which flight personnel are exposed all throughout their work activity. In the perspective of worldwide studies on radiation exposure of the civil aviation flight personnel, all the available results from previous studies on flight personnel radiation exposure have been examined in various ways (i.e. literature review, meta-analysis) to evaluate possible significant associations between atmospheric ionizing radiation environment and health risks, and to assess directions for future investigations. The physical characteristics of the atmospheric ionizing radiation environment make the results obtained for atmospheric flight personnel relevant for space exploration.

INTRODUCTION

For future manned space missions, with envisaged stays in Lower Earth Orbit (LEO) (Messerschmid and Bertrand, 1996) or deep space (Nealy et al., 1997; Cucinotta et al, 2001a) environment of at least several months or more (for example, the International Space Station crewmembers (SAAM, 1996)) the risk for possible health effects from low dose rate radiation exposure needs to be assessed (NCRP, 1989). Risk assessment techniques for possible health effects from low dose rate radiation exposure should combine knowledge of both radiation environment and biological response (NCRP, 1987), whose effects (e.g. carcinogenesis) are generally evaluated through mathematical models and/or animal and cell experiments (BEIR V, 1990). Data on human exposure to low dose rate ionizing radiation and its effects are not so readily available, especially with regards to stochastic effects (Jablon, 1984), related to carcinogenesis and therefore to cancer risks, for which the event probability increases with increasing radiation exposure (Kiefer, 1989). In distinction, for deterministic effects the level of injury severity increases with increasing radiation exposure (Kiefer, 1993). The largest source of such low dose rate data might be flight personnel (Foelsche et al., 1974), if considered as enrolled in epidemiological cohorts for studies on health effects induced by the cosmic-ray generated atmospheric ionizing radiation. The crew total dose, increasing over the years, might cause delayed radiation-induced health effects, with the high-LET and highly ionizing neutron component typical of atmospheric radiation (Wilson et al. Chapter 2) contributing so much to the effective dose equivalent (Sinclair, 1985) and being more similar in effects to space radiation than the normal terrestrial low-LET radiation (Singleterry

and Thibeault, 2000), which generally radiobiological studies are based on (Kiefer, 1989). In this way the human response database for low dose rate radiation exposure might be significantly augmented (BEIR V, 1990), with benefic effects on space radiation-related risk assessment techniques, both for LEO scenarios (Wu et al., 1996) and for interplanetary mission cruise phases (e.g., Letaw et al., 1989; Obe et al., 1999; Turner and Badhwar, 1999). Moreover, consideration of significant Solar Particle Events (SPEs), although infrequent (Shea and Smart, 1990), is of paramount importance for risk assessment techniques both for atmospheric flight (Wilson, 1981; O'Brien et al., 1994) and space flight (Petrov et al., 1994; Badhwar, 1997; Tripathi et al., 2001). Such events are to be studied in terms of received doses, generally massive, and possible delayed effects observed on crewmembers (Wilson et al., 1991). Another aspect for the significance of atmospheric flight results for space flight scenarios is the fact that the high altitude aircraft radiation environment is expected to be similar to the radiation environment found at the surface of Mars (Wilson et al., 1999), in spite of the constituent and pressure difference between the two atmospheres, air and 1013 mbar for the Earth, and mainly CO_2 and about 6 mbar for Mars (Zurek, 1992), being of little relevance on this respect (Singleterry and Thibeault, 2000), the neutron component at the surface of Mars being generated mainly due to a surface-generated backward flux (Wilson et al., 1999). Therefore any information gathered about terrestrial atmospheric aircraft flight may be applied to studies for manned Mars targeted missions, particularly with regards to landings on Mars, in the planet exploration phase (Weaver et al., 1993), and for planning habitats suitable to the Martian environment and which therefore can safely host a crew, as shelters, or a permanent base (Hoffman and Kaplan, 1997), or settlements for planet colonization (Zubrin, 1997).

In this study all the available results from previous epidemiological studies on flight personnel exposures have been considered in different ways to evaluate the association between atmospheric flight environment and health risks, with a particular regard to cancer induction, and to assess features and needs of future investigations. The physical characteristics of the atmospheric ionizing radiation environment have been described elsewhere (Wilson et al. Chapter 2), as well as the techniques for the evaluation of the exposure (Wilson et al., 2000), so they will be not further discussed in this paper.

ANALYSIS TECHNIQUES

A) LITERATURE REVIEW

The discussion on aircraft flight personnel radiation-related health issues has started already long ago (Winter, 1968). In 1990, aircraft flight personnel have been given the status of "occupationally exposed to radiation" by the International Commission for Radiation Protection (ICRP, 1991), with a received radiation dose that is at least twice larger than that of the general population (Wilson et al., 1994). Starting from this, in several countries epidemiological studies on the health status of civilian airlines crewmembers were promoted (see, e.g. Band et al., 1990; Kaji et al., 1993; Pukkala et al., 1995). These pioneering studies were limited in scope and cohort size, so no conclusive answers on disease risk were found, as better shown below. Moreover, in all these studies no information whatsoever on radiation occupational exposure (e.g. radiation dose, flight hours, route haul, etc.) were used in the analysis, so no correlation was possible between atmospheric ionizing radiation and (possibly radiation-induced) observed health effects, nor has it been possible to discriminate between radiation-induced effects and those of

potential occupational confounding risk factors, as exposure to jet fuels and volatiles (Seldén and Ahlborg, 1995), to disinfection and disinfestations products (Wartemberg et al., 1998 and 1999), to ozone (Reed et al., 1980), to cabin air pollutants (NRC, 1986), including passive smoking in the past (Ryan, 1991), to electromagnetic fields (Kaune, 1993), circadian rhythms disruption (Suvanto et al., 1990), and other factors related to lifestyle (Haugli et al., 1994) and leisure activities (Vågerö et al., 1990). Conversely no account could have been taken of possible synergies among concomitant exposures to different agents (Wu et al., 1996), in terms of risk increase because of the possible interaction mechanisms between radiation and the involved exposure agent, if the latter shows radiomimetic properties (USEPA, 1986). Spacecraft show the same kind of situation (Wu et al., 1996; James, 1997), with the crew member exposed simultaneously to radiation and to many other possible contamination sources (NRC, 1992), even if for spacecraft the infrequent occurrence and the low concentration of the airborne contaminants suggest minimal risk (NRC, 2000), with the simultaneous effects of these low concentration agents and radiation expected to be less than additive due to the concomitant repair of macromolecular lesions at different target sites (James, 1997).

So all the available information on aircraft flight personnel may be only evaluated on the basis that the exposure to the "flight environment" (i.e. exposure to atmospheric cosmic radiation and other physical or chemical agents not evaluated in more precise terms than the implicit fact of being aircraft flight personnel members who are exposed to the atmospheric ionizing radiation environment and to the civilian airline crew members occupational and leisure lifestyle) may pose health risk for flight personnel members.

Thorough literature reviews on epidemiological studies among pilots and cabin attendants have been published, mostly related to cancer risk (Krauss, 1985; Blettner et al., 1998; Blettner and Zeeb, 1999; Ballard et al., 2000; Boice et al., 2000; De Angelis et al., 2001a). In these reviews are considered studies aiming at obtaining results of incidence and mortality in the form of relative risk (RR), i.e. the ratio of the risk of the exposed population of interest and the risk of a reference population taken as the unexposed one (see, e.g. Kleinbaum et al., 1982), with its confidence limits. As a study design, the cohort study approach is generally selected, i.e. the selection and follow-up of an exposed population to obtain data of incidence and mortality. Case-control studies have played until now a minor role in investigations on aircraft flight personnel (Blettner et al., 1998), apart from nested case-control studies among the US Air Force crew members on brain and nervous system cancer (Grayson, 1996; Grayson and Lyons, 1996), mostly related to electromagnetic field exposure. Hoiberg and Blood (1983) compared hospitalization rates for male US Navy pilots and other flying crewmembers with non-flying officers, with flying officers having higher rates for both total hospital admissions and most of the major diagnostic categories. As for cancer endpoints, hospitalization rates for the Hodgkin disease and testis cancer were higher for the flying crewmembers, but numbers and rates were not reported in the paper. Depending on the study design, and dealing with mortality, the relative risk can be approximated through the odds ratios (see, e.g. Rothmans, 1986), namely the Standardized Mortality Ratio (SMR), when it is possible to calculate the ratio between the observed number of deaths in the cohort and the expected number of deaths in the cohort, the latter obtained through mortality data available for the reference population, or the Proportional Mortality Ratio (PMR), when only the relative frequencies of death in the exposed and the unexposed population are known and can be compared, but no personal information is available. In the case

of incidence results, the mortality data are just replaced by the incidence data to obtain the Standardized Incidence Ratio (SIR).

From these comprehensive reviews no clear picture with regards to disease patterns emerges, with individual studies being unrelated to exposures from the flight environment, lacking statistical power to indicate clear trends due to the small number of people enrolled in the considered cohorts, with the consequence of having cancer site-specific incidence increased in some studies and not increased in other ones due just to random effects due to the too small a sample size. The problem is complicated by the fact that for the flight personnel as a group the health risks of this selected group of individuals are low ("healthy worker effect", for the specific case of aircrew members see De Angelis et al., 2001a). The authors of a recent work on mortality for USA pilots and flight engineers (Nicholas et al., 1998), besides showing with their PMR analysis a significantly increased mortality for kidney and renal pelvis cancer, motor neuron disease, and various external causes, along with not statistically significant indications for mortality rate increase for various other causes, put into evidence the impossibility to obtain meaningful results on radiation without considering in detail both environment and work history. In their paper it is clearly stated: "…to determine if these health outcomes are related to occupational exposures, it will be necessary to quantify each exposure separately, to study the potential synergy of effects, and to couple this information with disease data on an individual basis".

In more recent studies, not yet included in most reviews, use has been made of some information related to exposure of the individual crewmember, although in most cases obtained in rudimentary ways. Irvine and Davies (1999) used a 'long/short haul' route characterization, Gundestrup and Storm (1999) used overall flight hours and a 'jet/non-jet' aircraft type characterization, Haldorsen et al. (2000, 2001) and Hammar et al. (2002) overall flight hours and specific aircraft type characterization, and Rafnsson et al. (2000) '>5h/<5h flight length' route characterization, overall flight hours and full aircraft type characterization. In the papers by Haldorsen et al. (2000, 2001) and Rafnsson et al. (2000, 2001) a tentative evaluation of the individual cumulative dose equivalent has been performed with the statistical approach proposed in Tveten (1997), but unfortunately the obtained values for radiation doses and exposures cannot be used for radiation-related investigations, because in Haldorsen et al. (2000, 2001) for dose evaluation the authors used the FAA CARI-3N software package (Friedberg et al., 1992), a version which does not include in the calculations and therefore in the dose results most of the atmospheric neutron component, i.e. about or more than 50% of the observed dose equivalent (O'Brien et al., 1994) depending on time and the considered flight path, whereas in Rafnsson et al. (2000, 2001) the dose is obtained by multiplying individual block-hours with mean hourly dose values averaged on flights of an airline company different from that whose aircrew members have been considered in the analysis.

From the health effects point of view, Rafnsson et al. (2000, 2001) have to cope with extremely small aircrew and reference populations like those of Iceland, and therefore they report only a significant incidence increase for malignant melanoma for both cockpit and cabin personnel, but on the basis of only few cases detected, in Haldorsen et al. (2000, 2001) significant excess risks is reported for only few cancer sites, which the authors interpret as due to leisure lifestyle, and incidence rates for other cancer sites very close to those of the Norwegian general population

they used as a reference. Irvine and Davies (1999) and Hammar et al. (2002) report only excess risk for melanoma skin cancer, and in Gundestrup and Storm (1999) the authors report significant excess risk for malignant melanoma and non-melanoma skin cancer, which they also attribute to leisure activities rather than occupational exposure, and increased risks for acute myeloid leukemia and total cancer incidence for crew members with more than 5000 hours of flight time. Even if these excess risks are to be considered as very slight due to the so large confidence intervals shown by these results (both very close to RR=1 on the confidence interval left side), this phenomenon due to the small numbers for incident cases for each different cause due to the rather small sample enrolled in their Danish flight personnel cohort. In a previous study on Danish cabin attendants, Lynge (1996) found a non-significant excess risk for breast cancer, 1.6 (0.9-2.7).

As for more recent US studies, Wartenberg and Stapleton (1998, 1999) reported a very slightly significant excess risk for breast cancer among female cabin attendant, and suggested it was due to the use of disinfestations products and pesticides as dicophane (DDT) used to get rid of insects onboard planes. The frequency and magnitude of exposures to pesticides for aircrew members are unknown, but probably limited (Pukkala et al., 1995), used only on international flights to very few destinations, so this exposure was certainly rare and is unlikely to have contributed to the observed incidence. Nicholas et al. (2001) performed a study on self-reported diseases from a health and lifestyle survey on active and retired commercial airline pilots. A questionnaire was mailed to 10678 pilots, of which only 6609 answered, the overwhelming majority (99.1%) being men. For cancer endpoints the main outcome was a self-reported age-adjusted incidence rate, whereas for non-cancer endpoints the main outcome was a self-reported prevalence rate. Increased morbidity with respect to the general population was found only for melanoma skin cancer, motor neuron disease, already found in Nicholas et al. (1998) with a PMR analysis, and ocular cataracts. Recently, a positive association between cataracts and space radiation exposure, both as increased incidence and earlier onset with respect to the general population, has been reported for US astronauts by Cucinotta et al. (2001b). Reynolds et al. (2002) performed a study based on the California cancer registry and including both male and female cabin crewmembers. They report an excess risk among female cohort members for breast cancer and skin melanoma, and, like in Haldorsen et al. (2001), an excess risk among male flight attendants for Kaposi's sarcoma skin cancer, in both papers considered as related to lifestyle only. In the paper by Haldorsen et al. (2001) the same can be said about the reported excess risks for esophagus and liver cancers.

In the Italian national study (De Angelis et al., 2001; Ballard et al., 2002) a retrospective cohort mortality study, still unrelated to radiation exposure evaluation, was conducted among Italian commercial airline cockpit crewmembers and cabin attendants with work history within the 1965-1996 years. The cohort was composed of 3,022 male cockpit crewmembers, and 3,418 male and 3,428 female cabin attendants. Cause-specific standardized mortality ratios (SMR) and 95% confidence intervals (CI) were calculated as estimates of the relative risk. No exposure variables other than length of employment was used in this mortality study. Causes of death were grouped into three mutually exclusive categories – (1) malignant neoplasms (ICD9 codes 140-209), (2) non-cancer and non-injury causes including infectious diseases, benign tumors, chronic diseases, and unknown causes (ICD9 codes 001-139, 210-799), and (3) external causes (ICD9 codes E800-E999). Cancer mortality was reduced for both male cockpit crew and cabin attendants (SMR 0.58 and 0.67 respectively) with respect to the Italian general population,

but only slightly less than expected for female cabin attendants (SMR 0.90). These are the first reported results about mortality for cabin attendants. No significant excess risk has been found for mortality for any cancer site. There was no increasing trend of the SMR for all-sites cancer or for breast cancer by duration of employment at any exposure lag. The SMR for leukemia was somewhat elevated (SMR 1.72; CI: 0.74-3.40) among male flight personnel based on 8 deaths, with a positive but non-significant trend by length of employment. No excess mortality was noted for non-cancer and non-injury causes, and, with the exception of acute myocardial infarction, SMRs for most other causes were well below one. Mortality from aircraft crashes was highly elevated (SMR 102.7; CI: 60.8-162), which is not surprising given the rarity of this cause of death in the general population. Additionally, an excess of death by suicide was seen among female cabin attendants (SMR 3.38; CI: 1.24-7.35). Other studies on the cohort of the Italian flight personnel are underway, including a detailed assessment of cosmic radiation exposure, a prospective study on disease incidence, an investigation of occupational risk factors for non-tumor outcomes, including psychological distress and circadian rhythms disruption, and an investigation on reproductive disorders and outcomes of female cabin attendants, similar in both philosophy and practice to that by NIOSH/FAA discussed below (Grajewski et al. 1994, 2002; Whelan 2002).

All cancer sites with significant positive association for civilian airline flight personnel crewmembers found in published studies are reported in Table 1 as from each study with its confidence limits (90 or 95 percent, depending on study).

B) FLIGHT PERSONNEL MORTALITY AND CANCER INCIDENCE META-ANALYSIS

As mentioned above, increased cancer risk among flight personnel have been noted in individual studies, but without the statistical power to identify increased risks with any statistical significance. In order to increase the precision of the estimated association between occupation as flight personnel crew member and observed morbidity patterns, different aircrew member cohorts have been selected for a meta-analysis process, in the way proposed in Blair et al. (1995). The studies to be considered were mortality and incidence cohort studies, divided into studies targeted to male pilots and female flight attendants. No proportional mortality studies were included in the analysis, and the same for military pilots studies. The results of the individual selected studies were combined by study outcome (mortality or incidence) for cause of death and/or cancer incidence sites with an excess risk in at least one of the individual studies and for which there were at least five cases in total among eligible studies. Calculations for combined relative risks for selected causes have been performed with a fixed effect model with inverse variance weighting of the log risk ratios (Greenland, 1987), with an evaluation of potential selection biases and heterogeneity among the combined groups, and with estimate and adjustment for possible sources of confounding, e.g. by socioeconomic status (SES). For male pilots, results from two to four individual studies per subcategory have been included to estimate the combined risks for nine cause of death or cancer incident sites, resulting in increased adjusted relative risks for mortality from melanoma and brain cancer and for incidence from prostate and brain cancer. For female cabin attendants, results from two individual studies were combined for incidence of all cancers, of melanoma and breast cancer, and excess risks were found for all sites. The results showing only excess risks are shown in Table 2. However even in the meta-analysis process for both male and female crew members the obtained

RRs show quite large confidence intervals, very close to RR=1 and even well below this on the confidence interval left side, so the results must be interpreted with caution. This work has been published in Ballard et al. (2000).

DISCUSSION

From all the above studies, a need comes out of further investigations to be performed over much larger cohorts, to reduce all uncertainties, and with a much better description of the flight environment to which aircrew members are exposed, in terms of a dose reconstruction as accurate as possible. The latter implies an in-depth knowledge of the atmospheric ionizing radiation environment and of its variation with location, altitude and time, a knowledge as detailed as possible for each individual crew member of his flight history, possibly in terms of the details for each work day of the individual flights on which each considered crew member was onboard, and a knowledge as detailed as possible on the flight paths of each individual flight in terms of timing, geographic coordinates, and altitudes, to calculate the dose along the profiles. The use of proxies for exposure evaluation like the use of the overall work hours (i.e. length of employment) instead of radiation doses gives only partly satisfactory results (Hammer et al., 2000).

As for health risk issues, also in individual small size studies excess disease risks have been found, but it has never been possible to confirm these results due to the lack of power of these studies (De Angelis et al., 2001b). Much larger enrolled cohorts such as those composed of the whole flight personnel of a civilian airline are needed to provide more conclusive answers and results, with consideration in detail of the flight environment, in terms of atmospheric ionizing radiation environment, crew employment history, and aircraft route profiles, to reconstruct individual doses. This can provide more solid clues on disease morbidity patterns by exposure to atmospheric ionizing radiation and on risk analysis. A need for a multi-part or an international study in order to obtain a much larger cohort size with the radiation exposure patterns considered in detail came out long ago (see e.g. Friedberg et al., 1991). Two collaborative multi-national efforts are underway, one, called ESCAPE (European Study on Cancer risk among Airline Pilots and cabin crEw), with the participation of nine European countries (namely Denmark, Finland, Germany, Greece, Iceland, Italy, Norway, Sweden and United Kingdom), as composed of individual national-level projects, then pooled together in a joint analysis following a jointly agreed protocol (as sketched in Blettner et al., 1998), with about 30 000 pilots and 45 000 cabin crews as cohort members, with the mortality from cancer as goal. The other study, the Nordic one, called NO-ESCAPE (Northern European Study on Cancer risk among Airline Pilots and cabin crEw), is composed of cohorts from five northern European countries (namely Denmark, Finland, Iceland, Norway and Sweden), with smaller numbers of cases, and incidence of cancer as the end point (all Nordic countries have national cancer registries with full national coverage). These studies are expected to provide results with reduced incertitude on the issue. Most of the national-level studies are presently completed or close to completion, at least in their basic contents. The joint data analysis phase for the two above mentioned studies is close to completion. As for US research project, the only large effort currently underway is the NIOSH/FAA Study of Reproductive Disorders in Female Flight Attendants. This study, in which female primary school teachers of the same age distribution as the female cabin attendant are used as a control group, is performed in three parts: a questionnaire to be filled by each cabin attendant on reproductive outcomes, the study of the

ovulation function by using hormone testing, and an environmental assessment of the cabin space (Whelan 2002). In the framework of the same study, Grajewski et al. (2002) developed an algorithm to evaluate whether effects of cumulative doses could be distinguished analytically from effects of circadian rhythm disruption for crewmembers as cabin attendants, for which generally only limited flight history details are available. An evaluation in terms of radiation doses of the exposure for pregnant female cabin attendant has been performed by Nicholas et al. (2000a), with the technique presented in Nicholas et al. (2000b), in which the mother's body has been modeled with a soft-tissue slab phantom at various thicknesses (from 0 to 30 cm): the results was that in this model the body of the mother provides no significant shielding to the embryo from atmospheric ionizing radiation

The obtained data sets would provide potentialities for interesting side studies, like an assessment on effects of prenatal exposure, to obtain clues about possible embryonic damages and/or lethality (and/or possible association with childhood disease) and radiation exposure deterministic effects during organogenesis, especially due to high-LET radiation (see e.g. BEIR V, 1990), onset of radiation-related ocular cataract (Grahn, 1973; Cucinotta et al., 2001b), and an association to cellular studies to associate observed cell damages or chromosomal aberrations to a quantitative and qualitative evaluation of radiation exposure, to assess on possible evaluation of radiation doses on an individual level on the basis of lymphocyte chromosomal analysis (for recent reviews and discussions on these topics see e.g. Edwards, 1997, Wolf et al.., 1999), in particular on possible radiation myelopoiesis and lymphopoiesis alterations (see, e.g. Jones et al., 1991). Recently Gundestrup et al. (2000), basing their analysis on 7 cases only, reported aircrew members who had myelodysplasia or acute myeloid leukemia showing the same cytogenetic abnormalities as non-aircrew-members patients of the same disease treated with radiotherapy alone, suggesting that these abnormalities could be indicators of previous radiation exposure.

ACKNOWLEDGEMENTS

The authors are grateful to Prof. V. Rafnsson for his invaluable help and support.

This work is dedicated to the memory of Maria Teresa Nicoletti.

REFERENCES

Badhwar, G. D. (1997). The Radiation Environment in Low Earth Orbit. *Radiat. Res.,* **148 (Suppl.)**, S3-S10.

Ballard, T.J., S. Lagorio, G. De Angelis, and A. Verdecchia (2000). Cancer Incidence and Mortality among Flight Personnel: A Meta-Analysis. *Aviat. Space Environ. Med.,* **71**, 216-224.

Ballard, T.J., S. Lagorio, M. De Santis, G. De Angelis, M. Santaquilani, M. Caldora, and A. Verdecchia (2002). A Retrospective Cohort Mortality Study of Italian Commercial Airline Cockpit Crew and Cabin Attendants 1965-96. *Int. J. Occup. Environ. Health* **8**, 87-96.

Band, P.R., J.J. Spinelli, V.T.Y. Ng, J. Moody, and R.P. Gallagher (1990). Mortality and Cancer Incidence in a Cohort of Commercial Airline Pilots. *Aviat. Space & Environ. Med*., **61**, 299-302.

Band, P.R., N.D. Le, R. Fang, M. Deschamps, A.J. Coldman, R.P. Gallagher, and J. Moody (1996). Cohort Study of Air Canada Pilots: Mortality, Cancer Incidence, and Leukemia Risk. *Am. J. Epidemiol.,* **143**, 137-143.

BEIR V (5th Committee on the Biological Effects of Ionizing Radiations) (1990). *Health Effects of Exposure to Low Levels of Ionizing Radiation.* National Academy Press, Washington DC.

Blair, A., J. Burg, J. Foran, et al. (1995). Guidelines for Application of Meta-Analysis in Environmental Epidemiology. *Reg. Toxicol. Pharmacol.*, **22**, 189-197.

Blettner, M., and H. Zeeb (1999). Epidemiological Studies among Pilots and Cabin Crew. *Radiat. Prot. Dos.,* **86,** 269-273.

Blettner, M., B. Grosche, and H. Zeeb (1998). Occupational Cancer Risk in Pilots and Flight Attendants: Current Epidemiologic Knowledge. *Radiat. Environ. Biophys.,* **37,** 75-80.

Boice, J.D., Jr., M. Blettner , and A. Auvinen (2000). Epidemiologic Studies of Pilots and Aircrew. *Health Phys*., **79**, 576-584.

Cucinotta, F.A., W. Schimmerling, J.W., Wilson, L.E. Peterson, G.D. Badhwar, P. Saganti, and J.F. Dicello (2001a). Space Radiation Cancer Risks and Uncertainties for Mars Missions. *Radiat. Res*., **156**, 682-688.

Cucinotta, F.A., F.K. Manuel, J. Jones, G. Iszard, J. Murrey, B. Djojonegro, and M. Wear (2001b). Space Radiation and Cataracts in Astronauts. *Radiat. Res*., **156**, 460-466.

De Angelis, G., M. Caldora, M. Santaquilani, R. Scipione, and A. Verdecchia (2001a). Health Risks from Radiation Exposure for Civilian Aviation Flight Personnel: a Study of Italian Airline Crew Members. *Radiat. Res.,* **156**, 689-694.

De Angelis, G., M. Caldora, M. Santaquilani, R. Scipione, and A. Verdecchia (2001b). Radiation-Induced Biological Effects on Crew Members: A Combined Analysis on Atmospheric Flight Personnel. *Phys. Med.,* **17**, **Suppl. 1**, 175-176.

Edwards, A. A. (1997). The Use of Chromosome Aberrations in Human Lymphocytes for Biological Dosimetry. *Radiat. Res.,* **148 (Suppl.)**, S39-S44.

Foelsche, T., R.B. Mendell, and J.W. Wilson (1974). *Measured and Calculated Neutron Spectra and Dose Equivalent Rates at High Altitudes: Relevance to SST Operations and Space Research.* NASA Technical Note TN D-7715.

Friedberg, W., D.N. Faulkner, L. Snyder, et al. (1991). The Cosmic Radiation Environment at Air Carrier Altitudes and Possible Associated Health Risks. In *Proceedings of the Workshop 'Radiation Exposure of Civil Aircrew' (Reitz, G., K. Schnuer, and K. Shaw, Eds.)*, **EUR 14964**, Luxembourg.

Friedberg, W., D.N. Faulkner, L. Snyder, E.B. Darden, and K. O'Brien (1992). *Radiation Exposure of Air Carrier Crewmembers.* Federal Aviation Administration, Office of Aviation Medicine, Report No. DOT/FAA/AM-92/2.

Grahn, D. (Ed.) (1973). *HZE Particle Effects in Manned Sopace Flight*. National Academy of Sciences, Washington, DC.

Grajewski, B., E.A. Whelan, M.A. Waters, J.S. Kesner, and T.M. Schnorr (1994). Overview of the Proposed NIOSH-FAA Study of Reproductive Disorders in Female Flight Attendants. Paper presented at the *42nd Annual Meeting of the Radiation Research Society*, Nashville, TN.

Grajewski, B., M.A. Waters, E.A. Whelan, and T.F. Bloom (2002). Radiation Dose Estimation for Epidemiologic Studies of Flight Attendants. *Am. J. Industr. Med.* **41**, 27-37.

Grayson, J.K. (1996). Radiation Exposure, Socioeconomic Status, and Brain Tumor Risk in the US Air Force: a Nested Case-Control Study. *Am. J. Epidemiol.*, **143**, 480-486.

Grayson, J.K., and T.J. Lyons (1996). Brain Cancer, Flying, and Socioeconomic Status: a Nested Case-Control Study of USAF Aircrew. *Aviat. Space Environ. Med.,* **67**, 1152-1154.

Greenland, S. (1987). Quantitative Methods in the Review of Epidemiologic Literature. *Epidemiol. Rev.*, **9**, 1-30.

Gundestrup, M., and H.H. Storm (1999). Radiation-Induced Acute Myeloid Leukaemia and Other Cancers in Commercial Jet Cockpit Crew: A Population-Based Cohort Studies. *Lancet,* **354**, 2029-2031.

Gundestrup, M, M. Klarskov Andersen, E. Sveinbjornsdottir, V. Rafnsson, H.H. Storm, and J. Pedersen-Bjergaard (2000). Cytogenetics of Myelodysplasia and Acute Myeloid Leukaemia in Aircrew and People Treated with Radiotherapy. *Lancet*, **356**, 2158 (letter).

Haldorsen, T., J.B. Reitan, and U. Tveten (2000). Cancer Incidence among Norwegian Airline Pilots, *Scand. J. Work Envir. Health*. **26,** 106-111.

Haldorsen, T., J. Reitan, and U. Tveten (2001). Cancer Incidence among Norwegian Airline Cabin Attendants. *Int. J.Epidemiol.* **30**,825-830.

Hammar, N., A. Linnersjö, L. Alfredsson, B.-G. Dammstrom, M. Johansson, and H. Eliasch (2002). Cancer Incidence in Airline and Military Pilots in Sweden 1961-1996. *Aviat. Space Environ. Med.,* **73**, 2-7.

Hammer G.P., H. Zeeb, U. Tveten, and M. Blettner (2000). Comparing Different Methods of Estimating Cosmic Radiation Exposure of Airline Personnel. *Radiat. Environ. Biophys.*, **39**, 227-231.

Haugli, L., A. Skogstadt, and O.H. Hellesoy (1994). Health, Sleep and Mood Perceptions Reported by Airline Crews Flying Short and Long Hauls. *Aviat. Space Environ. Med.,* **65,** 27-34.

Hoffman, S.J., and D.L. Kaplan (Eds.) (1997). *Human Exploration of Mars: The Reference Mission of the NASA Mars Exploration Study Team*. NASA SP-6107.

Hoiberg, A., and C. Blood (1983). Age-Specific Morbidity among Navy Pilots. *Aviat. Space Environ. Med.* **54**, 912-918.

ICRP (International Commission on Radiological Protection) (1991). *1990 Recommendations of the International Commission of Radiological Protection*. ICRP Publication **60**, Pergamon Press, Oxford, United Kingdom.

Irvine, D., and D.M. Davies (1999). British Airways Flightdeck Mortality Study. *Aviat. Space Environ. Med.,* **70**, 548-555.

Jablon, S. (1984). Epidemiologic Perspectives in Radiation Carcinogenesis. In *Radiation Carcinogenesis: Epidemiology and Biological Significance (Boice, J.D., and J.F. Fraumeni Jr, Eds.)*, Raven Press, New York, NY.

James, J.T. (1997). Carcinogens in Spacecraft Air. *Radiat. Res.,* **148 (Suppl.)**, S11-S16.

Jones, T.D., M.D. Morris, and R.W. Young (1991). A Mathematical Model for Radiation-Induced Myelopoiesis. *Radiat. Res.*, **128**, 258-266.

Kaji, M., T. Tango, I. Asukata, et al. (1993). Mortality Experience of Cockpit Crewmembers from Japan Airlines. *Aviat. Space Environ. Med.,* **64**, 748-750.

Kaune, W.T. (1993). Introduction to Power-Frequency Electric and Magnetic Fields. *Environmental Health Perspective Supplements,* **101 (Suppl. 4)**, 73-81.

Kiefer, J. (1989). *Biological Radiation Effects*. Springer-Verlag, Berlin, Germany.

Kiefer, J. (1993). On the Biological Significance of Radiation Exposure in Air Transport. *Radiat. Prot. Dos.*, **48**, 107-110.

Kleinbaum, D., L. Kupper, and H. Morgerstern (1982). *Epidemiological Research*. Lifetime Learning Publications, Belmont, CA.

Kraus, J.F. (1985). Epidemiological Studies on Health Effects in Commercial Pilots and Flight Attendants: A Review. *Sangyo Ika Dagaiku Zasshi*, **7 (Suppl.)**, 32-44.

Letaw, J.R., R. Silberberg, and C.H. Tsao (1989). Radiation Hazards on Space Missions Outside the Magnetosphere. *Adv. Space Res.*, **9**, 285-291.

Lynge, E. (1996). Risk of Breast Cancer is Also Increased among Danish Female Airline Cabin Attendants. *Br. Med. J.,* **312**, 253.

Messerschmid, E., and R. Bertrand (1999). *Space Stations Systems and Utilization*. Springer-Verlag, Berlin, Germany.

NCRP (National Council on Radiation Protection and Measurements) (1987). *Recommendations on Limits for Exposure to Ionizing Radiation.* NCRP Report No. 91, Bethesda, MD.

NCRP (National Council on Radiation Protection and Measurements) (1987). *Guidance on Radiation Received in Space Activities.* NCRP Report No. 98, Bethesda, MD.

Nealy, J.E., L.C. Simonsen, and G.D. Qualls (1997). SEI Analysis of Deep Space Vehicle Shielding. In *Shielding Strategies for Human Space Exploration (Wilson, J.W., J. Miller, A. Konradi, and F.A. Cucinotta, Eds.)*, NASA CP-3360.

Nicholas, J.S., D.T. Lackland, M. Dosemeci, L.C. Mohr, Jr., J.B. Dunbar, B. Grosche, and D.G. Hoel (1998). Mortality among US Commercial Pilots and Navigators. *J. Occup. Environ. Med.*, **40**, 980-985.

Nicholas, J.S., K. Copeland, F.E. Duke, W. Friedberg, and K. O'Brien (2000a). *Galactic Cosmic Radiation Exposure of Pregnant Flight Crewmembers*. *Aviat. Space Environ. Med.,* **71**, 647-648.

Nicholas, J.S., K. Copeland, F.E. Duke, W. Friedberg, and K. O'Brien (2000b). *Galactic Cosmic Radiation Exposure of Pregnant Aicrew Members.* Federal Aviation Administration, Office of Aviation Medicine, Report No. DOT/FAA/AM-00/33.

Nicholas, J.S., G.C. Butler, D.T. Lackland, G.S. Tessier, L.C. Mohr Jr., and D.G. Hoel (2001). Health among commercial airline pilots. *Aviat. Space Environ. Med.* **72**, 821-826.

NRC (National Research Council, Committee on Airliner Cabin Air Quality, Commission for Life Sciences) (1986). *The Airliner Cabin Environment: Air Quality and Safety*. National Academy Press, Washington DC.

NRC (National Research Council, Committee on Toxicology, Commission for Life Sciences) (1992). *Guidelines for Developing Spacecraft Maximum Allowable Concentrations for Space Station Contaminants*. National Academy Press, Washington DC.

NRC (National Research Council, Committee on Toxicology, Commission for Life Sciences) (2000). *Spacecraft Maximum Allowable Concentrations for Selected Airborne Contaminants*. National Academy Press, Washington DC.

Obe, G., R. Facius, G. Reitz, I. Johannes, and C. Johannes (1999). Manned Missions to Mars and Chromosome Damage. *Int. J. Radiat. Biol.,* **75,** 429-433.

O'Brien, K., W. Friedberg, H.H. Sauer, and D.F. Smart (1994). Atmospheric Cosmic Rays and Solar Energetic Particles at Aircraft Altitudes. *Environment International,* **22 (Suppl.1)**, S9-S44.

Petrov, V.M., V.S. Makhmtov, N.A. Panova, V.A. Shurshakov, Ts.P. Dachev, J.V. Semkova, and Yu.P. Matvijchuk (1994). Peculiarities of the Solar Proton Events of 19 October 1989 and 23 March 1991 According to the Measurements onboard the Mir Space Station. *Adv. Space Res.*, **14**, 645-650.

Pukkala, E., A. Auvinen, and G. Wahlberg (1995). Incidence of Cancer among Finnish Airline Cabin Attendants. *Br. Med. J.,* **311**, 649-652.

Rafnsson, V., J. Hrafnkelsson, and H. Tulinius (2000), Incidence of Cancer among Commercial Airline Pilots. *Occup. Environ. Med.*, **57**, 175-179.

Reed, D.S., S. Glaser, and J. Kaldor (1980). Ozone Toxicity Symptoms among Flight Attendants. *Am. J. Ind. Med.*, **1**, 43-54.

Reynolds P., J. Cone, M. Layfesky, D.E. Goldberg, and S. Hurley (2002). Cancer Incidence in California Flight Attendants (United States). *Cancer Causes Control,* **13**, 317-324.

Rothman, K. (1986). *Modern Epidemiology*. Little, Brown & Company, Boston, MA.

Ryan, P. (1991). Smoking and Commercial Airline Flights in Europe. *Eur. J. Cancer*, **27**, 1348-1350.

SAAM (Subsystem Analysis and Analytical Models) (1996). *ISS Integrated Traffic Model Report (DAC 4 Final)*. Boeing-Report NASA-JSC-Contract NAS15-10000.

Seldén, A., and G. Ahlborg (1995). Mortality and Cancer Morbidity after Exposure to Military Aircraft Fuel. *Aviat. Space Environ. Med.,* **62**, 789-794.

Shea, M.A., and D.F. Smart (1990). A Summary of Major Solar Proton Events. *Solar Physics*, **127**, 297-320.

Sinclair, W.K. (1985). Experimental RBEs of High-LET Radiations at Low Doses and the Implications for Quality Factor Assignment. *J. Rad. Prot. Dos.,* **13**, 319-326.

Singleterry, R.C., and S.A. Thibeault (2000). *Materials for Low-Energy Neutron Radiation Shielding*. NASA Technical Paper TP-2000-210281.

Suvanto, S., M. Partinen, M. Haermae, and J. Ilmarinen (1990). Flight Attendants' Desynchronosis after Rapid Time Zone Changes. *Aviat. Space Environ. Med.,* **61,** 543-547.

Tripathi, R.K., Wilson, J.W., Cucinotta, F.A., Nealy, J.E., Clowdsley, M.S., and Kim, M.H.Y. (2001). *Deep Space Mission Shielding Optimization*. Society for Automotive Engineers, Paper SAE 2001-01-2326.

Turner, R.E., and G.D. Badhwar (1999). Mars 2001 Cruise Phase Radiation Measurements. In "*Proceedings of the Workshop on Mars 2001: Integrated Science in Preparation for Sample Return and Human Exploration"* (Lunar and Planetary Institute, Houston TX, October 2-4, 1999), Lunar and Planetary Institute, Houston, TX.

Tveten, U. (1997). *Cosmic Radiation and Airline Pilots: Exposure Patterns of Norwegian SAS Pilots 1960 to 1994*. Report IFE/KR/E-96/008, Institute for Energy Technology, Kjeller, Norway.

USEPA (United States Environmental Protection Agency) (1986). Guidelines for Carcinogen Risk Assessment, *Fed. Regist.*, **51**, 33992-34003.

Vågerö, D., A.J. Swerdlow, and V. Beral (1990). Occupation and Malignant Melanoma: A Study Based on Cancer Registration Data in England and Wales and in Sweden, *Br. J. Industr. Med.,* **47**, 317-324.

Wartenberg D., and C.P. Stapleton (1998). Risk of Breast Cancer is also Increased among Retired US Female Airline Cabin Attendants. *Br. Med. J.,* **316**, 1902 (letter).

Wartenberg D., and C.P. Stapleton (1999). Risk of Breast Cancer among Female Airline Cabin Attendants. *Br. Med. J.,* **318**, 126 (letter).

Weaver, D.B., M.B. Duke, and B.R. Roberts (1993). Mars Exploration Strategies: A Reference Design Mission. Paper IAF 93-Q.1.383, presented at the 44th Congress of the International Astronautical Federation, held in Graz, Austria, in 1993.

Whelan, E.A. (2002). *The Working Women's Health Study: the NIOSH/FAA Study of Reproductive Disorders in Female Flight Attendants*. National Institute for Occupational Safety and Health, Status Reports Q2-2002.

Wilson, J.W. (1981). Solar Radiation Monitoring for High Altitude Aircraft. *Health Phys.,* **41**, 607-617.

Wilson, J.W. (2000). Overview of Radiation Environments and Human Exposures. *Health Phys*., **79**, 470-494.

Wilson, O.J., B.F. Young, and C.K. Richardson (1994). Cosmic Radiation Doses Received by Australian Commercial Flight Crews and the Implications of ICRP. *Health Physics,* **66**, 493-502.

Wilson, J.W., L.W. Townsend, W. Schimmerling, G.S. Khandelwal, F. Khan, J.E. Nealy, F.A. Cucinotta, L.C. Simonsen, J.L. Shinn, and J.W. Norbury (1991). *Transport Methods and Interactions for Space Radiations,* NASA Reference Publication #1257.

Wilson, J.W., M.Y. Kim, M.S. Clowdsley, J.H. Heinbockel, R.K. Tripathi, R.C. Singleterry, J.L. Shinn, and R. Suggs (1999). Mars Surface Ionizing Radiation Environment: A Need for Validation. In "*Proceedings of the Workshop on Mars 2001: Integrated Science in Preparation for Sample Return and Human Exploration"* (Lunar and Planetary Institute, Houston TX, October 2-4, 1999), Lunar and Planetary Institute, Houston, TX.

Wilson, J.W., D.L. Maiden, P. Goldhagen, H. Tai, and J.L. Shinn, this book. Overview of Atmospheric Ionizing Radiation (AIR). In "*Proceedings of the Workshop Atmospheric Ionizing Radiation (AIR) Investigators' Workshop: Preliminary Results and Lesson Learned from the June 1997 Flights"* (NASA Langley Research Center, Hampton VA, March 30-31, 1998), this book.

Winter, P.M. (1968). Aviator's Cancer. *Lancet* **2**, 285 (letter).

Wolf, G., R. Pieper, and G. Obe (1999). Chromosomal Alterations in Peripheral Lymphocytes of Female Cabin Attendants. *Int. J. Radiat. Biol.,* **75,** 829-836.

Wu, H., W. Atwell, F.A. Cucinotta, and T.C. Yang (1996). *Estimates of Space Radiation-Induced Cancer Risks for International Space Station Orbits.* NASA Technical Memorandum #104818, NASA Center for Aerospace Information, Linthicum Heights, MD.

Zubrin, R. (1997). *The Case for Mars: the Plan to Settle the Red Planet and Why We Must*. Touchstone Books, Simon & Schuster Publishing, New York, NY.

Zurek, R.W. (1992). Comparative Aspects of the Climate of Mars: An Introduction to the Current Atmosphere. In *Mars (Kieffer, H.H., B.M. Jakowsky, C.W. Snyder, and M.S. Matthews, Eds.),* Univ. of Arizona Press, Tucson, AZ.

Table 1. Cancer Sites with significant positive association for civilian airline flight personnel crew members. Confidence limits are 90 or 95 percent depending on study.

Cancer Site	Sex	Job	Type	Confidence Limits		Source
All Sites*	M	CA	SIR	1.3	2.2	Haldorsen et al. (2001)
All Sites*	F	CA	SIR	1.0	1.6	Rafnsson et al. (2001)
Bone	F	CA	SIR	1.8	54.4	Pukkala et al. (1995)
Brain	M	P	SIR	1.2	7.9	Band et al. (1990)
Brain	M	P	SMR	1.4	9.5	Band et al. (1990)
Breast	F	CA	SIR	1.2	2.2	Pukkala et al. (1995)
Breast	F	CA	SIR	1.0	4.3	Wartenberg et al. (1998, 1999)
Breast	F	CA	SIR	1.09	1.83	Reynolds et al. (2002)
Esophagus	M	CA	SIR	2.7	11.4	Haldorsen et al. (2001)
Hodgkin Lymphoma	M	P	SIR	1.2	11.7	Band et al. (1990)
Kidney and Pelvis	M+F	P	PMR	1.18	3.06	Nicholas et al. (1998)
Leukemia – AML	M	P	SIR	2.1	9.3	Band et al. (1996)
Leukemia – Myeloid	M	P	SIR	1.4	5.5	Band et al. (1996)
Liver*	M	CA	SIR	1.3	39.2	Haldorsen et al. (2001)
Prostate	M	P	SIR	1.4	2.5	Band et al. (1996)
Rectum	M	P	SMR	1.2	11.2	Band et al. (1990)
Skin – Melanoma	M	P	SMR	1.5	6.3	Irvine & Davies (1999)
Skin – Melanoma	M	P	SIR	1.1	2.7	Haldorsen et al. (2000)
Skin – Melanoma	M	P	SIR	5.0	36.5	Rafnsson et al. (2000)
Skin – Melanoma	M	CA	SIR	1.1	6.4	Haldorsen et al. (2001)
Skin – Melanoma	M	P	SIR	2.85	4.23	Nicholas et al. (2001)
Skin – Melanoma	F	CA	SIR	1.2	6.7	Rafnsson et al. (2001)
Skin -- Melanoma	M	P	SIR	1.27	4.54	Hammar et al. (2002)
Skin -- Melanoma	F	CA	SIR	1.28	4.38	Reynolds et al. (2002)
Skin – Other Cancers	M	P	SIR	1.1	2.2	Band et al. (1990)
Skin – Other Cancers	M	PE (jets)	SIR	2.1	4.2	Gundestrup & Storm (1999)
Skin – Other Cancers	M	P	SIR	1.3	4.0	Haldorsen et al. (2000)
Skin – Other Cancers*	M	CA	SIR	4.5	18.8	Haldorsen et al. (2001)
Skin – Other Cancers*	M	CA	SIR	5.18	15.36	Reynolds et al. (2002)
Prostate#	M	P	SIR	1.19	2.29	Ballard et al. (2000)
Skin – Melanoma#	M	P	SMR	1.02	3.82	Ballard et al. (2000)

*cancer outcome possibly related to lifestyle only;
results from meta-analysis of previous studies, then adjusted for socio-economical status;

AML = Acute Myeloid Leukemia;

CA = Cabin Attendants;
P = Pilots only;
PE = Pilots and flight Engineers;

PMR = Proportional Mortality Ratio;
SIR = Standardized Incidence Ratio;
SMR = Standardized Mortality Ratio

Table 2. Results for cancer sites with adjusted RRs showing excess risk (results from Ballard et al., 2000).

Results for Male Pilots		Results for Female Flight Attendants	
Cancer Site	RR (95% CI)	Cancer Site	RR (95% CI)
COLON (mortality)	**1.05 (0.71-1.53) ***	ALL-SITES (incidence)	**1.29 (0.98-1.70)**
MELANOMA (mortality)	**1.97 (1.02-3.82) #**		
MELANOMA (incidence)	**1.07 (0.55-2.10) #**	MELANOMA (incidence)	**1.54 (0.83-2.87) ^**
PROSTATE (mortality)	**1.11 (0.70-1.75) ***		
PROSTATE (incidence)	**1.65 (1.19-2.29) ***	BREAST (incidence)	**1.35 (1.00-1.83) #**
BRAIN (mortality)	**1.45 (0.75-2.80) §**		
BRAIN (incidence)	**1.74 (0.87-3.30) §**		

---

* SES factor 1.1 # SES factor 1.5 § SES factor 1.2 ^ SES factor 1.3

Chapter 19: Developing of a New Atmospheric Ionizing Radiation (AIR) Model

John M. Clem [1] , Giovanni De Angelis [2,3], Paul Goldhagen [4], John W. Wilson [2]

[1] Bartol Research Institute University of Delaware, Newark, DE
[2] NASA Langley Research Center, Hampton, VA
[3] Istituto Superiore di Sanita', Rome, Italy
[4] Environmental Measurements Laboratory, US Department of Energy, New York

Towards a New Atmospheric Ionizing Radiation (AIR) Model

Preface

As a result of the research leading to the 1998 AIR workshop and the subsequent analysis, the neutron issues posed by Foelsche et al. and further analyzed by Hajnal have been adequately resolved. We are now engaged in developing a new atmospheric ionizing radiation (AIR) model for use in epidemiological studies and air transportation safety assessment. A team was formed to examine a promising code using the basic FLUKA software but with modifications to allow multiple charged ion breakup effects. A limited dataset of the ER-2 measurements and other cosmic ray data will be used to evaluate the use of this code.

INTRODUCTION

The earth is continually bathed in high-energy ionizing radiation that comes from outside the solar system, called galactic cosmic rays which consist of roughly 90% protons and 8% helium nuclei (also called alpha particles, though of different origin) with the remainder being heavier nuclei and electrons [Gaisser, 1990]. When these particles penetrate the magnetic fields of the solar system and the Earth and reach the Earth's atmosphere, they collide with atomic nuclei in air and create cascades of secondary radiation of every kind [Reitz, 1993]. The intensity of the different particles making up atmospheric cosmic radiation, their energy distribution, and their potential effect on avionics and aircraft occupants vary with altitude, location in the geomagnetic field, and time in the sun's magnetic activity cycle [Reitz, 1993; Wilson, 2000; Heinrich et al., 1999]. The atmosphere provides shielding, which at a given altitude is determined by the mass thickness of the air above that altitude, called atmospheric depth. The geomagnetic field provides a different kind of shielding, by deflecting low-momentum charged particles back into space. The minimum momentum per unit charge (magnetic rigidity) a vertically incident particle can have and still reach a given location above the earth is called the geomagnetic vertical cutoff rigidity (vertical cutoff) for that point.

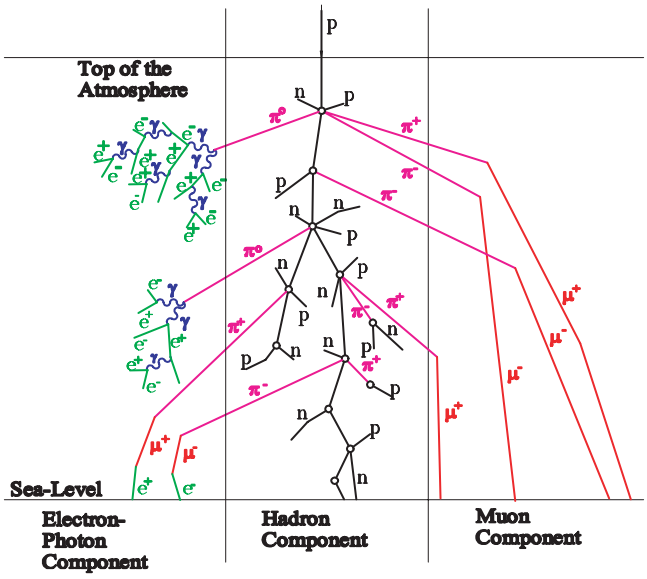

Fig. 1 Cascading particles produced by high-energy protons at the top of the atmosphere.

The local flux of incident cosmic rays at a given time varies widely with geomagnetic location and the solar modulation level. When solar activity is high, GCR flux is low and vice versa. Anti-correlation between cosmic rays fluxes and the level of solar activity (solar modulation) is caused by magnetic field irregularities in the solar wind that push charged particles out of the solar system or decelerate them [Clem et al., 1996 and references therein]. Solar modulation of cosmic ray fluxes has roughly a 22-year cycle, which must be considered to accurately predict the spectrum at any given time. The modulated spectrum is generally determined by solving the Fokker-Planck equation for a spherical symmetric model of the heliosphere incorporating diffusion, adiabatic acceleration and convection.

METHOD

The propagation of primary particles through the Earth's atmosphere has been calculated with a three dimensional Monte Carlo transport program FLUKA [Fasso, et al., 1993; Clem and Dorman, 2000]. Primary protons and alphas are generated within the rigidity range of 0.5GV-20TV uniform in $\cos^2\theta$. For a given location, primaries above the effective cutoff rigidity are transported through the atmosphere. Since FLUKA does not transport nuclei, helium ions are initially transported with a separate package called HEAVY to simulate fragmentation [Engel et al., 1992]. This package interfaces with FLUKA to provide interaction starting points for each nucleon originating from a helium nucleus

The primary cosmic ray spectrum used in this calculation was determined through an analysis of simultaneous proton and helium measurements made on high altitude balloon flights [Seo et al., 1991; Papini et al., 1993; Boezio et al., 1999; Menn et al., 2000; Sanuki et al., 2000] or space craft [Alcaraz, et al., 2000a; 2000b] as shown in Figure 2. These flights occurred during different times and different levels of solar modulation resulting in a variation of spectra shapes. To provide a continuous relationship between solar modulation level and the expected spectra shape for both cosmic ray protons and helium, a global fit was performed on this data using the solution to the Fokker-Plank equation assuming the shape of the spectrum of cosmic rays in the local interstellar medium (outside the solar system) is a power law in rigidity multiplied by an ionization energy loss term to account for the effects expected

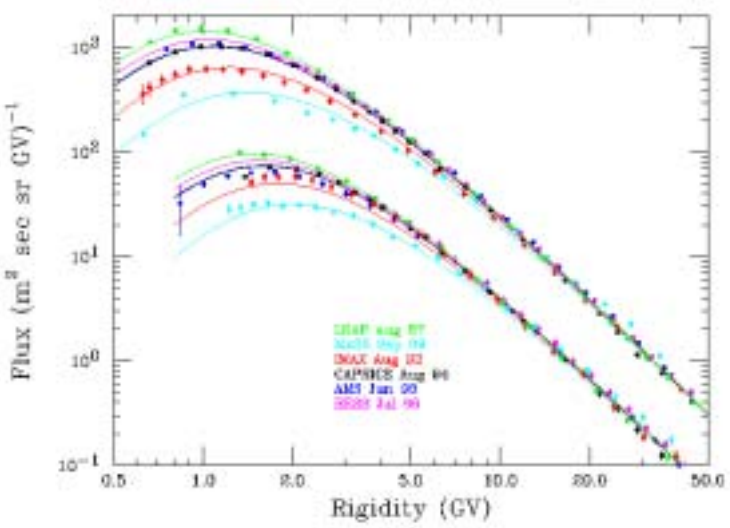

Figure 2. Results of balloon and space-craft measurements of the rigidity spectra of primary cosmic ray protons (upper spectra) and Helium ions (lower spectra) above of the Earth's atmosphere (points) and global fit to all the spectra (curves).

$$dF/dR = k1R^{-k2} \quad (1-e^{-k3\beta})$$

from galactic propagation. The free parameters (k1, k2, k3) in the fit include the power index and normalization of the local interstellar spectra of protons and alpha particles. Initially, the diffusion coefficient ($\boldsymbol{\kappa}$) was modeled in the standard way as

$$\boldsymbol{\kappa} = \boldsymbol{\kappa}_0 \, e^{(r-1)/rd} \beta R$$

where R is the rigidity of the particle, β is the speed of the particle normalized to the speed of light, r is the distance from the sun in astronomical units and rd is the diffusion length scale. In this model, the quantities $\boldsymbol{\kappa}$ and $\boldsymbol{\kappa}_0$ are vectors and each component of $\boldsymbol{\kappa}_0$ is a free parameter representing the diffusion coefficient value for each data set (same value for both particle species) used in the global fit. Although this unique method provided promising results, the chi square of the fits had a rigidity dependence resulting in systematic errors. As an attempt to reduce the systematic effects, the above diffusion coefficient model is modified to

$$\boldsymbol{\kappa} = \boldsymbol{\kappa}_0 \, e^{(r-1)/rd} \beta \, f_n(R)$$

where $f_n(R)$ is an nth order polynomial in rigidity with the lowest order term forced to zero and the coefficient on the linear term forced to one. Second order results are shown in Figure 2. Even though this technique has decreased the chi square per degree of freedom by ~30%, the average residual (the difference fit - data divided by the data error) is 3.5 sigma based on the published errors of the spectra. Therefore, some work is needed to improve this procedure including the possibility of modifying the current local interstellar spectrum model. The recent work of Badhwar et al. [2001] may be helpful.

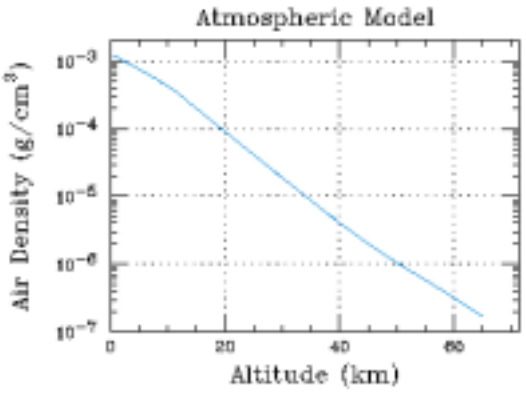

Fig. 3 Standard atmosphere density as a funciton of altitude.

The atmosphere is divided into 180 (bottom boundary radius = 6378.14km) concentric spherical shells with differing radii and density to simulate the actual density profile with a vertical total 1035g/cm2 column density for sea level and 305g/cm2 for 9.1km (30,000ft) [4]. Air density changes ~5% with each adjacent spherical shell, but within each shell the material has a uniform density. Above 2000 meters the atmospheric composition is constant with a 23.3% O2, 75.4% N2 and 1.3% Argon distribution by mass while below 2000 meters a varying addition of H2 from 0.06% at sea-level to 0.01% by mass at 2000 meters is included to account for the abundance of water vapor. The outer air-space boundary is radially separated by 65 kilometers from the inner ground-air boundary. A single 1cm2 element on the air-space boundary is illuminated with primaries. This area element defines

a solid angle element with respect to the center of the Earth which subtends a slightly smaller area element at different depths. Particle intensity at various depths is determined by superimposing all elements on the spherical boundary defining the depth. Due to rotational invariance this process is equivalent to illuminating the entire sky and recording the flux in a single element at ground level, but requires far less computer time [5]

COMPARISON WITH OBSERVATION

As a check, the calculated particle fluxes are compared to published data. The absolute normalization of the simulated flux is determined from the number of generated primaries, weighted according to the expected primary spectrum (no free parameters in the comparison). The particle types compared are muons, protons and neutrons. The neutron measurements were performed aboard an ER-2 high altitude airplane by Goldhagen's group during one of the lowest solar modulation periods (highest radiation levels) of the previous solar cycle (Jun-13 1997) [6]. As shown observations were taken at 56.5 and 101g/cm2 atmospheric depths at high latitude locations with rigidity cutoffs less than 1GV. The calculation agrees fairly well particularly in high energy regime, however the flux measurements are systematically higher at lower energies. This discrepancy could be the result of T value used for the ambient temperature and/or treatment of the thermalization process. Also shown are observations of sea-level protons and muons as published in Allkofer and Grieder 1984 [7]. Again the calculation seems to agree with the observations fairly well however there are systematic differences. These difference could be explained by the limitation of a digitized atmospheric model that produces an enhancement in pion interactions. In any case, it appears that the use of this version of FLUKA is a reasonable choice.

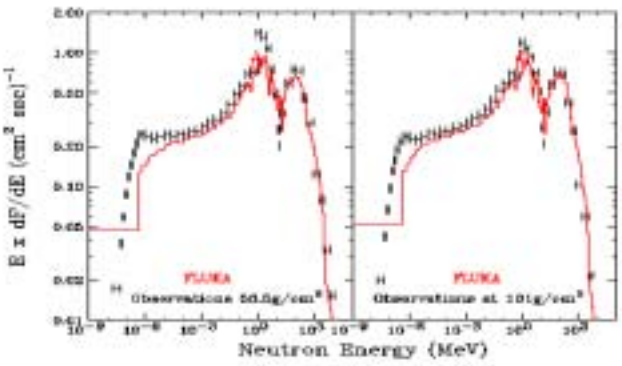

Figure 4. Measured and calculated neutron spectra at 20 km altitude and 0.8 GV cutoff.

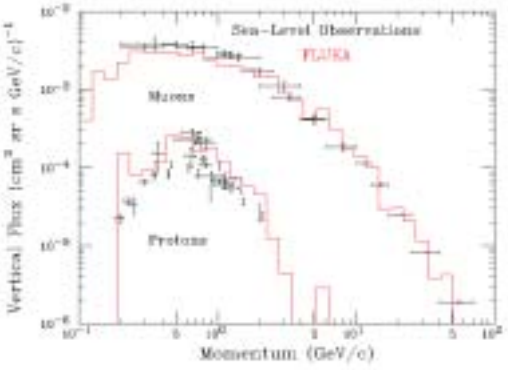

Figure 5. Sea-level observations of protons and muons [Allkofer and Grieder 1984] compared to this calculation.

REFERENCES

Anon. (1976) US Standard Atmosphere, USAF, NOAA, NASA, US Commerce Dept.

Alcaraz, J., et al. (2000a). "Cosmic Protons," Physics Letters B 490, 27.

Alcaraz, J., et al. (2000b). "Helium in Near Orbit," Physics Letters B 494, 193.

Allkofer, O.C. and Grieder, P.K.F. (1984). Cosmic Rays on Earth, Physics Data No. 25-1 (Fachinformationszentrum Energie, Physik, Mathematik, Karlsruhe, Germany).

Clem, J. and L. Dorman (2000) "Neutron Monitor Response Functions," Space Science Reviews, 93, 335.

Clem, J.M., D.P. Clements, J. Esposito, P. Evenson, D. Huber, J. L'Heureux, P. Meyer, and C. Constantin (1996). "Solar Modulation of Cosmic Electrons," Astrophysical Journal 464, 507.

Clem, J.M., J.W. Bieber, P. Evenson, D. Hall, J.E. Humble, M. Duldig (1997). "Contribution of obliquely incident particles to neutron monitor counting rate," Journal of Geophysical Research, 102, 26919

Fasso, A., A. Ferrari, A. Ranft, P.R. Sala, G.R. Stevenson ad J.M. Zazula (1993). "A comparison of FLUKA simulations with measurements of fluence and dose in calorimeter structures," Nuclear Instruments and Methods, A 332, 459-468.

Ferrari, A., M. Pelliccioni, T. Rancati (2001). "Calculation of the radiation environment caused by galactic cosmic rays for determining air crew exposure," Radiat. Prot. Dosim. 93, 101-114.

Gaisser, T., (1990). Cosmic Rays and Particle Physics, Cambridge University Press.

Reitz, G., K. Schnuer, K. Shaw, "Editorial--Workshop on radiation Exposure of civil aircrew." *Radiat. Prot. Dosim.* **48**, 3 (1993).

Wilson, J.W. Overview of radiation environments and human exposures. *Health Phys*. **79**: 470-494 (2000).

Chapter 20: Radiation Weighting Factors for High Energy Neutron, Proton, and Alpha Particles

N. Yoshizawa

Mitsubishi Research Institute Inc., Otemachi, Chiyoda-ku, Tokyo, 100-8141, Japan

Radiation Weighting Factors for High Energy Neutron, Proton, and Alpha Particles

Preface

Traditionally, radiation protection has relied on radiation dependent modifying factor Q(L) based on linear energy transfer L of the local tissue charged particle environment. In 1991, the International Commission on Radiological Protection (ICRP, Report Number 60) recommended a nonlocal exposure field quantity W_r to emphasize the uncertainties in knowledge of the appropriate modifying factor. The use of W_r simplifies dosimetry in many field applications but complicates the evaluation using some computational procedures. An alternate quantity has been defined by the International Commission on Radiological Units (ICRU, Report Number 51) as "organ dose equivalent" calculated in the traditional way using Q(L). Exceptions to the ICRP recommended W_r for protons has been made by the National Council on Radiation Protection and Measures (NCRP Report Number 116) on the basis of "organ dose equivalent." The present paper will fully address these issues and provide conversion factors for relavant radiation for any of the evaluation systems.

Introduction

Estimation of radiation exposure against high-energy neutron above 20 MeV is very important to radiation protection around high energy and large intensity proton accelerators. For aircrew of high-altitude flight, radiation exposure from high-energy neutron and proton has come to be an important problem (Wilson et al. 1995). High energy neutron, proton, and alpha exposure must be also estimated for radiation protection concerning the astronauts staying for a long time in a space station (NCRP 1997).

In ICRP 60 (1991), the organ equivalent dose is defined as the averaged organ absorbed dose multiplied by a radiation weighting factor appropriate for the external radiation type and incident energy on the body rather than the radiation type and energy distributions in the body. The introduction of the radiation weighting factor for high energy radiation was discussed(4). For high energy neutron, proton, and alpha irradiation, several different types of radiations are produced from nuclear interaction in the body. National Council on Radiation Protection and Measurements (NCRP) defined the value of w_R for proton as 2 (NCRP 1993). This value is less than the half of recommended value of 5 in ICRP 60 (1991).

We have reported dose conversion coefficients about two different types of effective doses, one was the effective dose using w_R and the other one is the effective dose using $Q-L$ relationship(Yoshizawa et al. 1998, to be published). In this paper, we propose modified radiation weighting factors for high energy neutron, proton, and alpha particles.

EFFECTIVE DOSE AND MEAN QUALITY FACTOR FOR THE WHOLE BODY

In ICRP60, the effective dose is defined as a summation of the equivalent doses for organs, with the term for each organ multiplied by an appropriate tissue weighting factor:

$$E_{w_R} = \sum_T w_T H_T = \sum_T w_T \sum_R w_R D_{T,R} \quad (1)$$

where H_T : equivalent dose in organ T
w_T : tissue weighting factor for T (values recommended in ICRP 60)
w_R : radiation weighting factor for radiation R (also recommended in ICRP 60)
$D_{T,R}$: absorbed dose of radiation R averaged over T.

We call the above E_{w_R} calculated using w_R "the effective dose using radiation weighting factor" to distinguish from E_{Q-L}, defined later. In the same ICRP60, it is recommended to replace the relationship given in ICRP 26 (1977) with a new $Q-L$ relationship (Q: quality factor, L : unrestricted linear energy transfer in water). The effective dose calculated using the $Q-L$ relationship is given by

$$E_{Q-L} = \sum_T w_T \hat{H}_T \quad (2)$$

where $\hat{H}_T$: dose equivalent averaged over organ T (diacritic mark ^ added to distinguish organ dose equivalent from equivalent dose). In order to obtain the organ dose equivalents, the energies deposited in the regions were weighted with the averaged quality factor in accordance with the methodology described by Yoshizawa et al. (1998).

In this study, the mean quality factor for the whole body is given by

$$\overline{Q}_{body} = \frac{E_{Q-L}}{\sum_T w_T D_T} \quad (3)$$

The difference between $\overline{Q}_{body}$ and w_R can be considered the factor that distinguishes E_{Q-L} from E_{w_R}.

METHOD OF CALCULATION

In this study, an adult hermaphroditic anthropomorphic phantom——modified MIRD5——was adopted for calculating the mean absorbed dose and the mean dose equivalent of an organ. Calculations were performed on whole-body irradiation with parallel broad monoenergetic beams incident on an anthropomorphic phantom placed in vacuum. Organ absorbed doses and organ dose equivalents were calculated by the HETC-3STEP (Yoshizawa et al. 1995) and the MORSE-CG/KFA (Cloth et al. 1988) in

the HERMES code system(Cloth et al. 1988). In Yoshizawa et al. (1998), the detailed method of calculation is described.

RESULTS AND DISCUSSION

Effective Dose Conversion Coefficients for high energy neutron, proton, and alpha particles have been already reported by Yoshizawa et al. (1998, to be published). Figure 1 plots the ratios E_{w_R}/E_{Q-L} for neutron, proton, and alpha particles. It is found large differences between E_{w_R} and E_{Q-L} .

As shown in Figure 1, E_{w_R} overestimates E_{Q-L} for neutron, proton, and alpha above 20 MeV. In ICRP60, w_R for neutron is defined as a continuous function of neutron energy as follows:

$$w_R(E_n) = 5 + 17\exp\left(-(\ln(2E_n))^2/6\right) \quad \text{(in ICRP 60)} \tag{4}$$

Siebert et al.(1994) described modification of w_R to reconcile a difference between w_R and $Q-L$. Pelliccioni (4) also proposed radiation weighting factors for high energy neutron, proton, negative pions, positive pions, negative muons, and positive muons. For neutron above 20 MeV, the adjustment of w_R as a function of neutron energy E_n given by Eq. (5) will make an agreement between E_{w_R} and E_{Q-L} within 40%.

$$w_R(E_n) = 4 + 26\exp\left(-(\ln(2E_n))^2/6\right) \quad 20MeV \le E_P \le 10GeV \tag{5}$$

In Eq. (5), only two coefficients in Eq. (4) are adjusted from 5 to 4 and from 17 to 26, respectively. Modified w_R given by Eq. (5) was shown in **Fig. 2**. comparing with $\overline{Q}_{body}$.

Differences between E_{w_R} and E_{Q-L} for proton and alpha are larger than those for neutron. The main reason is that w_R for proton is 5 and alpha is 20 in ICRP 60 independent on incident energy. For proton above 20 MeV, the adjustment of w_R as a step function of proton energy E_p given by the equation (6) will make an agreement between E_{w_R} and E_{Q-L} within about 70%.

$$w_R(E_p) = \begin{cases} 2.5 & 20MeV \le E_P < 30MeV \\ 2 & 30MeV \le E_P \le 10GeV \end{cases} \tag{6}$$

Modified w_R given by Eq. (6) was shown in **Fig. 3** to compare with $\overline{Q}_{body}$. NCRP 116 (1993) recommends that w_R is 2 for proton independent on its energy. Above 30 MeV, adjusted w_R in this study is equal to the value in NCRP 116. However, E_{Q-L} will underestimate E_{w_R} for proton with $w_R = 2$ below 30 MeV.

For alpha above 20 MeV, the adjusted w_R as a step function of alpha energy E_a is given by the equation (7).

$$w_R(E_a) = \begin{cases} 5 & 20MeV \le E_a < 30MeV \\ 3 & 30MeV \le E_a \le 10GeV \end{cases} \quad (7)$$

Modified w_R given by Eq. (7) was shown in **Fig. 4** to compare with $\overline{Q}_{body}$.

CONCLUSION

Effective doses using w_R and effective doses using $Q-L$ relationship were compared. It was found that effective doses using w_R overestimate effective doses using $Q-L$ relationship for neutron, proton, and alpha. Modifications of w_R were proposed. Proposed radiation weighting factors are summarized in **Table 1.**

Table 1 Proposed Radiation Weighting Factors for High Energy Neutron, Proton, and Alpha particles

Radiation	Radiation Weighting Factor	
	ICRP60	Proposed Radiation Weighting Factor
Neutrons	$5+17\exp(-(\ln(2En))^2/6)$ En: neutron energy (MeV)	$4+26\exp(-(\ln(2En))^2/6)$ $20MeV \le En \le 10GeV$ En: neutron energy (MeV)
Protons	5	2.5 $20MeV \le Ep < 30MeV$ 2 $30MeV \le Ep \le 10GeV$ Ep: proton energy(MeV)
Alpha Particles	20	5 $20MeV \le Ea < 30MeV$ 3 $30MeV \le Ea \le 10GeV$ Ea: alpha particle energy (MeV)

ACKNOWLEDGEMENT

Drs. Iwai and Sakamoto kindly accorded the author useful discussions.

REFERENCES

Cloth, P., et al. *KFA-IRE-EAN* 12/88(1988).

International Commission on Radiological Protection *"Recommendations of the International Commission on Radiological Protection,"* ICRP Publication 26, Pergamon Press, Oxford (1977).

International Commission on Radiological Protection *"1990 Recommendations of the International Commission on Radiological Protection,"* ICRP Publication 60, Pergamon Press, Oxford, (1991).

National Council on Radiation Protection and Measurements *NCRP Symposium Proceedings No.3,"Acceptability of Risk from Radiation – Application to Human Space Flight,"* NCRP Publ., Bethesda, (1997).

National Council on Radiation Protection and Measurements *"Limitation of Exposure to Ionizing Radiation,"* NCRP Report No.116 NCRP Publ., Bethesda, (1993).

Pelliccioni., M. *Radiat. Prot. Dosim.,* **80**, 371 (1998).

Siebert, B.R.L. *Radiat. Prot. Dosim.*, **54**[3/4], 193 (1994).

Wilson, J.W., et al. *NASA Technical Paper* 3524, (1995).

Yoshizawa, N. et al. *J. Nucl. Sci. and Technol.*,**35**, 928(1998).

Yoshizawa, N. et al. "*Fluence to Dose Conversion Coefficients for High-Energy Neutron, Proton and Alpha Particles*," Proc. of the 9th International Conference on Radiation Shielding, Oct.17-22,1999 *J. Nucl. Sci. and Technol.S1*,865(2000).

Yoshizawa, N. et al. *J. Nucl. Sci. and Technol.,***32**,601(1995).

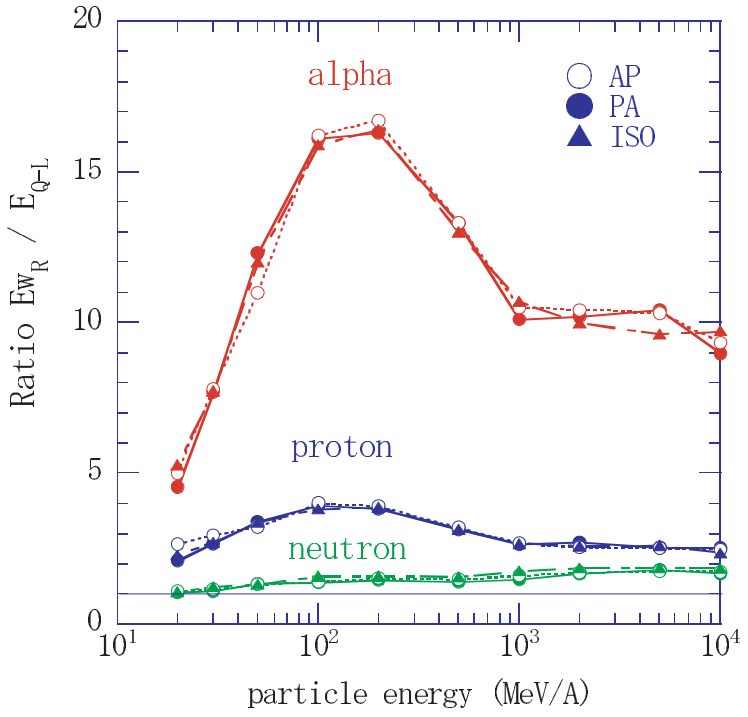

Fig. 1 Ratio between Ew_R and E_{Q-L} for neutron, proton, and alpha particle incident energy.

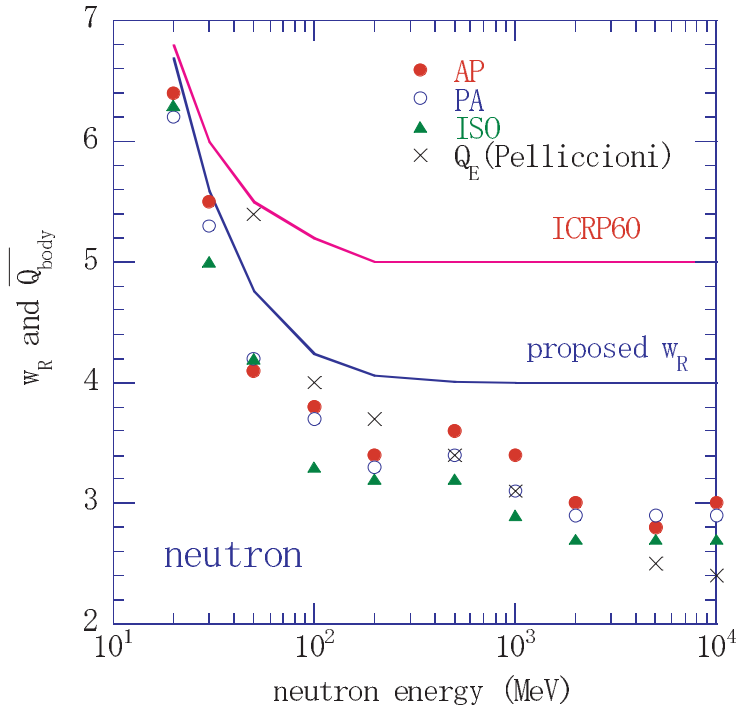

Fig. 2 Mean quality factor for whole body irradiated by neutron and proposed w_R.

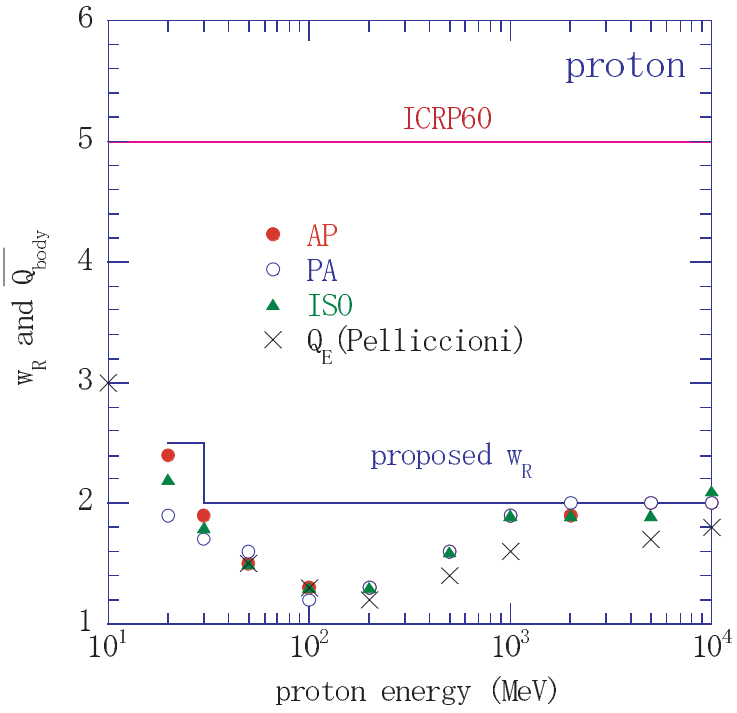

Fig. 3 Mean quality factor for whole body irradiated by proton and proposed w_R.

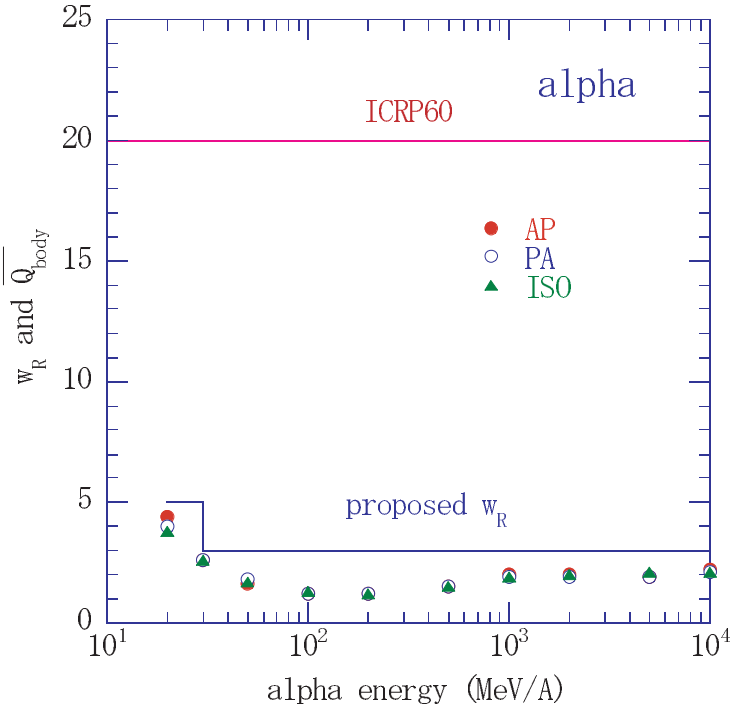

Fig. 4 Mean quality factor for whole body irradiated by alpha and proposed w_R.

Chapter 21: Summary of Atmospheric Ionizing *AIR* Research: SST-Present

J.W. Wilson[1], P. Goldhagen[2], V. Rafnsson[3], J. M. Clem[4], G. De Angelis[5,6] W. Friedberg,[7]

[1]NASA Langley Research Center, Hampton VA 23681 USA
[2]DOE Environmental Measurements Laboratory, New York NY 10014 USA
[3]University of Iceland, Reykjavik, Iceland
[4]Bartol Research Institute, University of Delaware, Newark DE 19716 USA
[5]Old Dominion University, Norfolk VA 23508 USA
[6]Istituto Superiore di Sanita', Rome, Italy
[7]Civil Aerospace Medical Institute, FAA, Oklahoma City, OK 73125 USA

SUMMARY OF ATMOSPHERIC IONIZING *AIR* RESEARCH: SST-PRESENT

ABSTRACT

The Supersonic Transport (SST) program, proposed in 1961, first raised concern for the exposure of pregnant occupants by solar energetic particles (SEP), and neutrons were suspected to have a main role in particle propagation deep into the atmosphere. An eight-year flight program confirmed the role of SEP as a significant hazard and of the neutrons as contributing over half of the galactic cosmic ray (GCR) exposures, with the largest contribution from neutrons above 10 MeV. The FAA Advisory Committee on the Radiobiological Aspects of the SST provided operational requirements. The more recent lowering of the radiation exposure limits by the International Commission on Radiological Protection with the classification of aircrew as "radiation workers" renewed interest in GCR background exposures at commercial flight altitudes and stimulated epidemiological studies in Europe, Japan, Canada and the USA. The proposed development of a High Speed Civil Transport (HSCT) required validation of the role of high-energy neutrons, and this resulted in ER-2 flights at solar minimum (June 1997) and studies on effects of aircraft materials on interior exposures. Recent evaluation of health outcomes of DOE nuclear workers resulted in legislation for health compensation in year 2000 and recent European aircrew epidemiological studies of health outcomes bring renewed interest in aircraft radiation exposures. As improved radiation models become available, it is imperative that a corresponding epidemiological program of US aircrew be implemented.

INTRODUCTION

After the discovery of radiation emanating from certain materials, the source of background radiation observed in the atmosphere was thought to have exclusively originated from the ground, however Hess's series of balloon flights from 1911-1913 showed that an additional component originating from the sky was also present in this background. In 1925, Millikan coined this newly discovered radiation as cosmic rays.

The fact that the cosmic rays consisted in part of charged particles was directly demonstrated by coincidence experiments using Geiger-Mueller tubes and resolving individual charged particle tracks within a Wilson cloud chamber. The cloud chamber lead to the discovery of the positron as part of the cosmic rays, followed by the discovery of the charged mesons, and further shed light on the important neutron component of cosmic radiation in the atmosphere (Bethe et al. 1940). Worldwide surveys of cosmic ionization during the years 1931-1932 were made by several groups and Hess of Austria studied time variations associated with solar activity cycle on a mountaintop from 1931-1937. Global radiation levels correlated well with the expected effects of the geomagnetic deflection of cosmic radiation. A worldwide network of stations began to develop leading to observed short-term fluctuations in the global ionization rates simultaneously in both the southern and northern hemispheres and correlated with solar

disturbances (Hess and Eugster 1949). Observed large increases in the ionization rates would be attributed to particles coming directly from the solar events (Fig. 1). More modest decreases over a few days, as seen for the July-August 1946 event, were attributed to disturbance of the local interplanetary medium by which approaching cosmic rays were excluded from the local Earth environment (Forbush decrease). It was now clear that extraterrestrial radiation from both the sun and the galaxy were contributing to the atmospheric ionization levels. The next-to-last piece of important evidence from a human exposure perspective was the discovery of heavy ion tracks by Phyllis Frier and coworkers (1948) using nuclear emulsion track detectors in high altitude balloon flight. Although the initial emphasis of this discovery was the ability to sample cosmic matter, attention would turn to the possibility of human exposure by these ions in high-altitude aircraft and future space travel (Armstrong et al. 1949, Schaefer 1950, 1952, 1959, Allkofer and Heinrich 1974).

When the possibility of high-altitude supersonic commercial aviation was first seriously proposed, Foelsche brought to light a number of concerns for the associated atmospheric radiation exposure due to penetrating cosmic rays (CR) from the galaxy (GCR) and the sun (SCR, also referred to as solar particle events, SPE) including the secondary radiations produced in collision with air nuclei (Foelsche 1961, Foelsche and Graul 1962, Foelsche 1965). Subsequently, a detailed study of the atmospheric ionizing-radiation component at high altitudes was conducted from 1965 to 1971 at the NASA Langley Research Center (LaRC) by Foelsche et al. (1969, 1974). Prior to that study the role of atmospheric neutrons in radiation exposure was generally regarded as negligible (ICRP 1966). The LaRC studies revealed the neutron radiation to be the major contributor to commercial aircraft GCR exposure. Still the exposure levels were comfortably below allowable exposure limits for the block hours typical of airline crews of that time except during a possible solar particle event (less than 500 block hours were typical of the 1960's although regulations allowed up to 1000 hours). As a result, the US Federal Aviation Agency (FAA) Advisory Committee on the Radiobiological Aspects of the SST issued recommendations that crew members will have to be informed of their exposure levels, maximum exposures on any flight be limited to 5 mSv, development of airborne radiation monitors, development of a satellite monitoring system, and development of a solar event forecasting service (FAA 1975, see also Foelsche et al. 1974).

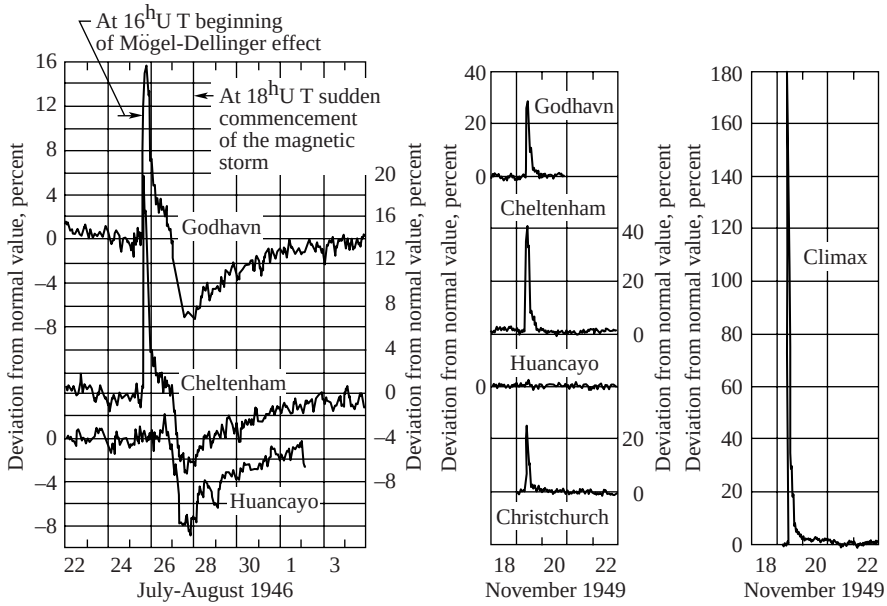

Fig. 1 Ground level ion chamber observations of solar particle events of 1946 and 1949. (From Foelsche et al. 1974)

Several factors have changed since those early studies: (a) the highly ionizing components are found to be more biologically damaging than previously assumed and the associated quality factors for fatal cancer have been increased (ICRU 1986, ICRP 1991); (b) recent studies on developmental injury in mice embryo indicate larger quality factors are required for protection in prenatal exposures (Jiang et al. 1994); (c) recent epidemiological studies (especially the data on solid tumors) and more recent A-bomb survivor dosimetry have resulted in higher radiation risk coefficients for γ rays (UNSCEAR 1988, BEIR V 1990, ICRP 1991) resulting in lower proposed permissible limits (ICRP 1991, NCRP 1993); (d) "an urgent need is recognized for better estimates of the risk of cancer from low levels of radiation" (anon. 1993); (e) subsequent to deregulation of the airline industry, flight crews are logging greatly increased flight hours (Bramlett 1985, Wilson and Townsend 1988, Friedberg et al. 1989, Barish 1990); (f) a new class of long haul commercial aircraft is being developed on which personnel for two crew shifts will be simultaneously aboard a single flight leading to increased exposures for a fixed number of flight duty hours (Lebuser 1993); (g) US airline crew members are now classified as radiation workers (McMeekin 1990, ICRP 1991); (h) NASA is developing technology for a High Speed Civil Transport (HSCT) to begin service in the twenty-first century; and (g) there are plans to introduce a revolutionary commercial transport (Mach 0.98 Sonic Cruiser) with operating altitudes from 45,000-51,000 ft (Boeing 2002). In recognition of the potential impact of several of these factors on present day

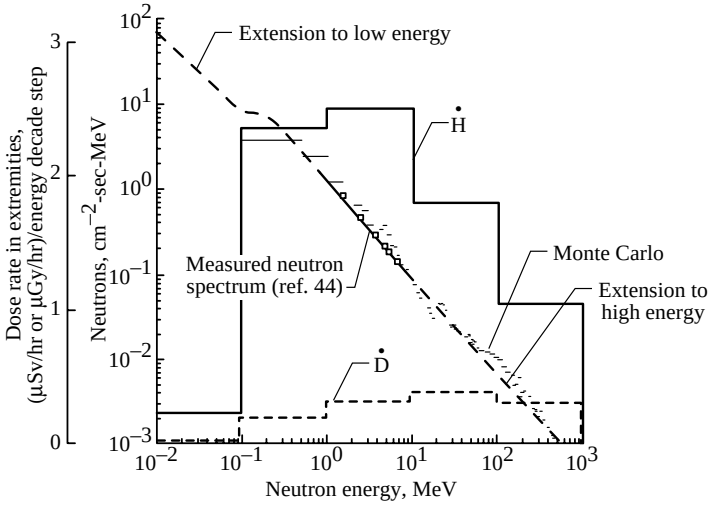

Fig. 2 Neutron spectrum at 70,000 ft over Ft. Churchill on August 3, 1965.

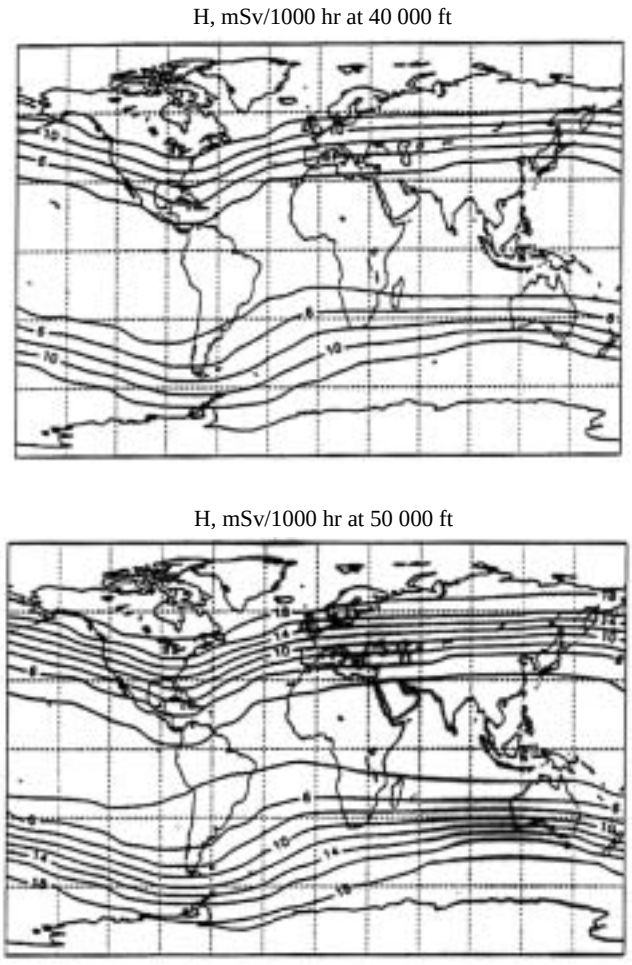

Fig. 3 Background exposure levels (*AIR* model) in atmosphere at solar minimum (1965).

crew exposures, the Commission of the European Communities organized a Workshop on Radiation Exposure of Civil Aircrew (Reitz et al. 1993). The workshop conclusions (mainly for subsonic exposures) are that the environment is not adequately known for reliable estimates of dose equivalent resulting mainly from uncertainty in the neutron spectra at high energies and a re-evaluation of the heavy ion component should be made. More recently the International Civil Aviation Organization (ICAO) has recommended that "All airplanes intended to be operated above 15 000 m (49 000 ft) shall carry equipment to measure and indicate continuously the dose rate of total cosmic radiation being received (i.e., the total of ionizing and neutron radiation of galactic and solar origin) and the cumulative dose on each flight. The display unit of the equipment shall be readily visible to a flight crew member" (ICAO 1995). More recently Japanese flight crews have requested from their government, health benefits on the basis that their exposures are "far greater than the exposure of the average nuclear power plant worker" (Fiorino 1996). Added emphasis comes from epidemiological studies of health outcomes among Department of Energy contractors (NEC 2000) leading to the *Energy Employees Occupational Illness Compensation Program Act of 2000*. Finally, it is clear that the development of advanced high-altitude commercial aircraft (such as the HSCT) requires some attention to the past concerns of high-altitude flight but in terms of current day knowledge and uncertainty in that knowledge (Wilson et al. 1995). In a prior report, we reviewed the status of knowledge of human occupational exposures and related uncertainties in health risks (Wilson 2000). It was clear that exposures among aircrew were generally higher than other terrestrial occupationally exposed groups and the aircrew risk uncertainties were high since a large fraction of the exposure is from high-LET radiations.

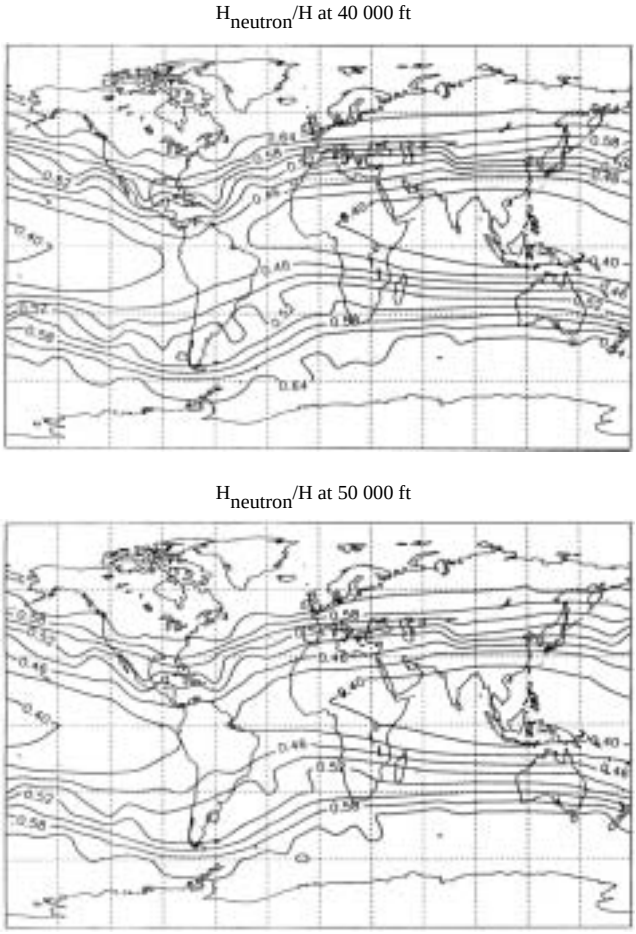

Fig. 4 Fraction of dose equivalent (AIR model) due to neutrons at solar minimum (1965).

In this paper we will review key historical developments in our understanding of atmospheric ionizing radiation and its impact on commercial operations. Although such a review cannot be made without reference to work outside the US, we leave the thorough review of European research to O'Sullivan et al. (2003) in this issue. A brief overview of ongoing research in the US is given with special emphasis on future requirements.

PAST *AIR* STUDIES

The primary concern for commercial aircraft radiation exposures began with the Supersonic Transport with a projected high operating altitude (20-km) for service on transoceanic flights. Foelsche raised concern on vulnerability on the high-latitude routes from the US eastern seaboard to Europe where extraterrestrial particles easily penetrate the geomagnetic field and intense solar particle events could induce unacceptable exposures on a single high-altitude flight. It was assumed that the neutrons produced in nuclear reactions with atmospheric nuclei would play an important role in carrying the dose equivalent deeper into the atmosphere and potentially contribute to background exposures. A measurement program was initiated by NASA at the Langley Research Center (LaRC) to resolve these issues in July 1964.

The LaRC commissioned over 300 flights over most of the duration of solar cycle 20 on high-altitude aircraft and balloons to study both background radiation levels over the solar cycle and to make measurements during a solar particle event. The Langley flight package consisted of a 1–10 MeV neutron spectrometer, tissue equivalent ion chamber, and nuclear emulsion for nuclear reaction rates in tissue. Monte Carlo calculations (Wilson et al. 1970, Lambiotte et al. 1971) for incident GCR protons were used to extend the neutron spectrum to high energies (Fig. 2). Also shown in Fig. 2 are the contributions to dose and dose equivalent from neutrons on individual energy decades. The measured data was integrated into a parametric Atmospheric Ionizing Radiation (*AIR*) model scaled with Deep River neutron monitor count rate and geomagnetic vertical cutoff rigidity (Wilson et al. 1991). The solar minimum global exposures are shown in Fig. 3 at two altitudes. Over half of the neutron dose is from neutrons above 10 MeV and an accurate knowledge of the high-energy neutron quality factors is critical to evaluation of dose equivalent. About half of the dose equivalent is from neutrons as shown in Fig. 4. Additional high-LET components come from the nuclear reactions caused by the charged hadrons so that well over half of the exposures in commercial operations are from high-LET events which leaves large uncertainties in the associated health risks (Wilson 2000, Cucinotta et al. 2001) even if the radiation levels are accurately known.

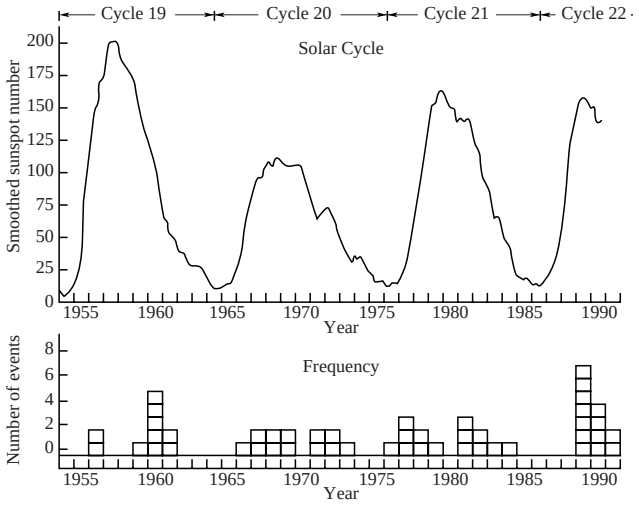

Fig. 5 Temporal distribution of ground level solar particle events for the past 40 years. (Shea and Smart 1993).

The only solar particle events of interest are those capable of ground level observations with ion chambers (Fig. 1) or neutron monitors. The rates of occurrence of such events (Shea and Smart 1993) are shown in Fig. 5. The ground

level events vary greatly in intensity and only the most intense events are important to high-altitude aircraft protection. The largest ground level event yet observed occurred on Feb. 23, 1956 in which neutron count rates rose to 3,600 percent above background. Two of the aforementioned over 300 flights were made out of Fairbanks, Alaska during the event of March 30-31, 1969 with results shown in Fig. 6. If the ground level increase for the March 1969 event is used to scale other historical ground level events, we conclude that high-levels (1 cSv or more) of radiation exposure were present at aircraft altitudes in the past. The uncertainties in the proton spectra for the Feb. 1956 event are large but upper and lower bounds estimated by Foelsche result in dose equivalent rates from Monte Carlo calculations (Foelscheet al. 1969, Wilson et al. 1970, Armstrong et al. 1969) in qualitative agreement with those derived from simply scaling the March 1969 data. The Monte Carlo results are shown in Fig. 7 as calculated by the Langley code (Wilson et al. 1970) and Armstrong et al. (1969) at Oak Ridge National Laboratory using the High Energy Transport Code (HETC). The results in the figure use the maximum surface dose equivalent conversion factors for a 30-cm tissue slab geometry. Dose equivalent averaged over the 30-cm slab is approximately a factor of 2-3 lower for solar particle events (Foelsche et al. 1974). It was clear from these results that exposures to crew and passengers on high-latitude routes of the SST flying at 58 g/cm^2 would be unacceptable unless decent to subsonic altitudes was possible to minimize exposures during such a large event. The importance of such events is limited to the Polar Regions.

The main concern of these early studies was the potential prenatal injury in high-altitude flight especially during such a possible large solar event since crew and passengers included women of childbearing age. It is seen in Fig. 3 that flights from the US northeast to Europe fly along the edge of the polar region and are subject to solar particle event exposures (Wilson et al. 1995). An advisory committee to the Federal Aviation Administration (FAA 1975) recommended that a satellite early-warning/monitoring system be established, active onboard monitoring devices be included in the aircraft design, and that operational procedures be developed to insure that exposures on a given flight be limited to 5 mSv. Although many ground level events occur, only a few have been of such intensity as to be of concern to near term high-altitude air traffic. The *second* largest ground level event observed over the last 60 years is the event on September 29, 1989. This event was similar to the February 23, 1956 event in its time course and spectral content but of an order of magnitude lower intensity (on the order of 1 mSv/hr) and of less concern to supersonic operations. Since the February 23, 1956

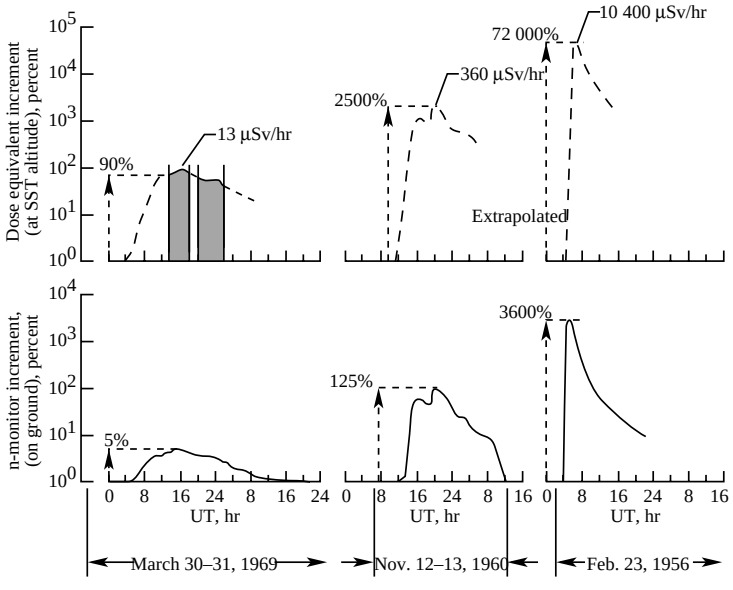

Fig. 6 . Energetic solar events measured on the ground and at SST altitude.

event is the only outstanding event, it leaves a heavy operational overhead requirement for such an unlikely occurrence. Yet, it is likely such an event will occur again and perhaps an even larger event. It is fortunate that high-altitude aircraft requirements are largely met by the space program and weather service requirements providing potential cost sharing (Wilson 1981).

RECENT *AIR* STUDIES

Many factors relative to aircraft exposures have changed over the last decade as recounted in the introduction. There are continued studies of a possible hypersonic air transport, which will bring a host of new issues as reviewed elsewhere (Wilson 2000). Two key events had an important impact on requirements for atmospheric ionizing radiation research over the last decade: the ICRP (1991) included aircrew among the defined occupationally exposed and NASA initiated a technology assessment for a possible second-generation supersonic transport (High Speed Civil Transport, HSCT).

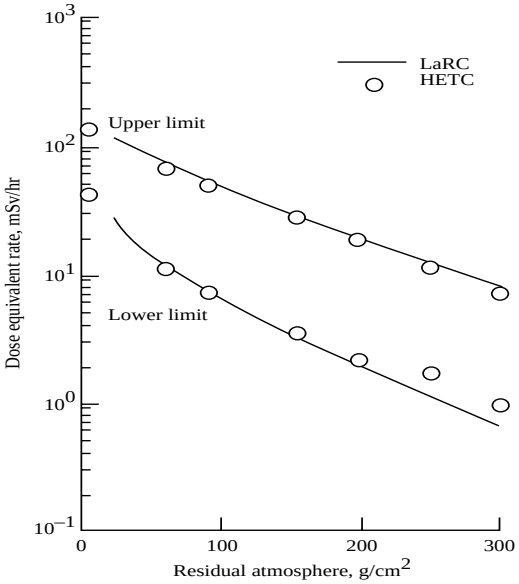

Fig. 7 Calculated upper and lower limits for dose equivalent rate at high latitude for the Feb. 23, 1956

Although a consistent data set over much of the Earth's surface and most of solar cycle 20 has been measured by the LaRC SST program, many of the individual components were not resolved due to instrument limitations at the time of measurement (circa 1964) and the major portion of the neutron spectrum depended on theoretical calculations for proton interactions with the atmosphere (Foelsche et al. 1974). Hewitt et at. (1978) measured the neutron spectrum using a Bonner sphere set up at subsonic altitudes and analyzed the data assuming a simple power spectrum and confirmed the importance of the high-energy neutrons but left the exact nature of the spectrum uncertain due to limitations of the analysis methods. Ferenc Hajnal of the DOE Environmental Measurements Laboratory developed new analysis techniques for unfolding Bonner sphere neutron spectral data and found important structural features in Hewitt's data near 100 MeV (see Fig. 8) that have important implications for aircraft exposures (Hajnal and Wilson 1991, 1992). A quick survey of published atmospheric neutron spectra shows considerable uncertainty in our knowledge and the impact of these uncertainties are analyzed elsewhere (Wilson et al. 1995, Wilson 2000). The status of knowledge of atmospheric ionizing radiation was reviewed by the NCRP (1996) providing a basis for continued studies in support of the HSCT technology assessment activity.

Further studies were started at the Langley Research Center. An instrument package was developed in accordance with the NCRP recommendations through an international guest investigator collaborative project, thereby ensuring

the availability of the numerous instruments required measuring the many components of the radiation spectra and providing a calibration platform for dosimetry. Selection criteria included: (a) the instruments had to fit within the cargo bay areas of the ER-2 airplane and be able to function in that environment, (b) the instruments had to be provided at no cost to meet budget constraints, (c) each instrument must have a principal investigator with independent resources to conduct data analysis, and (d) the instrument array must be able to measure all significant radiation components for which the NCRP (1996) had established minimal requirements. Also, the flight package had to be operational and the first flight to occur before or near the maximum in the galactic cosmic ray intensity (spring/summer 1997) and continued through the next cosmic ray minimum.

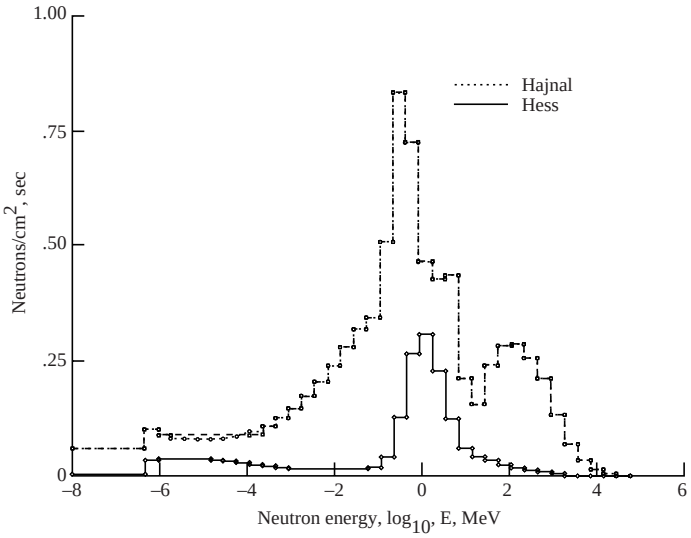

Fig. 8 Hajnal unfolded neutron spectrum from Hewitt data measured at 17.46°N at 23.5 km compared to Hess (1961) spectrum.

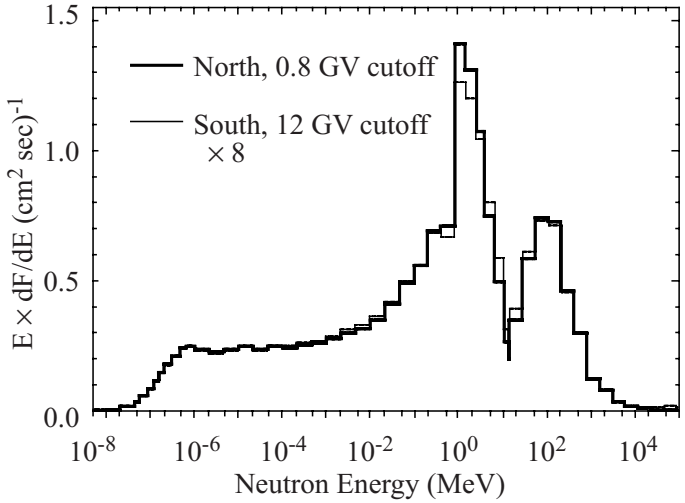

Fig. 9. Cosmic-ray neutron spectra measured at the northern end (54°N, 117°W, 0.8 GV cutoff, 56 g cm^{-2} atmospheric depth) and at the south end (19°N, 127°W, 12 GV cutoff; 54 g cm^{-2} atmospheric depth). The south spectrum is multiplied by 8.

The flight package was a collaboration of fourteen institutions in five countries and consisted of eighteen instruments able to separate the various physical components and tested various dosimeters (Goldhagen et al. 2000). The flight plan was established using the first *AIR* model (Tai et al. 1998) and concentrated on north/south surveys with an altitude profile at the northern extremity. The first flight series in June 1997 met with considerable success with the loss of only one instrument in the data flow. The flight program ended with the decision that technology was not ready to develop a competitive high-speed civil transport but the data analysis continues to this day including corrections for the ER-2 flight platform structure. Preliminary neutron spectra (Goldhagen et al. 2002) are shown in Fig. 9 and tend to confirm the results of Hajnal's analysis (Fig. 8). Note that the neutron spectra of the northern and southern flight extremes, where the geomagnetic cutoffs differ by more than an order of magnitude, are similar in spectral content with different magnitude. This corresponds well

with the more limited results of Foelsche et al. (1974), who likewise concluded that the spectrum has negligible differences in the upper atmosphere as a function of altitude and latitude.

A preliminary comparison of the first *AIR* model with the high-pressure argon ion chamber is given in Fig. 10. This was approximately a six and one-half hour flight starting June 13, 1997 at 15:52 from NASA Ames Research Center on a prescribed sequence of northern, western, and southern headings. This was the second northern flight and the aim was to approximately repeat the radiation measurements as a function of geomagnetic latitude to as far north as possible with altitude excursions along a constant-radiation, geomagnetic latitude line near Edmonton, Canada. During the westward portion of the flight, an altitude excursion was made as an altitude survey as evident in the figure. The AIR model using the recorded flight trajectory is shown in the figure for comparison with the measured flight data.

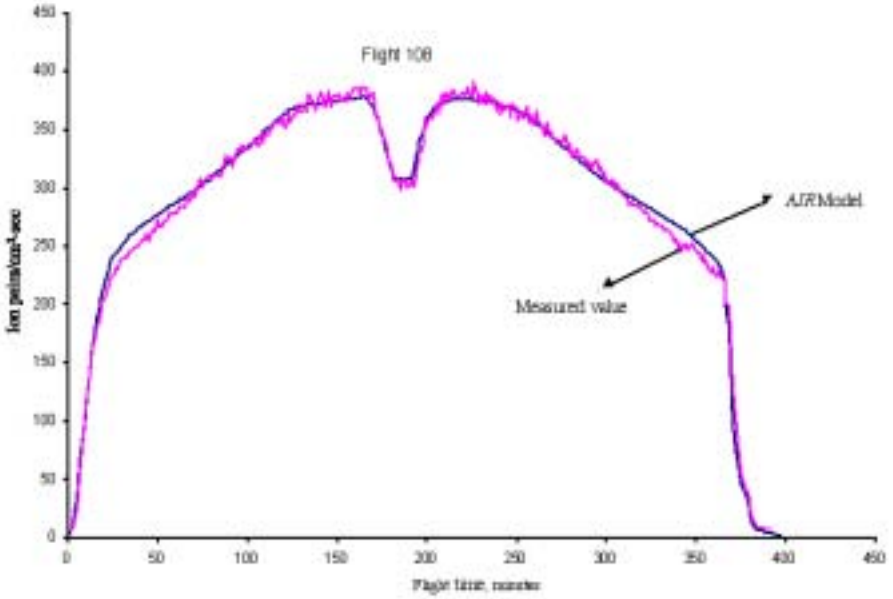

Fig. 10 Predicted and measured value of Air Ionization Rate as function of time for Flight 97-108, June 13, 1997.

A preliminary summary of European activity is given by McAulay et al. (1996). Further study of the atmospheric neutron spectrum lead by H. Schraube of GSF in Neuherberg has been funded by the Directorate General XII. The experimental component consists of a Bonner sphere spectrometer with a ^{3}He proportional counter

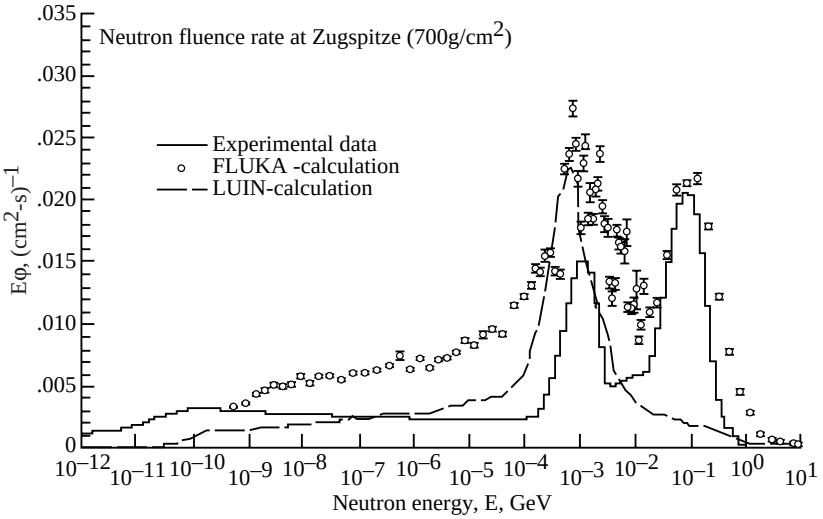

Fig. 11 Spectral neutron fluence rate obtained by measurements and calculations on top of Zugspitze (by permission of Schraube et al. 1998).

(Schraube et al. 1998) on a mountaintop (Zugspitze). The theory portion of the study uses the FLUKA code, currently maintained at CERN, and the known cosmic rays incident on the atmosphere (the multiple charged ions are assumed to be dissociated into nucleonic constituents (Roesler et al. 1998). It is interesting to note that the structure expected from the analysis of Hajnal at 100 MeV (Fig. 8) appears in both the measurements and the FLUKA calculation (see Fig. 11). Note that this feature is absent from the version of the LUIN code at the time of the study which depended on the Hess et al. (1961) spectrum for guidance, as the LUIN code is not a basic physics model in that information outside the basic LUIN transport model is used to patch an answer into the final values (O'Brien and Friedberg 1994). The importance of the Schraube et al. (1998) study is that the neutron ambient dose equivalent is about a factor of two larger than that estimated using the LUIN code (Schraube et al. 1998) and the added contributions are from high energy neutron interactions with tissue nuclei resulting in an array of high-LET reaction products at each collision event. Very little biological data exist on such radiations (Wilson et al. 1990, Wilson 2000, Cucinotta et al. 2001).

It was determined by Foelsche et al. (1974) using simultaneous flight measurements with a research aircraft and a balloon that local neutron production in materials of a small research aircraft added 10 percent to the measured neutron field. Later measurements by Wilson et al. (1994) onboard commercial subsonic transports found that the radiation levels varied by up to 30 percent within the aircraft cabin space. These results give incentive to evaluation of aircraft materials as a means to providing limited control of the interior environment. Evaluation of aircraft design alternatives requires a physics-based *AIR* model for which the transmission properties of aircraft materials can be folded into the design process.

POLICY & EPIDEMIOLOGY

Aside from the question of more restrictive regulatory requirements resulting in a FAA advisory (McMeekin 1990) there is increased concern for potential health outcomes among the crew in commercial aviation. The health outcomes are undoubtably related to environmental factors including radiation. Studies continue to expand giving greater statistical resolving power (De Angelis et al. 2001a). Although as a group the health risks of this select group of individuals are low (healthy worker effect, for the specific case of aircrew members, see De Angelis et al. 2001b), Band (1990) found increased risks of several types of cancer among Canadian commercial pilots. Further concern for some of the most sensitive occupants of commercial aircraft, the US National Institute for Occupational Safety and Health continues a study of early pregnancy outcomes among commercial flight attendants (Grajewski et al. 1994, Whelan 2002).

Table 1. *Cancer Sites with significant positive association for civilian airline flight personnel crewmembers. Confidence limits are 90 or 95 percent depending on study.*

Cancer Site	Sex	Job	Type	Confidence Limits		Source
All Sites*	M	CA	SIR	1.3	2.2	Haldorsen et al. (2001)
Bone	F	CA	SIR	1.8	54.4	Pukkala et al. (1995)
Brain	M	P	SIR	1.2	7.9	Band et al. (1990)
Brain	M	P	SMR	1.4	9.5	Band et al. (1990)
Breast	F	CA	SIR	1.2	2.2	Pukkala et al. (1995)
Breast	F	CA	SIR	1.0	4.3	Wartenberg et al. (1998, 1999)
Breast	F	CA	SIR	1.09	1.83	Reynolds et al. (2002)
Esophagus	M	CA	SIR	2.7	11.4	Haldorsen et al. (2001)
Hodgkin Lymphoma	M	P	SIR	1.2	11.7	Band et al. (1990)
Kidney and Pelvis	M+F	P	PMR	1.18	3.06	Nicholas et al. (1998)
Leukemia – AML	M	P	SIR	2.1	9.3	Band et al. (1996)
Leukemia – Myeloid	M	P	SIR	1.4	5.5	Band et al. (1996)
Liver*	M	CA	SIR	1.3	39.2	Haldorsen et al. (2001)
Prostate	M	P	SIR	1.4	2.5	Band et al. (1996)
Rectum	M	P	SMR	1.2	11.2	Band et al. (1990)
Skin – Melanoma	M	P	SMR	1.5	6.3	Irvine & Davies (1999)
Skin – Melanoma	M	PE	SIR	1.1	2.7	Haldorsen et al. (2000)
Skin – Melanoma	M	P	SIR	5.0	36.5	Rafnsson et al. (2000)
Skin – Melanoma	M	CA	SIR	1.1	6.4	Haldorsen et al. (2001)
Skin – Melanoma	M	P	SIR	2.85	4.23	Nicholas et al. (2001)
Skin – Melanoma	F	CA	SIR	1.2	6.7	Rafnsson et al. (2001)
Skin—Melanoma	M	P	SIR	1.27	4.54	Hammar et al. (2002)
Skin--Melanoma	F	CA	SIR	1.28	4.38	Reynolds et al. (2002)
Skin – Other Cancers	M	P	SIR	1.1	2.2	Band et al. (1990)
Skin – Other Cancers	M	PE (jets)	SIR	2.1	4.2	Gundestrup & Storm (1999)
Skin – Other Cancers	M	P	SIR	1.3	4.0	Haldorsen et al. (2000)
Skin – Other Cancers*	M	CA	SIR	4.5	18.8	Haldorsen et al. (2001)
Prostate#	M	P	SIR	1.19	2.29	Ballard et al. (2000)
Skin – Melanoma#	M	P	SMR	1.02	3.82	Ballard et al. (2000)

*cancer outcome possibly related to lifestyle only; # results from meta-analysis of previous studies, then adjusted for socio-economical status; AML = Acute Myeloid Leukemia; CA = Cabin Attendants;
P = Pilots only; PE = Pilots and flight Engineers; PMR = Proportional Mortality Ratio;
SIR = Standardized Incidence Ratio; SMR = Standardized Mortality Ratio

Although not a study of commercial aircrew, the report of the National Economic Council (NEC) Panel on *Occupational Hazards Associated with Nuclear Weapons Production* (NEC 2000) has important implications for commercial aviation. The US President requested the NEC to assess "whether there is evidence of occupational illness in current and former contract workers at the US Department of Energy (DOE) from exposures to occupational hazards unique to nuclear weapons production and evaluate the strength of that evidence." The NEC Panel (Task Group 1) found only modest average annual exposures of the DOE contractor workforce, 1.5 to 2 mSv to 1960, a slow decline from 1.5 mSv to 1 mSv in 1978 through 1988, followed to a rapid decline to a few tenths of a mSv past 1990 (compared to an estimated annual aircrew exposure (e.g., Chicago-to-NY) of 2.72 mSv, Friedberg

et al. 2002). Mortality studies among the DOE contractors showed a healthy worker effect but increased standard mortality and incident ratios (SMRs, SIRs) with 90-95 percent confidence intervals above unity (statistically significant) for cancer of the thyroid, breast, pharynx, esophagus, stomach, small intestine, pancreas, bile ducts, gall bladder, and liver as well as leukemia, multiple myeloma, and lymphomas (except Hodgkin's) as identifiable work related illnesses as concluded by the panel. A compensation program for this entire list of illnesses was set up with some limitations related to possible causality. Furthermore, several cancer sites showed positive correlations with radiation exposures while other cancer sites were assumed to be related to other environmental factors. As a result, the NEC recommended legislation for worker compensation for this restricted list of illnesses which were found with statically significant elevated SMRs and SIRs, leading to the *Energy Employees Occupational Illness Compensation Program Act of 2000* passed by the US Congress and signed into law.

A few studies of populations in high-altitude cities have concluded an inverse effect with radiation exposure although Weinberg et al. (1987) argues that oxygen effects may be the source of decreased adverse health risks at *high* altitudes. More recently studies of US Air Force pilots showed statistically significant elevated risks of cancer in genitals, testis, and urinary systems (Grayson and Lyons 1996). A recent study of mortality among US commercial pilots and navigators found statistically significant elevations of kidney and pelvic cancers (Nicholas et al. 1998). Many European epidemiological studies on health outcomes of aircrew have been in progress for several years (see e.g. Rafnsson et al. 2000, 2001, Ballard et al. 2002, and for reviews Ballard et al. 2000, De Angelis et al. 2001a, 2001b) and provide additional concern for the need for further studies in the US. It is well established that elevated standard mortality and incidence ratios with 90 to 95 percent confidence intervals above unity is observed among European aircrew as shown in Table 1 along with limited US studies. Even so, one might argue that the SMR and SIR depend on the control group and there are even regional differences as observed in the DOE contractor studies (NEC 2000) and the data still rests on relatively few occurrences in many cases (Friedberg et al. 2002). Still, establishment of policy and science are different issues and the data in Table 1 meets the selection criteria of the NEC panel for compensation (NEC 2000). It is anticipated that US crews who fly generally closer to the magnetic pole than European crews will have both different radiation exposure patterns and distribution of cancers with elevated SMRs. It appears the situation justifies that US aircrews are probably due illness compensatory legislation but insufficient data exists on which to write such legislation. It is imperative that US aircrew epidemiological studies are expanded to correct the current lack of data on cancer incidence and mortality among US aircrew in preparation of required legislation. This impetus follows since, "it is clear that there are health risks associated with a career of flying." (Friedberg et al. 2002)

CONTINUING US ACTIVITY

Three issues continue to be addressed within the US: development of the basic *AIR* model including experimental validation, testing of potential aircraft material transmission properties, and epidemiological studies. The extent of the ongoing activity will be briefly reviewed in this section.

The continued analysis of the ER-2 flight data has concentrated on establishing corrections to the neutron spectrum due to packaging into the flight racks and the surrounding aircraft structure (Goldhagen et al. 2003). This will be followed by analysis of the other instruments used on the flights including the high-pressure ion chamber, the various scintillators, and particle telescopes. Collaboration with the Bartol Research Institute at the University of Delaware and their unique augmentation of FLUKA to include collisional source terms for multiple charged ions is being evaluated for use in deriving a new physics-based *AIR* model (Clem et al. 2003). Preliminary comparisons of the altitude survey at the northern extreme of the ER-2 flight shown in Fig. 12 are encouraging. The new *AIR* model will include a dynamic geomagnetic transmission model for years 1945 to 2020 including geomagnetic storm effects (De Angelis et al. 2003). The fundamental model will be for the particle fields allowing introduction of aircraft geometry and human geometry for final exposure evaluation. One use of the model will be to evaluate single event effects on avionics in future aircraft design. With the historic variation of the geomagnetic transmission factors, the model will enable exposure assessment in retrospective health outcome studies.

The transmission properties of materials in such a complicated environment are poorly understood. The effects of the surrounding aircraft materials and payload on the exposures within the cabin space and on the flight deck are largely unknown. As a result we have designed a flight experiment for the ER-2 aircraft for evaluation of material effects on the local radiation environment. The experiment uses cross-calibrated TEPCs to measure effects on the lineal energy spectra as a function of material type. One rack of the basic apparatus is shown in Fig. 13. There are two such racks that fill the two well-isolated superpod tailcones mounted on the midwings of the ER-2. The measured change in lineal energy spectral content as a function of shield material will give us a degree of measure of the change in the physical fields within the shielded region to evaluate computational shielding models. Fundamental to this usage is an improved understanding of the TEPC response in such mixed radiation fields (Shinn et al. 2001).

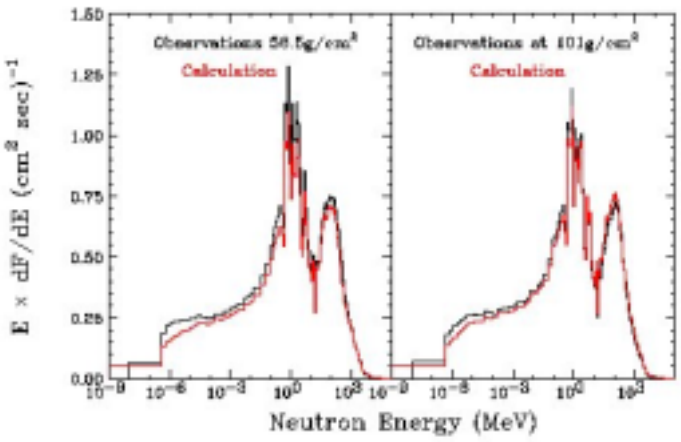

Fig. 12 Comparison of the augmented FLUKA evaluated neutron spectra at the northern extreme of June 1997 ER-2 flight measurements.

The NIOSH/FAA Study of Reproductive Disorders in Female Flight Attendants remains as the only US led epidemiological effort of which we are aware. The study is in three parts: data on reproductive outcomes by questionnaire, ovulation function study using hormone testing, and an environmental assessment of the cabin space (Whelan 2002). Primary school teachers of the same age distribution are being used as a control group for the study.

Fig. 13 Aircraft shield materials experiment rack being prepared for ER-2 flight.

CONCLUDING REMARKS

SST related studies of atmospheric ionizing radiation quantified the exposure fields, established neutrons as the dominant component of radiation health hazard, and identified solar particle event exposures of pregnant occupants as a major health issue. Even then it was recognized that background exposures of commercial aircrew placed them among the most highly exposed occupational groups. As cancer risk coefficients were revised to greater values and corresponding new safety standards implemented, concern over potential health risks led to a number of studies of the radiation environment and corresponding studies of health risks at subsonic commercial transport altitudes. Although unrelated, identifiable added health risks were found in epidemiological studies of nuclear weapons workers, who were generally less exposed to ionizing radiation than commercial aircrew. The resulting legislation for the US nuclear weapon contractors has strong implications for aircraft safety. Extensive studies of European aircrews have resulted in a database adequate for compensation of European aircrew. However, the corresponding database on US aircrew is lacking. An accurate physics based *AIR* model is required to evaluate reference exposures for epidemiological studies and evaluation of potential design features of future aircraft to improve safety. The development of such a model has been the focus of the NASA Langley Research Center for the last several years. A comprehensive flight measurements program is required to validate the *AIR* model and evaluate the transmission properties of aircraft materials.

REFERENCES

Allkofer, O. C., W. Heinrich, Measurement of galactic cosmic ray nuclei at supersonic transport altitudes and their dosimetric significance. *Health Phys*. **27**, 543-551, 1974.

Anon. Report on a workshop to examine methods to arrive at risk estimates for radiation-induced cancer in the human based on laboratory data. *Radiat Res* **135**, 434-437,1993.

Armstrong, H., H. Haber, H.Strunghold, Aero medical problems of space travel-panel meeting, School of Aviation Medicine, *J Aviation Med* **20**, 383-417, 1949,

Armstrong, T. W., R.G. Alsmiller, and J. Barish, Calculation of the radiation hazard at supersonic aircraft altitudes produced by an energetic solar flare. *Nucl Sci Eng* **37**, 337-342, 1969.

Ballard, T.J., S. Lagorio, M. G. De Angelis, and A. Verdecchia. Cancer Incidence and Mortality among Flight Personnel: a Meta-Analysis, *Aviat Space Environ Med* **71**, 216-224, 2000.

Ballard, T.J., S. Lagorio, M. De Santis, G. De Angelis, M. Santaquilani, M. Caldora, and A. Verdecchia. "A retrospective cohort mortality study of Italian commercial airline cockpit crew and cabin attendants, 1965-96", *Int. J. Occup. Environ. Health* **8**, 87-96, 2002.

Band, P.R., J.J. Spinelli, V.T.Y. Ng, J. Moody, and R.P. Gallagher. Mortality and cancer incidence in a cohort of commercial airline pilots. *Aviat Space Environ Med* **61**, 299-302, 1990.

Band, P.R., N.D. Le, R. Fang, M. Deschamps, A.J. Coldman, R.P. Gallagher, and J. Moody. "Cohort study of Air Canada Pilots: mortality, cancer incidence, and leukemia risk. *Am J Epidemiol* **143**, 137-143, 1996.

Barish, R. J. Health physics concerns in commercial aviation. *Health Phys.* **59**, 199-204, 1990.

BEIR, *Health effects of exposure to low levels of ionizing radiation: BEIR V*. Natl. Acad. Press, 1980.

Bethe, H. A., S.A. Korff, and G. Placzek, On the interpretation of neutron measurements in cosmic radiation, *Phys. Rev*. **57**, 573-587, 1940.

Boeing, http://biz.yahoo.com/n/b/ba.html, 2002.

Bramlitt, E. T. Commercial Aviation Crewmember radiation doses. *Health Phys.* **49**, 945-948, 1985.

Clem, J., G. De Angelis, P. Goldhagen, J.W. Wilson, Validation of computational procedures for a new atmospheric ionizing radiation (*AIR*) model. *Adv. Space Res*. This issue, 2003.

Cucinotta, F.A., W. Schimmerling, J.W., Wilson, L.E. Peterson, G.D. Badhwar, P. Saganti, J.F. Dicello, Space radiation cancer risks and uncertainties for Mars missions. *Radiat. Res*. **156**: 682-688, 2001.

De Angelis, G., M. Caldora, M. Santaquilani, R. Scipione, and A. Verdecchia. Radiation-Induced Biological Effects on Crew Members: A Combined Analysis on Atmospheric Flight Personnel, *Phys. Med.* **17**, **Suppl. 1**, 175-176, 2001a.

De Angelis, G., M. Caldora, M. Santaquilani, R. Scipione, and A. Verdecchia. Health risks from radiation exposure for civilian aviation flight personnel: a study of Italian airline crew members, *Radiat. Res.* **156**, 689-694, 2001b.

De Angelis, G., J.M. Clem, P. Goldhagen, J.W. Wiilson, A new dynamical atmospheric ionizing radiation (AIR) model for epidemiological studies. *Adv. Space Res*. This issue, 2003.

FAA, Cosmic radiation exposure in supersonic and subsonic flight. *Aviat Space Environ Med* **46**, 1170-1185, 1975.

Fiorino, F. Airline outlook, Radiation Limits, Aviat. Week and Space Tech. p. 23, June 3, 1996.

Foelsche, T. *Radiation Exposure in Supersonic Transports*. NASA TN D-1383, 1961.

Foelsche, T., and E.H. Graul, Radiation Exposure in Supersonic Transports, *Atompraxis*, **8**, 365-380, 1962.

Foelsche, T. SST report on the space radiation effects on the Apollo mission. *Second Symposium on Protection Against Radiations in Space,* Arthur Reetz, ed., NASA SP-71, 139-156, 1965.

Foelsche, T., R. Mendell, R.R. Adams, J.W. Wilson, Measured and Calculated Radiation Levels Produced by Galactic and Solar Cosmic Rays in SST Altitudes and Precaution Measures to Minimize Implecations at Commercial SST-Operations. NASA paper prepared for *the French-Anglo United States Supersonic Transport VII Meeting*, Paris, France, Mar. 3, 1969.

Foelsche, T., R. Mendell, J.W. Wilson, R.R. Adams, *Measured and calculated neutron spectra and dose equivalent rates at high altitudes: relevance to SST operations and space research*, NASA TN D-7715, 1974.

Friedberg, W., D.N. Faulkner, L. Snyder, E.B. Darden, K. O'Brien, Galactic cosmic radiation exposure and associated health risks for air carrier crewmembers. *Aviat., Space, and Environ. Med.* **60**, 1104-1108, 1989.

Friedberg, W., K. Copeland, F.E. Duke, J.S. Nicholas, E.B. Darden, K. O'Brien, Radiation exposure of aircrews. Occupational Medicine: State of the Art Reviews **17**: 293-309, 2002.

Frier, P., E.J. Lofgren, E.P. Ney, and F. Oppenheimer, The heavy component of the primary cosmic rays. *Phys. Rev*. **74**, 1818-1827, 1948.

Goldhagen, P., Overview of aircraft radiation exposure and recent ER-2 measurements. *Health Phys*.**79**: 526-544, 2000.

Goldhagen, P., M. Reginatto, T. Kniss, J.W. Wilson, R.C. Singleterry, I.W. Jones, W. Van Steveninck, Measurement of the energy spectrum of cosmic-ray induced neutrons aboard an ER-2 high-altitude airplane. *Nucl. Inst. & Meth*. A **476**: 42-51, 2002.

Goldhagen, P., J.M. Clem, J.W. Wiilson, Recent results on measurements of the energy spectrum of cosmic-ray neutrons aboard a ER-2 airplane and on the ground. *Adv. Space Res*. This issue, 2003.

Grajewski, B., E.A. Whelan, M.A. Waters, J.S. Kesner, and T.M. Schnorr, Overview of the proposed NIOSH-FAA study of reproductive disorders in femal flight attendants. Paper presented at the *42nd Annual Meeting of the Radiation Research Society*, Nashville, TN, April-May 1994.

Grayson, J.K., T.J. Lyons, Cancer incidence in United States Air Force aircrew, 1975-89. *Aviat., Space, & Environ. Med***. 67**: 101-104, 1996.

Gundestrup, M., and H.H. Storm, Radiation-Induced Acute Myeloid Leukaemia and Other Cancers in Commercial Jet Cockpit Crew: a Population-Based Cohort Studies, *Lancet,* **354**, 2029-2031, 1999.

Hajnal, F., and J.W. Wilson, High-altitude cosmic-ray neutrons: a significant contributor to the radiation exposures at aircraft altitudes. *Seventh Symposium on Neutron Dosimetry*, Berlin, October 14-18, 1991.

Hajnal, F., and J.W. Wilson, High-altitude cosmic ray neutrons: probable source for the high energy protons at the earth's radiation belts. In proc. *8th Congress Intl. Radiat. Prot. Ass.* Montreal, p 1620, 1992.

Haldorsen, T., J. Reitan, and U. Tveten. Cancer incidence among Norwegian airline pilots. *Scand. J. Work. Environ. Health* **26**,106-111, 2000.

Haldorsen, T., J. Reitan, and U. Tveten. Cancer incidence among Norwegian airline cabin attendants. *Int. J.Epidemiol.* **30**,825-830, 2001.

Hammar N, Linnersjo A, Alfredsson L, Dammstrom B-G, Johansson M, Eliasch H. Cancer incidence in airline and military pilots in Sweden 1961 ˆ 1996. Aviat Space Environ Med 73:2-7, 2002.

Hess, V. F., and J. Eugster, *Cosmic Radiation and Its Biological Effects*, Fordham University Press, New York, 1949.

Hess, W. N., E.H. Canfield, and R.E. Lingenfelter, Cosmic-ray neutron demography. *J. Geophys. Res.* **66**, 665-667, 1961.

Hewitt, J. E., L. Hughes, J.W. Baum, A.V. Kuehner, J.B. McCaslin, A. Rindi, A.R. Smith, L.D. Stephens, R.H. Thomas, R. V. Griffith, and C.G. Welles, Ames collaborative study of cosmic ray neutrons mid-latitude flights. *Health Phys.* **34**, 375-384, 1978.

ICAO "Annex 6: To the converntion on International Civil Aviation, Part I: International Commercial Air Transport-Aeroplanes" *International Standards and Recommended Practices*. Sixth Edition of Part I, July 1995. International Civil Aviation Organization, 1995.

ICRP Task Group Radiobiological aspects of the supersonic transport. *Health Phys*. **12**, 209-226, 1966.

ICRP *The 1990 Recommendations of the International Commission for Radiological Protection*, ICRP Report 60, Pergamon Press, Oxford, UK, 1991.

ICRU *The quality factor in radiation protection*. ICRU Rep. 40, Bethesda, M.D., 1986.

Irvine, D., and D. Davies. British Airways Flightdeck Mortality Study, 1950-1992. *Aviat. Space Environ. Med.* **70**, 548-555, 1999.

Jiang, T.-N., B.L. Lord, J.H. Hendry, Alpha particles are extremely damaging to developing hemopoiesis compared to gamma irradiation. *Radiat. Res.* **137**, 380-384, 1994.

Lambiotte, J. J., J.W. Wilson, and T.A. Filipas, *PROPER-3C: A Nucleon-Pion Transport Code.* NASA TM X-2158, 1971.

Lebuser, H. J. Round table discussion. *Radiat. Prot. Dosim.* **48**, 136-138, 1993.

McAulay, I. R., D.T. Bartlett, G. Dietze, H.G. Menzel, K. Schnuer, and U.J. SCHREWE, *Exposure of air crew to cosmic radiation.* European Radiation Dosimetry Group, EURADOS report 1996-01, 1996.

McMeekin, R. R. *Radiation exposure of air carrier crewmembers.* FAA Advis. Circ. No. 120-52, Mar. 1990.

NCRP *Limitation of exposure to ionizing radiation.* NCRP Rep. 116, Bethesda, MD., 1993.

NCRP *Radiation exposures and high-altitude flight.* NCRP commentary No. 12, NCRP, Bethesda, MD., 1996.

NEC http://www.eh.doe.gov/benefits/nec/necreport1.pdf, 2000.

Nicholas, J.S., D.T. Lackland, M. Dosemeci, L.C. Mohr Jr., J.B. Dunbar, B. Grosche, and D.G. Hoel. Mortality among US commercial pilots and navigators. *J. Occup. Environ. Med.* 40, 980-985, 1998.

Nicholas et al., G.C. Butler, D.T. Lackland, G.S. Tessier, L.C. Mohr Jr., and D.G. Hoel. Health among commercial airline pilots, *Aviat. Space Environ. Med.* **72**, 821-826, 2001.

O'Brien, K., and W. Friedberg, Atmospheric cosmic rays at aircraft altitudes. *Environ Internat'l* **20**, 645-663, 1994.

O'Sullivan, D. The DOSEMAX Team ..The radiation field at aircraft altitudes-A decade of progress. *Adv. Space Res*. This issue, 2003.

Pukkala, E., A. Auvinen, and G. Wahlberg, Incidence of Cancer among Finnish Airline Cabin Attendants, *Br. Med. J.* **311**, 649-652, 1995.

Rafnsson, V, J. Hrafnkelsson, and H. Tulinius. Incidence of cancer among commercial airline pilots. *Occup. Environ. Med.* **57**, 175-179, 2000.

Rafnsson, V, H. Tulinius, J.G. Jonasson, and J. Hrafnkelsson. Risk of breast cancer in female flight attendants: a population-based study (Iceland). *Cancer Causes Control* **12**, 95-101, 2001.

Reitz, G., K. Schnuer, K. Shaw, "Editorial--Workshop on radiation Exposure of civil aircrew." *Radiat. Prot. Dosim.* **48**, 3, 1993.

Reynolds P, Cone J, Layfesky M, Goldberg DE, Hurley S. Cancer incidence in California flight attendants (United States). Cancer Causes Control 13:317-324, 2002.

Roesler, S., W. Heinrich, and H. Schraube, Calculation of Radiation Fields in the Atmosphere and Comparison to Experimental Data. *Radiat. Res.* **149**, 87-97, 1998.

Schaefer, H. J. Evaluation of present-day knowledge of cosmic radiation at extreme altitude in terms of the hazard to health, *J. Aviation Med*. **21**, 375-94, 1950.

Schaefer, H. J., "Exposure hazards from cosmic radiation beyond the stratosphere and in free space." *J. Aviation Med.* **23**, 334-344, 1952.

Schaefer, H.J., Radiation and man in space. *Adv. Space Res*. **1**: 267-339, 1959.

Schraube, H., G. Leuthold, S. Roesler, and W. Heinrich, Neutron spectra at Flight Altitudes and Their Radiological Estimation. *Personal communication,* 1998.

Shea, M. A., and D.F. Smart, History of energetic solar protons for the past three solar cycles including cycle 22 update. *Biological Effects and Physics of Solar and Galactic Cosmic Radiation,* C. E. Swenberg, G. Horneck, G. Stassinopoulos, eds. Plenum Press, 37-71, 1993.

Shinn, J.L., J.W. Wilson, M.S. Xapsos*, An Improved Analytical Model for Microdosimeter Response.* NASA/TP-2001-211040, 2001.

Tai, H.; J.W. Wilson, and D.L. Maiden*, Atmospheric Ionizing Radiation (AIR) ER-2 Preflight Analysis*, NASA Technical Paper 1998-208422, June 1998.

UNSCEAR, United Nations Scientific Comm. on Effects of Atomic Radiation: *Sources, effects and risks of ionizing radiation-1988 report to the General Assembly,* United Nations, 1988.

Wartenberg D, Stapleton CP. Risk of breast cancer is also increased among retired US female airline cabin attendants. BMJ 316:1902, 1998.

Wartenberg D, Stapleton CP. Risk of breast cancer among female airline cabin attendants. BMJ 318:126, 1999.

Weinberg, C. R., K.G. Brown, D.G. Hoel, Altitude, Radiation, and Mortality from Cancer and Heart Disease. *Radiat. Res*. **112**: 381-390, 1987.

Whelan, E.A. *The Working Women's Health Study: The NIOSH/FAA Study of Reproductive Disorders in Female Flight Attendants*. National Institute for Occupational Safety and Health, Status Reports Q2 2002.

Wilson, J. W., J.J. Lambiotte, T. Foelsche and T.A. Filippas, *Dose Response Functions in the Atmosphere Due to Incident High-Energy Protons with Application to Solar Proton Events.* NASA TN D-6010, 1970.

Wilson, J. W., Solar Radiation Monitoring for High Altitude Aircraft. *Health Physics* 41:607, 1981.

Wilson, J. W., L.W. Townsend, Radiation Safety in commercial air traffic: a need for further study. *Health Phys.* **55**, 1001-1003; **56**, 973-974, 1988.

Wilson, J. W., J.L. Shinn, and L.W. Towsend, Nuclear reaction effects in conventional risk assessment for energetic ion exposures. *Health Phys*. **58**, 749-752, 1990.

Wilson, J. W., L.W. Townsend, W. Schimmerling, G.S. Khandelwal, F. Khan, J.E. Nealy, F.A. Cucinotta, L.C. Simonsen, J.L. Shinn, J. W. Norbury*, Transport methods and interactions for space radiation.* NASA RP-1257, 1991.

Wilson, J. W., J.E. Nealy, F.A. Cucinotta, J.L. Shinn, F. Hajnal, M. Reginatto, and P.Goldhagen, *Radiation safety aspects of commercial high-speed flight transportation.* NASA TP-3524, 1995.

Wilson, J.W. Overview of radiation environments and human exposures. *Health Phys*. **79**: 470-494, 2000.

Wilson, O.J., B.F. Young, and C.K. Richardson, Cosmic radiation doses received by Austrlian commercial flight crews and the implications of ICRP 60. *Health Phys*. **66**: 493-502, 1994.

Appendix A: The AIR Team

NASA LaRC
Aerospace Electronic Systems Division
David Terray
Donna Gallaher
Keith Harris
Mark Hutchinson
Peter Huynh
Dan Norfolk
Otis Riggins
Lloyd Spangler
Keith Woodman

Aerospace Mechanical Systems Division
Charles Bailey
Frank Boyer
Terry Clark
Keith Davis
Robert Davis
Irby Jones
Tommy Leffel
Vernon Marshall
Sonny Overbay
Ross Phillips
Richard Shearer
Robin Tutterow

Materials Division
Hsaing Tai
Judy Shinn
John Wilson

Fabrication Division
Thomas Abbott
Dolye Arboneaux
Wayne Barfoot
Carlos Castillo
Wayne Davis
Ronald Deans
William Drummond
James Firth
Robert Gage
Warren Hartraft
Charlie Haynes
Noel Hudgins
William Jones
Bruce Little
Franklin Mayhew
Eugene Robbins
Donald Smith
James Smith
Michael Smock
Ronald Topping
Mark Wynkoop

Flight Operations and Support Division
Mike Klebitz

HSRPO
Don Maiden
Allen Whitehead

LaRC Contractor Support
NYMA
Jennifier Allen
Sheryl Johnson
Raytheon
Brenda Adams
Ted Allen
Jeri Carter
Karen Cruz
Kent Davis
Tom Feigh
Mick Hartzheim
Larry Harvey
Carol Hayes
Viola Jackson
Mike Jenkins
Mary Jo Waterton
Cathy Kern
Arlene Knick
June Lawerance
Tom Luck
Vanessa Massengill
Peggy McCloud
Delores Russell
Rick Taylor
Rick Thomas
Paul Timbrell
Sam Tucker
Willie Wilson

NASA -ARC
NASA
Steve Patterson
Andrew Roberts
Jim Barrilliaux

Lockheed Martin Skunk Works
John Baca
James Barnes
Ken Broda
Gil Cagonot
Jeff Cohen
Paul Cole
Bill Collette
Mark Davis
Steve Geary
Rick Goodyear
Dave Gutierrez
Conrad Hornak
Harvey Kent
Hector Martinez
Jerry Moya
Ron Norris
Jay Nystrom

Ray Parada
Dee Porter
James Porter
Robert Porter
Greg Prince
Walt Prouty
Larry Robello
Larry Salter
Jim Sokolik
John Tilley
Floyd Whitmill
Bob York
Myron Yorks

Simco Electronics
Sue Tolley

U.S. Department of Energy
Environmental Measurements Laboratory
Paul Goldhagen
Marcel Reginatta

NASA HQ
Jim Huning Code Y
Walter Schimmerling Code UL

FAA Civil Aeromedical Inst.
Wallace Friedberg

NASA Johnson Space Center
Dr. Gautam Badhwar

National Radiation Protection Board, UK
Dr. David Bartlett

Royal Military College of Canada
Dr. L. G. I. Bennett
Lt. Martin Pierre

University of San Francisco
Dr. Eugene Benton

The Boeing Company
Dr. Alexander Chee

Defense Research Establishment Ottawa
Dr. Tom Cousins
Trevor Jones

University of Pisa, Italy
Dr. Francesco d'Errico

German Aerospace Research Establishment
Dr. Guenther Reitz

University of Kiel
Dr. Rudolf Beaujean

Appendix B: Workshop Participants

Last Name	First Name	Affiliation
Armstrong	Glenford Whit	DOT-Canada
Badhwar	Gautam	NASA Johnson Space Center
Bartlett	David	Natl. Radiological Protection BD – UK
Bennet	Les	RMC Canada
Benton	Eric	U. of San Francisco
Bloom	Thomas F.	NIOSH
Brady	Leslie A.	Texas A&M Univeristy
Bushnell	Dennis	NASA Langley Research Center
Chee	P. Alexander	Boeing-Seattle
Clowdsley	Martha	Old Dominion University
Copeland	Kyle	FAA
d'Errico	Francesco	U. of Pisa/Yale U.
De Angelis	Giovanni	Istituto Superiore di Sanita' - Italy
Friedberg	Wallace	FAA
Goldhagen	Paul	Evironmental Measurements Lab.-DOE
Huston	Stuart L.	Boeing-Huntington Beach
Jones	Irby	NASA Langley Research Center
Kim	Myung-Hee	NASA Langley Research Center
Lawton	Ralph M.	Prairie View A&M
Lewis	Brent	RMC Canada
Maiden	Don	NASA Langley Research Center
Menzel	Hans-Georg	European Commission-Belgium
Moore	Al	NASA Langley Research Center
Normand	Eugene	Boeing-Seattle
Pierce	Martin	RMC Canada
Reitz	Guenther	DLR-Germany
Sakamoto	Yukio	Japan Atomic Energy Research Inst.
Schimmerling	Walter	NASA Headquarters
Shinn	Judy	NASA Langley Research Center
Singh	Jay	NASA Langley Research Center
Singleterry	Robert	NASA Langley Research Center
Stassinopoulos	E. G.	NASA Goddard Space Flight Center
Tai	Hsiang	NASA Langley Research Center
Tripathi	Ram	Hampton University
Tume	Pamela	RMC Canada
Walker	L. Scott	Los Alamos National Laboratory
Whitehead	Allen	NASA Langley Research Center
Wilhite	Alan	NASA Langley Research Center
Wilson	John	NASA Langley Research Center
Wrobel	Mark	U.S. Air Force
Yoshizawa	Nobuaki	Mitsubish Research Inst.-Japan

REPORT DOCUMENTATION PAGE

Form Approved
OMB No. 0704-0188

1. REPORT DATE *(DD-MM-YYYY)*	2. REPORT TYPE	3. DATES COVERED *(From - To)*
01- 02 - 2003	Conference Publication	

4. TITLE AND SUBTITLE

Atmospheric Ionizing Radiation (AIR): Analysis, Results, and Lessons Learned From the June 1997 ER-2 Campaign

5a. CONTRACT NUMBER

5b. GRANT NUMBER

5c. PROGRAM ELEMENT NUMBER

6. AUTHOR(S)

Wilson, J. W.; Jones, I. W.; Maiden, D. L.; and Goldhagen, P.

5d. PROJECT NUMBER

5e. TASK NUMBER

5f. WORK UNIT NUMBER

784-50-00-01

7. PERFORMING ORGANIZATION NAME(S) AND ADDRESS(ES)

NASA Langley Research Center
Hampton, VA 23681-2199

8. PERFORMING ORGANIZATION REPORT NUMBER

L-18242

9. SPONSORING/MONITORING AGENCY NAME(S) AND ADDRESS(ES)

National Aeronautics and Space Administration
Washington, DC 20546-0001

10. SPONSOR/MONITOR'S ACRONYM(S)

NASA

11. SPONSOR/MONITOR'S REPORT NUMBER(S)

NASA/CP-2003-212155

12. DISTRIBUTION/AVAILABILITY STATEMENT

Unclassified - Unlimited
Subject Category 93
Availability: NASA CASI (301) 621-0390 Distribution: Standard

13. SUPPLEMENTARY NOTES

Wilson, Jones, and Maiden: NASA Langley Research Center, Hampton, VA; Goldhagen: DOE Environmental Measurements Laboratory, New York, NY
An electronic version can be found at http://techreports.larc.nasa.gov/ltrs/ or http://techreports.larc.nasa.gov/cgi-bin/NTRS

14. ABSTRACT

The United States initiated a program to assess the technology required for an environmentally safe and operationally efficient High Speed Civil Transport (HSCT) for entrance on the world market after the turn of the century. Due to the changing regulations on radiation exposures and the growing concerns over uncertainty in our knowledge of atmospheric radiations, the NASA High Speed Research Project Office (HSRPO) commissioned a review of "Radiation Exposure and High-Altitude Flight" by the National Council on Radiation Protection and Measurements (NCRP). On the basis of the NCRP recommendations, the HSRPO funded a flight experiment to resolve the environmental uncertainty in the atmospheric ionizing radiation levels as a step in developing an approach to minimize the radiation impact on HSCT operations. To minimize costs in this project, an international investigator approach was taken to assure coverage with instrument sensitivity across the range of particle types and energies to allow unique characterization of the diverse radiation components. The present workshop is a result of the flight measurements made at the maximum intensity of the solar cycle modulated background radiation levels during the month of June 1997.

15. SUBJECT TERMS

Atmospheric ionizing radiation; Aircrew health; Aircraft exposures.

16. SECURITY CLASSIFICATION OF:			17. LIMITATION OF ABSTRACT	18. NUMBER OF PAGES	19a. NAME OF RESPONSIBLE PERSON
a. REPORT	b. ABSTRACT	c. THIS PAGE			STI Help Desk (email: help@sti.nasa.gov)
					19b. TELEPHONE NUMBER *(Include area code)*
U	U	U	UU	424	(301) 621-0390